ICPIG XXXV
Egmond aan Zee
2023

July 9th – 14th, 2023

Hotel Zuiderduin, Egmond aan Zee,

The Netherlands.

www.icpig2023.com

Version: July 12, 2023

TU/e

Contents

1 ICPIG — a forum for discussion

1.1 History and mission

The International Conference on Phenomena in Ionized Gases (ICPIG), now in its XXXV edition, since 1953 has been a forum for the discussion of nearly all fields of plasma science, covering modelling and experiments, from the fundamentals of elementary processes, basic data and discharge physics (including transport and interaction with walls), to applications. Topics include plasma processing of surfaces and particles, high pressure and thermal plasma processing, development of radiation sources, plasma medicine, atmospheric and stellar plasmas, environmental protection and pollution control, plasma aerodynamics, and non-thermal plasmas in fusion devices.

In response to the Covid crisis, and to stay in an interchanging schedule with the ESCAMPIG, ICPIG XXXV has been postponed from July 2021 to July 2023. We are looking forward to resuming direct scientific exchange in a pleasant atmosphere.

1.2 Selection of talks

General and topical invited talks have been suggested and selected by the International Scientific Committee. The ISC also elected the winner of the von Engel and Franklin prize. The 36 selected talks have been selected by the ISC from the 125 abstracts whose authors applied for it; criteria were the scientific impact and a proper representation of participating countries. Other abstracts are presented as posters. The special session has been organised by the Local Organising Committee.

1.3 von Engel and Franklin prize

The 2023 winner of the von Engel and Franklin prize is:

Jean-Pierre Boeuf of Université P. Sabatier in Toulouse, France.

He was elected by ICPIG's international scientific committee. He will deliver his prize-lecture at the ICPIG on Friday morning. The "von Engel and Franklin Prize" was established in 1998. It is sponsored by the "Hans von Engel and Gordon Francis Fund" and is administered by the Board of Physical Sciences, University of Oxford. The prize is named in honour of two distinguished colleagues who had a major role in ICPIG and its community since the first meeting in 1953.

The prize is awarded every two years to an individual for work in the field of physics and technology of plasmas and ionized gases, as covered by ICPIG meetings. The selection is conducted by the International Scientific Committee, based either on long-standing and important contributions to the field, or an outstanding achievement giving rise to a new field, or both.

1.4 Information for Presenters

Selected orals are 20 minutes (16 min + 4 min questions), topical invited orals and special session invited orals are 30 minutes (25 min + 5 min questions), general invited orals are 45 minutes (40 min + 5 min questions) and the von Engel and Franklin prize is 60 minutes (55 min + 5 min questions). Orals will be presented from a modern Windows laptop, including Office 365 and Adobe Reader. Please upload your presentation to the laptop in the lecture hall well in advance of your scheduled presentation block.

Posterboards will be 1.25 meter high and 1.00 meter wide. Posters can be mounted before a poster session and should be removed in time before the next poster session.

1.5 Conference Topics

T1 Elementary processes and fundamental data

T2 Thermodynamics and transport phenomena

T3 Plasma wall interactions, electrode and surface effects

T4 Collective and nonlinear phenomena

T5 Modeling and simulation techniques

T6 Plasma diagnostic methods

T7 Astrophysical, geophysical and other natural plasmas

T8 Low pressure plasmas

T9 High frequency and pulsed discharges

T10 Non-equilibrium plasmas and microplasmas at high pressures

T11 Plasmas in/with liquids

T12 Thermal plasmas

T13 Complex and dusty plasmas, ion-ion plasmas, mixed phase plasmas

T14 Plasma created by external sources of ionization

T15 Plasma processing of surfaces and particles

T16 High pressure and thermal plasma processing

T17 Medical, biological, environmental and aeronautical applications

T18 Plasma power and pulsed power technology, particle and radiation sources

T19 Other applications

1.6 Local Organizing Committee

Ute Ebert (chair), Centre for Mathematics and Computer Science (CWI) Amsterdam and Eindhoven University of Technology (TU/e)

Sander Nijdam (co-chair), TU/e

Jannis Teunissen CWI

Jan van Dijk TU/e

Job Beckers TU/e

Baohong Guo CWI

Hemaditya Malla CWI

Conference organisation is supported by:
Ms. Inge Sanders and Ms. Evy Koenen - van Elderen - Conferences department of the Eindhoven University of Technology.
Student assistants: Francesco Botta, Jesse Delbressine, Wouter Holman and Marcel Mińkowski.

1.7 International Scientific Committee

Masaharu Shiratani (Chair) Japan

Igor Adamovich USA

N. Yu. Babaeva Russia

Christine Charles Australia

Gilles Cartry France

Uwe Czarnetzki Germany

Giorgio Dilecce Italy

Francisco J. Gordillo Vázquez Spain

Jon Tomas Guðmundsson Iceland

Sander Nijdam The Netherlands

Deborah O'Connell Ireland

Joanna Pawlat Poland

Marija Radmilovic Radjenovic Serbia

Tlekkabul Ramazanov Kazakhstan

1.8 Sponsors

ICPIG XXXV is sponsored by:

2 Practical information

2.1 Venue

The conference will take place at Hotel Zuiderduin (www.zuiderduin.nl) in Egmond aan Zee, 100 meter from the sand beach along the coast of Holland. Egmond is an old fishermen's village with many restaurants, pubs and hotels, and is well visited in the summer.

Free WIFI is available throughout the hotel using the ZDuinWIFI network. No password is required.

2.2 International travel and local transport

Air and land travel would approach Amsterdam airport or Amsterdam station. From there it is about an hour by public transport to the venue. The closest railway station is **Heiloo**, from which we will provide transportation by shuttle bus and coach, see below. However, the Alkmaar railway station is larger and has more taxis, which may be beneficial for participants arriving at other times.
We will provide:

- On Sunday July 9th, we will be driving our own van regularly to and from Heiloo station between 11:00 and 22:00 at least every half hour and no reservation is necessary.
- On other days our shuttle service is available between 8:00 and 22:00 (Friday only until 14:00), but a reservation is required.
  For reservations for pick-up, please send an email to icpig.shuttlereservation@gmail.com including your expected date and time of arrival at Heiloo station and your mobile phone number. Return transfers can be arranged in the same way, or by directly contacting Jesse or Wouter during the conference.
- On Friday July 14th, immediately after the end of the program, (12:30) we will provide coaches towards Heiloo station. There is no need for a reservation.

The pick-up location at Heiloo railway station is on the West side near the large bicycle parking. Google maps link: goo.gl/maps/rHu2hR6g36hhTySG9. Coordinates: 52.60038N, 4.70107E. Approximate address: Stationsweg 96, Heiloo, NL.

Floor 1

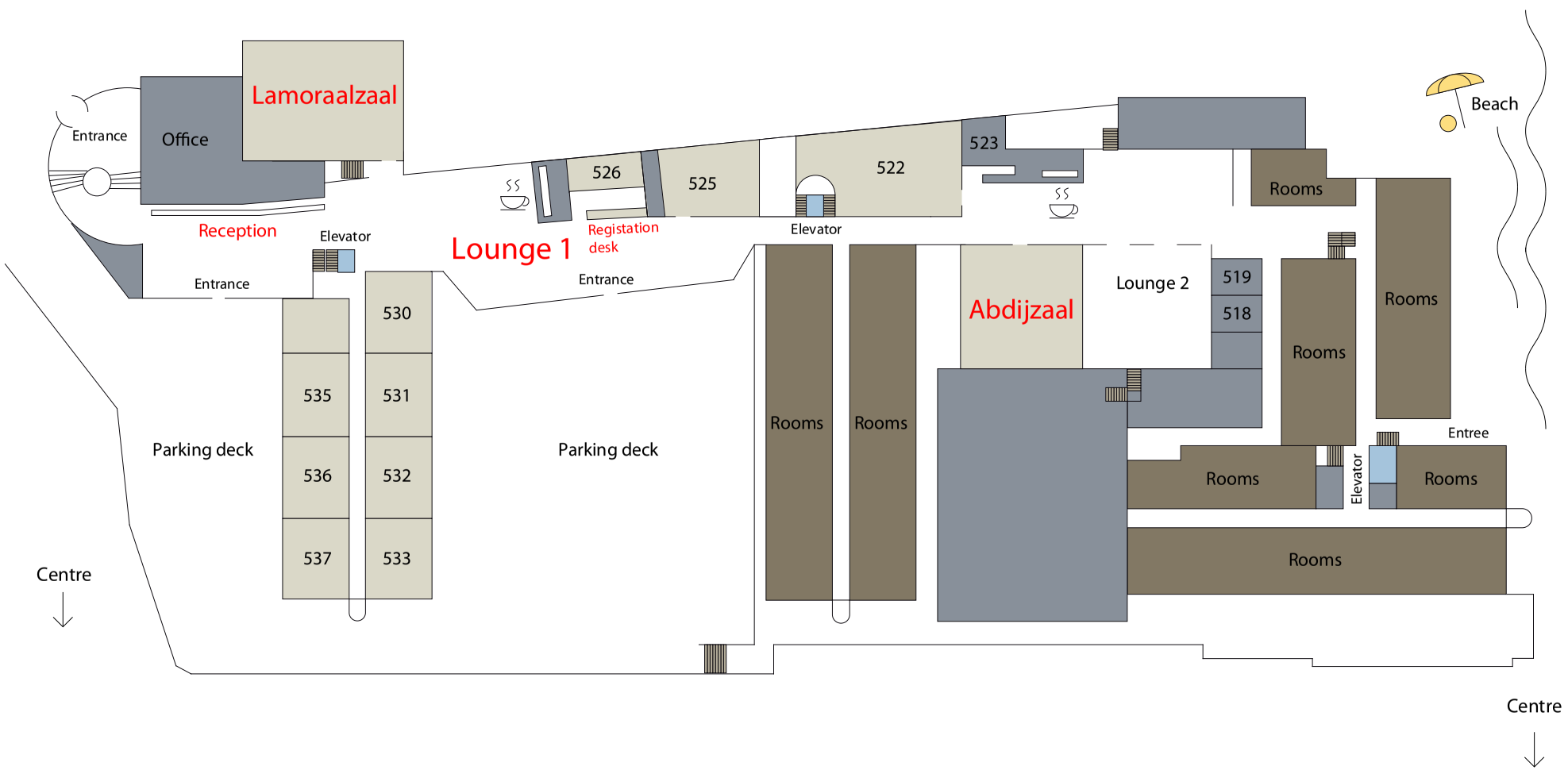
Lamoraalzaal
Entrance
Office
Reception
Elevator
Entrance
Lounge 1
Registation desk
526
525
522
523
Elevator
Entrance
Beach
Rooms
530
535
531
536
532
537
533
Parking deck
Parking deck
Rooms
Rooms
Abdijzaal
Lounge 2
519
518
Rooms
Rooms
Entree
Rooms
Elevator
Rooms
Rooms
Centre
Centre

Floor 0

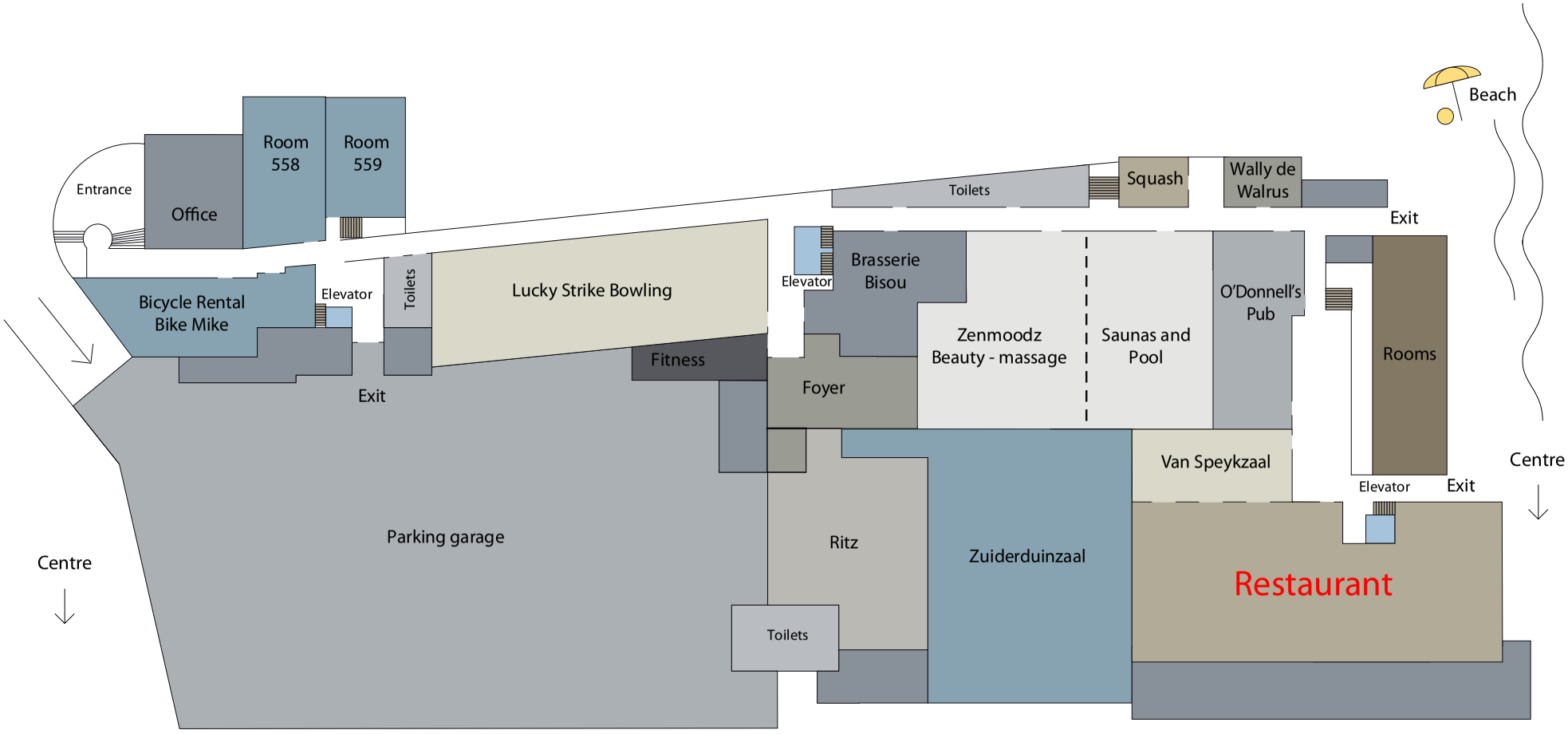
Entrance
Office
Room 558
Room 559
Toilets
Squash
Wally de Walrus
Exit
Beach
Bicycle Rental Bike Mike
Elevator
Toilets
Lucky Strike Bowling
Elevator
Brasserie Bisou
Zenmoodz Beauty - massage
Saunas and Pool
O'Donnell's Pub
Rooms
Fitness
Foyer
Exit
Van Speykzaal
Elevator
Exit
Centre
Parking garage
Ritz
Zuiderduinzaal
Restaurant
Toilets
Centre

3 Program

3.1 Program table

Mon, Jul 10			Tue, Jul 11			Wed, Jul 12			Thu, Jul 13			Fri, Jul 14		
09:00	Registration		09:00	**Tue1-1** **Kenji Ishikawa**		09:00	Wed1A-1 Chng	Wed1B-1 Benilov	09:00	**Thu1-1** **Zdenko Machala**		09:00	Fri1A-1 González-	Fri1B-1 Oliva
09:20	Opening					09:30	Wed1A-2 Limburg	Wed1B-2 Gonçalves				09:30	Fri1A-2 Ramazanov	Fri1B-2 Reuter
09:45	**Mon1-1** **Annemie Bogaerts**		09:45	**Tue1-2** **Achim von Keudell**		09:50	Wed1A-3 Leduc	Wed1B-3 Wang	10:30	**Thu1-2** **Pascal Chabert**		09:50	Fri1A-3 Adamovich	Fri1B-3 Miyazaki
						10:10	Wed1A-4 Herrmann	Wed1B-4 Dias				10:10	Fri1A-4 Gablier	Fri1B-4 Meyer
10:30	Coffee break		10:30	Coffee break		10:30	Coffee break		10:30	Coffee break		10:30	Coffee break	
11:00	Mon2A-1 Stamate	Mon2B-1 Choe	11:00	Tue2A-1 Takashima	Tue2B-1 Laurita	11:00	Wed2A-1 Skočić	Wed2B-1 Brault	11:00	Thu2A-1 Takeda	Thu2B-1 Michau	11:00	**von Engel and Franklin prize lecture:** **Jean-Pierre Boeuf**	
11:30	Mon2A-2 Vialetto	Mon2B-2 Chiu	11:30	Tue2A-2 Martini	Tue2B-2 Orel	11:30	Wed2A-2 Khan	Wed2B-2 Poli	11:30	Thu2A-2 Gerakis	Thu2B-2 Donders			
11:50	Mon2A-3 Guerra	Mon2B-3 Kutasi	11:50	Tue2A-3 Saito	Tue2B-3 Wagenaars	11:50	Wed2A-3 Wubs	Wed2B-3 Litch	11:50	Thu2A-3 Pajdarová	Thu2B-3 Peláez			
12:10	Mon2A-4 Shen	Mon2B-4 Walker	12:10	Tue2A-4 Toyoda	Tue2B-4 Agus	12:10	Wed2A-4 Lepikhin	Wed2B-4 Li	12:10	Thu2A-4 Kumagai	Thu2B-4 Bruggeman	12:00 - 12:30	Poster Prizes + Closing ceremony	
12:30			12:30	COST PlAgri		12:45 - 18:00	Excursion		12:30	Lunch		12:30 - 13:00	Bus transport to railway	
13:15	Diversity session	Lunch	13:15	Data Session	Lunch									
14:00	Poster session P1		14:00	Poster session P2					13:45	Poster session P3				
16:00	Short coffee break		16:00	Short coffee break					15:45	Short coffee break				
16:15	Mon3A-1 Bhattacharjee	Mon3B-1 Sobota	16:15	Tue3-1 Atsushi Komuro					16:00	Thu3A-1 Takahashi	Thu3B-1 Ussenov			
16:45	Mon3A-2 Shinoda	Mon3B-2 Robert	16:45	Tue3-2 Anne Bourdon					16:30	Thu3A-2 Cvelbar	Thu3B-2 Lazzaroni			
17:15	Mon3A-3 Taccogna	Mon3B-3 Jinno	17:15	Tue3-3 Mark van de Kerkhof					17:00 - 19:00	Poster session P4				
17:45	Mon3A-4 Ritchie	Mon3B-4 Garrigues	17:45 - 18:15	Tue3-4 Carmen Guerra-Garcia										
18:15 - 18:45	Mon3A-5 Engeln	Mon3B-5 Luque												
19:00 - 21:30	Welcome reception								19:30 - 00:00	Conference dinner				

General Invited Topical Invited Selected Special Session

3.2 Detailed program including social program

Sun, July 9

15:00 - 18:00 Registration. Location: Lounge 1.

Mon, July 10

09:00 - 09:20 Registration. Location: Lounge 1.

Session: Mon1 Chair: **Leanne Pitchford**. Location: Lamoraalzaal.

09:20 - 09:45 Opening.

09:45 - 10:30 Mon1-1 General Invited: **Annemie Bogaerts** (T17)
University of Antwerp, Belgium.
CO_2 conversion and N_2 fixation into value-added chemicals and fuels

10:30 - 11:00 Coffee break. Location: Lounge 1.

Session: Mon2A Chair: **Eric Robert** . Location: Lamoraalzaal.

11:00 - 11:30 Mon2A-1 Topical Invited: **Eugen Stamate** (T3)
Technical University of Denmark, Denmark.
Three-dimensional plasma sheath lenses: concept and applications

11:30 - 11:50 Mon2A-2 Selected: **Luca Vialetto** (T3)
University of Kiel, Germany.
Multiscale plasma-surface model applied to reactive magnetron sputtering

11:50 - 12:10 Mon2A-3 Selected: **Vasco Guerra** (T3)
IPFN, IST, Universidade de Lisboa, Portugal.
Atomic wall recombination in oxygen-containing plasmas

12:10 - 12:30 Mon2A-4 Selected: **Qinghao Shen** (T5)
Dutch Institute for Fundamental Energy Research, Netherlands.
Non-thermal chemical dissociation of CO_2: a modelling approach

Session: Mon2B Chair: **Masaharu Shiratani**. Location: Abdijzaal.

11:00 - 11:30 Mon2B-1 Topical Invited: **Wonho Choe** (T11)
Korea Advanced Institute of Science and Technology (KAIST), Korea, Republic Of.
Electric wind and water surface stabilization under impingement of an atmospheric pressure plasma jet

11:30 - 11:50 Mon2B-2 Selected: **Pohsien Chiu** (T11)
Department of Mechanical Engineering, National Yang Ming Chiao Tung University, Hsinchu, Taiwan.
DBD-Streamer Mode Transition of Atmospheric-Pressure Plasma Jet Applied on Water with Changed Distance and AC Power

11:50 - 12:10 Mon2B-3 Selected: **Kinga Kutasi** (T11)
Wigner Research Centre for Physics, Hungary.
Surface-wave microwave discharge in contact with liquids

12:10 - 12:30 Mon2B-4 Selected: **Roxanne Walker** (T11)
University of Michigan, United States of America.
Plasma Discharge Modifications Over a Rough Dielectric Liquid Surface

12:30 - 14:00 Lunch. Location: Restaurant.

13:15 - 14:00 Diversity session. Gerrit Kroesen and Cyndi Long Location: Lamoraalzaal.
In 2018, TU/e and its physics department set out on a long-term program to improve the diversity balance among students and staff. The main aspects of this program were based on examples from other universities, like the University of Michigan and Groningen university. It has proven to be successful. During the session, material will be presented that illustrates the effectiveness of various approaches and ingredients, and the audience will be engaged in a discussion of future options that could further improve inclusiveness and diversity in all its dimensions.

14:00 - 16:00 Poster session P1 Location: Lounge 1.
Poster titles and abstracts on page 20.

16:00 - 16:15 Short coffee break. Location: Lounge 1.

Session: Mon3A Chair: **Emile Carbone**. Location: Lamoraalzaal.

16:15 - 16:45 Mon3A-1 Topical Invited: **Sudeep Bhattacharjee** (T10)
Indian Institute of Technology (IIT) - Kanpur, India.
Potential fluctuation dynamics in cold atmospheric pressure microplasmas

16:45 - 17:15 Mon3A-2 Topical Invited: **Kazunori Shinoda** (T15)
Hitachi, Ltd., Japan.
Selective atomic layer etching of thin films using cyclic plasma exposure and infrared irradiation

17:15 - 17:45 Mon3A-3 Topical Invited: **Francesco Taccogna** (T3)
CNR, Italy.
Role of electron-induced secondary electron emission from the walls in RF breakdown

17:45 - 18:15 Mon3A-4 Topical Invited: **Grant Ritchie** (T8)
University of Oxford, United Kingdom.
High resolution spectroscopy of simple molecular plasmas

18:15 - 18:45 Mon3A-5 Topical Invited: **Richard Engeln** (T6)
Tech RES SCAN Plasma Physics, ASML Netherlands B.V., The Netherlands.
A diagnostic study of the CO_2 vibrational kinetics in a glow discharge

Session: Mon3B Chair: **Wonho Choe**. Location: Abdijzaal.

16:15 - 16:45 Mon3B-1 Topical Invited: **Ana Sobota** (T10)
Eindhoven University of Technology, Netherlands.
The interaction of non-thermal atmospheric pressure plasmas with substrates

16:45 - 17:15 Mon3B-2 Topical Invited: **Eric Robert** (T17)
GREMI, CNRS/Université d'Orléans, France.
Plasma electrode DBD for low power, large surface applications

17:15 - 17:45 Mon3B-3 Topical Invited: **Masafumi Jinno** (T17)
Ehime University, Japan.
Spontaneous external molecular/gene introduction with random genome integration free by complex stimuli generated by plasma and its applications

17:45 - 18:15 Mon3B-4 Topical Invited: **Laurent Garrigues** (T5)
Laplace/CNRS-Universite de Toulouse, France.
Low temperature plasmas modeling using the Sparse-PIC algorithm

18:15 - 18:45 Mon3B-5 Topical Invited: **Alejandro Luque** (T5)
Instituto de Astrofísica de Andalucía (IAA-CSIC), Spain.
Towards coarse-grained models for extensive streamer coronas in thunderclouds

19:00 - 21:30 Welcome reception. Location: Lounge 1.
Here we will also offer a variety of street food from all over the world (dinner replacing).

Tue, July 11

Session: Tue1 Chair: **Jon Tomas Gudmundsson**. Location: Lamoraalzaal.

09:00 - 09:45 Tue1-1 General Invited: **Kenji Ishikawa** (T15)
Nagoya University, Japan.
Frontiers of Plasma Etching Technology for Advanced Semiconductor Devices

09:45 - 10:30 Tue1-2 General Invited: **Achim von Keudell** (T8)
Ruhr University Bochum, Germany.
Transport from target to substrate in High Power Impulse Magnetron Sputtering Plasmas

10:30 - 11:00 Coffee break. Location: Lounge 1.

Session: Tue2A Chair: **Luca Vialetto**. Location: Lamoraalzaal.

11:00 - 11:30 Tue2A-1 Topical Invited: **Keisuke Takashima** (T9)
Tohoku University, Japan.
Generation of Vibrationally Excited Nitrogen in a DC-Superimposed Repetitive Nanosecond Pulse Discharge

11:30 - 11:50 Tue2A-2 Selected: **Luca Matteo Martini** (T9)
University of Trento, Italy.
Spectroscopic investigation of the time evolution of CO_2 dissociation in a nanosecond plasma-discharge.

11:50 - 12:10 Tue2A-3 Selected: **Atsushi Saito** (T15)
AGC Inc., Japan.
Propagation of radicals and carbon particles in CH_4 plasma at atmospheric pressure

12:10 - 12:30 Tue2A-4 Selected: **Hirotaka Toyoda** (T9)
Nagoya University, Japan.
Time-dependent measurement of ion composition in a capacitively-coupled $Ar/C_4F_8/O_2$ power-modulated VHF plasma

Session: Tue2B Chair: **Joanna Pawlat**. Location: Abdijzaal.

11:00 - 11:30 Tue2B-1 Topical Invited: **Romolo Laurita** (T19)
Alma Mater Studiorum - University of Bologna, Italy.
On the potential use of plasma for food processing

11:30 - 11:50 Tue2B-2 Selected: **Inna Orel** (T17)
GREMI, Université d'Orléans, France.
Synergetic effect of carbon monoxide (CO) and cold atmospheric Helium/CO_2 MHz and kHz plasmas on bacterial disinfection for biomedical applications

11:50 - 12:10 Tue2B-3 Selected: **Erik Wagenaars** (T9)
York Plasma Institute, University of York, United Kingdom.
Formation of O and H radicals in an atmospheric-pressure nanosecond pulsed discharge in helium with admixtures of water vapour

12:10 - 12:30 Tue2B-4 Selected: **Rita Agus** (T17)
EPFL (Swiss Plasma Center), École polytechnique fédérale de Lausanne, Switzerland.
Plasma-treated water inactivation mechanisms of Escherichia coli

12:30 - 14:00 Lunch. Location: Restaurant.

12:30 - 12:45 COST PlAgri. Location: Abdijzaal.
COST Action: CA19110 - Plasma applications for smart and sustainable agriculture

13:15 - 14:00 Workshop on Input data for Low-Temperature Plasma Science. Location: Lamoraalzaal.

This lunch event aims to bring together ICPIG participants with an interest in input data creation and dissemination. It will feature a demonstration of the new version of the LXCat database and a discussion on the path towards full-chemistry databases. Organized by Jan van Dijk and Emile Carbone.

14:00 - 16:00 Poster session P2 Location: Lounge 1.

Poster titles and abstracts on page 24.

16:00 - 16:15 Short coffee break. Location: Lounge 1.

Session: Tue3 Chair: **Luís Alves**. Location: Lamoraalzaal.

16:15 - 16:45 Tue3-1 Special Session Invited: **Atsushi Komuro** (T5)
The University of Tokyo, Japan.
Simulation of the chemical reaction induced by a streamer discharge and its validation study

16:45 - 17:15 Tue3-2 Special Session Invited: **Anne Bourdon** (T10)
LPP, France.
Why are 2D axisymmetric ionization waves generated in a simple point-to-plane geometry in atmospheric pressure air still studied?

17:15 - 17:45 Tue3-3 Special Session Invited: **Mark van de Kerkhof** (T14)
ASML, Netherlands.
EUV-induced Hydrogen Plasma: Pulsed Mode Generation and Consequences in Lithographic Scanner

17:45 - 18:15 Tue3-4 Special Session Invited: **Carmen Guerra-Garcia** (T10)
Massachusetts Institute of Technology, United States of America.
Two-Way Coupling of Plasma-Assisted Combustion

Wed, July 12

Session: Wed1A Chair: **Sander Nijdam**. Location: Lamoraalzaal.

09:00 - 09:30 Wed1A-1 Topical Invited: **Tat Loon Chng** (T6)
National University of Singapore, Singapore.
Recent Developments in the Electric Field-Induced Second Harmonic Generation (EFISH) Method for Non-Equilibrium Plasmas

09:30 - 09:50 Wed1A-2 Selected: **Anne Limburg** (T6)
Eindhoven University of Technology, Netherlands.
E-FISH data analysis for electric field measurements on single channel streamers

09:50 - 10:10 Wed1A-3 Selected: **Alexandre Leduc** (T6)
LPP, France.
Collisional Radiative Model as plasma diagnostic for Hall-effect thrusters

10:10 - 10:30 Wed1A-4 Selected: **Anja Herrmann** (T6)
DIFFER, Netherlands.
Determining the dependency of radical density on position by dual thermocouple radical probe

Session: Wed1B Chair: **Alejandro Luque**. Location: Abdijzaal.

09:00 - 09:30 Wed1B-1 Topical Invited: **Mikhail Benilov** (T5)
Universidade da Madeira, Portugal.
Is there a place for good math in gas discharge science? A personal view

09:30 - 09:50 Wed1B-2 Selected: **Duarte Gonçalves** (T5)
LPGP, University Paris-Saclay & IPFN, Instituto Superior Técnico, France.
Coupled reactive-flow simulation of plasma jets

09:50 - 10:10 Wed1B-3 Selected: **Zhen Wang** (T5)
Centrum Wiskunde & Informatica (CWI), Amsterdam, The Netherlands, Netherlands.
Quantitative modeling of streamer discharge branching in air and experimental validation

10:10 - 10:30 Wed1B-4 Selected: **Tiago Cunha Dias** (T5)
Instituto de Plasmas e Fusão Nuclear, Instituto Superior Técnico, Lisboa, Portugal.
Assessment of time-locality assumptions on the modelling of nanosecond-pulsed discharges

10:30 - 11:00 Coffee break. Location: Lounge 1.

Session: Wed2A Chair: **Richard Engeln**. Location: Lamoraalzaal.

11:00 - 11:30 Wed2A-1 Topical Invited: **Miloš Skočić** (T6)
Faculty of Physics University of Belgrade, Serbia.
Measurement of plasma parameters at the very beginning of the laser induced breakdown

11:30 - 11:50 Wed2A-2 Selected: **Waseem Khan** (T6)
Masaryk University, Czech Republic.
Fluorescence (TALIF) Measurement of Ground State Atomic Nitrogen Concentration in an Argon RF Plasma Pencil measured using a Picosecond Laser.

11:50 - 12:10 Wed2A-3 Selected: **Jente Wubs** (T6)
Leibniz Institute for Plasma Science and Technology (INP), Germany.
Comparison between THz absorption spectroscopy and ps-TALIF measurements of atomic oxygen densities

12:10 - 12:30 Wed2A-4 Selected: **Nikita Lepikhin** (T6)
Ruhr University Bochum, Germany.
Anomalous $N_2^+(B^2\Sigma_u^+)$ population in APPJ in nitrogen

Session: Wed2B Chair: **Atsushi Komuro**. Location: Abdijzaal.

11:00 - 11:30 Wed2B-1 Topical Invited: **Pascal Brault** (T5)
GREMI CNRS - University of Orleans, France.
Molecular dynamics simulations: A virtual microscope for studying plasma processes

11:30 - 11:50 Wed2B-2 Selected: **Davide Poli** (T5)
Universidad Carlos III de Madrid, Spain.
Fluid vs kinetic simulation of the Penning discharge

11:50 - 12:10 Wed2B-3 Selected: **Evan Litch** (T15)
University of Michigan, United States of America.
Redeposition in High Aspect Ratio Plasma Etching

12:10 - 12:30 Wed2B-4 Selected: **Xiaoran Li** (T5)
Xi'an Jiaotong University, China.
Particle-in-cell modelling of positive streamers in CO_2: the role of photoionization

12:35 - 12:45 Group photo. Location: TBD.

12:45 - 18:00 Excursion to *De Zaanse Schans*.

The busses will leave at 13:00 from the hotel, and lunch packages will be provided for the bus ride. The excursion will take you to Zaanse Schans, a water-rich landscape below sea level, where daily life and crafts of the 18th and 19th centuries are brought to life, with windmills, workshops, wooden houses and barns. In the different workshops you can see how wooden shoes are made, or barrels, cloth, cheese and alike, or you can go for a hike through the historic settlement or through nature.

Zaanse Schans was the first industrial area of Europe. It was processing the goods that Dutch ships brought from overseas; it was conveniently located for transport over water and fully based on wind power for transport (sailing) and production (windmills).

You will get a booklet with a map and a voucher for various entries: windmills (choose 2 from paint mill De Kat, wood sawing mill 't Jonge Schaap or oil mill De Bonte Hen), a barrel maker, a weaver's house, Zaans Museum (processing of overseas products, living and clothing at about 1850, and a cookie factory from about 1930), clock museum "Zaanse Tijd" (strongly recommended!), and the windmill museum. Many other attractions are free to visit.

Nature: a round trip hike along the dyke and through the "polder" is about 3 km. There is a nature viewing tower behind the Zaans Museum, and a painting of the landscape by Claude Monet in the museum. Observe that the water behind the dyke is higher than the "land" in the polder. Windmills would maintain the height difference.

The windmills and the musea close at 17:00. Workshops, souvenir shops, Zaans Museum with Cafe and restaurant De Kraai will stay open until the busses leave at 17:30 , bringing you back to the hotel at about 18:00.

Thu, July 13

Session: Thu1 Chair: **Anne Bourdon**. Location: Lamoraalzaal.

09:00 - 09:45 Thu1-1 General Invited: **Zdenko Machala** (T11)
Comenius University in Bratislava, Slovakia.
Transport of Reactive Species from Plasma Discharges into Water Determines the Plasma-Activated Water Properties and Applications

09:45 - 10:30 Thu1-2 General Invited: **Pascal Chabert** (T8)
LPP, CNRS, Ecole Polytechnique, France.
Recent challenges in electric (plasma) propulsion

10:30 - 11:00 Coffee break. Location: Lounge 1.

Session: Thu2A Chair: **Ana Sobota**. Location: Lamoraalzaal.

11:00 - 11:30 Thu2A-1 Topical Invited: **Keigo Takeda** (T6)
Meijo University, Japan.
Spectroscopic diagnostics of surface reactions of atomic species in non-thermal plasma

11:30 - 11:50 Thu2A-2 Selected: **Alexandros Gerakis** (T6)
Luxembourg Institute of Science & Technology, Luxembourg.
Single shot, non-resonant, four-wave mixing laser diagnostics of heavy species in low temperature plasmas.

11:50 - 12:10 Thu2A-3 Selected: **Andrea Dagmar Pajdarová** (T6)
University of West Bohemia, Czech Republic.
Cavity ring-down spectroscopy in HiPIMS discharge during the sputtering of the titanium target

12:10 - 12:30 Thu2A-4 Selected: **Shinya Kumagai** (T17)
Meijo University, Japan.
Plasma-on-Chip: A Microdevice for Direct Plasma Exposure of Cultured Cells

Session: Thu2B Chair: **Job Beckers**. Location: Abdijzaal.

11:00 - 11:30 Thu2B-1 Topical Invited: **Armelle Michau** (T13)
LSPM CNRS, France.
Particle formation and dusty plasma effect in non-equilibrium discharges

11:30 - 11:50 Thu2B-2 Selected: **Tim Donders** (T13)
Eindhoven University of Technology, Netherlands.
Decay of additional electron density released by laser-induced photodetachment as a diagnostic tool for dust particle size in a low-pressure nanodusty plasma

11:50 - 12:10 Thu2B-3 Selected: **Ramón Peláez** (T13)
CSIC, Spain.
Monitoring the carbonaceous interstellar dust analogues growth in cold plasmas by light scattering

12:10 - 12:30 Thu2B-4 Selected: **Peter Bruggeman** (T11)
University of Minnesota, United States of America.
A Model of Plasma-Enabled Gold Nanoparticle Synthesis in Microdroplets

12:30 - 13:45 Lunch. Location: Restaurant.

13:45 - 15:45 Poster session P3 Location: Lounge 1.
Poster titles and abstracts on page 29.

15:45 - 16:00 Short coffee break. Location: Lounge 1.

Session: Thu3A Chair: **Giorgio Dilecce**. Location: Lamoraalzaal.

16:00 - 16:30 Thu3A-1 Topical Invited: **Kazunori Takahashi** (T8)
Tohoku University, Japan.
Fundamental studies and applications of magnetic nozzle plasma

16:30 - 17:00 Thu3A-2 Topical Invited: **Uros Cvelbar** (T8)
Jozef Stefan Institute, Slovenia.
Plasmas for nano and facilitating next generation energy storage

Session: Thu3B Chair: **Igor Adamovich**. Location: Abdijzaal.

16:00 - 16:30 Thu3B-1 Topical Invited: **Yerbolat Ussenov** (T10)
Princeton University, United States of America.
Dynamics of microdischarges in a volume DBD under airflow

16:30 - 17:00 Thu3B-2 Topical Invited: **Claudia Lazzaroni** (T15)
USPN - LSPM CNRS UPR3407, France.
Micro Hollow Cathode Discharges in Ar/N_2 for boron nitride PECVD

17:00 - 19:00 **Poster session P4** Location: Lounge 1.
Poster titles and abstracts on page 33.

19:30 - 00:00 Conference dinner.
Location: restaurant Nautilus aan Zee, on the beach about 100 meters from the conference hotel.
BBQ, free drinks, and disco with a DJ in the later evening.

Fri, July 14

Session: Fri1A Chair: **Laurent Garrigues**. Location: Lamoraalzaal.

09:00 - 09:30 Fri1A-1 Topical Invited: **Olmo González-Magaña** (T1)
UNAM, Mexico.
Photodetachment of negative ions drifting in the Townsend Avalanche: Experimental and numerical study in O_2 and N_2O.

09:30 - 09:50 Fri1A-2 Selected: **Tlekkabul Ramazanov** (T1)
Al-Farabi Kazakh National University, IASIT, Kazakhstan.
Scattering and transport properties of dense plasmas

09:50 - 10:10 Fri1A-3 Selected: **Igor Adamovich** (T1)
Ohio State University, United States of America.
Semiclassical Analytic Model of Nonadiabatic Energy Transfer in Atomic Collisions

10:10 - 10:30 Fri1A-4 Selected: **Renaud Gablier** (T10)
Laboratoire EM2C, CentraleSupélec - CNRS, Université Paris-Saclay, France.
Effect of hydrodynamic regimes on the cumulative heating induced by NRP discharges in plasma-assisted combustion

Session: Fri1B Chair: **Inna Orel**. Location: Abdijzaal.

09:00 - 09:30 Fri1B-1 Topical Invited: **Manuel Oliva** (T17)
Universidad de Sevilla, Spain.
On the role of reaction mechanisms and metal catalysts during the plasma-assisted ammonia synthesis

09:30 - 09:50 Fri1B-2 Selected: **Stephan Reuter** (T11)
Polytechnique Montreal, Canada.
Coupling of a microfluidic device with a reference cold plasma jet

09:50 - 10:10 Fri1B-3 Selected: **Toshiaki Miyazaki** (T11)
Hokkaido University, Japan.
Control of self-organized luminous pattern formation in atmospheric-pressure dc glow discharge

10:10 - 10:30 Fri1B-4 Selected: **Mackenzie Meyer** (T11)
University of Michigan, United States of America.
Modelling of PFAS Removal From Water by Plasma Treatment: C3F8 as a Surrogate

10:30 - 11:00 Coffee break. Location: Lounge 1.

Session: Fri2 Chair: **Gilles Cartry/Khaled Hassouni**. Location: Lamoraalzaal.

11:00 - 12:00 Fri2-1 von Engel and Franklin prize lecture: **Jean-Pierre Boeuf** (T1)
CNRS, University of Toulouse, France.
Nonlinearity and complexity of low-temperature plasmas. Self-organized filaments, striations, and spokes

12:00 - 12:30 Poster Prizes + Closing ceremony.
Poster prize award ceremony and closing session of the conference.

3.3 Posters

3.3.1 Poster session P1, Mon, Jul 10, 14:00 - 16:00

P1-1 - **Jaime de Urquiijo** (T1)
Universidad Nacional Autónoma de México, Mexico.
Effective ionisation and three-body attachment swarm coefficients in H_2O-dry air gas mixtures

P1-2 - **Rui Manuel Santos Almeida** (T1)
Universidade da Madeira, Portugal.
Validating Townsend criterion for the ignition of volume electrical discharges

P1-3 - **Roman W. Schrittwieser** (T4)
University of Innsbruck, Austria.
Space charge structures on gridded coaxial cylinders

P1-4 - **Harry Philpott** (T4)
Eindhoven University of Technology, Netherlands.
Hysteresis Effects in Shielded kHz Atmospheric Pressure Plasma Jet

P1-5 - **YaZhen Wang** (T10)
Xi'an Jiaotong University, China.
Modelling the role of the leftover charged species on the subsequent discharges

P1-6 - **Bahram Mahdavipour** (T5)
University of Iceland, Iceland.
The influence of secondary electron emission on a capacitive chlorine discharge

P1-7 - **Baohong Guo** (T5)
Centrum Wiskunde & Informatica (CWI), Netherlands.
Modeling energy efficiency of plasma chemistry by streamers in air

P1-8 - **Swati Swagatika Mishra** (T5)
Indian Institute of Technology Kanpur, India.
Molecular dynamics simulations of confined microplasmas at cryogenic temperatures

P1-9 - **Hemaditya Malla** (T5)
Centrum Wiskunde & Informatica, Netherlands.
Double-pulse streamer simulations for varying interpulse times in air

P1-10 - **Borja Bayón Buján** (T5)
Universidad Carlos III de Madrid, Spain.
Data-driven Identification of the Breathing Mode governing equations

P1-11 - **Jannis Teunissen** (T5)
Centrum Wiskunde & Informatica (CWI), Netherlands.
Overview of the afivo-streamer and afivo-pic simulation codes

P1-12 - **Felix Smits** (T5)
Leiden University, Netherlands.
Flow and microwave design of the Topological Reactor

P1-13 - **Diego García-Lahuerta** (T5)
UC3M, Spain.
Modeling the effect of background pressure on magnetic nozzle performances

P1-14 - **Rutger Bell** (T6)
Eindhoven University of Technology, Netherlands.
Surface charge deposition on dielectric surfaces using an X-ray ionizer

P1-15 - **Mina Farahani** (T6)
University of West Bohemia, Czech Republic.
Ion and atom fluxes during HiPIMS deposition of NbC from a compound target

P1-16 - **Anne Limburg** (T6)
Eindhoven University of Technology, Netherlands.
Invasiveness of picosecond and nanosecond laser diagnostics on plasma bullets in nitrogen

P1-17 - **Dae-Woong Kim** (T6)
Korea Institue of Machinery & Materials, Korea, Republic Of.
Patch-type microwave resonance sensor for obtaining plasma electron density in low-pressure plasmas

P1-18 - **Paolo Francesco Ambrico** (T6)
CNR ISTP, Italy.
The Breakdown Development of a Plane-to-Plane Nanosecond Pulsed Discharge in Humid Air

P1-19 - **Francisco J Gordillo-Vázquez** (T6)
IAA-CSIC, Spain.
Corona discharges in thunderclouds as detected from space by ASIM: Types, properties, and worldwide geographical distributions

P1-20 - **Lex Kuijpers** (T6)
Eindhoven University of Technology, Netherlands.
Determination of atomic oxygen density and reduced electric field in oxygen-containing plasmas through OES methods

P1-21 - **Volker Schulz-von der Gathen** (T6)
Experimental Physics II, Ruhr-Universität Bochum, Germany.
Evolution of mean electron energy and dissociation over the initial pulses in a micro cavity plasma array

P1-22 - **Xingyu Chen** (T8)
DIFFER, Netherlands.
Experimental Study of the Plasma Enhanced Oxygen Reduction and Permeation of LSM|YSZ|LSM Solid Oxide Electrolyte Cell

P1-23 - **Jion Ogaki** (T10)
Tokyo Metropolitan University, Japan.
Density measurement of atomic oxygen in pulsed discharges formed under sub-atmospheric pressure pure oxygen

P1-24 - **Deepika Behmani** (T10)
Indian Institute of Technology Kanpur, India.
Electric field fluctuations in a cold micro-plasma jet under different flow modes

P1-25 - **Ivan Tsonev** (T10)
University of Antwerp, Belgium.
Glow and arc discharges in atmospheric pressure nitrogen

P1-26 - **Ryo Ono** (T10)
The University of Tokyo, Japan.
Quantitative measurements of the effects of OH, O, and O_3 on surface treatments of polymers using VUV photodissociation method

P1-27 - **Sebastian Wilczek** (T10)
Ruhr University Bochum, Germany.
Simulation of surface dielectric barrier discharges: Streamer and gas dynamics

P1-28 - **Duarte Gonçalves** (T10)
LPGP, University Paris-Saclay & IPFN, Instituto Superior Técnico, France.
Ar(1s5) density modulation by N_2-O_2 shielding of an atmospheric pressure argon plasma jet

P1-29 - **Yihao Guo** (T10)
Eindhoven University of Technology, Netherlands.
Stereophotography of streamer discharges in $N_2/O_2/CO_2$ mixtures

P1-30 - **David Prokop** (T10)
Masaryk University, Czech Republic.
Spatio-temporal spectroscopic investigation of a nanosecond-pulsed barrier discharge in argon

P1-31 - **Piotr Jamroz** (T11)
Wroclaw Univeristy of Science and Technology, Poland.
The spectroscopic characteristics of pulse-modulated radio-frequency atmospheric pressure glow microdischarge generated in contact with liquid

P1-32 - **Hiroshi Akatsuka** (T11)
Tokyo Institute of Technology, Japan.
Velocity change of non-transferred arc jet released into water

P1-33 - **Roberto Montalbetti** (T11)
Alma Mater Studiorum - University of Bologna, Italy.
A study on plasma active water from a new hybrid source for tomato growth in hydroponic conditions

P1-34 - **Oleksandr Galmiz** (T11)
Comenius University Bratislava, Slovakia.
Quantification of chemical species produced by the Surface Dielectric Barrier Discharge with liquid electrodes

P1-35 - **Giulia Laghi** (T15)
Alma Mater Studiorum - University of Bologna, Italy.
Control strategies for polymerization processes assisted by atmospheric pressure plasma jets

P1-36 - **Alice Remigy** (T15)
LSPM, France.
Investigation of gas flow pattern in a Micro-Hollow Cathode Discharge-based deposition reactor using planar Laser Induced Fluorescence.

P1-37 - **Yutaro Nakano** (T15)
Kyushu University, Japan.
Sputter epitaxy of atomically flat (ZnO)x(InN)1-x films on sapphire substrates using ZnO(N) buffer layers fabricated by Ar/N_2 discharges

P1-38 - **Ondrej Jasek** (T15)
Masaryk University, Czech Republic.
Influence of plasma instability on gas-phase synthesis of N-graphene in dual-channel microwave plasma torch at atmospheric pressure

P1-39 - **Tomoyuki Nonaka** (T15)
Samco Inc, Japan.
Chemical composition and surface morphology of films polymerized by C_4F_8 plasmas in Bosch process

P1-40 - **Jong Keun Yang** (T15)
Korea Institute of Fusion Energy, Korea, Republic Of.
Plasma-based Lithium recovery process

P1-41 - **Michihiro Otaka** (T15)
Kyushu University, Japan.
Effects of tailored voltage waveform discharges on deposition of hydrogenated amorphous carbon films by CH_4/Ar capacitively coupled plasma

P1-42 - **Ji Hun Kim** (T15)
Korea Instiitute of Fusion Energy, Korea, Republic Of.
Production of micro-sized metal powder using plasma-gas hybrid atomization system

P1-43 - **Manon Soulier** (T17)
Sorbonne Unviersité, Laboratoire de Physique des Plasmas, France.
Investigating the performances of cold plasma endoscopy for cholangiocarcinoma local treatment

P1-44 - **Anna Dzimitrowicz** (T17)
Wroclaw University of Science and Technology, Poland.
Application of non-thermal plasma for production of antiphytopathogenic plasma-activated liquid

P1-45 - **Ravi Patel** (T17)
Eindhoven University of Technology, Netherlands.
Optimizing nanosecond repetitively pulsed discharges for ignition stabilized combustion

P1-46 - **Tetsuji Shimizu** (T17)
National Institute of Advanced Industrial Science and Technology, Japan.
Albumin aggregation by cold atmospheric plasma between needle electrode and surface of albumin solution

P1-47 - **Shinya Kumagai** (T17)
Meijo University, Japan.
A plasma-assisted microperfusion culture system for promoted cell growth

P1-48 - **Kiran Ahlawat** (T17)
Indian Institute of Technology, Jodhpur, Rajasthan, India.
An efficient Far UV-C (222 nm) krypton chlorine excimer lamp

P1-49 - **Borui Zheng** (T17)
Xi'an University of Technology, China.
Turbulent skin-friction drag reduction by annular DBD plasma synthetic jet actuator

P1-50 - **In Je Kang** (T6)
Korea Institute of Fusion Energy, Korea, Republic Of.
Measurement of enthalpy probe on plasma temperature in atmospheric pressure microwave plasma jet for CO_2 reforming system

P1-51 - **InSun Park** (T3)
Korea Institute of Fusion Energy, Korea, Republic Of.
Development of Simulator for Interaction of Materials and PLasma (SIMPL) in Korea Institute of Fusion Energy

P1-52 - **Chang Hyun Cho** (T16)
Korea Institute of Fusion Energy, Korea, Republic Of.
Development of atmospheric pressure microwave plasma generator with gas preheating structure for dry reforming system.

P1-53 - **František Krčma** (T17)
Brno University of Technology, Czech Republic.
COST Action: CA19110 - Plasma applications for smart and sustainable agriculture

P1-54 - **Shin-ichi Aoqui** (T17)
Sojo University, Japan.
Characteristic Changes in Pumpkin Seeds by Atmospheric Pressure Gliding Arc Plasma Irradiation

3.3.2 Poster session P2, Tue, Jul 11, 14:00 - 16:00

P2-1 - **Daan Boer** (T1)
Eindhoven University of Technology, Netherlands.
LXCat 3: A novel data platform for low-temperature plasma physics

P2-2 - **Andrei Smolyakov** (T1)
University of Saskatchewan, Canada.
ExB heating and transport in magnetized plasmas with ionization and charge-exchange effects

P2-3 - **Thierry Dufour** (T1)
Sorbonne Université, France.
Triggering self-organization of guided streamers in a cold plasma jet

P2-4 - **Jaime de Urquiijo** (T2)
Universidad Nacional Autónoma de México, Mexico.
Measurement of the flux drift velocity of electrons in THF-H_2O mixtures

P2-5 - **Karima Bendib-Kalache** (T2)
University of Sciences and Technology HB, Algeria.
Semicollisional transport coefficients for relativistic plasmas

P2-6 - **Gilles Cartry** (T3)
Aix-Marseille Université, France.
Correlation between the negative ion surface production efficiency and the surface work function in low pressure hydrogen plasmas

P2-7 - **Shu Zhang** (T5)
Laboratoire de Physique des Plasmas (LPP), CNRS, École polytechnique, Institut Polytechnique de Paris, France.
Drift-Diffusion models for RF-CCPs at intermediate pressure: estimating transport coefficients

P2-8 - **Aleksandr Pikalev** (T5)
Dutch Institute for Fundamental Energy Research (DIFFER), Netherlands.
Collisional-radiative model of low-pressure He-O_2 plasma

P2-9 - **Jan Tungli** (T5)
Masaryk University, Czech Republic.
Modelling of magnetron plasma using fluid dynamics

P2-10 - **Jesper Janssen** (T5)
Plasma Matters B.V., Netherlands.
Modelling radiation using PLASIMO

P2-11 - **Anatole Berger** (T5)
CNRS, Ecole Polytechnique, France.
Multi-fluid modeling of a weakly-ionized confined plasma: ion-neutral collision term

P2-12 - **Karim Saber** (T5)
Materials and Renewable Energies Laboratory, Physics Department, Ibn Zohr University, Morocco.
Effect of multi-tip reactor parameters on energy efficiency using the electrical model equivalent to corona discharge

P2-13 - **Laurent Garrigues** (T5)
Laplace/CNRS-Universite de Toulouse, France.
Benchmark of particle-in-cell simulations of a Penning-type discharge: Preliminary results

P2-14 - **Rick Budé** (T5)
Eindhoven University of Technology, Netherlands.
ECR simulations on unstructured meshes

P2-15 - **Mate Vass** (T5)
Ruhr University Bochum / Wigner Research Centre for Physics, Germany.
Determination of the atomic oxygen density distribution in an RF-driven He/O_2 microplasma jet at atmospheric pressure using an efficient 2D hybrid simulation method

P2-16 - **Tarek Ben Ben Slimane** (T5)
Laboratoire de Physique des Plasmas (LPP), CNRS, Sorbonne Université, Ecole polytechnique, Institut Polytechnique de Paris, France.
Insights on Hall effect thruster using Xe Collisional Radiative Model

P2-17 - **Gregory Daly** (T5)
University of Exeter, United Kingdom.
Surrogate collisional radiative models for fluorocarbon plasmas from optical diagnostics data using deep autoencoders

P2-19 - **Maria Mitrou** (T6)
Laboratory of Subatomic Physics and Cosmology, University Grenoble Alpes, France.
Laser-induced photo-detachment diagnostic for interrogating pulsed ECR-driven plasmas: Application to H- and D- negative ions

P2-20 - **Tomas Hoder** (T6)
Masaryk University, Czech Republic.
Theoretical and experimental analysis of 2p states kinetics in barrier discharge in argon

P2-21 - **Benjamin Esteves** (T6)
CNRS, Sorbonne Université, Université Paris-Saclay, Observatoire de Paris, ?Ecole polytechnique, Institut polytechnique de Paris, France.
Development of optical diagnostics to study neutral species in low-pressure iodine plasmas: application within a gridded thruster.

P2-22 - **Horacio Fernandes** (T6)
Instituto de Plasmas e Fusao Nuclear, Portugal.
RF Plasma source characterization for an EM cavity

P2-23 - **Toma Sato** (T6)
Kyushu university, Japan.
Optical tweezers technique for electric field strength and fluctuation measurements in plasma using a fine particle

P2-24 - **Lukáš Kusýn** (T6)
Masaryk University, Czech Republic.
Spatiotemporally resolved electric field and temperatures in positive streamers

P2-25 - **Arne Meindl** (T6)
Max Planck Institute for Plasma Physics, Germany.
1D TALIF of atomic oxygen in the effluent of a CO_2 microwave discharge

P2-26 - **Koichi Sasaki** (T6)
Hokkaido University, Japan.
Estimation of vibrational temperatures of CO_2 in dielectric barrier discharges by deep ultraviolet absorption spectroscopy

P2-27 - **Gabi Daniel Stancu** (T6)
Laboratoire EM2C, CentraleSupelec, France.
Microwave discharges under thermal control for generation of nitric oxide

P2-28 - **Gwenael Fubiani** (T8)
CNRS, France.
3D Particle-in-Cell simulation of the $E \times B$ electron drift instability in Hall thrusters

P2-29 - **Quentin Delavière–Delion** (T8)
Laplace - Université de Toulouse Paul Sabatier - CNRS - INPT, France.
Experimental observation of the coupling of low frequency instabilities at different scales in a Hall thruster

P2-30 - **Thomas Maho** (T8)
INU Champollion - DPHE, France.
Characterization of a low-pressure microwave plasma in multisource configuration for surface decontamination applications

P2-31 - **Guangyu Sun** (T8)
Swiss Plasma Center, EPFL, Switzerland.
Improved negative ion source extraction efficiency using highly emissive inverse sheath for NBI heating in fusion

P2-32 - **Charlie Kniebe-Evans** (T8)
University of Oxford, United Kingdom.
Investigating the spatial distribution of nitrogen plasma species using saturated cavity ring-down spectroscopy

P2-33 - **Davide Maddaloni** (T8)
Universidad Carlos III de Madrid - EP2 research group, Spain.
Experimental investigation of oscillations in a magnetic nozzle

P2-34 - **Scott Doyle** (T8)
University of Michigan, United States of America.
Simulating Transformer Coupling and kHz Pulsing in a Toroidal Wave Heated Remote Plasma Source

P2-35 - **Lucas Fuster** (T9)
Laplace / CEA Gramat / Isae-Supaero, France.
Leaky wave discharges in a printed transmission line

P2-36 - **Erik Wagenaars** (T9)
York Plasma Institute, University of York, United Kingdom.
Effect of pulse repetition frequency on reactive oxygen species production in a pulsed He + H_2O plasma

P2-37 - **Maria Mitrou** (T10)
Laboratory of Subatomic Physics and Cosmology, University Grenoble Alpes, France.
Cylindrical SDBD of well-defined expansion area for standardized studies

P2-38 - **Alexandra Brisset** (T10)
CNRS, France.
Electron density and temperature in a diffuse nanosecond pulse discharge in air at atmospheric pressure

P2-39 - **Tatsuru Shirafuji** (T10)
Osaka Metropolitan University, Japan.
Shape Control of Surface-Launched Plasma Bullets

P2-40 - **Olivera Jovanović** (T11)
Institute of Physics Belgrade, Serbia.
The influence of non-thermal Ar plasma jet on physicochemical properties of treated liquid

P2-41 - **Zimu Yang** (T11)
University of Michigan, United States of America.
Spatially resolved spectra in an atmospheric pressure DC glow plasma emission with liquid anode

P2-42 - **Cas van Deursen** (T12)
DIFFER, Netherlands.
Effluent nozzles in Reverse-vortex-stabilized microwave plasmas for performance enhancement

P2-43 - **Volodymyr Nosenko** (T13)
DLR Institute of Materials Physics in Space, Germany.
Two-dimensional complex plasma with active Janus particles

P2-44 - **Kunihiro Kamataki** (T13)
Kyushu University, Japan.
Investigation of particle charge and interparticle interaction in a plasma

P2-45 - **Yerbolat Ussenov** (T13)
Princeton University, United States of America.
Optimization of nanoparticle growth in RF discharge plasma

P2-46 - **Hisato Yabuta** (T15)
Kyushu university, Japan.
Non-equilibrium nitrogen incorporation into ZnO films by rf-magnetron sputtering: stabilization of amorphous phase and noteworthy local structure in crystalline phase by solid phase crystallization

P2-47 - **Iori Nagao** (T15)
Kyushu University, Japan.
Control of ion trajectory in high aspect ratio trenches by using amplitude modulated rf discharges

P2-48 - **Jayashree Majumdar** (T15)
Indian Institute of Technology, Kanpur, India.
Studies on changes in surface morphology of materials under plasma environment and their potential applications in field emission

P2-49 - **Kazunori Koga** (T15)
Kyushu University, Japan.
Coverage control of carbon nanoparticles on substrate using capacitively coupled plasma chemical vapor deposition

P2-50 - **Didar Batryshev** (T15)
Kazakh-British Technical University, Kazakhstan.
Chondro-like particles in the plasma environment: formation mechanisms and properties

P2-51 - **Sushanta Barman** (T15)
Indian Institute of Technology Kanpur, India.
Controlled guiding and focusing of intense plasma ion beams by micro-glass capillaries beyond the self-focusing limit

P2-52 - **Sagi Orazbayev** (T15)
Al-Farabi Kazakh National University, Kazakhstan.
Superhydrophobic surfaces production by PECVD method

P2-53 - **Lucie Janů** (T15)
CEITEC, Brno University of Technology, Czech Republic.
Improve adhesion of electrospun nanofibers to plasma-treated polypropylene textile

P2-54 - **Hiromi Alwi Yamamoto** (T17)
Meijo University, Japan.
Bactericidal species in electrically-neutral oxygen radical irradiated solution

P2-55 - **Inna Orel** (T17)
GREMI, Université d'Orléans, France.
Carboxyhemoglobin creation in hemoglobin solution following treatment by pulsed DBD kHz plasma jet in Ar-CO_2 for plasma medicine applications

P2-56 - **Borui Zheng** (T17)
Xi'an University of Technology, China.
Paper sheet disinfection and sterilization by non-thermal atmospheric-pressure plasma

P2-57 - **Thomas Vazquez** (T17)
Comenius University in Bratislava, Slovakia.
Combined effects of cold atmospheric plasma and photocatalysis for indoor air decontamination

3.3.3 Poster session P3, Thu, Jul 13, 13:45 - 15:45

P3-1 - **Wouter Graef** (T1)
Plasma Matters, Netherlands.
The 2023 status report on the LXCat project

P3-2 - **Octavio Emmanuel Hernández Alvarez** (T1)
Charles University, Czech Republic.
Nuclear-Spin-Changing Collisions Between H_3^+ and H_2 in an Ion Trap Experiment

P3-3 - **Jean-Paul Booth** (T1)
CNRS, France.
Oxygen atom and ozone kinetics in the afterglow of a pulse-modulated DC discharge in pure O_2: an experimental and modelling study

P3-4 - **Miroslava Kassayová** (T1)
Charles University, Czech Republic.
Spectroscopy and recombination of H_2D^+ and HD_2^+ ions

P3-5 - **Juan Miguel Gil** (T1)
Universidad de Las Palmas de Gran Canaria (ULPGC), Spain.
Simulation and characterization of the interaction of fast quasi-monoenergetic ion beams and deuterium-tritium plasma

P3-6 - **Ayesha Nanda** (T2)
Indian Institute of Technology Kanpur, India.
Power balance in an anisotropic dipole plasma: thermodynamical insights

P3-7 - **Stephen Muhl** (T3)
Instituo de Investigaciones en Materiales, UNAM, Mexico.
Photothermic Infrared Emission of Sputtering Targets

P3-9 - **Jiansyun Lai** (T3)
Kyushu university, Japan.
Effects of lower discharge frequency on ion energy distribution function in dual frequency plasma studied by particle-in-cell/Monte Carlo method

P3-10 - **Codrina Ionita-Schrittwieser** (T3)
University of Innsbruck, Austria.
Diamond-coated probes for diagnostics in hot and hazardous plasmas

P3-11 - **Jon Tomas Gudmundsson** (T5)
University of Iceland, Iceland.
On surface effects in a capacitive argon discharges

P3-12 - **Kevin Michael Rettig** (T5)
scia Systems GmbH, Germany.
Modeling the extraction of a focused broad ion beam from an inductively coupled plasma source.

P3-13 - **Hans Höft** (T5)
INP Greifswald, Germany.
Investigation of self-pulsing discharges in argon at atmospheric pressure

P3-14 - **Kevin van 't Veer** (T5)
Plasma Matters B.V., Netherlands.
Atmospheric pressure high current diffuse glow-like dielectric barrier discharges in argon

P3-15 - **Richard Christian Bergmayr** (T5)
Max Planck Institute for Plasma Physics, Germany.
Corona modelling for ro-vibrationally resolved spectra analysis in low-temperature hydrogen plasmas

P3-16 - **Ilija Simonović** (T5)
Institute of Physics Belgrade, University of Belgrade, Serbia.
Axisymmetric streamer model in the AMReX environment

P3-17 - **Ataollah Eivazpour Taher** (T5)
Universidade da Madeira, Instituto de Plasmas e Fusão Nuclear, Lisboa, Portugal.
On stability of negative corona discharges

P3-18 - **Dennis Bouwman** (T5)
Centrum Wiskunde & Informatica (CWI), Netherlands.
Estimating the physics of single positive air streamers from measurable parameters

P3-19 - **Laura Chauvet** (T6)
Ruhr Universty Bochum, Germany.
Mass spectrometry of an atmospheric pressure plasma jet interacting with a dielectric surface

P3-20 - **Jean-Paul Booth** (T6)
CNRS, France.
Oxygen atom TALIF : temperature dependence of fluorescence quenching

P3-21 - **Yuya Yamashita** (T6)
Tokyo Institute of Technology, Japan.
Diagnosis of spatial distribution of electron temperature and electron density of argon inductively coupled plasma by tomographic optical emission spectroscopic measurement

P3-22 - **Jesse Laarman** (T6)
Eindhoven University of Technology, Netherlands.
Electric field analysis of single channel stable streamers using E-FISH

P3-23 - **Marion Henkel** (T6)
Leibniz-Institut für Plasmaforschung und Technologie e.V. (INP), Germany.
Laser-induced plasma formation in water with up to 600 bar hydrostatic pressure and up to 400 millijoule double-pulse LIBS

P3-24 - **Vasco Guerra** (T8)
IPFN, IST, Universidade de Lisboa, Portugal.
Development of a reaction mechanism for CO_2-N_2 plasmas

P3-25 - **Shu Zhang** (T9)
Laboratoire de Physique des Plasmas (LPP), CNRS, École polytechnique, Institut Polytechnique de Paris, France.
RF CCPs at intermediate pressure: Dissociation trends in O_2/Ar

P3-26 - **Jon Tomas Gudmundsson** (T9)
University of Iceland, Iceland.
On working gas rarefaction in high power impulse magnetron sputtering

P3-27 - **Gita Revalde** (T9)
University of Latvia, Latvia.
Investigation of radiation of Hg 198 isotope lamp

P3-28 - **Yusuke Nakagawa** (T10)
Tokyo Metropolitan University, Japan.
Behavior of atomic oxygen in pulsed barrier discharge under sub-atmospheric pressure He/O_2 mixture

P3-29 - **Hans Höft** (T10)
INP Greifswald, Germany.
Interaction of two single-filament, pulsed-operated dielectric barrier discharges

P3-30 - **David Schulenberg** (T10)
Ruhr University Bochum, Germany.
On the influence of the gas temperature on electron power absorption in atmospheric pressure micro radio frequency plasma jets

P3-31 - **Nikola Skoro** (T11)
Institute of Physics Belgrade, Serbia.
Characterization of a plasma system with microwave launcher used for treatment of liquids

P3-32 - **Saeed Kooshki** (T11)
Comenius University Bratislava, Slovakia.
Plasma-Activated Water (PAW): Sustainable Technology for Wastewater Treatment and its Reuse as a Green Fertilizer

P3-33 - **Judith van Huijstee** (T13)
Eindhoven University of Technology, Netherlands.
Microparticle charge in a spatio-temporal afterglow plasma: influence of an externally applied electric field

P3-34 - **Kazuo Takahashi** (T13)
Kyoto Institute of Technology, Japan.
Ion bombardment on microorganism in dusty plasmas

P3-35 - **Kseniia Leonova** (T15)
ChIPS, University of Mons, Belgium.
Influence of target heating on the growth of Nb coatings during hot magnetron sputtering

P3-36 - **Shinjiro Ono** (T15)
Kyushu University, Japan.
Deposition characteristics of cumene plasma CVD for high-speed deposition of high-density a-C:H films

P3-37 - **Kizuku Ikeda** (T15)
Kyushu University, Japan.
Effects of Ne mixing on plasma enhanced chemical vapor deposition of a-C:H films using CH_4/Ar/Ne capacitively coupled discharges

P3-38 - **Mitsuaki Maeyama** (T15)
Saitama University, Japan.
Effects of electrode geometries and materials on a water purification using the ball lightning discharge

P3-40 - **Emilio Martines** (T17)
University of Milano-Bicocca, Italy.
Optical emission spectroscopy of a plasma jet for biomedical applications

P3-41 - **Anda Abola** (T17)
Institute of Atomic Physics and Spectroscopy, University of Latvia, Latvia.
Zeeman AAS - a means to assess mercury pollution in the environment through artefacts of wild birds

P3-42 - **Yasumasa Mori** (T17)
Meijo University, Japan.
Nitric oxide radicals penetrates into fibroblast cells to promote proliferation

P3-43 - **Satoshi Uchida** (T17)
Tokyo Metropolitan University, Japan.
Permeation characteristics of hydrogen peroxide through biological membranes by applying electric field

P3-44 - **Ryo Ono** (T17)
The University of Tokyo, Japan.
Treatments of cancer tumors in mice using streamer discharge

P3-45 - **Ana Sainz-García** (T17)
University of La Rioja, Spain.
Bactericidal activity against Listeria spp using Plasma Activated Water

P3-46 - **Perla Trad** (T17)
INRS/LPGP, France.
Coupling of a non-thermal plasma to a membrane process for the treatment of n-hexane

P3-47 - **Korentin Géraud** (T17)
LPP, Sorbonne Université, France.
Cold plasma therapy applied to non-small cell lung cancer: deciphering the relevant plasma parameters to induce antitumor effects

P3-48 - **Yoshihisa Ikeda** (T17)
Ehime University, Japan.
Mechanism of molecular introduction into plant cells using plasma treatment

P3-49 - **Takamasa Okumura** (T17)
Kyushu University, Japan.
Measurement of electric field, UV photons, and long-lifetime reactive species generated by atmospheric pressure air plasma for plasma bio applications

P3-50 - **Paolo Francesco Ambrico** (T17)
CNR ISTP, Italy.
The inhibitory effect of volume dielectric barrier discharge on phytopathogenic fungi.

P3-51 - **Aysegul Uygun Oksuz** (T17)
Suleyman Demirel University, Turkey.
Determination of antibacterial effectiveness rate of plasma activated physiological saline (PAIS) solution (0.9% NaCl)

P3-52 - **Richard Cimerman** (T17)
Comenius University in Bratislava, Faculty of mathematics, physics and informatics, Slovakia.
Nonthermal plasma regeneration and repetitive use of deactivated catalysts

P3-53 - **Filippo Capelli** (T19)
Alma Mater Studiorum - University of Bologna, Italy.
Plasma assisted decontamination of food packaging

P3-54 - **Kunihiro Kamataki** (T19)
Kyushu University, Japan.
Prediction of plasma process conditions via machine learning

P3-55 - **Pohsien Chiu** (T19)
Department of Mechanical Engineering, National Yang Ming Chiao Tung University, Hsinchu, Taiwan.
Stabilize Voltage and Transmit Power by Atmospheric-Pressure Plasma Jet in Streamer Mode

3.3.4 Poster session P4, Thu, Jul 13, 17:00 - 19:00

P4-1 - **Guadalupe Espinosa Vivas** (T1)
Universidad de Las palmas de Gran Canaria, Spain.
Microscopic properties of xenon plasmas in a wide range of plasma conditions.

P4-2 - **Robert Carman** (T1)
Macquarie University, Australia.
Inelastic momentum transfer cross-sections from inelastic differential cross-sections for electron-impact excitation in Helium and in Argon

P4-3 - **Rafael Rodriguez** (T1)
Universidad de Las Palmas de Gran Canaria, Spain.
Effects of impurities on beam-plasma interaction and hot spots properties in fast ignition nuclear fusion

P4-4 - **Yui Okuyama** (T2)
National Institute of Technology, Tomakomai College, Japan.
Simulation of negative ion mobility at atmospheric pressure in O_2 by Monte Carlo method using rate coefficients of ion-molecule reactions

P4-5 - **Andrei Smolyakov** (T4)
University of Saskatchewan, Canada.
Plasma acceleration in the magnetic nozzle

P4-6 - **Luís L. Alves** (T5)
IPFN/IST, Portugal.
The LisbOn KInetics simulation tools

P4-7 - **Carlos Pintassilgo** (T5)
IPFN, Portugal.
Effect of the magnetic field on the electron kinetics under AC/DC electric fields

P4-8 - **Nicolas Lequette** (T5)
LPP, France.
Comparison of 1D particle-in-cell simulations with Langmuir probe measurements of a low-pressure inductively-coupled discharge

P4-9 - **Alejandro Malagón Romero** (T5)
Centrum Wiskunde & Informatica (CWI), Netherlands.
A physics-informed neural network to accelerate Montecarlo streamer simulations

P4-10 - **Tsanko Vaskov Tsankov** (T5)
Ruhr University Bochum, Germany.
First-principles simulation of optical emission spectra for low-pressure argon plasmas and its experimental validation

P4-11 - **Federico Petronio** (T5)
LPP Ecole Polytechnique - SAFRAN, France.
Two-dimensional electrostatic instabilities in Hall thrusters

P4-12 - **Hiroshi Akatsuka** (T6)
Tokyo Institute of Technology, Japan.
Spatial distribution of vibrational and rotational temperatures of N_2 ICP by tomographic optical emission spectroscopic measurement

P4-13 - **Irene van de Haar** (T6)
Eindhoven University of Technology, Netherlands.
A Numerical Algorithm to Restore the Electric Field Distribution from E-FISH Signals

P4-14 - **Laurent Invernizzi** (T6)
Laboratoire des Sciences des Procédés et des Matériaux, France.
Challenges of ps-TALIF measurements using a streak camera

P4-15 - **Ibrahim Baraze Abdoul Razak** (T6)
DPHE / INU Champollion, France.
Experimental characterization of a Kr-Cl DBD lamp for surface irradiance distribution study including simple photon transfer simulation.

P4-16 - **Zhan Shu** (T6)
Laboratoire de Physique des Plasmas, France.
Time-resolved absolute density of atomic oxygen in the early afterglow of a nanosecond CO_2 plasma

P4-17 - **Waseem Khan** (T6)
Masaryk University, Czech Republic.
Fluorescence (LIF) measurement of atomic antimony concentration in a planar dielectric barrier discharge.

P4-18 - **Dejan Dojić** (T6)
University of Belgrade, Serbia.
Absorption properties of Laser Induced Plasma

P4-19 - **Isabel Tanarro** (T8)
CSIC -Consejo Superior de Investigaciones Científicas, Spain.
Relevance of N_2 addition in the ion composition of C_2H_2 glow discharges

P4-20 - **Tiago Cunha Dias** (T8)
Instituto de Plasmas e Fusão Nuclear, Instituto Superior Técnico, Lisboa, Portugal.
A reaction mechanism for oxygen plasmas

P4-21 - **Scott Doyle** (T8)
University of Michigan, United States of America.
Structural and Electrical Enhancement of Radial Homogeneity in Wide Aspect Ratio Capacitively Coupled Plasma Processing Sources

P4-22 - **Anda Abola** (T9)
Institute of Atomic Physics and Spectroscopy, University of Latvia, Latvia.
Self-modulation in arsenic high-frequency electrodeless lamps

P4-23 - **Swaminathan Prasanna** (T9)
Universite Paris Sorbonne Nord, France.
Evidence of a significant N-atom metastable population by ns-TALIF in pulsed N_2 microwave plasma

P4-24 - **Zheng Zhao** (T9)
Xi'an Jiaotong University, China.
Streamer discharge instabilities under repetitive nanosecond pulses

P4-25 - **Denis Eremin** (T9)
Ruhr University Bochum, Germany.
The electron power absorption mechanism due to the sheath motion in a microwave-driven plasmaline discharge

P4-26 - **María C García** (T9)
Universidad de Córdoba, Spain.
Generating non-filamented argon plasma columns at atmospheric pressure using a surfatron consuming low 2.45 GHz microwave power

P4-27 - **Quentin Gutierrez** (T9)
Laboratoire de Physique Subatomique et de Cosmologie (CRPMN), France.
Discharge sustained by HF cathode for fluorescent lamp applications

P4-28 - **Victor Lafaurie** (T10)
LPP, France.
Nanosecond Surface Dielectric Barrier Discharge: Experimental study of high-pressure streamer to filament transition with varying gas composition

P4-29 - **Corentin Bajon** (T10)
Laplace - Université de Toulouse Paul Sabatier, France.
Study of Townsend Dielectric Barrier Discharge in CO_2

P4-30 - **Jun Sup Lim** (T10)
Plasma Bioscience Research Center (PBRC), Kwangwoon Univ, Korea, Republic Of.
Effect of charge accumulation on the ionized gas propagation in atmospheric pressure plasma jet

P4-31 - **Rui Manuel Santos Almeida** (T10)
Universidade da Madeira, Portugal.
Breakdown characterization in device with dielectric spacer in air at 1 atm

P4-32 - **Yoshinobu Inagaki** (T11)
Hokkaido University, Japan.
Effects of rf power and potential of water jet on quantum yield of laser-induced desolvation in inductively coupled plasma

P4-33 - **Takuma Uemura** (T11)
The University of Tokyo, Japan.
Electrical potential and luminescence distribution measurements of repetitive surface dielectric barrier discharges in N_2 and O_2 mixture gases

P4-34 - **Lara Alomari** (T11)
PPRIME Institute, France.
Needle-to-liquid DC and AC dielectric barrier discharges in atmospheric air: electrical characteristics and chemical analysis

P4-35 - **Ramón Peláez** (T13)
CSIC, Spain.
Behaviour of interstellar dust analogues under interstellar conditions.

P4-36 - **Guido Klaassen** (T13)
Eindhoven University of Technology, Netherlands.
Photodetachtment experiments on Plasma Confined Micro-Particles

P4-37 - **Corné Rijnsent** (T15)
TNO, Netherlands.
First Mirror cleaning in ITER Edge Thomson Scattering diagnostic system using 40.68-MHz discharge in hydrogen

P4-38 - **Yoshiharu Wada** (T15)
Kyushu University, Japan.
Sputter deposition of low resistive 30-nm-thick ZnO:Al films using ZnO seed layers grown via solid-phase crystallization

P4-39 - **Ryota Narishige** (T15)
Kyushu University, Japan.
Pseudomorphic growth of (ZnO)x(InN)1-x films on ZnO substrates by magnetron sputtering using $Ar/N_2/O_2$ discharges

P4-40 - **Takafumi Yunoue** (T15)
Kyushu University, Japan.
Sputter epitaxy of Zn1-xMgxO films on lattice-mismatched sapphire substrates utilizing ZnO(N)/MgO buffer layers fabricated by Ar/N_2 and Ar/O_2 discharges

P4-41 - **Shih-Nan Hsiao** (T15)
Nagoya University, Japan.
Atomic layer etching of SiN films with CF_4/H_2 surface modification and H_2/N_2 plasma exposure

P4-42 - **Jianyu Feng** (T15)
Masaryk University, Czech Republic.
Temperature-friendly remote atmospheric pressure plasma source for plasma activation of materials

P4-43 - **Joanna Pawlat** (T15)
Lublin University of Technology, Poland.
Nonthermal plasma impact on NaCMC/glauconite suspension properties

P4-44 - **Yuma Yamamoto** (T15)
Kyushu University, Japan.
Relation between Spatial Distribution of Optical Emission Intensity and SiO_2 Film Property in TEOS-PECVD

P4-45 - **Murugesh Munaswamy** (T15)
Hokkaido University, Japan, Japan.
Challenges in obtaining uniform distribution of core shell Tin nano-particles using dc magnetron sputtering plasma

P4-46 - **Tamiko Ohshima** (T15)
National Institute of Technology, Sasebo College, Japan.
Plasma processing of Al-doped zinc oxide thin films using powder targets

P4-47 - **Pasquale Isabelli** (T17)
Alma Mater Studiorum, Italy.
Cold plasma systems for bioaerosol decontamination: comparison between a Rotating Dielectric Barrier Discharge plasma source and a commercial device

P4-48 - **Manuel Oliva** (T17)
Universidad de Sevilla, Spain.
Unraveling surface effects for improving the germination of barley seeds: from drying to air plasma treatments

P4-49 - **Etienne Michaux** (T17)
ICARE CNRS, France.
Fractal Dimension of cathode spots in a Vacuum Arc Thruster

P4-50 - **Cristina Muja** (T17)
I.N.U. J.F. Champollion, University of Toulouse, France.
Sensitivity of Deinococcus radiophilus and Escherichia coli to UVC radiation generated by a plasma lamp combined with phosphors

P4-51 - **Yoshihito Yagyu** (T17)
National Institute of Technology, Sasebo College, Japan.
Development of a novel plasma device for cancer treatment and irradiation effects on the hepatoblastoma-derived cell, Hep G2

P4-52 - **Ramavtar Jangra** (T17)
Indian Institute of Technology Jodhpur, India.
Deactivation efficiency analysis of airborne microorganisms using a Dielectric Barrier Discharge (DBD) based plasma system

P4-53 - **Roxanne Walker** (T17)
University of Michigan, United States of America.
Nonthermal Plasma Interactions with Microplastics in a Polymer-Water Matrix

P4-54 - **Leonardo Zampieri** (T17)
Università degli Studi di Milano-Bicocca, Italy.
Combining diagnostics for characterizing antibacterial effect of a cold atmospheric plasma source

P4-55 - **Shin-ichi Aoqui** (T10)
Sojo University, Japan.
Discharge space expansion in single-phase atmospheric pressure gliding arc discharge

4 Abstracts

Nonlinearity and complexity of low-temperature plasmas Self-organized filaments, striations, and spokes

J.P. Boeuf

LAPLACE, Université de Toulouse, CNRS, INPT, UPS, 118 Route de Narbonne, 31062 Toulouse, France

Low-temperature non-equilibrium plasmas are characterized by a variety of nonlinear phenomena, which can lead to the emergence of stationary patterns or structures with complex dynamics. As stated in Ref. [1], "Every good model starts from a question. The modeler should always choose the correct level of detail to answer the question", and "Don't model bulldozers with quarks". The purpose of this presentation is to illustrate the emergence of self-organized structures in low-temperature plasmas through a few examples, and demonstrate how relatively simple yet well-thought-out models, i.e. at the right level of description, can offer a comprehensive understanding of the physics underlying the formation of complex structures.

Low-temperature non-equilibrium plasmas are complex systems where the transport of charged particles interacts with electromagnetic fields, neutral transport, chemistry, and surfaces. The complexity of plasmas is not specific to hot plasmas and some recommendations on how to face complexity in hot plasmas in Ref.[2] are worth reading and also apply to low-temperature plasmas.

This presentation will focus on the coupling between charged particles and fields and its significant role in the emergence of self-organized structures and patterns (the chemistry of neutral species can vastly increase the complexity of low-temperature plasmas and is crucial for some applications but will not be discussed here). Examples of low-temperature plasma structures include well-known Lichtenberg figures, streamer branching [3], dynamic filamentary patterns in dielectric barrier discharges [4, 5] or microwave breakdown [6], moving striations in positive columns [7], and rotating micro or macro-plasma structures in magnetized plasmas [8,9,10]. The presentation will utilize some of these examples to showcase how combining various levels of models with the right level of complexity can provide an in-depth understanding of the physics underlying plasma structuration. A good example of the importance of choosing the right level of description is the modelling of streamer branching by Luque and Ebert [3], who used discharge tree models based on results and insights from fluid and kinetic models. As Anderson put it [11] (quoted in Ref. [3]), "Each new level in such a hierarchy usually contains nontrivial, sometimes surprising, physics that is not immediately apparent from our understanding of the lower levels".

References

[1] Goldenfeld N. and Kadanoff L.P., Simple lessons from complexity, Science 284, 87-89 (1999).

[2] Escande, D.F.. How to face the complexity of plasmas?, in: Leoncini, X., Leonetti, M. (eds), From Hamiltonian Chaos to Complex Systems. Nonlinear Systems and Complexity, vol **5**. pp. 109-157, Springer, New York, NY (2013).

[3] Luque, A. and Ebert, U., Growing discharge trees with self-consistent charge transport: the collective dynamics of streamers, New. J. Phys. **16** 013039 (2014).

[4] Callegari, T., Bernecker, B., Boeuf, J.P., Pattern formation and dynamics of plasma filaments in dielectric barrier discharges, Plasma Sources Sci. Technol. **23** 054003 (2014).

[5] Trelles, J.P., Pattern formation and self-organization in plasmas interacting with surfaces, J. Phys D: Appl. Phys. **49** 393002 (2016).

[6] Boeuf, J.P., Chaudhury, B., Zhu, G.Q., Theory and Modeling of Self-Organization and Propagation of Filamentary Plasma Arrays in Microwave Breakdown at Atmospheric Pressure, Phys. Rev. Lett. **104** 015002 (2010).

[7] Boeuf, J.P., Ionization waves (striations) in a low-current plasma column revisited with kinetic and fluid models, Phys. Plasmas **29** 022105 (2022).

[8] Boeuf, J.P., Rotating structures in low temperature magnetized plasmas - insight from particle simulations, Front. Phys. **2** 1 (2014).

[9] Boeuf J.P. and Takahashi M., Rotating Spokes, Ionization Instability, and Electron Vortices in Partially Magnetized E×B Plasmas, Phys. Rev. Lett. **124** 185005 (2020).

[10] Boeuf J.P. and Smolyakov A., Physics and instabilities of low temperature E×B plasmas for spacecraft propulsion and other applications, Phys. Plasmas, to be published (2023).

[11] Anderson, P.W., More is different, Science **177**, 393 (1972).

XXXV ICPIG, July 9-14, 2023, Egmond aan Zee, The Netherlands Topic number 17

CO_2 conversion and N_2 fixation into value-added chemicals and fuels

A. Bogaerts

Research group PLASMANT, Dept. Chemistry, University of Antwerp, Antwerp, Belgium

Plasma-based CO_2 and CH_4 conversion, as well as N_2 fixation are very promising. In this talk, I will first give a brief overview of the state-of-the-art on these applications, with the different types of plasma reactors typically used, discussing the opportunities and main challenges. Subsequently, I will present some recent results obtained in our group PLASMANT in this domain, including experiments to improve the performance, and modeling for a better understanding of the underlying mechanisms.

1 General

Plasma technology is gaining increasing interest for various gas conversion applications, such as CO_2 and CH_4 conversion into value-added compounds, and N_2 fixation for fertilizer applications [1-4]. Indeed, the electrons are mainly heated by the applied electric field, due to their small mass, and they activate the gas molecules by electron impact ionization, excitation and dissociation, creating new ions, excited species and radicals. These are very reactive, so they can easily produce new products. Hence, thermodynamically or kinetically limited reactions can proceed at mild conditions, i.e., atmospheric pressure and introducing the gas at room temperature. Furthermore, plasma reactors can quickly be switched on/off, and because they operate with electricity, they are very suitable to be combined with (fluctuating) renewable electricity, hence for electrification of chemical reactions.

To improve these applications in terms of conversion, energy efficiency and product formation, a good insight is needed in the underlying mechanisms. We try to obtain this by computer modelling and experiments.

2 Plasma-based CO_2 (and CH_4) conversion

Warm plasmas, such as microwave (MW), gliding arc (GA) and atmospheric pressure glow discharges (APGDs) are quite energy efficient for converting CO_2 into CO and O_2, but the overall conversion is typically limited, among others by recombination of CO with O/O_2 after the plasma. In this talk, I will show how a quenching nozzle can improve the performance, due to changing as flow dynamics and fast cooling, to avoid these recombination reactions.

Furthermore, I will show how a carbon bed placed after a GA plasma reactor can help to increase the CO_2 conversion (by a factor 2) and the CO yield (even by a factor 3), due to trapping the O/O_2 on the carbon bed, thereby avoiding these recombination reactions [5]. Likewise, also the energy efficiency increases by roughly a factor 2. Moreover, if the temperature is high enough, also the reverse Boudouard reaction can occur ($CO_2(g) + C(s) \leftrightarrow 2CO(g)$). In addition, the carbon bed allows to remove O_2 and obtain a (more or less) pure CO_2/CO stream, which reduces separation costs.

3 Plasma-based N_2 fixation

I will also show some recent examples of successful NO_x formation from air plasma, again in GA and MW plasmas, reaching very low energy cost (down to 2 MJ/mol) and quite high NO_x concentrations (up to 6%). In addition, I will show how a low-power pulsed plasma jet can reach record-low energy cost of 0.48 MJ/mol, close to the theoretical energy limit, due to efficient vibrational-translational non-equilibrium. Although the NO_x concentration in this case was quite low (~ 200 ppm), this was no problem when combined with lean-NO_x trap for very energy-efficient NH_3 synthesis, as I will explain in more detail in my talk.

References

[1] Snoeckx, R., Bogaerts, A. Plasma technology – a novel solution for CO_2 conversion? Chem. Soc. Rev. **46**, 5805-5863 (2017).

[2] Bogaerts, A., Neyts, E. Plasma technology: An emerging technology for energy storage. ACS Energy Lett. **3**, 1013-1027 (2018).

[3] Rouwenhorst, K. H. R., Engelmann, Y., van 't Veer, K., Postma, R. S., Bogaerts, A., Lefferts, L. Plasma-driven catalysis: green ammonia synthesis with intermittent electricity, Green Chemistry. Green Chemistry, 20, 6258-6287 (2020).

[4] Rouwenhorst, K. H. R., Jardali, F., Bogaerts, A., Lefferts, L. From the Birkeland–Eyde process towards energy-efficient plasma-based NO_X synthesis: a techno-economic analysis, Energy Envir. Sci., 14, 2520-2534 (2021).

[5] Girard-Sahun, F., Biondo, O., Trenchev, G., van Rooij, G., Bogaerts, A. Carbon bed post-plasma to enhance the CO_2 conversion and remove O_2 from the product stream, Chem. Eng. J. **442**, 136268 (2022).

Frontiers of Plasma Etching Technology for Advanced Semiconductor Devices

Kenji Ishikawa[1], T-T-N Nguyen[1], T. Tsutsumi[1], S-N. Hsaio[1], N. Britun[1], M. Sekine[1] and M. Hori[1]

[1] *Center for low-temperature plasma sciences, Nagoya University, Japan*

In the semiconductor device fabrications, plasma technologies are indispensable for mass-production of high-aspect-ratio features controlling at atomic scales. To develop continuously, mechanisms on the hierarchiral comlex plasma-surface reactions should be elucidated comprehensively on the basis of measurements using *in situ* plasma diagnosis at real time.

Low-temperature plasma processes occur at the heterogeneous interface between the plasma and the surface, that is, the "process architecture" comprises plasma, sheath, and a geometrical surface [1].(Fig. 1) The hierarchical systems of bulk plasma, sheath transport, and surface reactions should be handled in the plasma etching technology.

The plasma etching reactions are produced by the synergistic effect of radicals and ions. These reactive species are transported toward reaction surface. The radicals promote to form volatile products. To fabricate high-aspect ratio features, the reactions inside the features are important for controling the plasma etching reactions. For this purpose, it is necessary of plasma diagnostic techniques that are both easy to use and sufficiently accurate, combining various plasma measurement techniques such as spectroscopy. Builiding a scientific database accumulating reliable experimental data under a well-defined experimental system is indispensable.

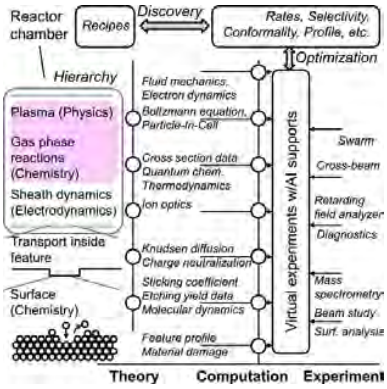

Fig. 1 Discovery of processing recipes through the combination of theory, computation, and experiments [1].

In the autonomous cotrol of etched feature profiles, the challenge is to control dimensions of the pattern (minimum critical dimension: CD) and properties of the materials (damage suppression) after the etching process [2].

The etched feature profiles were modified by a real time control of radical densities on the basis of substrate temperature change. Practically, etchant radical density of H atom increased in early stage with low substrate temperature and passivation radical density of N atom increased at later stage with high substrate temperature, enabling autonomously to be controlled by monitoring densities for H and N atom in the H_2 and N_2 mixture plasma in real time [3]. A feedback controller system can maintain these densities and substrate temperature, even when chamber wall conditions were disturbed. The etched featured profiles were tailored by lateral etching amount in a trend of processing time, operating feedback of on-off sequences of plasma and bias powers [4].

In the Nanoscale dry processes for controlling atomic layer reactions, cyclic processes of modification and removal are called atomic layer process (ALE). Isotropic ALE enables us to control removal thickneses at atomic level. Binary compounds such as gallium nitride (GaN) films are issued on etching with maintenance of their stoichiometric compositions [5]. Furthermore, the ALE of ternary compounds such as TaAlC films has been demonstrated by medium pressure (ranged from 1 kPa to 100kPa) plasma processes [6].

We are approaching the elucidataion of the mechanism by which etching reactions proceed selectively on the suraface of materials, including unfamiliar, complex structured materials in semiconductor procesing.

Acknowledgement

The authors would like to thank Dr K. Shinoda, Dr M. Izawa, Dr Tanide, Dr S. Nakamura, Dr M. Shiratani, and Dr K. Koga for fruitful disscussion and the Hori-Ishikawa laboratory members for technical assistances. This study was partly supported by JSPS-KAKENHI nos. 20H00142, 21H01073, and 21H04451.

References

[1] M. Kambara *et al*., Jpn. J. Appl. Phys. **62**, SA0803 (2023).
[2] K. Ishikawa *et al*., Jpn. J. Appl. Phys. **57**, 06JA01 (2018).
[3] T. Suzuki *et al*., J. Phys. D: Appl. Phys. **47**, 422001 (2014).
[4] Y. Fukunaga *et al*., Jpn. J. Appl. Phys. **58**, 020906 (2019).
[5] S. Nakamura *et al*., J. Appl. Phys. **133**, 043302 (2023).
[6] T-T-N. Nguyen *et al*., Sci. Rep. **12**, 20394 (2022).

Transport from target to substrate in High Power Impulse Magnetron Sputtering Plasmas

J. Held, M. George, W. Breilmann, V. Schulz-von der Gathen, A. von Keudell

Chair for Experimental Physics II. Reactive Plasmas, Ruhr University Bochum, Bochum, Germany

The transport in high power impulse magnetron plasmas is strongly affected by the dynamic of these plasmas. Spectroscopic techniques reveal the appearance of instabilities on various temporal and spatial scales that affect the cross field transport. Most prominent are spokes that rotate above the racetrack of a magnetron target and mitigate the return effect. This presentation highlights the nature of these spokes and their impact on heavy particle transport.

High power impulse magnetron sputtering (HIPIMS) is an important technology to synthesize high performance coatings. In these plasmas, a short high power pulse with of typically 100 µs and power densities on the target of a few kW/cm^2 is used to create plasma with a very high ionization degree and thus a very energetic particle fluxes towards the substrate enabling these excellent film qualities. The plasmas are operated at a duty cycle of below 1% to keep the thermal load on the target manageable. These HIPIMS plasmas, however, exhibit a big disadvantage with respect to conventional dc magnetron sputtering (DCMS). If normalized to the same average power density on the target, the deposition rate in HIPIMS is often much smaller compared to DCMS since ions are drawn back to the target in the magnetic pre-sheath of the plasma. This is coined ‘’return effect’’

The high plasma density in these discharges and steep gradients induce a wide range of instabilities and plasma patterns. The most prominent ones are spokes, bright ionization zones which rotate in the ExB or anti-ExB direction depending on the power density [1] with a typical velocity of 10 km/s or 30 kHz on a 2’’ circular target. It can be observed, that the return effect is significantly mitigated when these spokes emerge. The creation of these ionization zones is stochastic in nature, which makes a direct quantification of the plasma densities and electron temperatures inherently difficult. In this presentation, we will show how these plasmas can be quantified and how the transport from target to substrate is affected by the occurrence of these plasma patterns as evaluated by various diagnostics [1-4].

The temporal analysis of the Langmuir probe data reveals that the electron density in the ionization zones reaches values up to 10^{20}m^{-3} and a plasma potential close to the potential in front of the substrate [1]. Thereby, the electric field in the magnetic presheath is almost eliminated and the return effect mitigated. However, this reduction of the electric field in the magnetic pre-sheath occurs only in a time window of the moving ionization zone and has to correlate with the ion transit time through the magnetic trap region. The ionization zones can also be controlled by an external periodic signal, which is in sync with the travelling spokes. Within a window of a few kHz around the natural rotation frequency, the spokes can be accelerated or slowed down. Thereby the ion transport will be altered, because the temporal correlation between the ion transit and the spoke movement is affected. These detailed plasma parameters are also compared to a global model similar to the ionization region model (IRM), good agreement has been found.

Acknowledgments

The work is supported by the German Science Foundation within the project SFB TR 78.

References

[1] J. Held, A. von Keudell, Pattern formation in high power impulse magnetron sputtering (HiPIMS) plasmas, Plasma Chemistry Plasma Physics 40, 643 (2020)

[2] J. Held, M. George, A. von Keudell, Spoke-resolved electron density, temperature and potential in direct current magnetron sputtering and HiPIMS discharges, Plasma Sources Sci. Technol 31, 85013 (2022)

[3] P. Maaß, V. Schulz-von der Gathen, A. von Keudell and Julian Held, Synchronising optical emission spectroscopy to spokes in magnetron sputtering discharges, Plasma Sources Science and Technology 30, 125006 (2021)

[4] M. George, W. Breilmann, H. Held, A. von Keudell, Control of spoke movement in DCMS plasmas, Plasma Source. Sci. Technol. 31, 83004 (2022)

Transport of Reactive Species from Plasma Discharges into Water Determines the Plasma-Activated Water Properties and Applications

Zdenko Machala[1], Mostafa E. Hassan[1,2], Pankaj Pareek[1], Saeed Kooshki[1], Oleksandr Galmiz[1], Patrik Štípala[1], Karol Hensel[1], Mario Janda[1]

[1]*Faculty of Mathematics, Physics, and Informatics, Comenius University Bratislava, Slovakia*
[2] *now with Institut Pprime (CNRS UPR 3346-Université de Poitiers-ENSMA), Chasseneuil Futuroscope, France*

1 General

Atmospheric air plasma produces a cocktail of reactive oxygen and nitrogen species (RONS) with various lifetimes, reactivities, and multiple functions. The plasma chemistry is initiated by elementary processes of ionization, excitation, and dissociation; thus it leads to the formation of radicals and other RONS, and induces their mutual reactions. Specific composition of plasma gaseous RONS depends on the plasma discharge type and its power and geometry, the feed gas, its flow rate, the presence of water, and other environmental parameters. For example, low-power air discharges (corona, streamers, surface DBD) dominantly produce ozone, while the main products of high-power discharges (sparks, volume DBD, glow discharge, gliding arc, and arcs) are nitrogen oxides [1]. Besides these long-lived gaseous RONS, plasma also creates short-lived ones (e.g. hydroxyl $OH^{\bullet}$, atomic oxygen $O^{\bullet}$, superoxide $O_2^{-\bullet}$ radicals, or molecular singlet delta oxygen $^1O_2$) that strongly influence the plasma reactivity and its effects, although their diagnostics are challenging. These long- and short-lived RONS are not only formed directly in air plasmas but also in plasma rare gas jets with effluents into the ambient air.

Once plasma interacts with a liquid, either by operating the discharge completely submerged in liquid, or at the gas-liquid boundary, or in hybrid gas-liquid aerosol or bubble systems, gaseous RONS are transported into the liquid and the evaporation strongly influences the plasma processes [2]. The transport of RONS to the liquid phase through the plasma–liquid interface can be significantly enhanced by increasing the interface area, e.g. by converting bulk water to aerosol microdroplets [3]. The solubility of various plasma RONS does not perfectly match with the equilibrium of Henry's law. We verified the applicability of Henry's law coefficients for plasma–liquid interaction with bulk water vs. charged electrosprayed vs. non-charged aerosols [4].

In the liquid, the plasma-formed, as well as the new ionic RONS diffuse and undergo further reactions. They are crucial when the plasma-treated (activated) liquid interacts e.g. with organic pollutants, biomolecules, live cells, tissues, or plant seeds.

2 Results

We compare various air plasma discharges interacting with water solutions (DC and ns-pulsed driven streamer corona and transient spark, atmospheric glow discharge, surface, and volume DBDs), by analysing their gaseous and aqueous RONS. While low power streamers and DBDs in air produce dominantly ozone, higher power air discharges generate more $OH^{\bullet}$, hydrogen peroxide H_2O_2, NOx, and nitric/nitrous acids. However, due to various gas-liquid transport rates, even ozone-dominated plasma will not generate high liquid ozone concentrations but rather H_2O_2 and some NO_3^-, which can be still efficient against microorganisms or cancer cells. On the contrary, NOx-dominated plasma makes RNS-dominated plasma-activated water, which can be strongly antimicrobial if both H_2O_2 and nitrites NO_2^- are present and form peroxynitrites. Or RNS-dominated PAW can be used as a NO_3^--rich fertilizer and plant growth promoter in sustainable agriculture.

The selection of the discharge regime and its operational environmental parameters strongly influence the properties of the plasma-activated water and determines its suitability for specific applications. This fundamental knowledge can lead to optimized designs of plasma–water interaction systems for multiple applications.

Acknowledgement

This work was supported by Slovak Research and Development Agency APVV-17-0382 and APVV-22-0247, and Slovak Grant Agency 1/0596/22.

References

[1] M.J. Pavlovich et al., *Plasma Sources Sci. Technol.* 23, 2014, 065036.
[2] P.J. Bruggeman et al., *Plasma Sources Sci. Technol.* 25, 2016, 053002.
[3] Z. Machala et al. *J. Phys. D Appl. Phys.* 52, 2019, 340023.
[4] M.E. Hassan et al., *Water* 13, 2021, 182.

Recent challenges in electric (plasma) propulsion

[1]P. Chabert, [1]B. Esteves, [1]F. Petronio, [1]T. Ben Slimane, [1]N. Lequette, [1]A. Leduc, [1]A. Bourdon, [1]C. Drag, [1]A. Alvarez Laguna, [2]T. Lafleur

[1]LPP, CNRS, Institut Polytechnique de Paris, Sorbonne Université, Ecole Polytechnique 91128 Palaiseau, France
[2]School of Engineering and Information Technology, UNSW Canberra 2600, Australia

Electric (plasma) propulsion is a key technology in the space industry and for the deep space exploration programs. Research in this field has always been active and basic plasma physics is needed to understand the complexity of the plasma engines. The research involves gas discharge physics, such as ionization instabilities and secondary electron emission from the walls, and basic magnetized plasma physics including drifts in ExB fields and related instabilities and anomalous transport. Recently, the need for alternative propellants (because xenon and krypton that are currently used in plasma engines are rare and expensive) has increased the research effort on molecular gases, such as iodine. The talk will give an overview of the research conducted in the last decade and a few ideas for the near future.

Plasma propulsion has been used for a long time [1] but it is only recently, i.e. about ten years ago, that it has become the mainstream technology for satellite station keeping and even orbit transfer. Historically, the two main engines used (ion-gridded thrusters and Hall thrusters) were in the kilowatt range, and they produced thrust around 10-100 mN for a specific impulse typically in the range 1500-4000s (the specific impulse is the propellant ejection velocity divided by *g*, the acceleration due to gravity on the earth's surface). These numbers are adequate for station keeping of satellites in the GEO orbit. However, there is now a need for higher power thrusters for orbit transfer (typically 5kW and above), and lower power thrusters for smaller satellites in the LEO orbits. This diversity is not easily achieved and the equipment manufacturers need intense R&D efforts to have better scaling laws and even numerical simulations tools to optimize their design.

The talk will first give an overview of the recent research carried out on Hall thrusters operated in xenon [2]. There has been tremendous progress in the modelling of Hall thrusters and in particular on a better description of instabilities responsible for anomalous transport in the thruster channel and in the near plume. This progress relies both on 2D (even 3D) particle-in-cell simulations and on kinetic theory [3,4]. It will also be shown that synthetic diagnostics, i.e. "experimental" signals produced by numerical simulations, is a powerful tool for simulation validation. Classical experimental signals such has coherent Thompson scattering can be synthetically generated from PIC simulations allowing a detailed and precise comparison between synthetic and real signals [5]. The same applies for optical emission spectroscopy.

In a second part, the talk will also address the hot topic of alternative propellants. Xenon, and even krypton, used in classical plasma thrusters, have become rare and too expensive. The space industry is therefore investigating alternatives. This talk will show that iodine could be a possible candidate [6].

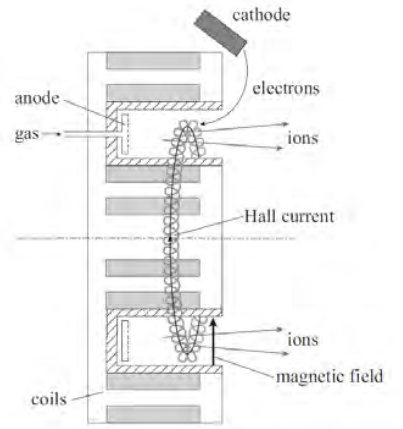

Figure 1: A schematic of a Hall Thruster

References

[1] D. M. Goebel and I. Katz, Fundamentals of Electric Propulsion: Ion and Hall Thrusters, JPL Space Science and Technology Series (Wiley, 2008).
[2] I. Kaganovich et.al, Physics Plasmas **27** (2020) 120601
[3] T. Lafleur and P. Chabert, Plasma Sources Sci. and Technol. **27** (2018) 015003
[4] F. Petronio et al. Phys. of Plasmas, 30 (2023) 012103 and 012104
[5] T. Ben Slimane et al., Phys. Plasmas, **29** (2022) 023501
[6] B. Esteves et al. Plasma Sources Sci. Technol. **31** (2022) 085007

Three-dimensional plasma sheath lenses: concept and applications

E. Stamate[1]

[1] *DTU Nanolab, Technical University of Denmark, Kgs. Lyngby-2800, Denmark*

The concept of three-dimensional plasma-sheath-lenses is discussed in connection with modal and discrete ion focusing effects, including phenomenology and applications. The investigation is then extended to magnetized plasma-sheath-lenses and other plasma processes where three-dimensional aspects are gaining relevance.

1 Introduction

Modal and discrete ion focusing effects are manifesting for 3D plasma-sheath-lens structures through the presence of passive surface, active surface, impact radius, modal lines, modal spots, and additional fine structures, such as modal rings and modal rays. [1,2] The focusing effects are dependent on plasma parameters, electrode shape and bias, and the electrode-insulator interface. For disk and square electrodes one can obtain very well-defined patterns, corelated with the 2D distribution of the ion current density. The measurable patterns can be used as a fingerprint of the entire plasma-presheath-sheath-electrode system for extracting additional information. It was demonstrated that modal and discrete ion focusing effects are also manifesting for negative ions.[1,2] So far, several applications have been proposed, including plasma diagnostics, ion beam extraction, and mass separation. [3]

This work reviews the status of 3D plasma-sheath-lenses and presents new results on the magnetic field effect on modal and discrete ion focusing effects. Furthermore, the concept of 3D plasma-sheath-lens is extended to magnetron sputtering where oxygen negative ions are focused to a location on the substrate correlated with the erosion track of the target. [4]

2 Modal and discrete ion focusing effects

One can obtain a potential structure with highly curved equipotential profiles by realizing a biased electrode-insulator interface as presented in Fig. 1 where in (a) the biased-electrode immersed in plasma is surrounded by an insulator and in (c) only the rear-side of the electrode is insulated. It was demonstrated by simulations that such structures exhibit very distinct ion kinetics that can be recorded experimentally by electrode sputtering/etching as presented in Fig. 1 (b) and (d) where 10×10 mm^2 silicon electrodes were etched in Ar/SF_6 plasma (–300 V bias and 10^{15} m^{-3} plasma density). The modal ion focusing involves ions entering the sheath from its rear-side and exhibits very well-defined modal lines, two for each corner. The discrete ion focusing involves ions entering the sheath from the lateral-side and provide a sharp delineation between the passive surface (near the electrode edge) and the active surface. Fig. 1 also helps understanding the importance of separating the two focusing effects. The focusing effects are affected by the presence of an external magnetic field and simulations predicted the formation of an additional disk passive-surface, at the center of disk electrodes, with a mass dependent radius. [3]

Experimental results and simulations for magnetized 3D plasma-sheath-lenses will be presented for disk as square electrodes immersed in multi-ion species plasmas.

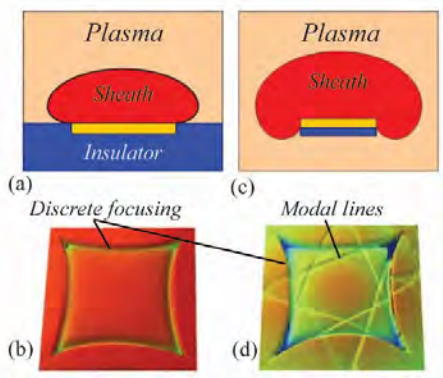

Fig. 1 Modal and discrete ion focusing effects for square electrodes.

3 References

[1] E. Stamate and H. Sugai, Phys. Rev. Lett. 94 (2005) 125004.

[2] E. Stamate and H. Sugai, Phys. Rev. E 72 (2005) 036407.

[3] E. Stamate, Plasma Phys. Control. Fusion 54 (2012) 124048.

[4] K. Norrman, P. Norby and E. Stamate, J. Mater. Chem. C 10 (2022) 14444.

Electric wind and water surface stabilization under impingement of an atmospheric pressure plasma jet

Wonho Choe[1], Sanghoo Park[1], Hyungyu Lee[1], Joo Young Park[1], Jinwoo Kim[1], Se Youn Moon[2], Uroš Cvelbar[3]

[1] *Korea Advanced Institute of Science and Technology, Daejeon, Republic of Korea*
[2] *Chonbuk National University, Jeonju, Republic of Korea*
[3] *Jožef Stefan Institute, Ljubljana, Slovenia*

Stabilizing water by physical processes has been a longstanding challenge and has led to profound insights into water properties. We present the peculiar deformation and stabilization of water surfaces with weakly ionized helium gas jets. Case studies have been designed to reveal the major origin of the plasma-induced force acting on the water surface. We have experimentally and numerically demonstrated that the electrohydrodynamic force generated inside the formed cavity causes cavity extension while maintaining stability, despite the critical gas flow rate being on the verge of unstable oscillation. This study demonstrates the dynamics of liquids subjected to a plasma-induced force, offering insights into physical processes and revealing an interdependence between weakly ionized gases and deformable dielectric matter, including plasma– liquid systems.

1 Introduction

An electric wind or ionic wind is a neutral gas flow that occurs in weakly ionized gases due to the charged particle–neutral coupling [1]. In atmospheric pressure plasmas, although the convective flow of neutrals by electric winds can significantly contribute to the transport of chemically active species, it has not been considered so far and must be considered. For gas-liquid two phase systems, for example water under impingement of an atmospheric pressure plasma jet, these electric winds also give rise to many interesting physical phenomena. Gas jets can create dimple-like depressions in the liquid surface. As the speed of the gas jet increases, the cavity becomes unstable and starts bubbling and splashing.

2 Results

Our study, for the first time, revealed that an ionized gas jet (or atmospheric pressure plasma jet) blowing onto water produces a more stable interaction with the water surface compared to a neutral gas jet [2]. It has been found that when a gas jet with plasma is impinged toward the water surface, deeper digging of the water surface by the electric wind generated by the plasma occurs. At the same time, the cavity undergoes a damped oscillation of about 100 Hz, which eventually becomes stable, i.e., the stability of the surface is improved despite the deeper digging of the water surface by the electric wind generated by the plasma. We found out that the Kelvin-Helmholtz instability, caused by the large velocity difference between gas and water at the boundary, becomes stabilized due to the strong electric field parallel to the water surface produced by high-speed ionization waves, i.e., plasma bullets. The experimental observation was confirmed by computational modelling for the plasma jet and water surface. In the developed plasma model, the plasma characteristics were analyzed by calculating the spatiotemporal change of the plasma, and the electric field in the direction of the surface increased by the plasma was quantitatively obtained by calculating the electric field near the water surface. From this computational modelling, the experimentally identified improvement in surface stability and deepening of the water surface cavity was cross-validated.

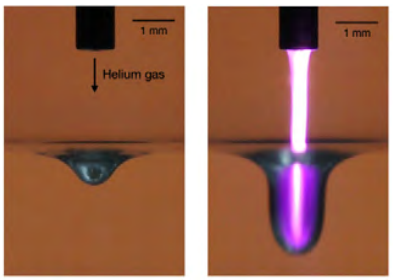

Figure 1 Cavity formation at water surfaces with and without a plasma jet

References

[1] Park, S., Cvelbar, U., Choe, W., Moon, S. Y. The creation of electric wind due to the electrohydrodynamic force. Nature Comm. **9**, 371 (2018).

[2] Park, S., Choe, W., Lee, H., Park, J., Kim, J., Moon, S. Y., Cvelbar, U. Stabilization of liquid instabilities with ionized gas jets. Nature **592**, 49 (2021).

Potential fluctuation dynamics in cold atmospheric pressure microplasmas

Sudeep Bhattacharjee[1], Michael Keidar[2] and Deepika Behmani[1]

[1]*Department of Physics, Indian Institute of Technology, Kanpur 208016, India*
[2]*Dept. of Mech. & Aerospace Engineering, The George Washington University, Washington, DC 20052, USA*

Frequency locked measurements of the plasma floating potential have been carried out in an atmospheric pressure microplasma jet interacting with substrates of varying electrical permittivity. Particular attention is paid to amplitude and frequency content of the fluctuations in the axial and poloidal directions of the jet. The results are compared with the peak value of the fluctuations determined from time series and fast Fourier transform. Investigation of fluctuations are critical to the generation and kinetics of RONS including particle and energy transport in the jet.

1 Introduction

Cold atmospheric pressure microplasmas are non-equilibrium plasmas with widely different electron (~ 6000 K) and ion temperatures (~ 300 K). These plasmas, created in the form of jets, have become attractive for a variety of applications, due to the rich atmospheric chemistry leading to the generation of reactive oxygen and nitrogen species (RONS) and novel surface interaction effects [1].

Our recent work indicated that the jet is prone to fluctuations in the plasma floating potential (FP) [2], that lie in the range 0.5 – 9 kHz, and depend upon experimental parameters such as applied voltage and gas flow rate. The importance, may be understood from the typical time scales for the development of RONS in the discharge which are around 0.5 – 1 ms in RF [3], and ~1 ns – 100 µs in pulsed jets [4]. These time scales correspond well to the observed fluctuation frequencies (~ 0.1 – 1 ms) in the experiments. Hence, fluctuations can influence RONS development, and affect particle and energy transport.

In this work, the fluctuations are investigated for a jet interacting with substrates of varying permittivity such as conductor (Cu), p-type semiconductor (Si), insulator (quartz and teflon) and biological tissue (goat skin). Besides the time series, FFT and correlation analysis, we report amplitude of the FP through frequency locked measurements, which helps to determine the precise value of the potential at the reference frequency, chosen from among the range of fluctuation frequencies (0.5 – 9.5 kHz). The results of the frequency locked measurements are compared with the peak value of the fluctuation frequencies determined from the time series and FFT.

2 Experimental

A schematic of the setup is shown in figure 1. A ring-to-ring electrode configuration is employed [2] for generating the jet with He as the input gas. The applied voltage is of 10 kHz and peak-to-peak amplitude of 11 kV. After ignition, the plasma emerges out from the orifice of the capillary tube as a fine jet [2]. The plasma plume is diagnosed by a single-pin probe [2], whose signal (voltage or current) is fed to the input of a lock in amplifier for FP and current measurements, as a function of the reference signal using a Keithley multimeter.

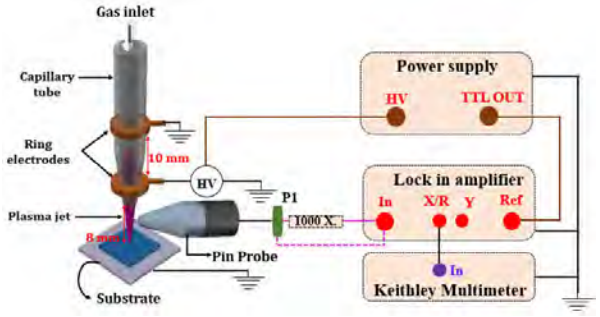

Figure 1: Schematic diagram of the experimental setup to measure fluctuations in the jet interacting with a substrate

References

[1] Johnson, M. J. *et al.*, Spatio-temporal characterization of a pulsed DC atmospheric pressure plasma jet interacting with substrates. Journal of Physics D: Applied Physics **54**, 085202 (2020).

[2] Behmani, D. *et al.*, Fluctuations of plasma potential in atmospheric pressure micro-plasma jets. AIP Advance **11**, 085128 (2021)

[3] Gaens, W. V. *et al.*, Kinetic modelling for an atmospheric pressure argon plasma jet in humid air. Journal of Physics D: Applied Physics **46**, 275201 (2013).

[4] Barni, R. *et al.*, Chemical kinetics simulations for atmospheric pressure air plasmas in a streamer regime. Journal of Applied Physics **97**, 073301 (2005).

Selective atomic layer etching of thin films using cyclic plasma exposure and infrared irradiation

K. Shinoda[1], S. Fujisaki[1], N. Miyoshi[1], H. Kobayashi[1], M. Izawa[2], K. Ishikawa[3], and M. Hori[3]

[1] *Research and Development Group, Hitachi, Ltd., Tokyo, Japan*
[2] *Nano-Technology Solution Business Group, Hitachi High-Tech, Tokyo, Japan*
[3] *Center for Low-temperature Plasma Sciences, Nagoya University, Nagoya, Japan*

An isotropic atomic layer etching (ALE) process for thin films using cyclic plasma exposure and infrared irradiation was developed. Dry chemical removal (DCR), a novel 300-mm tool composed of an inductively coupled plasma (ICP) source and infrared lamps, was produced to facilitate rapid thermal desorption of the modified surfaces. The key advantage of this process is that it utilizes two different temperatures: low temperature for surface modification and high temperature for desorption of the modified surface. This aspect makes the process suitable for a high degree of selectivity control as well as smooth etched surfaces. This talk will review the selective ALE of a variety of thin films (Si_3N_4, TiN, W, SiGe, and Co) with a focus on surface reactions analyzed by in situ x-ray photoelectron spectroscopy (XPS).

To fabricate miniaturized three-dimensional (3D) devices, precise control of the etching is required, not only for anisotropic but also for isotropic etching. The conventional method for isotropic etching is wet chemical etching, which has drawbacks such as inaccuracy in etched amount and a higher possibility of pattern collapse due to the higher surface tension of the wet chemical solution. One response to this challenge is isotropic atomic layer etching (ALE). We developed an isotropic ALE process composed of cyclic surface modification by plasma exposure and rapid removal of the modified surface by infrared irradiation [1]. A dry chemical removal (DCR) tool, which has both an inductively coupled plasma (ICP) source and infrared (IR) lamps, was developed to facilitate the ALE process. In this talk, we present the selective isotropic ALE of various materials (Si_3N_4, TiN, W, SiGe, and Co) with particular emphasis on surface atomic layer reactions examined by in situ x-ray photoelectron spectroscopy (XPS).

The DCR tool utilized in this study consists of a processing chamber, cooling stage for a 300-mm wafer, ICP source, IR lamps, and in situ ellipsometer. A wafer was placed on an electrostatic chuck cooled by a circulator and then exposed to radicals to modify the surface of the film. After that, the wafer was heated by IR lamp irradiation to remove the modified surface of the film. Surface analysis was carried out in an XPS system that was connected to a plasma treatment chamber via an ultrahigh vacuum wafer handling system.

Selective ALE of Si_3N_4 and TiN films over SiO_2 and poly-Si was performed using cyclic hydrofluorocarbon-based plasma exposure and IR lamp irradiation. The mechanism underlying the selective etching was analyzed by in situ XPS on the films after each step of the ALE cycles. We found that ammonium salt-based modified layers were formed only on nitride films after plasma exposure. The modified layers were removed when the samples were heated because the ammonium salt decomposes at the elevated temperatures.

One advantage of the thermal cyclic process is that material selectivity can be significantly controlled by changing the IR heating time [2]. For example, selective ALE of tungsten (W) over TiN is obtained when the IR irradiation time is 8 sec, while nonselective ALE of W and TiN is obtained when the IR irradiation time is 20 sec. This controllability is owing to the difference in the desorption temperature of the modified layers of the materials. Selective ALE of SiGe over Ge was also demonstrated based on the ammonium salt-based chemical reactions by using nitrogen added gas mixtures.

Another benefit of the thermal cyclic process is smooth etched surfaces for the ALE of metals. For example, ALE of Co with a smooth etched surface was demonstrated by utilizing cyclic plasma oxidation at low temperature and organometallization at elevated temperature [3]. The low temperature oxidation step is an important key in producing the smooth Co oxide.

In summary, thermal cyclic ALE of various thin films using our DCR tool was demonstrated. We conclude that ALE has great potential for the manufacturing of next-generation semiconductors.

References

[1] K. Shinoda et al., J. Phys. D: Appl. Phys. **50**, 194001–1–194001–13 (2017).
[2] K. Shinoda et al., J. Vac. Sci. Technol. B **40**, 022201–1–022201–11 (2022).
[3] S. Fujisaki et al., Appl. Phys. Lett. **121**, 122102-1-122102-5 (2022).

Role of electron-induced secondary electron emission from the walls in RF breakdown

F. Taccogna and D. Bruno

Institute for Plasma Science and Technology (ISTP), CNR, Bari, Italy

We report the results of Monte Carlo model of the electrical breakdown of hydrogen in radio-frequency (RF) electric fields taking into account the effect of electron-induced secondary electron emission from the walls.

A specific characteristic of RF breakdown is that the self-sustained discharge may be merely maintained through the α contribution (volumetric gas ionization by electrons), since the heavy ions do not respond to the RF field and just slowly diffuse towards all the surfaces without inducing the acceleration of ion-induced secondary electrons iSEE towards the anode (γ mechanism) as in the DC case. Nevertheless, by analysing the amplitude of electron oscillation under the RF electric field, it is evident how at relatively low pressure and low frequency, the electron-induced secondary electron emission (eSEE) can play an important role for sustaining the electron cascade during the gas breakdown. In recent years, different Particle-in-Cell Monte Carlo Collisions (PIC-MCC) simulations [1-3] have calculated the breakdown voltage as a function of the driving frequency and pressure in the RF modified Paschen curve.

In this work we present results of a 1D Monte Carlo simulation of H_2 RF breakdown with the implementation of a sophisticated SEE module. The electron/ion trajectories are obtained by integrating their equations of motion (with a time step $\Delta t = 10^{-10}$ s) in the presence of the applied electric field. The occurrence of collisions is checked at every time step Δt, for each electron. The types of collisions and the scattering processes are treated in a classical stochastic Monte Carlo Collision (MCC) manner. When electrons and ions hit the bulb walls, SEE is considered by using energy dependant yield data for the electron-induced emission e-SEE $\gamma_e(E)$ and by using a fixed yield $\gamma_i = 0.4$ for the iSEE [4]. Data refers to SiO_2 material.

The simulation time is set to 50 RF cycles and the number of electrons in continuously monitored. The number of electrons N_e during the last RF 20 cycles is checked (to avoid possible memory effects related to the initial seed electron distribution injected at the beginning) and fitted by a straight line. Separate simulations are carried out with slightly increased voltage amplitudes V_0, and the breakdown event is recognized when: i) the slope of the line $N_e(t)$ is positive; ii) the volumetric ion production rate (by electron gas ionization) is larger than the ion diffusion loss on the bulb walls (both averaged over the last 20 RF period).

Fig. 1 shows the RF breakdown voltage amplitude for a H_2 gas with electrode gap of L = 2 cm and working frequency ν_{RF} = 10 MHz.

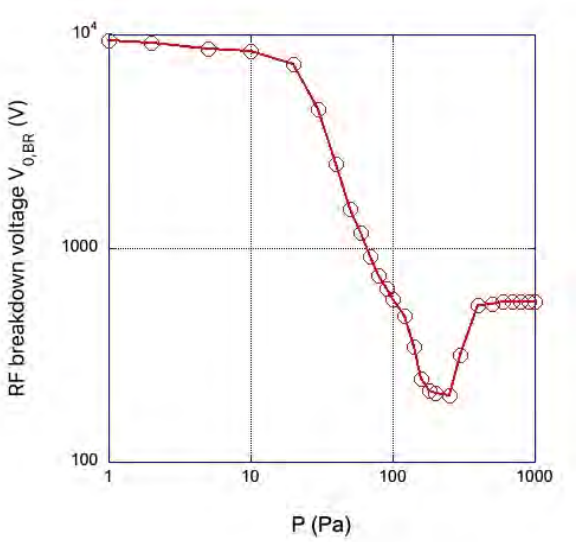

Fig. 1 – RF amplitude breakdown voltage as a function of H2 gas pressure for an electrode gap of L=2 cm and working frequency ν_{RF}=10 MHz.

References

[1] Smith, H. B., Charles, C. and Boswell, R. W. *Phys Plasmas*, **10(3)**, 875-881 (2003).
[2] Korolov, I. and Donko, Z. *Phys Plasmas*, **22(9)**, 093501, (2015).
[3] Puac, M., Maric, D., Radmilovic-Radjenovic, M., Suvakov, M. and Petrovic, Z. *Plasma Sources Sci. Technol.* **27(7)**, 075013 (2018).
[4] Booth, J. P., Curley, G., Maric, D. and Chabert, P. *Plasma Sources Sci. Technol.*, **19(1)**, 015005 (2009).

High resolution spectroscopy of "simple" molecular plasmas

C.V. Kniebe-Evans[1], A. Vitos[1], R. Peverall[1], S.D. Rogers[1,2], and G. A. D. Ritchie[1]

[1] *Department of Chemistry, University of Oxford, Oxford, United Kingdom*
[2] *Wolfson Atmospheric Chemistry Laboratory, Department of Chemistry, University of York, United Kingdom*

This contribution details the application of sensitive optical absorption techniques to probe inductively coupled plasmas of oxygen and nitrogen. Radio frequency plasmas formed from these simple molecular species have found an increasingly important role in many industrial applications and high-resolution spectroscopy allows their chemistry to be probed with unrivalled specificity and sensitivity. In particular, this work uses cavity ringdown spectroscopy to detect atomic, ionic and electronically excited molecular species as a function of plasma operating conditions. The data are supplemented with observations of plasma emission spectra and interpreted by volume averaged kinetic modelling. The modelling is complemented by spatially resolved measurement of ion densities.

1 General

The first part of this contribution concerns oxygen plasma and presents cavity ringdown spectroscopy (CRDS) measurements of $O(^3P)$ and $O_2(a^1\Delta_g)$, which reveal dissociation fractions as high as 15%, metastable molecule fractions of 5% and translational temperatures up to 450 K [1,2]. The two species, by virtue of their different threshold energies for electron impact production, provide insight into different regions of the electron energy distribution function (EEDF). As a result, measurements of $O(^3P)$ and $O_2(a^1\Delta_g)$ in combination with a volume averaged kinetic plasma model allow changes in the EEDF to be investigated as the plasma transitions from the (capacitive) E- to the (inductive) H-mode of operation [3]. One important kinetic parameter for the model, *i.e.* the chamber specific wall loss rate for the two species, is deduced from lifetime measurements following plasma extinction.

Volume averaged modelling, although quantitatively useful, neglects spatial inhomogeneity within the plasma, a characteristic that has been investigated by measuring $O_2(X^3\Sigma^-_g)$. These observations reveal a vibrational temperature (amongst the low v states) of $\approx 750 \pm 150$ K under plasma conditions of 100 mTorr pressure and 300 W power and we show that a 1D model exhibiting physically reasonable line of sight variations in plasma temperature and composition corroborates these measurements.

The second part of this contribution concerns nitrogen plasma and focuses on CRD measurements of the molecular cation, $N_2^+(X\,^2\Sigma^+_g)$, and the electronically excited metastable $N_2(A^3\Sigma^+_u)$ state. Notably, in these cases the use of large intracavity radiation intensities to probe allowed transitions results in optical saturation, the effects of which must be accounted for when determining species temperatures and densities. With adjustments made for the effects of optical saturation the CRD measurements show ion (and therefore electron) densities of the order of $10^9 - 10^{10}$ cm^{-3} in the plasma bulk (depending on operating conditions) and metastable densities an order of magnitude higher. Interestingly the two species show rather different translational temperatures with that for the ions typically ≈ 1000 K and for the metastables ≈ 600 K. Again, the absolute density measurements are interpreted in terms of a volume averaged kinetic model.

In addition, spatially resolved measurements of the same nitrogen species are presented, with particular reference to how ion densities change as the edge of the chamber is approached *i.e.* in the plasma – surface boundary layers: the pre-sheath and sheath. Measurements with a spatial resolution of ≈ 100 μm show that the ion density is reduced by almost an order of magnitude close to the chamber's lower electrode. Finally, the effects of saturation on the CRD spectra are explored and the contributions to the Lamb dip structures quantified.

References

[1] Rogers SDA, Peverall R, Ritchie GAD, Quantitative measurement of oxygen atom and negative ion densities in a low pressure oxygen plasma by cavity ringdown spectroscopy, Plasma Sources Sci. Technol. **29** 045004 (2020).

[2] Rogers SDA, Bond A, Peverall R, Hancock G, Ritchie GAD, Quantitative measurements of singlet molecular oxygen in a low pressure ICP. Plasma Sources Sci. Technol. **30** 09LT02 (2021).

[3] Rogers SDA, Bond A, Rhodes BJ, Peverall R, Hancock G, Ritchie GAD, Cavity ringdown studies of the E-H transition in an inductively coupled oxygen plasma: comparison of spectroscopic measurements and modelling. Plasma Sources Sci. Technol. **31** 115006 (2022).

A diagnostic study of the CO_2 vibrational kinetics in a glow discharge

R. Engeln[1]

[1] *Tech RES SCAN Plasma Physics, ASML Netherlands B.V.*

During the presentation results of diagnostic studies into the (ro)vibrational excitation and relaxation mechanisms in a CO_2 glow discharge and the effect of common impurities in the CO_2 gas flow on this excitation and relaxation will be presented. In particular the effects of the addition of N_2, O_2 and H_2O to the CO_2 gas flow will be discussed. The results are obtained using absorption spectroscopy with quantum cascade lasers, Raman, Fourier Transform and laser induced fluorescence spectroscopy.

1 Introduction

The research that will be presented is performed in the field of solar fuels, where energy from renewable sources is stored in the chemical bonds of high energy-density hydrocarbon fuels, with CO_2 as the carbon resource. One of the crucial steps in the synthesis of hydrocarbon fuels is the dissociation of CO_2 to form CO, which is an energy costly step. The aim of the research is to improve understanding of the fundamental mechanisms that lead to CO_2 dissociation and the role of the vibrations of CO_2 in this process and the effects of impurities in particular.

During the presentation the effects of the addition of molecular nitrogen, oxygen and water will be discussed. These effects are studied in a pulsed DC glow discharge (50 mA, 5 ms on, 10 ms off). The glow discharge was selected since it provides easy diagnostic accessibility and an excellent homogeneity in the positive column.

1.1 Results

In a CO_2 glow discharge a non-equilibrium has been found between the various vibrational modes of CO_2 and CO [1,2]. When pulsing the discharge, i.e. 5 ms on, 10 ms off, the asymmetric stretch vibrational temperature, T_3, of CO_2 and the vibrational temperature of CO, T_{CO}, show an initial fast rise, before reaching a maximum after about 1 ms and decreasing towards the end of the on-time. In contrast, the time evolution of the rotational temperature, T_{rot}, a combined temperature for the symmetric stretch and bending modes, T_{12}, and T_{gas} was characterized by a much slower increase towards the end of the on-time. The order of the measured temperatures always follows $T_{CO}>T_3>T_{12}>T_{rot}=T_{gas}$. The addition of N_2 has been studied since it is suggested to allow easy energy transfer towards the asymmetric stretch mode of CO_2. Addition of N_2 shows a significant enhancement of the vibrational non-equilibrium, with T_3 and T_{CO} reaching 2250 K and 3700 K respectively for N_2 admixtures up to 90%. These peak temperatures were reached significantly later than for a pure CO_2 gas flow, suggesting that N_2 causes V-T relaxation to become significantly lower with respect to the excitation of the vibrational levels by electron impact and V-V interactions [3]. During the presentation also results on the effects on the different temperatures and CO_2 conversion when admixing molecular oxygen [4] or water [5,6] to the CO_2 gas flow will be discussed.

1.2 Acknowledgments

The results presented have been obtained in a long-standing collaboration of the experimental groups in Paris (LPP, Guaitella) and Eindhoven (PMP, Klarenaar, Damen, Budde, Martini, van de Sanden, Vervloedt, Brescia), and the modeling group in Lisbon (IST, Guerra, Grofulović). This work was partly supported by NWO, under project numbers 713.013.003 and 15325, partly by LABEX Plas@par receiving financial aid managed by the Agence Nationale de la Recherche under the reference ANR-11-IDEX-0004-02, and partly funded from the European Union's Horizon 2020 research and innovation programme under the Marie Skłodowska-Curie grant agreement No 813393 (*co2pioneer.eu*).

References

[1] B.L.M. Klarenaar, A.S. Morillo-Candas, M. Grofulović, M.C.M. van de Sanden, R. Engeln, O. Guaitella, Plasma Sources Sci. Technol. **28**, 035011(2019)
[2] T. Silva, M. Grofulović, B.L.M, Klarenaar, A.S. Morillo-Candas, O. Guaitella, R. Engeln, C.D. Pintassilgo, V. Guerra, Plasma Sources Sci. Technol. **27**, 015019 (2018)
[3] M. Grofulović, B.L.M. Klarenaar, O. Guaitella, V. Guerra and R. Engeln, Plasma Sources Sci. Technol. **28**, 045014 (2019)
[4] S. C. L. Vervloedt, M. Budde and R. Engeln, Plasma Sources Sci. Technol. **32**, 015004 (2023)
[5] M.A. Damen, L.M. Martini and R. Engeln, Plasma Sources Sci. Technol. **29**, 095017 (2020)
[6] M. Budde, L.M. Martini, M. Ceppelli, S. Quercetti, R. Engeln, Plasma Sources Sci. Technol. **31**, 055002 (2022)

The interaction of non-thermal atmospheric pressure plasmas with substrates

A. Sobota[1], O.J.A.P. van Rooij[1], J.R. Wubs[1,2], O.I.M. Ahlborn[1], P.A. Viegas[3], E.T. Slikboer[1,3,4], O. Guaitella[3], A. Bourdon[3] and E. Garcia-Caurel[4]

[1] *Departmet of. Applied Physics, Eindhoven University of Technology, Eindhoven, The Netherlands*
[2] *Leibniz Institute for Plasma Science and Technology (INP), Greifswald, Germany*
[3] *LPP, CNRS, Ecole Polytechnique, UPMC, Université Paris-Saclay, 91128 Palaiseau, France*
[4] *LPICM, CNRS, Ecole Polytechnique, Université Paris-Saclay, 91128 Palaiseau, France*

Plasma-substrate interactions are of interest primarily because of potential applications like medicine, agriculture, water cleaning, plasma-assisted catalysis etc. However, because of lack of understanding in this field, they are also interesting from the fundamental point of view, to elucidate mechanisms that play a role in the interaction.

This talk addresses two types of interaction: the interaction of non-thermal atmospheric pressure plasma with a liquid substrate and with a dielectric substrate.

The research of the interaction with the dielectric substrate focuses on the charge dynamics on the substrate during the contact time with the plasma and outlines some consequences of the results, such as the way to control charging of a dielectric substrate.

The research into the interaction of the plasma and the liquid substrate focuses on the gas phase properties and shows how they evolve over time.

Plasma electrode DBD for low power, large surface applications

F. do NASCIMENTO[1], A. STANCAMPIANO[2], K. TREBULOVA[3], K.G. KOSTOV[1], S. DOZIAS[2], J.M. POUVESLE[2] and E. ROBERT[2]

[1] *Faculty of Engineering in Guaratinguetá, São Paulo State University-UNESP, Guaratinguetá 12516-410, Brazil*
[2] *GREMI, UMR7344, CNRS/Université d'Orléans, BP 6744, 45067 Orléans, France*
[3] *Brno Univ Technol, Fac Chem, Purkynova 118, Brno 61200, Czech Republic*

This work reports on the development of a conical-shaped atmospheric pressure plasma discharge serving as the powered electrode for a large surface Dielectric Barrier Discharge (DBD) device, the second grounded electrode being a metallic grid. As the powered electrode is transient, active only when the discharge in the cone is ignited, the capacitive coupling is limited allowing for the generation of the air-DBD from a low power (a few Watt) pulsed power supply. This latter delivers microsecond duration voltage pulses, a few kV in amplitude, of either positive or negative polarity with pulse repetition rate ranging from a few hundreds of Hz to a few tens of kHz. The first objective is the parametric characterization of this innovative DBD prototype through electric, fast imaging, and spectroscopic diagnostics. Then the device is used either to generate plasma treated solutions or to investigate its disinfecting potentialities on agar-plated pathogens. The measurement of DBD generated reactive species is under investigation.

Based on the conical-shaped atmospheric pressure discharge developed at UNESP [1] for polymer treatment, this work investigates the use of a new device for the generation of large surface DBD as sketched in Fig.1. The discharge is ignited in quartz cones (large cone of 25 cm height, 13 cm wide at its base, small cone of 15 cm height and 7 cm wide at its base) equipped with a needle electrode, the tip of this latter being set at various distances from the cone base. The cone is flushed with argon at a few L/min. The needle is powered with microsecond Gaussian-like voltage pulses with peak amplitude ranging from 5 to 20 kV and pulse repetition rate ranging from a few hundreds of Hz to 20 kHz. The base of the cone is set fraction of mm above a glass plate, with thicknesses ranging from 1 to 5 mm. 0.5 mm below this glass plate, a grounded grid served as the counter electrode for the air-DBD reactor. ICCD imaging on ns time scale characterize the discharge development inside the cone, along the bottom plate and on the other side of this plate where the air–DBD is generated. The top electrode of the DBD consists in the plasma developing from the needle electrode to the bottom plate. This "plasma" electrode is inherently transient and has various shape depending on the voltage amplitude, needle to plate gap and voltage pulse polarity. In any case, the power delivered to the whole device is of the order of a few W and current measurement coupled with ICCD imaging reveals the timing for the discharge development and the DBD ignition.

Liquid solution treatment or agar-plated pathogen decontamination are performed a few mm below the air-DBD zone. Preliminary results show high potential for large surface decontamination for both prokaryotic bacteria Escherichia coli and the eukaryotic yeast Candida glabrata as model targets.

Work is ongoing to characterize the generation of reactive species with a special emphasis on the time resolved analysis of ozone production for the two polarities and different input powers.

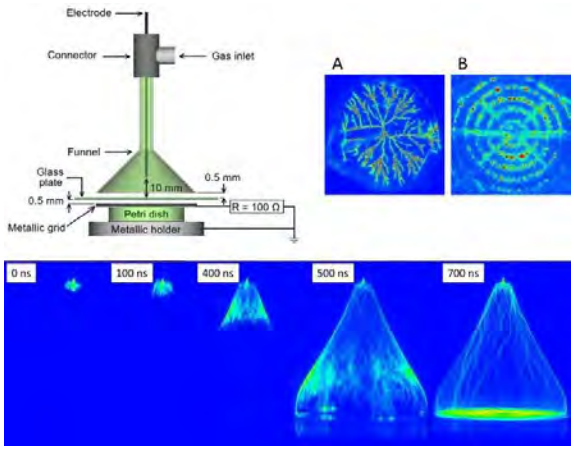

Fig.1 Top left: DBD configuration. A: 50 ns ICCD image of the argon discharge on the top surface of the cone base, B: 50 ns ICCD image of the DBD discharge on the outside surface of the cone base. Bottom are side-on 50 ns ICCD snapshots of the argon discharge development inside the cone at different indicated delays.

Acknowledgments The microbiological part of the work and KT were supported by the COST action CA20114.

Reference

[1] FVP Kodaira, BHS Leal, TF Tavares, A Quade, LRO Hein, W Chiappim and KK Kostov, Polymers 15 (2), 461 (2023).

Spontaneous external molecular/gene introduction with random genome integration free by complex stimuli generated by plasm and its applications

M. Jinno[1], S. Satoh[1] , Y. Kido[1], Y. Ikeda[1]and H. Motomura[1]

[1] *Dept. Electrical and Electronic Eng. Ehime Univ., Ehime, Japan*

In the plasma molecular/gene introduction, a spontaneous uptake of cells is induced by endocytosis. Both the electrical and the chemical stimuli are required to evoke endocytosis. The plasma treatment is proven to introduce plasmid DNA without random genome integration. The Genome Integration-Free characteristics are unique and expected to be a valuable tool for genome editing.

1 Molecular/gene introduction by plasma

We tried various plasma sources for gene/molecular introduction into cells. We found that the micro-discharge plasma with a counter electrode simultaneously achieved the highest transfection efficiency and cell viability. Since the plasma treatment time is short as 10^{-2} s or less, damages to cells and plasmid DNA are suppressed. We also found that surface discharge plasma achieves higher introduction efficiency and cell viability.

2 Spontaneous introductions by complex stimuli

The Zeta potential measurement shows that cells are charged up positively after plasma treatment. Since plasmid DNA, which is naturally charged in negative, is attracted to the positively charged cells by Coulomb force, the collision frequency between plasmid DNA and cell increases. We also experimentally found that large-size molecules such as plasmid DNA are transferred into cells by endocytosis. and ROS and electrical stimuli are required to trigger endocytosis. In the plasma methods, large molecules are transferred into cells by endocytosis, spontaneous cell membrane transfer, by complex stimuli of electric current and ROS[1,2].

3 Random genome integration free

In genome editing, the editing molecules should be introduced into cells without any random genome integration. The plasma method is expected to be free from random genome integration because it causes endocytosis, and cells spontaneously take external DNA molecules up into themselves. The authors experimentally proved that the plasma method is random genome integration-free.

The GFP gene-coded plasmid DNA was introduced into target cells using plasma, electro-poration, or lipofection. The cells are continuously passaged every 3 or 4 days as they reach confluence. As shown in Fig. 2, after the passage for 25 days, many colonies are formed by the electroporation and lipofection method. On the other hand, only a few

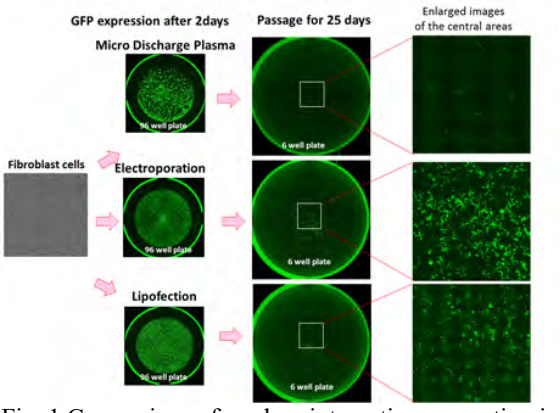

Fig. 1 Comparison of random integration generation in various gene transfer methods [7].

colonies are formed by the plasma method. These results show that plasma treatment introduces a plasmid DNA without random genome integration, so-called “Genome Integration-free.”

4 Conclusion

The plasma induces the spontaneous uptake of cells by endocytosis. Both the electrical and the chemical stimuli are required to evoke endocytosis. The plasma treatment is proven to introduce plasmid DNA without random genome integration. The Genome Integration-Free characteristics are unique and expected to be a valuable tool for genome editing.

Acknowledgments

JSPS supported part of this work by JSPS KAKENHI Grant Number 21H04455, 17H01068, 15H00896, 25108509.

References

[1] M. Jinno et al., *Plasma Sources Sci. and Tech.*, **26**(6) 065016 (2017).
[2] Y. Kido et al., *PLoS ONE*, **16**(1) e0245654 (2021).
[3] M. Jinno et al. *Jpn. J. Appl. Phys.*, **60**(3) 030502 (2021).

Low temperature plasmas modeling using the Sparse-PIC algorithm

L. Garrigues[1]

[1] *LAPLACE, Université de Toulouse, CNRS, INPT, UPS, Toulouse, France*

Explicit Particle-In-Cell (PIC) used to model low temperature plasmas are time consuming. We show that a new Sparse PIC method based on sparse grid approaches combined with the combination technique offers a promising alternative to reduce the computational time keeping a high precision in the modeling results.

1 Motivation

The simulation under real conditions of low temperature plasmas by the Lagrangian approach using the powerful Particle-In-Cell (PIC) method [1], [2] requires considerable computing resources for large plasma densities, even on high performance computing machines.

This is explained by two main limitations. First, stability conditions that constrain the numerical parameters to resolve the small space and time scales related to the electron properties. These numerical parameters are the mesh size of the grid used to compute the electric field and the time step between two consecutive computations. Second, PIC methods rely on a sampling of the distribution function by numerical particles whose motion is time integrated in the self-consistent electric field. The reduction of the statistical error associated with the numerical noise induced by the finite number of particles evolves slowly with this latter as $\sqrt{Nh_n^d}$ where N is the total number of particles, h_n is the grid spacing and d the dimension.

2 Sparse PIC approach

The introduction of a sparse grid in the discretization of a problem for large dimension d was proposed in the 1960s to solve the constraints related to the memory size of the computers. It relies on the use of a hierarchy of grids with an increasing resolution. The different numerical approximations carried out on each of them allow the reconstruction of the solution on a refined grid, with very good precision and extreme efficiency. The cost of computation is weakly dependent on the dimension d of the problem, while it increases exponentially for the conventional approach with a regular grid. This saving in computational time is accompanied by lower memory requirements. For an identical number of particle-per-cell as that of the regular grid of the standard PIC algorithm, reducing the number of cells induces a drastic reduction of the total number of particles in the simulation, and hence a speed up of the computational time, accordingly. By applying the sparse grid method to the PIC approach, Ricketson and Cerfon [3] have shown that this error remains acceptable in the context of Landau damping and diocotron instability. We have extended this approach to the study of low temperature plasmas, including collisions, ion motion, appropriated boundary conditions [4], [5]. More recently, the algorithm has been extended to model magnetized plasma with more accuracy [6]. One efficient parallelization strategy on shared memory architectures also has been proposed and validated in Ref. [7].

3 Benchmark verification

We will present comparisons between the standard and Sparse PIC algorithms in the context of low temperature plasmas including partially magnetized plasmas.

Acknowledgments

This research was funded by l'Agence Nationale de la Recherche (ANR), project ANR-22-CE46-0012. This work was granted access to the HPC resources of CALMIP supercomputing center under the allocation 2013-P1125. L.G. wants to thank G. Fubiani, M. Chung-To-Sang, from Laplace, and F. Deluzet, J. Narksi and C. Guillet from the Institut Mathématiques de Toulouse for fruitful discussions.

References

[1] R. W. Hockney and J. W. Eastwood, Computer simulation using particles (IOP Publish. Ltd, 1989).
[2] C. K. Birdsall and A. B. Langdon, Plasma physics via computer simulation (Taylor and Francis, 2005).
[3] L. F. Ricketson and A. J. Cerfon, Plasma Phys. Control. Fusion **59**, 024002 (2017).
[4] L. Garrigues, B. Tezenas du Montcel, G. Fubiani, F. Bertomeu, F. Deluzet, and J. Narski, J. Appl. Phys. **129**, 153303 (2021).
[5] L. Garrigues, B. Tezenas du Montcel, G. Fubiani, and B. Reman, J. Appl. Phys. **129**, 153304 (2021).
[6] F. Deluzet G. Fubiani, L. Garrigues, C. Guillet, and J. Narski, ESAIM: Math. Model. Numer. Anal. **56**, 1809 (2022).
[7] F. Deluzet, G. Fubiani, L. Garrigues, C. Guillet, and J. Narski., J. Comput. Phys. **480**, 112022 (2023).

Towards coarse-grained models for extensive streamer coronas in thunderclouds

A. Luque[1]

[1]*Instituto de Astrofísica de Andalucía, (IAA-CSIC) Granada, Spain*

We motivate and introduce coarse-grained models for the study of large streamer systems such as those that are present in strongly convective thunderstorms.

1 Introduction and motivation

There is strong evidence of the presence of massive streamer coronas in very active thunderstorms. They are likely composed by around a hundred to a thousand million streamers [1] that propagate for hundreds of meters within some tens of microseconds. These large streamer outbursts are called *fast breakdown* [2, 3, 4] in the atmospheric electricity literature and are responsible for short electromagnetic pulses of Very High Frequency (VHF) radiation called Narrow Bipolar Events (NBEs) and for bright, blue flashes in the cloudtops that can be observed from space (BLUEs) [5, 6].

The large number of streamers inside fast breakdown events motivates the development of discharge models where streamers are not considered as individual channels but instead are treated as a continuum with an evolving density.

There are several approaches to develop such a description of fast breakdown, each with its own challenges. We will start from a simple stochastic growth model for a tree of streamer channels and derive reaction-drift-diffusion equations for the large-scale dynamics of the streamer system, accountig also for how the propagation of the streamer system modifies the underlying, coarse-grained conductivity of air.

References

[1] Li, D. *et al.* Blue Flashes as Counterparts to Narrow Bipolar Events: The Optical Signal of Shallow In-Cloud Discharges. *J. Geophys. Res. (Atmos.)* **126**, e2021JD035013 (2021).

[2] Rison, W. *et al.* Observations of narrow bipolar events reveal how lightning is initiated in thunderstorms. *Nature Communications* **7**, 10721 (2016).

[3] Tilles, J. N. *et al.* Fast negative breakdown in thunderstorms. *Nature Communications* **10**, 1648 (2019).

[4] Li, D. *et al.* Multi-Pulse Corona Discharges in Thunderclouds Observed in Optical and Radio Bands. *Geophys. Res. Lett.* **49**, e98938 (2022).

[5] Chanrion, O. *et al.* Profuse activity of blue electrical discharges at the tops of thunderstorms. *Geophys. Res. Lett.* **44**, 496–503 (2017).

[6] Soler, S. *et al.* Blue Optical Observations of Narrow Bipolar Events by ASIM Suggest Corona Streamer Activity in Thunderstorms. *J. Geophys. Res. (Atmos.)* **125**, e32708 (2020).

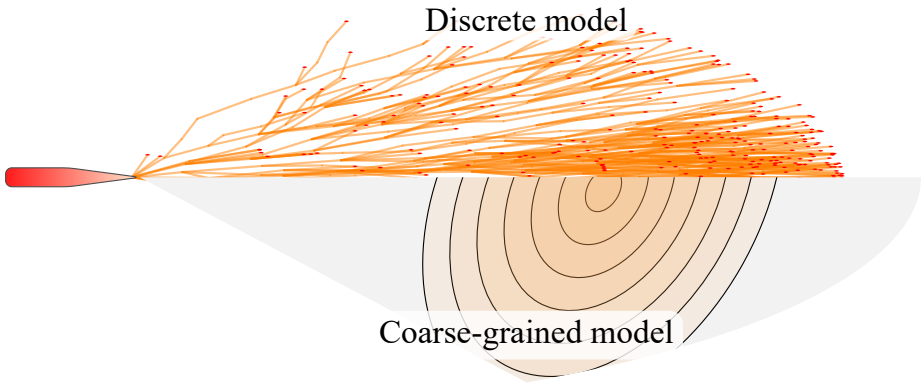

Figure 1: A coarse-grained model represents an extensive streamer discharge (above) as an evolving continuum density (below).

Generation of Vibrationally Excited Nitrogen in a DC-Superimposed Repetitive Nanosecond Pulse Discharge

K. Takashima[1], Y. Kunishima[1] and T. Kaneko[1]

[1] *Graduate School of Engineering, Tohoku Univ., Japan*

Some reaction pathways in the plasma nitrogen-fixation include vibrationally excited nitrogen molecules, often noted as a key for a sustainable nitrogen-fixation to improve the net efficiency. This work focuses on building a concrete basis to study chemical reactivity of vibrationally excited nitrogen. Significant power input at a reduced electric field below the self-sustaining discharge condition is realized by a developed DC superimposed nanosecond pulse discharge system for vibrational excitation. The superimposed DC voltage is found to populate vibrational level higher than v = 8 estimated by spontaneous Raman spectroscopy and elevates the vibrational temperature without significant gas heating effects from the rotational and vibrational Raman spectra fitting. Fluid dynamical and vibrational relaxation modelling in the pulse intervals supports our arguments that the superimposed DC plays a key role in efficient generation of vibrationally excited nitrogen.

Recently, plasma nitrogen fixation, synthesizing nitrogen compounds with plasma, is gaining interest as a sustainable technology [1,2] unlike the current nitrogen fixation, dependent on Haber-Bosch process with fossil fuel. Previously, we have reported selective plasma synthesis of dinitrogen pentoxide exclusively from air [3], whose production efficiency was limited by the nitrogen dissociation processes. Zel'dovich mechanism and dissociative attachment process of the vibrationally excited nitrogen $N_2(v)$ on solid surface are expected to play a key role in the plasma nitrogen fixation [2]. Therefore, a plasma reactor selectively activating the dissociation pathway with vibrationally excited nitrogen can potentiate the efficient and sustainable plasma nitrogen fixation. Plasma for nitrogen fixation accompanies significant gas heating resulting in fluid dynamical effects as well as density drop affecting the reduced electric field (*E/N*) and reaction processes of the vibrationally excited states (V-V and V-T). This unavoidable thermo-fluid dynamical complexity in plasma generation is hardly resolved if the entire nitrogen fixing reactions undergo in the plasma volume as in the earlier studies.

Our efforts have been made to untangle the complex processes for the nitrogen dissociative reactions of $N_2(v)$ from plasma generation. A non-self-sustaining (NSS) DC discharge with spontaneous Raman measurements enables to control the plasma nitrogen vibrational excitation and the following reactions [4, 5]. A developed plasma source with a single electrode pair, powered by both a lab-built repetitive nanosecond pulse generator with a superimposed DC high voltage, enables NSS DC discharge to control the apparent reduced electric field *E/N* in the discharge volume up to 5.5 Td [5] at 0.2 atm. A pulse burst consisting fifty of nanosecond pulses at a repetition rate of 5 kHz are fully synchronized with Nd:YAG laser output beam at 532 nm at 10 Hz. The Raman scattering for $\Delta v = +1$ from the center of the discharge volume is measured and fitted with a synthetic spectrum composed of Q, S, O-branches in every vibrational state. The least square error sum of the residuals (LSQ) gives the vibrational population and the rotational temperature T_{rot} in the spectrum fitting. Vibrational temperature T_{v01} , slope in vibrational population v = 0 to 1, was significantly increased by the superimposed DC voltage in a middle of the burst from T_{v01} ~ 3000 K to 4000 K and vibrational level v > 8 clearly appeared. The rotational temperature T_{rot} simultaneously obtained from the Raman spectra was found around 1000 K and was insignificantly increased with the superimposed DC when the vibrational population is well-developed. This can be interpreted that the DC discharge power is selectively loaded to the nitrogen vibrational states. Further details will be presented, including our fluid dynamical and vibrational relaxation modelling which supports our arguments that the superimposed DC plays a key role in efficient generation of $N_2(v)$.

Acknowledgements

This work has been supported by JSPS KAKENHI (Grant Nos. JP20H01890, JP20J20527).

References

[1] B. S. Patil, et al., Catalysis Today **256,** 49 (2015).
[2] E. C. Neyts, et al., J. Phys. D: Appl. Phys.**47,** 22401 (2014).
[3] S. Sasaki, et al., Ind. Eng. Chem. Res. **60**, 798 (2020).
[4] M. Nishihara, et al., AIAA J. **50**, 2255 (2012).
[5] Y. Kunishima, et al., Jpn. J. Appl. Phys. **58**, 060908 (2019).

On the potential use of plasma for food processing

Romolo Laurita[1], Alina Bisag[1,2,3], Filippo Capelli[1,2,3], Caterina Maccaferri[1], Giorgia Gozzi[4], Silvia Tappi[3,4],Beatrice Cellini[4], Jessica Genovese[3], Sauro Vittori[5], Pietro Rocculi[3,4], MarcoDalla Rosa[3,4], Lucia Vannini[3,4] Junior Bernardo Molina-Hernandez[6], Jessica Laika[6], Lilia Neri[6], Clemencia Chaves-López[6], Antonella Ricci[6], Massimo Mozzon[7], Lama Ismaiel[7], Ancuta Nartea[7], Cinzia Mannozzi[7], Luca Belleggia[7], Cristiana Cesaro[7], Roberta Foligni[7], Matteo Gherardi [1,3,8] Vittorio Colombo[1]

[1] Department of Industrial Engineering, University of Bologna, Italy [2] AlmaPlasma s.r.l., Italy [3] Interdepartmental Centre for Agri-Food Industrial Research, University of Bologna, Italy [4]Departmentof Agricultural and Food Sciences, University of Bologna [5] School of Pharmacy, University of Camerino, Italy [6]Faculty of Bioscience and Technology for Food, Agriculture and Environment, University of Teramo, Italy [8]Interdepartmental Center for Industrial Research forAdvanced Mechanics and Materials, University of Bologna, Italy

Cold atmospheric plasma (CAP) and plasma-activated water (PAW) are increasingly used as non-thermal methods to decontaminate food products due to new pathogens, production changes, and consumer preferences. CAP and PAW have shown promise in inactivating food pathogens and microorganisms, but their impact on food matrices and consumer safety requires further research.

Cold Atmospheric Pressure (CAP) plasmas and Plasma Activated Water (PAW) have become increasingly popular as a non-thermal methods for decontaminating food products. This is due to the emergence of new pathogens in food products, changes in production technologies, and evolving consumer lifestyles and preferences. CAP technology has shown promise in several studies as an effective means of inactivating food pathogens, degradative enzymes, and spoilage and spore-forming microorganisms.

However, research on the impact of CAP on food matrices and its effect on consumer safety is still needed before this technology can be widely applied, indeed, even if preliminary results on the use of CAP on food matrices have shown its feasibility for food decontamination, but further research is required to assess its impact on nutritional profiles. The aim of this talk is to provide information concerning the state of the art related to the use of CAP and PAW in food treatment, showing results concerning a systematic review.

Moreover, results concerning CAP treatment of food products and its effect on nutritional profiles will be shown. For instance, a study assessed the effect of surface barrier discharge (SBD)-generated CAP on dried tomatoes contaminated with *Aspergillus rugulovalvus*, and *Aspergillus niger*. [1]. Results showed that the spore germination was reduced and spore viability was impacted, while the physicochemical parameters and antioxidant activity of sundried tomatoes were not affected. Additionally, pistachio kernels were exposed to plasma, which did not significantly alter their composition, including fatty acids and alcoholic constituents of unsaponifiable matter. [2]

In addition, PAW allowed an average reduction of mesophilic and psychrotrophic bacteria and *Enterobacteriaceae* on rocket leaves, with minimal variation of qualitative and nutritional parameters [3]

CAP is a promising novel tool in the field of food sanitation, but efforts have to be spent in order to identify and evaluate the effects induced by plasma treatment on the physicochemical parameter, antioxidant activity, and changes in composition.

Acknowledgements

The present work is funded by the Italian Ministry of University and Research (PRIN 2017, Project "PLASMAFOOD").

References

[1] Molina-Hernandez JB, Laika J, Peralta-Ruiz Y, Palivala VK, Tappi S, Cappelli F, Ricci A, Neri L, Chaves-López C. Foods. **713**,11,210 (2022)

[2] Foligni, R.; Mannozzi, C.; Ismaiel, L.; Capelli, F.; Laurita, R.; Tappi, S.; Dalla Rosa, M.; Mozzon, M. Foods, **11**, 419. https://doi.org/ 10.3390/foods11030419 (2022)

[3] Romolo Laurita et. alii Innovative Food Science & Emerging Technologies. **73**, 102805 (2021)

XXXV ICPIG, July 9-14, 2023, Egmond aan Zee, The Netherlands Topic number 6

Recent Developments in the Electric Field-Induced Second Harmonic Generation (EFISH) Method for Non-Equilibrium Plasmas

T. L. Chng[1], and E. S. Sugeng[1]

[1] *Department of Mechanical Engineering, College of Design and Engineering, National University of Singapore*

The E-FISH method has generated considerable research interest for its utility as an electric field measurement tool. It complements other techniques such two-line molecular nitrogen (N_2) emission as well as stark shift spectroscopy using helium or neon gas. In this work, we describe some of the primary limitations of this method as well as some recent advances in its development.

1 Electric Field-Induced Second Harmonic (E-FISH) Generation

Electric field induced second harmonic generation, or E-FISH, is a laser-based diagnostic which has recently been repurposed for the measurement of electric fields in non-equilibrium plasmas [1,2]. This method involves probing a non-polar gas sample with laser light, and quantifying its second harmonic response to an externally applied electric field that is to be measured. This second harmonic signal varies quadratically with the applied field strength squared, and is otherwise absent (for a non-polar gas) if no field is imposed. Calibration may be performed in a known electrostatic field (see figure 1) so as to obtain absolute field information, for instance in a plasma. Key advantages of the E-FISH method include its versatility, excellent signal localization in time, and relatively straightforward implementation. The versatility of the method is demonstrated by its non-resonant nature - the technique is in theory applicable to any non-polar gas or gas mixture (except gases with low non-linear hyperpolarizability such as helium), and does not demand a specific probe laser wavelength. The temporal resolution of the measurement is only physically limited by the laser pulse duration since the signal generation is effectively instantaneous, with pulses as short as 50 fs being shown to yield good signals. This duration is deemed more than sufficient for existing non-equilibrium plasma problems. Finally, as a single-beam technique, E-FISH does not require any complex alignment, and the signal path can easily be traced using an appropriate non-linear, second harmonic crystal.

Yet, recent work has also shown that the E-FISH diagnostic possesses certain limitations with respect to the spatial origin of the signal. This is due to the coherent nature of the signal generation, which builds up along the direction of beam propagation, and makes it sensitive to the Gouy phase shift present in the probe beam along this path. This results in the signal being dependent on the entire electric field profile along the beam path, rather than just the local value within the beam focus [3].

2 Recent Advances in E-FISH

In this talk, I will describe some of the applications of the E-FISH method, particularly to nanosecond pulsed plasmas, but more importantly elaborate on some of the solutions that have been explored to address the shortcomings of this method [4]. E-FISH continues to be a viable method for electric field measurements in plasmas, and an update on efforts to extend its applicability through high-repetition rate field measurements and obtaining the *direction* of the electric field vector using homodyne detection will also be provided.

References

[1] Dogariu, A., Goldberg, B.M., O'Byrne, S. and Miles, R.B., Species-independent femtosecond localized electric field measurement. Physical Review Applied, **7(2)**, p.024024 (2017).

[2] Goldberg, B.M., Chng, T.L., Dogariu, A. and Miles, R.B., Electric field measurements in a near atmospheric pressure nanosecond pulse discharge with picosecond electric field induced second harmonic generation. Applied Physics Letters, **112(6)**, p.064102 (2018).

[3] Chng, T.L., Starikovskaia, S.M. and Schanne-Klein, M.C., Electric field measurements in plasmas: how focusing strongly distorts the E-FISH signal. Plasma Sources Science and Technology, **29(12)**, p.125002 (2020).

[4] Chng, T.L., Pai, D.Z., Guaitella, O., Starikovskaia, S.M. and Bourdon, A., 2022. Effect of the electric field profile on the accuracy of E-FISH measurements in ionization waves. Plasma Sources Science and Technology, **31(1)**, p.015010 (2022).

Is there a place for good math in gas discharge science? A personal view

M. S. Benilov

Departamento de Física, FCEE, Universidade da Madeira, Funchal, Portugal
Instituto de Plasmas e Fusão Nuclear, Instituto Superior Técnico, Universidade de Lisboa, Lisbon, Portugal

A representative example of good mathematics in gas discharge science is the theory of high-voltage capacitive RF sheaths, developed in the 1980s. Unfortunately, there is currently a lack of such high-level theoretical works in the discharge science. There are many papers with endless transformations with obscure mathematical sense, without a clear statement of the problem, clear objectives, and understandable physical results. In many papers, asymptotic features of the solution are confused with physical facts. One could try to reverse this trend, for example, by promoting research with good mathematics in gas discharge journals and at conferences. To this end, a consensus needs to be reached in the gas discharge community as to what exactly constitutes good mathematics. This talk aims to give a personal opinion on this issue and hopefully spark a discussion.

An excellent example of good mathematics in gas discharge science is the theory of high-voltage collisionless capacitive RF sheaths [1,2]. The presentation in the paper [2] is especially impressive: the analytical theory of a complex phenomenon is presented transparently and understandably in just seven journal pages!

Unfortunately, papers written in this style are in short supply nowadays. There are many papers with endless transformations with obscure mathematical sense and without a clear statement of the problem, clear objectives, and understandable physical results. In many papers, asymptotic features of the solution are confused with physical facts. The classical Bohm criterion is a good example: although this criterion is asymptotic in nature, it is assumed in most works concerned with the theory of plasma-sheath transition that there is a well-defined point in space, the “sheath edge”, where the Bohm criterion should be applied, i.e., the ion speed should be set equal to the Bohm (ion sound) speed. This confusion has originated, in particular, numerous attempts to “modify” or "generalize" Bohm's criterion to account for collisions and geometric effects; search of Web of Science with "modified Bohm criterion" or "generalized Bohm criterion" in the field “Topic” returned a list of 78 papers (12.04.2023). (Of course, not all the papers on the list give new versions of generalized or modified Bohm criterion and *vice versa*; nevertheless, the number of papers on the list gives an idea.) However, no widely accepted definitions of the sheath edge and collisionally modified Bohm criterion have emerged, in spite of efforts invested by able researchers over decades. The reason is clear: such definitions cannot be introduced otherwise than arbitrarily, which is consequence of the asymptotic nature of the Bohm criterion.

Of course, the criteria of good math is a matter of personal taste of the researcher. In view of this author, the most important criteria are:

(1) The essence of the work and its results should be understandable to researchers who are more interested in physics than in math;
(2) The mathematical sense of the treatment should be clearly identified and only standard mathematical methods should be used.

An interesting example illustrating the importance of the first criterion is the work [3], where the plasma-sheath transition in low-pressure discharges was studied. The ratio of the Debye length to the transversal dimension of the discharge was considered as a small parameter and the method of matched asymptotic expansions was used. The treatment [3] was (and remains) almost impeccable. Unfortunately, the physics was not considered, and [3] did not have the impact it could have had.

It this talk, the above criteria will be illustrated and discussed using the Bohm criterion as an example.

The work was supported by FCT of Portugal under Project UIDP/50010/2020 and by European Regional Development Fund through the Operational Program of the Autonomous Region of Madeira 2014 - 2020 under Project PlasMa-M1420-01-0145- FEDER-000016.

References

[1] Godyak, V. A. Soviet Radio Frequency Discharge Research. Falls Church: Delphic, 1986.
[2] Lieberman, M. A. Analytical solution for capacitive RF sheath. IEEE Trans. Plasma Sci. **16**, 638–644 (1988).
[3] Franklin, R. N. and Ockendon, J. R. Asymptotic matching of plasma and sheath in an active low pressure discharge. J. Plasma Phys. **4**, 371-385 (1970).

Measurement of plasma parameters at the very beginning of the laser induced breakdown

M. Skočić, N. Nedić, L. Rajačić, D. Dojić and S. Bukvić

University of Belgrade, Faculty of Physics, Serbia

The target was illuminated by a 1064 nm Nd:YAG harmonic while monitoring the bright area with a bifurcated optical cable equipped with identical SMA collecting lenses. Simultaneous detection on the camera CCD was achieved by arranging the fiber cores of the two legs in line at the common end of the cable. According to the results, the temperature range of the copper surface was found to be between 7400-11200 K. These findings are consistent with the existing data in the literature regarding the critical temperature of copper. Plasma temperature exceeded 50000 K after its creation, measured from continuous spectra emitted from the laser-illuminated bright spot.

This paper presents a technique for measuring the temperature of a copper surface at the very beginning of a Laser Induced Breakdown experiment, before the creation of plasma, see Fig 1. The experiment was conducted using a Nd:YAG laser at three different irradiances: 1.4×10^9, 3.2×10^{11}, and 3.7×10^{12} W/cm^2, at a residual atmosphere of 0.05 mbar.

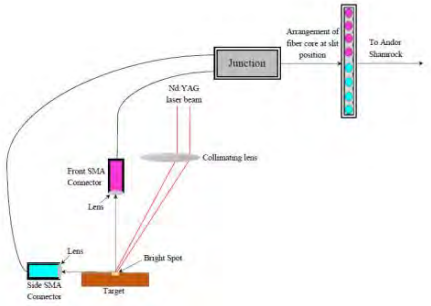

Fig 1. The experimental setup involved illuminating the target with the 1064 nm Nd:YAG harmonic while monitoring the bright area using two legs of a bifurcated optical cable. The purple leg is used to measure the surface temperature, while the blue one is used to monitor the creation of the plasma.

The results show that the temperature of the copper surface is in the range of 7400-11200 K, which is consistent with the most data available in the literature for the critical temperature of copper [1]. The relaxation time of electron and ion temperature necessary to achieve equilibrium via elastic collisions is estimated to be less than 1 ns, while the relaxation time among the internal electronic degrees of freedom via inelastic collisions is estimated to be below 10 ps. Following the creation of the plasma, the temperature significantly increases, reaching values over 50000 K. It is worth noting that all temperature measurements were obtained by analyzing the continuous spectra emitted from the bright spot illuminated by the laser, see Fig 2.

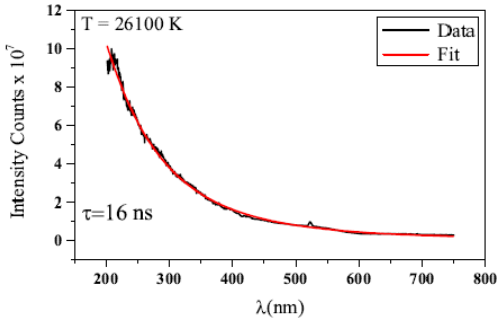

Fig 2. Plasma temperature obtained from the Planck's spectrum.

Additionally, electron number density and temperature were measured inside the plasma measuring attenuation of the two lasers HeNe at 633 nm and the diode laser at 400 nm wavelength, applied side on. Assuming that inverse bremsstrahlung is the dominant absorption mechanism [2] and comparing absorption coefficients for the two lasers, we derived values for electron density and electron temperature inside the plasma. Electron density and temperature at 150 μm from the target are 3.5×10^{25} m^{-3} and 19000 K, respectively.

This research provides valuable insights into the plasma parameters at the very beginning of laser-induced breakdown, which can have significant implications for various fields, including material processing and laser-based spectroscopy.

References

[1] A. L. Horvath, Critical temperature of elements and the periodic system, Journal of Chemical Education **50**, 335-336 (1973).

[2] A. Dalgarno and N. F. Lane, Free-free transitions of electrons in gases, Astrophysical Journal **145**, 623 (1966).

Molecular dynamics simulations: A virtual microscope for studying plasma processes

P. Brault[1]

[1] *GREMI, CNRS - Université d'Orléans, Orléans, France*

As plasma processes are atomic and molecular by nature, simulations at the molecular level will be relevant for providing us with insights into core and interface plasma chemistry basic phenomena. Moreover, statistical averaging allows to provide/predict macroscopic data as reaction rates, diffusion coefficients, ... directly comparable with experiment outputs. Recent developpments relevant for plasma processing and applications to plasma assisted sputtering deposition, nanoparticle growth and reactivity on plasma produced reactive oxygen species on pollutant molecules in water are reviewed.

Among all the available molecular simulation tools, reactive and ab-initio molecular dynamics (MD) simulation techniques are a good compromise between quantum mechanical and kinetic Monte-Carlo methods, especially due to the availability of robust and accurate reactive force fields and fast quantum chemistry methods such as numerous DFT (Density Functional Theory) variants. Moreover, such semi-empirical or quantum calculated reactive forcefields are also determining partial charges at any relevant times using charge equilibration algorithm. In the context of plasma chemistry this will allow to address charge transfer mechanisms. Using these forcefields, MD simulations can calculate the trajectories of a set of particles, by solving the appropriate set of Newton equations of motion leading to the ability of these simulations to address reactivity of relatively large molecular systems (up to 10^9 atoms). It is now possible to directly include the electrons, but it is limited to some specific situations as plasma breakdown. Nevertheless, MD simulations can be carried out with initial conditions including expected plasma composition (ions, neutrals) from experimental measurement, such as mass spectrometry or fluid models. Addressing reactive plasma processes remains a quite challenging and useful task. Three examples nicely illustrate the interest of carrying out reactive molecular dynamics simulations: i) Plasma sputtering and deposition, ii)nanoparticle growth in the context of plasma sputtering iii) plasma-liquid interaction, especially effects of plasma produced reactive oxide species on organic molecules in water.

1) Plasma sputtering deposition
Selection of initial velocity conditions can be done from either experimental data (energy resolved mass spectrometry) or SRIM simulations of sputtered atom energy distribution (EDF) for thermal evaporation, dc magnetron, HiPIMS and bipolar HiPIMS. This is expected to give a step forward for improving MD simulation prediction ability of sputtered film properties, such as morphology, composition, structure, tribology etc. Moreover, it is possible to describe, in a single MD simulation, sputtering, transport and deposition using scaling arguments.
2) Nanoparticle growth
The simulation box is composed of the plasma forming gas (Argon here), a metal vapor (Pd, Pt, Bi, Ni, Cu, or Au) originated from a sputtered target and, if relevant, a reactive gas (O_2 here). The composition and morphology of NPs are consistent with experimental findings, especially catalytic properties.
3) Insight into plasma-liquid interactions: effects of ROS on pollutant molecules in water.
There are available reactive force fields to describe chemical reactions: reaxFF and COMB3, which address bond breaking and formation, via a distance-dependent bond order. ReaxFF method will be used for addressing pollutant molecules containing only C, H, O and N atoms. Molecules having additional atoms such as sulphur, chlorine, fluorine, or phosphorus will be treated with a DFT scheme coupled to MD method. For all these molecules the MD simulated degradation products are compared with available experimental results.

Spectroscopic diagnostics of surface reactions of atomic species in non-thermal plasma

K. Takeda[1], K. Masuda[1], M. Hiramatsu[1], T. Tsutsumi[2], K. Ishikawa[2], M. Hori[2]

[1] *Depatment of Electrical and Electronic Engineering, Meijo University, Nagoya, Aichi, Japan*
[2] *Center fir Low-temperature Plasma Sciences, Nagoya University, Nagoya, Aichi, Japan*

Plasma processes are achieved by the interaction between neutral species and ions on material surfaces. In our group, the loss probabilities of atomic species on material surface in afterglow plasmas have been measured by vacuum ultraviolet absorption spectroscopy. In this time, the surface loss probabilities of H atoms on material surfaces under continuously plasma irradiation were estimated. From the results, it is experimentally confirmed the surface loss probability depends on the ion flux.

1 Introduction

Feature of plasma process is determined by surface reactions due to neutral and charged species generated by the plasma. However, there is not enough knowledge about the surface reaction of each species in the plasma processes, and the interaction between neutral species and ions on material surfaces are often unknown. For the further technological innovation of plasma processes, understanding them is strongly required. In our group, the loss probabilities of atomic species on material surface have been quantitatively measured by vacuum ultraviolet absorption spectroscopy (VUVAS) [1]. In the experiments, the surface loss probabilities were estimated from the decay of the density in afterglow plasmas. The material processes with plasmas are frequently performed under irradiations of not only neutral species but also ions in the steady state of continuous discharge plasma. Therefore, the surface loss probability of neutral species under ion irradiation interests us very much. In this study, from the spatial density distributions of H atoms supplied from inductively coupled hydrogen plasma (H_2 ICP) measured by VUVAS, the surface loss probability of H atoms on the material surface continuously irradiated by plasma was estimated.

2 Experiments

The experimental apparatus consists of a vacuum chamber equipped with an ICP source and a sample stage, and VUVAS system. The stage made of stainless-steel is a circular shape with a diameter of 200 mm. The stage was located at 300 mm apart from the ICP source. The flow rate of H_2 gas introducing into the ICP source was fixed at 50 sccm. The H_2 ICP was generated by applying an RF power (13.56 MHz) to the ICP antenna keeping a chamber pressure.

The VUVAS system was composed of a VUV monochromator and a micro discharge hollow cathode lamp as a light source [2]. The absorption line of H atom used in this study was Lyman α line at a wavelength of 121.56 nm The absorption length at which the VUV light was absorbed by the H atom inside the chamber was fixed at 221 mm.

3 Results

In this study, from the spatial density distributions of H atoms on the stage measured by VUVAS, the surface loss probability of H atoms on the material surface was estimated on the basis of Milne boundary condition. Figure 1 shows the surface loss probabilities of H atom on the SUS and SiO_2 surfaces as a function of flux ratio of ion to H atom onto the stage. The ion flux incident to the stage was measured by commercially available retarding field analyzer (RFA) (SEMION from Impedans). As shown in Fig.1, the surface loss probabilities of H atom on each surface increased with the increase in the flux ratio and then was saturated. From the results, it is considered that the ion impact affects the surface reaction of H atom such as recombination and so on.

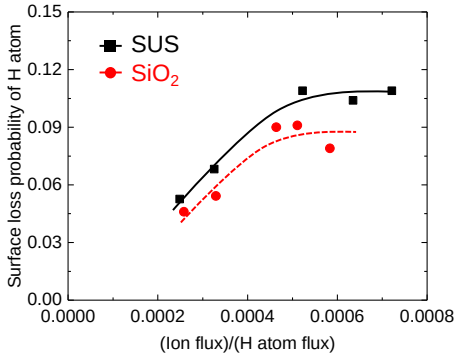

Fig.1 Surface loss probabilities of H atom on stainless-steel and SiO_2 surfaces as a function of flux ratio of ion to H atom.

References

[1] Takeda, K. Ishikawa, K. Hori, M. Reviews of Modern Plasma Physics, 6, 13:1-32 (2022).
[2] Takashima, S. et al., Appl. Phys. Lett., 20, 3929-3931 (1999).

Particle formation and dusty plasma effect in non-equilibrium discharges

A. Michau[1], G. Tetard[1], P. Swaminathan[1], C. Arnas[2] and K. Hassouni[1]

[1] *Université Sorbonne Paris Nord, Laboratoire des Sciences des Procédés et des Matériaux, LSPM, CNRS, UPR 3407, F-93430, Villetaneuse, France*

[2] *Laboratoire PIIM, CNRS, Aix-Marseille université, Centre Saint-Jérôme, 13397 Marseille, France*

Particle nucleation in reactive plasmas is performed through the dissociation of primary precursor that results in the formation of small neutral and charged species that are involved in surface deposition and molecular growth processes. This later depends not only on the chemistry taking place in the discharge but also on transport phenomena such as convective flow or drift effects. This implies that growth may occur following different routes depending of the precursor and plasma conditions.

Once large molecular precursors are formed, solid particle nucleates. They are subsequently subject to charging and transport phenomena, as well as growth by both coagulation and surface deposition. These processes that are function of the local plasma conditions are sketched in figure 1 in the case of acetylene/argon RF discharge [1].They usually results in complex particle-size distributions (PSD) as illustrated in figure 2 in the case of carbon dust particles produced by sputtering in DC a discharge with a graphite cathode [2] .

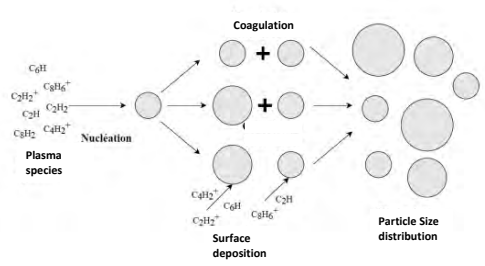

Figure 1 : schematic of particle formation and growth in an RF Ar/C_2H_2 discharge

Eventually, once the particle charge becomes significant, the aerosols affect the discharge dynamics with a subsequent feed-back on molecular growth and nucleation processes. This is called the dusty plasma effect that can be observed for example in RF discharges with the so-called 'void' creation.

We propose to discuss particle formation in different plasma sources and discharge conditions as inferred from dusty plasma models that couples a discharge model, a molecular growth (nucleation) model and an aerosol dynamic model. We especially discuss the molecular growth in low-pressure DC discharges where carbon particles are obtained through the sputtering of a graphite electrode [2], RF [1] discharges with acetylene precursor or microwave hydrocarbon discharges. In such cases nucleation may occur through different routes and dynamics which may differ from the well-known silane RF dusty plasma discharges [3]. We also discuss the dust particle dynamics and analyse the influence of the particle on the plasma discharge equilibrium.

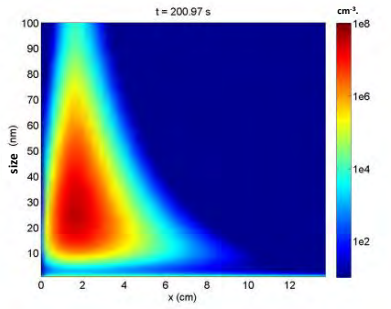

Figure 1 : numerical simulation of particle size distribution obtained after 200 s in a DC discharge

References

[1] Tetard G, Michau A, Prasanna S, Mougenot J, Brault P, Hassouni K. Molecular growth paths and dust-particles nucleation precursors in Ar/C2H2 low pressure discharges. Plasma Processes and Polymers 2022;19.

[2] Dominique C, Arnas C. Cathode sputtering and the resulting formation of carbon nanometer-size dust. Journal of Applied Physics 2007;101:123304-8.

[3] Bouchoule A, Boufendi L. Particulate formation and dusty plasma behaviour in argon-silane RF discharge. Plasma Sources Science and Technology 1993;2:204-13.

Fundamental studies and applications of magnetic nozzle plasma

Kazunori Takahashi[1,2]

[1] *Dept. Electrical Engineering, Tohoku Univ., Sendai, Japan*
[2] *Interdisciplinary Research Center for Non-Equilibrium Plasma, Sendai, Japan*

Plasma expanding in a divergent magnetic field includes many aspect of physics and its physical processes play crucial roles in development of a new type of electric propulsion devices, being called a magnetic nozzle rf plasma thruster, where the low-pressure plasma is produced by a rf discharge and accelerated in the magnetic nozzle. Here the studies on the plasma dynamics in the magnetic nozzle plasma thruster is presented.

A magnetic nozzle is a key element for a high-power electric propulsion device called a helicon plasma thruster [1]. The plasma produced in the source is transported along the field lines to the source exit and subsequently expands along the magnetic nozzle as can be seen in Fig.1, where the plasma is spontaneously accelerated. A number of studies have been conducted to understand the thrust generation mechanisms [2-5]. Although the magnetic nozzle itself does not transfer the energy to the plasma, it has been demonstrated that the momentum conversion process in the magnetic nozzle increases the axial thrust force, where a Lorentz force induced by an electron diamagnetic drift current and a radial magnetic field is responsible for the increase in the axial thrust. The internal plasma current is affected by spatial structure of the plasma parameters such as the density and the electron temperature; the plasma transport in the magnetic nozzle and the thermodynamic properties of the electrons are critical issues for the thruster performance [6,7,8].

Since the magnetic field lines are closed and turn back to the thruster, the plasma has to be detached from the field lines; otherwise, no net thrust can be obtained in boundary-free space. The plasma detachment has been a challenging problem [8], especially when electrons have a gyro-radius smaller than the system's scale.

Here the thrust generation mechanisms and current status of the thruster development are reviewed [9]. Furthermore, we experimentally demonstrate that a cross-field transport of the electrons toward the main nozzle axis is induced by the spontaneously excited wave having the frequency considerably higher than the ion cyclotron frequency and driving an ExB drift that only effects the electrons [10]. The density and electric field fluctuations are simultaneously measured, and the direction and the magnitude of the cross-field electron flux are assessed and compared with the cross-field ion flux induced by the electrostatic field. Wave-induced transport and loss have been one of many important issues in plasma physics over the past several decades. Conversely, the presently observed electron inward transport has a beneficial effect on the detachment by neutralizing the ions deviating from the field lines.

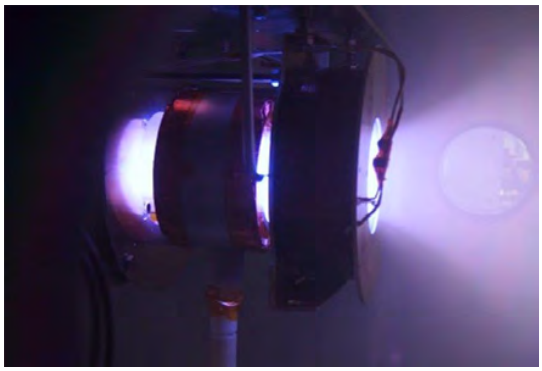

Fig.1: Photograph of laboratory experiment of the magnetic nozzle rf plasma thruster.

References

[1] K. Takahashi, Rev. Mod. Plasma Phys. **3**, 3 (2019).
[2] K. Takahashi *et al.*, Phys. Rev. Lett. **107**, 235001 (2011).
[3] A. Fruchtman *et al.*, Phys. Plasmas **19**, 033507 (2012).
[4] K. Takahashi *et al.*, Phys. Rev. Lett. **110**, 195003 (2013).
[5] K. Takahashi *et al.*, Phys. Rev. Lett. **114**, 195001 (2015).
[6] K. Takahashi *et al.*, Phys. Rev. Lett. **120**, 045001 (2018).
[7] K. Takahashi *et al.*, Phys. Rev. Lett. **125**, 165001 (2020).
[8] J. Y. Kim *et al.*, Plasma Sources Sci. Technol. *submitted*.
[9] K. Takahashi, Sci. Rep. **12**, 18618 (2022).
[10] K. Takahashi *et al.*, Sci. Rep. **12**, 20137 (2022).

Plasmas for nano and facilitating next generation energy storage

U. Cvelbar [1] and N. M. Santhosh[1]

[1] *Department of Gaseous Electronics (F6), Jožef Stefan Institute, Jamova cesta 39, SI-1000 Ljubljana, Slovenia*

Global energy demand is expected to double in the next fifty years due to projected population and economic growth. Therefore, it is crucial to develop renewable energy sources at low cost to provide sufficient energy to meet the needs of consumers. Among the various energy sources, energy storage devices that can shop and provide electricity for consumer needs have promising potential. Batteries (metal-ion, multivalent and metal-air) and supercapacitors are considered next-generation energy storage devices. The overall performance and efficiency of such devices are largely determined by the electrode materials used. Most of the active electrode materials currently in use are in the form of nanostructures, as they can be used to tailor the electrical and electrochemical properties. The strategies implemented so far to improve the efficiency and performance of energy storage devices are: the development of nanostructures at low cost, the tailoring of structures with surface defects and heteroatoms, and the improvement of surface and intrinsic properties. All these processes can be achieved individually or simultaneously through the development of hybrid nanostructures.

Several approaches have already been developed to design and simultaneously adapt advanced carbon nanostructures for energy storage. However, an all-encompassing method for designing advanced nanostructures is still challenging. Therefore, plasma-based technologies that can rapidly and simultaneously design and customise the materials have emerged as a fast-growing approach for the development of advanced energy storage materials [1]. The advantages of plasma are that ecologically advantageous carbon nanostructures can be assembled directly on a substrate from a gaseous to a solid or from a solid to a solid form with predefined orientation (vertical or horizontal), dimension (1D-3D) and morphology [2]. Furthermore, the surface structure can be modified in a controlled manner using plasmas with the desired functional/heteroatoms in an environmentally friendly approach [3]. Experimental evidences suggest the advantages of various plasma-assisted processes such as deposition, etching, forming, transformation, exfoliation, defect engineering and surface processing to design and customise advanced nanomaterials for next-generation energy storage devices. Recent and best performing cases of hybrid carbon nanostructures with superior energy storage performance are also highlighted. [4-8]

References

[1] H. Liang, et al. Applications of Plasma in Energy Conversion and Storage Materials, Advanced Energy Materials **8**, 1801804 (2018).

[2] N. M. Santhosh, et al. Label-free mycotoxin Raman identification by high-performing plasmonic vertical carbon nanostructures, Small **17**, 2103677 (2021).

[3] N. M. Santhosh, et al. N-graphene nanowalls via plasma nitrogen incorporation and substitution : the experimental evidence, Nano-Micro Letters **12**, 53 (2020).

[4] J. Dias, et al. N-graphene-metal-oxide(sulfide) hybrid nanostructures : single-step plasma-enabled approach for energy storage applications, Chemical Engineering Journal **430**, 1 (2022).

[5] N. M. Santhosh, et al. Advanced carbon-nickel sulfide hybrid nanostructures : extending the limits of battery-type electrodes for redox-based supercapacitor applications, ACS Applied Materials and Interfaces **13**, 20559 (2021).

[6] N. M. Santhosh, et al. Advancing Li-ion storage performance with hybrid vertical carbon/Ni_3S_2-based electrodes, Journal of Energy Chemistry **67**, 8 (2021).

[7] N. M. Santhosh, et al. Widening the limit of capacitance at high frequency for AC line-filtering applications using aqueous carbon-based supercapacitors, Carbon **203**, 686 (2023).

[8] N. Shaji, et al. Moving toward smart hybrid vertical carbon/MoS_2 binder-free electrodes for high-performing sodium-ion batteries, ACS Sustainable Chemistry & Engineering **11**, 8, 3260-3269 (2023).

Dynamics of microdischarges in a volume DBD under airflow

Y.A. Ussenov[1,*], A.I. Ashirbek[1,2], M.K. Dosbolayev[1,3], M.T. Gabdullin[4], Yu. S. Akishev[5] and T.S. Ramazanov[3]

[1]*NNLOT, Al-Farabi Kazakh National University, Almaty, Kazakhstan*
[2] *Institute of Apllied Sciences and IT, Almaty, Kazakhstan*
[3]*NNLOT, Al-Farabi Kazakh National University, Almaty, Kazakhstan*
[4]*Kazakh British Technical University, Almaty, Kazakhstan*
[5]*State Research Center TRINITI, Troitsk-Moscow, Russia*
**Currently with the Department of Mechanical and Aerospace Engineering, Princeton Univeristy, USA*

A detailed understanding of microdischarge dynamics in DBD is crucial for the accurate interpretation of the underlying physics of discharge regimes, surface and volume "memory" effects, and pattern formation. This contribution reports on the impact of external (forced) and convective (natural) airflow on the collective dynamics of microdischarge channels in the volume DBD with rail type and parallel plate electrode arrangements.

1 Introduction

The dielectric barrier discharge (DBD) at ambient room conditions, operating with the air as the plasma-forming gas, usually exists in the form of randomly distributed thin microdischarge (MD) channels. There is growing interest in the study of microdischarge dynamics within DBD driven by a requirement to better understand the collective behavior of MD filaments, memory effects, and the emergence of self-organized patterns. This study examined the microdischarge dynamics (MD) of atmospheric pressure air dielectric barrier discharge (DBD) when subjected to both forced external gas flow and natural convective flow.

2 Experiment and results

Both rail-type and parallel-plate discharge electrode arrangements are utilized in the experiments. By observing the discharge between rail electrodes in an external airflow along the electrodes, we were able to gain insight into the role of both volume plasma and surface charges in the memory effect of MD channels. The gas flow regime transitions from laminar to turbulent, resulting in the intricate dynamics of MD filaments. The trajectories of these filaments are observed to move both downstream and upstream in the direction of the gas flow. The study also examined the influence of convective flow on a parallel-plate electrode arrangement, which occurs due to the temperature difference between the discharge cell electrodes and the surrounding ambient air. As the thermal gradient increased, the velocity of the convective gas flow increased, and the MD channels aligned with the direction of the gas flow (Figure 1). The velocity of the convective flow was estimated by the computational fluid dynamics (CFD) simulation and compared with the average velocity of the MD channels obtained via the particle image velocimetry (PIV) method.

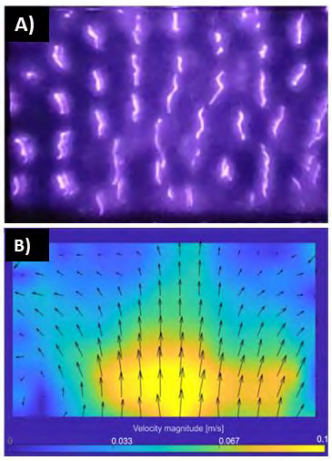

Figure 1. Images of MD filaments of vertical DBD cell (A) at ΔT_{max}=87.9 K temperature gradient and the corresponding velocity map from PIV analysis (B).

3 Acknowledgments

The work supported by the grant (AP09258963.) of Ministry of Higher Education and Science of Kazakhstan.

References

[1] Usenov E.A. et.al., The memory effect of microdischarges in the barrier discharge in airflow. Plas. Phys. Rep., **46**, 459–464 (2020).

[2] YA Ussenov, AI Ashirbek, AR Abdirakhmanov, MK Dosbolayev, MT Gabdullin, TS Ramazanov, Microdischarge dynamics of volume DBD under the natural convection flow. arXiv preprint arXiv:2212.02760 (2022).

Micro Hollow Cathode Discharges in Ar/N_2 for boron nitride PECVD

C. Lazzaroni, A. Remigy, M. Jacquemin, H. Kabbara, S. Kasri, B. Menacer, K. Gazeli, V. Mille, and G. Lombardi

Université Sorbonne Paris Nord, Laboratoire des Sciences des Procédés et des Matériaux, LSPM, CNRS, UPR 3407, F-93430, Villetaneuse, France

A Plasma Enhanced Chemical Vapor Deposition (PECVD) process based on Micro Hollow Cathode Discharges (MHCDs) is used for boron nitride deposition (hexagonal and amorphous). To optimize and better understand the PECVD process it is necessary to characterize the discharge and to study in particular the production and the transport in the deposition chamber of the atomic nitrogen density, a key parameter in the process. The characterisation has been performed through experimental and modelling tools and the results can be related to the properties of the deposited films.

A Plasma Enhanced Chemical Vapor Deposition (PECVD) process based on Micro Hollow Cathode Discharges (MHCDs) in Ar/N_2 mixture has been developed. The process, illustrated in figure 1a, is based on a two-chamber reactor, the MHCD being located in between. The targeted material is hexagonal boron nitride (h-BN) which is highly demanded for electronic and optoelectronic applications, and more recently for quantum technologies [1]. The Ar/N_2 is injected in the higher pressure upstream chamber to favour the dissociation of N_2 and the boron precursor, boron tribromide (BBr_3), is injected in the lower pressure downstream chamber where the substrate holder is localized. The polarization of the substrate-holder allows the expansion from the hole to the substrate in the so-called Micro Cathode Sustained Discharge (MCSD) configuration.

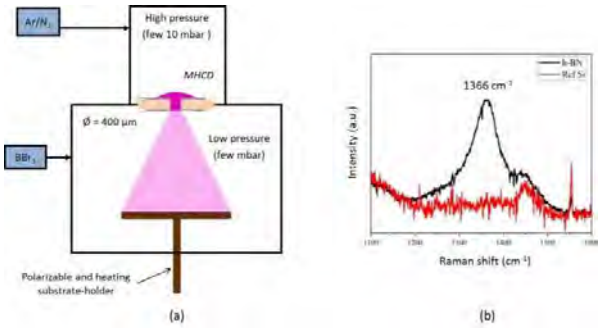

Figure 1: (a) Schematic of the PECVD reactor and (b) Raman spectrum of h-BN film on a silicon substrate (in black) obtained by a 7h deposition (the Si reference spectrum is given in red).

We have shown the feasibility of h-BN deposition on large area substrates (2 inches) at relatively low temperature (800°C) compared to more conventional deposition processes, with a Raman spectrum clearly showing the h-BN signature at 1366 cm^{-1} (see figure 1b) [2]. The corresponding stoichiometry is close to one with 55% of B and 45% of N. It turns out that the distance between the MHCD source and the substrate has an important effect on the stability and the stoichiometry of the deposited films. Moreover, the injection of hydrogen in the deposition chamber allows the preferential orientation of the process (h-BN or amorphous a-BN) to be selected.

In order to optimize and better understand the PECVD process, the discharge has been characterized experimentally and also modelled using global models in Ar/N_2 chemistries. We focused in particular on the production and the transport of atomic nitrogen density, a key parameter in the deposition process. Experimentally, the density has been measured in various configurations (with or without a pressure differential between the two sides of the MHCD, with or without a third electrode in front of the MHCD) by means of nanosecond Two-photon Absorption Laser Induced Fluorescence (ns-TALIF) and Vacuum Ultra Violet (VUV) Fourier Transform Spectrometry (FTS) [3]. Given the high spatial resolution of the diagnostic, the TALIF measurements allow a mapping of the atomic nitrogen density in the deposition chamber, from the MHCD to very near the substrate's surface. The results obtained in the different configurations are compared to the results of the model and related to the properties of the BN thin films.

References

[1] Sajid A. *et al.* Rep. Prog. Phys. **83**, 044501 (2020).
[2] Kabbara H. *et al.* Appl. Phys. Lett. **116**, 171902 (2020).
[3] Remigy A. *et al.* Phys. Plasmas **29**, 113508 (2022).

Photodetachment of negative ions drifting in the Townsend Avalanche: Experimental and numerical study in O_2 and N_2O.

O. González-Magaña[1], J. de Urquijo[1], E. Basurto[2] and A M Juárez

[1]*Instituto de Ciencias Físicas, Universidad Nacional Autónoma de México, 62210, México*
[2]*Universidad Autónoma Metropolitana – Azcapotzalco, Ciudad de México, México*

In this talk, we shall present and discuss recent results on the photodetachment of negative ions of O_2 and N_2O formed inside a Townsend Avalanche. In addition, experimental results are compared with our recently modified avalanche simulator SIMAV to consider the effect of photodetachment.

The presence of negative ions in a gas discharge can considerably influence its space charge distribution and temporal development due to electron detachment from unstable negative ions. Therefore, an accurate quantification of the density of negative ions is of great importance when performing diagnostics and simulations on a low-temperature plasma containing electronegative gases [1, 2]. A review can be found in [3].

In this work, the negative ions under study are formed using a pulsed Townsend apparatus (PTA), which has been used for decades for the measurement of electron/ion transport, ionization, attachment and, under carefully selected conditions, ion molecule reaction rates over wide ranges of the density-normalized electric field intensity E/N and gas pressures [4]. The electron component the avalanche allows the determination of the transport and ionization coefficients [5] whereas an Avalanche simulator (SIMAV) permits the analysis of far more complex ionic transient pulses [6,7]. Recently, we have upgraded the simulator by including the influence of a negative ion photodetaching laser pulse on the measurable current. This addition has proven particularly useful when two or more negative species are present in the avalanche, such as O^- and O_2^- for molecular oxygen; or O^- and NO^- for N_2O gas discharges.

Measurements were made for the photodetachment signal of O_2 as a function of time delay for firing the photodetaching laser at E/N=112 Td, where the ionization equals attachment. We use a Nd:YAG laser at wavelengths of 1064 and 532 nm to photodetaching O^- and O_2^- . We correspondingly record the photodetaching signal on the waveform. For example, at 1064 nm the measured photodetachment cross sections [8] are $\sigma(O^-) = 0$ and $\sigma(O_2^-) = 0.5\text{x}10^{-18}$ cm^2. Using a wavelength of 532 nm, electrons from both O^- and O_2^- are released, with corresponding photodetachment cross sections being $\sigma\ (O^-) = 6.5\text{x}10^{-18}$ cm^2 and $\sigma(O_2^-) = 1.7\text{x}10^{-18}$ cm^2.

This is an interesting finding since O^- is not detachable with 1,064 nm, and is congruent with $\sigma(O^-)=0$ at this wavelength. Changes in the ion pulse shapes with time and wavelength will be shown and discussed.

This information is currently used to calibrate SIMAV. In the case of N_2O, the measurement was made at E/N= 16 Td, where only negative ions form in the avalanche.

Current and future work deals with photodetachment of negative ions at low E/N in CH_4, CO_2, and H_2O, combining the photodetachment experiment and SIMAV.

References

[1] Oudini N, et al. Physics of Plasmas 25 053510 (2018)
[2] Bacal M. Review of Scientific Instruments 71 3981–4006 (2000)
[3] H. Amemiya and T. Suzuki, Jpn. J. Appl. Phys. 29 L1712 (1990)
[4] J L Hernández-Ávila, et al. J. Phys. D: Appl. Phys. 35, 2264–2269 (2002).
[5] Brambring J 1964 Z. Physik 179 532
[6] de Urquijo J, et al., IEEE Trans. Plasma Science, 35 1204-9 (2007)
[7] Bekstein, A., Urquijo, J. et al. J. Phys. Conf. Ser 370, 012006 (2012).
[8] L. C. Lee and G. P. Smith. J. Chem. Phys. 70, 1727 (1979)

Project supported by UNAM-PAPIIT IA101922. Thanks are due to A. Bustos and G. Bustos for their technical assistance.

On the role of reaction mechanisms and metal catalysts during the plasma-assisted ammonia synthesis

A. Gómez-Ramírez[1,2], P. Navascués[2], J. Garrido-García[2], M. Oliva-Ramírez[1,2], J. Cotrino[1,2], A. R. González-Elipe[2]

[1] *Departamento de Física Atómica, Molecular y Nuclear, Universidad de Sevilla, Avda. Reina Mercedes, E-41012 Seville, Spain*

[2] *Laboratory of Nanotechnology on Surfaces and Plasma. Instituto de Ciencia de Materiales de Sevilla (CSIC-Universidad de Sevilla), Avda. Américo Vespucio 49, E-41092 Seville, Spain*

The incorporation of catalysts into packed-bed plasma reactors has been demonstrated to be a useful strategy to increase the performance of different plasma-driven chemical processes. In this work, we analyse the factors that hinder higher nitrogen conversions and better energy performances as well as the effect of a Ru-catalyst on the plasma-assisted ammonia synthesis, with the aim of determining the role of pure catalytic or plasma interactions during the process, which is a key issue to overcome the current energy efficiency limitations of the plasma-assisted ammonia synthesis.

1 General

Current studies on ammonia synthesis by means of atmospheric pressure plasmas respond to the urgent need of developing less environmentally aggressive processes than the conventional Haber−Bosch catalytic reaction. Nevertheless, and although many plasma devoted research groups are working on this topic, energy efficiencies and chemical yields are still under those provided by the classical method.[1-5]

In this work we analyse the ammonia synthesis process in a ferroelectric packed-bed reactor, paying special attention to the factors that hinder higher nitrogen conversions and better energy performances. Firstly, we analyse the occurrence of the reverse reaction (it is, destruction of ammonia by the plasma after being formed) and inefficient exchange reactions (ammonia can exchange H atoms with H_2 molecules in the plasma bulk or –OH groups at the surfaces). With the aim of quantifying the occurrence of those energy wasting processes, we apply an isotope labelled technique. By using different reactive gases (composed by NH_3, H_2, N_2, D_2 or their mixtures) and varying their residence time in the plasma reactor we have obtained valuable information about reaction mechanisms. Our results point to an important proportion of decomposed ammonia, that alternatively can be seen as a hydrogen production process, and a high number of H↔H inefficient exchanges. This methodology allows us to quantify, for the first time up to our knowledge, the relative amount of processes taking place in the plasma bulk or at the ferroelectric surface. Secondly, we study the effect of incorporating a ruthenium (Ru) metal catalyst, one of the most widely used metal catalyst for the thermal and plasma-catalytic synthesis of ammonia, into the ferroelectric barrier. In this case our results suggest that the incorporation of Ru nanoparticles provokes a negligible enhancement in reaction yield or in energy efficiency, even working at 190ºC. Although ruthenium may contribute to ignite more intense plasmas by modifying the electric properties of the discharge it can be also detrimental for the ammonia synthesis through the promotion of undesired reactions, as the ammonia decomposition or hydrogen exchange processes. All these processes seem to hide possible catalytic effects induced by the ruthenium nanoparticles.

Acknowledgements

The authors acknowledge projects PID2020-114270RA-I00 and PID2020-112620 GB-I00 funded by MCIN/AEI/10.13039/501100011033, project TED2021-130124A-I00 funded by MCIN/AEI/10.13 39/501100011033 and the European Union NextGeneration EU/PRTR, projects US-1380977 and US-1381045 funded by Fondo Europeo de Desarrollo Regional (FEDER) and Consejería de Transformación Económica, Industria, Conocimiento y Universidades de la Junta de Andalucía, within Programa Operativo FEDER 2014-2020.

References

[1] J. Hong et al. Sustainable Chem. Eng **6**, 15−31 (2018).

[2] Carreon, M. L. J. Phys. D: Appl. Phys **52**, 483001 (2019).

[3] Y. Gorbanev, et al. ACS Sustainable Chem. Eng. **8**, 2996–3004 (2020).

[4]. Navascués, P. et al. ACS Sustainable Chemistry & Engineering **8**, 14855–14866 (2020).

[5] Navascués, P. et al. ACS Sustainable Chemistry & Engineering **11**, 3621-3632 (2023)

Simulation of the chemical reaction induced by a streamer discharge and its validation study

A. Komuro, and R. Ono

[1] *Dept. Advanced Energy, The University of Tokyo, Japan*

Atmospheric pressure streamer discharges are expected to be used in many industries as an effective chemical reaction field, and the development of simulators to accurately predict the production distribution and density of chemically active species is long awaited. This study presents the work of our group on validation studies in streamer discharge simulation, with particular emphasis on the generation characteristics of chemically active species.

Atmospheric pressure streamer discharges can easily form chemically active reaction fields and are expected to be used in various industrial fields [1]. The chemical reaction fields generated by streamer discharges start from the behaviour of electrons and undergo various chemical reaction processes, from the generation of molecularly excited species to their de-excitation processes, so numerical simulations are very useful to elucidate the whole picture. In recent years, streamer simulation itself is no longer so special, due to the development of computational techniques and improvements in the power of the computers themselves. One of the challenges for the future of streamer simulation is how to construct highly systematic streamer simulation models, for which validation and verification (V&V) studies are becoming increasingly important. Our group has been conducting a validation study of streamer discharge simulation since around 2011, and this presentation describes the contents of the study.

In the simulation, we use a classical two-dimensional (2D) fluid model based on the drift-diffusion model for electrons and positive and negative ions coupled with Poisson's equation. The simulations were performed with a 13 mm gap point-to-plane electrode configuration in N_2/O_2(21%) at atmospheric pressure and $T = 293$ K, according to our experimental setup. The experiments used the special electrode configuration capable of producing a pseudo-2D axisymmetric single-filament pulsed positive streamer discharge [2]. The ozone density was measured by laser spectroscopy and compared with the simulation. Part of the results are shown in Figure 1. The results show that the length of the high ozone density region is slightly different between the experiment and the simulation, although the ozone production characteristic that ozone is mainly produced in the secondary streamer is well reproduced. The reason for this discrepancy is discussed in terms of the formation mechanism of the secondary streamer and the effects of the oxygen concentration in N_2/O_2 on ozone formation [3].

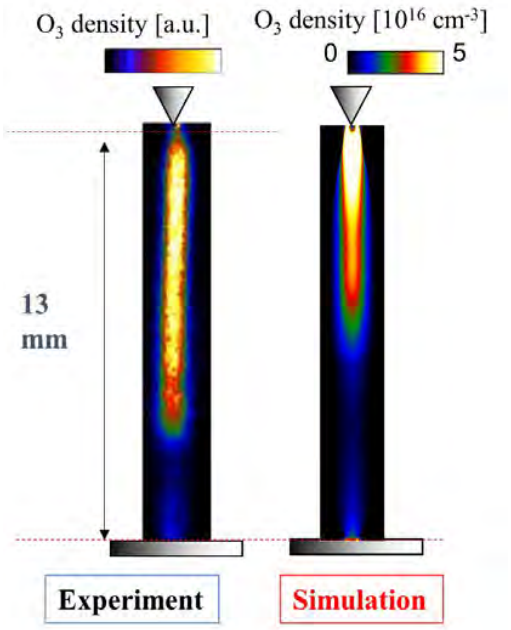

Figure 1 Distributions of ozone obtained from the experiment and simulation [2].

References

[1] Adamovich I, Agarwal S, Ahedo E, et al. The 2022 Plasma Roadmap: low temperature plasma science and technology J. Phys. D: Appl. Phys. **55** 373001 (2022).

[2] Ono R and Komuro A Generation of the single-filament pulsed positive streamer discharge in atmospheric-pressure air and its comparison with two-dimensional simulation J. Phys. D: Appl. Phys. **53** 035202(2020).

[3] Komuro A, Yoshino A, Wei Z, et al. 2023 Effects of oxygen concentration on streamer propagation and ozone production in a single-filament streamer discharge at atmospheric pressure J. Phys. D: Appl. Phys. 56 185201.

Why are 2D axisymmetric ionization waves generated in a simple point-to-plane geometry in atmospheric pressure air still studied?

A. Bourdon[1]

[1] *Laboratoire de Physique des Plasmas (LPP), CNRS, Sorbonne Université, Ecole polytechnique, Institut Polytechnique de Paris, 91120 Palaiseau, France*

The development of high voltage generators, diagnostic techniques and numerical simulations have allowed in recent years to better understand some key characteristics of ionization waves or streamers in atmospheric pressure air as ignition, branching and conditions to obtain 2D axisymmetric discharges in point-to-plane geometry. In this work, we discuss the influence of the maximal value of the applied voltage, the shape of the applied voltage, the polarity, the gap size, the shape of the point electrode and its holder on the discharge ignition, propagation and morphology.

1 Introduction

Ionization waves also called streamers are transient discharges that are precursors of sparks and lightning leaders. Many experimental and numerical studies of these discharges have been carried out in atmospheric pressure air in a simple point-to-plane geometry. As reviewed in [1] streamer discharges in air often branch and quantifying streamer branching is a challenging topic. In this work, we focus on 2D axisymmetric air streamer discharges in a point-to-plane geometry.

2 On the different conditions to obtain 2D axisymmetric streamer discharges in air

In the 1970s, in point-to-plane geometry in air gaps of about 1 cm at atmospheric pressure, with positive DC voltages of up to 20kV [2], stable and repetitive 2D axisymmetric discharges were obtained and studied. In the following, these streamer discharges are called “low DC voltage streamer discharges”.

Recently, several experimental and numerical studies in point-to-plane geometry in air gaps of about 1 cm at atmospheric pressure have reported images of axisymmetric diffuse discharges with maximum radius of several centimeters as reviewed in [3,4]. These discharges are obtained with nanosecond pulsed applied voltages. In the following, these discharges are called “nanosecond pulsed high voltage streamer discharges”.

3 Characteristics of 2D axisymmetric streamer discharges in air

During the propagation of “low DC voltage streamer discharges”, the maximum electric field in the ionization front is in the range of 100 to 150 kV/cm and the radius of the discharge channel behind the front is rather constant and is of a few 100s μm. The average propagation velocity of the ionization front is about 0.1-0.2 mm/ns.

As an example of “nanosecond pulsed high voltage streamer discharges”, in [5], for a point-to-plane geometry with a 1.5 cm gap and a positive voltage of 250 kV applied to the point electrode with a subnanosecond voltage front, a discharge radius of up to 1 cm and a propagation velocity in the range of 10 to 100 mm/ns, is simulated and in good agreement with experiments. In [6] the influence of the electrode set-up geometry on the morphology of nanosecond pulsed positive ionization waves in air was studied. In this work we discuss the influence of the maximal value of the applied voltage, the shape of the applied voltage, the polarity, the gap size, the shape of the point electrode and its holder on the discharge ignition, propagation and morphology.

References

[1] Nijdam S. et al, The physics of streamer discharge phenomena *Plasma Sources Sci. Technol.* 29, 103001 (2020).

[2] Marode E, The mechanism of spark breakdown in air at atmospheric pressure between a positive point and a plane. I. Experimental: nature of the streamer track *J. Appl. Phys.* **46,** 2005–15 (1975)

[3] Naidis G V et al 2018 Subnanosecond breakdown in high-pressure gases *Plasma Sources Sci. Technol.* **27**, 013001 (2018)

[4] Babaeva N Y and Naidis G. V., Universal nature and specific features of streamers in various dielectric media *J. Phys. D: Appl. Phys.* **54** 223002 (2021)

[5] Babaeva N Y and Naidis G V Simulation of subnanosecond streamers in atmospheric-pressure air: effects of polarity of applied voltage pulse, *Phys. Plasmas* **23**, 083527 (2016)

[6] Bourdon A. et al. Morphology of positive ionization waves in atmospheric pressure air: influence of electrode set-up geometry, *Plasma Sources Sci. Technol.* **30**, 105022 (2021)

Tue3-3

EUV-induced Hydrogen Plasma: Pulsed Mode Generation and Consequences in Lithographic Scanner

Mark van de Kerkhof[a,b]

a) ASML Netherlands B.V., De Run 6501, 5504 DR Veldhoven, The Netherlands
b) Department of Applied Physics, Eindhoven University of Technology, Eindhoven, The Netherlands

ABSTRACT

In the past years, EUV lithography scanner systems have been widely adopted for manufacturing of state-of-the-art Integrated Circuits (IC), with critical dimensions down to 10 nm. This technology uses 13.5 nm EUV radiation, which is shaped and transmitted through a near-vacuum H_2 background gas. This gas is excited into a low-density H_2 plasma by the EUV radiation, as generated in high-frequency pulsed mode operation by the Laser-Produced Plasma (LPP) in the EUV Source.
Thus, in the confinement created by the walls and mirrors within the scanner system, a reductive plasma environment is created that must be understood in detail to maximize mirror transmission over lifetime and to minimize molecular and particle contamination in the scanner. Besides the irradiated mirrors, reticle and wafer, also the plasma and radical load to the surrounding construction materials must be considered.
This presentation will provide an overview of the EUV-induced plasma in scanner context. Special attention will be given to the plasma parameters in a confined geometry. It will be shown that plasma confinement and resulting contributions from secondary electron emission delay the formation of the plasma sheath and thereby reduce the peak ion energies, to below the sputtering threshold for mirrors and construction materials. Also, the spectrum of the EUV Source may be relevant in this respect.
Furthermore, for a confined pulsed plasma with a pulse period shorter than the decay time of the plasma, the plasma will consist of a quasi-steady-state cold background plasma, and periodic transient peaks in ion energy and ion flux. In terms of modeling, this means no assumptions can be made on the electron distribution functions, and a (Monte-Carlo) Particle-in-Cell (PIC) model is needed. We will present an extension of the PIC model approach to complex 3D geometries and to multiple pulses, by using a Hybrid PIC-diffusion approach.

Keywords: Lithography, EUV, EUV-induced Plasma, Pulsed Discharge, PIC, Hybrid PIC

Two-Way Coupling of Plasma-Assisted Combustion

C. Guerra-Garcia[1] and C. A. Pavan[1]

[1] *Department of Aeronautics and Astronautics, Massachusetts Institute of Technology, Cambridge, MA, USA*

Plasma actuation is a promising technology to address challenges in combustion, ranging from extending lean limits, to controlling dynamics, igniting supersonic flows, or facilitating burning of ammonia. Whereas the goal is to modify combustion through plasma assistance, the combustion process can also modify the plasma, and this backward interaction is oftentimes overlooked. In this contribution we present experiments and model results of the interaction of a mesoscale flame with nanosecond pulsed discharges in a dielectric barrier discharge configuration. This platform is ideal to study the two-way interaction, thanks to the comparable length scales of plasma and flame. The impact of the plasma on the flame is manifested as flame speed modifications, and enhanced flame wrinkling. The plasma regime, whether uniform or micro-discharges, and the energy deposition, are controlled by the flame dynamics. Experiments isolating different mechanisms are presented and the implications for industrially relevant systems are discussed.

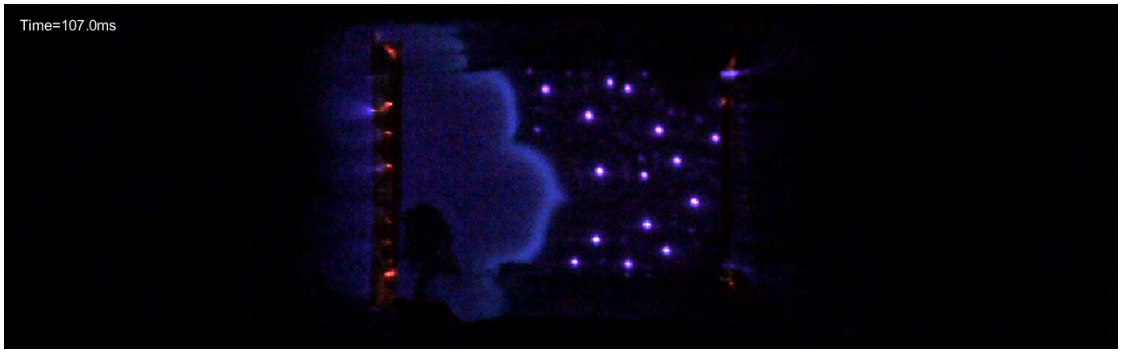

Fig. 1: Photograph of a methane-air laminar flame travelling left to right interacting with a dielectric barrier discharge under pulsed nanosecond voltage. Upstream of the flame, micro-discharges are observed. Downstream of the flame, a uniform discharge takes place. The visualization of the interaction is enabled using transparent electrodes.

From a scientific perspective, plasma-assisted combustion presents a challenging two-way coupled problem between the gas discharge physics and the reactive background gas of the flame. The forward problem, i.e., the impact of plasma on combustion, provides the motivation for the research and can result in beneficial outcomes in terms of emissions reductions or broader operational envelopes of propulsion systems. The backward problem, i.e., the impact of combustion on plasma, can affect the actuation authority of the plasma as it drives the energy deposition pathways. Whereas the forward problem has been extensively studied, the backward problem has attracted significantly less attention.

In this contribution we present experiments that exemplify the relevance of accounting for the feedback of the combustion environment on the electrical breakdown process. The image presented in Fig. 1 shows an example of a dielectric barrier discharge, under pulsed nanosecond voltage, interacting with a premixed laminar methane-air flame [1]. The initially filamentary discharge occurring ahead of the flame transitions into a uniform discharge as the flame progresses. The mechanisms of the interaction are linked to the highly non-uniform background gas, in terms of temperature gradients, spatially dependent flow fields, and variations in composition. These mechanisms are isolated in a series of experiments and the fully coupled problem is studied in the mesoscale platform from experimental and theoretical perspectives. The contribution will conclude with examples of the practical implications of these studies [2].

This work was supported by the Office of Naval Research under grant N00014-21-1-2571, and by the Lockheed Martin Corporation.

References

[1] Pavan, C. A., Guerra-Garcia, C. Nanosecond pulsed discharge dynamics during passage of a transient laminar flame, Plasma Sources Science and Technology 31 (11), 115016 (2022).

[2] Shanbhogue, S., Pavan, C., Weibel, D., Gomez del Campo, F., Guerra-Garcia, C., Ghoniem, A. Control of Large-Amplitude Combustion Oscillations Using Nanosecond Repetitively Pulsed Plasmas, Journal of Propulsion and Power, 1-13, (2023).

Multiscale plasma-surface model applied to reactive magnetron sputtering

L. Vialetto[1], C. Stüwe[1], T. Gergs[2], T. Mussenbrock[2], and J. Trieschmann[1]

[1] *Theoretical Electrical Engineering, Department of Electrical and Information Engineering, Kiel University, Kaiserstraße 2, 24143 Kiel, Germany*

[2] *Chair of Applied Electrodynamics and Plasma Technology, Department of Electrical Engineering and Information Science, Ruhr University Bochum, 44780 Bochum, Germany*

Reactive magnetron sputtering for deposition of silicon oxide thin films is studied via Particle-In-Cell with Monte Carlo Collisions simulations. Dynamic coupling of the plasma with surfaces is taken into account by including a deterministic model for surface kinetics. Whereas the coupled plasma-surface model is generic, its application is exemplified by a low-pressure capacitively coupled radio-frequency discharge operated with Ar and O_2. The work highlights the relation between surface properties during deposition and discharge characteristics.

1 Introduction

Reactive radio-frequency (RF) sputter processes are highly relevant for thin film deposition, but a complete understanding of their fundamentals and operation is still missing [1, 2]. In fact, the dynamics of multi-component plasmas in contact with solid surfaces is extremely complex, involving a large number of processes in the plasma and in the solid, as well as fluxes across the interface. Therefore, numerical studies on the mutual influence of surface properties and discharge characteristics are needed.

2 Method and discussion

In this work, a novel numerical model for low-pressure partially-magnetized discharges is presented, which establishes a dynamic coupling of the plasma and the surfaces. The code has been developed within the modern object-oriented OpenFOAM framework [3], which enables parallel simulations and the use of arbitrary geometries. The toolbox features have been extended by including a multi-dimensional Particle-In-Cell with Monte-Carlo-Collisions (PIC/MCC) scheme for charged particles, energetic neutrals, and sputtered atoms, which may be coupled to a system of fluid equations for the neutral background plasma species. The surface evolution is described through a system of rate equations for the predominant adsorbed atoms and vacancies, which takes into account physical sputtering, chemisorption, physisorption, and surface diffusion of adatoms [4]. As an example, the newly developed coupled model is applied to a low-pressure RF magnetron discharge for the sputter deposition of silicon oxide thin films using Ar gas with variable admixtures of O_2. Figure 1 shows the corresponding time-averaged charged species number density profiles obtained from 2d3v PIC/MCC simulations with 90% Ar and 10% O_2 at a gas pressure of 1 Pa, 13.56 MHz driving frequency, and 175 V RF bias. As a results of this work, the link between discharge characteristics, such as applied RF power and gas composition, and surface processes, such as target poisoning, is investigated.

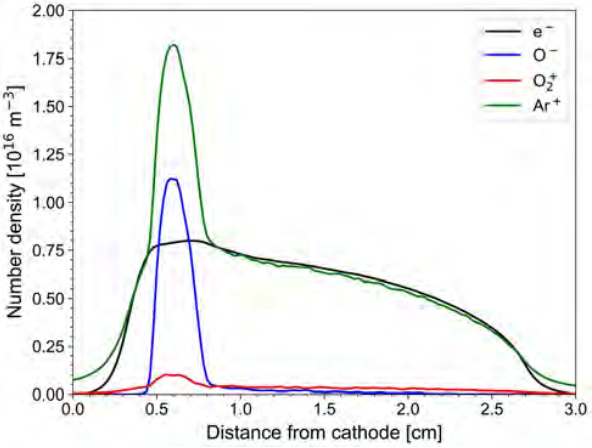

Figure 1: Time-averaged number density profiles of charged particles obtained with PIC/MCC simulations for a magnetron operated with a background gas of 90% Ar and 10% O_2 at 1 Pa, 13.56 MHz, and 175 V RF bias.

Acknowledgements

This work was supported by the Deutsche Forschungsgemeinschaft (DFG, German Research Foundation) - Project-ID 434434223 - SFB 1461.

References

[1] I. Adamovich *et al.*, *J. Phys. D: Appl. Phys.* **55** (2022) 373001

[2] J. Roggendorf *et al.*, *Plasma Sources Sci Technol*. **31** (2022) 065007

[3] https://github.com/OpenFOAM/OpenFOAM-10 (last access 24th February 2023)

[4] Guerra and Marinov, *Plasma Sources Sci. Technol.* **25** (2016) 045001

Atomic wall recombination in oxygen-containing plasmas

P. Viegas[1], J. Afonso[1] , J. Silveira[1], A. S. Morillo-Candás[2] , L. Vialetto[3] and V. Guerra[1]

[1] *Instituto de Plasmas e Fusão Nuclear, Instituto Superior Técnico, Universidade de Lisboa, Portugal*
[2] *Laboratoire de Physique des Plasmas (UMR 7648), CNRS, Univ. Paris-Saclay, Sorbonne Université, École Polytechnique, France*
[3] *Theoretical Electrical Engineering, Faculty of Engineering, Kiel University, Germany*

Atomic oxygen recombination on a Pyrex surface in an oxygen glow discharge plasma is studied via numerical simulations and comparisons with experiments, for pressures between 0.2 Torr and 8 Torr and several current values. The surface kinetics simulations reproduce the experimental measurements and point out the main recombination mechanisms at each experimental condition. Moreover, this work highlights the presence of plasma-induced reversible surface modifications at low pressures.

1 General

Heterogeneous surface kinetics plays a role in most plasma processes, where surfaces interact either with active discharges or their afterglow. It can affect both plasma and surface properties. In particular, in oxygen-containing discharges, the adsorption and recombination of atomic oxygen on reactor surfaces determine the gas composition, the availability of O for important volume reactions (e.g.: $CO_2 + O \rightarrow CO + O_2$; $CO + O + M \rightarrow CO_2 + M$) and eventually the flux of reactive oxygen species (ROS) towards target surfaces.

In Booth et al. (2019) [1], the wall loss frequencies of O atoms have been measured in the positive column of an oxygen glow discharge in a Pyrex tube (borosilicate glass) of 10 mm inner radius, for several pressures and currents. However, the surface mechanisms determining recombination are not fully known yet. In particular, the increasing recombination with decreasing pressure below 1 Torr (see figure 1) is not understood. In this work we employ deterministic and Kinetic Monte Carlo methods [2-4] to simulate the surface kinetics of atomic oxygen in the experimental conditions of Booth et al. (2019) and highlight the relevant mechanisms.

The newly developed model describes the experimental dependence of the atomic oxygen recombination probability on pressure, current, gas temperature and wall temperature and allows to identify the most important recombination mechanisms for each condition. Moreover, this work demonstrates that the plasma has important effects on the surface at low pressures. This is due to fast particles that produce new chemisorption sites on the surface, where O atom recombination can take place without an energy barrier [5]. Figure 1 shows the effect of these sites on the atomic oxygen surface recombination frequency below 1 Torr, agreeing with experimental measurements.

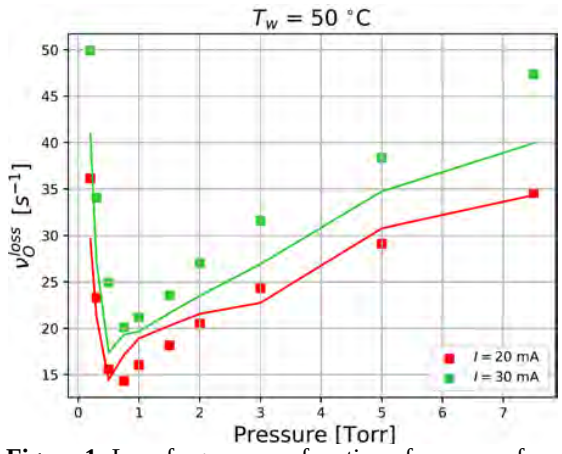

Figure 1: Loss frequency as function of pressure, for a wall temperature of 50 ºC and discharge currents of 20 mA and 30 mA. Results from experiments [1] (square symbols) and simulations employing the deterministic method (full lines).

Acknowledgements

This work was partially supported by the Portuguese FCT-Fundação para a Ciência e a Tecnologia, under projects UIDB/50010/2020, UIDP/50010/2020 and PTDC/FISPLA/1616/2021 (PARADiSE).

References

[1] Booth *et al., Plasma Sources Sci. Technol.* **28** (2019) 055005
[2] Guerra, *IEEE Transactions on Plasma Science* **35** (2007) 1397
[3] Guerra and Marinov, *Plasma Sources Sci. Technol.* **25** (2016) 045001
[4] Marinov *et al., Plasma Process. Polym.* **14** (2017) 1600175
[5] Schwartzentruber *et al., AIAA International Space Planes and Hypersonic Systems and Technologies Conference* (2015) 3567

Non-thermal chemical dissociation of CO_2: a modelling approach

Q. Shen[1], F. J. J. Peeters [2] and M. C. M. van de Sanden[1,3]

[1] *Dutch Institute for Fundamental Energy Research, Eindhoven, TheNetherlands*

[2] *Leyden Jar company, Eindhoven, The Netherlands*

[3] *Department of Applied Physics, Eindhoven Institute of Renewable Energy Systems, Eindhoven University of Technology, Eindhoven, The Netherlands*

In this contribution, we present a non-thermal model, i.e., the vibrational temperature is different from the gas and rotational temperature, for the decomposition of CO_2. The model is based on a zero-dimensional continuous stirred-tank reactor (CSTR) and the chemistry contains four chemical reactions and their reverse reactions. The entire vibrational manifolds of CO_2, CO and O_2 are included, and a novel procedure to calculate the reaction rate constants under these non-thermal conditions is proposed. In all cases, the Boltzmann distribution is assumed for the vibrational states and the effect of the activation barrier for the chemical reactions is taken into account using a Fridman-Macheret expression [1]. The different non-thermal reaction rates change as a function of gas and vibrational temperature. The results illustrate the beneficial effect of higher vibrational than gas temperature on CO_2 conversion and energy efficiency. This work aims to provide more insights into the dissociation and recombination reactions in CO_2 conversion under non-thermal conditions and paves the way for multi-dimensional non-thermal modelling in the future.

1 General

CO_2 conversion by vibrational excitation, followed by vibrational-vibrational relaxation to the highest levels, is in theory the most energy-efficient CO_2 dissociation process. In the present work, 10548, 26 and 80 vibrational levels of CO_2 molecules, O_2 molecules, and CO molecules have been considered, whose vibrational energy is not higher than the dissociation energy separately. A new method to illustrate the effect of non-thermal conditions on CO_2 conversion is proposed. The molecules have a Boltzmann distribution characterized by a vibrational temperature different from the gas temperature. The eight reaction rates in the non-thermal plasma model are calculated by weighted algebraic expressions rather than complex differential equations, which could save computing time dramatically.

The energy utilization ratio in the different channels at different vibrational and gas temperatures, including dissociation, thermal energy for heat loss, and storing in molecules as vibrational energy is analysed. This heating term is usually ignored for non-thermal conditions but can drastically affect the calculated energy efficiencies.

As an example, Figure 1 shows the energy utilization change for different gas temperatures at a fixed (higher) vibrational temperature, residence time, and pressure.

Because the dissociation process is sluggish at low gas temperature, most energy is still stored in CO2 molecules at low gas temperature even though the vibrational energy is promoting dissociation of the CO_2 molecules. As the gas temperature increases, the accelerated dissociation reaction rate promotes more and more CO_2 molecules absorbing enough energy to split, which raises the energy used for dissociation. However, continually increasing gas temperature also accelerates energy waste in the thermal energy or storing in molecules, which reduces the energy efficiency. According to the calculation, the efficiency hits a peak of 66 % for T_{vib} = 5000 K and T_{gas} = 1300 K when the resident time is 1 ms. In addition, the model compares maximum efficiency for different residence times. With the increment of residence time, the peak of efficiency goes up, whereas the vibrational and gas temperature for which the maximum efficiency is reached both reduce. In the end, compared with the stationary time for different vibrational and gas temperatures, raising vibrational and gas temperatures could significantly accelerate CO_2 dissociation.

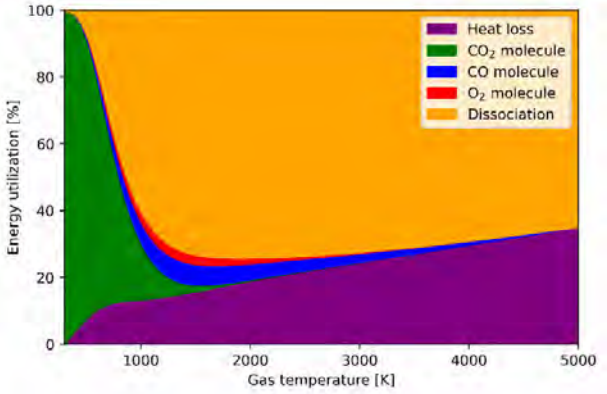

Figure 1: Relative contribution of the main processes responsible for the energy utilization as a function of the gas temperature, for a vibrational temperature of 5000 K, resident time of 1 ms, and a pressure of 100 mbar

References

[1] Fridman A A. Plasma chemistry. Cambridge University Press (2008).

DBD-Streamer Mode Transition of Atmospheric-Pressure Plasma Jet Applied on Water with Changed Distance and AC Power

Po-Hsien Chiu and Jong-Shinn Wu*

Department of Mechanical Engineering, National Yang Ming Chiao Tung University, Hsinchu, Taiwan

This study systematically analysed the electrical properties of the APPJ device to provide a reference to facilitate the improvement of the PAW system. The snapshots of images of dielectric barrier discharge (DBD) and the streamer discharge were captured by the intensified charge-coupled device (ICCD) to analyse the relationship between the discharge and the timings in a period. The results showed that the APPJ device performed equivalent to either a capacitor or a resistor electrically. This study also found that discharge showed a clear transition between DBD and streamer based on the absorption ratio by changing electrode-to-exit distance and AC power. Thus, the absorption ratio is a reference to check the discharge mode of an APPJ device. Further, when the discharge is streamer, the voltage amplitude is similar for different consumed power or absorption power. Therefore, the APPJ device has the potential to serve as the voltage stabilizer in the power supply system.

1. INTRODUCTION

APPJ devices can generate dielectric barrier discharge (DBD) and streamer discharge to produce acidic solutions with RONS. Foster et al [1] found that the voltage controls the switch from DBD to streamer based on the voltage-current waveforms. However, there is a lack of the quantitative information to investigate an extensive scope.

2. EXPERIMENTAL METHODS

Fig. 1 shows that the study circulated the water flow to pass under a APPJ device to create the low-pressure region to draw ambient air into the APPJ device. The entrained air was charged inside the APPJ device by an AC power source to produce plasma and reactive species.

3. RESULTS AND DISCUSSION

Fig. 2 shows that when the discharge is streamer, the voltage amplitude is similar for different consumed power or absorption power. Therefore, the APPJ device has the potential to serve as the voltage stabilizer in the power supply system.

Fig. 3 shows a clear transition between DBD and streamer based on the absorption ratio by changing electrode-to-exit distance and AC power. When the discharge was in the form of DBD, the absorption ratio was less than 50%. When the discharge was in a form of streamer, the absorption ratio increased up to 99.9%. Thus, the absorption ratio is a reference to check the discharge mode of an APPJ device.

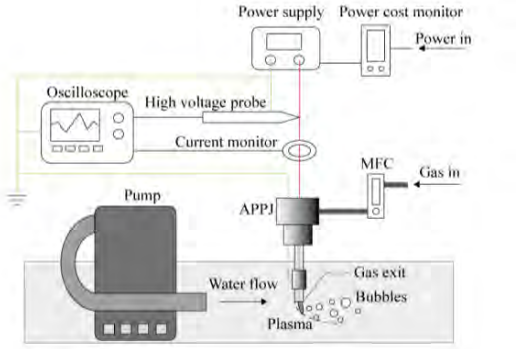

Fig. 1. APPJ device treating the water.

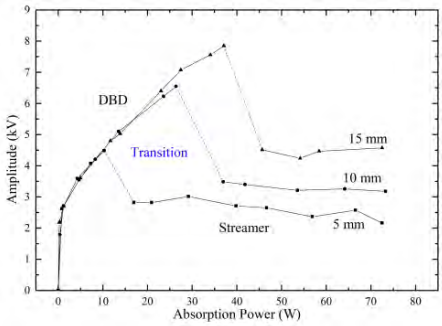

Fig. 2. The voltage amplitude as a function of the absorption power for electrode-to-exit distances.

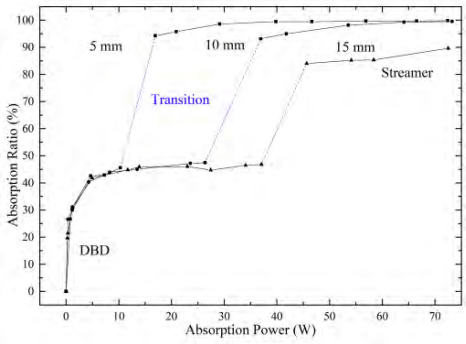

Fig. 3. The absorption ratio is the ratio of the absorption power to the consumed power.

References

[1] J. E. Foster, B. Weatherford, E. Gillman and B. Yee, "Underwater operation of a DBD plasma jet," Plasma Sources Science and Technology, vol. 19, no. 2, 2010.

Surface-wave microwave discharge in contact with liquids

Kinga Kutasi, Péter Hartmann

Wigner Research Centre for Physics, POB 49, H-1525 Budapest, Hungary

A surface-wave microwave discharge generated by using a surfatron wave launcher is put in contact with water under batch and flowing conditions. The effect of the different operation modes of the discharge on the plasma-water interaction and species deposition into the water is investigated. It is shown that the species deposition under given plasma conditions is determined only by the plasma-water interaction time.

The surface-wave microwave discharge generated by using the surfatron wave launcher has been shown to be very efficient in deposition of reactive species into the liquids under batch conditions [1,2]. The work investigates the interaction of the discharge with the liquid and the deposition of the species under flowing conditions, as illustrated in Fig.1.

Fig.1. Surface-wave microwave discharge in contact with water flowing in a 9 mm trapezoid channel.

The atmospheric pressure surface-wave microwave discharge is ignited with the help of a *surfatron* (Sairem, Surfatron 80) in a quartz tube of outer diameter 6 mm and I.D. 4 mm, using Ar gas at 2000 sccm flow rate and MW input power of 25 W. The characteristics of the plasma plume at the interaction surface can be tuned with the initial gas mixture composition, input power and the tube to surface distance. By tuning the density of electrons and NO_x species at the plasma-liquid interface, the creation of NO_2^-, NO_3^- and H_2O_2 species in the liquid can be controlled [1]. Generally, the density of electrons decreases along the plasma column, while that of the NO and NO_2 molecules increase, due to the air influx into the plasma outside the discharge tube.

At the chosen operating conditions the discharge is predominantly ignited in the (0,0) mode with the plasma column filling the central part of the discharge tube, as illustrated in Fig. 2. During operation the filamentation of the discharge can occur. The random appearance, the moving and collapsing of the filaments can be observed at μs scale. The filamentation of the discharge in contact with the water flowing in a trapezoid channel is shown in Fig. 2. The filaments can cover the whole width of the 9 mm channel. PTFE and copper trapezoid channels of 9 mm width, 60° and 5 mm depth are used to put flowing water in contact with the plasma plume. The water flow is provided by a peristaltic pump which results in a pulsating flow. The smallest adjustable flow rate is 13 ml min^{-1}. It is found that under flowing conditions the concentrations of the deposited species are similar as under batch conditions when treating the same volume for the same length of time. No difference is found between the floating and grounded channels.

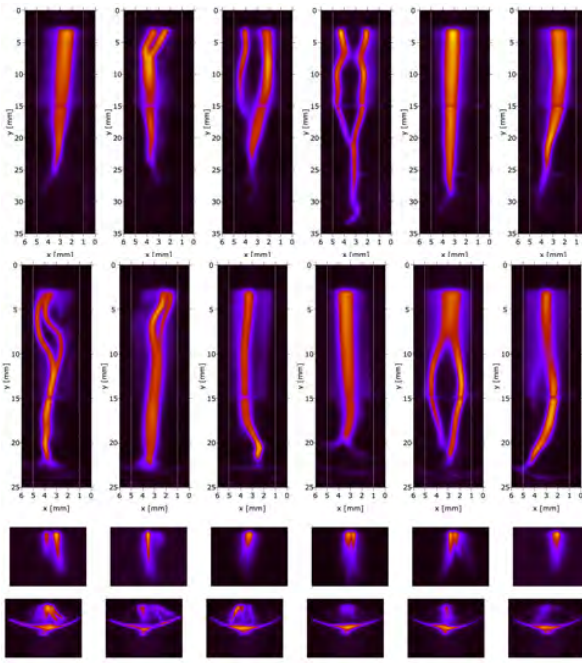

Fig. 2. The ICCD images of the plasma plume in free air (1st row) and in contact with water at 6 mm distance from the discharge tube (2nd row) recorded with 50 μs exposition time. The images of the plume end in free air (3rd row) and in contact with water flowing in copper channel at 12 mm distance recorded with 5 ms exposition time.

References

[1] Kutasi, K. *et al.* Plasma Sources Sci. Technol., **28,** 095010 (2019); Kutasi, K. e*t al.* Plasma Sources Sci. Technol., **30,** 045015 (2021); Kutasi, K. *et al.* Plasma Process. Polym., **20**, 2200143 (2023)

[2] Kutasi, K., Tombácz, E. Plasma Process. Polym., **19,** 2100077 (2022)

Plasma Discharge Modifications Over a Rough Dielectric Liquid Surface

R.Z. Walker[1], M. Meyer[2], S. Doyle[2], M.J. Kushner[2], and J.E. Foster[1]

[1] *Dept. Nuclear Engineering and Radiological Sciences, Univ. of Michigan, Ann Arbor, MI, United States*
[2] *Dept. Electrical Engineering and Computer Science, Univ. of Michigan, Ann Arbor, MI, United States*

Plasma discharge attachment to the surface of a turbulent liquid interface is explored. In general turbulence at the plasma liquid interface not only affects mass transport through mixing and droplet formation but also it influences the magnitude of the local electric field and thus E/N driven chemistry. This work aims to understand the changes in discharge morphology and plasma chemistry for a pulsed corona atmospheric pressure discharge over a liquid water (dielectric) surface in response to induced changes in liquid interfacial morphology in a controlled fashion where perturbations are of order size of discharge footprint. This perturbed surface is used as a surrogate for the rough surface produced under turbulent conditions. An understanding of the discharge chemistry and dose for turbulent flow may be important for plasma water purification applications.

1 General

To date, much emphasis has been placed on diffusive transport of plasma species from the gas phase into the liquid. An opportunity for increased mass transport is the enhancement of collection surface area and mixing via the introduction of turbulence at the plasma-liquid interface. Indeed, the importance of fluid dynamical effects in plasma-liquid treatment systems remains to be fully explored.

In turbulent flow, where momentum diffusion produces eddies of varying length scales, there are numerous effects that can occur, including 1) enhanced surface area, 2) local electric field enhancements, 3) islands of trapped surface charge, and 4) significant mixing. Previous work has shown the sensitivity of plasma attachment mode and dose delivered fluid regime [1]. Turbulent flow was found to be associated with a more diffuse discharge, with more peroxide produced and less nitrogen species, compared to the laminar flow case.

Acoustic excitation is used to introduce interfacial perturbations in a controlled fashion so that discharge response and dose delivered can be assessed. Here, sound waves promote the growth of surface capillary waves, where surface tension and the frequency of the sound waves determine the wavelength of the surface perturbation.

Electric field simulations, shown in Figure 1, show the enhancement of the electric field (10 kV applied) at the surface of the simulated perturbations. These electric field enhancements are expected to change the local plasma attachment and E/N, altering the plasma chemistry (and therefore possible dose to the water). Preliminary optical emission spectroscopy observations, shown in Figure 2, align with previous observations of a more diffuse discharge (lower intensity), with less nitrogen plasma. This work explores the plasma characteristics of a pulsed corona discharge over a rough dielectric (water) surface.

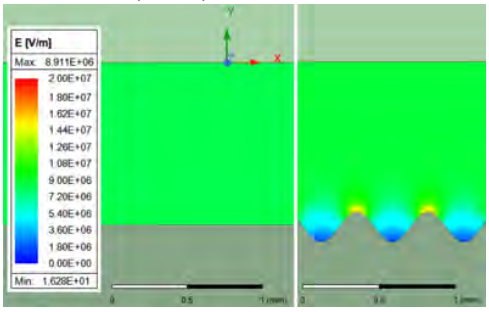

Figure 1. Enhanced electric field on a rough dielectric (water) surface, simulated in ANSYS Maxwell.

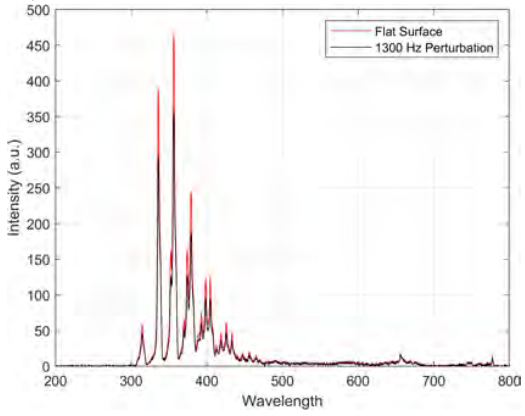

Figure 2. OES indicates a decrease in intensity of nitrogen emission for a rough surface.

Acknowledgements

This work was supported by NSF GRFP, NSF ECLIPSE Award No. 2206039, and DOE EERE Award No. DE-EE0009945.

References

[1]Walker, R. Z., & Foster, J. E. (2023). Journal of Applied Physics **133**, 093301 (2023)

Spectroscopic investigation of the time evolution of CO_2 dissociation in a nanosecond plasma-discharge.

L.M. Martini[1], C. Montesano[1], T.P.W. Salden[2,1], G. Dilecce[3,1] and P. Tosi[1,3]

[1] *Department of Physics, University of Trento, Trento, Italy*
[2] *Dept. Applied Physics, Eindhoven Univ. Techn., Eindhoven, The Netherlands*
[3] *CNR Institute for Plasma Science and Technology, Bari, Italy*

Plasma-driven conversion of major greenhouse gases (CO_2, CH_4, etc.) represents a promising way to simultaneously store renewable energy and convert the greenhouse gases into value-added compounds. Nanosecond repetitively pulsed discharges have shown high efficiency in CO_2 reduction to CO, and O_2[1, 2]. To gain further insights into the physical and chemical mechanisms of CO_2 dissociation in the first microseconds after the discharge pulse, collisional energy transfer laser-induced fluorescence (CET-LIF) and time-resolved optical emission spectroscopy have been employed to probe the evolution of the gas composition and the translational temperature, respectively.

1 Introduction

The successful and widespread use of gas discharges is due to the possibility of inducing out-of-the-equilibrium conditions. Understanding the mechanisms of plasma dissociation is necessary to improve the efficiency of the technology.

2 Experimental

CET-LIF [3] has been applied to probe the gas composition in the first microseconds of a discharge generated by a 10 ns high-voltage (HV) pulse applied between two pin electrodes at atmospheric pressure. For CET-LIF measurements, a small flow of water is added to the CO_2 gas to promote the generation of OH into the discharge. The information on the gas composition (CO_2 conversion) is derived from the analysis of the fluorescence spectra of the OH(A) state that is excited by a tunable pulsed dye laser at different delays with respect to the HV pulse. To determine the translational gas temperature, a 5 % of N_2 is admixed to the CO_2 stream, and the nitrogen's second positive system (SPS) emission is recorded and analyzed[4].

3 Results

Up to 80 ns after the breakdown, CO_2 conversion values are lower than 8 %; after 5 µs, the CO_2 dissociation is about 45%. Similarly, the translational gas temperature does not exceed 1200 K in the first 80 ns, is estimated to be around 2400 K at 3 µs, and decreases with higher delays. The progressive increase of the molecular dissociation after the breakdown suggests that the direct excitation to a dissociative state by electron impact is not the primary dissociation mechanism. On the other hand, the delayed dissociation with respect to the discharge phase indicates that the leading dissociation channel is an indirect mechanism mediated by CO_2 excitation and, most likely, with a predominant role of vibrationally-mediated processes.

References

[1] Montesano, C., Quercetti, S., Martini, L. M., Dilecce, G. & Tosi, P. The effect of different pulse patterns on the plasma reduction of CO_2 for a nanosecond discharge. *Journal of CO2 Utilization* **39**, 101157 (2020).

[2] Delikonstantis, E. *et al.* Exceeding equilibrium CO_2 conversion by plasma-assisted chemical looping. *ACS Energy Letters* **7**, 1896–1902 (2022).

[3] Martini, L. M., Gatti, N., Dilecce, G., Scotoni, M. & Tosi, P. Laser induced fluorescence in nanosecond repetitively pulsed discharges for CO_2 conversion. *Plasma Physics and Controlled Fusion* **60**, 014016 (2017).

[4] Ceppelli, M., Salden, T. P. W., Martini, L. M., Dilecce, G. & Tosi, P. Time-resolved optical emission spectroscopy in CO_2 nanosecond pulsed discharges. *Plasma Sources Science and Technology* **30**, 115010 (2021).

Propagation of radicals and carbon particles in CH_4 plasma at atmospheric pressure

A. Saito[1], Y. Hayashi[1], T. Miyazaki[2], N. Shirai[2], K. Sasaki[2]

[1] *Innovative Technology Laboratories, AGC Inc.,Yokohama, Japan*
[2] *Division of Quantum Science and Engineering, Hokkaido University, Sapporo, Japan*

The propagation of radicals and carbon particles on CH_4 decomposition with nonequilibrium atmospheric-pressure plasma was investigated using laser-induced fluorescence measurements and the Schlieren technique. The results show that CH radicals, C_2 radicals, and carbon particulates propagate towards the ground electrode independent of the gas flow. Regarding the energy efficiency, during the CH_4 decomposition and H_2 generation, the influence of plasma propagation is negligible, but the generation of carbon particles is influenced by plasma propagation. We investigated the effect of the plasma-propagation and electric fields on the energy efficiency.

1 Introduction

As a H_2 production process with low CO_2 emissions, CH_4 decomposition by the thermal plasma has been investigated [1]. Nonequilibrium plasma is also being studied to further improve energy efficiency and produce carbon particles generated simultaneously [2]. Many studies on the verification of energy efficiency and the analysis of generated carbon particles have been conducted. We investigated the propagation of CH and C_2 radicals via laser-induced fluorescence (LIF) measurements and the flow of plasma-containing carbon particles using the Schlieren technique.

2 Experimental methods

The electrode structure consisted of a pipe electrode placed horizontally on the upper part, which also served to receive CH_4, and a rod electrode on the lower part. A high AC voltage of 17 kHz and 5 kV p-p was applied to the electrode. LIF measurements were used to investigate the distribution of CH and C_2 radicals. The wavelengths of the laser introduced into the plasma were 363.7 nm for CH and 516.5 nm for C_2. The Schlieren technique was used to visualize the plasma flow.

3 Results and discussion

Figure 1 shows the experimental setup, plasma photograph, radical distribution by LIF, and Schlieren images. In Fig. 1(a), (c), (d), (g), and (h), the ground electrode is on the horizontal part, and in Fig. 1(b), (e), (f), (i), and (j), the ground electrode is on the bottom part. Fig. 1(a) and (b) show the configuration of the electrodes. Plasma photographs are shown in Fig. 1(c) and (e). The Schlieren images are shown in Fig. 1(d) and (f). In the plasma photographs and Schlieren images, although the shapes were different, both extended to the ground electrode. The distribution of C_2 radicals (Fig. 1(g) and (i)) and CH radials (Fig. 1(h) and (j)) show significant differences. However, the plasma spreads toward the ground electrode for all radicals. This is attributed to the effect of ionic wind from the high-voltage electrode to the ground electrode.

The energy efficiency was not affected by the electrode arrangement for CH_4 decomposition and H_2 generation. However, for the carbon particle generation, the setting with a high voltage applied to the bottom electrode was four times larger. This suggests that the coupling of the particle flow and electric field influences the particle growth of carbon.

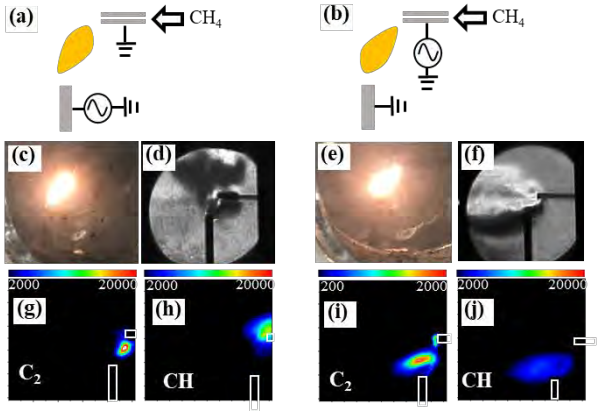

Fig. 1. Comparison of plasma appearance and radical distribution depending on electrode arrangement. (a) and (b) show the electrode setups. (c) and (e) show the photographs of the plasma. (d) and (f) are Schlieren images. (g)–(j) are the radical distributions obtained via LIF measurements. (a), (c), (d), (g), and (h) correspond to the case in which the ground electrode is on top, whereas (b), (e), (f), (i), and (j) correspond to the case wherein the ground electrode is on the bottom.

References

[1] Laurent Fulcheri et al., International Journal of Hydrogen Energy. 48.2920. (2023)
[2] Ruipeng Zhong et al., Chemical Engineering Journal. 387. 124102. (2020)

Time-dependent measurement of ion composition in a capacitively-coupled Ar/C_4F_8/O_2 power-modulated VHF plasma

H. Toyoda[1,2,3], H. Kato[1], Y. Seki[1], S. Kuboi[1] Y. Akatsuka[1] and H. Suzuki[1,2]

[1]Department of Electronics, Nagoya University, Nagoya, Japan
[2]Center for Low-temperature Plasma Sciences, Nagoya University, Nagoya, Japan
[3]National Institute of Fusion Science, Toki, Japan

Time-dependent ionic composition of a power-modulated Ar/C_4F_8/O_2 capacitively-coupled VHF plasma were investigated by mass spectrometry, focusing on influence of pulse power waveform on the ion composition. Importance of the plasma density increase accompanied with momentary increase of the electron temperature was suggested as a reason of the ion composition change.

1 Introduction

One of the most important technologies in 3D memory fabrication is high aspect ratio (HAR) reactive ion etching (RIE) of silicon dielectric films, and pulse-modulated dual-frequency capacitively-coupled plasma (DF-CCP) is commonly used. In the chemical reaction process of HAR RIE, high surface reaction probability of neutral radicals makes their transport to the hole bottom difficult. As a result, energy and composition of the irradiated ions are important as a precursor to the etching reaction on the etch front.

We have reported time dependence of ionic composition in pulse-modulated Ar/C_4F_8/O_2 DF-CCP by time-resolved mass spectrometry and have pointed out importance of time-variation of electron energy during the pulse operation [1,2]. In this study, we report influence of power modulation waveform on the ion composition, i.e., change of the power waveform from on-off to high-low.

2 Experimental apparatus

Plasma is produced by applying 40 MHz power to an RF electrode (diameter: 110 mm). Grounded electrode is placed 30 mm away from the RF electrode. Ar/C_4F_8/O_2 gases (flow rates: 34/4/2 sccm) are fed to the chamber at a total pressure of 4.0 Pa. The 40 MHz power is high (100 W)-low (50 W) modulated at a frequency of 1 kHz and a duty ratio of 50 %. Time dependence of ions in the plasma is measured by a differentially-pumped quadrupole mass spectrometer (QMS) equipped with an energy analyzer and an orifice. For the measurement of time-dependent ion composition, ion transit time in the QMS and ion energy distribution are taken into account.

3 Results and Discussion

In the previous study of on-off-modulated DF-CCP, strong time variation of the ion composition was observed[1,2]. In the present case of high-low power modulation, Ar^+ is the dominant ion immediately after the power is increased to 100 W, and after then, Ar^+ ions decreased, while $C_2F_4^+$ and $C_3F_5^+$ ions increased. The result is similar to that of the on-off pulse-modulated plasma. In this study, however, initial Ar^+ increase becomes moderate compared to that of on-off power modulation.

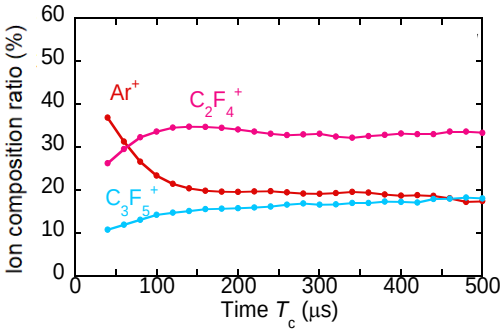

Fig. 1. Time-resolved ion composition measurement of high-low power-controlled plasma.

Measured time-dependent ion variation is considered as follows. Immediately after the power is increased, ionization rate is increased to increase the plasma density, as well as increase in high-energy component of the EEDF. Then, the high energy component of the EEDF returns close to its steady state. Meanwhile, ionization rates of Ar and C_4F_8 drastically change by the electron temperature variation. At high electron temperatures, the Ar ionization rate is relatively large compared with dissociative ionisation rate of C_4F_8. This induces Ar^+ increase immediately after increasing the VHF power. Transient time of the ion composition is probably determined by ion confinement time of the plasma, which is influenced by ion diffusion loss.

References

[1] S. Kuboi, et al, *43rd Int. Sympo. Dry Process* (Osaka, 2022) A-5.
[2] S. Kuboi et al., Jpn. J. Applied Phys., to be published.

Synergetic effect of carbon monoxide (CO) and cold atmospheric Helium/CO_2 MHz and kHz plasmas on bacterial disinfection for biomedical applications

I. Orel[1], E. Mestre[1], D. Henze[2], L. Chauvet[2], S. Burhenn[2], J. Golda[2], S.Dozias[1], F. Brulé-Morabito[3], T.Gibert[1] and C.Douat[1]

[1] *GREMI UMR7344 CNRS/Université d'Orléans, Orléans, France*
[2] *Experimental Physics II, Ruhr-Universität Bochum, 44801 Bochum, Germany*
[3] *Centre de Biophysique Moléculaire (CBM), CNRS UPR 4301, 45071 Orléans, France*

The present work reports CO production rates in Helium/CO_2 non-equilibrium atmospheric-pressure plasmas from two plasma sources: a MHz jet of the COST reactor and a kHz-jet of an in-house made external electrodes DBD reactor. It has been observed that both plasma sources can produce CO in tunable amounts that are comparable with those used in clinical application for CO inhalation. In particular, at 0.3% of CO_2, kHz-jet demonstrates more efficient CO_2 to CO conversion than MHz jet at the same specific deposited energy. The antibacterial efficiency of CO-containing plasmas was studied on *Escherichia coli* at various plasma parameters.

1 Introduction

Non-equilibrium atmospheric-pressure plasmas had shown antibacterial, vasodilatory and antiproliferative effects [1] that makes them attractive for numerous applications including plasma medicine. CO is a stable signaling gasotransmitter specie that plays anti-inflammatory role and can be produced by CO_2 dissociation in plasma [2]. In spite of the fact that both, plasma and CO are known for beneficial effect in medical field, their simultaneous action is yet to be studied.

The aim of this work is twofold. Firstly, to compare the CO production between a sinusoidal MHz discharge provided by COST plasma jet [3], and a kHz pulsed discharge provided by a coplanar-coaxial DBD plasma jet (kHz-jet), both fed with He/CO_2. Secondly, to evaluate synergetic plasma-CO bactericide effect on the example of *E. coli* at various plasma parameters.

2 Results

Fig. 1 shows that the COST jet and the kHz-jet were capable to produce from a couple of ppm to respectively hundreds and thousands of ppm of CO, which is the range used in clinical application with CO inhalation. Thus, both reactors are CO-safe.

In log-log scale, the concentration of CO produced by plasma as a function of specific energy input, SEI, follows a linear trend. This result lead to the conclusion that SEI is a scaling parameter for CO_2 conversion. At 0.3% CO_2 for the same SEI, the COST jet is less efficient in terms of CO_2 conversion compared to the kHz-jet.

K-12 strain of *E. coli* was used for *in vitro* plasma treatment on semi-solid medium. Petri dishes with uniform bacterial layer were prepared by inundation method, treated immediately and left overnight for incubation at 37 °C. Inhibition of bacterial proliferation was studied as a function of CO concentration for both plasma sources at fixed SEI.

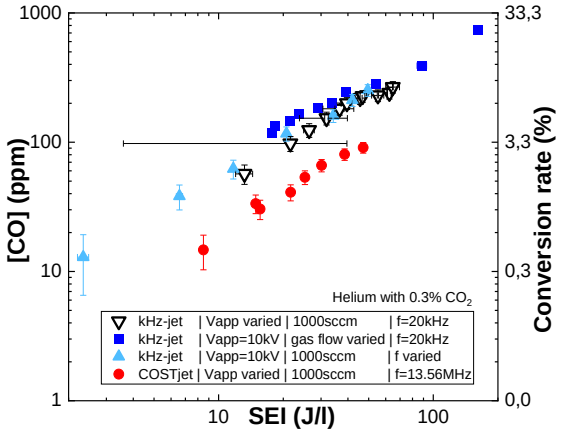

Fig. 1. CO concentration (left) and conversion rate of CO_2 into CO (right) in the COST jet and in the kHz-jet as a function of specific energy input (SEI) at 0.3% of CO_2.

3 Acknowledgements

The authors thank the French Research Agency, ANR, (MediCO-Plasma | ANR-21-CE19-0005) and the French program PHC Procope (48122NF) for research funding and the German program DAAD for funding collaboration's travel expenses. Bacterial material was acquired as a kind courtesy of FBM. EM thanks the MESRI for founding her PhD thesis.

References

[1] E. Carbone, C. Douat, Plasma Med, **8**:1 (2018).
[2] C. Douat, P. Escot Bocanegra, S. Dozias, É. Robert, and R. Motterlini, Plasma Process Polym **18:**2100069 (2021).
[3] J. Golda et al., J. Phys. D: Appl. Phys., **49**:8, (2016).

Formation of O and H radicals in an atmospheric-pressure nanosecond pulsed discharge in helium with admixtures of water vapour

A. Brisset[1,3], M. Bieniek[2,4], L. Invernizzi[1,5], J. Walsh[1,2], M. Hasan[2], E. Wagenaars[1]

[1] *York Plasma Institute, School of Physics, Engineering and Technology, University of York, York, UK*
[2] *Department of Electrical Engineering and Electronics, University of Liverpool, Liverpool, UK*
[3] *EM2C, CNRS, CentraleSupélec, Université Paris Saclay, Gif-sur-Yvette, France*
[4] *The University of Antwerp, Department of Chemistry, Campus Drie Eiken, Wilrijk, Belgium*
[5] *Laboratoire des Sciences des Procédés et des Matériaux, LSPM, CNRS, Université Sorbonne Paris Nord, Villetaneuse, France*

Atmospheric pressure plasmas (APPs) have applications in areas such as surface processing, assisted combustion, and plasma medicine. O and H are highly reactive species in these plasmas and are key precursors of long-living species such as NOx, O_3 and H_2O_2 which are used in applications of APPs. Their quantification is therefore necessary to unravel the chemical pathways in pulsed APPs. In this work, the formation of O and H radicals in a pulsed pin-to-pin discharge in He with water vapour admixtures was studied by experiment (TALIF) and modelling (1D fluid). It was found that the O and H densities peak about 1 µs after the end of the 90 ns HV pulse. They remain nearly constant over 10 µs before decaying. Modelling explains the reaction pathways that lead to this behaviour: the built up of O and H densities continues after electron-impact dissociation processes during the HV pulse, with significant additional afterglow processes contributing to the formation of O and H, well into the afterglow.

1 Introduction

Plasmas that produce O-, H- and N-species are extensively studied for applications. For example, water containing plasmas are studied for the production of reactive species such as OH, H_2O_2, HO_2. Atomic oxygen and hydrogen radicals play a crucial role in these plasmas. Understanding the kinetics of O and H is the aim of this work.

2 Methodology

The plasma has a pin-to-pin electrode geometry with a gap of 2.2 mm. A discharge in Helium with a water vapour content of 0.1% – 0.25% is created through a positive high-voltage nanosecond pulse to one of the pins. The pulse has a voltage of about 2 kV, 35 ns rise time (10-90%) and 90 ns duration FWHM. The energy dissipated in the discharge is 90 µJ and the repetition rate is 5 kHz.

Two-photon Absorption Laser Induced Fluorescence (TALIF) is used to measure the densities of O and H radicals. Details of this method can be found in [1]. The 1D plasma fluid model used is based on a system of differential equations: continuity of the flux density of electrons, electron energy, ions, and neutral species, and Poisson's equation. Full details can be found in [1]

3 Results and discussion

The experimental results as shown in figure 1. The most striking feature is that for both admixtures the main production of O and H occurs after the voltage pulse has finished. From the modelling, it is clear that there is a distinct change in reaction mechanisms during the discharge cycle. During the voltage pulse O is predominantly produced through electron-impact dissociation of O_2. For H, the dominant mechanism is electron-impact dissociation of H_2O. However, most of the O and H radicals are produced in the early afterglow (up to 1 µs) through recombination processes. The conclusion is that not only the discharge itself, but also the (early) afterglow of pulsed discharges need to be considered when studying O and H-based plasma chemistries.

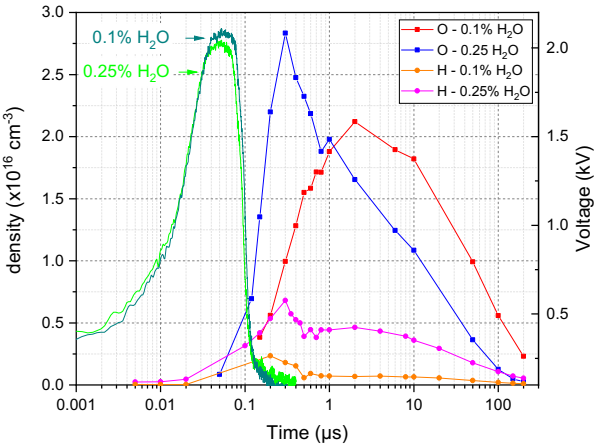

Fig. 1: Temporal evolution of O and H densities measured with TALIF for 0.1% and 0.25% water admixture.

References

[1] A. Brisset, *et al.* Plasma Sources Sci. Technol. submitted (2023).

Plasma-treated water inactivation mechanisms of *Escherichia coli*

R. Agus[1], F. Avino[1] and I. Furno[1]

[1] *EPFL - (Swiss Plasma Center), École polytechnique fédérale de Lausanne, CH-1015 Lausanne, Switzerland*

Despite bactericidal properties of plasma treated liquids have been widely reported in the literature, the bacteria inactivation mechanisms are still subject of debate [1,2]. The understanding of microorganism's inactivation pathways by **Plasma Treated Water** (PTW) would bring various benefits to the plasma medicine community: it would allow to tune the reactors in order to enhance the production of specific Reactive Oxygen and Nitrogen Species (RONS) [3], and address the plasma resistance issue. We have developed and characterized an in-house PTW reactor, optimized for disinfection purposes. The design of the reactor allows modulating the water flow and tuning the samples chemistry. PTW samples have been tested on E. coli and the **log-reduction curve** has been measured. The investigation of inactivation mechanisms is on-going by coupling three diagnostics: Scanning Electron Microscopy (**SEM**), **flow cytometry** and **single cell microscopy** (Section 1.2).

1 Experimental setup

PTW is produced by exposing ultra-pure deionized water to cold atmospheric plasma, generated by a surface dielectric barrier discharge (SDBD) in ambient air. The discharge power, measured as the area of the Lissajous figure, corresponds to 38 W.

The log-reduction curve of non-pathogenic *E. coli* (K-12 strain MG1655) is measured by Colony Forming Unit counting experiments by exposing the bacteria culture to different PTW samples for 10, 30 and 50 minutes.

Single cell microfluidic experiments are performed on an inverted Nikon Eclipse Ti-2 microscope by depositing cells on a specific PDMS microchip designed for bacteria time-lapse microscopy. [4] Flow Cytometry experiments are performed by means of apposite staining targeting bacteria integrity and metabolism.

1.1 Water chemical characterization

Chemical characterization of PTW samples is performed for different water treatment times by measuring the concentrations of hydrogen peroxide, nitrite ions and nitrate ions through colorimetric methods.

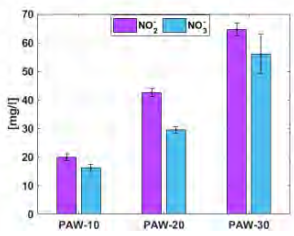

Figure 1. Example of PTW chemical characterization: nitrite and nitrate ions concentration measured for different treatment times (10, 20, 30 minutes).

pH, electrical conductivity (EC) oxidation-reduction potential (ORP) are also measured.

1.2 Bacteria treatments and investigation of inactivation mechanisms

The efficacy of PTW treatments can vary from about 1-log reduction up to 6-log reduction depending on the sample chemistry and treatment time.

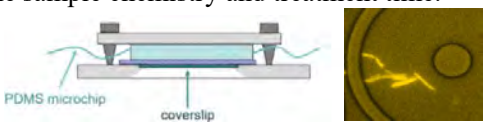

Figure 2. (a) Schematic of the microfluidic device for single cell time lapse microscopy. (b) Example of fluorescent acquisition of *E. coli*.

To shed light on the inactivation mechanisms, three different diagnostics are coupled together for the first time: single-cell phase contrast and fluorescence time-lapse microscopy [4] for the observation of the real time effect of PTW on bacterial size and duplication rate, SEM for the identification of outer bacteria membrane damage and morphology modification, and flow cytometry for the discrimination of specific cell death pathways through specific fluorescent dyes. In light of the above-mentioned measurements, we propose a mechanism for the bacteria inactivation by PTW, which will be a key factor for the design and optimization of future disinfection applications.

References

[1] Zhou R. et al., Journal of Physics D: Applied Physics, (2020), **53**, 10.1088/1361-6463/ab81cf

[2] Mai-Prochnow A., Zhou R., et al., npj Biofilms and Microbiomes, (2021), **7**, pag. 1-12, 10.1038/s41522-020-00180-6

[3] Machala Z. et al, Journal of Physics D: Applied Physics, (2019), **52**, 10.1088/1361-6463/aae807

[4] Dhar N. et al., Methods in Molecular Biology, Humana Press Springer, (2015), **241**, 10.1007/978-1-4939-2450-9_14

E-FISH data analysis for electric field measurements on single channel streamers

A.A.A. Limburg, I.D. van de Haar, J.H. Laarman, Y. Guo and S. Nijdam

Dept. Applied Physics, Eindhoven Univ. Techn., Eindhoven, The Netherlands

Electric field induced second harmonic generation (E-FISH) is a recently introduced technique to obtain the electric field of any type of plasma. As a result of the simply obtained signal and the possibility to obtain the electric field in areas with little to no light emission, the technique is embraced by the plasma community and widely used. However, in the translation of the E-FISH signal to an electric field distribution, several mistakes are often made related to the laser beam properties and the shape of the electric field which can result in faulty conclusions. This research presents a significant improvement in the E-FISH data analysis by including all phase variations. Finally, E-FISH is applied to a repetitive single channel streamer in ~100 mbar air to obtain the electric field distribution of a streamer. All in all, this enables reliable application of E-FISH to cylindrically symmetric plasmas.

1 Introduction

One of the most important parameters of a plasma is its electric field. It defines quantities such as particle transport, gas temperature, electron energy distribution function and creation of energetic particles. Recently, a promising laser-based optical diagnostic technique is introduced for electric field measurements called Electric Field Induced Second-Harmonic generation (E-FISH). In this technique, a pulsed, focused laser beam interacts non-linearly with the ambient electric field in a medium, which results in frequency doubled light. The intensity of these second harmonics scales quadratically with the magnitude of the electric field. In this way, a polarization resolved electric field distribution can be obtained for (almost) any kind of plasma.

In literature, the implementation of E-FISH and interpretation of the results is described as straight-forward and easy. However, omission of the influence of the properties of the laser beam and the electric field shape in E-FISH data analysis might have led to incorrect conclusions in previous work. [1]

The goal of this research is to improve the data analysis to be able to reliably determine the electric field distribution of a repetitive and cylindrically symmetric single channel streamer using E-FISH.

2 Methods

A deconvolution method is used to translate an E-FISH signal to an electric field distribution for a cylindrically symmetric plasma. This method includes the Gouy phase shift caused by focusing the laser beam and the wavevector mismatch induced phase shift. Firstly, an E-FISH signal is obtained experimentally using a focused Gaussian beam. Secondly, a piecewise polynomial fit is made through the E-FISH data. Finally, the deconvolution model is used to obtain an electric field distribution. To test the method, this distribution is compared to the electric field distribution obtained in COMSOL Multiphysics for the same electric field configuration. Ultimately, the electric field distribution of a repetitive single channel streamer in ~100 mbar air is obtained and compared to field simulations and measurements from [2] on the same streamer.

3 Results

In Fig. 1, it is shown that a simulated input electric field, similar in shape to the field of a single channel streamer, is in great agreement with the restored electric field using the developed deconvolution model.

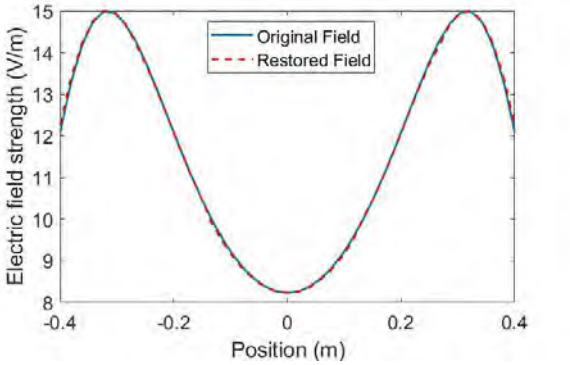

Fig. 1: Input and restored radial electric field distribution.

4 Conclusion

This newly developed method opens up the possibility of a trustworthy analysis of E-FISH data, obtained with a focused Gaussian beam, to determine the electric field of cylindrically symmetric plasmas.

References

[1] Chng et al.. Electric field measurements in plasmas: how focusing strongly distorts the E-FISH signal. PSST, 29(12):125002 (2020).

[2] Dijcks et al. High-resolution electric field and temperature distributions in positive streamers. Front. Phys. 1120284 (2023)

Collisional Radiative Model as plasma diagnostic for Hall-effect thrusters

A. Leduc[1], T. Ben Slimane[1], L. Schiesko[1], A. Bourdon[1], and P. Chabert[1]

[1] *Laboratoire de Physique des Plasmas (LPP), CNRS, Sorbonne Université, École Polytechnique, Institut Polytechnique de Paris, Palaiseau, France*

Hall Effect Thrusters (HETs) are increasingly used for space propulsion [1]. Even if the HETs operation is well understood, HETs are still the subject of many researches for: new geometry, new fuel, optimization, or instabilities studies... For the plasma characterization, in this work, the choice is made to use a non-invasive method: the analysis will use the light emitted by the plasma atoms using a spectrometer and a Collisional Radiative Model (CRM) in order to derive the physical parameters out of the spectra. The exploration of the plasma parameters allows the CRM to reproduce the optical emission spectra and to deduce the values of density and electron temperature. It was thus possible to study the variations of plasma parameters in the thruster plume, but also to explore the thruster channel plasma.

1 General

Hall Effect Thrusters (HETs) are increasingly used for space propulsion [1]. For the study of the thruster, the plasma characterization is essential, and for this reason, in this work, optical emission spectroscopy measurements, coupled to a Collisional Radiative Model (CRM) have been developed.

1.1 Collisional Radiative Model

A CRM aims to produce an optical emission spectrum from the plasma parameters (electron density and temperature, gas density and temperature, and optical thickness) [2]. In this work, we have developed a CRM for Xe plasmas, with a focus on the atomic radiative transitions (putting aside the ionic ones).

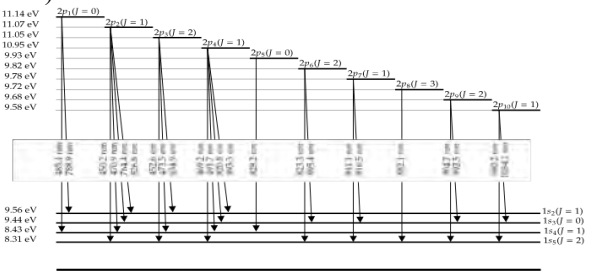

The CRM is a 0D model and therefore does not consider transport or diffusion of species. It includes 15 atomic levels (14 excited levels and the fundamental level) and the 23 associated transitions (as illustrated on the first figure). To populate and depopulate the levels, it considers the effective cross sections of excitation and radiative decay by electronic impact [3]. The total radiative decay is corrected for radiation trapping and absorption based on the Mewe approximation [4].

1.2 Plasma Parameters Values

After the CRM development and validation, it has been used to produce optical emission spectra. The CRM associates an optical emission spectrum to each set of plasma parameters.

Using an optical fiber and a spectrometer (with a HET Xe plasma, at LPP), it is possible to acquire optical emission spectra. By fitting the calculated spectra to the experimental ones, it is possible to deduce the plasma parameters. By reproducing optical emission spectra at different positions, the parameters spatial variations can be studied. Analysis are performed on the plasma plume, which corresponds to the thruster's exhaust, one on the plasma plume axis, the other on the vertical plane. The OES with the CRM gave some results, coherent with other estimations of the plasma parameters (typically from PIC simulation).

By targeting the thruster channel with another optical setup, a similar study can be made. The CRM highlights an electron temperature above 20eV and a significant gradient between the inner and outer walls of the channel (highlighted on the figure below).

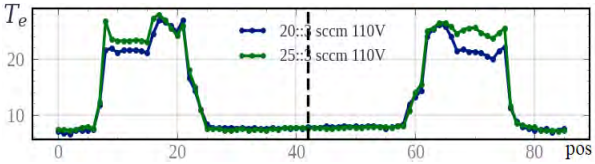

References

[1] O'Reilly, D. & al., "Electric Propulsion Methods for Small Satellites: A Review," Aerospace, Vol. 8, No. 1, (2021)

[2] Karabadzhak, G. F. & al., Passive optical diagnostic of Xe propelled Hall thrusters. II. Collisional radiative model. Journal of applied physics, 99(11), (2006)

[3] BSR database,", Jan. 2022. https://fr.lxcat. net

[4] Mewe, R., "Relative intensity of helium spectral lines as a function of electron temperature and density," British Journal of Applied Physics, Vol. 18, No. 1, p. 107 (1967)

Determining the dependency of radical density on position by dual thermocouple radical probe

A. Herrmann[1], P. Krebaum[2], S. Bera[1], M.N. Tsampas[1] and M.C.M. van de Sanden[1]

[1] *Dutch Institute for Fundamental Energy Research (DIFFER), Eindhoven, The Netherlands*
[2] *Fontys Hogeschoolen Technische Natuurkunde, Eindhoven, The Netherlands*

Radical probes help determining radical densities through monitoring temperature changes of a catalytic surface on which radical recombination creates heat. Dual probe systems have been suggested to eliminate issues with distinguishing recombination heating from other interactions with the systems causing heating or cooling. We describe the use of a dual radical probe in a RF inductively coupled flow reactor in N_2 gas, observing the impact of radiative, convective and conductive heat fluxes on the probe's temperature readings as well as characterizing the change in radical density in the remote part of a Nitrogen plasma.

The density of radicals is an important factor determining the reaction rates in plasma reactors. It is desirable to quantify the radical density and flux to obtain a complete description and improvement of processes in plasma reactors. One option for measuring radical densities are radical probes, which monitor the temperature of a catalytic surface on which radicals exothermically recombine. The radical density can be deduced from the heat flux of these radical recombinations using a few assumptions on recombination rate, -heat and heat fluxes from other sources [1].

According to Quermi et al.[2], adding an identical reference without catalytic surface can reduce uncertainty from assumptions on heating and cooling mechanisms. We, however, see that thermal fluxes impact the measuring result.

We analyse the impact of conductive, convective and radiation heat flows on the measured temperatures and estimate the change in radical density with distance from the afterglow in a RF inductively coupled flow reactor in N_2 gas. A schematic of the setup is shown in Figure 1. The probe consisting of two thermocouples is mounted through an adjustable feedthrough, allowing for measurements at differing distance from the plasma glow. Copper is sputtered on the tip of one thermocouple as catalytic surface for Nitrogen recombination. The temperature of the glass tube is simultaneously monitored with an IR camera to monitor the impact of radiative heat on the measurements. The bottom of Figure 1 shows the temperature difference between the thermocouples with distance from the coil measured at a pressure of 76 Pa and flow rate of 3 sccm.

We observe the probe's lifetime to be roughly 8h. Radical densities in the visible glow region are in the range of 10^{19} to 10^{20} m^{-3}. Monitoring of the glass tube temperature shows that heat flux from radiation affects the temperature measurements and needs to be accounted for in in the evaluation.

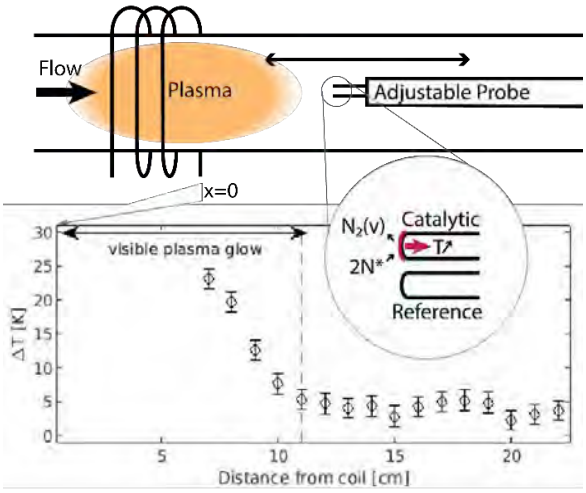

Figure 1 Top: Schematic of the setup: Probe consisting of two thermocouples (reference and catalytic) can be adjusted in position with respect to the plasma, Bottom: measured data of temperature difference between the reference and Catalyst-coated thermocouple

Acknowledgements

This project is part of the European project ORACLE, which has received funding from the European Union's Horizon 2020 Research and Innovation Programme under grant agreement No 101022738.

References

[1] Mozetic, M., Vesel, A., Cvelbar, U. et al. An Iron Catalytic Probe for Determination of the O-atom Density in an Ar/O2 Afterglow. Plasma Chem Plasma Process 26, 103–117 (2006).

[2] Qerimi, D., Shchelkanov, I., Panici, G., Jain, A., Wagner, J., Ruzic, D. (2021). Radical probe system for in situ measurements of radical densities of hydrogen, oxygen, and nitrogen. Journal of Vacuum Science & Technology A. 39. 023003.

Coupled reactive-flow simulation of plasma jets

D. Gonçalves[1,2], S. Pasquiers[2], J. Santos Sousa[2], M. Lino da Silva[1], L. L. Alves[1]

[1] *Instituto de Plasmas e Fusão Nuclear, Instituto Superior Técnico, Universidade de Lisboa, Lisboa, Portugal*
[2] *Université Paris-Saclay, CNRS, Laboratoire de Physique des Gaz et des Plasmas, Orsay, France*

In this work we simulate plasma jets using a computational fluid dynamic model. This model solves the 2D axisymmetric compressible reactive Navier-Stokes equations with free-electrons at a non-equilibrium temperature, including kinetic source terms.
As a test case, we simulate an atmospheric-pressure co-axial plasma jet, consisting of a 1slm central argon jet, shielded by a 3slm annular co-flow of N_2-O_2. The interaction of the flows is described by an Ar-N_2-O_2 reactive kinetic scheme. The electrons are excited by applying an external electric field (~500 Td, 20KHz, 1μs), representing the ionization wave responsible for electron temperatures of eVs and excited species densities comparable with measurements, e.g. [Ar($1s_5$)] ~ 10^{13}cm^{-3}.

Plasma jets can be produced by repetitive ionization waves propagating in a jet flow. The modelling of plasma jets is usually focused on the ionization wave. This complex task is usually simplified by considering a static flow model [1], which does not account for synergistic plasma-flow effects, e.g. acoustic waves, flow instabilities and fast-heating. Also, advection (bulk transport) and dissipation (viscosity and diffusion) over multiple pulses can modify the spatiotemporal distribution of species, which in turn changes the initial gas mixture. Describing these interactions requires a high-fidelity modelling of the flow, which is done here using a modified version of the code SPARK [2].

Accordingly, we simulate a multi-species flow with a simplified discharge model. The discharge model consists of an effective electric field describing the electron energy deposition by the ionization wave. Advective-diffusive-reactive processes are calculated according to the 2D-axisymmetric compressible Navier-Stokes equations with reactive processes defined by a kinetic scheme. The model further includes the electron energy balance equation, that allows for a non-equilibrium two temperature description, for the electrons and the gas.

The code SPARK is preconditioned to simulate subsonic flows. Furthermore, we include Strang splitting to describe fast (discharge) and slow (transport) processes. Other adaptations include code parallelization and a low-dissipation flux model.

As a test case we simulate a co-axial plasma jet composed by a 1slm central argon jet, shielded by a 3slm annular co-flow of N_2-O_2. An external electric field pulse (~500 Td, 20KHz, 1μs) excites electrons to temperatures of eVs, which in turn excite heavy species to densities comparable to measurements, e.g. [Ar($1s_5$)] ~ 10^{13}cm^{-3}[3], see Fig 1. Subproducts, e.g. O_3, are formed mainly at the boundary of the jet with the co-flow, with densities increasing over multiple pulses.

This modelling strategy includes electrons and allows to model the plasma and the jet flow over a wide range of spatiotemporal scales (ps to s, μm to cm). Adopting the reactive compressible Navier-Stokes equations accounts for other processes such as (fast) gas-heating, flow-instabilities and acoustic waves.

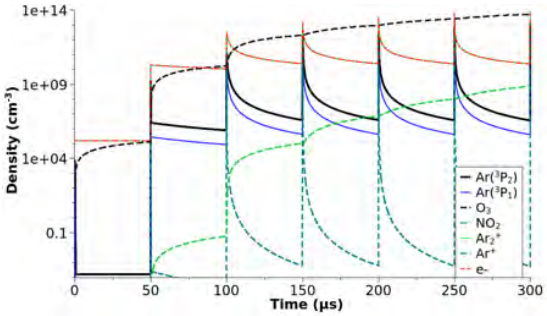

Fig. 1. Temporal evolution of the density of different species over multiple applied pulses, for one cell at the center of the plasma jet.

Acknowledgement
Work supported by the Portuguese FCT through projects UIDB/50010/2020 & UIDP/50010/2020, and grant PD/BD/142972/2018 (PD-F APPLAuSE).

References

[1] P. Viegas *et al.*, Plasma Sources Sci. Technol. **31** 053001 (2022)
[2] B. Lopez and M. Lino da Silva, 46th AIAA Thermophysics Conference, 4025 (2016)
[3] D. Gonçalves *et al.*, Ar($1s_5$) density modulation by N_2-O_2 shielding of an atmospheric pressure argon plasma jet, ICPIG XXXV, The Netherlands (2023)

Quantitative modeling of streamer discharge branching in air and experimental validation

Z. Wang[1,3], S. Dijcks[2], Y. Guo[2], M.van der Leegte[2], A. Sun[3], U. Ebert[1,2], S. Nijdam[2] and J. Teunissen[1]

[1] *Centrum Wiskunde & Informatica (CWI), Amsterdam, The Netherlands*
[2] *Eindhoven University of Technology, Eindhoven, The Netherlands*
[3] *Xi'an Jiaotong University, Xi'an, 710049, China*

Streamer discharges are the primary mode of electric breakdown of air in lightning and high voltage technology. Streamer channels branch many times, which determines the developing tree-like discharge structure. We simulate branching of positive streamers in air using a 3D fluid model with stochastic photoionization. The distributions of branching angles and branching locations agree quantitatively with dedicated experiments. The simulated branching is remarkably sensitive to the photoionization coefficients, which confirms the validity of the classical photoionization model.

1 Introduction

Streamer discharges are the first stage of electric breakdown of air (or of other gases) when suddenly exposed to high electric fields. As an integral part of streamer dynamics, branching could be found in both natural and experimental environments [1]. To understand the mechanism of branching and to predict multi-streamer behavior by macroscopic breakdown models, streamer branching needs to be characterized quantitatively.

2 Simulation model and condition

We use a 3D drift-diffusion-reaction fluid model in which a Monte-Carlo photoionization model is implemented. Electron transport coefficients are assumed to be functions of the local electric field, and they are computed from electron-neutral cross sections using BOSIG+. Ions are assumed to be immobile. For photoionization, a Monte-Carlo version of Zheleznyak's model with discrete photons. The simulations and dedicated experiments are performed in synthetic air (80% N_2, 20% O_2, no humidity) at 233 mbar and 300 K, under applied voltages of 15 kV, 17 kV and 19 kV. More detailed information can be found in [2].

For each applied voltage 60 simulations and 128 experiments were performed, and we quantitatively compared the results based on the morphorlogy, the distribution of branching angle and first branching location. The sensitivity of simulated branching behavior to the photoionization coefficient ξ of Zhelenyak's model is also tested.

3 Results

We have found quantitative agreement between simulations and experiments of positive streamer branching in air, from which we draw three main conclusions: First, we have demonstrated that photoionization is the main mechanism that triggered the branching observed in our cases, as this was the only source of stochastic fluctuations in the simulations. Second, our comparison is one of the first sensitive tests for Zheleznyak's photoionization model, since the branching probability was shown to be very sensitive to the photoionization coefficients, in contrast to other streamer properties like velocity. Third, the presented validation of the model opens the opportunity to computationally study streamer branching.

References

[1] Nijdam, S., Teunissen, J. & Ebert, U. The physics of streamer discharge phenomena. *Plasma Sources Science and Technology* **29**, 103001 (2020).

[2] Wang, Z. *et al.* Quantitative prediction of streamer discharge branching in air (2022). URL `https://arxiv.org/abs/2208.07279`.

Assessment of time-locality assumptions on the modelling of nanosecond-pulsed discharges

T. C. Dias, V. Guerra

Instituto de Plasmas e Fusão Nuclear, Instituto Superior Técnico, Universidade de Lisboa, Portugal

This work analyzes the impact of the local-field and local-energy approximations (LFA and LEA) in the modelling of the electron kinetics. These approximations are compared with an accurate time-dependent Monte Carlo solution. It is shown that their validity is highly dependent on the electric-field pulse, pressure and background gas, LFA failing dramatically at lower pressures.

The interest in nanosecond-pulsed discharges (NPD) has been growing quickly due to their remarkable non-equilibrium properties. However, their potential comes together with great complexity and a detailed study of the fundamental processes in the discharge is necessary to find the most efficient configuration for a determined application. NPD are characterized by very high reduced electric fields, *E/N* (~1000 Td), with rising times on the nanosecond timescale, which turns their modelling deeply challenging, specially in what regards the electron kinetics and their coupling with the heavy species.

The electron kinetics in gas discharges is described by the electron Boltzmann equation (EBE) and is often solved following one of two assumptions: the local-field approximation (LFA), also known as the quasi-stationary approximation, which identifies the solution of the EBE with the steady-state calculation assuming locality in space and time, being satisfactory when the electron energy relaxation is sufficiently fast; and the local-energy approximation (LEA), where the rate-coefficients and the electron power distribution along the different collisional channels depend on the local value of the electron mean energy. In the latter the EBE is typically solved for a wide range of *E/N* in steady-state conditions and, then the results are converted into a lookup table as a function of the electron mean energy. Moreover, an additional equation for the electron mean energy is included, using the input power from the electric field and the power losses obtained from the lookup table.

In this work we focus on time-locality and evaluate the impact of the LFA and LEA assumptions on the temporal evolution of the electron kinetics in a NPD. We use the electron kinetics Monte Carlo solver LoKI-MC [1]. The initial version of the code solves only configurations with homogeneous DC electric fields. Here, we generalize the formulation to time-dependent electric fields to obtain an accurate solution in a nanosecond pulse. Then, this solution is compared against the LFA and LEA, in various pulses, pressures and background gases.

Figure 1 shows a comparison of the electron mean energy and ionization coefficient for an electric-field pulse in air at 10 Torr, using the time-dependent and the LFA approaches. The results underline the importance of comparing the electron energy relaxation time with the characteristic times of the pulse before using the LFA. The LEA succeeds significantly more due to the presence of the "memory" effect introduced by the additional equation for the electron energy, as it will be shown in the conference.

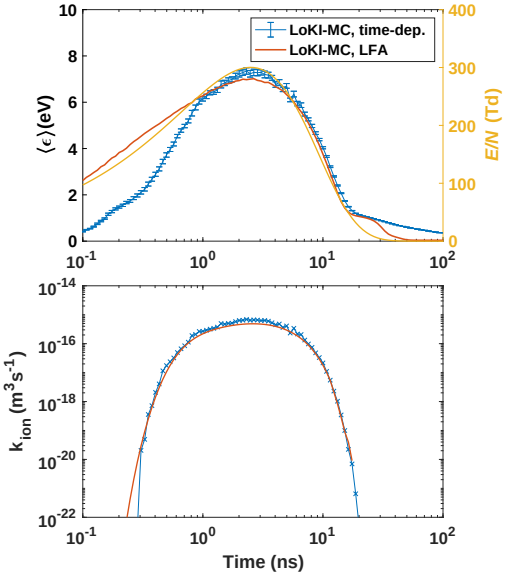

Figure 1: Comparison between time-dependent and LFA solutions for an electric-field pulse in air at 10 Torr.

Acknowledgements

This work was supported by the Portuguese FCT - Fundação para a Ciência e a Tecnologia, under projects PTDC/FISPLA/1616/2021, UIDB/50010/2020, UIDP/50010/2020 and grant PD/BD/150414/2019, and ESA under project I-2021-03399.

References

[1] Dias, T. C., Tejero-del-Caz, A., Alves, L. L., Guerra, V. The LisbOn KInetics Monte Carlo solver. Computer Physics Communications **282**, 108554 (2023).

Fluorescence (TALIF) Measurement of Ground State Atomic Nitrogen Concentration in an Argon RF Plasma Pencil measured using Picosecond Laser

W. Khan, P. Dvořák, N. Bolouki and M. Mrkvičková

Dept. of Physical Electronics, Faculty of Science, Masaryk University, Brno, Czech Republic

The average density of ground-state atomic nitrogen (N) and its spatial distribution in a plasma jet plume was analyzed using the picosecond two-photon absorption laser-induced fluorescence (TALIF) method. The plasma jet is a device used as a source of reactive species (H, O, OH, N, NO), having many applications in nitriding metal and surface modification. In our case, the jet is driven at radio frequency (RF) voltage and ignited in argon at atmospheric pressure. The measurements were performed in pure argon and argon with an admixture of nitrogen. In the case of Ar with nitrogen admixture, most atomic nitrogen production is found near the capillary, where the plasma starts blowing out into the atmosphere. On the contrary, in pure argon discharge, the absolute concentration increases with distance from the capillary up to 15 mm and then decreases up to the end of the plume. The average concentration of atomic nitrogen in pure argon discharge is estimated to be 10^{15} cm $^{-3}$. The average concentrations with an admixture of nitrogen gas 20 and 80 sccm are estimated to be 10^{16} cm ^{3}. The results show that the plasma jet has a high ability to generate atomic nitrogen.

A plasma pencil is an atmospheric plasma jet driven at rf (13.56 MHz) voltage. It is a capacitively coupled discharge with a silica capillary (outer and inner diameters are 4.3 mm and 2 mm, respectively) acting as a thin dielectric barrier that separates the powered electrode from the plasma. The plasma was ignited inside a silica capillary in Ar (3.20 slm) and Ar/N_2 (3.20 slm/20, 80 sccm) admixture, as shown in Fig. 1.

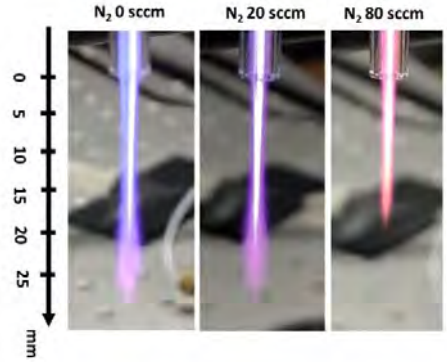

Fig. 1 Plasma plume in pure Ar and Ar/N_2 admixture.

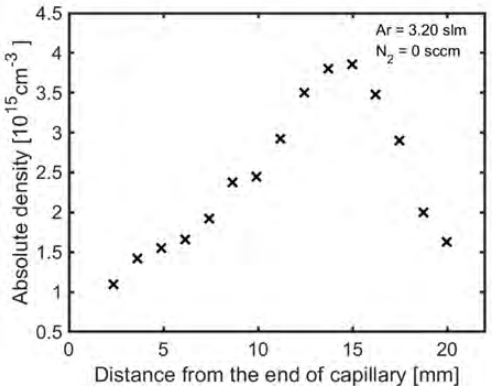

Fig.2. Spatial profile of average N concentration in Ar discharge.

The spatial distribution of N concentration in the plume of rf-jet was calculated from the TALIF measurement. The TALIF signal of N was calibrated by the TALIF measurement of Kr, which has the nearest excitation level. It is a well-known method reported in [1] and in many papers for concentration measurement of atomic species.

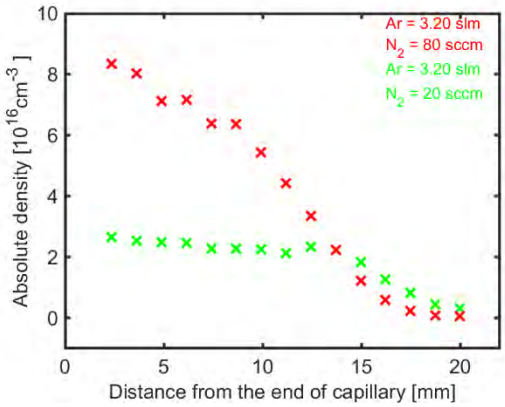

Fig. 3. Spatial profile of average N concentration in Ar/N_2.

The spatial concentration profiles of N in an Ar and Ar/N_2 admixture plasma discharge are shown in Fig. 2 and 3, respectively. In Ar discharge, the maxima of N concentration is found at 15 mm from the capillary. In the case of N_2 admixture, the maximum N is located near the capillary. In both cases, the RF plasma jet is a promising candidate for N production and crucial for nitride material and for treating organic polymers' surfaces.

Acknowledgment:

This research has been supported by the Czech Science Foundation under Contract 23-05974K and by the Project LM2018097 funded by the Ministry of Education, Youth and Sports of the Czech Republic.

References [1]

Niemi, K., Schulz-Von Der Gathen, V. and Döbele, H.F: Journal of Physics D: Applied Physics, **34** 2330 (2001).

Comparison between THz absorption spectroscopy and ps-TALIF measurements of atomic oxygen densities

J. R. Wubs[1], L. Invernizzi[2], K. Gazeli[2], G. Lombardi[2], U. Macherius[1], K.-D. Weltmann[1], and J. H. van Helden[1]

[1] *Leibniz Institute for Plasma Science and Technology (INP), Greifswald, Germany*
[2] *Laboratoire des Sciences des Procédés et des Matériaux (LSPM), CNRS, Université Sorbonne Paris Nord, Villetaneuse, France*

Atomic oxygen densities measured with THz absorption spectroscopy are compared to those obtained from ps-TALIF measurements on the same low-pressure CCRF oxygen discharge. The results are in very good agreement, and it can be concluded that THz absorption spectroscopy is an accurate and reliable diagnostic for determining atomic oxygen densities in plasmas.

Terahertz (THz) absorption spectroscopy with quantum cascade lasers (QCLs) has recently been developed and implemented as a novel diagnostic technique for investigating atomic oxygen densities in plasmas [1]. It is based on the detection of the $^3P_1 \leftarrow {}^3P_2$ fine structure transition at approximately 4.75 THz ($\approx 158\,\mathrm{cm}^{-1}$), using a tunable QCL as THz source [2] and a bolometer for detection. A typical example of a measured absorption profile is shown in figure 1. THz absorption spectroscopy allows for direct measurements (i.e. no calibration procedure required) of absolute ground-state atomic oxygen densities. Its accuracy depends almost exclusively on the the accuracy to which the transition line strength is known. Furthermore, the high spectral resolution and narrow laser linewidth (below 10 MHz) make it possible to determine the temperature of oxygen atoms from the measured absorption profiles as well. These features make THz absorption spectroscopy an attractive diagnostic for atomic oxygen density measurements in plasmas.

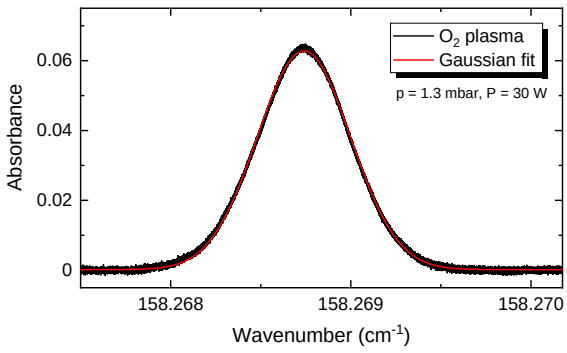

Figure 1: Typical example of an absorption profile of atomic oxygen measured with THz absorption spectroscopy in a CCRF oxygen discharge.

A possible way to validate this new method is by a comparison with two-photon absorption laser induced fluorescence (TALIF), as this is currently the most established method for measuring atomic oxygen densities in plasmas [3]. To this end, both THz absorption spectroscopy and TALIF measurements were performed on the same capacitively coupled radio frequency (CCRF) discharge generated in pure oxygen, for a variation of the applied power (20–100 W) and gas pressure (0.7–1.3 mbar). The TALIF measurements were done using a picosecond (ps) laser system and a streak camera for detection, and they were calibrated using xenon gas.

In this contribution, a comparison is presented between atomic oxygen densities obtained with the two different diagnostics. The results (all of the order of $10^{14}\,\mathrm{cm}^{-3}$) overlap very well. This validates THz absorption spectroscopy as an accurate and reliable diagnostic for determining atomic oxygen densities in plasmas.

References

[1] Wubs, J. R. *et al.* Terahertz absorption spectroscopy for measuring atomic oxygen densities in plasmas. *Plasma Sources Sci. Technol.* **32**, 025006 (2023).

[2] Lü, X. *et al.* Terahertz quantum cascade lasers for high-resolution absorption spectroscopy of atoms and ions in plasmas. *Semicond. Sci. Technol.* **38**, 035003 (2023).

[3] Gazeli, K. *et al.* Progresses on the use of two-photon absorption laser induced fluorescence (TALIF) diagnostics for measuring absolute atomic densities in plasmas and flames. *Plasma* **4**, 145–171 (2021).

Anomalous $N_2^+(B^2\Sigma_u^+)$ population in APPJ in nitrogen

N. D. Lepikhin[1], N. A. Popov[2], D. Luggenhölscher[1], N. Sadeghi[3] and U. Czarnetzki[1]

[1] *Institute for Plasma and Atomic Physics, Ruhr University Bochum, Bochum, Germany*
[2] *Skobeltsyn Institute of Nuclear Physics, Moscow State University, Moscow, Russia*
[3] *Laboratoire Interdisciplinaire de Physique, LIPhy, CNRS, UMR 5588, Université de Grenoble-Alpes, Grenoble, France*

Anomalously high relative density of the $N_2^+(B^2\Sigma_u^+,v{=}0)$ state is observed in the plasma bulk of the nanosecond near-atmospheric pressure plasma jet in nitrogen during its quasi-DC phase and afterglow. Numerical kinetic modeling is used to identify possible mechanisms of additional $N_2^+(B^2\Sigma_u^+,v{=}0)$ formation.

1 Introduction

Recently, it has been shown that a nanosecond near-atmospheric pressure plasma jet (APPJ) after the breakdown is characterized by uniform and stationary space structure as well as constant electric field and weakly varying electron density [1, 2, 3]. Uniformity of the discharge allows to consider it as a 0D system making the ns-APPJ a convenient tool for plasma studies. In the present work this tool is applied to investigate the evolution of electronically excited states of nitrogen.

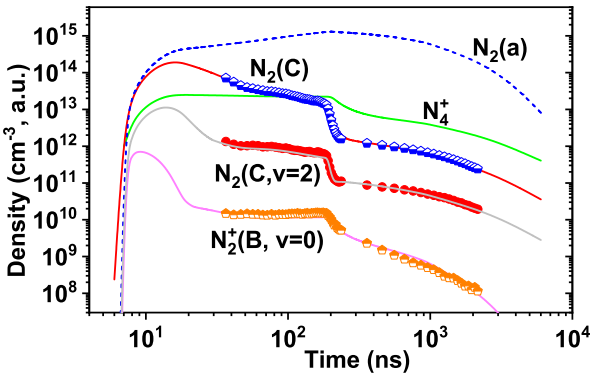

Figure 1: Relative densities of the $N_2^+(B^2\Sigma_u^+,v{=}0)$ and $N_2(C^3\Pi_u,v)$ states in a.u. measured experimentally together with the results of the kinetic modeling in cm^{-3}. Pure N_2, 200 mbar, 340 K.

2 Results

The results of the Optical Emission Spectroscopy measurements are presented in Fig. 1, where the relative densities of the $N_2^+(B^2\Sigma_u^+,v{=}0)$ and $N_2(C^3\Pi_u,v)$ states are shown in arbitrary units. The measured relative intensity of First Negative System (FNS) is about 100 times higher than the intensity expected from empirical formula derived in [4] at E/N=85 Td measured by EFISH technique. Moreover, significant density of the $N_2^+(B^2\Sigma_u^+,v{=}0)$ state is observed in the afterglow similarly to $N_2(C^3\Pi_u)$ populated in the pooling reaction. Thus, the experimental data clearly indicate additional population of the $N_2^+(B^2\Sigma_u^+)$ state besides direct electron impact. Numerical kinetic modeling similar to [5] has been used to identify possible mechanisms of additional $N_2^+(B^2\Sigma_u^+)$ formation. Kinetic calculations including two new processes, $N_2(C^3\Pi_u) + N_2(a^1\Pi_g) \rightarrow N_2^+(B^2\Sigma_u^+) + N_2 + e$ and $N_4^+ + N_2(a^1\Pi_g) \rightarrow N_2^+(B^2\Sigma_u^+) + N_2 + N_2$, describe adequately the FNS(0-0) emission dynamics and the high (relative to $N_2(C^3\Pi_u)$) density of the $N_2^+(B^2\Sigma_u^+,v{=}0)$ state, see Fig. 1.

Acknowledgements. The work is supported by the DFG funded SFB1316 Project "Transient atmospheric plasmas - from plasmas to liquids to solids".

References

[1] Lepikhin, N. D. *et al. J. Phys. D: Appl. Phys.* **54**, 055201 (2020).

[2] Kuhfeld, J. *et al.* PIC/MCC simulation for a ns-pulsed glow discharge in nitrogen at sub-atmospheric pressureand analysis of its quasi-steady state physics. *submitted to PSST* (2023).

[3] Lepikhin, N. D. *et al.* Breakdown and quasi-DC phase of a nanosecond discharge. comparison of optical emission spectroscopy measurements with numerical simulations. *submitted to PSST* (2023).

[4] Paris, P. *et al. J Phys. D: Appl. Phys.* **38**, 3894 (2005).

[5] Lepikhin, N. D. *et al. PSST* **31**, 084002 (2022).

Fluid vs kinetic simulation of the Penning discharge

D. Poli[1], E. Bello-Benítez[1], L. Garrigues[2], P. Fajardo[1] and E. Ahedo[1]

[1] *Dept. Aerospace Engineering, Universidad Carlos III de Madrid, Madrid, Spain*
[2] *LAPLACE, Université de Toulouse, CNRS, INPT, UPS, Toulouse, France*

The investigation of turbulent phenomena and instabilities in ExB devices has motivated the in-house development of 2D full particle-in-cell and multi-fluid plasma codes. Due to the intrinsic differences in the captured physics and modelling techniques, a direct comparison of the results obtained simulating a Penning-like discharge is presented. Finally, the triggering mechanism of the observed rotating spokes is investigated.

1 Motivation and Background

The understanding of the physics behind turbulence and instabilities in Hall-thruster, Penning and other ExB plasmas is of great importance, mainly due to their role on anomalous electron transport and performances. Even if fundamental linear stability theory [1, 2] is useful to provide physical insight, a full understanding can only be reached when together with nonlinear simulations. Conventional electron fluid models miss some of the kinetic effects behind some relevant instabilities (e.g., the electron-cyclotron drift instability) but are able to capture other instabilities in a wide spectrum of frequencies and scales (e.g., ionization instabilities [3], collisionless Simon-Hoh instability[1, 2], among others). These differences have motivated the recent development in our group of in-house 2D full particle-in-cell (PIC) and multi-fluid magnetized plasma codes.

2 Methodology

In this work, results from the full PIC and the multi-fluid models are compared. The analysed scenario consists of a collisionless plasma column in a Penning-like 2D configuration, consisting in a plasma enclosed in a grounded perfectly-conducting box where a uniform perpendicular magnetic field is applied. Such a configuration is known to be unstable under certain conditions and the formation of rotating spokes is usually observed and generally attributed to the onset of the collisionless Simon-Hoh instability [4]. This test case is proposed due to the relative simplicity compared to other devices (e.g., magnetic field inhomogeneity of Hall-thruster-like simulations is avoided) and because the physics behind the Simon-Hoh instability are captured by both kinetic and fluid electron formulations.

3 Anticipated Results

The onset of the instability, the long-term behavior and impact of oscillations on electron transport are analysed in both the fluid and kinetic models. A parametric study is presented in order to assess the trigger mechanism of the rotating spokes and whether it can be attributed to the Simon-Hoh instability. The direct comparison of the results is used to understand the potentiality and limits of fluid codes compared to the more computationally expensive PIC simulations in the frame of ExB discharges.

References

[1] Ramos, J. J., Bello-Benítez, E. & Ahedo, E. Local analysis of electrostatic modes in a two-fluid E x B plasma. *Physics of Plasmas* **28**, 052115 (2021). URL `https://doi.org/10.1063/5.0039341`.

[2] Simon, A. Instability of a partially ionized plasma in crossed electric and magnetic fields. *The Physics of Fluids* **6**, 382–388 (1963).

[3] Poli, D., Bello-Benítez, E., Fajardo, P. & Ahedo, E. Non stationary fluid modelling of plasma discharge in Hall thrusters. In *Space Propulsion Conference 2022*, 116 (2022). URL `available at https://ep2.uc3m.es`.

[4] Powis, A., Carlsson, J., Kaganovich, I., Raitses, Y. & Smolyakov, A. Scaling of spoke rotation frequency within a penning discharge. *Physics of Plasmas* **25**, 072110 (2018). URL `https://doi.org/10.1063/1.5038733`.

XXXV ICPIG, July 9-14, 2023, Egmond aan Zee, The Netherlands Topic number 15

Redeposition in High Aspect Ratio Plasma Etching*

Evan Litch[1], Hyunjae Lee[3], Sang Ki Nam[3] and Mark J. Kushner[2]

[1]*Nuclear Engr. & Radiological Sci., University of Michigan, Ann Arbor, Michigan, USA*
[2]*Electrical Engr. & Computer Sci., University of Michigan, Ann Arbor, Michigan, USA*
[3]*Mechatronics Research, Samsung Electronics Co., Ltd., Republic of Korea*
elitch@umich.edu, hj0928.lee@samsung.com,sangki.j.nam@samsung.com, mjkush@umich.edu

In the transition from 2D to 3D semiconductor devices, fabrication of high aspect ratio (HAR) features by plasma etching is becoming a more critical process. With aspect ratios now approaching 100, transport of etch products out of the feature and their redeposition becomes problematic. In this paper, results from multi-scale modeling (reactor and feature scale) of plasma etching of HAR-DTI (deep trench isolation) features will be discussed with a focus on the consequences of reposition of etch products.

1 Introduction

Plasma etching of semiconductors is primarily performed by ion-enhanced chemical sputtering of the substrate producing both saturated and radical etch products. Shrinking microelectronic features has shifted fabrication from 2-dimensional architectures towards 3D devices having high aspect ratio (HAR) features. One such feature is the deep trench isolation (DTI) etched in Si and back-filled with dielectric [1]. The DTI prevents interaction between adjacent logic devices. DTI etching is typically performed in inductively coupled plasmas (ICP) of tens of mTorr sustained in halogen containing gases with a substrate bias of up to several kV. O_2 is often added to the gas mixture to reduce sidewall etch rate by forming a thin oxide layer.

When using $Ar/Cl_2/O_2$ gas mixtures for Si HAR etching, unsaturated etch products must diffuse from the bottom of the feature out the top, undergoing hundreds collisions on the sidewalls. These numerous collisions allow for redeposition to take place. The redeposition provides temporary passivation against lateral etching as it is weakly attached to the surface. However, too much redeposition can lead to tapering of the feature as occurs with large oxygen fraction.

1.1 Simulation of HAR-DTI Plasma Etching

In this presentation, results will be discussed from a computational investigation on ICPs sustained in $Ar/Cl_2/O_2$ mixtures of tens of mTorr having a substrate bias for etching DTI features in Si. Emphasis is on consequences of redeposition of etch products on feature profiles. Feature scale simulations were conducted using the Monte Carlo Feature Profile Model (MCFPM) [2]. Ion and neutral energy and angular distributions onto the substrate were obtained from reactor scale simulations performed with the Hybrid Plasma Equipment Model (HPEM) [2]. Parametric studies were performed varying ICP power, substrate bias, and oxygen fraction. (See Figure 1.)

The etch products consist of physically sputtered Si and SiO_x (from passivation of the sidewalls); physically and chemically enhanced sputtered $SiCl_x$ and $SiOCl_x$; and thermally etched $SiCl_4$. As a saturated molecule $SiCl_4$ does not redeposit as it diffuses out of the feature. However, the non-saturated (radical) etch products do have some finite probability of depositing on surfaces in diffusing out of the feature. With there being up to hundreds of reflections from sidewalls in diffusing out of a HAR feature, a sticking probability of a fraction of a percent will result in sticking. The sticking is likely not chemisorption but rather strong physisorption that is susceptible to removal by both sputtering and thermal etching. The redeposition produces tapering of the feature, which then increases the aspect ratio and the number of reflections for diffusing out of the feature. This then increases the likelihood for sticking.

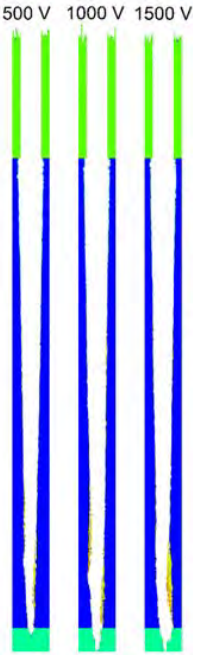

Figure 1 -Predictions for DTI features in Si for a 100 nm mask etched to AR=20 for different substrate bias voltage.

1.2 References

[1] K. Mumba, et al. *IEEE 22nd Intl. Conf. on Nanotechnology (NANO)* Spain, 2022, pp. 271-274.
[2] S. Huang, et al., J. Vac. Sci. Technol. A **38**, 023001 (2020).

* This work was supported by Samsung Electronics, Lam Research, U.S. National Science Foundation (2009219) and the Department of Energy Fusion Energy Sciences (DE-SC002023).

Particle-in-cell modelling of positive streamers in CO_2: the role of photoionization

Xiaoran Li[1, 2], Anbang Sun[1] and Jannis Teunissen[2]

[1] *State Key Laboratory of Electrical Insulation and Power Equipment, School of Electrical Engineering, Xi'an Jiaotong University, Xi'an, China*

[2] *Centrum Wiskunde & Informatica (CWI), Amsterdam, The Netherlands*

We investigate the effect of photoionization on positive streamer propagation in CO_2 with 2D particle-in-cell simulations. For positive streamers to propagate, they require a supply of free electrons in front of them. Photoionization in CO_2 is significantly weaker than in air due to the reduced number of ionizing photons produced and the shorter distance over which they are absorbed, which is orders of magnitude smaller. Our results demonstrate that even a small amount of photoionization can sustain positive streamer propagation in CO_2, but a higher electric field is needed around the streamer head than in air.

Streamer discharges are a common initial stage of electrical discharges, playing an important role for electric breakdown in high voltage technology. CO_2 is increasingly used as an insulating gas in high-voltage equipment, and it constitutes a major component in various substitutes to SF_6 [1]. In this study, we focus on a particular question: whether photoionization can sustain positive streamer propagation in CO_2.

We simulate the propagation of positive streamers in CO_2 at 300 K and 1 bar with a 2D particle-in-cell model based on afivo-pic [2]. A Monte Carlo photoionization model was implemented based on experimental data retrieved from [3], in which photons with wavelengths of 83-89 nm contribute to the photoionization of CO_2. The number of ionizing photons produced per impact ionization ($\xi\omega/\alpha_{\mathrm{eff}}$) is between 0.6×10^{-4} to 4.8×10^{-4} and absorption coefficients are in the range of 0.34 to 2.2 $\mathrm{cm^{-1}Torr^{-1}}$. Compared to air, there are fewer ionizing photons, and they are absorbed at much shorter distances.

We simulate streamer propagation in a parallel-plate electrode geometry with a needle protrusion of 2.1 mm long. A high voltage of 32 kV is applied over a 16 mm gap. Figure 4 shows the electron density evolution for a positive streamer in CO_2 between 5 ns and 35 ns. In our simulations, streamer propagation can be sustained by photo-electrons in a background electric field of 2 kV/mm. We analyze these results and discuss uncertainties in the photoionization model.

References

[1] Seeger M. Perspectives on Research on High Voltage Gas Circuit Breakers. Plasma Chem Plasma Process **35**, 527–41 (2015).

[2] Teunissen J, Ebert U. 3D PIC-MCC simulations of discharge inception around a sharp anode in nitrogen/oxygen mixtures. Plasma Sources Sci. Technol. **25**(4), 044005 (2016).

[3] Pancheshnyi S. Photoionization produced by low-current discharges in O_2, air, N_2 and CO_2. Plasma Sources Sci. Technol. **24**, 015023 (2014).

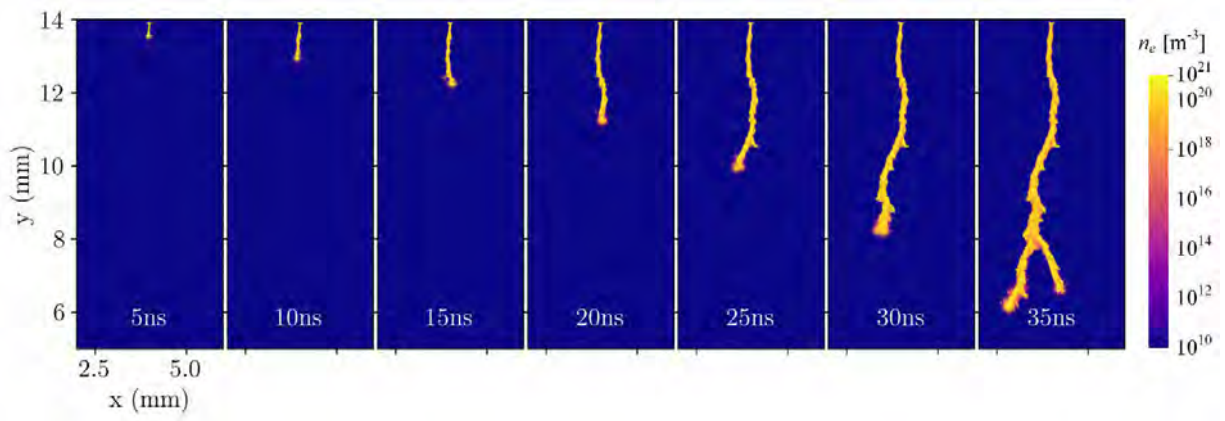

Figure 1. The electron density evolution for a positive streamer in CO_2 in a background electric field of 2 kV/mm.

Single shot, non-resonant, four-wave mixing laser diagnostics of heavy species in low temperature plasmas

R. Randolph[1], S. Suzuki[2], K. Hara[2] and A. Gerakis[1,3]

[1]*Dept. of Aerospace Engineering, Texas A&M University. College Station, Texas, USA*
[2]*Dept. of Aeronautics & Astronautics, Stanford University, Stanford, California, USA*
[3]*Materials Research & Technology Dept., Luxembourg Institute of Science & Technology, Belvaux, Luxembourg*

Single shot coherent Rayleigh-Brillouin scattering (CRBS), a non-linear, four-wave mixing laser diagnostic technique, is applied to measure the translational temperature and density of neutral species in a low pressure (15 Torr), xenon, DC glow discharge. The single shot CRBS configuration scans the entire velocity distribution function of the neutral species in the medium in the duration of a single laser shot (approximately 150 ns), allowing for rapid spectral acquisition. Experimentally obtained spectral lineshapes show good agreement when compared to simulated ones. Single shot CRBS exhibits the significant advantages of being able to measure at both low densities and optically noisy environments. The CRBS measurements within a glow discharge presented here can lead to diagnostics of neutral species in similar environments such as arc discharges, flames, plasma torches, etc.

1 General

We experimentally demonstrate the use of single shot coherent Rayleigh-Brillouin scattering (CRBS) for the measurement of the velocity distribution function (VDF) of neutral species in a glow discharge, from which macroscopic quantities, such as the flow velocity, density and translational temperature can be extracted. In CRBS, a four-wave mixing technique, a high energy optical lattice of precisely tailored chirped frequency interacts with the medium, such as neutral or ionized gas. The variation of the CRBS signal intensity at different optical lattice phase velocities allows for the restoration of the VDF and the resulting CRBS lineshape is a direct mapping of the medium's VDF. CRBS has already been demonstrated to be the coherent analogue of spontaneous Rayleigh-Brillouin scattering and has already been demonstrated in the measurement of nanoparticles in an arc discharge [1].

Single-shot CRBS is applied to measure simultaneously the temperature and density of neutral species in a weakly ionized DC glow discharge plasma. The DC glow discharge is generated at a pressure range of 15 Torr using xenon gas. For this application, we employ a newly developed dual-color CRBS scheme [2, 3] where the frequency doubled 532 nm beam serves as a probe beam to achieve a higher signal-to-noise ratio at the low-pressure environment versus the most employed single color CRBS approach. The temperature and density of neutral xenon particles inside the DC glow discharge is evaluated simultaneously by analyzing the resolved single-shot CRBS lineshapes as a function of the discharge currentA multiscale fluid simulation model of the glow discharge is also developed and there is good agreement between the simulation and the experimental measurements in the glow discharge. Finally, we report on the progress towards extending the technique axially, along the column of the discharge, prior to extending detection capabilities into discharges with higher degrees of ionization.

References

[1] Gerakis, A. *et al.* Four-wave-mixing approach to in situ detection of nanoparticles. *Phys. Rev. Appl.* **9**, 014031 (2018).

[2] Bak, J., Randolph, R. & Gerakis, A. Dual color, frequency, pulse duration and shape agile laser system for particle spectroscopy and manipulation. *Opt. Express* **30**, 41709–41723 (2022).

[3] Bak, J., Randolph, R. & Gerakis, A. Torr-level, seedless, non-resonant velocity distribution function measurement with a dual-color, single-shot coherent rayleigh–brillouin scattering scheme. *Journal of Physics D: Applied Physics* **56**, 074001 (2023).

Cavity ring-down spectroscopy in HiPIMS discharge during the sputtering of the titanium target

A.D. Pajdarová, T. Kozák, and J. Čapek

Department of Physics and NTIS – European Centre of Excellence, University of West Bohemia, Univerzitní 8, 301 00 Plzeň, Czech Republic

We have applied cavity ring-down spectroscopy (CRDS) together with laser-induced fluorescence (LIF) in high-power impulse magnetron sputtering (HiPIMS) discharge. We have measured the density and spatial distribution of Ti atom and ion ground-state densities near the target during the HiPIMS voltage pulse and after its termination. A significant difference between spatial distributions of Ti atoms and ions was found during the HiPIMS voltage pulse. The highest energy levels of the ground-state multiplets show a population inversion that is strong for Ti^+ ions.

Cavity ring-down spectroscopy (CRDS) is a laser absorption technique where the decay time of a laser pulse bouncing between two spherical mirrors forming an optical cavity is measured. From the decay time, the absolute average density of absorbing species over the cavity length may be calculated [1]. High-power impulse magnetron sputtering (HiPIMS) discharges are characterized by very high-power densities (around 1 kW/cm^{-2}) delivered to the sputtered target in the form of voltage pulses (with duration ~10–100 µs and repetition frequencies ~100 Hz). Such powers produce large fluxes of the sputtered target material with a high ionization degree allowing the deposition of high-quality densified films [2].

We have applied the CRDS technique close to a 100 mm in diameter cylindrical Ti target (at 10 mm from its surface) sputtered by a HiPIMS discharge in argon gas at a pressure of 1 Pa [3]. The average power in a period was the same for the repetition frequencies of voltage pulses f_r = 50, 100, 200 and 500 Hz. The densities of energy levels belonging to the ground-state multiplets (GSM) of Ti atoms and Ti^+ ions were measured in the wavelength range of 335–339 nm. From the laser-induced fluorescence (LIF) images taken by an emICCD camera, the density distributions of the Ti atom and ion ground state along the laser path were constructed.

Figure 1 shows the densities of individual energy levels averaged over the length of 14 cm above the target for the regime with f_r = 100 Hz (a regime with a higher peak power density of 500 W/cm^{-2}). A typical result is that the GSM levels with higher energy have a higher density leading (especially in the case of ions) to a significant inversion in the populations. The LIF measurements (not shown here) revealed that between Ti atoms and Ti^+ ions, there is a significant difference in their distributions. Ti^+ ions have maximum density directly above the target racetrack during the voltage pulse, moving toward the target edge after the pulse end. The maximum density of Ti atoms is located above the target center, and close to the racetrack position, there is a deep decrease of their density (especially for f_r = 100 Hz).

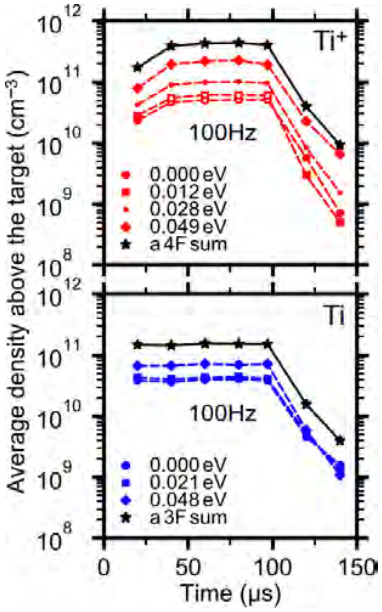

Figure 1 The time evolution of the average Ti atom and ion ground-state density in 10mm above the target surface during and after the HiPIMS voltage pulse.

References

[1] Berden, G., Engeln, R. *Cavity Ring-Down Spectroscopy: Techniques and Applications*, Wiley (2009).

[2] Anders, A., *Tutorial: Reactive high power impulse magnetron sputtering (R-HiPIMS)*, J. Appl. Phys. **121**, 171101 (2017).

[3] Pajdarová, A.D., Kozák, T., Čapek, J., Tölg, T. *On density distribution of Ti atom and ion ground states near the target in HiPIMS discharge using cavity ring-down spectroscopy and laser induced fluorescence*, Plasma Sources Sci. Technol. **31**, 05LT04 (2022).

Plasma-on-Chip: A Microdevice for Direct Plasma Exposure of Cultured Cells

Shinya Kumagai[1], Mime Kobayashi[2], Tetsuji Shimizu[3] and Minoru Sasaki[4]

[1] *Meijo University, Nagoya, Japan*
[2] *Osaka Medical and Pharmaceutical University, Takatsuki, Japan*
[3] *National Institute of Advanced Industrial Science and Technology, Tsukuba, Japan*
[4] *Toyota Technological Institute, Nagoya, Japan*

We developed a microdevice "*Plasma-on-Chip*" which enables direct plasma exposure of cultured cells. The *Plasma-on-Chip* is used to elucidate how plasma affects cells for controlling cell fate. Fabrication process of the device and application for cell analysis are reported.

1 General

Since non-thermal atmospheric pressure plasma (NTAPP) was applied in biomedical research, excellent results have been reported leading to many innovations: selected cell killing [1], promoted cell proliferation [2] as well as differentiation [3]. However, it had been unclear how NTAPP affects cells. What is actually happening inside the cells? To answer this issue, we have developed a microdevice referred to as the *Plasma-on-Chip* which enables direct plasma exposure of cultured cells.

2. Idea of direct plasma exposure to cultured cell

Plasma-on-Chip device is shown in Fig. 1. It consists of two parts; microwells for cell culture and micro plasma sources for generating active species such as reactive oxygen and nitrogen species [4, 5]. In between, at the bottom of the microwells, there is a small through-hole. When cell-containing liquid medium is put in the microwell, liquid does not leak because of the surface tension. When a NTAPP is generated at the backside of the microwell, the plasma-generated active species are delivered into the liquid via the gas-liquid interface. The *Plasma-on-Chip* enables direct plasma exposure of cells.

3. Results and Discussions

Plasma-on-Chip was fabricated using MEMS technology [4] and assembled with Teflon holders for easy handling.

For the cell experiment, L929 murine fibroblast cells were used. L929 cells were cultured in MEM (10% FBS, 1% Penicillin-Streptomycin). Before cell injection, surface of *Plasma-on-Chip* device was modified with 3-aminopropyltriethoxysilane to display amino groups. The amino groups improved L929 adhesion onto the device surface through electrostatic interaction.

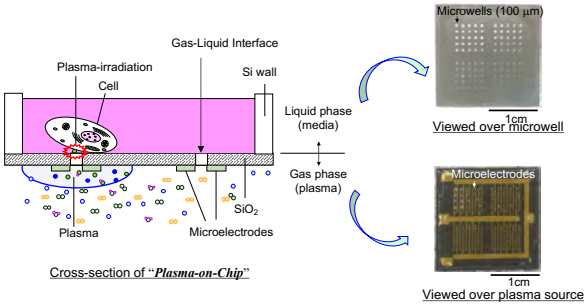

Fig. 1: Structure of *Plasma-on-Chip*.

After injection, L929 cells adhered well to the *Plasma-on-Chip* showing their filopodium (Fig. 2(a)). With increasing plasma exposure time, filopodium decreased due to the effects of plasma-generated active species. We also investigated Ca signalling in L929 cells upon plasma exposure. L929 cell in the vicinity of the through-hole emitted green fluorescence which was derived from Ca ions induced by plasma exposure. The *Plasma-on-Chip* device developed here will open up new research fields of plasma-bio science.

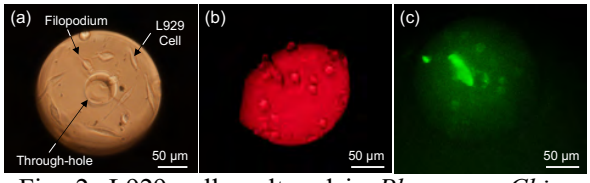

Fig. 2: L929 cells cultured in *Plasma-on-Chip*. Phase contrast microscopy images (a) before and (b) after plasma exposure. (c) Fluorescence microscopy image. Plasma stimulated a cell and green fluorescence of Ca ion signalling.

Acknowledgements

This study was partially supported by the Hibi Foundation , the Nitto Foundation, and the joint usage / research program of center for Low-temperature Plasma Sciences, Nagoya University.

References

[1] H. Tanaka et al., Sci. Rep. **9**, 13657 (2019).
[2] Y. Hori et al., Plasma Process Polym. 2021; 18:e2000225
[3] M. Kobayashi et al., Heliyon 2022, DOI: 10.1016/j.heliyon.2022.e12009.
[4] S. Kumagai et al., Jpn. J. Appl. Phys. Vol. 55, 01AF01 (2016), (OPEN ACCESS).
[5] S. Kumagai et al., JSAP Review (OPEN ACCESS), DOI: 10.11470/jsaprev.220417.

Decay of additional electron density released by laser-induced photodetachment as a diagnostic tool for dust particle size in a low-pressure nanodusty plasma

T.J.M. Donders[1], T.J.A. Staps[1] and J. Beckers[1]

[1] *Dept. Applied Physics, Eindhoven Univ. Techn., Eindhoven, The Netherlands*

One of the key parameters in a nanodusty plasma is the dust particle size. In this work, we use a combination of laser-induced photodetachment (LIPD) and microwave cavity resonance spectroscopy to follow the transient behaviour of the free electron density in the plasma after interaction with a short UV laser pulse. Here we show that the decay time of the additional free electron density released by LIPD can be used to determine the dust particle size using OML theory. Furthermore, a measurement scheme was developed to measure the dust particle size in real-time with minimal invasiveness.

1 Introduction

Apart from neutrals, ions and electrons, a dusty plasma also consists of charged solid dust particles, from which the size can range from a few nanometers up and until a few micrometers. These types of plasma exist in nature, in the form of interstellar clouds or in the rings of Saturn. In the laboratory environment, a nanodusty plasma can be created by igniting a plasma in a mixture of a noble background gas and a reactive gas. Generally in these systems, polymerization of reactive species will lead to the formation of large clouds of monodisperse dust particles, with a typical size in the order of 100 nm. It is interesting to note that the presence of dust particles in the plasma induces widely different behavior compared to the situation in a pristine plasmas. The most important effect is *electron depletion*, i.e. the loss of free electrons in the plasma due to charging of the dust particles. Two key parameters in a nanodusty plasma are the *dust charge* and *dust particle size*. In this work we show the development of a novel method to determine the dust particle size, making use of the fact that they are charged.

2 Determining the dust particle size

In these experiments we use an ultraviolet ($\lambda = 266$ nm) pulsed laser to detach charge from the dust particles, and follow the decay of the additional electron density as a function of time using microwave cavity resonance spectroscopy (MCRS). Figure 1 shows the released electron density Δn_e as a function of time. As the laser pulse is fired at $t = 0$ s, a sharp increase in the free electron density is observed, which is attributed to photodetachment events. Subsequently, a decay towards the equilibrium value is observed, which is attributed to the (re-)charging of the dust particles after their charge has been disturbed.

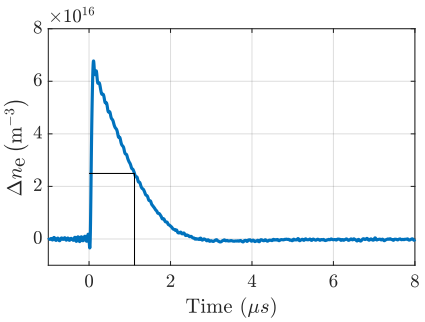

Figure 1: Timetrace of the photodetached electron density. The decay time (here the $1/e$-time $\tau = 1.1\,\mu$s, indicated in black) is related to the recharging of the dust particles.

Using the widely accepted OML theory, one can calculate the charging timescale for a particle with a certain size a suspended in the plasma bulk. By matching of the measured decay timescales to the theoretically obtained charging timescale, one can determine the mean dust particle size. Furthermore, we will show that a single laser pulse is enough to determine the dust particle size and that this enables to monitor the particle size in real-time during the dust growth process.

Monitoring the carbonaceous interstellar dust analogues growth in cold plasmas by light scattering

R. J. Peláez[1], M. Jiménez-Redondo[1,2], B. Maté[1], V. J. Herrero[1] and I. Tanarro[1]

[1] *Instituto de Estructura de la Materia (IEM), CSIC, Serrano 121-123, 28006 Madrid, Spain*
[2] *Max Planck Institut für Extraterrestrische Physik, Gießenbachstraße 1, 85748 Garching, Germany*

We monitored the growth of interstellar hydrocarbon dust analogues in cold RF acetylene plasmas using a laser scattering imaging technique. Laser absorption, self-bias voltage, or time resolved mass spectrometry were also recorded during the growth process. The results showed a sudden initial growth of dust followed by a slower increase. Evolution of the number density of grains and the electronic density and temperature were also obtained. Furthermore, the particle sizes estimated by light scattering agreed with those obtained from SEM images, and the comparison of both techniques allowed for the estimation of the optical index of dust. This latter result is very significant in astrophysical dust models.

1. Introduction

The interstellar dust grains play an important role in the stellar cycle of matter. Infrared absorption bands in some diffuse clouds are assigned to amorphous hydrogenated carbons. Moreover, these grains can serve as catalyst agents, favoring the formation of molecules. The production of interstellar dust analogs in cold RF plasmas using acetylene as a precursor gas has been extensively described [1]. In this work, the growth of these dust analogs was monitored. We focused on the process of nanoparticle (NP) growth from tens to hundreds of nanometers.

2 Experiment and results

The experimental setup consisted of a capacitively coupled RF reactor [2]. Flows of 5 sccm Ar and 2 sccm C_2H_2 were employed at pressures of 0.26 mbar. The growth period analysed in this work lasted for 14 seconds. Subsequently, the plasma was turned off for 6 seconds during which the NPs fell on the substrate and the precursor gas mixture was recovered. Then, the plasma was turned back on, the particles grew, and the cycle started again.

A green laser planar beam, a CCD and two polarizers were used to obtain 90° scattering images of the dust at different times during the growth process. Polarization-sensitive laser light scattering (PSLLS) was employed to obtain the spatio-temporal evolution of the nanoparticles [3]. In addition, the laser light absorption, the evolution of the DC self-bias voltage, the spectral optical emission, and the evolution of neutral species by quadrupole mass spectrometry with a mass range of 1–100 u were also monitored. Finally, dust samples collected after several cycles were analyzed ex-situ. The IR absorption features observed are in agreement with those of interstellar carbonaceous dust. SEM images were also used to analyze the morphology and size of the NPs.

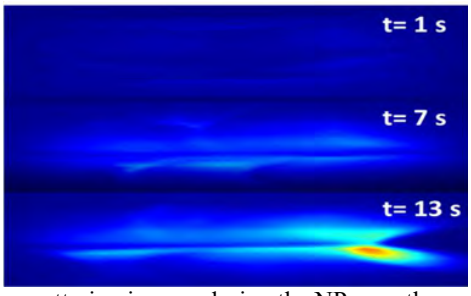

Laser-scattering images during the NP growth process

The optical index was estimated from the comparison between the sizes of the NPs obtained through PSLLS and those obtained through SEM images. The results agree with the optical index obtained in a previous work [4]. The NPs grew monotonically in two phases. Firstly, they grew rapidly within approximately 3 seconds until they reached a diameter of 100 nm. Later on, they grew slowly, reaching 140 nm at the end of the 14 seconds cycle. The evolution of the grains and electronic density, the species concentration, and the electronic temperature were obtained from these complementary measurements. The trends and values agreed with the previous results from literature.

4. Acknowledgements

This work has been funded by the Ministerio de Ciencia e Innovación of Spain under grant PID2020-113084GB.

References

[1] Herrero, V. J. et al Front. Astron. Space Sci. **9**:1083288, (2022).
[2] Jiménez-Redondo, M. et al. J. Phys. Chem. A **123** 8135–47 (2019).
[3] Byoung Chai, K. et al, New J. Phys. **11** 103006 (2009)
[4] Peláez R J et al. Plasma Sources Sci. Technol. **27** 035007 (2018)

A Model of Plasma-Enabled Gold Nanoparticle Synthesis in Microdroplets

Jaehyun Nam[1], Gaurav Nayak[1], Stephen Exarhos[1] and Peter Bruggeman[1]

[1] *Department of Mechanical Engineering, University of Minnesota, Minneapolis, MN, USA*

Plasma-driven solution electrochemistry is an alternative method to synthesize nanoparticles and is an intrinsically green and fast process. To study the gold nanoparticle particle synthesis mechanisms enabled by plasma, we developed a microdroplet plasma reactor in which microdroplets were transported by a gas flow through a well-characterized homogeneous RF-driven plasma. The *ex-situ* characterization of plasma-treated droplets was carried out and a 1-D reaction-diffusion model was developed to simulate the experimental results of particle mean diameter, concentration, and reduced precursor concentration. The model showed good agreement with the experiments. The timescale analysis of the simulation revealed that nucleation is enabled by fast reduction of gold ions, and autocatalytic growth mainly determines the particle size leading to an 100-1000 times enhancement of precursor reduction compared to electrons only.

1. Introduction

Plasma-driven solution electrochemistry is an alternative approach to conventional wet chemistry to generate nanomaterials and has been extensively studied in the plasma community [1]. The synthesis of nanoparticles enabled by plasma-liquid interactions has considerable advantages over conventional processes as it can be much faster and does not require the addition of often harmful reducing agents. Nonetheless, the mechanisms of liquid phase ion precursor reduction and the particle growth mechanism enabling the formation of metal particles remain unclear.

Inspired by the work of Maguire et al [2], we designed an on-demand microdroplet plasma reactor to study the formation of gold nanoparticles and complement these measurements with a model to explain the underpinning mechanisms of nanoparticle formation.

2. Methods

The microdroplet plasma reactor enables the production of a train of droplets with a fixed size of 40 μm through a homogeneous atmospheric pressure RF-driven plasma [3]. The experiment allows us to estimate the electron flux to the droplet from the measured electron density by analysing the continuum radiation from the plasma [4]. Furthermore, *ex-situ* analysis of plasma-treated droplets was performed. Guided by these experiments, we developed a 1-D reaction-diffusion model of the plasma-enabled reduction of Au^{3+} ions including particle nucleation and growth. The model incorporates classical nucleation theory as a nucleation model, diffusion-limited monomer absorption, and autocatalytic surface growth. The mean particle diameter, nanoparticle concentration, and reduced ion concentrations are calculated by the model.

3. Results

The model shows that the mean particle diameter increases with decreasing reducing species flux, which qualitatively agrees with the experimental trends. Using a reported solubility of Au and an estimated nanoparticle concentration from experiments, a critical reducing species flux is in the range of 10^{11} to 10^{12} s^{-1}. The experimentally obtained electron flux does not exceed 10^{10} s^{-1} which implies a possible role of other reducing species such as VUV photons.

The model suggests that the nucleation process occurring within 10 ms is enabled by fast electron-induced reduction possibly augmented by VUV photons while the particle growth is mainly enabled by autocatalytic growth mediated by plasma-produced H_2O_2 that continues after the droplet exits the ionizing plasma region. This autocatalytic growth process can lead to the enhancement of plasma-produced reduction by factor 100-1000 compared to electrons only.

4 Conclusions

The modelling results reported in this work show excellent agreement with the experiment and provide insights into the timescales and growth process for the synthesis of gold nanoparticles in droplets. These insights will be helpful in the development of plasma-enabled synthesis processes.

5 Acknowledgements

This work was supported by the Army Research Office under Grant Number W911NF-20-1-0105.

References

[1] Q. Chen et al., J. Phys.D, **48**, 42, 424005 (2015).

[2] P. Maguire et al., Nano Lett. **17, 3**, 1336–1343 (2017).

[3] G. Oinuma, G. Nayak, Y. Du, and P.J. Bruggeman, Plasma Sources Sci. Technol. **29** 095002 (2020)

[4] G. Nayak, J. Wang, R. Li, D. Aranzales, S. Mededovic Thagard and P.J. Bruggeman, Plasma Process Polym. e2200222 (2023)

Scattering and transport properties of dense plasmas

T.S. Ramazanov [1,2], S.K. Kodanova [1], M.K. Issanova [1], M.T. Gabdullin[1,3], M.M. Muratov [1]

[1] *Al-Farabi Kazakh National University, IETP, NNLOT, al-Farabi av., 71, Almaty, 050040, Kazakhstan*
[2] *Institute of Applied Sciences and Information Technology, Almaty 050438, Kazakhstan*
[3] *Kazakh-British Technical University, Tole bi str., 59, Almaty, 050000, Kazakhstan*

A pseudopotential approach was used to study the electron–ion scattering in dense plasmas. Screening of the ion charge is taken into account using the density response function in the long wavelength limit. Additionally, the effect of electronic non-ideality is included using the compressibilty sum-rule connecting the local field correction and the exchange-correlation part of the electronic free energy density. Using a screened pseudopotential, we have computed electron–ion scattering phase shifts, the total and transport elastic scattering cross sections and transport properties of dense plasma.

Among the plasma diversity, a non-ideal dense plasma is particularly difficult object to study due to the presence of strong interparticle correlations and quantum degeneracy effects in the system. Dense plasmas are routinely generated at modern high-energy-density-plasma science facilities such as NIF, [1] where the dense plasmas are created by compressing and heating a target by a laser or intense charged particle beams [2]. Knowledge about transport properties of such dense plasmas is needed to understand experimental results and to design new experiments. Therefore, a large amount of effort has been out into understanding the scattering phenomena at extreme plasma conditions.

Dense plasma occurs in many astrophysical objects and modern high-technological facilities. Therefore, study of physical properties of dense plasmas is the important topic in the physics of inertial confinement fusion, warm dense matter and high-power lasers physics [3].

The results of calculations of the scattering and transport properties of dense plasma are presented in this work. In the mentioned cases effective potentials should take into account both quantum and collective (screening) effects for dense, nonideal, nonisothermal plasma. In order to describe the interactions between particles several effective potentials are used. These potentials take into account quantum mechanical, screening and polarizations effects in dense plasmas [3-8]. A pseudopotential approach was used to study the effect of an ionic core on the electron-ion scattering in dense plasmas. The effective potentials between particles in dense nonisothermal plasmas are derived on the basis of the method of dielectric response functions and multipole expansion. The non-ideality effects for electrons is calculated by method of local field corrections. On the basis of proposed effective potentials the electron-ion scattering phase shifts, the total and transport elastic scattering cross sections have been computed. Based on scattering properties we have studied the transport coefficients of dense plasma. It is found that taking into account the above mentioned effects leads to significant changes in physical properties of plasma. Comparisons with results obtained by other approaches are given.

References

[1] O. Hurricane, D. A. Callahan, D. T. Casey, P. M. Celliers, C. Cerjan, E. L. Dewald, T. R. Dittrich, T. Doppner, D. E. Hinkel, L. F. Berzak Hopkins et al., Nature 506, 343 (2014).
[2] S. Kawata, T. Karino, and A. I. Ogoyski, Matter Radiat. Extremes 1, 89 (2016).
[3] T.S. Ramazanov, S.K. Kodanova, Zh. A. Moldabekov, and M. K. Issanova. Phys. Plasmas, 20, 112702 (2013).
[4] Z.A. Moldabekov, T. Dornheim, M. Bonitz. Contrib. Plasma Phys. e202000176 (2021).
[5] D.O. Gericke, J. Vorberger and K. Wünsch. Phys. Rev. E 81, 065401(R) (2010).
[6] T.S. Ramazanov, S.K. Kodanova, M.M. Nurusheva, M.K. Issanova. Phys. Plasmas 28 (9), 092702 (2021).
[7] M.K. Issanova, S.K. Kodanova, T.S. Ramazanov, and D.H.H. Hoffmann. Contrib. Plasma Phys. 56, 425 (2016).
[8] T.S. Ramazanov, M.K. Issanova, Ye.K. Aldakul, S.K. Kodanova, Phys. Plasmas 29 (11), 112706 (2022).

Semiclassical Analytic Model of Nonadiabatic Energy Transfer in Atomic Collisions

I. V. Adamovich[1] and J. W. Rich[1]

[1] *Department of Mechanical and Aerospace Engineering, Ohio State University, Columbus, OH, USA*

A previously developed semiclassical analytic theory on nonadiabatic energy transfer is used to predict the cross sections of electronic excitation and associative ionization in atomic collisions. The predictions are compared with the quantum scattering calculations, for the same interaction potentials and nonadiabatic coupling, and with the experimental data. The cross section of electronic excitation, $O(^3P)+O(^3P) \rightarrow O(^3P)+O(^1D)$, exhibits good agreement with the quantum scattering predictions. The energy dependence of the associative ionization cross section, $N(^2D) + O(^3P) \rightarrow NO^+ + e^-$, differs from the experimental data, likely due to the effect of the multi-channel energy transfer, which has not been incorporated into the present model. The results demonstrate the significant potential of the analytic theory for the prediction of the rates of heavy particle impact excitation and ionization in atomic collisions.

The objective of the present work is the development of a semiclassical analytic model of nonadiabatic energy transfer in atom-atom collisions, using the generalized Landau-Zener-Stückelberg theory [1]. The accuracy of the theory is tested by analyzing the electronic excitation in collisions of two O atoms, $O(^3P)+O(^3P) \rightarrow O(^3P)+O(^1D)$. The analysis includes non-zero angular momentum (impact parameter) collisions. The predictions of the semiclassical theory are compared with the exact quantum solution [2], for the same interaction potentials and nonadiabatic coupling. Fig. 1 illustrates the dominant effect of the collision angular momentum, which changes the phase shift between the incoming and ongoing waves and results in the oscillatory behavior of the transition probability. The analytic theory reproduces this effect very well. The excitation cross section, obtained by summing the probability over the collision angular momentum, is also in very good agreement with the quantum solution. The results illustrate the significant potential of the semiclassical theory for the prediction of the rates of electronic excitation in atom-atom collisions. Since the theory has been demonstrated to be applicable for multi-channel energy transfer, this suggests that electronic excitation in atomic collisions involving multiple interaction channels can also be predicted accurately. The feasibility of extending this approach to atom-molecule collisions with complex potential energy surfaces will need additional work.

The second, considerably more challenging, test of the semiclassical theory is the prediction of the cross section of associative ionization, $N(^2D) + O(^3P) \rightarrow NO^+ + e^-$. The cross section of this process was predicted by quantum scattering [3], yielding good agreement with the data [4] near the threshold energy. The cross section predicted by the present model over a wide range of collision energies differs from the experimental data. A likely reason for this is the coupling with the Rydberg states of NO. The comparison of the semiclassical theory with quantum scattering, for the same potential energy surfaces and electronic coupling matrix elements, will provide additional insight and elucidate the factors controlling the behavior of the cross section.

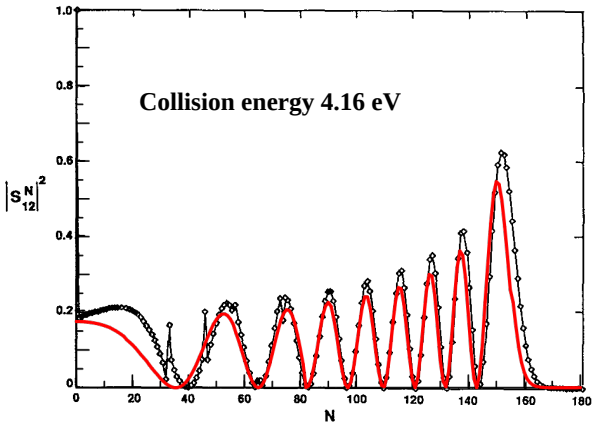

Figure 1. Electronic excitation transition probability vs. orbital angular momentum quantum number: quantum scattering [2] (black) vs. analytic model (red).

The support of the US Office of Naval Research is gratefully acknowledged.

References

[1] C. Zhu, Y. Teranishi, and H. Nakamura, Adv. Chem. Phys. **117** 127-233 (2001)

[2] Sun, Y., and Dalgarno, A., J. Chem. Phys. **96** 5017-5019 (1992)

[4] Golubkov, M.G., Ozerov, G.K., Adamson, S.O., Golubkov, G.V., Malyshev, N.S., and Dementiev, A.I., Chem. Phys. **462** 28-34 (2015)

[3] Ringer, G., and Gentry, W.R., J. Chem. Phys. **71** 1902-1909 (1979)

Effect of hydrodynamic regimes on the cumulative heating induced by NRP discharges in plasma-assisted combustion

Renaud Gablier, Arthur Salmon, Victorien Blanchard, and Christophe O. Laux

Laboratoire EM2C, CentraleSupélec, CNRS, Université Paris-Saclay, France

This work presents the study of a toroidal hydrodynamic regime induced by Nanosecond Repetitively Pulsed (NRP) discharges in flames. Thanks to OH Planar Laser-Induced Fluorescence (PLIF) experimental visualizations of toroidal structures are reported for the first time in Plasma-Assisted Combustion (PAC) conditions using the Mini-PAC burner. The gas temperature measured between the electrodes by Optical Emission Spectroscopy (OES) of the (0,2) vibrational band of N2(C-B) for experimental conditions involving toroidal recirculation is about 1950 K. This value is close to the adiabatic flame temperature and shows the absence of cumulative heating effect by the repetitive discharges, far from previous experimental and numerical literature results reporting values around 3500 K. Such a drop in the inter-electrode temperature should lead to a decrease of thermal NO_X produced by the plasma but has not been observed yet.

1 Introduction

Plasma-assisted combustion (PAC) aims at reducing the production of combustion-related pollutants, mainly NO_X. The most efficient way to do so is by generating the plasma with Nanosecond Repetitively Pulsed (NRP) discharges [1]. However, the high pulse repetition frequency may lead to a cumulative significant heating of the gas located between the electrodes [2], measured to be about 1500 K [3] in the literature. The plasma is thus also producing thermal NO_X.

A promising way to prevent cumulative heating is to use the properties of a post-discharge toroidal hydrodynamic regime [4]. In particular, the toroidal recirculation structures draw surrounding gases between the electrodes. The surrounding gases are cooler than the hot core where the plasma was formed and will likely limit NO_X production.

2 Results

Toroidal structures induced by nanosecond discharges were previously observed in air [4] at room temperature. In this work, toroidal structures are observed with OH PLIF for the first time in configurations suitable for PAC, in the 13-kW methane-air flame of the Mini-PAC burner. This diagnostic allows us to find experimental conditions permitting both toroidal recirculation and flame assistance.

Temperature measurements of the gas in the inter-electrodes gap are undertaken by Optical Emission Spectroscopy (OES) of the (0,2) vibrational band of the N_2(C-B) transition. The measured temperature between the electrodes is 1950 K, like the adiabatic methane-air flame temperature for a fuel equivalence ratio of 0.8, and far from the literature values of around 3500 K. This shows that the toroidal regime prevents cumulative heating of the gas in the inter-electrode gap.

Finally, the NO_X concentration is measured using a commercial gas analyzer (ECOM J2KN). The expected abatement of the plasma NO_X production was not observed. Other mechanisms of NO_X production are suspected to be fostered by the new experimental conditions of the plasma corresponding to the toroidal structures.

3 Future work

We plan to further investigate the reduction of cumulative heating thanks to the presence of the toroidal structures. This work will be performed by optimizing the PLIF setup in order to observe the toroidal structures in a plasma-assisted flame with a high pulse repetition frequency.

Acknowledgments

This work has received funding from the European Research Council (ERC) under the European Union's Horizon 2020 research and innovation program (grant agreement No. 101021538).

References

[1] C. Kruger *et al.*, "Nonequilibrium discharges in air and nitrogen plasmas at atmospheric pressure", *Pure Appl. Chem.*, 74, nº 3, 337-347, janv. 2002.

[2] D. L. Rusterholtz *et al.*, "Ultrafast heating and oxygen dissociation in atmospheric pressure air by nanosecond repetitively pulsed discharges", *J. Phys. Appl. Phys.*, 46, nº 46, 464010, nov. 2013.

[3] V. Blanchard *et al.*, "Experimental and numerical characterization of a lean premixed flame stabilized by nanosecond discharges", in *AIAA SCITECH 2022 Forum*.

[4] C. Dumitrache *et al.*, "Hydrodynamic regimes induced by nanosecond pulsed discharges in air: Mechanism of vorticity generation", *J. Phys. Appl. Phys.*, 52, nº 36, juill. 2019.

Coupling of a microfluidic device with a reference cold plasma jet

J. Bissonnette-Dulude[1], P. Heirman[2], S. Coulombe[3], A. Bogaerts[2], T. Gervais[1], S. Reuter[1]

[1]*Department of Engineering Physics, Polytechnique Montreal, Montreal, Canada*
[2]*Department of Chemistry, University of Antwerp, Antwerp, Belgium*
[3]*Department of Chemical Engineering, McGill University, Montreal, Canada*
email: stephan.reuter@polymtl.ca

We present a novel plasma-microfluidic platform that combines plasma at atmospheric pressure with liquids in a multiphase flow. The plasma source is a COST capacitive plasma jet operated in helium. This jet is coupled with a simple microfluidic channel. Plasma-generated species are brought into contact with the liquid in a gas bubble-liquid droplet flow within the microfluidic channel. The coupling of the jet with the microfluidic channel can be modified to any position within the jet's plasma or effluent region. We supported the design of the plasma-microfluidic platform with a novel model that assumes plug flow conditions in the gas phase and uses 2D chemical and flow kinetics in the liquid phase. By measuring discharge power and H_2O_2 concentration in the liquid, we were able to show that the plasma-microfluidic platform is well suited to study aspects of plasma-liquid interaction e.g., for plasma medicine.

1 Aim of the work

Plasma-liquid interaction is a field of increasing interest among the plasma research community. With liquids being ubiquitous in living organisms, plasma-liquid interaction is of high relevance for applications of plasma science such as water decontamination, agriculture and medicine [1]. A promising diagnostic tool for plasma-liquid interaction lies in microfluidic devices. Microfluidic devices, often referred as lab-on-a-chip (LOC) technologies, have been used to reproduce standard chemical and biological experiments with a very small footprint. Three-dimensional cell cultures embedded in microfluidic devices have been found very useful for studying different cancer treatments such as chemotherapy and radiotherapy [2]. The high parallelization potential of LOCs makes the technology ideal for testing different treatments and selecting the optimal one rapidly. With the objective of using LOC technologies for studying the treatment of cancer by plasma, we developed a platform that enables the coupling of microfluidic devices with an atmospheric pressure plasma jet [3].

2 Experimental Setup

The plasma device is based on the COST reference microplasma jet [4]. It uses a capacitively coupled discharge excited at 13.56 MHz with two stainless steel electrodes clamped between a glass plate and a microfluidic device. The plasma channel has a volume of 30×1×1 mm^3. The effluent of the same dimensions is confined by dielectric walls. The feed gas is helium with variable admixture of O_2, N_2 and H_2O. The 3D-printed microfluidic channel allows high control on the position of the plasma-liquid interface and on the velocity of the liquid. The microfluidic device can be operated with a continuous liquid multiphase flow for increased reactive species transfer.

The developed plasma-microfluidic platform is to our knowledge the first demonstration of the coupling of a reference biomedical application-focused plasma jet with a microfluidic device. The platform provides high control over the delivery of plasma-produced reactive oxygen and nitrogen species and is a very powerful diagnostic tool for tailoring plasma reactivity in biomedical applications.

3 Results

The dissipated discharge power was determined using the subtractive power measurement method [5] and was on the order of 1W. The zone of interaction of the plasma with the liquid contained in the microfluidic channel was set to two positions: inside the plasma-forming region and in the plasma effluent.

The H_2O_2 concentrations, colorimetrically determined in the liquid collected from the microfluidic channel, is higher when the plasma-liquid interaction zone is located in the effluent region, compared to plasma-forming region. This is due to the fact that in the effluent, OH radicals quickly recombine to form H_2O_2 and that in the discharge region, H_2O_2 is destroyed by electron impact dissociation.

In conclusion, we have demonstrated the successful development of a plasma-microfluidic platform of reduced complexity that allows description by reaction kinetics models. With our work, we want to pave the way to standardized plasma-liquid interaction studies and promote a novel research approach in plasma medicine and plasma-liquid interaction.

References

[1] P. J. Bruggeman et al. PSST. 25 053002 (2016).
[2] Patra, B., Lafontaine, J., Bavoux, M. et al. Sci Rep 9, 2214 (2019).
[3] J. Bissonnette-Dulude et al. PSST (2023) submitted
[4] J. Golda et al. J. Phys. D: Appl. Phys. 49 084003 (2016).
[5] V. A. Godyak, R. B. Piejak, "In situ simultaneous radio frequency discharge power measurements," V8(5) 3833 (1990)

Control of self-organized luminous pattern formation in atmospheric-pressure dc glow discharge

T. Miyazaki, N. Shirai and K. Sasaki

Division of Applied Quantum Science and Engineering, Hokkaido University, Sapporo, Japan

In this work, to control the luminous pattern formation, we changed various experimental conditions, such as the gas condition, the external electric field, and the surface tension of the liquid anode in a dc glow discharge. We observed various luminous patterns depending on the experimental conditions. We were able to intentionally control the pattern formation in this work.

1 Introduction

The formation of self-organized luminous patterns is one of interesting phenomena observed in an atmospheric-pressure dc glow discharge. However, the mechanism of the pattern formation has not been understood in detail. The pattern is only observed above the anode, and the presence of electro-negative gases is important to form the patterns [1]. Therefore, we expected the densities of electron and negative ion are two formation factors in the reaction-diffusion system which is a mathematical model to describe self-organized patterns [2]. In this work, we changed various experimental conditions to change the reaction and the diffusion (the transport).

2 Experiment procedure

Figure 1 shows the experimental setup to generate an atmospheric-pressure dc glow discharge. The electrode structure is the same as that in reference [1]. To control the ambient gas atmosphere, nitrogen or oxygen sheath gas was flowed around the discharge column. The flow rates of helium and the sheath gas were 150-350 and 1000-2000 sccm, respectively, and the discharge current was changed between 20-120 mA. The external electric field was applied by placing a metal ring electrode above the anode coaxially. A surfactant (polyoxyethylene (23) lauriether) was added to the liquid anode to reduce the surface tension.

3 Results and discussion

Figure 2 shows various pattern formations above the liquid anode. These patterns were observed by controlling the gas flow rates and the voltage applied to the ring electrode. The number of luminous spots and the shape of the pattern were controlled by the experimental conditions. The pattern immediately changed when the external electric field was applied. The pattern gradually changed with the flow rate of helium. When the surface tension was reduced, we observed a protrusion on the surface of the liquid anode in the area in contact with the plasma. When the protrusion was formed, the surface area with the self-organized luminous pattern became narrower. It

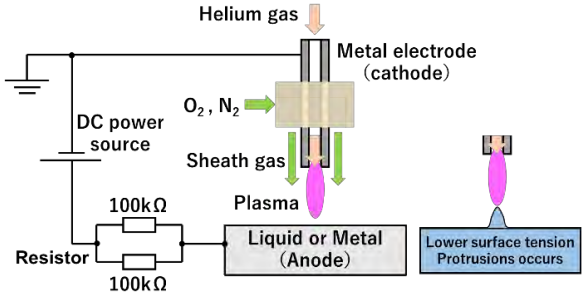

Fig.1 Experimental setup.

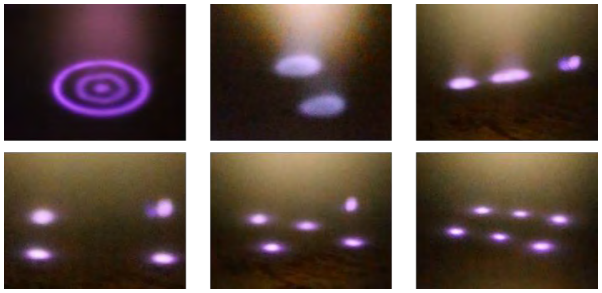

Fig.2 Various patterns observed above the anode.

is reported that the conductivity of the liquid and the type of the electrolyte affect the luminous pattern formation [3]. In this work, we were able to intentionally control the pattern formation by controlling the gas composition, by applying the external electric field, and by changing the shape of the anode. In addition, the experimental results suggest that the luminous pattern formation is controlled by the ratio of negative ion to electron densities and by the radial transport of the negatively charged species.

References

[1] N. Shirai, et al., Plasma Sources Sci. Technol. 23, 054010 (2014).
[2] A. Turing, Phil. Trans. R. Soc. B237 37-72 (1952).
[3] J. E. Foster, et al., Plasma Sources Sci. Technol. 29, 034004 (2020).

Modelling of PFAS Removal From Water by Plasma Treatment: C_3F_8 as a Surrogate *

Mackenzie Meyer[1], Mikhail Vasilev[2], Stephen Olson[3], Katharine Hunter[3], Selma Mededovic Thagard[2], and Mark J. Kushner[1]

[1] *Electrical Engineering and Computer Science Department, University of Michigan, Ann Arbor, MI, USA*
[2] *Department of Chemical and Biomolecular Engineering, Clarkson University, Potsdam, New York, USA*
[3] *3M Company, Saint Paul, MN, USA*

Plasmas can be utilized to efficiently treat water containing PFAS. Since PFAS are found on the surface of the liquid, they can be degraded by gas phase electrons and radicals as well as aqueous reactive species. Modelling the removal of PFAS from water, using C_3F_8 as a surrogate molecule, is discussed. Modifications were made to the 2-dimensional model to enable gas phase reactants to degrade liquid phase surfactants. The resulting C_3F_8 removal, and translating these results to PFAS removal, will be discussed.

1 Introduction

Water containing perfluoroalkyl and polyfluoroalkyl substances (PFAS) is increasingly being investigated due to the strength of the C-F bonds. Plasma treatment has been shown to remove organic contaminants in water, including PFAS. The mechanism of removal of PFAS is not solely due to aqueous reactive species. Since some PFAS are surfactants, PFAS may be removed by gas phase species, including electrons, at the interface between the gas and liquid [1]. To better understand trends in PFAS removal by plasma treatment, removal of a surrogate molecule C_3F_8 is modelled in this work. This molecule was chosen based on it being an alkane-like C_xF_y molecule and the availability of electron-impact dissociative cross-sections, shown in Figure 1 [2-4].

1.1 Model Description

The 2-dimensional model employed in this work is *nonPDPSIM* [5]. Poisson's equation is solved with continuity equations for charged species on an unstructured mesh. Electron and gas temperatures are obtained using their respective energy equations. Boltzmann's equation is solved to generate a look-up table of electron-impact rate coefficients. Henry's law governs transport between the gas and liquid. Modifications were made to the plasma-liquid interactions to account for surfactants. The rates of reactions between the gas phase species and surfactants are based on the electron or gas temperature and rate coefficient at a neighboring gas phase node and the flux of the gas phase reactant to the liquid phase node.

1.2 C_3F_8 Removal

The plasma is formed in humid Ar with a pulsed negative voltage applied to a pin electrode. A surface ionization wave forms above 5 mm of water. The removal of C_3F_8 over one pulse will be discussed. The different fragments, both neutral and charged, will be examined. The role of gas phase radicals, solvated electrons, and liquid phase radicals in C_3F_8 removal will also be assessed. Applications of these results to PFAS removal will be discussed.

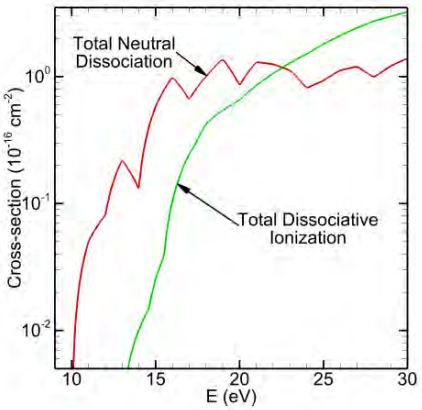

Figure 1. Dissociative cross-sections for C_3F_8.

References

[1] Stratton, G. R. *et al.* Environmental Science and Technology 51, 1643 (2017).
[2] Baio, J. E. *et al.* Journal of Physics D: Applied Physics **40**, 6969 (2007).
[3] Janev, R. K. and Reiter, D. Physics of Plasmas **11**, 780 (2004).
[4] Jiao, C. Q. *et al.* Chemical Physics Letters **325**, 203 (2000).
[5] Norberg, S. *et al.* Plasma Sources Science and Technology **24**, 035026 (2015).

* This work as supported by 3M, Inc., the U.S. Department of Energy Fusion Energy Sciences (DE-SC0020232), Army Research Office (W911NF-20-1-0105), and National Science Foundation (2032604). **Each author certifies that their freedom to design, conduct, interpret, and publish research was not compromised by the sponsor.**

Effective ionisation and three-body attachment swarm coefficients in H_2O-dry air gas mixtures

J de Urquijo[1], O. González[1], E. Basurto[2], A.M. Juárez[1]

[1]Instituto de Ciencias Físicas, Universidad Nacional Autónoma de México, México
[2]Universidad Autónoma Metropolitana – Azcapotzalco, Ciudad de México

We present the measurement of the effective ionisation and three-body attachment coefficients in H_2O-dry air mixtures. The three-body attachment coefficients were measured over the E/N range 1-30 Td and H_2O-dry air mixtures from 1%-50% H_2O. A pulsed Townsend apparatus was used.

This contribution is part of a long-term project dealing with the measurement of transport and ionisation properties of electrons in atmospheric gases. We have included H_2O as an important component in gaseous mixtures of CO_2, O_2, N_2 and dry air. The present contribution deals only with the dry air- H_2O mixture or in other words, humid air. Briefly, three-body attachment proceeds in two stages, the first of which involves an electron captured by a molecule into a vibrationally excited negative ion state, followed by a collision with a third body which removes the excess energy.

Previous work done in the direction of electron drift velocities and ionisation coefficients is abundant; however, little experimental work has been done in the line of electron diffusion and attachment, and in particular three-body attachment, an important phenomenon firstly proposed by Bloch and Bradbury [1] and further studied by Pack and Phelps [2] and Grünberg [3], the latter using a Pulsed Townsend apparatus with integration of the displacement current. These studies were made with pure oxygen.

Our Pulsed Townsend apparatus [4] was used for the measurement of the flux electron drift velocity, v_e, the effective ionisation coefficient, $(\alpha-\eta)/N$, and the density-normalised flux longitudinal coefficient, ND_L. All these coefficients will be presented in the conference.

The three-body attachment coefficient could be measured over the density-normalised electric field intensity, E/N, from 1-30 Td. First of all, a well defined gas pressure dependence was observed when plotting η/N as a function of E/N, with the curves fanning out regularly with the H_2O concentration and pressure. More precisely, for a given mixture ratio, η/N was observed to be clearly dependent on the total gas pressure (density). Provided that this is a three-body collision process, it is expected that the parameter η/N^2 be pressure independent, of course, within the experimental uncertainties. Indeed, the above is shown in Fig. 1, where the three-body attachment coefficient is shown plotted as a function of E/N. For the dry air and 2% H_2O-dry air measurements there is very good agreement between our values and those of Van Lint [5]. Our measurements of η/N^2 could be extended to mixtures containing up to 50% H_2O. It is noteworthy pointing out that water enhances three-body attachment at low E/N values by up two orders of magnitude in comparison with dry air. The uncertainties in our measurements for η/N^2 range between 6-14%

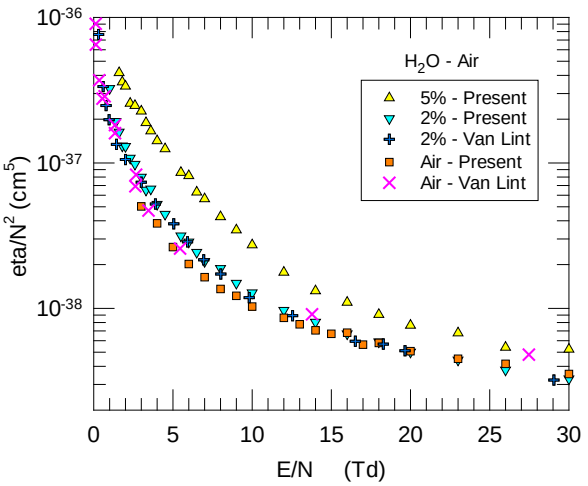

Fig. 1 The three-body attachment coefficient normalised to the square of gas density, η/N^2, in dry air and its mixtures with H_2O.

References

[1] F. Bloch and N. Bradbury, *Phys. Rev.* 48, 689 (1935).
[2] J. L. Pack and A. V. Phelps, *J. Chem. Phys.* 44, 1870 (1966).
[3] R. Grunberg, Z. Naturforsch. 24a, 1039 (1969).
[4] J L Hernàndez-Ávila, et al. *J. Phys. D: Appl. Phys.* **35,** 2264–2269 (2002).
[5] van Lint, V.A.J., *Theoretical Note 345* (1982) Westinghouse Electric Corporation

Validating Townsend criterion for the ignition of volume electrical discharges

R. M. S. Almeida[1,2], P. G. C. Almeida[1,2], G. V. Naidis[3], M. S. Benilov[1,2]

[1] *Departamento de Física, FCEE, Universidade da Madeira, Funchal, Portugal*
[2] *Instituto de Plasmas e Fusão Nuclear, Instituto Superior Técnico, Universidade de Lisboa, Lisboa, Portugal*
[3] *Joint Institute for High Temperatures, Russian Academy of Sciences, Moscow, Russia*

The Townsend self-sustainment criterion is extended to include the effect of negative ions and non-homogeneous electric fields in multidimensional geometries. The formulated extended criterion is validated against the exact solution of the eigenvalue problem describing the ignition of self-sustained discharges.

1 Introduction

In accurate mathematical terms, the ignition voltage (IV) of electrical discharges in gases is governed by an eigenvalue problem describing the ion and electron transport in the applied electric field [1]. On the other hand, the main tool for a quick evaluation of the IV, which is a key characteristic of high-voltage devices, is still some or other form of the Townsend criterion. A link between these two approaches is established in this work.

2 The formulation

At ignition of a self-sustained discharge, the discharge current is very low, multistep processes are irrelevant, and the charged particle conservation equations are linear. If diffusion, photoionization, and detachment reactions are neglected, and the local-field approximation adopted, then a partial integration of the system of conservation equations along the electric field lines gives a necessary condition for existence of a non-trivial solution,

$$e^{K(z_a)} + \int_0^{z_a} \eta e^{K(z)} dz = 1 + \frac{1}{\gamma'}, \quad (1)$$

$$K(z) = \int_0^z (\alpha - \eta) dz,$$

where α is the ionization coefficient, η is the electron attachment coefficient, γ' an effective secondary electron emission coefficient, coordinate z is measured along a field line from the cathode ($z = 0$) to the anode ($z = z_a$), and both integrals are evaluated along a field line. Equation (1) represents the extended Townsend criterion. It is reduced to the classical Townsend expression if no negative ions are considered, $\eta = 0$ (and the electric field is uniform).

While the classical form of Townsend criterion neglects the effect of negative ions on the IV, equation (1), which was derived without account of detachment, provides an upper estimate of the effect.

3 Results and discussion

The approach was validated against the exact solution of the eigenvalue problem describing the ignition of a self-sustained discharge, which was computed by the resonance method [1]. The kinetic and transport coefficients are the same as in [1].

An example of validation is shown in the table. The IV values given by the resonance method in limiting cases *b)* and *c)* are very close to those given by the extended and classical Townsend criteria, as they should. With increase of pressure, the difference between the values obtained with and without account of attachment increases. The full model *a)*, accounting for ionization, attachment and detachment, gives an intermediate value between the two limiting cases. A very close value is given by the extended Townsend criterion, equation (1), if η is replaced with the effective attachment coefficient [2].

	Eigenvalue problem			Townsend criterion		
p (atm)	*a)*	*b)*	*c)*	Extended	Classical	*d)*
0.117	5.60	5.72	5.68	5.77	5.73	5.73
0.996	26.16	26.69	26.10	26.73	26.14	26.16
9.063	153.21	163.12	148.39	163.15	148.42	152.77

Table: Inception voltage of coaxial negative corona (in kV) with inner radius of 0.1195 cm and outer radius of 4.875 cm, for different values of pressure. *a)* Full model. *b)* No photoionization and no detachment. *c)* No photoionization and no attachment. *d)* Equation (1) with η replaced with the effective attachment coefficient introduced in [2].

The approach has been validated also for negative corona in point-to-plane geometry and a discharge between disc electrodes separated by a dielectric disc.

Acknowledgments

This work was supported by European Regional Development Fund through the program Madeira 2014–2020 under Project No. PlasMa-M1420-01-0145-FEDER-000016 and FCT of Portugal under Project No. UIDP/50010/2020 (UMa).

References

[1] Benilov, M. S. et al, J. Appl. Phys. **130**, 121101 (2021).
[2] Ferreira, N. G. C. et al, J. Phys. D: Appl. Phys. **52**, 355206 (2019).

Space charge structures on gridded coaxial cylinders

F. Enescu[1], R.G. Cucu[2], G. Dimitriu[3], C. Ionita[1], R.W. Schrittwieser[1]

[1]*Institute of Ion Physics and Applied Physics, University of Innsbruck, Austria*
[2]*Faculty of Applied Science and Engineering, Ovidius University of Constanta, Romania*
[3]*Faculty of Physics, Alexandru Ioan Cuza University of Iasi, Romania*

1 General

Complex space charge structures may appear in plasma regions if the localized electric field is modified. This causes the system to shift away from thermodynamic equilibrium showing both, steady and unstable regimes. The dynamics of the plasma structures involve complex oscillations of plasma parameters identified as chaotic states under certain experimental conditions [1,2].

In this experiment we have investigated various instabilities in a system consisting of two concentric cylindrical gridded cylinders with a common aperture on one side.

2 Setup and results

The experiments were carried out in a cylindrical stainless steel chamber of 92 cm length and 53,5 cm diameter (Figure 1).

The chamber was filled with argon (pressure $7{\cdot}10^{-2}$ to $7{,}5{\cdot}10^{-2}$ mbar). Two coaxial cylindrical gridded cathodes of stainless steel were inserted (mesh width 1,2×1,2 mm^2, wire diameter 0,6 mm), length of both cylinders 10 cm and 3 and 6 cm diameter, respectively. Both cylinders were open on the right side and simultaneous negatively biased from –50 V to –350 V.

We found an inverted fireball outside of the aperture of the cylinders, with a brief period of unstable pulsating behaviour. The transition from instability to stability and back was analysed and a hysteresis pattern appeared, as well as a chaotic regime.

Fig. 2 shows an exemplary cycle of the plasma instability starting with a discharge between the cathodes (Fig. 2a), followed by an increasing plasma structure between the cylinders (maximum in Fig. 2b), then a longer period of stability as seen in Fig. 2c; then the cycle repeats.

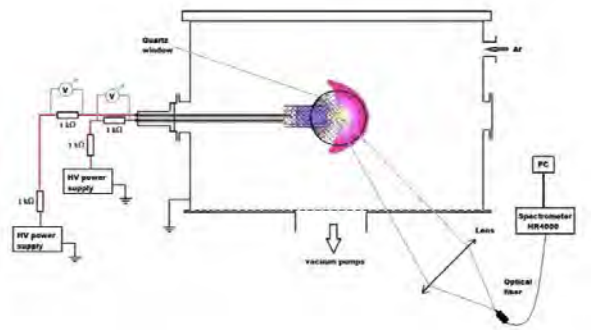

Figure 1. Experimental set-up.

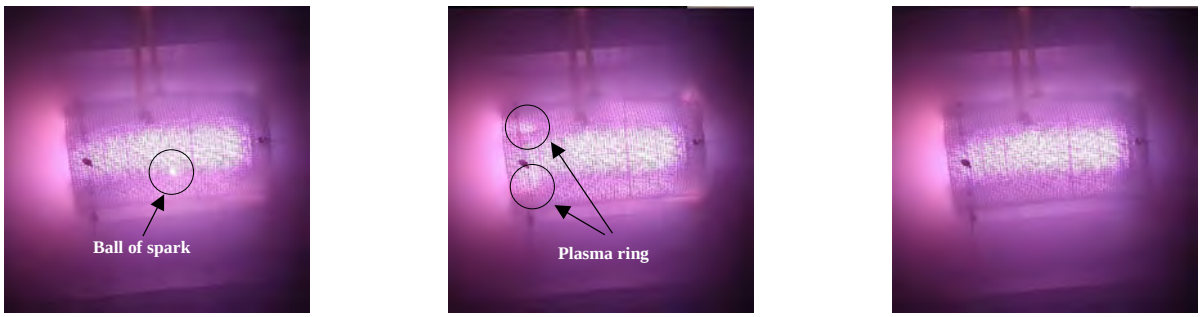

(a) **(b)** **(c)**

Figure 2. Photos of a cycle of plasma pulsation between two regimes: $p = 7{\cdot}10^{-2}$ mbar, $V_{inner} = -350$ V (kept constant), $I_{inner} = 30$ mA, $V_{outer} = -139{,}6$ V, I_{outer} 6 mA.

Acknowledgement

This work was supported by the CEEPUS (Central European Exchange Programme for University Studies) network AT-0063.

References

[1] R. Schrittwieser et al., *Phys. Scr.* **92** (2017) 044001.
[2] C.T. Konrad-Soare et al, *Plasma Sources Sci. Techn.* **30** (2021) 085006.

Hysteresis Effects in Shielded kHz Atmospheric Pressure Plasma Jet

H. Philpott[1,2], A. Sobota[1] and O. Guaitella[2]

[1] *Dept. Applied Physics, Eindhoven Univ. Techn., Eindhoven, The Netherlands*
[2] *Laboratoire de Physique des Plasmas (UMR 7648), CNRS, Univ. Paris Saclay, Sorbonne Université, École Polytechnique, France*

In this work we put forth results obtained from experimental measurements investigating hysteresis effects in a shielded coaxial atmospheric pressure plasma jet (APPJ) [1] using different shielding and working gas combinations. At present, the interaction of ionisation waves with complex dielectric materials (e.g. catalysts) is still not very well understood. Therefore an APPJ was chosen so that highly reproducible ionisation waves could be generated in a way that allowed for numerous diagnostic approaches. Specifically, we took measurements using optical emission spectroscopy (OES), oscilloscope traces, Schlieren imaging, intensified charge couple device (ICCD) imaging and images taken from a high definition webcam.

Our measurements involved placing a 5mm wide smooth glass disk angled at 45 degrees to our shielded plasma source, and 0mm distance from it. The target was held in place for 90 minutes as the plasma stabilised. We then moved the target away from the source, making measurements at 2, 4, 6 and 300mm (effectively infinite) distances, holding the target in place for 10 minutes before moving it to the next distance with the aid of a fine control stepper motor. We then performed the reverse of this operation, by moving the target towards the plasma source and measuring at the same positions. This procedure of moving the target away and then towards the plasma source was repeated for four different working/shielding gas combinations, which are as follows: He-N_2, He-CO_2, He/Ar-N_2, He-unshielded. In particular we find that the current peaks evolve over a long timescale as the applied voltage is held constant, and that the results at each position depends upon the direction of travel. However, these findings are very much dependent on the gas mixture used, with each combination exhibiting different effects, for example, in figure 1 we see a notable variation in the plasma within the capillary and on the target depending upon the direction of travel. This effect is not as strong with other shielding/working gas mixtures.

The overall aim of this investigation was to get a better understanding of how certain aspects of experimental measurement regimes can affect their reproducibility. The outcome of this investigation puts forth evidence that the plasma from a DBD source is not only dependent upon the current global parameters (e.g. gas temperature, humidity, applied voltage etc.), but also on their preceding values of those parameters, i.e. the plasma is capable of hysteresis. We posit that this hysteresis can arise from the charge storing properties of the dielectric barriers creating so-called “memory effects”[2] which impact subsequent discharges.

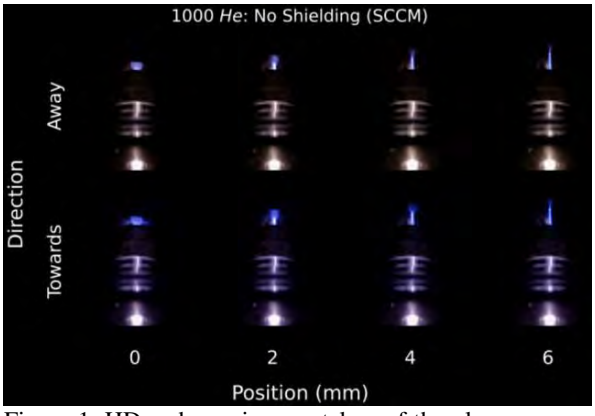

Figure 1. HD webcam images taken of the plasma source at various positions and directions of travel. The difference between the “away” and “towards” images is quite apparent, with the “away” showing a much whiter discharge inside the capillary and on the target surface.

References

[1] Narimisa, M. A poly-diagnostic study of the shield gas-assisted atmospheric pressure plasma jet propagation upon a dielectric surface. Plasma Processes and Polymers, **19**(6), 1–24 (2022).

[2] Kuthanová, L. Memory propagation in barrier discharge at water interface: Suspected Markov states and spatiotemporal memory effects. Plasma Sources Science and Technology, **31**(4) (2022).

Modelling the role of the leftover charged species on the subsequent discharges

Yazhen Wang[1], Yuan Li[1], Yifei Zhu[2], Guanjun Zhang[1]

[1] *School of Electric Engineering, Xi'an Jiaotong University, Xi'an 710049, People's Republic of China*
[2] *School of Mechanical Engineering, Xi'an Jiaotong University, Xi'an 710049, People's Republic of China*

In this paper, we report the simulation results of double-pulse discharges by zero and two-dimensional modelling, and quantitatively explain how residual charges and species created by previous streamer discharge affect the initiation and propagation of the subsequent discharge. The kinds and densities of the charged species decay as a function of the pulse delay time (Δt) and the dynamics determine the length changes of the 2nd streamer.

1 Introduction

Previous discharge significantly influences the subsequent discharges and this is especially pronounced in repetitively pulsed discharges, due to the residual charges and species created by previous discharge [1-2].

In previous work [3], we have performed double-pulse streamer experiments in pure nitrogen (N_2) and artificial air (20% O_2+80% N_2) at 66.7 mbar to 400 mbar pressure (1 mbar = 100 Pa) with a varying pulse delay (Δt) from 0.45 μs to 20 ms. It is found that the propagation distance of the 2nd pulse streamer can be elongated (66% longer than the 1st pulse in nitrogen, and 37% longer in artificial air under the same conditions). However, it was experimentally verified that it is not caused by a higher propagation velocity nor by fast gas heating of previous channels under the experimental conditions, but by faster initiation of the 2nd pulse streamers. More specifically, we found that the 2nd pulse streamer can initiate almost 150 ns earlier than the previous one (with respect to the voltage pulse) in N_2. In artificial air, the 2nd pulse streamers start at almost the same time to form the inception cloud but the inception cloud of the 2nd pulse streamer breaks up at least 120 ns earlier than the 1st pulse streamer, hence the 2nd pulse streamers have more effective propagation time and travel longer. The onset of every stage occurs at smaller Δt in air than in N_2 at the same pressure. Based on these observations, it can be safely assumed that different mechanisms work in N_2 and air, e.g., photoionization and attachment.

However, the current measurement conditions do not allow us to directly unveil the role of those assumed mechanisms and species in a quantitative manner. This paper follows up on previous work and further quantitative analyses the exact mechanism for the pulse delay times, especially on how the density and distribution of electrons, ions and metastable species influences the next discharge.

2 Simulation results and discussion

We incorporate a zero-dimensional kinetic model and two-dimensional multiphysics model based on the local approximation to describe the roles of electrons, ions and various metastable species. The zero-dimensional model employs the BOLSIG+ solver and includes 650 reactions of 53 species [4]. We cite [1] as a point of reference with respect to the excited neutrals, ground state neutrals, positive ions, and negative ions under consideration. Two distinctions between our work and the reference [1] are as follows: (i) in the current study, we place greater emphasis on the plasma decay phase, which refers to the period of time between the 1st pulse streamer and the 2nd pulse streamer and (ii) we place greater emphasis on neutrals, specifically metastable atoms and molecules.

The results of our simulation model quantitatively clarify that the density of electrons and ions in the previous discharge plasma channels are still considerably high to let the 2nd streamer continue the paths from the stopping point of previous streamer instead of that from the tip. Moreover, the mechanism of electron generation during the decay process of plasma in air and N_2 is elucidated.

References

[1] Nijdam S, Takahashi E, Markosyan A H, et al. Investigation of positive streamers by double-pulse experiments, effects of repetition rate and gas mixture[J]. Plasma Sources Science and Technology, 23(2): 025008 (2014).

[2] Li Y, Dijcks S, Sun G, et al. Characterizing streamer branching in N2–O2 mixtures by 2D peak-finding[J]. Plasma Sources Science and Technology, 29(3): 03LT02. (2020).

[3] Li Y, Van Veldhuizen E M, Zhang G J, et al. Positive double-pulse streamers: how pulse-to-pulse delay influences initiation and propagation of subsequent discharges[J]. Plasma Sources Science and Technology, 27(12): 125003 (2018).

[4] Flitti A, Pancheshnyi S. Gas heating in fast pulsed discharges in N2–O2 mixtures[J]. The European Physical Journal Applied Physics, 45(2): 21001 (2009).

The influence of secondary electron emission on a capacitive chlorine discharge

B. Mahdavipour[1] and J. T. Gudmundsson[1,2]

[1] *Science Institute, University of Iceland, Dunhaga 3, Reykjavik, Iceland*
[2] *Space and Plasma Physics, School of Electrical Engineering and Computer Science, KTH Royal Institute of Technology, Stockholm, Sweden*

A one-dimensional particle-in-cell Monte Carlo collision simulations are applied to explore the influence of secondary electron emission on a capacitively coupled chlorine discharge at different chlorine gas pressures.

The one-dimensional particle-in-cell Monte Carlo collision (PIC/MCC) code `oopd1` is used to explore a capacitively coupled chlorine discharge. The chlorine plasma discharge is located between two parallel, planar electrodes with the left electrode connected to a sinusoidal voltage source and the right electrode grounded. The feedstock gas is the Cl_2 molecule, which has a low threshold for dissociative attachment and low dissociation energy (2.5 eV), while the electron affinity is high (2.45 eV). The model is composed of the ground state molecule $Cl_2(X^1\sum_g^+, v = 0)$, the ground state atom $Cl(^2P_u)$, the negative ion $Cl^-(^1S_g)$, and the positive ions $Cl^+(^3P_g)$ and $Cl_2^+(^2\Pi_g)$. The reactions taken into account and the cross sections used are described in detail elsewhere [1]. Here, secondary electron emission due to both ion impact and electron impact is added to the discharge model. The cross sections for elecron impact excitation of the chlorine molecule, and therfore dissociation, which were earlier taken from the calculations of Rescigno [2] (old) are now replaced by more recent calculations of Hamilton *et al.* [3] (new). The Hamilton *et al.* [3] cross section data is used for all the calculations with secondary electron emission. The gap space was 2.54 cm and the discharge driven by a sinusoidal rf voltage of amplitude 222 V.

The results for the center electronegativity are shown in Figure 1, where the different cases are compared. All the cases have nearly the same electronegativity at pressure of 2 Pa. When the pressure is increased the electronegativity increases. When neglecting the secondary electron emission the Rescigno cross sections give slightly lower electronegativity than using the Hamilton *et al.* cross sections. We consider ion energy dependent electron emission $\gamma_i(\mathcal{E}_i)$ from Phelps and Petrović (actually for the Ar^+ ion) [4] and electron induced electron emission $\gamma_e(\mathcal{E}_e)$ [5]. At both pressures increasing the secondary electron emission yield lowers the electronegativity. At both 10 and 20 Pa, for high ion induced secondary electron emission yield ($\gamma_i = 0.5$) the elecronegativity is the lowest.

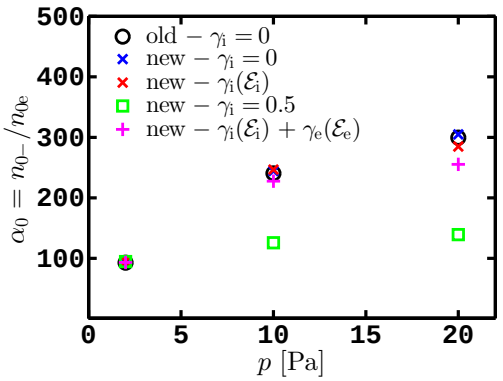

Figure 1: The electroegativity in the discharge center α_0 versus pressure for various secondary emission conditions.

References

[1] Huang, S. & Gudmundsson, J. T. *Plasma Sources Science and Technology* **22**, 055020 (2013).

[2] Rescigno, T. N. *Physical Review A* **50**, 1382 – 1389 (1994).

[3] Hamilton, J. R. *et al. Plasma Sources Science and Technology* **27**, 095008 (2018).

[4] Phelps, A. V. & Petrović, Z. L. *Plasma Sources Science and Technology* **8**, R21–R44 (1999).

[5] Vaughan, R. M. *IEEE Transactions on Electron Devices* **40**, 830 (1993).

Modeling energy efficiency of plasma chemistry by streamers in air

Baohong Guo[1], Ute Ebert[1,2] and Jannis Teunissen[1]

[1] *Centrum Wiskunde & Informatica (CWI), Amsterdam, The Netherlands*
[2] *Dept. Applied Physics, Eindhoven Univ. Techn., Eindhoven, The Netherlands*

We have studied the energy efficiency of species production by streamer discharges with a single voltage pulse in atmospheric dry air, using a 2D axisymmetric fluid model [1]. Sixty streamers are simulated by varying the electrode geometry, pulse duration and applied voltage. Between these cases, the streamer radius and velocity vary by about an order of magnitude, but the variation in maximal electric field is significantly smaller, about 30%. We find that G-values for the production of N(^{4}S), O(^{3}P), NO and N_2O, which have relatively high activation energies, vary by about 30% to 60%. This variation is mainly caused by two factors: differences in the fraction of energy deposited in the streamer head region, and differences in the maximal electric field at the streamer head, suggesting that energy efficiency can be increased by using short voltage pulses with a high applied voltage.

1 Introduction and simulation model

In streamer discharges, chemically active species are produced by collisions of energetic electrons with gas molecules. Due to their highly non-equilibrium nature, streamer discharges can efficiently produce species with a high activation energy without significant gas heating.

In this paper, we computationally study how streamer properties affect the energy efficiency with which chemically active species are produced. Simulations are performed at 300 K and 1 bar in a 40 mm plane-plane gap with a needle protrusion, using a 2D axisymmetric fluid model. Pulsed streamer discharges and their afterglows are simulated up to $t = 500$ ns using the open-source `Afivo-streamer` code. We have here constructed a set of 263 chemical reactions for streamer simulations in atmospheric dry air, considering relatively short time scales (up to several microseconds).

2 Simulation results and conclusions

Sixty different positive streamers were obtained by varying the electrode geometry, the applied voltage and the duration of the voltage pulse. The obtained streamers had diameters ranging from about 0.5 mm to 3.5 mm, velocities ranging from about 0.3×10^6 m/s to 5.7×10^6 m/s and maximal electric fields ranging from about 120 kV/cm to 150 kV/cm.

For species with a relatively high activation energy, such as N(^{4}S), O(^{3}P), NO and N_2O, G-values, which give the net number of atoms or molecules produced per 100 eV of deposited energy, were found to vary by about 30% to 60% between the 60 positive cases. The most important factors behind this variation were differences in the fraction of energy deposited in the streamer head region and variation in the maximal electric field at the streamer head. When accounting for both factors, good agreement was obtained with an analytic estimate for G-values proposed by Naidis [2].

Our results suggest two main ways to increase the energy efficiency with which species with a high activation energy are produced. First, Joule heating losses in the streamer channel can be reduced, and second, the maximal reduced electric field at the streamer head can be increased. Short voltage pulses with a high applied voltage can contribute to both factors.

References

[1] Guo, B. & Teunissen, J. A computational study on the energy efficiency of species production by single-pulse streamers in air. *Plasma Sources Science and Technology* **32**, 025001 (2023).

[2] Naidis, G. V. Efficiency of generation of chemically active species by pulsed corona discharges. *Plasma Sources Science and Technology* **21**, 042001 (2012).

Molecular dynamics simulations of confined microplasmas at cryogenic temperatures

Swati Swagatika Mishra[1], Pascal Brault[2] and Sudeep Bhattacharjee[1]

[1]*Department of Physics, Indian Institute of Technology, Kanpur 208016, India*
[2]*GREMI UMR 7344 CNRS Université d'Orléans, Cedex 2 France*

Molecular dynamics simulations (MDS) are performed to study the He microplasmas at cryogenic temperatures, employing the insights obtained from the study of confined He gas in equilibrium and non-equilibrium conditions. It is expected that these simulations will predict the role of plasma-surface, and plasma-gas interactions in determining the energetics and the structure of the plasma and the surfaces in contact.

1 Introduction

Confined noble gases such as He, Ne and Ar at cryogenic temperatures exhibit several interesting physical properties. In a recent work, we show how the gas temperature (T_g) guides the transport phenomena and near-wall behaviour of He in the cryogenic limit (30 – 150 K), employing equilibrium MDS [1]. At a lower T_g (< 50 K) near-wall accumulation of the gas particles is observed, which affects the heat transfer from the walls to the confined gas. This has been investigated through non-equilibrium MDS, dictated by the temperature difference between the wall and the gas.

In the present work, the above findings are applied in understanding the structure, dynamics and energetics of microplasmas created at cryogenic temperatures. Cryoplasmas are commonly generated in noble gases using a parallel plate dielectric barrier discharge [2]. Due to their weakly ionized nature, the background cold neutral gas plays an important role in deciding the structure and energetics. We investigate the roles of ions interacting with other ions, the ambient gas, and enclosing surfaces, including gas-surface interactions, in the formation of crystal structures and patterns in the He cryoplasma. Furthermore, the plasma dynamics and its energy distribution under bulk and confined conditions are studied.

2 Simulation details

All the MDS are performed using LAMMPS software package [3]. The gas region having dimensions 66^3 nm^3 is populated with He atoms interacting through Lennard-Jones potential [1]. Initial gas pressure is set at 1 atmospheric pressure whereas, initial T_g is chosen in the range 30 - 150 K. He^+ ions are introduced at the centre of the gas region, with ion temperature $\approx T_g$, with an initial Gaussian distribution, and can move randomly. For the bulk phase simulations, periodic boundary conditions are implemented in all the directions. To maintain the set T_g the He particles are coupled with a Nose-Hoover thermostat. However, the ions constitute a microcanonical ensemble with their number (N), volume (V) and energy (E) constant. Electron motion is not considered explicitly in the simulations, but they participate in the shielding process through the Yukawa potential. The ion-ion interaction is therefore guided by this potential and a modified form is used at low temperatures (< 40 K). For the ion-gas interaction an effective potential is taken [4].

For the confined case, a pair of parallel Fe walls is introduced along the X direction (cf. Fig. 2). Periodic boundary conditions are implemented along the two unbounded (Y and Z) directions. The Fe atoms interact through EAM potential, whereas, the gas-wall interactions are modelled by Morse potential [1]. The walls are coupled with a Nose-Hoover thermostat that maintain the set temperature of the whole system. Both the gas and the ions constitute a microcanonical ensemble.

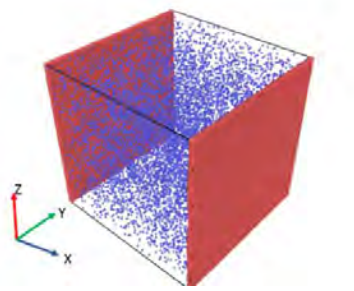

Fig. 1 Snapshot of the confined simulation system. Brown colour shows Fe walls and blue dots show He atoms.

References

[1] Mishra S. S. and Bhattacharjee, S. Chemical Thermodynamics and Thermal Analysis **7**, 100073 (2022).
[2] Noma, Y. et al. Journal of Applied Physics **109**, 053303 (2011).
[3] Plimpton, S. Journal of Computational Physics **117**, 1 (1995).
[4] Ramazanov, T. S. Physics of Plasmas **17**, 042703 (2010).

Double-pulse streamer simulations for varying interpulse times in air

H. Malla[2], A. Martinez[1,2], U. Ebert[1,2] and J. Teunissen[2]

[1] *Dept. Applied Physics, Eindhoven Univ. Techn., Eindhoven, The Netherlands*
[2] *Centrum Wiskunde & Informatica (CWI), Amsterdam, The Netherlands*

In this poster, we show how streamer discharges are influenced by a previous voltage pulse by peforming double-pulse positive streamer simulations. We do this in an axisymmetric model in dry air at 1 bar, varying the time between the pulses between 5 ns and 10 μs. For increasing interpulse times, we observe three regimes during the second pulse: streamer continuation, inhibited growth and streamer repetition (see figure 1). In the streamer continuation regime, a new streamer emerges from the tip of the previous one. In the inhibited regime, the previous channel is partially re-ionized, and almost no light emission. Finally, for the longest interpulse times, a new streamer forms that is similar to the first one. The remaining electron densities at which we observe streamer continuation agree with earlier experimental work. We introduce an estimate which relates streamer continuation to the dielectric relaxation time, the background field and the pulse duration. Furthermore, we show that for interpulse times above 100 ns several electron detachment reactions significantly slow down the decay of the electron density.

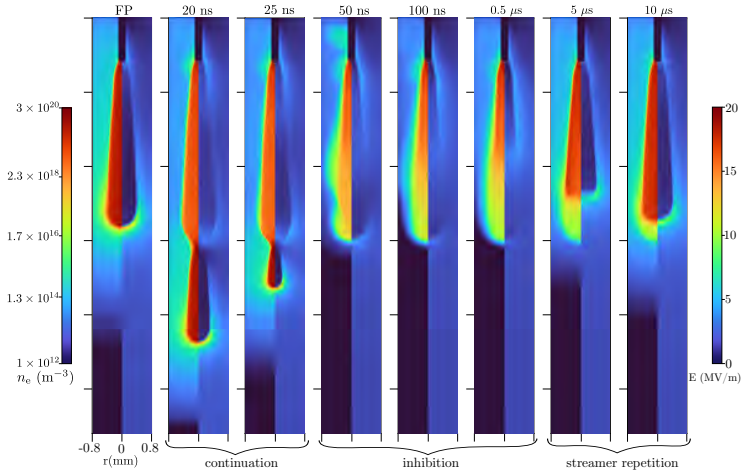

Figure 1: Plots of the first pulse (FP) streamer (left most column) and of the second streamer for interpulse times of 20 ns to 10 μs (as indicated above each column), for 20% O_2. Each column shows electron density and electric field. The three observed regimes, streamer continuation, inhibited growth and streamer repetition are indicated

Data-driven Identification of the Breathing Mode governing equations.

B. Bayón[1] and M. Merino[1]

[1] *Equipo de Propulsión Espacial y Plasmas (EP2), Universidad Carlos III de Madrid, Leganés, Spain*

We demonstrate the use of data-driven sparse regression techniques to obtain the Ordinary Differential Equations governing the neutral and ion density dynamics of the breathing mode in a Hall Effect Thruster, using PIC/fluid simulation data at 4 different operating points. Various models of different degree of complexity are obtained, with a focus on the physical explainability of the appearing terms. The resulting equations for the average densities in the ionization zone agree well with existing 0D models. On the other hand, point-wise density models show a dependency on the location in the discharge chamber, e.g. upstream vs downstream and channel centerline vs near the wall. While the point-wise ion density equation exhibits small variations along the channel, neutral density equations depend strongly on the location. We use ensemble methods to describe the uncertainty in the identified models. Finally, the variation of the model coefficients with the operating point is discussed.

1 General

Hall Effect Thrusters (HETs) are one of the most successful plasma space propulsion systems. However, their physics are still not fully understood and remains object of active research. The Breathing Mode (BM) instability consists of large, low-frequency discharge current oscillations and is operating point-dependent. If not accounted for, it can dominate the discharge, reduce performance, and increase wall erosion. Previous studies have described the BM as increasingly complex predator-prey dynamics between neutrals and the ionization process [1]. However, the BM still lacks a consistent model that can explain the instability's physics, such as its onset criteria and growth rate. Beyond theoretical and phenomenological approaches to obtaining governing equations, Machine Learning techniques show promise to unlock hidden insight from high-dimensional data, finding patterns without being constrained by researcher bias.

In this contribution we propose the use of the Sparse Identification of Non-linear Dynamics (SINDy) [2] framework to retrieve the governing equations of the plasma dynamics from microscopic data, following a similar approach to the one in [3]. We use SPT-100 simulation data generated by HYPHEN [4], a particle-in-cell / fluid hybrid axisymmetric 2D plasma simulation code. These data have been recently used to isolate the Breathing Mode oscillations from the rest of the dynamics using data-driven modal analysis [5].

Three main results are reported. First, the evolution of the average plasma and neutral densities in the channel are well described by simple differential equations. Various reduced models, ranging in complexity, are identified and discussed, with a focus on the physical interpretation of each term in them. Second, we expand our analysis to the point-wise densities in the discharge channel, to ascertain the domain in which simple BM laws are followed. Axial position in the channel and nearness of walls affects the identified model. Thirdly, we discuss the trend of the numerical value of the coefficients in the differential equations as the operating point of the HET is varied. The sparse regression method outlined here is shown to have the potential to be easily extended to the analysis of other thrusters and phenomena where prior knowledge is lacking.

References

[1] Hara, K., Sekerak, M. J. et al. Perturbation analysis of ionization oscillations in Hall effect thrusters. Physics of Plasmas **21**, 122103 (2014).

[2] Brunton, S. L.; Proctor, J. L.; Kutz, J. N. Discovering governing equations from data: Sparse identification of nonlinear dynamical systems. Proceedings of the National Academy of Sciences V113, **15** (2016).

[3] Alves, E. P.; Fiuza, F. Data-driven discovery of reduced plasma physics models from fully kinetic simulations. Physical Review Research **4**, 033192 (2022).

[4] Domínguez-Vázquez, A. Axisymmetric simulation codes for Hall effect thrusters and plasma plumes. PhD Thesis (2019).

[5] Maddaloni, D.; Domínguez-Vázquez, A.; Merino, M. Data-driven analysis of oscillations in Hall thruster simulations. Plasma Sources Science and Technology **31**, 4 (2022).

Overview of the afivo-streamer and afivo-pic simulation codes

J. Teunissen[1], D. Bouwman[1], U. Ebert[1], H. Francisco[1], B. Guo[1], X. Li[1], A. Malagon[1], H. Malla[1], Z. Wang[1]

[1] *Centrum Wiskunde & Informatica (CWI), Amsterdam, The Netherlands*

On this poster, we give an overview of the `afivo-streamer` and `afivo-pic` codes, which are used for the simulation of fast-pulsed discharges, primarily streamers, in 2D and 3D. The underlying `afivo` framework provides adaptive mesh refinement (AMR) and parallelization. We will discuss recent improvements, give examples of applications, and discuss design and practical considerations.

1 Introduction

In recent years, the number of available (open-source) discharge simulation codes has increased. Having more options can be beneficial, but it can also make it more difficult to choose the right code for a particular purpose. On this poster, two codes developed in the Multiscale Dynamics group at CWI are therefore presented in some detail: `afivo-streamer` and `afivo-pic` [1, 2, 3, 4]. They were primarily developed for simulating streamer discharges, although other applications are also possible. We will give an overview of the codes and discuss their respective benefits and drawbacks. We also present recent applications and provide an outlook on future development.

References

[1] Wang, Z., Sun, A. & Teunissen, J. A comparison of particle and fluid models for positive streamer discharges in air. *Plasma Sources Science and Technology* **31**, 015012 (2022).

[2] Teunissen, J. & Ebert, U. Afivo: A framework for quadtree/octree AMR with shared-memory parallelization and geometric multigrid methods. *Computer Physics Communications* **233**, 156–166 (2018).

[3] Teunissen, J. & Ebert, U. Simulating streamer discharges in 3D with the parallel adaptive Afivo framework. *Journal of Physics D: Applied Physics* **50**, 474001 (2017).

[4] Teunissen, J. & Ebert, U. 3D PIC-MCC simulations of discharge inception around a sharp anode in nitrogen/oxygen mixtures. *Plasma Sources Science and Technology* **25**, 044005 (2016).

Flow and microwave design of the Topological Reactor.

F.M.A. Smits[1], L. de Man[1], P.W.C. Groen[2], J.A.J.M. Disselhorst[1], E.J.Visser[1], E.L.Wiegers[1], C.F.A.M. van Deursen[2], D. Bouwmeester[1], M.C.M. van de Sanden[2] and W.A. Bongers[2]

[1] *Leiden Institute of Physics, Leiden University, Leiden, The Netherlands*
[2] *DIFFER, Eindhoven, The Netherlands*

Linear microwave plasma sources suffer from gas slippage (unprocessed gas flow), energy loss and back-reaction (burn back of products) mechanisms [1]. As a consequence, these reactors can either achieve high conversion or high energy efficiency, but not both at the same time [2]. The topological reactor is being designed to tackle these issues by processing the entire gas flow, eliminating the loss mechanisms, and applying controlled quenching. This is achieved by a helical flow topology around a microwave plasma. The flow topology forces nearly all gas through the processing region. The plasma shape remains inside the microwave cavity with increasing power, removing microwave losses. The large distance to the cavity walls and the absence of the heat radiation absorbing quartz tube reduce heat loss. The fast flow at the exhaust nozzle close to the product forming region must allow for quenching before back-reactions occur. The reactor design simulations demonstrate that the flow topology and microwave heating are feasible.

Microwave plasma reactors are a promising alternative to fossil fuel heating of chemical processes and can scale up for bulk chemistry [3]. Microwave reactors offer fast on/off switching, have no plasma to reactor contact and use no rare materials. Linear microwave plasma reactors suffer from gas slippage since part of the flow can pass by the processing region. Heat losses to the quartz tube by thermal heating and infrared radiation absorption of the quartz are transferred to the surroundings by convection and radiation. Finally, uncontrollable quenching occurs by mixing with surrounding gas, partly causing back-reactions. The reactor under test removes these problems with a flow that forces almost all gas to pass through the processing region, the absence of a quartz vessel, use of radiation reflection, and a high velocity flow over a short distance between the process region and the quenching zone.

Two concepts were investigated by COMSOL simulations: The first with internal quartz vessel to decouple the microwave design from the flow design. The second with a single metal vessel which serves as flow vessel and as microwave cavity at the same time, simplifying the mechanics and avoiding quartz vessel heat losses.

A single cavity design was found that supports both a microwave field generating a plasma that remains inside the vessel without touching the wall, and a stable flow through the plasma as well.

A turbulent flow model without chemistry is used and isolating walls were assumed. Plasma heating is simulated by a power deposition profile with a thickness equal to plasma thickness observed in Init-SF at DIFFER [4]. At input powers exceeding 4.5 kW and 50 slm flow, a region forms with temperatures of 4000 K and higher, which processes all the flow. This indicates the removal of slippage. Simulations converged to solutions with powers up to 12 kW.

Microwave simulations were performed on a range of geometries to design the cavity. The cavity was optimized for the largest difference between the resonance creating the desired plasma and resonances with competing plasma shapes.

The simulations showed that the desired plasma resonance frequency detuned depending on the plasma conductivity, while other resonances also detuned or remained constant. Various methods were found to avoid the additional resonances. As microwave sources cannot tune the frequency over this range, various cavity tuning methods were investigated. One of them produced the required tuning range while being compatible with the flow.

Additional heat management simulation work has started to include more realistic thermal boundary conditions. Further work will include simulations on plasma parameters corresponding to the trajectory from start-up to operational pressures. Three test set-ups are under development to validate the flow, microwave and thermal simulations.

This work was supported by The Netherlands Organization for Scientific Research (NWO) under project number 18978

References

[1] F.M.A. Smits et al., Proc. 48th EPS Conf. on Plasma Physics, (2022) 560, Maastricht, Netherlands, 2022/07/01,

[2] Bongers W.A. et al., Plasma Processes Polym. **14** (2017) 1600126

[3] Snoeckx R, Bogaerts A., Chem Soc Rev 2017; **46**(19):5805–63.

[4] A.J. Wolf et al, Plasma Sources Sci. Technol.(2019), **28**, 11.

Modeling the effect of background pressure on magnetic nozzle performances

Diego García-Lahuerta[1], Mario Merino[1] and Eduardo Ahedo[1]

[1] *Equipo de Propulsión Espacial y Plasmas (EP2), Universidad Carlos III de Madrid, Leganes, Spain*

Magnetic nozzles (MN) are a key feature in the operation of Electrodeless Plasma Thrusters (EPT). Here we use a simple two-fluid model to study the expansion of plasma in a magnetic nozzle immersed in a background of neutrals and the effect of the density of this background on nozzle performance.

1 Introduction

Electrodeless Plasma Thrusters (EPTs) promise many advantages over traditional electric propulsion devices. However, this kind of thrusters is still underperforming in terms of efficiency in comparison with mature technologies such as Hall-Effect Thrusters (HET) and Gridded-Ion thrusters (GIT).

One of the main characteritics of EPTs such as the Helicon Plasma Thruster (HPT) or the Electron-Cyclotron Resonance Thruster (ECRT)is the guided expansion of the low temperature plasma into a divergent magnetic field region known as the magnetic nozzle that confines the plasma radially and accelerates it axially. The acceleration of a plasma plume in a magnetic nozzle may suffer from facility effects [1] due to the fact that the acceleration region of ions in a MN is larger than that of a HET thrusters.

Some studies have pointed out that background pressure may affect the final velocity of ions leaving the nozzle [2]. Therefore measurements of common plasma properties and thruster characteristics such as thrust might be compromised by testing these kind of devices in vacuum chambers with insufficient pumping capabilities.

2 Model

In this study we model the plume as a two fluid plasma comprised of mass-less, warm, perfectly magnetised electrons and cold, weakly magnetised ions as in [3].

Collisions are not considered except of ionization collisions against the constant density background of neutrals.

3 Integration

In the model described above the equations for the inertia-less equaions are found to be algebraic, while the ion equations are integrated using a first order Discontinuous-Galerkin method. This way we obtain two-dimensional maps for the most relevant plasma properties and total magnetic thrust produced by the magnetic nozzle.

References

[1] Vialis, T., Jarrige, J. & Packan, D. Geometry optimization and effect of gas propellant in an electron cyclotron resonance plasma thruster. In *Proc. 35th Int. Electr. Propuls. Conf*, 1–12 (2017).

[2] Wachs, B. & Jorns, B. Background pressure effects on ion dynamics in a low-power magnetic nozzle thruster. *Plasma Sources Science and Technology* **29**, 045002 (2020).

[3] Ahedo, E. & Merino, M. Two-dimensional supersonic plasma acceleration in a magnetic nozzle. *Physics of Plasmas* **17**, 073501 (2010).

Surface charge deposition on dielectric surfaces using an X-ray ionizer

R. Bell[1], A.A.A. Limburg[1], G.G. van Eden[2] and S. Nijdam[1]

[1] *Dept. Applied Physics, Eindhoven Univ. Techn., Eindhoven, The Netherlands*
[2]*ASML Netherlands B.V.*

r.bell@student.tue.nl

Surface charges on dielectric surfaces induce challenges in industry. A tool capable of depositing quantitative amounts of surface charge can provide insight in the behaviour of surface charge residing on dielectric surfaces. This research contribution examines the potential of such a tool based on X-ray ionization to facilitate this surface charging in a controlled manner. The experimental results prove that the tool can, within seconds, deposit predictable, quantitative amounts of charge on dielectric surfaces for potential differences of either polarity up to 100 V.

1 Introduction

When a significant amount of surface charge resides on a dielectric surface, disruptive discharges can occur [1]. An electrical breakdown can disrupt, fail or completely shut off electric components, causing defects in all kinds of (small scale) technology. Since the reliability of these technologies is crucial for their success, preventing and managing charge accumulation as much as possible is a priority. To learn more about the behaviour of surface charge on dielectrics, a tool capable of depositing quantitative amounts of charge on dielectric materials can be insightful. In this research, such a tool based on an X-ray ionizer is built and qualified.

2 Methods

The setup used to deposit the surface charge is schematically depicted in Figure 1. Neutral atoms and molecules are ionized by the X-rays emitted by the ionizer, forming both positive and negative ions. The positive ions are attracted to the top surface of the dielectric as a negative bias voltage is applied to the conductive backside of the dielectric. Within a couple of seconds, the top surface of the dielectric sample is saturated with positive ions. Note that this process also works when the polarity of the bias voltage is reversed. In that case, the negative ions will accumulate on the top surface of the dielectric sample.

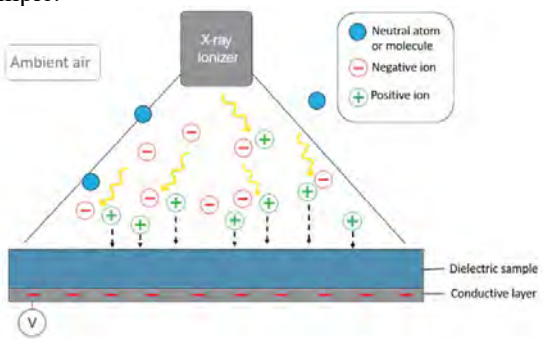

Fig. 1: Schematic drawing of surface charge deposition set-up using an X-ray ionizer.

3 Experimental Results

In Fig. 2, the voltage measured on the top surface of a 1 mm thick quartz sample is displayed as a function of the applied bias voltage. The bias voltage is ranging from -100 V to 100 V. The potential is measured using an electrostatic voltmeter (ESVM). The figure shows a clear linear relation with roughly a 13% voltage loss over the entire range which is probably due to ESVM calibration errors. This indicates that within this range of bias voltages, a desirable amount of surface charge can be accurately deposited on the top side of the quartz.

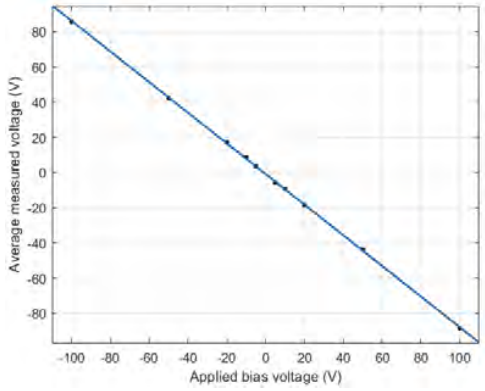

Fig. 2: Average measured voltage on the top surface of a 1 mm thick quartz sample as a function of the applied bias voltage. Measured using an ESVM.

4 Conclusion

A charge deposition technique using an X-ray ionizer enables users to study surface charge behaviour on solid dielectrics in detail. Charge can now be deposited quantitatively on a dielectric surface within a matter of seconds.

References

[1] Wang, Z. L., Lin, L., Chen, J., Niu, S., & Zi, Y. (2016). Triboelectrification. *Triboelectric Nanogenerators*, 1–19. https://doi.org/10.1007/978-3-319-40039-6_1.

Ion and atom fluxes during HiPIMS deposition of NbC from a compound target

M. Farahani[1], T. Kozák[1], A.D. Pajdarová[1]

[1] *Department of Physics and NTIS-European Centre of Excellence, University of West Bohemia*

Sputtered element ratio (Nb/C) in films deposited from a compound NbC target by non-reactive high power impulse magnetron sputtering (HiPIMS) operated at different frequencies and duty cycles have been investigated. Time-averaged mass spectrometry shows that the fluxes of sputtered target ions increase with increasing pulse power density (and decreasing pulse length) due to increasing the electron density and, hence, electron-impact ionization probability. Since Nb atoms have lower ionization energy and larger ionization cross-section than C atoms, the Nb ions dominate the flux of ions onto the film at all conditions. Neutrals were monitored by optical emission spectroscopy (OES) and showed a decrease by increasing pulse power density. In the case of 500 Hz, the Nb/C ratio varied from 0.6 to 0.95 by adjusting the length of HiPIMS pulses between 200 μs and 30 μs, achieving nearly stoichiometric composition for the lowest pulse length.

Over the past years, transition metal carbides have been widely studied as a material with high electrical conductivity, mechanical strength, and high chemical and thermal stability, with potential applications in the field of protective coatings, catalytic materials, and electronics. High-power impulse magnetron sputtering (HiPIMS) has been used for thin film deposition of NbC films from a single compound target utilizing high pulse power and short duty cycle (a few percent) to achieve more ionization in comparison to conventional dc magnetron sputtering for the same average power. The film composition (Nb/C ratio), microstructure, and, consequently, mechanical properties can be controlled by varying the power density in the pulse [1].

Within the presentation, the explanation of the observed compositional transition from C-rich films to stoichiometric NbC films in response to an increase in pulse power density is going to be the main topic. The sputtering rate and angular distribution, scattering off the process gas atoms, ionization in the high-density plasma, and return of ions onto the target or loss of them to chamber walls are some of the processes which collectively affect the transport of sputtered Nb and C atoms towards the substrate. Due to the different atomic masses and ionization potentials of the two elements, these processes are anticipated to appear differently for Nb and C. Understanding the sputtering of compound targets in HiPIMS discharges has yet to fully develop.

Time-averaged plasma diagnostic techniques were employed to study the impact of the aforementioned plasma processes on the transport of atoms and ions in the discharge and, ultimately, on the Nb/C ratio in the films. For this purpose, OES was employed to detect the ratios of sputtered species neutrals and ions at different locations in the discharge and mass spectroscopy to estimate Nb^+ and C^+ fluxes at the substrate position.

It is found that the density of Nb ions is significant even for low power densities due to lower ionization energy and larger ionization cross-section compared to C atoms. However, the film growth is still driven mainly by neutral C flux, which leads to much free C in the deposited film. Higher ionization efficiencies can be attained by enhancing the target power density [2], so more C species will be ionized as the power density increases. Ionized C might be affected by either the back-attraction effect to the target or by scattering to the wall [3], resulting in almost stoichiometric films obtained for the highest pulse power density (and shortest pulse length) [1]. For the repetition frequency of 500 Hz, when pulse power density increases from 0.1 $kWcm^{-2}$ to 0.6 $kWcm^{-2}$, the C and Nb deposition fluxes drop from 2.8×10^{15} $cm^{-2}s^{-1}$ to 1.3×10^{15} $cm^{-2}s^{-1}$ and 1.7×10^{15} $cm^{-2}s^{-1}$ to 1.2×10^{15} $cm^{-2}s^{-1}$ respectively. The Nb/C ratio varied from 0.6 to 0.95 by increasing pulse power density, achieving a nearly stoichiometric composition for the shortest pulse length.

References

[1] A. Bahr, T. Glechner, T. Wojcik, A. Kirnbauer, M. Sauer, A. Foelske, O. Hunold, J. Ramm, S. Kolozsvári, E. Ntemou, E. Pitthan, D. Primetzhofer, H. Riedl, R. Hahn. *Non-reactive HiPIMS deposition of NbC_x thin films: Effect of the target power density on structure-mechanical properties*. Surf. Coat. Technol. **444**, 128674 (2022).

[2] Anders, André. *Discharge physics of high power impulse magnetron sputtering*. Surface and Coatings Technology **205**, S1-S9 (2011).

[3] Tiron, Vasile, et al. *Optimization of deposition rate in HiPIMS by controlling the peak target current*. Journal of Physics D: Applied Physics **48.49**, 495204 (2015).

Invasiveness of picosecond and nanosecond laser diagnostics on plasma bullets in nitrogen

A.A.A. Limburg, T.E.W. Keur, B.E.T. Broekman, S.J. Dijcks and S. Nijdam

Dept. Applied Physics, Eindhoven Univ. Techn., Eindhoven, The Netherlands

This paper aims to reveal the effect of a high power, pulsed, focused laser beam, used as probe in a plasma diagnostic, on the plasma trajectory and thereby on the obtained results from the diagnostic. Ns and ps E-FISH is applied to plasma bullets in nitrogen in ambient air. Branching of the plasma into the laser beam path is observed by ICCD imaging for both laser types. However, only for the ns laser, the measured electric field distribution is affected. Therefore, nanosecond laser diagnostics cannot be considered non-invasive.

1 Introduction

Laser diagnostics are widely used to obtain plasma characteristics. For example, Thomson scattering is applied for determining the electron temperature and density. Recently electric field induced second harmonic generation (E-FISH) was introduced as a method to directly obtain the electric field of a plasma. In this new, simple and promising E-FISH technique, a pulsed, focused laser beam interacts non-linearly with the ambient electric field in a medium, which results in frequency doubled light. The intensity of these second harmonics scales quadratically with the electric field. In this way, a polarization resolved electric field distribution can be obtained for (almost) any kind of plasma.

So far, laser diagnostics were considered non-invasive when applied to plasma, which is advantageous over most other plasma diagnostics. Furthermore, laser diagnostics are not limited to the light emission of the plasma.

In this research, E-FISH is applied to non-thermal pulsed plasma jets in nitrogen flowing into atmospheric air to determine the invasiveness of this technique. A nano- and a picosecond pulsed 1064 nm laser are used as a source. For the first time, the field profiles measured with both lasers are compared to each other and the effect of the laser beam on the plasma is examined by using ICCD imaging.

2 Results

The camera images show the bullet branches when crossing the laser beam path, which is a consequence of the beam ionizing part of the molecules and atoms along its focus. Fig. 1. shows that after leaving the laser beam path, branches follow the background field lines. This work unfolds a direct correspondence of the determined electric field profile obtained with the nanosecond laser and the branching of the plasma. In Fig. 2. the E-FISH results are shown for both the ps and ns laser, whereby branching occurs over the width of the top hat profile.

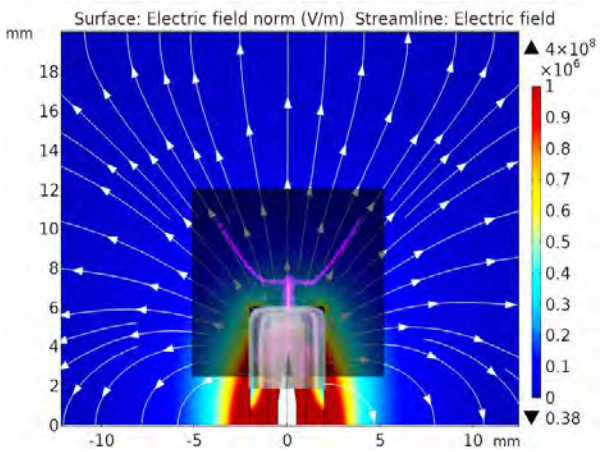

Fig 1: A COMSOL Multiphysics model of the electric field and streamlines for the used plasma nozzle. An ICCD image of the plasma trajectory is put on top (purple, ps laser).

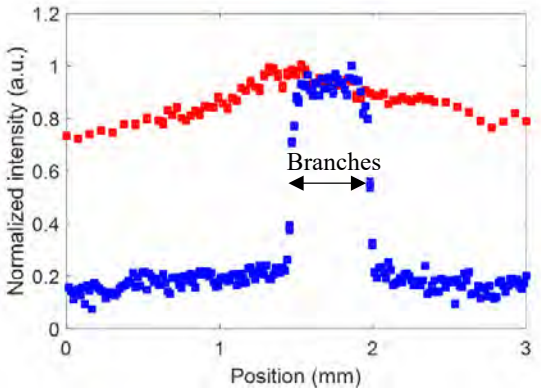

Fig 2: Radial profile of the line-integrated axial electric field component obtained with a nanosecond laser (blue) and picosecond laser (red).

3 Conclusions

The ns and the ps laser beam both induce branching of the plasma. The obtained electric field distribution obtained with the ns laser is affected by the branching. Ns E-FISH can, thus, be invasive and results need to be critically assessed.

Patch-type microwave resonance sensor for obtaining plasma electron density in low-pressure plasmas

Dae-Woong Kim[1], Sang-Ho Lee[1,2], Geon-Woong Eom[1,2], Si-Jun Kim[2], Shin-Jae You[2], Min Hur[1], Woo-Seok Kang[1]

[1] *Department of Plasma Engineering, Korea Institute of Machinery and Materials, Republic of Korea*
[2] *Department of Physics, Chungnam National University, Republic of Korea*

We propose a novel patch-type plasma microwave resonance sensor that is thin and flexible enough to be attached to the surface of a plasma chamber. The sensor measures the plasma electron density by deducing it from the plasma electron resonance peak frequency in the microwave transmission spectrum between two thin and flexible antennas based on active microwave spectroscopy. The antennas consist of two metal tips on a dielectric layer less than 100 μm thick, resulting in a flexible and lightweight design. The accuracy of the sensor was evaluated using 3-dimensional electromagnetic simulations. The results showed good agreement between the measured plasma electron density and the input electron density in the simulation. A comparison experiment between the patch sensor and a conventional planar cut-off probe was also carried out and showed good agreement between the two.

Active microwave spectroscopy (AMS) is a reliable and suitable technique for obtaining plasma electron density in low pressure plasmas. Many types of AMS have been developed, such as plasma resonance probe [1], hairpin probe [2], plasma absorption probe [3], multipole resonance probe [4], cutoff probe [5] and so on. However, the original model of these microwave probes is not applicable for in-situ monitoring of plasma processing discharges due to their invasive probe structures with respect to the plasma.

Therefore, non-invasive AMS probes have recently been proposed and analysed [6-9]. These probes have planar resonator or planar radiating and detecting tips that can be embedded in the chamber chuck or wall. Thanks to their non-invasive probe structure, a wide range of in-situ monitoring applications of AMS probes in plasma processing are possible.

In this paper, we propose a thin and flexible patch-type AMS sensor, called plasma patch sensor, for the measurement of plasma electron density in low pressure plasmas. The proposed plasma patch sensor is based on the detection of the plasma electron resonance peak frequency in the transmission spectrum. The plasma patch sensor is composed of flexible and thin tips of radiating and detecting two metal tips on a dielectric layer less than 100 μm thick, resulting in a flexible and lightweight design. The accuracy as a function of pressure and plasma electron density was evaluated using 3-dimensional electromagnetic simulation. The results showed that the plasma patch sensor has good accuracy in low pressure plasmas of less than a few hundred mTorr. In addition, a comparison experiment was carried out between the plasma patch sensor and a conventional planar cut-off probe, which is a transmission type plasma resonance AMS probe, and showed good agreement between the two.

References

[1] Harp, R. S., and F. W. Crawford., Journal of Applied Physics 35.12 (1964)
[2] RB Piejak, VA Godyak, R. Garner, and B. M. Alexandrovich, Journal of applied physics 95.7 (2004)
[3] Hikaru Kokura, Keiji Nakamura, Ivan P. Ghanashev and Hideo Sugai, Japanese journal of applied physics 38.9R (1999): 5262.
[4] Lapke, M., T. Mussenbrock, and R. P. Brinkmann., Applied Physics Letters 93.5 (2008): 051502.
[5] Kim, Jung-Hyung, D. J. Seong, J. Y. Lim, and K. H. Chung, Applied physics letters 83.23 (2003): 4725-4727.
[6] D. W. Kim, S. J. You, S. J. Kim, J. H. Kim, J. Y. Lee, W. S. Kang, and M. Hur, Plasma Sources Sci. Technol. 28, 015004 (2019).
[7] H. J. Yeom, J. H. Kim, D. H. Choi, E. S. Choi, M. Y. Yoon, D. J. Seong, Shin Jae You, and Hyo-Chang Lee, Plasma Sources Sci. Technol. 29, 035016 (2020).
[8] Lji Liang, Keiji Nakamura, and Hideo Sugai, Applied Physics Express, 4, 066101 (2011)
[9] Christian Schulz, Tim Stynoll, Peter Awakowicz, and Ilona Rolfes, IEEE Transactions on Instrumentation and Measurement, 64, 857 (2015).

The Breakdown Development of a Plane-to-Plane Nanosecond Pulsed Discharge in Humid Air

P.F. Ambrico[1], D. Aceto[1], G. Dilecce[1], L. Ibba[2], I. Furno[2], X. Yang[3] and I.V. Adamovich[3]

[1] *CNR – Institute for Plasma Science and Technology, Dipartimento Interateno di Física - Uniba – 70126 Bari – Italy*
[2] *Swiss Plasma Center (SPC), École Polytechnique Fédérale de Lausanne (EPFL), CH-1015 Lausanne, Switzerland;*
[3] *Department of Mechanical and Aerospace Engineering, The Ohio State University, Columbus, OH 43210, USA*

We used EFISH to measure the electric field evolution of a 200 ns pulse, dielectric barrier, plane-to-plane discharge in humid air. ICCD detected a uniform evolution of the discharge emission during the breakdown. Spectroscopic measurements tracked the N_2 second positive and first negative systems to infer the E/N evolution. EFISH measurements showed the electric field persistent during the entire HV pulse, with the residual field between pulses and the field inversion at the start and end of the HV pulse. Experimental data are consistent with simulations, with electron attachment and negative ion kinetics incorporated. Spectroscopic E/N determination showed time evolution at variance with the EFISH measurements, which may be due to the non-locality of the EEDF. Possible explanations will be discussed.

1 Introduction

Using low temperature plasmas on biological systems requires understanding the crucial physical factors such as the electric field. Estimating the electric field in low-temperature plasmas typically involves observing the N_2 first negative and second positive band emission [1]. Direct measurements in plasmas by electric field-induced second harmonic (EFISH) generation can be achieved with spatially localized, ultrashort pulsed lasers with sub-ns time resolution, but their availability limits their use. To overcome this, ns laser EFISH diagnostics can be performed by time-resolving the laser pulses and the EFISH signal [2]. Our study examines the time evolution of the electric field in a 1 kHz ns discharge in humid air, typically used to treat biological tissues. We also performed optical emission spectroscopy and imaging by ICCD, electrical measurements, and discharge modelling to understand the process involved in the E-field evolution.

2 Experimental

The 1064 nm output of a ns pulse Nd:YAG laser (Opotek, Opolette 355LD, pulse duration 7 ns FWHM, RR≤20 Hz) is sent between two parallel plane circular electrodes (ϕ = 2.00 cm, 1.95 mm gap), and is detected by an AlphaLas Fast Photodiode (UPD-200-UP, RT<175 ps). The EFISH signal is detected by Hamamatsu Fast PMT (H10721-04, rise time 0.57 ns). The signals are acquired by a Keysight Infiniivision MSOX-6004A Oscilloscope (1GHz BW, 20 GS/s). The field is calculated from Eq. 1,

$$E_{ext}(t) = A \frac{\sqrt{I^{(2\omega)}(t)}}{I^{(\omega)}(t)} \qquad (1)$$

where $I^{(2\omega)}(t)$, $I^{(\omega)}(t)$, and A are the time-resolved PMT and photodiode waveforms, and the calibration constant derived from the Laplacian field measurements, respectively.

Results

Figure 1 shows the experimental and simulated voltage, current and electric field at the gap centre. In summary the E-field measurements reveal a clear inversion at the beginning and at the end of the HV pulse, indicating that the effect of the field outside the plasma is negligible. The experimental field does not decrease to zero after the breakdown. The model can reproduce this behaviour if the attachment reactions are considered. The E/N inferred from the emission spectroscopy data exhibits disagreement with the direct EFISH measurements, suggesting that some additional processes may occur, leading to the excitation of $N_2(B^3\Pi)$ state. Possible explanation of the observed disagreement (such as the non-locality of the EEDF) will be discussed.

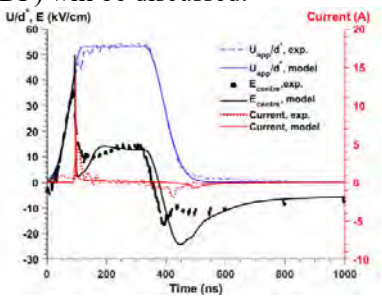

Figure 1. Time-resolved electric characteristics: experimental data (points) and kinetic modelling (lines) at the gap center.

Acknowledgment

D.A. thanks RIPARTI POC PUGLIA FESRTFSE 2014/2020, I.V.A. thanks CNR – STM2019 Program.

References

[1] Obrusník A, et al., 2018, *Plasma Sources Sci. Technol.* **27** 085013

[2] Adamovich I V., et al, 2020, *J. Phys. D. Appl. Phys.* **53** 145201

Corona discharges in thunderclouds as detected from space by ASIM: Types, properties, and worldwide geographical distributions

F. J. Gordillo-Vázquez[1], S. Soler [1], F. J. Pérez-Invernón[1], T. Neubert[2], V. Reglero[3], N. Ostgaard[4]

[1] *Instituto de Astrofísica de Andalucía, IAA - CSIC, Glorieta de la Astronomía s/n Granada, Spain*
[2] *National Space Institute, Technical University of Denmark (DTU-Space), Denmark*
[3] *Image Processing Laboratory, University of Valencia, Spain*
[4] *Department of Physics and Technology, Birkeland Centre for Space Science, University of Bergen, Norway*

We report on the systematic storm cloud corona discharge observations carried by the Atmosphere Space Interaction Monitor (ASIM) space mission of the European Space Agency (ESA) launched in April 2018. It is the first time that corona discharges in thunderclouds, characterized by their distinct bluish (337 nm) optical emissions, are mapped all over the planet. The results presented here describe some of their key features like, for instance, number of streamer and vertical extension, and their global geographical distribution. The knowledge of corona discharge activity in thunderclouds is important because they can inititate lightning and can also directly inject greenhouse gases (like ozone, O_3, and nitrous oxide, N_2O) that can influence the chemical balance of the atmosphere.

1 General

The presence of transient corona discharges occurring in thunderclouds has been suspected for a long time (early 1970s). Thunderstorm coronas can be observed as Blue LUminous Events (BLUEs) formed by a large number of streamers characterized by their distinct 337 nm light flashes with negligible (or absent) 777.4 nm optical emission (typical of lightning leaders). The Modular Multispectral Imaging Array (MMIA) of the Atmosphere-Space Interaction Monitor (ASIM) has successfully allowed us to characterize [1] and map BLUEs worldwide [2,3].

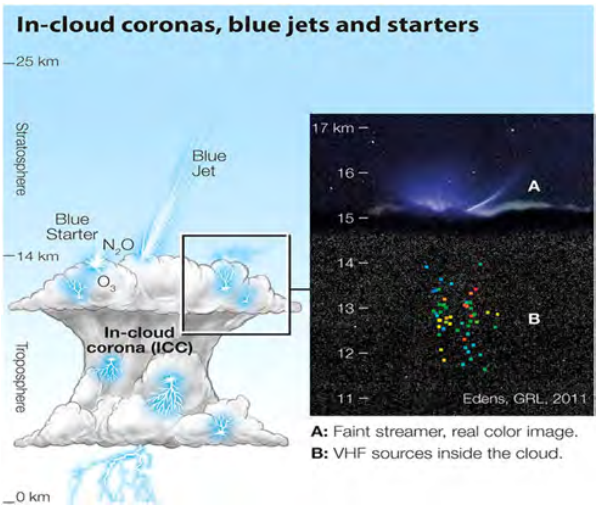

Figure 1: Schematic representation of in-cloud corona discharges in thunderclouds (Gordillo-Vázquez F. J. and Pérez-Invernón, Atmospheric Research, **252**, 2021). The inset is a true color photo of blue corona emissions (Edens, GRL, **38**, 2011), including a blue starter with their Very High Frequency (VHF) sources detected by a Lightning Mapping Array (LMA) as a function of time (coloured dots increasing in time from blue to red).

The results presented here include a global analysis of key properties of BLUEs such as their characteristic rise times and duration, their depth with respect to cloud tops, vertical length and number of streamers [3]. We also present two different global annual average climatologies of BLUEs depending on considerations about the rise time and total duration of BLUEs worldwide [2,3].

The altitude distribution of in-cloud corona discharges indicate that they are commonly present between cloud tops and a depth of $\leq$ 4 km in the tropics and $\leq$ 1 km in mid and higher latitudes. Impulsive single pulse BLUEs in the tropics are the longest (up to ~4 km height) and have the largest number of streamers (up to ~3×10^9) [3].

References

[1] S. Soler, F. J. Pérez-Invernón, F. J. Gordillo-Vázquez, *et al.*, "*Blue optical observations of narrow bipolar events by ASIM suggest corona streamer activity in thunderstorms*" (**Editor's Hightlight**), Journal of Geophysical Research - Atmospheres, **125**, 2020, doi: 10.1029/2020JD032708.

[2] S. Soler, F. J. Gordillo-Vázquez, *et al.*, "*Global Frequency and Geographical Distribution of Nighttime Streamer Corona Discharges (BLUEs) in Thunderclouds*", Geophysical Research Letters 2021, **48**, doi: 10.1029/2021GL094657.

[3] S. Soler, F. J. Gordillo-Vázquez, *et al.*, "*Global distribution of key features of streamer corona discharges in thunderclouds*", Journal of Geophysical Research: Atmospheres, **127**, 2022, doi: 10.1029/2022JD037535.

Determination of atomic oxygen density and reduced electric field in oxygen-containing plasmas through OES methods

L. Kuijpers[1], T. Silva[2], V. Guerra[2], E. Baratte[3], O. Guaitella[3], D. Sadi[3] and M.C.M. van de Sanden[1,4,5]

[1] *Dept. Applied Physics, Eindhoven Univ. Techn., Eindhoven, The Netherlands*
[2] *Instituto de Plasmas e Fusão Nuclear, Instituto Superior Técnico, Universidade de Lisboa, Portugal*
[3] *Laboratoire de Physique des Plasmas (UMR 7648), CNRS-Univ.Paris Sud-Sorbonne Universite -Ecole polytechnique 91128 Palaiseau, France*
[4] *Eindhoven Institute for Renewable Energy Systems, Eindhoven Univ. Techn., Eindhoven, The Netherlands*
[5] *Dutch Institute For Fundamental Energy Research, Eindhoven, The Netherlands*

This work presents an investigation of two diagnostic methods based on optical emission spectroscopy: Actinometry for the atomic oxygen density and the line ratio method for the reduce electric field. The methods are compared with experimental results of a DC glow discharge containing oxygen with trace argon and xenon. The discharge is operated at 0.55-5 Torr at a current of 40 mA. As both methods rely on a ratio of measured line intensities the investigation starts with the direct simulation of these line intensities. Using best found simulated line intensities and a correction for consistency between cross sections good agreement is found with experiment for the reduced electric field and atomic oxygen density.

Understanding of basic plasma parameters, such as gas temperature, vibrational temperature, dissociation fraction, etc. is often achieved through plasma diagnostics. Plasma diagnostics in CO_2 and O_2 plasmas are often expensive, active, complex and with high sensitivity to noise. In this work, the efforts were directed towards the investigation of two non-intrusive diagnostic approaches: oxygen actinometry [1] and the line ratio method for the reduced electric field [2]. Both methods are based on optical emission spectroscopy (OES) which is a powerful, yet non-intrusive characterization tool based on the measurement and analysis of light emitted by the spontaneous relaxation of excited species in the plasma.

The methods are based on the comparison of measured emission line ratios with simulated emission line ratios. The investigation starts with an attempt to calculate the line intensity of the emission lines directly. This is done for a glow discharge in oxygen with trace argon and xenon, operating at pressures in the range of 0.55-5 Torr and a current of 40 mA. The EEDF is calculated using the LisbOn KInetics Boltzmann solver (LoKI-B) [3], from which line intensities can be calculated assuming an extended corona model.

The calculated line intensities are tested against measured line intensities taken using OES. Best results are found using the Tayal and Zatsarinny electron impact excitation cross sections [4, 5]. The results exhibit excellent trend for the evolution of the line intensities as a function of discharge pressure. A correction factor is suggested to achieve agreement in the absolute values of the line intensities of different species.

The calculated reduced electric field is compared with the electric field measurements from experiment. The atomic oxygen density is found using actinometry and results are compared against Cavity Ring Down Spectroscopy measurements. For both methods the results based on consistent line intensities give good agreement with experimental values. Sensitivity to $O_2(a^1\Delta_g)$ and $O(^3P)$ populations is tested and remains low, allowing for the use of approximate or literature values.

The line ratio method and actinometry prove to give accurate results if the underlying line intensity calculations are good and consistent. Both absolute values and trend of the reduced electric field and atomic oxygen density over discharge pressure has been reproduced appropriately.

Acknowledgements

Part of this work was funded by Portuguese FCT (Fundação para a Ciência e a Tecnologia) under projects UIDB/50010/2020, UIDP/50010/2020, EXPL/FIS-PLA/0076/2021, and 2021.09150.CBM,

References

[1] D. Pagnon et al. 1995 J. Phys. D: Appl. Phys. **28** 1856

[2] X.M. Zhu and Y.K. Pu 2010 J. Phys. D: Appl. Phys. **43** 403001

[3] A. Tejero-Del-Caz, et al. 2019 Plasma Sources Sci. Technol. **28**, 043001

[4] S. Tayal and O. Zatsarinny 2016. Phys. Rev. A **94** 042707

[5] O. Zatsarinny and K. Bartschat 2013 J. Phys. B: At. Mol. Opt. Phys. **46** 112001

Evolution of mean electron energy and dissociation over the initial pulses in a micro cavity plasma array

H. van Impel[2], D. Steuer[2], V. Schulz-von der Gathen[1], M. Böke[1] and J. Golda[2]

[1] *Experimental Physics II, Ruhr-Universität Bochum, Bochum, Germany*
[2] *Plasma Interface Physics, Ruhr-Universität Bochum, Bochum, Germany*

Here, we investigate atomic oxygen production as a model system in a micro cavity plasma array, a customized surface DBD confined to geometrically arranged cavities of micrometer size. We study the discharge behaviour and the plasma chemical processes using optical emission spectroscopy methods. Using a multi-photomultiplier setup with synchronous narrow bandwidth detection of characteristic transitions and SEA, we measure the temporal evolution of the atomic oxygen density and the effective mean electron energy over the first ignitions.

1 Introduction

Micro cavity plasma arrays [1] have numerous applications, such as ozone generation or the treatment of volatile organic compounds (VOCs). A key to applications is the generation of reactive species within the plasma. In a DBD reactor configuration a large surface to volume ratio can be achieved that allows to improve the plasma conversation by surface enhanced processes via the incorporation of a catalyst.

To energetically optimise the conversion, the understanding of the generation processes and in particular of the temporal evolution of the species during the discharge phase is of greatest importance.

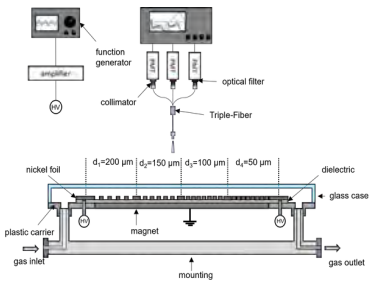

Fig. 1: Experimental setup for 3-photomultiplier SEA

Exemplarily, we investigate atomic oxygen densities and the mean electron energy with helium state enhanced actinometry (SEA) considering the limited optical access to the micro cavity array.

2 Experimental Setup

SEA makes use of three individual emission lines from helium, oxygen and known admixtures of argon to provide the degree of oxygen dissociation and the mean electron energy [2,3]. A set of three photomultiplier tubes in combination with narrowband filters (see figure 1) allows to simultaneously acquire the respective emission signals with a time resolution of about 1 µs. The micro cavity array is operated in helium with a varying molecular oxygen admixture of about 0.1% at atmospheric pressure using bursts at 15 kHz and about 600V triangular excitation voltage.

3 Results

From investigation of the various emission signals (see figure 2) the influence of an oxygen admixture on the discharge behaviour and the development over a discharge cycle can be understood. Subsequent ignitions are affected by a memory effect due to residuals. A nearly complete degree of dissociation is achieved within the array cavities already after the very first discharge pulses. The observed mean electron energy stays relatively constant at high values of about 5 eV.

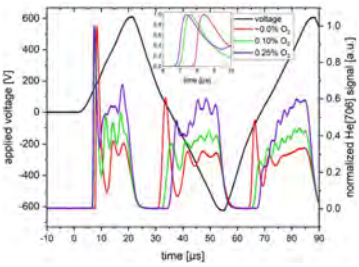

Fig. 2: Temporal evolution of the He 706 nm emission line for various oxygen admixtures

Acknowledgement

This project is supported by the DFG in the frame of the CRC 1316 in project A6.

References

[1] S. Dzikowski et al. 2020 Plasma Sources Sci. Technol. 29 035028
[2] D. Steuer et al. 2022 Plasma Sources Sci. Technol. 31 10LT01
[3] D. Steuer et al. 2023 Plasma Sources Sci. Technol. 32 025013

Experimental Study of the Plasma Enhanced Oxygen Reduction and Permeation of LSM|YSZ|LSM Solid Oxide Electrolyte Cell

X. Chen[1,2,3], A. Pikalev[2,4] , G.J. Zhang[1], V. Guerra[4] and M.C.M. van de Sanden[2,3]

[1] *School of Electrical Engineering, Xián Jiaotong University, Xián, China*
[2] *Dutch Institute of Fundemental Energy Research, Eindhoven, The Netherlands*
[3] *Dept. Applied Physics, Eindhoven Institute of Renewable Energy Systems, Eindhoven Univ. Techn., Eindhoven, The Netherlands*
[4] *Instituto de Plasmas e Fusão Nuclear, Instituto Superior Técnico, Universidade de Lisboa, Lisboa, Portugal*

In this contribution we present an experimental study of the plasma enhanced oxygen reduction reaction and permeation of the lanthanum strontium manganite (LSM)-yttria-stabilized zirconia (YSZ) solid oxide electrolyte cell (SOEC). Firstly, to determine the performance of the LSM|YSZ|LSM SOEC, a symmetric cell was characterized in air environment with homogenous heating via polarization curves and electrochemical impedance spectra. Then a He/O_2 low pressure glow discharge was used to provide a stable and homogeneous oxygen containing plasma environment for the SOEC. Finally, the oxygen reduction and permeation process of the SOEC exposed to the plasma were investigated under different operating conditions. Our purpose is to quantify the plasma-effect on SOEC performance and to gain physical insight into the plasma-enhanced oxygen reduction kinetics.

Non-thermal plasma has drawn great attention in CO_2 utilization due to the potential to activate CO_2 at reduced energy cost. However, it is difficult to obtain very high CO_2 conversion due to the unavoidable reverse reaction [1]. In-situ removal of oxygen or oxygen radicals from the plasma using oxygen transporting membrane SOEC can improve the CO_2 conversion by inhibiting the reverse reaction [2, 3]. A synergistic effect was also observed that not only the O_2 permeation flux through the membrane was improved in the CO_2 plasma compared to the same membrane without the plasma [4], but the SOEC material stability was also improved compared with the conventional electrolysis approach [5]. Despite the great potential of plasma-SOEC synergy, the fundamental surface kinetics involving the oxygen reduction reactions and oxygen permeation is still unclear and needs to be explored to further improve the overall energy efficiency and selectivity of the processes.

In this contribution, a novel plasma-SOEC integration system was built to characterize the influence of the plasma on the SOEC performance. A symmetrical cell was fabricated with an 8mol% YSZ electrolyte, with a thickness of 1.5mm. LSM ($La_{0.8}Sr_{0.2}MnO_{3-\delta}$) powders were used for electrodes. Firstly, we characterized the SOEC in a split tube oven in air, within a wide range of operating temperatures between 350°C and 800°C. Then we compared the oxygen partial pressure influence on the SOEC oxygen reduction reactions in the BABE plasma reactor [6], to determine the oxygen reduction reaction rate-limiting steps for the SOEC surface kinetics. Finally, a He/O_2 low pressure (~1Torr) glow discharge was generated in the BABE reactor to provide a stable and homogeneous oxygen containing plasma environment for the SOEC operation. We used the open circuit potential and the polarization curve to describe the oxygen permeation ability, and used the electrochemical impedance spectra to describe the oxygen reduction reactions on the working electrode exposed to plasma, to compare the plasma impact with different plasma power on the SOEC performance. In this way, we make important steps to develop an insight into the enhanced oxygen reduction and permeation process in the plasma-SOEC synergy.

This work was partially supported by the European Space Agency under Project I-2021-03399. VG was partially supported by the Portuguese FCT - Fundação para a Ciência e a Tecnologia, under projects UIDB/50010/2020 and UIDP/50010/2020.

References

[1] Bongers, W., Bouwmeester, H., Wolf, B., et al., Plasma processes and polymers **14**, 1600126 (2017).
[2] Mori, S., Tun, L. L., Plasma Processes and Polymers **14**, 1600153 (2017).
[3] Chen, G., Buck, F., Kistner, I., et al., Chemical Engineering Journal **392**, 123699 (2020).
[4] Buck, F., Wiegers, K., Schulz, A., et al., Journal of Industrial and Engineering Chemistry **104**, 1-7 (2021).
[5] Pandiyan, A., Kyriakou, V., Neagu, D., et al.,. Journal of CO_2 Utilization **57**, 101904 (2022).
[6] Ratynskaia, S., Dilecce, G., Tolias, P. Journal of Plasma Physics, **81**, 345810202 (2015).

Density measurement of atomic oxygen in pulsed discharges formed under sub-atmospheric pressure pure oxygen

J. Oogaki, Y. Nakagawa and F. Tochikubo

Dept. Elec. Eng. & Comp. Sci., Tokyo Metropolitan Univ., Tokyo, Japan

Atmospheric pressure plasma can produce high density radicals, whereas it leads to short lifetime of radicals and has difficulty in producing a uniform plasma. Sub-atmospheric pressure plasma, which is slightly depressurized from atmospheric pressure, has the potential to both delocalize the plasma and extend the lifetime of the radicals while maintaining the diversity of the target. Previous studies showed an improvement in the lifetime of atomic oxygens due to reduced pressure. Additionally, an increase in the amount of atomic oxygens produced on the dielectric cathode surface was observed. In this study, to clarify the cause of the phenomenon, the effect of pulse width and barrier existence on the atomic oxygen production were investigated. As a result, the steep increase in atomic oxygen production near the cathode only occurred in barrier discharges. In addition, it was also found that the increase in the atomic oxygen production occurred only in a small area in the vicinity of the cathode.

1 Introduction

Chemical processes using atmospheric pressure plasma can be applied in many fields such as surface treatment and environmental purification with rich radical production, whereas the radical lifetime is short owing to frequent collisional deactivation. The plasma in sub-atmospheric pressure, which is slightly reduced from atmospheric pressure, is expected to be effective in increasing the lifetime of radicals.

We observed the lifetime extension and a production enhancement of atomic oxygen (O) near the dielectric cathode in sub-atmospheric pressure pulsed DBD. In this study, we measured atomic oxygen in sub-atmospheric pure oxygen discharge by TALIF[1,2] under different conditions such as voltage pulse width and dielectric existence, in order to clarify the conditions for efficient atomic oxygen.

2 Experimental settings

A stainless needle anode and a stainless sphere cathode were used for positive pulse discharge. In the barrier discharge, a borosilicate glass hemisphere was placed on the cathode. The gap length between the needle and the top of cathode was 1.1 mm. Pure oxygen was flowed with a rate of 2 L/min in the reactor, and the pressure in the reactor was adjusted in the range of 20-95 kPa. Pulsed high voltage was applied at 10 pulses/s to the needle with pulse widths of 300 or 35 ns. The discharge energy was adjusted to 6.0 mJ for the long pulse(300-ns), and the energy of short-pulse (35 ns) discharges were approximately 0.59 mJ for both barrier cathode and metal cathode.

3 Results and Discussion

The O density under each condition at 50 kPa is shown in Fig.1. The O density is the averaged value over the horizontal area of observation, $5 \times 6.25 mm^2$

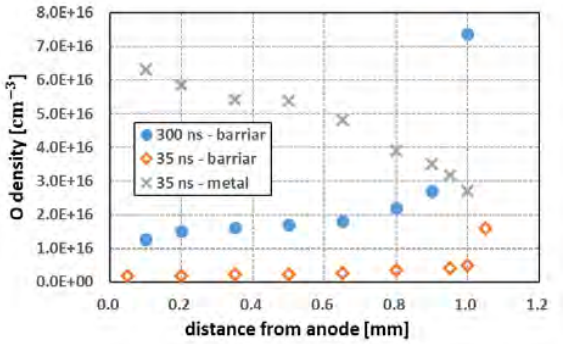

Fig.1 Density distribution of O atoms in barrier discharge at 50 kPa.

The steep increase in atomic oxygen near the cathode was observed only in barrier discharges. In addition, it was also found that the density increase was confined in the immediate vicinity of the spherical cathode. The maximum O density in 300-ns discharge was approximately 4 times larger than that in 35-ns discharge, indicating higher O-production efficiency considering the discharge energy. Possible reasons for the localized O distribution in the barrier discharges are the expansion of the discharge space, the increase in electrons exceeding the dissociation energy, and the adsorption of atomic oxygens on the dielectric, but the dominant factor cannot be identified from the present results. More detailed density profiles are needed to elucidate the cause of the increased production.

References

[1] W. K. Bischel *et al., Chem. Phys. Lett.,* 82, No. 1, p. 85 (1981).

[2] Y. Nakagawa *et al., J. Phys. D: Appl. Phys.*, 53, 135201 (2020).

Electric field fluctuations in a cold micro-plasma jet under different flow modes

Deepika Behmani, and Sudeep Bhattacharjee

Department of Physics, Indian Institute of Technology, Kanpur 208016, India

A spatial mapping of electric field fluctuations along the axial and poloidal direction of the jet has been carried out under different flow regimes such as laminar (1 lpm), transition (2.5 lpm) and turbulent (5 lpm). Special emphasis is put to comprehend the nature of fluctuations by phase space and correlation analysis. It has been observed that fluctuations tend to increase axially from the orifice of the capillary and get enhanced under turbulent conditions, due to induced instabilities caused by mixing of ambient air to the main helium plasma channel.

1. Introduction

Atmospheric pressure plasmas are 'non-equilibrium' in nature due to significantly differing electron ($T_e \sim 0.5 – 1$ eV) and ion ($T_i \sim 0.025$ eV) temperatures. The lower gas temperature and presence of reactive oxygen and nitrogen species (RONS) make them suitable for a variety of applications, especially in the biomedical field: bacterial deletion, sterilization, wound healing, and cancer cell treatment [1]. The plasma dosage i.e., the concentration of RONS is one of the crucial parameters which can influence the positive selectivity of desirable damaged cells [1]. Recently, it has been found that the time scale (~0.1-1 ms) of potential fluctuation [2] lies close to the time scale (~0.5-1 ms) of RONS evolution [3], hence fluctuations can alter the RONS concentration. Therefore, it is crucial to investigate the electric field fluctuations and their spatial asymmetry along the plasma plume for the uniform treatment of any intended surface, thereby improving the quality of the applications.

2. Experimental set-up

A ring-to-ring electrode configuration has been employed in this work, as shown in fig. 1. Helium gas is fed through a tapered glass capillary tube and ignited by applying a sinusoidal waveform of amplitude of 11 kV (pp) and frequency 10 kHz, [3]. After ignition, the plasma comes out from the orifice of the capillary as a fine jet of size ~ 0.6-0.8 mm. A double-pin probe has been employed to estimate the electric field fluctuations. Any axial and poloidal point inside the plasma plume can be accessed by a specially designed rotating frame having a rotatable arm (with XYZ stage) (cf. fig. 1).

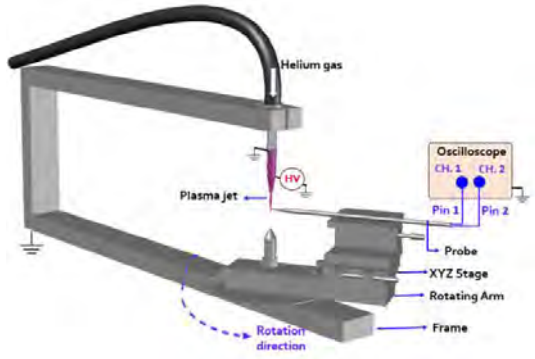

Fig.1. Schematic diagram of experimental setup of the cold micro-plasma jet with rotating frame

3. Results

The fluctuations in E_z and E_φ components of the electric field are scanned along the axial and poloidal direction of the jet under three different flow modes: laminar (1 lpm), transition (2.5 lpm), and turbulent (5 lpm). The frequency characterization has been done by fast Fourier transform. Fig. 2 shows the poloidal variation of the peak amplitude of E_φ fluctuations at different axial (z) positions in the transition regime (2.5 lpm). The fluctuations are comparatively lower and more symmetric near the orifice and tend to get enhanced with an increase in axial distance from the orifice of the capillary. Furthermore, the behaviour of fluctuations will be investigated by phase space analysis and correlation analysis.

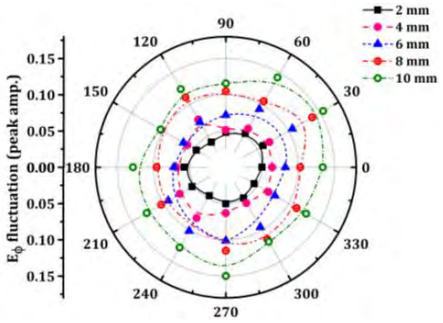

Fig.2. Variation of E_φ fluctuations (peak amp.) along the poloidal direction of the jet in the transition mode (2.5 lpm)

References

[1] Lin l. and Keidar M. Applied Physics Review 2021 **8**, 011306

[2] Behmani, D. *et al.*, AIP Advance **11**, 085128 (2021)

[3] Gaens, W. V. *et al.*, Journal of Physics D: Applied Physics **46**, 275201 (2013)

Glow and arc discharges in atmospheric pressure nitrogen

I. Tsonev[1], J. Boothroyd[1], S. Kolev[2], A. Bogaerts[1]

[1] *Research group PLASMANT, Department of Chemistry, University of Antwerp, Antwerp, Belgium*
[2] *Faculty of Physics, Sofia University, Sofia, Bulgaria*

In this work we developed a two-dimensional (2D) model for nitrogen plasma, which solves the Navier-Stokes equation coupled to the electron energy balance equation, heat balance equation, mean vibrational energy balance equation, the balance equations for the considered species and Poisson's equation in a self-consistent manner. The cathode emission mechanism was varied between field-enhanced thermionic emission (arc) and secondary electron emission (glow) and the results were compared for three different currents (80, 120 and 160 mA) for a gas velocity of 1 m/s. For a current of 80 mA, additional computations for a flow velocity of 1, 2 and 4 m/s were performed. No difference in the positive column was found between the glow and arc discharge, showing that at atmospheric pressure the near electrode regions can be neglected. Our model reveals that increasing the gas flow velocity strongly influences the radial contraction of the positive column but does not influence the peak gas temperature and electron density.

1 Introduction

Atmospheric pressure nitrogen arc and glow discharges have gained attention in recent years, due to their ability to successfully create a chemically active environment suitable for various applications [1,2]. Nonlinearities in the electron production and loss rates tend to contract the positive column, preventing large volume operation of the plasma. Such instability can be initiated by the cathode electron emission mechanisms during the transition from secondary electron emission (glow) to field-enhanced thermionic emission (arc). Although a significant number of works have modelled nitrogen discharges at atmospheric pressure, few include the self-consistent computation of Poisson's equation in order to resolve the sheath regions at atmospheric pressure. The main novelty of our model is thus the inclusion of the self-consistent computation of the cathode region. We compare the thermionic-field emission with the secondary electron emission in order to determine the influence of the cathode region on the positive column.

2 Results

No difference in the positive column was found between the glow and arc discharge, showing that at atmospheric pressure the near electrode regions can be neglected. Figure 1 shows the 2D electron density profiles, at three different currents, for the arc (a) and glow (b) regime, at $u_{g_0} = 1$ m s^{-1}. The 2D profiles of the electron density, at three different inlet flow velocities, for I = 80 mA in the arc regime are presented in figure 2. By varying the flow velocity for the 80 mA arc, only radial contraction is observed without significant influence on the peak electron density.

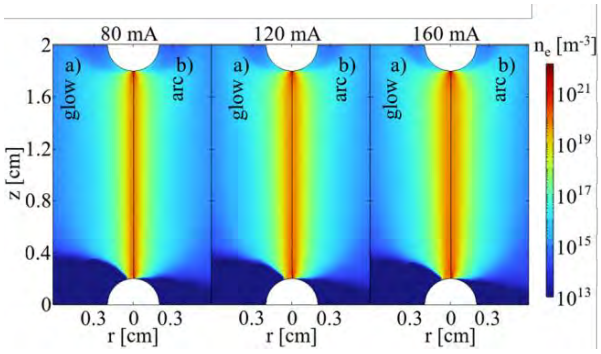

Figure 1. 2D electron density profile, at three different currents, for the arc (a) and glow (b) regime, at $u_{g_0} = 1$ m s^{-1}.

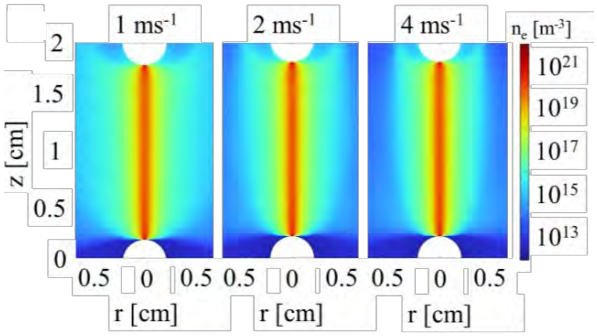

Figure 2. 2D profiles of the electron density, at three different inlet flow velocities, for I = 80 mA in the arc regime.

References

[1] Gorbanev Y, Nitrogen Fixation with Water Vapor by Nonequilibrium Plasma: toward Sustainable Ammonia Production *ACS Sustain. Chem. Eng.* **8** 2996–3004 (2020)

[2] Ji S H, Assessment of the Effects of Nitrogen Plasma and Plasma-Generated Nitric Oxide on Early Development of Coriandum sativum *Plasma Process. Polym.* **12** 1164–1173 (2015)

Quantitative measurements of the effects of OH, O, and O_3 on surface treatments of polymers using VUV photodissociation method

R. Ono, H. Du, and A. Komuro

Dept. Advanced Energy, The Univ. Tokyo, Tokyo, Japan

We have previously developed a method to selectively supply each type of reactive species such as OH and O to a surface placed in room air to quantitatively measure the surface treatment effect of the reactive species. Gas molecules (H_2O, O_2, and CO_2) flowing through a quartz tube are irradiated with VUV light to be photodissociated into reactive species (OH, H, and O), which are delivered to the surface from the quartz tube end. In this study, we demonstrate that this method is a powerful tool to quantitatively measure the effects of reactive species on surface treatments and to elucidate their surface reaction mechanisms. As an example, the effects of OH, O, and O_3 on polypropylene surface treatment were measured. The decay rate of water contact angle by O-atom treatment was determined to be 3.2×10^{-13}[O] degrees/s ([O] in cm^{-3}), which was 3.5 times faster than that of OH. The synergistic effect of O_3 with O for the surface modification and the surface reaction mechanisms were also discussed with ATR FTIR and XPS surface analysis results.

1 Introduction

Reactive species play important roles in the surface treatments using plasma, including polymers, living tissues, and liquids. However, the treatment effect of each type of reactive species has not been quantitatively determined due to the difficulty of such measurements. For this purpose, we have previously developed a method to selectively supply reactive species such as OH and O to a surface using vacuum ultraviolet (VUV) photolysis instead of using plasma, named VUV Photodissociation Reactive species Supply (PRS) method [1, 2]. This method was successfully applied to measure the effect of OH radicals on the surface modification of polypropylene (PP) [3]. In the present study, we demonstrate that this method is a powerful tool to quantitatively measure the effects of reactive species on surface treatments and to elucidate their surface reaction mechanisms. As an example, the effects of OH, O, and O_3 on PP surface treatment were measured.

2 VUV PRS method

Argon-buffered H_2O, O_2, or CO_2 gases flowing in a quartz tube (ID 2 mm, 0.3–3 L/min) is irradiated with VUV light (172 nm) to be photodissociated into OH, H, and O. The subsequent reactions produce additional reactive species (O_3, HO_2, etc.), and the resulting mixture flows to the PP surface from the quartz tube end. The reactive species densities are determined using simulation. The maximum densities of OH and O are 2×10^{13} cm^{-3} and 1×10^{14} cm^{-3}, respectively [2, 3].

3 Results and discussion

When the PP surface is treated with OH and O radicals, polar functional groups such as –OH and C=O are formed. The increase of polar functional groups increases the surface energy, and as a result decreases the water contact angle (WCA) on the PP surface. The decay rate of WCA is not determined by the flux of OH and O, but by their densities [OH] and [O]. This indicates that this is a surface-reaction-rate-limited process. Our measurements determined the decay rate of WCA by O atoms to be 3.2×10^{-13}[O] degrees/s ([O] in cm^{-3}), which is 3.5 times faster than that of OH. The surface reaction mechanisms of OH and O are discussed on the basis of this result, taking into account the much slower hydrogen abstraction from the PP surface by O than that by OH. The surface analysis results of ATR FTIR and XPS are also used for the discussion. In addition, the synergistic effect of O_3 with O for the PP surface modification and the production of low molecular weight oxidized materials are discussed.

The VUV PRS method can be used not only for polymers, but also for any sample such as living tissues. It is a promising tool for studying the effects of reactive species on surface treatments.

References

[1] Ono, R. et al., Comparison of measured and simulated chemical species densities in vacuum ultraviolet photolysis method of $Ar/H_2O/O_2$ mixture developed for selectively supplying reactive species. J. Photochem. Photobiol. A **387**, 112148 (2020).

[2] Ono, R. et al., Selective supply of atomic oxygen to a surface placed in room air using vacuum ultraviolet photolysis of carbon dioxide. Plasma Sources Sci. Technol., accepted.

[3] Ono, R. and Murakami, S., Quantitative measurement of the effect of OH radicals on the surface treatment of polymers. Plasma Process. Polym. **17**, 2000024 (2020).

Simulation of surface dielectric barrier discharges: Streamer and gas dynamics

S. Wilczek[1], G. Hübner[1], A. Böddecker[1], R.T. Nguyen-Smith[1], P. Awakowicz[1] I. Korolov[1] and T. Mussenbrock[1]

[1] *Chair of Applied Electrodynamics and Plasma Technology, Ruhr-University, Bochum, Germany*

In this work, a twin surface dielectric barrier discharge at atmospheric pressure in helium-nitrogen is studied for different voltage waveforms. The formation of streamers and the resulting gas dynamics are studied by means of 2D fluid simulations. It is shown that the dynamics of the streamers lead to different vortices in the gas flow.

1 General

Surface dielectric barrier discharges (SDBDs) play an essential role in environmental applications such as the decomposition of volatile organic compounds (VOCs). A dielectric material (Al_2O_3) is located in the center between two identical electrodes, which are powered by different voltage waveforms in the microsecond or nanosecond time scale[1]. The configuration limits the resulting non-thermal plasma to the surface of the dielectric material generating reactive species and heating the gas.

2 Simulation

In order to study the streamer as well as the gas dynamics of such a discharge setup, 2D fluid simulations are applied. In this work, the simulation code nonPDPSIM developed by Mark Kushner from the University of Michigan is used. A helium/nitrogen chemistry is implemented and various voltage waveforms are applied.

3 Results

The voltage amplitude of the waveform drastically affects the length of the streamer. As a result, the gas heats up at different positions, which results in the formation of vortices in the gas flow. The shorter streamer (4 kV) leads to the generation of one vortex with a downstream to the electrode (see figure 1 left). The longer streamer (5 kV) results in two vortices causing the gas to flow upwards from the electrode (see figure 1 right).

References

[1] Nguyen-Smith, R. T. *et al.* μs and ns twin surface dielectric barrier discharges operated in air: from electrode erosion to plasma characteristics. *Plasma Sources Science and Technology* **31**, 035008 (2022).

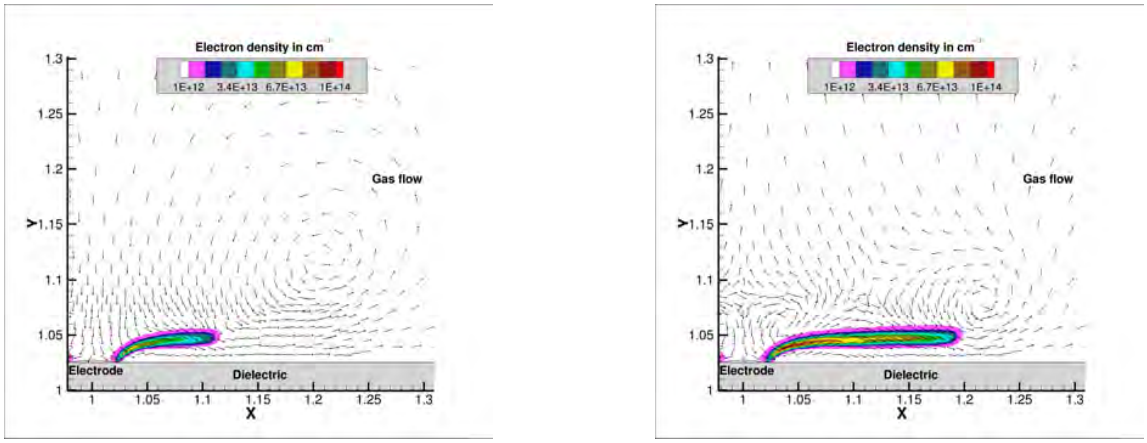

Figure 1: Streamer and gas dynamics for 4 kV and 5 kV voltage amplitude

Ar($1s_5$) density modulation by N_2-O_2 shielding of an atmospheric pressure argon plasma jet

D. Gonçalves[1,2], G. Bauville[1], P. Jeanney[1], M. Lino da Silva[2], L. L. Alves[2], S. Pasquiers[1], J. Santos Sousa[1]

[1] *Université Paris-Saclay, CNRS, Laboratoire de Physique des Gaz et des Plasmas, Orsay, France*
[2] *Instituto de Plasmas e Fusão Nuclear, Instituto Superior Técnico, Universidade de Lisboa, Lisboa, Portugal*

In this work, we used a co-axial reactor with a main jet of argon and a shielding of a nitrogen and oxygen gas mixture. Using laser absorption spectroscopy, we determined the density of the metastable Ar($1s_5$) in the Ar plasma jet created by applying high-frequency (20kHz) high-voltage (4kV) positive square pulses (1µs). The diagnostics were complemented by optical emission spectroscopy measurements.
A higher O_2 fraction in the co-flow leads to a higher Ar($1s_5$) density. The O_2 fraction modulates the longitudinal velocity at which Ar($1s_5$) is created, increasing this velocity on the first discharge (rising edge of the applied voltage) and decreasing on the second discharge (falling edge of the applied voltage). For the first discharge, there is a two-step increase of the Ar($1s_5$) density for higher O_2 fractions.

A plasma jet can be created by ionization waves propagating within an argon jet [1]. These streamers are born inside the tube and propagate along the flow direction exciting and ionizing different gas particles [2]. These discharges are transient and because the argon jet mixes with the ambient air, these streamers propagate in a varying Ar-Air gas mixture, both longitudinally and radially. Accordingly, we determined the temporal-radial density profiles of Ar($1s_5$), excited in an argon plasma jet shielded by different gas mixtures.

The flow consists of a center argon jet (1slm) shielded by an annular co-flow (3slm) of an N_2-O_2 mixture. We used a cylindrical DBD reactor composed by a metallic tube (exposed high-voltage electrode) mechanically forced inside a dielectric tube, which is wrapped by a copper foil strip on the outside (ground electrode). The plasma is produced by high-voltage high-frequency square pulses (4kV, 20kHz, 1µs long), resulting in a first discharge at the rising edge of each applied pulse, and another discharge at the falling edge of the pulse.

Using laser absorption spectroscopy, we measured the temporal absorbance profile of Ar($1s_5$). We then performed an Abel inversion of the temporal profiles to estimate the temporal-radial density profiles of Ar($1s_5$). These results are supported by optical emission spectroscopy data and by estimates from a computational fluid dynamic model [3]. The reproducibility of the absorbance is always above 75% (above 4mm from the nozzle), its lowest value being for a 100%N_2 co-flow, increasing significantly with the admixture of only 2%O_2 into the co-flow. The propagation velocity of the first (second) discharge increases (decreases) with the increase of the O_2 fraction in the co-flow. For both discharges, the Ar($1s_5$) peak density increases with increasing O_2 fraction in the co-flow. However, the peak density obtained in the first discharge is maintained only when the co-flow is composed of 100% O_2. For the first discharge, the temporal profiles show a two-step density increase of Ar($1s_5$) up to 14mm, see Fig. 1, with the duration of the second step increasing with the O_2 fraction.

These results allow us to discuss state-of-the-art hypothesis on flow dynamics, electronegative shielding, photoionization and quenching rates in argon plasma jets. They may also provide valuable data for the development and validation of models.

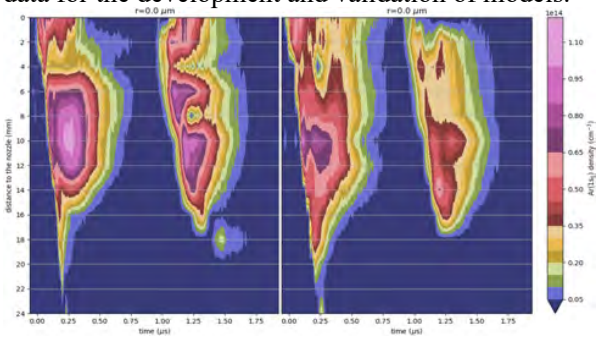

Figure 1. Local temporal density of Ar($1s_5$) along the centerline of the plasma jet, for a 100%O_2 shielding on the left, and a 50%O_2-50%N_2 shielding on the right.

Acknowledgement
Work supported by the Portuguese FCT UIDB/50010/2020 & UIDP/50010/2020, and grant PD/BD/142972/2018 (PD-F APPLAuSE).

References

[1] T. Darny *et al.*, Plasma Sources Sci. Technol. **30**, 105021 (2021)
[2] K. Gazeli *et al.*, Plasma Sources Sci. Technol. **27**, 065003 (2018)
[3] D. Gonçalves *et al.*, Coupled reactive-flow simulation of plasma jets, ICPIG XXXV, The Netherlands (2023)

Stereophotography of streamer discharges in $N_2/O_2/CO_2$ mixtures

Y. Guo and S. Nijdam

Dept. Applied Physics, Eindhoven Univ. Techn., Eindhoven, The Netherlands

A streamer channel usually breaks up into one or more branches during its development. It is known that photoionization plays an important role in streamer propagation and branching in N_2/O_2 mixtures, while with CO_2 admixture this process is inhibited. In this work, we have performed experiments on positive streamer discharges in $N_2/O_2/CO_2$ mixtures at pressures from 100 to 200 mbar in a protrusion-to-plane gap. We characterize the streamer discharges with stereoscopic and stroboscopic imaging and a 3D reconstruction algorithm. Based on the reconstructed 3D models, branching angles, propagation velocities, and radii of streamer channels for different conditions are analysed and compared.

1 General

Streamers are ionized fingers that propagate through dielectric media when a high voltage is applied quickly to a gap. They can then propagate through non-ionized areas due to the enhanced electric field created by the curved space charge layer around their heads. As the first stage of sparks, streamer discharges play an important role in high voltage applications where they are often to be avoided. Recently, CO_2 is considered to be one of the alternative gasses for SF_6 and thus its discharge properties are of great interest to researchers. However, as discharges in pure CO_2 are very dim, it is difficult to study them in great detail.

During its development, a streamer channel usually breaks up into one or more branches. The stochastic fluctuation of electron density ahead of the space charge layer can lead to streamer branching. In N_2/O_2 mixtures, such fluctuations are damped by photoionization, while in gasses containing CO_2, the process of photoionization is strongly inhibited.

In this work, we characterize streamer discharges in $N_2/O_2/CO_2$ mixtures by using stereophotography. Particularly, the effect of CO_2 addition on branching properties are studied.

2 Experimental method

Traditional imaging of streamer discharges usually results in 2D projections of these 3D phenomena, which leads to misunderstanding of the 3D structure of streamer discharges. Therefore, we have developed a method to semi-automatically reconstruct the streamers into 3D representations from stereoscopic and stroboscopic images [1]. We have performed experiments on positive streamer discharges in $N_2/O_2/CO_2$ mixtures at pressures from 100 to 200 mbar in a protrusion-to-plane gap with voltages between 8 and 11 kV. Branching angle, propagation velocity, and radius of streamer channels are then analysed based on the reconstructed 3D models for different experimental conditions.

3 Results and discussions

The general morphology of discharges for different conditions is shown in Fig. 1. The number of branches decreases as O_2 content increases in N_2/O_2 mixtures. Also, the discharge channels become smoother and the feather-like structures fade away for increasing O_2 content. When CO_2 is added into synthetic air, the number of branches grows and small branches appear again for an increasing CO_2 fraction.

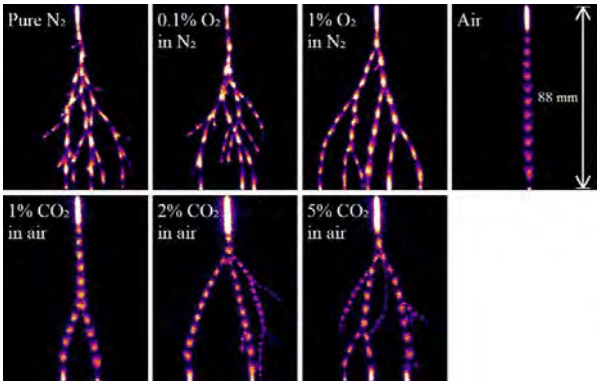

Fig. 1. Stroboscopic images of the general morphology of streamer discharges in different $N_2/O_2/CO_2$ mixtures (V = 9 kV, p = 133 mbar).

From the calculated 3D models, the branching angles for different conditions are distributed statistically. Furthermore, the average branching angles become smaller as O_2 content decreases in N_2/O_2 mixtures and as CO_2 content increases in air/CO_2 mixtures. This is because the relevant photons for photoionization are strongly absorbed by CO_2, which makes the electron density in front of the streamer head lower.

References

[1] Dijcks et al. Imaging and reconstruction of positive streamer discharge tree structures. Under review.

Spatio-temporal spectroscopic investigation of a nanosecond-pulsed barrier discharge in argon

L. Kusýn[1], D. Prokop[1], Z. Navrátil[1] and T. Hoder[1]

[1] *Department of Physical Electronics, Faculty of Science, Masaryk University, Brno, Czechia*

In this contribution, we have studied a nanosecond-pulsed barrier discharge in atmospheric pressure argon. We have performed electrical and ICCD measurements to obtain an overview emission spectra for all ten 2p (Paschen notation) radiative states. Apart from dominant 2p states lines in the range of 680-920 nm, we have also detected emission from 3p states in the range of 410-470 nm. From the overview spectra, we have selected two spectral lines to obtain spatio-temporal scans of the investigated discharge. From the highly resolved time-correlated single photon counting (TCSPC) optical emission spectra, we were able to distinguish between different phases of the discharge. The presented measurements reveal also the spatiotemporally resolved relative $2p_{1-10}$ state densities, which are analysed and mechanisms responsible for their population are discussed.

1 General

Nanosecond pulsed discharges are currently used as unique sources of non-equilibrium transient plasma and offer interesting possibilities for their application in various fields of plasma science [1]. Apart from the geometrical and electrical specifications, the use of appropriate gas mixtures in the fundamental research as well as in the applied, utilization of pulsed plasmas is a crucial part for tailoring of the intended plasma physical and chemical effects. A special role has an argon gas as it serves in many cases as the carrier gas for various precursors, whether in surface treatment or setting of the gas chemistry. Therefore, proper diagnostic methods coupled with advanced data processing algorithms are needed in order to fully understand these phenomena [2].

2 Experiment & results

The volume barrier discharge was ignited in the glass tube between metal and dielectrics-covered electrodes with hemispherical tips that were 1.5 mm apart. Micro discharges were produced by applying high voltage nanosecond pulses with a rise time of almost about 40 ns and an amplitude of 5600 V, with a repetition frequency of 10 kHz. The optical emission spectra were recorded utilizing the time-correlated single photon counting (TCSPC) technique. From the obtained single line data, displayed in Fig. 1, several fundamental trends of the investigated nanosecond pulsed discharge are deduced. The space between the electrodes is the most relevant investigated area which can be divided into four basic phases. The transitions from rapid electron avalanching to streamer and to transient glow discharge were observed. The discharge ended with a surface discharge upon reaching the lower electrode.

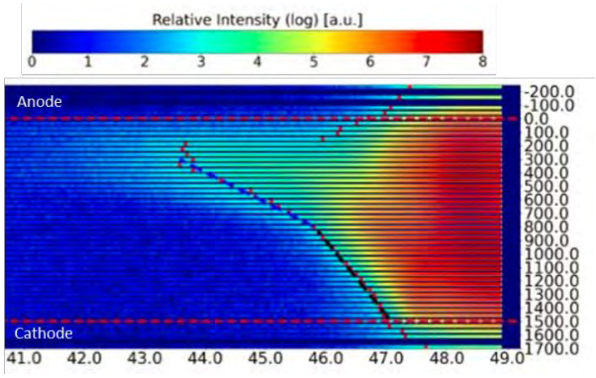

Fig. 1.: Spatio-temporal TCSPC scan of the emission from $3p_9$ state.

Acknowledgment

This research has been funded by Czech Science Foundation under contract no. 21-16391S and supported by the project LM2023039 funded by the Ministry of Education, Youth and Sports of the Czech Republic.

References

[1] Brandenburg R, Bruggeman P J and Starikovskaia S M 2017 Plasma Sources Science and Technology 26 020201.

[2] Šimek M, Ambrico P F, Hoder T, Prukner V, Dilecce G, De Benedictis S and Babicky V. 2018 Plasma Sources Science and Technology 27 0963-0252.

The spectroscopic characteristics of pulse-modulated radio-frequency atmospheric pressure glow microdischarge generated in contact with liquid

P. Jamroz[1], T. Klis[1], K. Swiderski[1] and P. Pohl[1]

[1]*Department of Analytical Chemistry and Chemical Metalurgy, Faculty of Chemistry, Wroclaw University of Science and Technology, Wroclaw, Poland*

The miniaturized pulse-modulated radio-frequency atmospheric pressure glow discharge (pm-rf-APGD) generated in contact with liquid electrodes as a new atomization/excitation microsource in analytical atomic spectrometry was investigated in details. The spectroscopic characterization of the plasma microsource was performed by optical emission spectroscopy (OES). The important plasma parameters, *i.e.*, optical temperatures (rotational and vibrational) as well as the electron number density, were determined and compared for various experimental conditions to elucidate elementary processes in the plasma zone, responsible for the atomization of liquid samples.

The atmospheric pressure glow-like discharges (APGDs) generated in contact with liquid electrodes have been intensively studied in recent years due to their potential applications in environmental engineering [1,2], agriculture [1,3], food processing [4] as well as in nanotechnology for the synthesis of metal nanoparticles [5]. Their miniaturization give an opportunity to use them as unique excitation/atomization sources in analytical atomic spectrometry. Moreover, they are considered nowadays as one of the most promising excitation sources for optical emission spectrometry (OES) [6,8] as well as high performance sample introduction systems for inductively coupled plasma-optical emission spectrometry/mass spectrometry (ICP-OES/ICP-MS) [7,8]. Different constructions of liquid electrodes, means of their polarization as well as modifications of their composition, e.g. by the addition of low weight organic compounds, were applied to improve the analytical performance of APGD sources [6]. It should be noted that to ignite and sustain APGD systems usually high voltage (HV) direct current (dc) power supplies were applied. Low interest was devoted to APGD sources generated in contact with liquids that were sustained by radio frequency power generators [6].

The main aim of this contribution was the spectroscopic diagnostics of a miniaturized pm-rf-APGD microsource generated in contact with flowing liquids as well as the elucidation of the elementary (atomization/excitation) plasma processes in this microsource. The active species, such as NO, OH, N_2, O, H, were identified in the emission spectra of pm-rf-APGD. Additionally, the atomic lines of selected metals, dissolved in liquids, were identified. The vibrational temperature of OH (4000-4200K) and the rotational temperature of OH (3000-4000K), determined for pm-rf-APGD, were higher than the respective rotational temperature of N_2 (1200-1500K) and compared with those reported for other plasma sources. A relatively high value of the electron number density (~4-6)×10^{14} cm^{-3} was also determined and noted to be comparable with other plasma sources generated in contact with liquids [1].

Acknowledgements

The financial support of the National Science Centre (Poland) is gratefully acknowledged (UMO-2019/33/B/ST4/00356).

References

[1] Kovacevic V.V., Sretenovic G.B., Obradovic B.M., Kuraica M.M., Journal of Physics D: Applied Physics, **55**, 473002 (2022).

[2] Jamroz P., Greda K., Pohl P., Zyrnicki W., Plasma Chemistry and Plasma Processing, **34**, 25–37 (2014).

[3] Dzimitrowicz A., Jamroz P., Pohl P., Babinska W., Terefinko D., Sledz W., Motyka-Pomagruk A., International Journal of Molecular Sciences, **22**, 4813 (2021).

[4] Pohl P., Dzimitrowicz A., Cyganowski P., Jamroz P., Food Chemistry **375**, 131831 (2022).

[5] Dzimitrowicz A., Jamroz P., Pogoda D., Nyk M., Pohl P., Plasma Processes and Polymers, **14**, 1600251 (2017).

[6] Pohl P., Jamroz P., Greda K., Gorska M., Dzimitrowicz A., Welna M., Szymczycha-Madeja A., Analytica Chimica Acta **1169**, 338399 (2021).

[7] Pohl P., Greda K., Dzimitrowicz A., Welna M., Szymczycha-Madeja A., Lesniewicz A., Jamroz P., TrAC Trends in Analytical Chemistry, **113**, 234-245 (2019).

[8] Swiderski K., Welna M., Greda K., Pohl P., Jamroz P., Analytical and Bioanalytical Chemistry, **412**, 4211–4219 (2020).

Velocity change of non-transferred arc jet released into water

H. Akatsuka[1,2], J. Kawamura[2], S. Mori[3] and A. Nezu[1,4]

[1] *Inst. Innov. Res., Tokyo Tech, Tokyo, Japan,* [2] *Dept. Elec. Electron. Eng., Tokyo Tech., Tokyo, Japan*
[3] *Dept. Chem. Sci. Eng., Tokyo Tech., Tokyo, Japan,* [4] *Open Facil. Cent., Tokyo Tech, Tokyo, Japan*

A non-transferred atmospheric-pressure argon arc jet is ejected into water from an anode nozzle and examined by optical emission spectroscopy measurement to study thermohydraulic characteristics. The plasma temperature dropped sharply at 10–13 mm downstream measured from the nozzle. Since the arc diameter was found to be almost constant, the arc velocity can be traced from the mass-flux conservation. The velocity dropped sharply at the aforementioned region, where its velocity approximately agreed with the sonic velocity in the water. It is considered that energy dissipation occurred near the sonic velocity of water.

Aiming at the application to the decommissioning of the Fukushima Daiichi Nuclear Power Plant, research is being conducted to measure the underwater thermohydraulic characteristics of non-transferred atmospheric-pressure argon arc jet, by applying optical emission spectroscopy (OES) measurement. Following the measurement of electron temperature and density changes [1], remarkable results are found on the velocity change of the atmospheric pressure argon arc plume released into water from the kinetic considerations, which will be presented.

40 L/min of argon gas was fed to an arc torch under atmospheric-pressure, and a non-transferred DC arc plasma was steadily generated with its discharge current of $80 - 160$ A. Subsequently, it was released continuously from the anode nozzle with an inner diameter of 6.7 mm into water out of the nozzle immersed in the water. The plasma was in the state of thermodynamic equilibrium, and the electron temperature and density were obtained by OES, and their changes in the downstream direction were investigated. Figure 1 (left) shows the electron temperature. At the position $10 - 13$ mm in the downstream direction of the nozzle, the electron temperature dropped steeply compared to other places.

In this study, since the arc column diameter is almost constant, velocity change can also be tracked from mass flux conservation. If the electron temperature at each position is known, the mass density is uniquely determined from the thermal equilibrium conditions. Then, the flow velocity at each measurement position can also be calculated from the conservation of the mass flow rate of the supplied gas, which is shown in Fig. 1 (right).

As a result, it was found that the velocity is subsonic and monotonic deceleration at all observation positions, However, the velocity also decreases sharply at the temperature discontinuity position. Just before approaching this rapid deceleration region, it was found that the plasma jet reaches a sound speed in water of about $1400 - 1500$ m/s. This result can be interpreted that when the plasma flow velocity decelerates and reaches the speed of sound in water, energy dissipation occurs more rapidly than in the upstream region, resulting in a rapid drop in velocity and temperature. That is, in the case of an underwater arc, even subsonic plasma may change its flow characteristics at the speed of sound of the surrounding water [2].

References

[1] Suzuki, R. *et al.* Spectroscopic measurement of arc-discharge argon plasma plume injected into water. *IEEJ Trans. Elec. Electron. Eng.* **16**, 364–373 (2021).

[2] Kawamura, J. *et al.* Heat transfer and thermohydraulic characteristics of arc-discharge argon plasma plume injected into water. *IEEJ Trans. Elec. Electron. Eng.* **17**, 1396–1408 (2022).

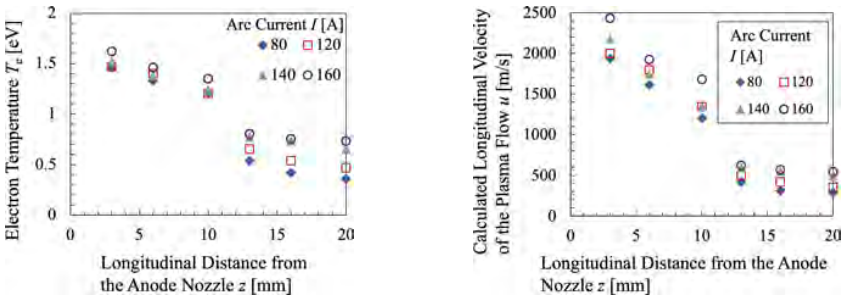

Figure 1: Electron temperature of underwater arc (left) obtained by OES measurement and its velocity (right) calculated from mass flux conservation [1, 2].

A study on plasma active water from a new hybrid source for tomato growth in hydroponic conditions

R. Montalbetti[1], F. Capelli[1,6], F. Orsini[2], N. Contaldo[2,3], A. Pistillo[2], A. Bertaccini[2], G.Pennini[2], V. Colombo[1,4,5,6], M. Gherardi[1,5] and R. Laurita[1,4].

[1]*Department of Industrial Engineering,* Alma Mater Studiorum - *University of Bologna, Bologna, Bologna, Italy*

[2]*Department of Agricultural and Food Science,* Alma Mater Studiorum - *University of Bologna, Bologna, Italy*

[3]*Institute for Sustainable Plant Protection (IPSP), National Research Council of Italy (CNR), Bari, Italy.*

[4]*Interdepartmental Centre for Industrial Research Health Sciences and Technologies,* Alma Mater Studiorum - *University of Bologna, Ozzano dell'Emilia, Bologna, Italy*

[5]*Interdepartmental Centre for Industrial Research Advanced Mechanical Engineering Applications and Materials Technology,* Alma Mater Studiorum - *University of Bologna, Bologna, Italy*

[6]*Alma Plasma S.r.l., Bologna, Italy*

This work presents an innovative cold atmospheric plasma (CAP) source for the production of large volumes of plasma-activated water. Plasma-activated water produced by this atmospheric plasma source is used for the growth of tomato (*Solanum lycopersicum* L.) to evaluate the effectiveness of PAW on plant growth.

1 Aim of the work

The environmental and medical applications of non-thermal atmospheric plasma in and in contact with liquids make plasma-activated liquids a central topic within the atmospheric plasma applications [1]. 'Scopus' and 'Web of science' were used as database to find articles and reviews focused on plasma activated water (PAW) published until December 31, 2022. Over the past 2 decades, the use of PAW in agriculture has shown the effectiveness of these treatments for plant growth and seedling germination [2,3]. The biological activity of PAW is strictly related to the concentration of reactive species of oxygen and nitrogen (RONS) in the aqueous phase [4]. These reactive species are produced within the aqueous medium or at the interface between liquid and gas phases [5]. The production of these reactive species depends on typical parameters of the atmospheric plasma sources such as type of gas used and flow rate, average discharge power, type of liquid used and volume, treatment time, and discharge gap. Therefore, the type of atmospheric plasma source used for plasma treatment significantly affects the chemistry of the treated liquid and the RONS concentration [1]. This study, in addition to presenting a new atmospheric plasma source for treatment of large volumes of water, will also show the results of PAW applied to the growth of *Solanum lycopersicum* L. in hydroponic environment. The new atmospheric plasma source used is a hybrid source composed of a Dielectric Barrier Discharge - rod (DBD-rod) source and a Corona one. The two atmospheric plasma sources work alternately for a total treatment time of 34 minutes and allow treating a volume of 6 litres of tap water.

2 Results

Types of plasma sources, gas and liquid most widely used, RONS concentration within the scientific community will be shown. The results of the electrical characterization of the hybrid source and chemical characterization of the treated water will be presented. In addition, the results of efficacy of PAW produced with the new device on the growth, production and phenotypic characteristics of *S. lycopersicum* will be presented.

3 References

[1] Renwu Zhou, "Plasma-activated water: generation, the origin of reactive species and biological applications" J. Phys. D: Appl. Phys. (2020) 53: 10.1088/1361-6463/ab81cf

[2] David B. Graves, " Plasma activated organic fertilizer " Plasma Chem. Plasma Proc. (2019) 39:1–19.

[3] Pietro Ranieri, "Plasma agriculture: review from the perspective of the plant and its ecosystem" Plasma Process Polym. (2021);18:e2000162

[4] Valeria Veronico, "The active role of organic molecules in the formation of long-lived reactive oxygen and nitrogen species in plasma treated water solutions" Plasma Process Polym. (2022) 19:e2100158.

[5] Corina Bradu, "Reactive nitrogen species in plasma-activated water: generation, chemistry and application in agriculture" J. Phys. D: Appl. Phys. (2020) 53:22300.

4 Acknowledgment

The research leading to this publication has received funding from the Italian Ministry of Education and Research (MUR), within the Research Projects of National Interest (PRIN), project "VFARM - Sustainable Vertical Farming" (Project : 2020ELWM82, CUP:J33C20002350001).

Quantification of chemical species produced by the Surface Dielectric Barrier Discharge with liquid electrodes

O. Galmiz[1], M. Janda[1] and Z. Machala[1]

[1]*Division of Environmental Physics, Faculty of Mathematics, Physics and Informatics, Comenius University Bratislava, Slovakia*

Results on quantification of chemical species produced in gas and liquid phase during the surface dielectric barrier discharge with liquid electrode depending on different experimental conditions will be presented.

1 General

Despite the quickly-growing applications of low temperature plasma physics and technology, many plasma processes are far from being completely understood, particularly the physical and chemical interaction of plasmas with solids and liquids. It is therefore essential to diagnose the fluxes of the generated species, to identify the relevant reaction pathways, to be able to tailor the reaction products for specific applications and to gain further insight into plasma-induced reactivity.

It has been previously reported that Surface Dielectric Barrier Discharge (SDBD) generating gas plasma at the interface with conductive liquids serving as electrodes was used for the treatment of hollow dielectric bodies such as polymer tubes [1-3]. Several potential applications of SDBD discharge were tested, but dedicated experiments under well-defined conditions is needed to better understand the discharge and to fully discover its applicability in emerging plasma technologies, especially for material processing.

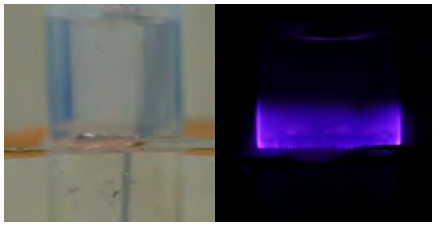

Figure 1. Surface Dielectric Barrier Discharge with liquid electrodes.

Plasma-treated liquids containing a mixture of various reactive oxygen and nitrogen species (RONS) with potentially beneficial chemical or biological effects are broadly referred to as plasma-activated liquids (PAL). Gaseous reactive plasma species such as OH, O_3, NO, and NO_2 are mainly responsible for the biocidal effects in plasmas generated in air [4, 5] and can influence the chemical reactions that take place during the plasma treatment of studied targets.

The aim of this work is to investigate the electrical discharge generating cold plasma with liquid electrodes, where the plasma activated liquid is created. Identification and quantification of the chemical species produced in the discharge and delivered into the liquid is performed.

Acknowledgement

Slovak Research and Development Agency grants APVV-17-0382 and APVV-22-0247. Oleksandr Galmiz was supported by Marie S. Curie Action Personal Fellowship under Horizon 2021 with grant agreement number 101066764.

References

[1] Galmiz, O. et al. Hydrophilization of outer and inner surfaces of Poly(vinyl chloride) tubes using surface dielectric barrier discharges generated in ambient air plasma. Plasma Process. Polym. **14**, 1600220 (2017).

[2] Pavliňák, D. et al. Design and evaluation of plasma polymer deposition on hollow objects by electrical plasma generated from the liquid surface. Plasma Process. Polym. **15**, 1–12 (2018).

[3] Galmiz, O. et al. Plasma treatment of polyethylene tubes in continuous regime using surface dielectric barrier discharge with water electrodes. J. Phys. D. Appl. Phys. **51**, 195201 (2018).

[4] Brandenburg, R. et al. Antimicrobial Treatment of Heat Sensitive Materials by Means of Atmospheric Pressure Rf-Driven Plasma Jet. Contrib. Plasma Phys. **47**, 72 (2007).

[5] Machala, Z. et al. Plasma agents in bio-decontamination by dc discharges in atmospheric air. J. Phys. D: Appl. Phys. **43,** 222001 (2010).

Control strategies for polymerization processes assisted by atmospheric pressure plasma jets

G. Laghi[1], S. Watson[2], R. Laurita[1,3], S. Reuter[2], M. R. Wertheimer[2] and M. Gherardi[1,4]

[1]*Department of Industrial Engineering, Alma Mater Studiorum - University of Bologna, Bologna, Italy*
[2]*Department of Engineering Physics, Polytechnique Montreal, Montreal, Canada*
[3]*Interdepartmental Centre for Industrial Research Health Sciences and Technologies, Alma Mater Studiorum - University of Bologna, Ozzano dell'Emilia, Italy*
[4]*Interdepartmental Centre for Industrial Research Advanced Mechanical Engineering Applications and Materials Technology, Alma Mater Studiorum - University of Bologna, Bologna, Italy*

This work explores the possible control strategies for a polymerization process assisted by an atmospheric pressure single electrode plasma jet and two different silicon-based precursors, aiming to advance the comprehension and the understanding of the process.

1 Aim of the work

Nowadays, polymerization processes assisted by atmospheric pressure (AP) plasma jets are receiving interest in numerous industrially relevant sectors since they allow to coat complex 3D substrates without requiring expensive vacuum systems [1,2]. Therefore, finding proper strategies to control polymerization processes supported by AP plasma jets has become a high priority research topic.

The Yasuda parameter W/FM (W: discharge power; FM: precursor molar flow rate multiplied by precursor molecular weight) is a consolidated controlling parameter for low pressure plasma polymerization processes [3,4]. Despite several research groups attempted to extend its application also to the AP case [5,6], the validity of W/FM as a controlling parameter at AP has been questioned because 1) the precursor is usually highly diluted in an inert gas flow and 2) the measurement of the discharge power is often non-trivial. As a more accurate alternative to the Yasuda parameter, Nisol et al. developed a methodology (based on the resolution of an electrical equivalent circuit model) for measuring the energy absorbed per precursor molecule, E_m, in AP plasma polymerization processes [7]. Nevertheless, this methodology is still limited to planar dielectric barrier discharges and to gaseous and vaporized precursors.

In this work, a study of the validity of W/FM as a controlling parameter in a polymerization process assisted by a single electrode AP plasma jet and an aerosolized fluorinated silane precursor is proposed. The chemical and physical properties of thin films deposited under different W/FM values are assessed by means of numerous surface characterization techniques (ATR-FTIR, XPS, SEM, etc.).

Furthermore, the development of a methodology for measuring the energy of reactions in the polymerization process assisted by the same AP plasma jet and vaporized hexamethyldisiloxane is presented. The values of E_m are calculated through the identification and resolution of a suitable electrical equivalent circuit model. To validate the methodology, these E_m values are correlated to the bond energies of the precursor molecule and to the properties of the deposited thin films.

2 Results

About W/FM, surface characterization techniques reveal the presence of the so-called energy-deficient and monomer-deficient domains, thus suggesting the validity of W/FM as a controlling parameter. In addition, the key role of W/FM in the process is further demonstrated since coatings deposited under the same W/FM exhibit similar properties, regardless of how W/FM is obtained.

Regarding the new methodology proposed, it is shown that both precursor fragmentation and coating characteristics can be successfully explained according to the calculated E_m values.

Through a detailed discussion of the limits and the potentialities of the explored control strategies, this work provides useful insights into the control of polymerization processes assisted by AP plasma jets.

References

[1] X. Lu et al., Plasma Sources Sci. Technol., **21**, 3 (2012).
[2] S. Bornholdt et al., Eur. Phys. J. D, **60**, 3 (2010).
[3] H. Yasuda et al., J. Polym. Sci. Polym. Chem. Ed., **16**, 4 (1978).
[4] H. Yasuda, J. Polym. Sci. Macromol. Rev., **16** (1981).
[5] R. Morent et al., Plasma Process. Polym., **6**, 1 (2009).
[6] A. Kakaroglou et al., RSC Adv., **5**, 35, (2015).
[7] B. Nisol et al., Plasma Process. Polym., **13**, 3 (2016).

Investigation of gas flow pattern in a Micro-Hollow Cathode Discharge-based deposition reactor using planar Laser Induced Fluorescence.

A. Remigy[1], B. Menacer[1], A. Halfaoui[2], G. Bauville[2], L. Invernizzi[1], K. Gazeli[1], G. Lombardi[1], S. Iseni[3], J. Santos Sousa[2] and C. Lazzaroni[1]

[1] *Université Sorbonne Paris Nord, Laboratoire des Sciences des Procédés et des Matériaux, LSPM, CNRS, UPR 3407, F-93430, Villetaneuse, France*
[2] *Université Paris Saclay, CNRS, Laboratoire de Physique des Gaz et des Plasmas, 91405, Orsay, France*
[3] *GREMI-Groupe de Recherches sur l'Energétique des Milieux Ionisés, UMR 7344, CNRS/Université d'Orléans, France*

A micro-hollow cathode discharge (MHCD), ignited in an Ar/N_2 gas mixture, is used to produce atomic nitrogen in a Plasma Enhanced Chemical Vapor Deposition (PECVD) reactor for hexagonal boron nitride synthesis. To expand the plasma volume of the MHCD and transport the species onto the substrate, a pressure differential is introduced between the two sides of the MHCD, creating a plasma jet. Two dimensional spatial mappings of the atomic nitrogen density in the deposition chamber showed an unexpected density profile, presumably due to the gas flow pattern. To better understand the gas flow effect, Planar Laser Induced Fluorescence is used on acetone to visualize the gas flow structure in the deposition chamber.

Hexagonal Boron Nitride (h-BN) is a strategic material for electronic and optoelectronic applications, as it is an atomically flat insulator with a crystalline structure close to that of graphene (1% mismatch). Such applications require the synthesis of high-quality h-BN films of controlled thickness over large surfaces (2 inches diameter). To that end, our team developed a Plasma Enhanced Chemical Vapor Deposition (PECVD) process using a Micro-Hollow Cathode Discharge (MHCD) as a plasma source [1]. Our MHCD consists of a dielectric layer glued in-between two electrodes, with a 400-µm hole drilled through them. When a DC voltage is applied between the electrodes, a plasma ignites inside the hole and expands on the cathode surface. As a precursor for the nitrogen (N) atoms needed for h-BN deposition, The MHCD is operated in an Ar/N_2 gas mixture, N2 being the nitrogen (N) atoms precursor (essential for h-BN deposition). Previous measurements revealed that the plasma inside the hole generates high electron densities (10^{13} cm^{-3}) as well as high N atoms densities (10^{14} cm^{-3}) [2].

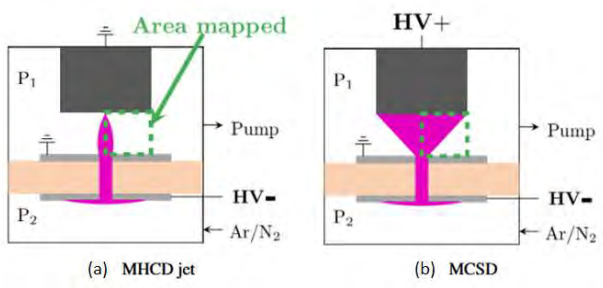

Figure 1: Scheme of (a) the MHCD plasma jet and (b) the MCSD configurations. HV: High voltage.

With the goal of large area deposition, two different strategies for the expansion of the plasma volume have been studied. The first route, presented in figure 1a, refers to the use of a grounded substrate and a pressure differential ($P_2>P_1$) to create a MHCD plasma jet. The second route, presented in figure 1b, is to apply a positive bias to the substrate, while still maintaining a pressure differential, and thus creating a Micro-Cathode Sustained Discharge (MCSD).

N atoms density mappings, in the area indicated by the dashed green line in figure 1, have been performed using nanosecond Two-Photons Absorption Laser Induced Fluorescence (TALIF) and revealed peculiar density profiles. In addition, to support the investigation of the N atoms density distribution, we admixed acetone to the Ar gas and use it as a tracer to perform Planar Laser Induced Fluorescence (P-LIF) [3].
P-LIF allowed us to visualize the gas flow pattern inside the deposition chamber and in particular the turbulences and/or vortices created by the jet impinging onto the substrate. Optimisation of the gas flow pattern and the resulting N-atom density profile is crucial for the deposited h-BN films to be homogeneous over the whole substrate.

References

[1] Kabbara H. et al. Appl. Phys. Lett. **116**, 171902 (2020).
[2] Remigy A. et al. J. Phys. D: Appl. Phys. **55**, 105202 (2022).
[3] Iseni S. et al. J. Phys. D: Appl. Phys. **47** 152001

Sputter epitaxy of atomically flat $(ZnO)_x(InN)_{1-x}$ films on sapphire substrates using ZnO(N) buffer layers fabricated by Ar/N_2 discharges

Y. Nakano[1], R. Narishige[1], N. Yamashita[1], K. Kamataki[1], T. Okumura[1], K. Koga[1,2], M. Shiratani[1], H. Kiyama[1], H. Yabuta[1] and N. Itagaki[1]

[1] *Graduate School of Information Science and Electrical Engineering, Kyushu University, Fukuoka, Japan*
[2]*National Institutes of Natural Sciences, Tokyo, Japan*

Epitaxial $(ZnO)_x(InN)_{1-x}$ (hereafter ZION) films have been successfully grown on 18%-lattice mismatched sapphire substrates using ZnO(N) buffer layers fabricated by radio-frequency magnetron sputtering. We observed that the buffer layers lead to change in ZION growth mode from three dimensional to two dimensional one, and even ZION films of 300 nm thick have atomically-flat surfaces with the root-mean-square roughness of 0.44 nm when the films grow on the buffers. We consider that this is because the buffer layers provide lattice-relaxed nucleation centres, smooth surfaces, and low interfacial energy between the films and the buffers, all of which promote 2D growth of the subsequent ZION films.

1. Introduction

$(ZnO)_x(InN)_{1-x}$ (hereafter ZION) are promising materials for optoelectronic devices because of the high exciton binding energies of 30–60 meV and tuneable band gaps (1.5–3.4 eV) [1]. Growth of ZION films with high crystal quality on cost-effective sapphire substrates has been, however, challenging because of their large lattice mismatch over 18%. Recently, we have succeeded in epitaxial growth of ZnO films on 18%-lattice mismatched sapphire substrates using ZnO(N) buffer layers [2]. The latter consist of strain-relaxed nano-sized three dimensional (3D) islands, where the islanding cost is reduced by adsorbed N atoms that are produced through dissociation of N_2 molecules in Ar/N_2 discharges. On the buffers, films grow in 2D mode, forming atomically flat terraces [2]. Here we apply the ZnO(N) buffers to epitaxial growth of ZION films on lattice mismatched sapphire substrates and investigate their effects on ZION growth mode, observing the temporal evolution of film morphology.

2. Experimental

All films were fabricated by magnetron sputtering. First, 10-nm-thick-ZnO(N) buffer layers were deposited on c-plane sapphire substrates at 900ºC in Ar/N_2 atmosphere. Then, ZION films were deposited on the buffer layers at 450ºC in $Ar/N_2/O_2$ atmosphere. The thickness (d_{ZION}) were 35–300 nm.

3. Result and discussion

We found that the ZnO(N) buffer layers lead to drastic change in ZION growth mode. Figures 1 (a) and (b) show atomic force microscope (AFM) images of 35- and 300-nm-thick ZION films fabricated with buffer layers, respectively. For comparison, AFM images of 35- and 300-nm-thick ZION films fabricated without buffers are shown in Figs. 1 (c) and (b), respectively. The film without buffer grows in 3D mode, where the root mean square (RMS) roughness increases from 1.07 to 9.08 nm with increasing the film thickness from 35 to 300 nm. This is because islanding occurs during ZION growth so that the lattice strain due to the lattice mismatch between ZION and sapphire is released. Remarkably, however, no such increase in the surface roughness is observed for ZION film on the buffer, and the RMS roughness rather decreases from 0.69 to 0.44 nm with increasing the thickness. This indicates that the film with ZnO(N) buffer grows in 2D mode, where the buffer layer provides lattice-relaxed nucleation centres, smooth surface, and low interfacial energy between the film and the buffer, all of which promote 2D growth of the subsequent ZION film. In addition, even very thin ZION film of 35 nm thick shows small full-width at half maximum of (002) plane x-ray rocking curve of 0.8º, indicating that the buffers bring about excellent out-of-plane alignment of ZION films.

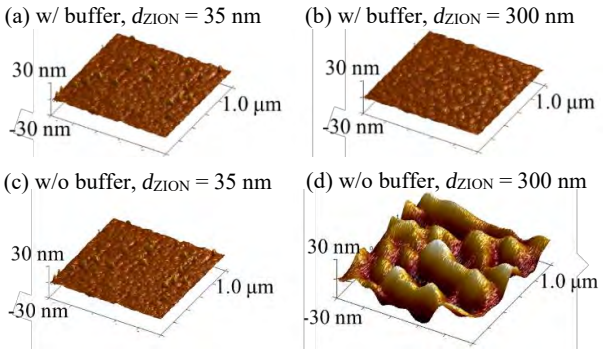

Fig. 1. AFM images of ZION films. The films are with buffers ((a), (b)) and without buffer ((c), (d)). The film thickness are 35 nm ((a), (c)) and 300 nm ((b), (d)).

Acknowledgments

This work was supported by JSPS KAKENHI Grant Numbers JP21H01372, JP21K18731, JP22H05000, and The Murata Science Foundation.

References

[1] N. Itagaki *et al.*, Master. Res. Express, 1, 36450 (2014).
[2] N. Itagaki *et al.*, Sci. Rep. 10 4669 (2020).

Influence of plasma instability on gas-phase synthesis of N-graphene in dual-channel microwave plasma torch at atmospheric pressure

O. Jasek[1], J. Jurmanova[1], D. Vsiansky[2], D. Nejezchleba[1] and Z. Navratil [1]

[1] *Department Of Physical Electronics, Faculty of Science, Masaryk University, Brno, Czech Republic*
[2] *Department of Geological Sciences, Faculty of Science, Masaryk University, Brno, Czech Republic*

The influence of plasma instability of on the gas-phase synthesis of nitrogen-doped graphene (N-graphene) was investigated using dual-channel microwave plasma torch at atmospheric pressure. Plasma plume instability was controlled by delivered microwave power and the interplay of Ar central channel flow rate and gas flow rates of precursors (C_2H_2 and N_2) delivered into electrode's secondary channel. The lateral size of N-graphene nanosheets increased and the number of defects in its structure decrease with delivered microwave power, however, concentration of nitrogen in the N-graphene structure decreased as well and was strongly depended on stability of plasma plume. Plasma was monitored by optical emission (OES) and Fourier transform infrared spectroscopy (FTIR). Graphene was analyzed by scanning electron microscopy (SEM), Raman, and X-ray photoelectron electron spectroscopy (XPS) and thermogravimetry (TGA).

1 Introduction

The process of organic precursors decomposition and subsequent formation of carbon nanostructures in the gas-phase is strongly dependent on the temperature [1] and plasma plume stability of the environment formed by the plasma discharge [2]. Nitrogen-doped graphene (N-graphene) synthesis strongly depends on used precursor and method of its injection during the synthesis. N-graphene was prepared at atmospheric pressure using N_2/Ar/ethanol mixture in MW SWD with low content of 0.2 at% of N atoms bonded to C atoms [3]. Improvement was achieved using CH_4 and CH_3-NH_2 as nitrogen precursors, 8 at% of N, and different approaches for NH_3 injection were also studied and showed high importance of different plasma zones with different gas temperatures during the synthesis [4].

2 Experimental

Organic precursor (C_2H_2) decomposition was carried out in a dual-channel microwave plasma torch discharge at atmospheric pressure enclosed in a quartz tube reactor. The discharge was ignited in Ar, 360 - 700 sccm, flowing through the central channel (Q_c) applying microwave power (P_W) of 180 - 350 W. C_2H_2 flow rate was varied from 6 to 19 sccm in secondary channel. N_2 admixture flow rate was 13 sccm. After the synthesis, the nanopowder was scrapped from the reactor's wall. OES was carried out using a Jobin Yvon Triax 550 with 1200 gr/mm grating and effluent gases were analyzed by FTIR using Bruker Vertex80V in the range 3500 - 550 cm^{-1}. N-graphene was characterized by SEM with Tescan MIRA3 and XPS was carried out by Thermo Scientific ESCALAB 250Xi device. Raman spectra were measured by the HORIBA LabRAM HR Evolution system (532 nm) in the range from 500 to 3350 cm^{-1}. TGA was measured by a Setaram Sestys Evolution 2400 in air.

3 Results

Two main parameters studied were delivered microwave power and Ar central channel flow rate, at constant flow rate of N_2. At laminar flow regime (Q_c=360 sccm), graphene nanosheet's size increased from 20 nm to 200 nm with increase of P_W from 195 W to 270 W. Similarly, ID/IG Raman band ratio decreased from 1.6 to 0.7, respectively. However, formation of flame instability using higher Q_c=700 sccm resulted in formation of crystalline carbon nanoparticles with ID/IG ratio of 1.9. XPS analysis showed increasing content of nitrogen with increasing number of defects in the graphene's structure and the emission intensity of CN and HCN molecular band in OES and FTIR spectra, respectively, increased with P_W and Q_c as well.

4 Acknowledgement

This work was supported by project LM2023039 funded by the MEYS of the Czech Republic.

References

[1] A. Dato, Graphene synthesized in atmospheric plasmas - A review, Journal of Materials Research, **34**, 214–230 (2019).

[2] O. Jašek et al., Controlled high temperature stability of microwave plasma synthesized graphene nanosheets, J.Phys D:Appl. Phys., **54**, 165201 (2021).

[3] E. Tatarova et al. Towards large-scale in free-standing graphene and N-graphene sheets, Sci. Rep. **7**, 10175 (2017).

[4] D. Tsyganov et al., Microwave plasma-based direct synthesis of free-standing N-graphene, Phys. Chem. Chem. Phys. **22**, 4772 (2020).

Chemical composition and surface morphology of films polymerized by C_4F_8 plasmas in Bosch process

T. Nonaka[1,2], K. Takahashi[3], A. Uchida[1], S. Lundgaard[1] and O. Tsuji[1]

[1] *Research and Development Department, Samco Inc., Kyoto, Japan*
[2] *Department of Electronics, Kyoto Institute of Technology, Kyoto, Japan*
[3] *Faculty of Electrical Engineering and Electronics, Kyoto Institute of Technology, Kyoto, Japan*

In the Bosch process, a polymerized film deposited by C_4F_8 plasma is used for sidewall passivation. During processing (alternated deposition and etching), the polymerized film creeps and can lead to undesired etching of the silicon on the sidewalls. In this study, chemical compositions of the polymerized films deposited by C_4F_8 plasmas were analyzed before and after etching to examine changing in characteristics of the film surface due to the effect of F radicals. The surface morphology of polymerized films deposited with C_4F_8 plasma and also with an alternated C_4F_8 and SF_6 plasmas was observed. It was confirmed that the polymerized film surface was deformed by the F radicals.

1 Introduction

A silicon-deep-reactive-ion-etching (Si-DRIE) process which alternately switches a deposition of sidewall passivation film and the etching of silicon, is called the Bosch process [1]. The Bosch process uses C_4F_8 polymerized film for sidewall passivation. The polymerized film is etched by F radicals generated by SF_6 plasma during silicon etching [2] which causes changes in the chemical composition and surface morphology of the polymerized films. Therefore, as the processing time increases, localised breaks in the passivation film occurs and the silicon on the sidewall is etched even though there is a sufficiently thick polymerized film.

2 Experiment

An inductively Coupled Plasma (ICP) etcher RIE-800iPBC (Samco) for the Bosch process was used as the plasma generator.

Chemical compositions of the polymerized films were analyzed by x-ray photoelectron spectroscopy (XPS) which were deposited by C_4F_8 plasma and etched by F radicals generated from SF_6 plasmas.

Two surfaces of the films were observed by scanning electron microscopy (SEM). One was deposited by C_4F_8 plasma and another was deposited by alternating C_4F_8 and SF_6 plasmas over 100 loops to mimic Bosch process conditions.

3 Results and discussion

Comparing chemical composition of polymerized films before and after etching by F radicals, the bond fraction of CF_3 and CF_2 increase, while those of CF and C-CF_X decrease (Fig. 1). The CF and C-CF_X were converted to CF_2 by F radicals, resulting in making more straight polymer chains.

The surface of the polymerized film deposited by C_4F_8 plasma was smooth (Fig. 2(a)). However, a surface of the polymerized film deposited by alternating C_4F_8 and SF_6 plasma was rough and exhibited a porous structure (Fig. 2(b)). We believe that these changes in the polymerized film surface create localized thinned areas in the sidewall passivation from which F radicals penetrate and locally etch the silicon on the sidewall (Fig. 2(c)).

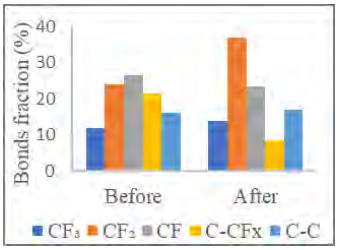

FIG.1. Bonds fraction of polymerized film before and after radical etching by SF_6 plasma.

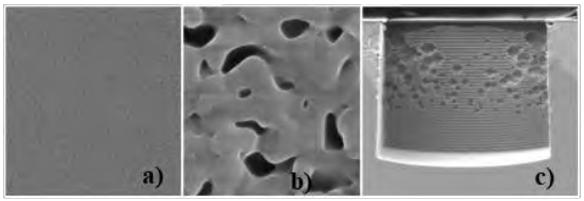

FIG.2. SEM images of the surface of the polymerized film deposited (a) by C_4F_8, and (b) by 100 cycles of alternating C_4F_8 and SF_6 plasma (30,000x). (c) an image of Bosch process with undesired sidewall etching (180x).

References

[1] F. Laermer, A, Schilp,
Patents DE4241045, US 5501893 and EP 625285

[2] D. Zhang, M. J. Kushner, J. Vac. Sci. Technol. A 18, 2661 (2000)

Plasma-based Lithium recovery process

Jong Keun Yang[1], InSun Park[1], Chang Hyun Cho[1], Inje Kang[1], and Ji Hun Kim[1]

[1] *Korea Institute of Fusion Energy, South korea*

This study is a plasma-based lithium recovery process for improving the efficiency of the carbonation reaction of lithium salt by CO_2 gas addition. It showed 3 times higher efficiency than the conventional method.

Carbonation reactions are used to recover lithium from lithium-containing solutions such as brines, including seawater, in order to mineralize the lithium present in nature into various forms such as Li_2CO_3 or Li_2O. There are two main methods for such reactions. One is using the carbonate compound and the other is using carbon dioxide gas.

The carbonated compounds addition method uses various carbonates such as Na_2CO_3, $NaHCO_3$, K_2CO_3, etc. to recover lithium carbonate (Li_2CO_3) from lithium-containing solutions. CO_2 gas addition method is a method of recovering precipitated lithium carbonate (Li_2CO_3) by adding carbon dioxide gas to a lithium-containing solution.

In the carbon dioxide gas adding, depending on the type of lithium salt, the reaction may not occur thermodynamically. One such lithium salt is LiCl. In order to solidify this LiCl-containing aqueous solution into lithium carbonate by CO_2 addition method, external factors such as catalyst, external energy, and additives are required. Nevertheless, even if additives are used, the recovery rate is low, so various research is needed to improve efficiency.

In this study, a plasma-based lithium recovery method was studied to recover lithium salts in brine and improve the recovery efficiency. The CO_2 plasma method shows the increase 300% efficiency than the just CO_2 gas and NaOH addition.

The plasma-based lithium recovery using global warming gases will contribute to the development of technologies in various fields such as seawater desalination waste liquid resource utilization, secondary batteries, waste batteries, CCUS, high value-added CO_2, and the development of nuclear fusion fuel manufacturing technologies.

Acknowledgment

This research was supported by R&D Program of "Plasma Convergence & Fundamental Research (EN2321)" through the Korea Institute of Fusion Energy (KFE) funded by the Government funds, Republic of Korea.

Effects of tailored voltage waveform discharges on deposition of hydrogenated amorphous carbon films by CH_4/Ar capacitively coupled plasma

M. Otaka[1], H. Otomo[1,2], K. Ikeda[1], J. Lai[1], K. Kamataki[1], T. Okumura[1], N. Yamashita[1], N. Itagaki[1], K. Koga[1], M. Shiratani[1], T. Shindo[2], S. Tanaka[2], T. Matsudo[2]

[1] *Graduate School and Faculty of Information Science and Electrical Engineering, Kyushu University, Japan*
[2] *Tokyo Electron Technology Solutions Limited, Japan*

We investigate effects of Tailored Voltage Waveform (TVW) discharges on deposition of hydrogenated amorphous carbon (a-C:H) films in CH_4/Ar capacitively coupled plasma. TVW discharges employ dual frequencies, by which ion bombardment energy and ion flux are controlled independently. Plasma enhanced chemical vapor deposition (PECVD) with TVW discharges realizes control mass density of a-C:H films with a nearly constant deposition rate.

1. Introduction

A novel discharge method using TVW in Capacitively Coupled Plasma (CCP) has been developed to offer new tuning knobs for controlling the plasma. TVW is synthesized, for instance, by phase-locked fundamental waveform and its second harmonic [1,2]. This method realizes independent control of Ion Bombardment Energy (IBE) and ion flux using phase between the dual frequencies. So far, rather few reports of thin film deposition using TVW discharges have been published. In this study, we have investigated effects of TVW discharges on deposition of a-C:H films by CH_4/Ar CCP.

2. Experimental

The experiments were performed using CCP with TVW discharges. The TVW discharges were sustained by a fundamental frequency (13.56 MHz) and a second harmonic (27.12 MHz) for phase shift of 0, 22.5, 45, 67.5 and 90 degree, respectively. CH_4 (5 sccm) and Ar (10 sccm) were supplied to the reactor. Total gas pressure was 30 mTorr. The a-C:H film properties were obtained by X-ray reflectometry (XRR), ellipsometry and Raman spectroscopy.

3. Results and discussion

Figure 1 shows (a) mass density and (b) deposition rate of a-C:H films fabricated by single fundamental RF frequency (13.56MHz) discharge (V_{PP} = 280 ~780 V) and TVW ones (V_{PP} = 360 and 480 V). The mass density depends on DC self-bias ($|V_{DC}|$) and has the maximum value at $|V_{DC}|$ ~180 V. The mass density changes from 1.54 g/cm^3 to 1.80 g/cm^3 as controlling the phase shift from 90 ($|V_{DC}|$ = 90 V) to 0 ($|V_{DC}|$ = 180 V) by the TVW method. The deposition rate of the film by the single frequency discharge increases with increasing the DC self-bias, whereas the deposition rate by TVW discharges is almost constant irrespective of the DC self-bias. In TVW discharges, DC self-bias is determined by phase shift while keeping the peak to peak discharge voltage, V_{PP} constant. Hence, the ion flux is constant while changing Vdc in TVW discharges. On the other hand, in the single frequency discharges, ion flux increases with the DC self-bias.

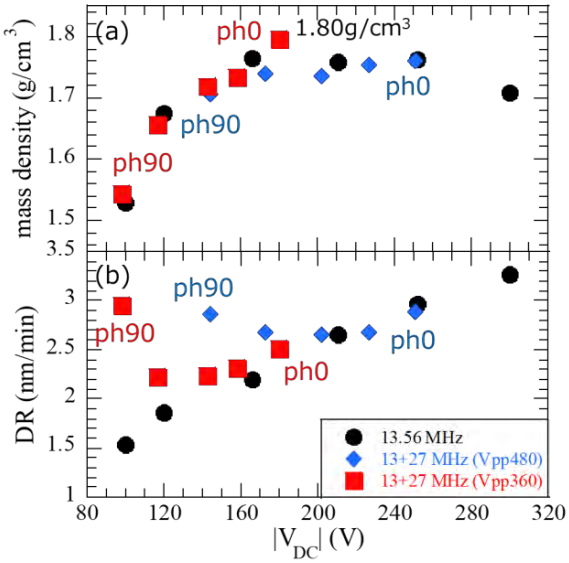

Fig. 1 (a) mass density, (b) deposition rate of a-C:H films deposited by PECVD with TVW discharges. ph stands for the phase between dual frequencies.

4. Conclusion

In this study, we investigated the effects of TVW discharges on deposition of a-C:H films. The TVW discharges realizes control of mass density from 1.54 to 1.80 g/cm^3 while maintaining a nearly constant deposition rate.

References

[1] J. Schulze, et. al, J. Phys. D: Appl. Phys. **43** 124016 (2010)
[2] L. Wang, et. al, Plasma Sources Sci. Technol. **30** 054001 (2021)

Production of micro-sized metal powder using plasma-gas hybrid atomization system

Jihun Kim[1], Injae Kang[1], Hyunjae Park[1], Changhyun Cho[1], Jongkeun Yang[1], Insun Park[1]
[1] *Institute of Plasma Technology, Korea Instituite of Fusion Energy*

The process of producing micro-sized spherical metal powders using a dispersed melt is called atomization [1]. Spherical metal powders are widely used in the automotive, medical, and aerospace industries using additive manufacturing. Micro-sized metal powders were produced by production methods of spherical metal powders such as WA (water atomization) [1] and GA (gas atomization) [2]. WA is one of the economical processes, but this technology is not suitable for producing spherical clean powders [3], and GA is suitable for producing spherical powders, but has difficulties in producing fine powders of less than 30 μm. To apply to 3D printing, metal powders of 20 μm or less are required. In order to make a smaller size metal powder, the temperature of the molten metal must be higher in the conventional atomizing method, and high energy is required in the collision between the molten metal and the gas. The DC arc plasma torch has the highest heat velocity compared to other heat sources, so it is advantageous to increase the temperature of the object to be treated in a short time. In this study, an optimized DC arc plasma torch (DCAPT) was applied to the GA to develop a novel HA system containing three DCAPTs, improving the general GA technique by using a higher superheat in a high-velocity plasma jet. DCAPT has an optimized anode structure and shows high thermal efficiency of about 80% for stable operation of DCAPT at power of 15~20kW and nitrogen gas flow rate of 80SLM. An experiment was conducted on the production of stainless steel metal powder by the developed HA system with three DCAPTs. As a result of scanning electron microscopy (SEM) analysis, high-quality spheroids were observed in the atomized stainless steel powder. The experiment was performed under the experimental conditions of the HA system in which the total power of three DC arc plasma torches was about 45 kW and the nitrogen gas injection pressure was 1.5 MPa. In the SEM images, the atomized tin and copper powders clearly show high-quality spherical shapes.

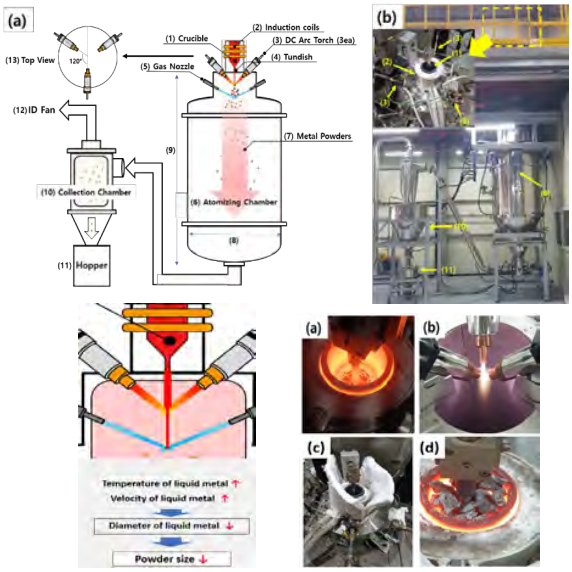

Fig. 1 A hybrid plasma atomization system

The size distribution of stainless powder showed a high particle size distribution below 10 μm. It is expected that this technology will be used as a 3D printing material in the future, and it will be applicable to various materials.

This work was supported by R&D Program of "Plasma Convergence & Fundamental Research" through the Korea Institute of Fusion Energy (KFE) funded by the Government fund

References

[1] Y. Liu, S. Niu, F. Li, Y. Zhu, and Y. He, *Powder Technol.*, vol. 213, pp. 36-40 (2011)
[2] S. Hussain, C. Cui, L. He, L. Mädler, and V. Uhlenwinkel, *J. Mater. Process. Technol.*, vol. 282 (2020)
[3] S. Lagutkin, L. Achelis, S. Sheikhaliev, V. Uhlenwinkel, and V. Srivastava, *Mater. Sci. Eng. A*, vol. 383, pp. 1-6 (2004)

Investigating the performances of cold plasma endoscopy for cholangiocarcinoma local treatment

M. Soulier[1*], A. Pavy[2*], H. Decauchy[1], K. Géraud[1], B. Lekbaby[2], L. Aoudjehane[2,3], M. Camus[2,4], L. Fouassier[2#] and T. Dufour[1#]

[1] *LPP. Sorbonne Université, CNRS, Ecole Polytechnique, Paris, France*
[2] *Sorbonne Université, INSERM, Centre de Recherche Saint-Antoine (CRSA), Paris, France*
[3] *Institute of Cardiometabolism and Nutrition (ICAN), Paris, France*
[4] *Sorbonne University, Endoscopic Unit, Saint-Antoine Hospital, AP-HP, Paris, France*
**Co-first authors, # co-leadership*

In 2020, 600 types of cancer have been identified by the World Health Organization, resulting in 10 million deaths worldwide. Cold atmospheric plasmas seem to be interesting alternative therapies because of their physicochemical properties and their great flexibility in the generation mode. In recent years, CRSA and LPP teams have been investigating a non-thermal plasma catheter for cholangiocarcinoma treatment [1,2]. Experiments conducted on murine subcutaneous models have shown a significant reduction in tumour volumes after 5 plasma treatments. *In vitro* studies have proven a high mortality of human and murine cholangiocarcinoma cell lines with over 70 % cell death after 5 minutes of treatment. The setup has been inserted into post-mortem porcine models, demonstrating the generation of plasma in a closed wet environment without any thermal or electrical hazards.

1 Context and aims

Cholangiocarcinoma (CCA) is a rare and aggressive biliary tract cancer with a very poor prognosis and, increasing incidence and mortality rates worldwide. CCA represents the second most current malignant liver tumour, accounting for about 15 % of all hepatic cancer, following hepatocellular carcinoma. It is a primary fibrous tumour that can grow all along the bile ducts. Asymptomatic in its early stages and poorly accessible for current treatments, only 35 % of patients could receive a curative therapy. Surgical resection is performed, often completed with adjuvant chemotherapy or radiotherapy.

The therapeutic effects of cold atmospheric plasma (CAP) on cancer models have been studied since the 2010s. CAP represent innovative technological approaches where the conventional ones seem limited. It can cause deleterious effects on cancer cells leading to cell death or dysfunction. Reactive oxygen species (ROS) generated by plasma cause oxidative stress, saturating the antioxidant system of cancer cells leading cell death [3]. Besides, electric field transporting plasma charged species can cause electroporation of the cell membrane [4].

This study provides proofs of concept about: (i) the efficacy of a CAP catheter *in vitro* against CCA cells and *in vivo* on CCA tumours, (ii) the feasibility of plasma generation when introducing such a device into the bile ducts, wet and confined atmosphere, and (iii) the recipient and endoscopic practitioner safety.

2 Investigation and results

An endoscopic plasma source generating a dielectric barrier discharge (Es-DBD) has been designed to assess CCA local treatments. A metallic wire ended by a dielectric is inserted inside a PTFE catheter of 2 mm inner diameter. Plasma is initiated with 1 slm helium flow passing throughout this catheter, and pulses of 5 kV, 10 kHz, 1 % duty cycle supplying the wire electrode.

To assess *in vivo* the antitumour effects of plasma, a subcutaneous syngenic murine model of CCA has been setup, and the tumours were exposed to CAP. After 5 repeated expositions to CAP, we assessed a significant decrease in the tumour burden compared to the control group.

In vitro, CCA tumour cell lines and CCA microenvironment cells including myofibroblasts have been treated by CAP to decipher its antitumour effects. IC50 (50% of survival inhibition) was reached after 2 or 3 minutes of CAP exposition, correlated with an increase of oxidative stress.

The plasma catheter has then been introduced in an endoscope to access the biliary tract of post-mortem porcine models. Electric and thermal measurements have been performed during the process to guaranty electrical and thermal safety, both for the recipient and endoscopic practitioner.

Further studies are conducted to investigate the plasma composition, reactive species production and deposited power.

References

[1] Decauchy, H. *et al*. Cold plasma endoscopy applied to biliary ducts: feasibility risk assessment on human-like and porcine models for the treatment of cholangiocarcinoma. J. Phys. D: Appl. Phys. **55**, 455401 (2022).
[2] Vaquero, J. *et al*. Cold-Atmospheric Plasma induces tumor cell death in preclinical in vivo and in vitro models of human cholangiocarcinoma. Cancers **12**, 1280 (2020)
[3] Mitra, S. *et al*. Impact of ROS generated by chemical, physical and plasma techniques on cancer attenuation. Cancers **11**, 1030 (2019).
[4] Napotnik, T. B. *et al*. Cell death due to electroporation – A review. Bioelectrochemistry **141**, 107871 (2021).

Application of non-thermal plasma for production of antiphytopathogenic plasma-activated liquid

A. Dzimitrowicz[1], A. Motyka-Pomagruk[2], W. Babinska[2], D. Terefinko[1], P. Jamroz[1], P. Pohl[1], E. Lojkowska[2] and W. Sledz[2]

[1] *Department of Analytical Chemistry and Chemical Metallurgy, Wroclaw University of Science and Technology, Wroclaw, Poland*

[2] *Intercollegiate Faculty of Biotechnology University of Gdansk and Medical University of Gdansk, University of Gdansk, Gdansk, Poland*

Production of the plasma-activated ammonium nitrate of the defined antimicrobial properties towards plant pathogens was the aim of this work. For the continuous fabrication of this solution, we have chosen the proper plasma source and tailored its operating conditions. It was found that the produced plasma-activated solution (PAS) in 25% concentration inhibited the growth of *Pectobacterium parmentieri* IFB5308, while in 50% it exhibited biocidal properties against this pest. We assume that the obtained PAS may find application as a plant-protecting agent in the future.

1. Introduction

Food security is endangered by political instability or impacted by natural disasters such as floods or droughts. In this view it is important that approx. 14.1% [1] of the crops is lost due to the activity of phytopathogens, *i.e.,* bacteria, viruses, or fungi. As European Union is restricting the policies associated with the available plant protection agents, it is highly challenging to limit the spread of phytopathogens effectively and in an eco-friendly manner. Therefore, our research group is examining the antiphytopathogenic actions of inorganic salts solutions activated by cold atmospheric plasma (CAP). Due to the fact that during CAP treatment reactive oxygen and nitrogen species, including O_3, H_2O_2, OH, NO_2^-, NO_3^- are generated, these solutions show different properties than the non-treated CAP solutions [2]. The main aim of this work was related to the development, adjustment, and use of a highly effective CAP-based system for production of a plasma-activated mineral salt solution of defined antimicrobial properties towards plant pathogenic bacterium belonging to the *Pectobacterium* genus.

2. Experimental

Pulse-modulated radio-frequency atmospheric pressure glow discharge (pm-rf-APGD), generated in contact with a flowing 0.5% ammonium nitrate solution (NH_4NO_3, Archem, Poland), was applied as a CAP source. The current-voltage parameters used for activation of NH_4NO_3 by CAP were as follows: frequency of modulation: 1300 Hz and duty cycle: 20%. The NH_4NO_3 solution was continuously introduced to the CAP-based system using a Masterflex L/S (Core Palmer) peristaltic pump with a flow rate of 3.0 mL min^{-1}, as was described in detail in ref [2]. After the CAP treatment, the solutions were gathered for further microbiological analyses involving delineation of minimal inhibitory concentration (MIC) and minimal bactericidal concentration (MBC). As a representative strain of phytopathogenic bacteria *Pectobacterium parmentieri* IFB5308 (OD=0.01) was used.

3. Results and Conclusions

Based on the conducted microbiological analyses, it was found that the CAP-activated NH_4NO_3 solution inhibits the growth of *P. parmentieri* IFB5308 if applied in the concentration higher than 25%. To show bactericidal properties towards this pest, 50% concentration of the synthesized CAP-activated NH_4NO_3 solution was required. Thus, we observed that the pm-rf-APGD-activated NH_4NO_3 solution showed similar phytopathogenic properties towards soft rot *Pectobacteriaceae* to the previously examined FLC-dc-APGD-treated NH_4NO_3 solution [2].

4. Acknowledgements

The presented research was financed by National Science Centre (Poland) in the frames of Opus 17 project (UMO-2019/33/B/NZ9/00940).

References

[1]https://www.cphdforum.org/index.php/2022/05/26/plant-disease-crop-loss/, accessed 11/04/2023.

[2] Dzimitrowicz, A., Jamroz, P., Pohl, P., Babinska, W., Terefinko, D., Sledz, W., Motyka-Pomagruk, A. Multivariate optimization of the FLC-dc-APGD-based reaction-discharge system for continuous production of a plasma-activated liquid of defined physicochemical and anti-phytopathogenic properties. International Journal of Molecular Sciences, **22**, 4813 (2021).

Optimizing nanosecond repetitively pulsed discharges for ignition stabilized combustion

R. Patel[1,2], N. Dam[2] and S. Nijdam[1]

[1] *Dept. Applied Physics, Eindhoven Univ. Techn., Eindhoven, The Netherlands*
[2] *Dept. Mechanical Engineering, Eindhoven Univ. Techn., Eindhoven, The Netherlands*

We present a plasma-assisted ignition stabilized burner. The burner uses a dielectric barrier discharge configuration such that plasma is produced in a methane-air flow. Because of the continuous ignition of the methane-air flow by the plasma filaments, we can extend the lean combustion operation regime significantly. In order to minimize plasma generated NO_X, optimization of plasma parameters is needed. This is achieved by measuring NO_X and CO emissions and flame length.

1 Introduction

Lean combustion is one of the possible ways to make combustion cleaner and more efficient. However, ignition and flame stabilization are challenging in these conditions. Over the last few decades, plasma-assisted combustion (PAC) has been demonstrated to ignite and stabilize lean combustion in extreme conditions. Nanosecond repetitively pulsed (NRP) discharges can enhance combustion by generating radicals and heat. Through which pathway plasma will enhance the combustion depends on the plasma type and the configuration. In our previous work, we demonstrated that NRP DBD plasma can ignite fuel-air mixture flows repetitively while maintaining plasma at low temperatures [1]. In this work, we investigate how this ignition source can stabilize combustion above conventional flame stabilization limits.

2 Experimental setup

Experiments are performed in a coaxial DBD flow reactor. Figure 1 shows a schematic and photograph of the reactor. Apart from digital camera imaging, we performed high-speed OH^* chemiluminance imaging and combustion exhaust gas analysis.

3 Results and conclusions

We have successfully demonstrated stable lean combustion above flame blow-out conditions. Optimal plasma pulse repetition rate and the number of pulses are identified to minimize plasma-induced NO_X production.

References

[1] Patel, R., van Oijen, J., Dam, N. & Nijdam, S. Low-temperature filamentary plasma for ignition-stabilized combustion. *Combustion and Flame* **247**, 112501 (2023).

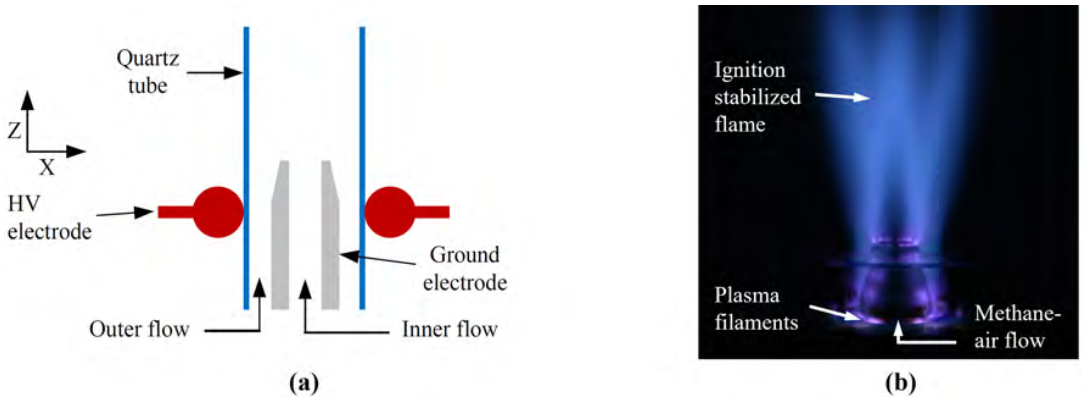

Figure 1: (a) A side-on cross-sectional view of the DBD plasma assisted ignition stabilized burner and (b) a digital camera photograph capturing the ignition stabilized flames above blowout conditions.

Albumin aggregation by cold atmospheric plasma between needle electrode and surface of albumin solution

T. Shimizu[1], Y. Ishihara[1,2] and H. Sakakita[1,2]

[1] *Research Institute for Advanced Electronics and Photonics, National Institute of Advanced Industrial Science and Technology (AIST), Ibaraki, Japan*

[2] *Dept. of Engineering Mechanics and Energy, Graduate School of Systems and Information Engineering, University of Tsukuba, Ibaraki, Japan*

Blood can be coagulated by a treatment using clod atmospheric plasmas. One of the coagulation mechanisms is aggregation of protein. In this study, albumin solution was treated by a plasma discharge between a needle electrode and solution surface since albumin is the most abundant protein in blood. The plasma exposure resulted in the albumin aggregation on the solution surface. In this contribution, the role of electrical parameters for plasma production in albumin aggregation will be discussed.

1 Introduction

Using cold atmospheric plasmas, there are several biomedical applications [1,2]. Blood coagulation is one of the possible applications proposed. By a plasma treatment, it is possible to coagulate blood in seconds [2]. In the plasma-induced blood coagulation, there are three main mechanisms such as aggregation of protein, aggregation of fibrinogen and platelets, and haemolysis [2].

We have investigated the aggregation of albumin (the most abundant protein in blood) by a plasma treatment in this study. In the reports so far, it is suggested that the deposition of charge on the solution surface plays a key role in the aggregation albumin [3,4].

In this contribution, we aim to understand the mechanism of albumin aggregation by the plasma treatment. As a plasma source, a plasma discharge between a needle electrode and surface of solution was used [5]. Electrical parameters for plasma production were controlled by changing the applied voltage, frequency, and waveforms.

2 Experimental setup

In a quartz dish on an electrically grounded metal plate, there was albumin solution filled as shown in Fig. 1. A needle electrode was placed 1 mm above the solution surface. By applying high voltage to the needle electrode, a plasma discharge was produced between the needle electrode and solution surface.

The albumin aggregation was monitored by digital cameras from diagonally above and the side. The chemical change in albumin solution was measured using a pH meter and UV-Vis absorption spectroscopy.

3. Experimental result

By the plasma treatment, a white substance (albumin aggregate) appeared on the surface of the albumin solution as shown in Fig.1. In general, longer plasma treatment results in larger size of albumin aggregate. In the conference, we discuss the role of electrical parameters on the albumin aggregation, especially the growth speed of aggregation and the shape of aggregate.

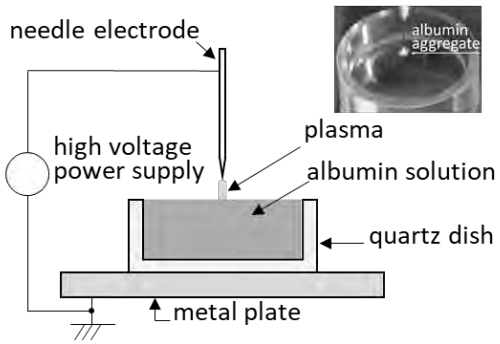

Figure 1: Experimental setup and albumin aggregation on the solution surface.

Acknowledgements

This work was partly supported by JSPS KAKENHI Grant Number 21K03527.

References

[1] Kong, M. G., Kroesen, G., Morfill, G., Nosenko, T., Shimizu, T., van Dijk, J., and Zimmermann, J. L. New Journal of Physics. **11**, 115012 (2009).

[2] Shimizu, T. and Ikehara, Y. Journal of Physics D: Applied Physics. **50**, 503001 (2017).

[3] Sakakita, H., Yamada, H., Shimizu, T., Fujiwara, M., Kato, S., Kim, J., Ikehara, S., Shimizu, N., and Ikehara, Y. Journal of Physics D: Applied Physics **54**, 215201 (2021).

[4] Shimizu, T., Fukui, T., and Sakakita, H. Japanese Journal of Applied Physics **61**, Si1016 (2022).

[5] Shimizu, T., Iwafuchi, Y., Morfill, G., and Sato, T. New Journal of Physics **13**, 053025 (2011).

A plasma-assisted microperfusion culture system for promoted cell growth

Hayata Okino[1] and Shinya Kumagai[1]

[1]*Meijo University, Nagoya, Japan*

A microperfusion cell culture system which used non-thermal atmospheric plasma exposure for promoted cell growth was developed. Here, fabrication process of the system was reported. For the demonstration, C2C12 murine myoblast cells were cultured in the system for promoted cell growth.

1 Introduction

Cell culture using microfluidic devices can simulate environments of human circulatory systems. Therefore, it is possible to supply medium, buffer solution, and air while removing waste products from cellular activity [1].

Recently, non-thermal atmospheric pressure plasma has been applied to biomedical research field. One of the excellent results is promoted cell growth. Plasma effects functioned as a trigger of cell growth [2]. In this study, a microperfusion culture system using plasma was developed for promoted cell growth.

2 Device Concept

A microperfusion culture system using plasma is schematically shown in Fig.1. A cell culture chamber is connected to microchannels for supplying fresh culture medium and removing exhausted medium. To supply plasma stimulation to cells cultured in the chamber, partially opened area (microgap) is prepared at the chamber. To make the opened area, two glass plates separated with a microgap were attached with the microchannel device. The microchannel device with glass plates was set on a planar plasma source. Using the microgap, plasma-generated active species such as reactive oxygen and nitrogen species are supplied to cells in the chamber for promoted growth.

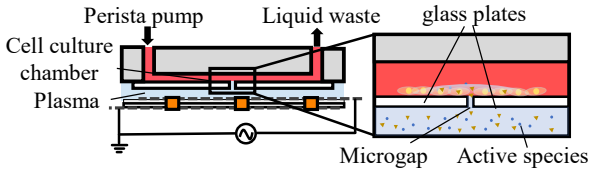

Fig. 1 Cross-sectional drawing of perfusion cell culture system.

3 Materials and Methods

Microperfusion system was fabricated by assembling a microchannel, a holder, and a planar plasma source. To make a microchannel, a mold made with 3D printer was set in a plastic case, PDMS was poured into the case. The PDMS was baked at 60°C. Then, the mold was removed, forming PDMS microchannel device. Two glass plates were closely attached with each other at the side edges. Due to the accuracy of glass-machining, a microgap formed between the plates. After, the PDMS microchannel was attached to the two glass plates. Then, the microchannel device with micro-gapped glass plates and a planar plasma source using a dielectric barrier discharge was assembled into a holder part. Electrodes of the planar plasma source was connected to high voltage source.

4 Results and Discussion

A microperfusion culture system is shown in Fig.2. Magnified image of a microgap between the glass plates is shown in Fig. 3. To test the delivery of plasma-generated active species, pH indicator of methyl red was injected into the microchannel. When a DBD plasma was generated, the methyl red solution changed its colour from yellow to red, indicating acidic conditions.

C2C12 murine myoblast cells were cultured and exposed with plasma for 30 sec and cultured under perfusion. As shown in Fig.4, cells were proliferated in perfusion culture after plasma exposure.

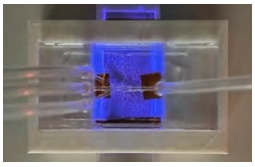

Fig. 2 Microperfusion system during plasma exposure.

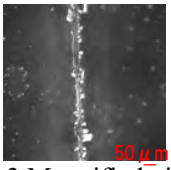

Fig. 3 Magnified view of microgap between glass plates.

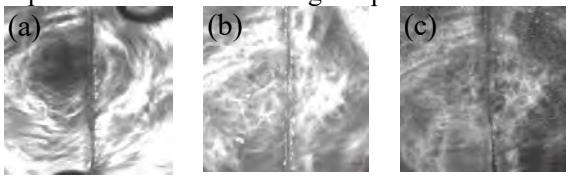

Fig. 4 C2C12 cells (a) before and (b) after plasma exposure. (c) 3day incubation.

Acknowledgements

This study was partially supported by the Hibi Foundation, the Nitto Foundation, and the joint usage / research program of center for Low-temperature Plasma Sciences, Nagoya University.

References

[1] M. L. Coluccio et al., Microfludic Engineering, **208**, (2019) pp.14-28.

[2] F. Tan et al., Stem Cell Res Ther, **11**, (2020) 368.

An efficient Far UV–C (222 nm) krypton chlorine excimer lamp

Kiran Ahlawat[1], Ramavtar Jangra[1] and Ram Prakash[1]

[1]*Department of Physics, Indian Institute of Technology Jodhpur, Jodhpur, Rajasthan, India, 342030*

In this work, a dielectric barrier discharge (DBD) plasma based Far UV-C light source has been designed, developed and optimized for the maximum absolute intensity by varying the different parameters such as gas pressure, applied voltage and frequency. A very narrow band peaking at the wavelength of the 222 nm has been obtained at low gas pressures of 140 mbar and the developed source has been tested for its bacterial efficiency on gram positive bacteria *S. aureus* and a complete reduction of initial concentration 10^7 CFU/ml has been achieved within 10 sec of ultraviolet (UV) treatment having an intensity of ~100 μW/cm^2.

1 Introduction

The COVID-19 pandemic has increased awareness of the need for strategies that provide active disinfection of transmittable disease pathogens, such as airborne and surface-associated viruses and bacteria. UV-C radiation is commonly used for air and surface disinfection and has been shown to be successful for reducing the incidence of infectious diseases that are spread by fomites in health care facilities and other occupied settings. However, these uses are limited by the necessity to reduce human exposure to UV-C radiation. Far UV-C radiation (207-230 nm) has demonstrated potential as an antibacterial and antiviral agent. In addition, there is evidence that far UV-C radiation damages skin and eye tissues at significantly lower rates than radiation from conventional UV-C sources [1]. Together, these characteristics of far UV-C radiation have the potential to fundamentally alter how and where UV-C radiation can be deployed for air and surface disinfection. So, an effort has been made for the development of Far UV-C excimer light source and study its bacterial inactivation efficiency.

1.1 Experimental Setup

Two cylindrical quartz tubes having length of 160 mm were fused coaxially to make an annular gap of 1.5 mm for gas filling. Two metal electrodes made up of aluminium were used to complete DBD configuration. Inner electrode was a screw type electrode having groves at a constant pitch and length, act as a high voltage electrode and outer electrode was aluminium cylinder having circular holes with equal apertures into it and acts as a ground electrode.

A mixture of krypton with a very small fraction of chlorine gas has been sealed-off into the gas gap as a working gas. When the high voltage was supplied to the DBD based excimer source, then the excitation and ionization of both the gases (Kr and Cl_2) takes place. The cations of krypton and anions of chlorine gas get involved in a three-body recombination reaction with an atom or molecule of buffer gas (M) and form the excited complex (KrCl*) which decomposes rapidly and emits photons having wavelength of 222 nm. For the absolute intensity measurement, Hamamatsu make UV power meter with a photodetector head (H9535-222) has been used. An Andor make PMT based monochromator has been used for spectroscopic analysis. Gam positive bacteria (*S. aureus*) having initial concentration 10^7 CFU/ml has been studied to check the bacterial inactivation efficiency.

1.2 Results and Conclusion

The maximum absolute intensity obtained from the lamp was 2.5 mW/cm^2. The input power of developed source has been obtained 31 W and the electrical to optical efficiency of the developed source has been obtained nearly 12%. A very narrow band spectrum (FWHM~2 nm) has been obtained at 222 nm as shown in Fig.1(b)

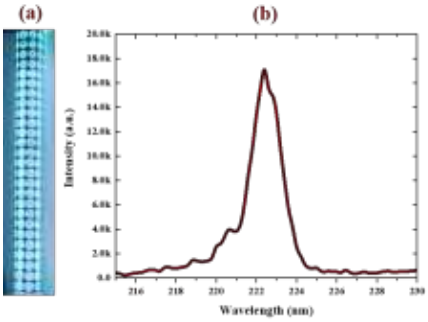

Fig. 1. (a) Pictorial view of developed source. (b) Optical spectra peaking at 222 nm of the developed source.

The developed source shows very high bacterial efficiency (7 log reduction in 10 sec) so it can be used for the inactivation of various bacteria and viruses on the surfaces and air in the occupied space.

Acknowledgements

KA and RJ would like to acknowledge the UGC for providing SRF. RP would like to acknowledge SERB for providing funding under **project No. S/SERB/RP/20200082.**

References

[1] K. Narita *et al.*, *J. Hosp. Infect.*, vol. 105, no. 3, pp. 459–467, 2020, doi: 10.1016/j.jhin.2020.03.030.

XXXV ICPIG, July 9-14, 2023, Egmond aan Zee, The Netherlands Topic number 17

Turbulent skin-friction drag reduction by annular DBD plasma synthetic jet actuator

Borui Zheng[1], Deling Lin[1], Yuanzhong Jin[1], Minghao Yu[1], Zhen Cui[1], Jingrui Luo[1]and Chang Ge[1]

[1] *Xi'an University of Technology, Xi'an, Shaanxi, People's Republic of China*

Turbulent skin-friction drag constitutes a significant component of the overall drag experienced by aircraft in transportation, and turbulent drag reduction (TDR) has the potential to result in energy conservation and decreased emissions. This thesis proposes the design of an annular dielectric-barrier-discharge plasma synthetic jet actuator (A-DBD-PSJA) that integrates the advantages of both pulsed DBD plasma actuation and synthetic jet. Wind tunnel experiments were conducted on a flat plate to assess the turbulence drag reduction capabilities of the proposed A-DBD-PSJA. The aerodynamic analysis of the unsteady flow field generated by the A-DBD-PSJA and the impact of pulsed plasma actuation on the turbulent boundary layer showed that the wall-normal jet located on the symmetry plane played a crucial role in controlling the turbulence. An increase in the duty cycle of plasma discharge resulted in a more steady and continuous wall-normal jet, which resulted in a reduction of the mean streamwise velocity profiles, wall-normal velocity gradient in the logarithmic region, velocity fluctuation level of the entire TBL, and turbulent shear stress.

1 Introduction

The principles of cost-effectiveness, environmental protection, and safety now govern the development of the civil aviation industry. To achieve commercial success, civil aircraft must possess both cost-effectiveness and ecological sustainability. Cost-effectiveness is a critical factor in selecting and purchasing aircraft, while environmental protection is becoming increasingly important as a requirement for accessing aviation markets. One significant aspect impacting these characteristics is aircraft drag, which plays a vital role in fuel consumption and carbon emissions. Viscous frictional drag is an essential contributor to the overall drag on an aircraft, especially during high Reynolds number cruising of large passenger aircraft, where the flow over the aircraft surface is predominantly turbulent. A reduction of just 10% in turbulent friction drag is estimated to result in global savings of $3 billion annually in fuel costs [1-2].

This study aimed to investigate the flow field characteristics induced by annular dielectric barrier discharge synthetic jet plasma actuators (A-DBD-PSJA) and evaluate their performance as a means of TBL control using techniques such as particle image velocimetry (PIV) and a hot wire anemometer in wind tunnel experiments. The study's results shed light on the underlying mechanisms of plasma actuators and provide a foundation for future research on the control of turbulent boundary layers (TBLs). The A-DBD-PSJA presents a promising solution for turbulence control in wind tunnel experiments by combining the benefits of pulsed plasma actuators and synthetic jet-blowing modes.

1.2 Conclusion

The A-DBD-PSJA's wall-normal jet located on the symmetry plane plays a dominant role in controlling the turbulent boundary layer. The duty cycle of plasma discharge determines the formation and evolution of the induced vortices. As the increase of the duty cycle, the induced jet continuously blows near the wall, transporting mass and momentum to the TBL unintermittent. A stable upwash flow zone is formed in the middle, and the upwash flow reduces the bottom velocity of the boundary layer. The reverse pressure gradient flow makes it slightly "stable". At the same time, the upwash flow also carries the low-velocity fluid of the bottom layer to the higher place, which significantly reduces the velocity in the logarithmic region, reduces the velocity fluctuation level of the whole boundary layer, and then reduces the turbulent shear stress.

References

[1] Guanghui Wu, Yingchun Chen. 2018, Investigation on the Principles and Methods of drag Reduction for Large Civil Aircraft (Shanghai Jiaotong University Press)(in Chinese)

[2] Graham M. D., Floryan D. 2021,Annual Review of Fluid Mechanics,53(1),227-253

Measurement of enthalpy probe on plasma temperature in atmospheric pressure microwave plasma jet for CO_2 reforming system

In Je Kang[1], Ji Hun Kim[1], Chang Hyun Cho[1], Jong Keun Yang[1], and In Sun Park[1]

[1]*Institute of Plasma Technology, Korea Institute of Fusion Energy, Gunsan, Republic of Korea*

In atmospheric pressure microwave plasma jet, the temperatures of CO_2 plasma were measured by using an enthalpy probe, for a contribution to the understanding of correlation between plasma temperatures and an energy efficiency for CO_2 dry reforming system. The mapping of the measured plasma temperatures was obtained with the variation of the specific energy input (SEI). For numerical estimation of plasma temperature, the result was approximately 2500 K at a core region (r = 0 and z = 50 mm) of plasma jet under the SEI of approximately 300 kJ/mol at atmospheric pressure.

For the microwave plasma jet under atmospheric pressure conditions, the experimental investigations are insufficient, and there are no clear results on characteristics of plasma parameters, although demand for the application of atmospheric pressure microwave plasma on CO_2 dry reforming process increases.

We introduce an enthalpy probe (EP) system for measurement on the distribution of plasma temperatures in atmospheric pressure microwave plasma jet, which allows for measurements on thermal plasmas [1]. With the variations of the specific energy input (SEI), an EP with thermocouples (K- and R-types) was scanned for the ranges of r-axis = 0 – 12 mm and z-axis = 50 – 250 mm. To estimate the plasma temperatures from the plasma enthalpy acquired by an EP, the tabular data using the local thermodynamic equilibrium was used. Because the predominant element of collisional plasmas is still neutral atoms due to the low degree of ionization in most collisional plasma sources, the overall flow behavior can be explained by conventional gas dynamic theory [2,3]. For consider it, the mapping of the measured plasma temperatures in CO_2 plasma was obtained by combining the laminar flow model and the heat transfer in the fluid model.

In this work, the experimental mapping results on plasma temperatures for CO_2 plasma jet generated by a microwave generator under atmospheric pressure were given with the SEI variations. For example, the result was approximately 2500 K at a core region (r = 0 and z = 50 mm) of plasma jet under the SEI of approximately 300 kJ/mol. Also, the effect of plasma temperature on the energy efficiency of the CO_2 dry reforming process was analyzed.

References

[1] Kim, K. S. et al. Enthalpy probe measurements and three-dimensional modelling on air plasma jets generated by a non-transferred plasma torch with hollow electrodes. Journal of Physics D: Applied Physics **41**, 065201 (2008).

[2] Vankan, P. et al, Inflow and shock formation in supersonic, rarefied plasma expansions. Physics of Plasmas **12**, 10230 (2005).

[3] Kang, I. J. et al. Measurement of Mach probe on plasma flow velocity in highly collisional plasma jet. Current Applied Physics **39**, 45-50 (2022).

Development of Simulator for Interaction of Materials and PLasma (SIMPL) in Korea Institute of Fusion Energy

In Sun Park[1], In Je Kang[1], Ji Hun Kim[1], Chang Hyun Cho[1], Jong Keun Yang[1] and Kyu-Sun Chung[2]

[1] *Institute of Plasma Technology, Korea Institute of Fusion Energy, Gunsan, South Korea*
[2]*Department of Electrical Engineering, Hanyang University, Seoul, South Korea*

Simulator for Interaction of Materials and PLasma (SIMPL) is developed for simulation of plasma-materials interaction (PMI) such as scrape-off layer (SOL), divertor, first wall and anti-plasma materials. The SIMPL has plasma parameters, which are electron temperature (T_e) ~ 10 eV, electron density (n_e) ~ $10^{12\text{-}14}$ cm^{-3} for Argon gas.

The plasma-materials interaction (PMI) has been studied for nuclear fusion reactor, semi-conductor and aerospace. The PMI study covered from low temperature (Semi-conductor) to high temperature (Nuclear fusion, Aerospace, Environment) plasma. Tungsten (W) and Silicon carbide (SiC) especially was important candidate plasma facing components, because of its thermal resistance (high melting temperature) and low chemical sputtering in nuclear fusion, aerospace and semi-conductor [1].

The magnetized linear plasma device, which is called Simulator for Interaction of Materials and PLasma (SIMPL) has been developed for PMI study, and it has the characteristics as the following: (1) geometry: length < 2530 mm, diameter < 240 mm (2) plasma source: LaB_6 DC (3) plasma parameter: plasma density (n_e) $10^{12\text{-}14}$ cm^{-3}, electron temperature (T_e) ~ 10-50 eV (Hydrogen, Helium) and 5-20 eV (Argon), ion temperature (T_i) ~ 0.01-0.2 (Argon) for Langmuir probe and triple electric probe (4) Magnetic field of electromagnet (B) < 3.5 kG.

We introduce process of development SIMPL (plasma source, reactor and etc), operating plasma condition and result of plasma ignition. A new developed SIMPL could be applied to plasma-wall physics, durability of materials test, steady-state and transient phenomena and etc.

References

[1] Hammond, K.D. Helium, hydrogen, and fuzz in plasma-facing materials Materials Research Express 4, 104002 (2017)

Development of atmospheric pressure microwave plasma generator with gas preheating structure for dry reforming system.

Chang Hyun Cho[1], Ji Hun Kim[1], Jong Keun Yang[1], In Sun Park[1], and In Je Kang[1]

[1] *Institute of Plasma Technology, Korea Institute of Fusion Energy, Gunsan, Republic of Korea*

To improve an energy efficiency of dry reforming process, the new concept of a microwave plasma source was developed by introducing gas preheating structure. The energy efficiencies of dry CO_2 reforming of CH_4 were investigated for the developed plasma source. As a result, the conversion rates of CO_2 and CH_4 were 91.8% and 83.9%, respectively, and the energy efficiency was 64.4% when the plasma power was applied up to 10 kW.

For protecting the parts of plasma generator from high heat flux of plasmas, conventional microwave plasma generators have used water, gas, oil cooling methods [1,2]. However, the method of cooling through the extra coolant loop reduces the thermal efficiency of plasma generators and complicates them.

In this work, a plasma generator with novel structure was developed to increase the energy efficiency for CO_2 reforming of CH_4 by using microwave plasmas, which has double helix structure so that the injection gases could be guided along the spiral from the source surface and enter the discharge tube. For CO_2 reforming of CH_4, it was experimentally investigated by comparing a typical microwave plasma generator. Plasma power was applied up to 10kW by using a 2.45 GHz microwave power supply. The CO_2 of 1800 NL/h was injected as discharge gas. The CH_4 of 1800 NL/h was injected between the plasma generator and the reforming reactor, which is the CO_2/CH_4 molar ratio of 1 required for dry reforming. The composition of the produced gases was investigated by using a gas analyzer. In addition, the total syngas flow rate was measured using a dry gas meter to estimate reforming efficiency.

As experimental results, the conversion rates of CO_2 and CH_4 were 91.8% and 83.9%, respectively, under the experimental conditions as follows: 10 kW of plasma power, and 6188 NL/h of total syngas flow rate. The CO and H_2 production rates were estimated as 338 g/kWh and 25.4 g/kWh, respectively, and the energy efficiency was 64.4%, which shows a 2% improvement compared to a conventional microwave plasma generator.

References

[1] Sina Mohsenian. et al. Carbon dioxide conversion by solar-enhanced microwave plasma: Effect of specific power and argon/nitrogen carrier gases. Journal of CO_2 Utilization **34,** 725-732 (2019).

[2] Guoxing Chen. et al. Plasma-catalytic conversion of CO_2 and CO_2/H_2O in a surface-wave sustained microwave discharge. Applied Catalysis B: Environmental **214,** 114-125 (2017).

COST Action: CA19110 - Plasma applications for smart and sustainable agriculture

F. Krčma[1], N. Puać[2]

[1] *Faculty of Chemistry, Brno University of Technology, Brno, Czech Republic*
[2] *Institute of Physics-National Institute of Republic of Serbia, University of Belgrade, Belgrade, Serbia*

The current society needs stable and sustainable production of food by modern environmentally friendly processes. There is a high demand to increase the production without or with at least moderate use of various harmful chemicals. Application of plasmas in the agriculture/food production chain can help to fulfil the demand pointed out above. There is necessary to coordinate research across Europe/world and share knowledge to tackle the best results as fast as possible. Due to this fact the broad world-wide research network was created recently under the support of COST Association. Details about Action and its activities can be found at its website plagri.eu.

Main goals

To advance the current understanding of the physical and biochemical changes induced by plasmas; To develop guidelines and protocols that can be adopted by the community working on plasma treatment of seeds, plants and soils; Identifying applications in the food production chain where plasma technology could have a potential application transferable to the industrial processing environment; Development of plasma sources and technologies with attention to legislative, energy consumption, food safety and food quality aspects.

Working groups and selected highlights

Cost Action work is organized by four scientific working groups that of course marrow co-operate each other. Additional WG (WG1) serves as platform for organization and dissemination).

WG2 focusses on non-thermal plasma treatment of seeds. The main aim is to advance the current understanding of the physical and biochemical changes induced by plasma treatments of seeds. The seeds are mainly treated by atmospheric pressure plasma systems operating in air (DBDs, corona) or various plasma jets. The studied effects are seed germination and plants early grow, surface changes, wettability, and water sorption, influence on plant hormones and signal compounds. The obtained results using various seeds generally show faster germination and grow with more branched roots. Pilot tests up to harvest demonstrated also higher production. Non-negligible effect is also seeds surface decontamination.

WG3 works on the definition of standard protocols and procedures for usage of plasma and/or plasma treated liquids aiming to speed up and increase plant growth and development resulting in better yields. The two main plasma effects are combined here: surface decontamination and fertilization because air plasma produces nitrogen in form better accessible for the plants. The pilot small field experiments showed that even one plasma treated liquid application can lead to the production increase up to 10 %. Part of the work is also given to the interaction of plasma treated liquids with soil to avoid its damage that start be an urgent problem.

WG 4 focusses on the procedures developing for efficient decontamination of wastewater of agricultural origin and for treatment of growth media. It is known that plasmas with liquids can decompose various pollutants in water. On the other hand, there is possible also introduces to water various new compounds (like hydrogen peroxide, nitrates and nitrides) that change solution properties. Recently, detailed studies of grow media modification were started.

The last WG (WG5) works on the identification of the applications in the food production chain transferable to the industrial processing environment. Studies focused on the surface decontamination (meat, vegetables, fruits, spices) or volume treatments of liquids (juices, wine) were successfully completed.

Acknowledgement

This publication is based upon work from COST Action “Plasma applications for smart and sustainable agriculture (PlAgri)”, supported by COST (European Cooperation in Science and Technology).

Characteristic Changes in Pumpkin Seeds by Atmospheric Pressure Gliding Arc Plasma Irradiation

S. Aoqui[1], O. V. Prysiazhna[1], K. Yamauchi[2], F. Mitsugi[3], M. Yamazato[4], H. Kawasaki[5], H. D. Stryczewska[6] and M. Shiratani[7]

[1]*Dept. of Computer and Information Sciences, Sojo Univ., Japan*
[2]*Graduate School of Eng., Sojo Univ., Japan*
[3]*Faculty of Advanced Science and Technology, Kumamoto Univ. Japan*
[4] *Faculty of Eng., Univ. of the Ryukyus, Japan*
[5] *Dept. of Electrical and Electronic Eng., National Institute of Tech., Sasebo College, Japan*
[6] *Dept. of Electrical Eng. and Electrotechnology, Lublin Univ. of Tech., Poland*
[7]*Graduate School of Information Science and Electrical Eng., Kyushu Univ., Japan*

Plasma irradiation for seeds can promote or inhibit germination and growth by altering the seed surface conditions. Because there are many different types of plant seeds with widely varying seed structures, individual studies are required to determine what conditions are optimal. In this study, pumpkin seeds were irradiated with atmospheric pressure gliding arc plasma to investigate changes in seed surface conditions and water absorption characteristics. For information on the interior of the seeds, the composition of the cross sections was analyzed using EDS.

1 Introduction

Atmospheric pressure gliding arc discharge (GAD) plasma can be used to treat organic matter and plants because the gas temperature is nearly room temperature. Dielectric Barrier Discharge (DBD) and micro plasma jet are similar in terms of low gas temperature, but GAD is overwhelmingly large in terms of power consumption and is suitable for large-scale processing. Many papers have been published on plasma irradiation for seeds using DBD, and most have confirmed growth enhancement. But, for many papers, the processing time was several tens of minutes or even longer, so processing time becomes a problem. In the case of GAD, the treatment time may be only a few seconds to a few dozen seconds, which is promising for agricultural applications. In this study, we investigated how the surface and internal conditions of Pumpkin seeds change by varying the type of introduced gas, the distance between electrode and seeds, and the irradiation time.

2 Experiment

The experimental setup for plasma irradiation is shown in Fig. 1. The electrodes were installed in an inverted position, and the working gas flows from above to below. Although not shown in the figure, the reaction tube was connected to a duct and the gas was discharged by a duct fan to avoid atmospheric contamination. The sample holder was rotated to ensure uniform plasma irradiation for seeds due to the single-phase electrode discharge. Argon, oxygen, and nitrogen gases were used. Fig. 2 shows a cross-sectional SEM image of a seed treated at a position directly exposed to argon (20 l/min) plasma. The right side was the plasma-exposed surface. 150 μm depth from the seed surface was analyzed for composition by EDS. Plasma irradiation caused changes in the structure of the tissue. Water droplet contact angles were measured, and it was confirmed that the wettability of the irradiated surface was improved. Plasma treatment reduced the contact angle of water droplets from 10% to 15%. It was confirmed that the seeds became hydrophilic.

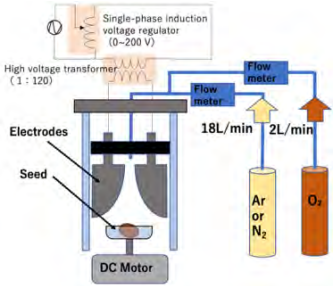

Fig. 1 Experimental setup for plasma irradiation

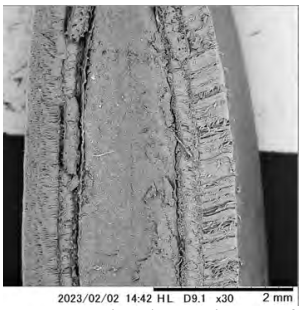

Fig. 2 Cross-sectional SEM image of seed

LXCat 3: A novel data platform for low-temperature plasma physics

D.J. Boer[1], S. Verhoeven[2], W.A.A.D. Graef[3], E.A.D. Carbone[4] and J. van Dijk[1]

[1] *Dept. Applied Physics, Eindhoven Univ. Techn., Eindhoven, The Netherlands*
[2] *Netherlands eScience center, Amsterdam, The Netherlands*
[3] *Plasma Matters BV., Campus Eindhoven Univ. Techn., Eindhoven, The Netherlands*
[4] *Centre Énergie Matériaux Télécommunications, INRS, Varennes, QC, Canada*

The amount of input data available for simulating low-temperature plasmas (LTPs) is ever-growing, and datasets become increasingly more complex. Proper management of these datasets requires advanced data platforms. This work presents a novel, open-source platform for the exploring, inspecting, managing, using and sharing of LTP input data. The project is developed in close collaboration with the LXCat team, and will result in a successor dubbed "LXCat 3" later this year.

Reliable input data is of key importance in any low-temperature plasma (LTP) simulation. The ability to access and share such data within the community is reliant on the presence of capable data platforms. However, current platforms are often very specific, enforcing a strict structure on states and reactions, severely limiting the range of data they support. Moreover, the lack of a proper data format and schema renders the data inconvenient to use in a general context.

This work presents a novel data platform for low-temperature plasma physics. It is designed and implemented from the ground up, using modern data science and web technology, and the experience of the well-established LXCat platform [1]. The primary accomplishment regards the ability to serve any complex atomic, or molecular state as a structured object, including compound and less well-defined state designations. As a result, the platform has excellent support for state-to-state, as well as less precise data. Whereas contributors can provide data describing individual interactions, self-consistent reaction mechanisms remain a core concept.

Previous contributions focused on the core technological choices and the development of a flexible system for schema generation for low-temperature plasma data. This contribution will focus on the first results that are made possible by establishing a solid technological base. The platform is nearing its initial public release, and the core functionality regarding cross section data is implemented. Visitors of the poster will be able to interact with different aspects of the platform, including: exploring and inspecting the available cross sections and cross section mechanisms, composing detailed mixtures of cross sections, creating and managing cross section mechanisms using interfaces specifically developed for contributors, and running Boltzmann calculations directly in the browser using BOLSIG+ [2] and LoKI-B [3].

All work regarding the platform is open-source and publicly available on GitLab [4]. In addition to cross section data, the platform has early-stage support for other types of data and accompanying tools, including e.g. potentials, and rate coefficients. The base infrastructure is developed such that the integration of new data types, and thus its goal to transition into a full-fledged chemistry platform, is not merely possible, but seemless.

Acknowledgements: part of this work has been supported by the Dutch Science Foundation NWO and the Netherlands eScience Center (project 'passing XSAMS') and by ASML.

References

[1] Carbone, E. *et al.* Data needs for modeling low-temperature non-equilibrium plasmas: The lxcat project, history, perspectives and a tutorial. *Atoms* **9**, 16 (2021). URL `http://dx.doi.org/10.3390/atoms9010016`.

[2] Hagelaar, G. J. M. & Pitchford, L. C. Solving the Boltzmann equation to obtain electron transport coefficients and rate coefficients for fluid models. *PSST* **14**, 722 (2005). URL `https://dx.doi.org/10.1088/0963-0252/14/4/011`.

[3] del Caz, A. T. *et al.* The LisbOn KInetics Boltzmann solver. *PSST* **28**, 043001 (2019). URL `https://dx.doi.org/10.1088/1361-6595/ab0537`.

[4] Boer, D., Verhoeven, S., Ali, S., Graef, W. & van Dijk, J. LXCat. URL `https://gitlab.com/LXCat-project/lxcat`.

XXXV ICPIG, July 9-14, 2023, Egmond aan Zee, The Netherlands Topic number 1/2

ExB heating and transport in magnetized plasmas with ionization and charge-exchange effects

A.Smolyakov[1], P. Yushmanov[2], S. Putvinski[2]

[1]*University of Saskatchewan, 116 Science Place, Saskatoon, SK, S7N 5E2 Canada*
[2]*TAE Technologies, 19631 Pauling, Foothill Ranch, CA, 92610 USA*

Conversion of cold neutrals into ions due to the ionization and charge-exchanges in magnetized plasmas is accompanied by the additional input of energy, the so-called ExB heating. The same mechanism creates additional ion current. These sources of energy and momentum can be substantial in the source driven plasma discharges. A system of fluid equations is formulated here describing energy and momentum balance and transport fluxes in magnetized plasmas with atomic processes such as ionization and charge-exchange interactions.

Magnetized plasmas rotating due to strong electric field are used in fusion schemes [1-3] and also in other technologies such as mass separation [4]. In this presentation we discuss a heating mechanism that occurs in a rotating plasma due to ionization and charge-exchange (CX) sources in presence of strong electric field.

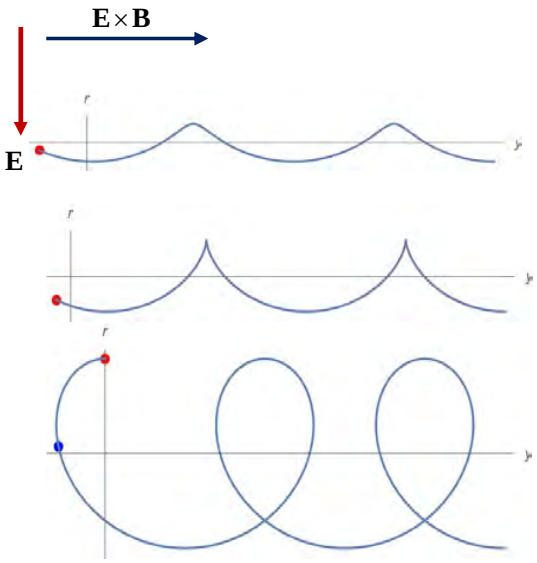

Fig. 1. Ion trajectories for ions drifting in crossed electric and magnetic field and born with different initial energy and different velocities; ionization/CX points are shown by red and blue dots. The net energy input is determined by the integral for all particles averaged over the distribution function.

Ions formed from cold neutrals acquire some energy due to the acceleration in the electric field, Fig. 1. For an ion ionized from the state with zero initial energy, the net energy gain is mV_E^2 split between the random thermal and kinetic energy of the directed flow with $V_E = E/B$, the velocity of the ExB drift. This mechanism also shifts the radial particle position resulting in the ion ionization current $J_i = qS^{ion}V_E/\omega_{ci}$ which is ultimately responsible for the energy exchange between plasma and electromagnetic field. Net heating power and momentum input have to be calculated by the integration over the particle distribution function. Moment (fluid) approach offers an insightful framework highlighting these mechanisms. We discuss the energy and momentum balance and present a system of transport equations that include the ionization and CX induced energy and momentum sources and sinks and relevant transport fluxes.

References

[1] Lehnert, B. (1971). "ROTATING PLASMAS." Nuclear Fusion **11**(5): 485-533.
[2] Gota, H., M. W. Binderbauer, T. Tajima, S. Putvinski, M. Tuszewski, et al (2019). "Formation of hot, stable, long-lived field-reversed configuration plasmas on the C-2W device." Nuclear Fusion **59**(11): 112009.
[3] Teodorescu, C., R. Clary, R. F. Ellis, A. B. Hassam, R. Lunsford, I. Uzun-Kaymak and W. C. Young (2008). "Experimental study on the velocity limits of magnetized rotating plasmas." Physics of Plasmas **15**(4).
[4] Gueroult, R., J. M. Rax, S. J. Zweben and N. J. Fisch (2018). "Harnessing mass differential confinement effects in magnetized rotating plasmas to address new separation needs." Plasma Physics and Controlled Fusion **60**(1): 014018.

Triggering self-organization of guided streamers in a cold plasma jet

T. Dufour[1], H. Decauchy[1]

[1] *LPP. Sorbonne Université, CNRS, Ecole Polytechnique, Paris, France*

Guided streamers are generated by a plasma jet device and interact with a mesh target at floating potential followed by a metal plate target. We show how this experimental setup can self-organize guided streamers with complex order (Ω) as high as 5. Besides, transient emissive phenomena are highlighted in the inter-target region. All phenomena are deciphered combining electrical probes and fast ICCD imaging.

1 Context

Self-organization can be defined as a process where the organization (constraint, redundancy) of a system spontaneously increases. It can also be defined as a dynamical/adaptive process where systems acquire and maintain structure without external control. In plasma physics, self-organized patterns have already been highlighted in cathode boundary layer micro-discharges, in DC pin electrodes interacting with liquids and in high power impulse magnetron sputtering.

2 Experimental setup

In this work, guided streamers are generated by a CHEREL (Capillary with inner Hollow Electrode and outer Ring ELectrode) supplied with helium and polarized by HV pulses (D_{Cycle}=10%, f_{rep}=5-10kHz, V=4-6kV). The CHEREL is completed by two targets placed in series: a metal mesh target (MM) at floating potential and a metal plate target (MP) connected to a 1.5 kΩ resistor that is grounded.

3 Results & Discussion

This experimental configuration allows to shift from the repetition of guided streamers to the emergence of their self-organization. Each of them is generated on the rising edge of a high-voltage pulse. Thus, self-organization patterns comprising up to 5 positive guided streamers can be generated one after the other, all distinct in space and time. Figure 1 compares guided streamers that are either repeated (Ω=1) or self-organized at third complexity order (Ω=3). In that later case, the α, β and γ streamers propagate at different velocities in the capillary (v_α = 75.7 km.s^{-1}, v_β = 66.5 km.s^{-1} and v_γ = 58.2 km.s^{-1}, before being accelerated in the vicinity of the MM target.

We also demonstrate the existence of transient emissive phenomena in the inter-target region, including the possibility of leader formation (dark domains Δ_α, Δ_β, Δ_γ in Fig. 2) driving to a primary ionizing event (Θ) that initiates filamentary discharge (Φ). We discuss how these phenomena are correlated with Ω and why they are only triggered on the rising edges of the voltage pulses.

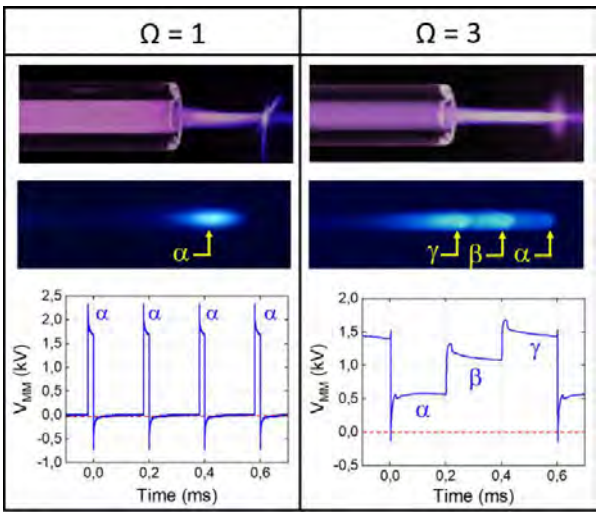

Fig. 1. Cold plasma jet analyzed by fast ICCD imaging to show a train of guided streamers either repeated (Ω=1) or self-organized (Ω=3) and correlated with voltage probe.

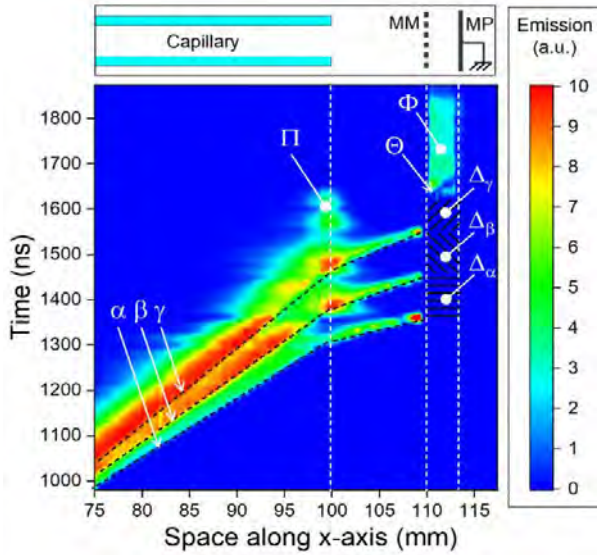

Fig. 2. Space-time-emission diagram of self-organized guided streamers and related emissive phenomena (Π: residual surface discharge, Δ: dark domains of leaders, Θ: primary ionizing event, Φ: filamentary discharge).

Measurement of the flux drift velocity of electrons in THF-H_2O mixtures.

G. Pérez[1,2], J. de Urquijo[1], O. González[1]

[1] *Instituto de Ciencias Físicas, Universidad Nacional Autónoma de México, 62210, México*
[2] *Instituto de Investigación en Ciencias Básicas y Aplicadas, Universidad Autónoma del Estado de Morelos, Av. Universidad 1001 C.P. 62209, Cuernavaca, Mor., México*

We present measurements of the flux drift velocity of electrons, v_e, in THF, H_2O and their mixtures in the gaseous phase over a wide range of pressures and of the density-normalised electric field intensity, E/N. Interestingly, all the velocity curves cross at E/N≈70 Td, a fact hitherto unobserved with any other binary mixtures.

Tetrahydrofuran (THF, C_4H_8O), a close analogue of the 2-deoxyribose [1] has been studied experimentally by swarm and beam techniques, out of which electron collision cross sections have been either derived and/or corrected.

The study of THF stems on its importance to explain the complex processes underlying DNA damage by slow electrons [2].

In this work we have used the swarm technique and, in particular, the Pulsed Townsend Technique (PTT). The apparatus and analytical procedures has been described in detail previously [3]. The PTT allows the measurement of ionization and transport parameters such as the flux electron drift velocity and longitudinal diffusion coefficient, the effective ionisation coefficient and, under some conditions, ion drift velocities and ion-molecule reaction rates.

Figure 1 shows the measured values of the flux electron drift velocity, v_e, in THF, H_2O and the 50% THF-H_2O mixture. Notice that the flux drift velocity curves cross at nearly the same E/N value, a feature hitherto not found with many other binary mixtures studied by this group. This finding is currently under study. Regarding the THF-H_2O mixtures, previously calculated values of White et al [4] disagree both in trend and value with the present measurements.

Qualitatively, one can understand lower flux drift velocities in H_2O than in THF at low E/N since there are several energy-loss rotational and electronic excitation channels at low electron collision energies which, on the other hand, are almost absent in THF. The comparatively higher drift velocities in H_2O than those for THF at high E/N may be explained in terms of a higher total momentum cross section in THF than in H_2O.

We have also measured and shall present the density-normalised flux longitudinal diffusion coefficients and the effective ionisation coefficients for the pure gases and their mixtures.

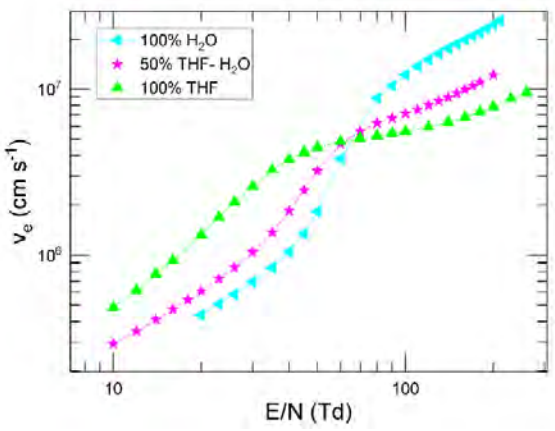

Fig. 1 The measured flux drift velocities of electrons in H_2O, THF and the 50% H_2O-THF mixture.

References

[1] P. W. Stokes, et al., *Plasma Sources Sci. Tech.*, **29,** 105008 (2020).
[2] R D White et al. *Plasma Sources Sci. Tech*, **27,** 053001 (2018).
[3] J L Hernandez- ´ Avila, et al. *J. Phys. D: Appl. Phys*. **35,** 2264–2269 (2002).
[4] R. D. White et al. *Eur. Phys. J. D*, **68:** 125 (2014).

Semicollisional transport coefficients for relativistic plasmas

K. Bendib-Kalache and A. Bendib

Laboratoire Electronique Quantique, Faculty of Physics, USTHB, Algiers, Algeria

A linear semicollisional transport theory in relativistic plasmas is presented. Non local expressions of the electron heat flux and the transfer of momentum from ions to electron have been established for arbitrary temperature value. In the limit of non relativistic temperature and high collisonal regime, the Spizer-Härm thermal conductivity [1], the frictional force [2] and the thermal force [2] were recovered. In the collisonless regime and arbitrary temperature values the result reported in Ref. 3 were also retrieved. New transport coefficients valid for arbitrary relativistic regime and collisionality were derived which can be used as reliable closure relations in fluid equations.

1 Introduction

With the advent of high power lasers, relativistic laser-plasma interactions have become a booming field of study, especially in the context of the inertial confinement fusion experiments (ICF). The transport properties have to be treat by taking into account the relativistic effects. The aim of this work is the determination of the semicollisional transport coefficients in relativistic plasmas.

2 Kinetic model

The basic equation of the model is the relativistic Fokker-Planck equation (FP). This equation is linearized, about the global thermal equilibrium defined by the Maxwell–Boltzmann–Jüttner (MBJ), f_{MBJ} distribution function. The perturbed state is defined by the electron distribution function (EDF) $\delta f(x,\vec{p},t)$, the density δn, the temperature δT, the electric field δE, the fluid velocity δV and the relative velocity of the electron with respect to the ions δu. Taking the spatial Fourier transform $(x \leftrightarrow k)$ and the temporal Laplace transform $(t \leftrightarrow s)$ of the perturbed FP equation it results the following equation

$$\lim_{s\to 0}(s\delta f) + ikc^2\frac{p_x}{\varepsilon}\delta f + e\delta E\frac{p_x}{m\varepsilon}zf_{MBJ} + ik\delta V\frac{p_x^2}{m\varepsilon} = C_{ee}(\delta f) + C_{ei}(\delta f) + \delta f(t=0) \qquad (1)$$

where m and e are the mass and charge the electron, $\vec{p}$ the relativistic momentum vector, ε, the total energy of the electrons, c the speed of light, $z = \frac{mc^2}{T}$, the relativistic parameter, where T is the electron temperature expresses in energy unit, C_{ee} and C_{ei} the electron-electron and the electron-ion collision operators respectively. To solve equation (1), we proceed as follows. First, the EDF $\delta f = \sum_{l=0}^{\infty}\delta f_l(p)\,P_l(\mu)$ is expanded in a series of Legendre polynomials $P_l(\mu)$ where $\mu = \frac{p_x}{p}$. It results an infinite set of equations, that we solved in the limit of high value of the ion charge and with the used of the continued fractions. In addition, the density and the energy conservation were taking into account by considering the initial value problem. We restrict our analysis to the transport coefficients defined by $P_1(\mu)$. Using the Branginskii notations [2] we calculated the non local expression of the electron heat flux, δq and the transfer of momentum from ions to electrons, δR_{ei}:

$$\delta q = -K_T n_e c\frac{ik}{k}\delta T + \alpha_u n_e T\delta u + \alpha_V n_e\delta V \qquad (2)$$

$$\delta R_{ei} = \beta_T n_e ik\delta T + \beta_u\frac{c}{\lambda_{ei}}n_e m\delta u \qquad (3)$$

where n_e is the electron density, λ_{ei} the electron mean free path, K_T, the thermal conductivity, $\alpha_{u,V}$ are the relative and convective velocities respectively; β_T and β_u are the coefficients of the thermal and the friction force respectively. Note here that these coefficients depend on both the Knudsen number $k\lambda_{ei}$ and the relativistic parameter z. Here, we illustrate our result in figure given above for the thermal conductivity K_T with respect of $k\lambda_{ei}$ for two values of the relativistic parameter z:

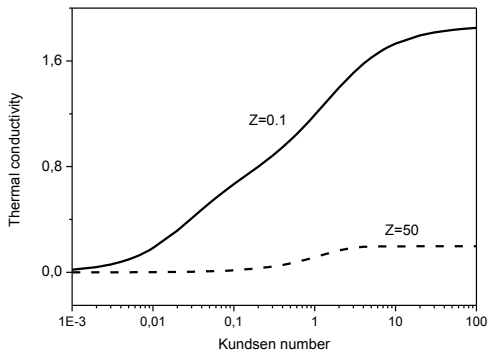

We can see that the relativistic effects tend to increase the thermal conductivity and thus the dissipation of plasma modes.

References

[1] L. Spitzer, Jr. and R. Ha¨rm, Phys. Rev. **89**, 977 (1953).

[2] S. I. Braginskii, in *Reviews of Plasma Physics*, edited by M. A. Leontovich (Consultants Bureau,NewYork, 1965),Vol. 1,p. 205.

[3] K. Bendib-Kalache, A. Bendib, and G. Matthieussent Phys. Plasmas **11**, 4254 (2004).

Correlation between the negative ion surface production efficiency and the surface work function in low pressure hydrogen plasmas

G. Cartry[1], R. MaGee[3], T. Gans[3], J. Dedrick[3], M. Sasao[2], H. Nakano[4], J.M. Layet[1]

[1] *Aix-Marseille Université, CNRS, PIIM, ISFIN, UMR7345, F-13013 Marseille, France*
[2] *Organization for Research Initiatives and Development, Doshisha University, Kyoto 602-8580, Japan*
[3] *York Plasma Institute, Dep. of Physics, University of York, Heslington, York, YO10 5DD, UK*
[4] *NIFS, Toki, Japan and Grad. School of Engineering, Nagoya University, Nagoya, Japan*

Low pressure negative-ion sources rely on the process of negative-ion surface production, a process in which positive ions or atoms scattered from a plasma wall capture one or two electrons from the surface and lead to the production of a negative ions. The negative-ion emission yield is depending strongly on the surface work function which in turns can be influenced by plasma exposure. Photoelectron yield spectroscopy (PYS) is used to perform in-situ work function (WF) measurements of samples submitted to low temperature hydrogen plasmas and correlate them with negative-ion yields.

1 Introduction

Low pressure negative-ion (NI) sources find applications in several fields such as particle injection in linear accelerators or cyclotrons, surface analysis such as SIMS, or neutral beam injection for magnetically confined fusion. These NI sources rely on the process of negative-ion surface production, a process in which positive ions or atoms scattered from a plasma wall capture one or two electrons from the surface and lead to the production of a NI. Plasma source wall materials having low-work function favour electron capture and NI emission yield. In many negative-ion sources a caesium vapour is injected in the plasma. The caesium on plasma walls and create a low work function layer which favour NI surface production. However, caesium drawbacks push to the use of other materials. In this contribution we are exploring several alternative materials for negative-ion surface production with the aim of detailing surface processes at play [2]. In order to collect in-situ information about changes of surface electronic properties due to plasma exposure a photoelectron yield spectroscopy (PYS) diagnostic has been developed to measure material work-function (WF). WF measurements are correlated with NI yields.

2 Experiment

Measurements are performed in an ICP reactor at 2 Pa and 150W injected power. A negatively biased sample is placed in the middle of the plasma chamber 40 mm away from a NI detector, being whether a magnetized retarding field energy analyser or a mass spectrometer. Positive ions from the plasma bombard the sample and form NI, which are then accelerated toward the detector. The photoelectron yield spectroscopy bench consists in a tuneable light source, an optical fibre and collimation lenses, as well as a light chopper, an ammeter and a lock-in detector. The photon energy is scanned from 1.12 eV (1200 nm) and 6.21 eV (200 nm). The photoemission threshold (i.e. the WF) is determined by measuring the sample current versus photon energy.

3 Results

Several alternative materials to caesium are investigated such as various diamond layers, graphite of a low work-function electride material named C12A7. In particular NI yield variation with surface temperature (30° to 800°C) have been measured both for graphite and diamond materials. They present very different trends with a yield continuously decreasing with temperature for graphite and a yield peaking at intermediate temperature of about 400°C for diamond. The plasma exposed graphite work-function has been observed to continuously increase from 3.9 eV to 4.5 eV between 200°C and 800°C in good agreement with NI yield variations. On the contrary there is no apparent direct correlation between WF measurements and NI yield for diamond layers.

Concerning the low-work function electride materials, the studies have focussed on the sample surface in-situ cleaning by argon plasma and on the effect of hydrogen plasma exposure on the work-function. The WF has been observed to decrease from 4.1 eV (as introduced) to 3.5 eV after 45 minutes' exposure of Argon plasma with positive ion impact at 60 eV energy. Hydrogen plasma exposure at floating potential seems to favour a decrease of the sample work-function.

4 References

[1] Cartry, G. et al (2017). New Journal of Physics, 19(2), 025010.
[2] M Sasao et al, Applied Physics Express, 11(6), 2018.
[3] Fowler, R.H et al (1931), Physical Review.

Drift-Diffusion models for RF-CCPs at intermediate pressure: estimating transport coefficients

S. Zhang[1], A. Alvarez Laguna[1] and J.P. Booth[1]

[1]*Laboratoire de Physique des Plasmas (LPP), CNRS, Sorbonne Université, École polytechnique, Institut Polytechnique de Paris, Palaiseau, 91120, France*

We compare different assumptions for the mobility and diffusion coefficients in fluid drift-diffusion models of intermediate-pressure radio-frequency capacitively coupled plasmas (RF-CCP). The differences are discussed and benchmarked against a particle-in-cell (PIC) simulation.

1 Introduction

RF-CCPs at gas pressures above ~1 Torr are often simulated by fluid models using the drift-diffusion approximation, since Particle-in-Cell (PIC) models are too computationally intensive. Fluid models require the electron transport coefficients (mobility, μ, diffusion, D, energy mobility μ_ε and energy diffusion D_ε), as well as rate constants (for ionisation, energy loss, etc.). These are calculated from the electron energy distribution function (EEDF), which is commonly estimated using either the local field approximation or by a simple Maxwellian distribution. We compare these approaches to a full PIC model in a 100V 13.56 MHz discharge in 100 Pa Ar.

2.1 Local field assumption

Here the EEDF is calculated, as a function of the electron mean energy <E>, using a Boltzmann solver such as BOLSIG or Loki. This assumption is well justified for homogeneous DC glow discharges, but its applicability to time-varying fields (e.g. RF-CCP) is more questionable.

When all four coefficients (μ, D, μ_ε and D_ε) are directly calculated from the local-field EEDF, the RF-CCP simulation gave unphysical negative values in the sheath for the electron density and energy, and thus failure of the simulation. A widely used solution for RF-CCP simulation [1] is to use the local field mobility, and calculate the other coefficients from the mean electron energy using the Einstein relations (which are only strictly valid for a Maxwellian distribution) assuming a constant momentum-transfer collision frequency. This solution gives improved numerical stability and convergence speed.

2.2 Maxwellian assumption

The transport coefficients and rates can be directly calculated for a Maxwellian EEDF assuming a constant collision frequency. The electron temperature is fixed by power balance during simulation. However, at intermediate pressures (1-10 Torr) the EEDF will deviate significantly from Maxwellian due to inelastic collisions.

3. Benchmark with PIC

The ion density profiles produced by the three models are compared in Fig.1 (a). The local field density is closer (but below) the PIC prediction, while the Maxwellian model density is much higher. The mean electron energy, <E>, is presented in Fig. 1 (b). The local field model strongly overestimates <E>, while the Maxwellian model underestimates it. This can be explained by EEDFs shown in Fig. 1 (c): the true EEDF (from PIC) is neither local nor Maxwellian. The local EEDF underestimates the population of high-energy electrons, while the Maxwellian EEDF overestimates them. Lastly, both fluid models predict flat <E> profiles, due to overestimation of electron energy diffusion in the sheath.

References

[1] Boeuf J P and Pitchford L C *Physical Review E* 1995 **51** 1376-1390

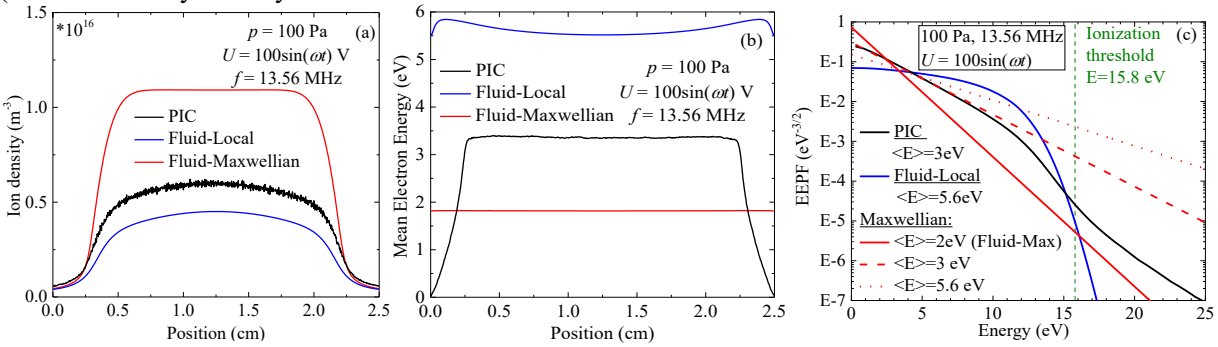

Fig. 1 (a) Ion density profile, (b) Mean electron energy and (c) EEPF for the different models

Collisional-radiative model of low-pressure He-O_2 plasma

A. Pikalev[1,2], D. Sadi[3], O. Guaitella[3], P. Viegas[2], T. Silva[2], A. Tejero-del-Caz[4], L. L. Alves[2], M.C.M. van de Sanden[1] and V. Guerra[2],

[1] *Dutch Institute for Fundamental Energy Research, Eindhoven, The Netherlands*
[2] *Instituto de Plasmas e Fusão Nuclear, Instituto Superior Técnico, Universidade de Lisboa, Lisboa, Portugal*
[3] *Laboratoire de Physique des Plasmas, École Polytechnique, Palaiseau, France*
[4] *Departamento de Física, Facultad de Ciencias, Universidad de Córdoba, Spain*

A collisional-radiative model of helium-oxygen plasma is developed using the LisbOn KInetics (LoKI) simulation tool for plasma chemistry and validated against electric field and optical emission spectra measured in a glow discharge positive column with pressures of 1–6 Torr and oxygen fractions of 5–20%. The calculated electric fields and ratios of spectral line intensities as functions of pressure are in agreement with the experiment.

Plasma in helium-oxygen mixture produces many highly reactive species and thus is used for surface treatment (in particular, for biomedical purpose) [1] or as a source of singlet molecular oxygen for oxygen-iodine lasers [2]. We adopt a low-pressure glow discharge in helium-oxygen to investigate the plasma interactions with a solid-oxide electrolysis cell (SOEC) used for oxygen separation [3]. Optical emission spectroscopy can provide essential data regarding the discharge conditions, however modelling is required to get quantitative results.

We develop a global model using the LisbOn KInetics (LoKI) chemical-Boltzmann solver. The Boltzmann equation is solved using the two-term approximation [4]. The electron density and the gas pressure are input parameters of the model. The reduced electric field is determined from the requirement of the creation-destruction balance for ions considering quasi-neutrality. The gas temperature is calculated considering heating by electrons and chemical reactions and cooling at the walls.

The chemical model is based on the model for pure helium by Alves et al. [5], the model for pure oxygen by Dias et al. [6] and helium-oxygen interactions from the model by Stafford and Kushner [2]. It is also supplemented with oxygen radiative states similar to [7].

The model is validated against the electric field and optical emission spectra measured in the positive column of a direct current glow discharge. The experiments are conducted with oxygen fractions of 5–20%, the gas pressures of 1–6 Torr and the discharge current of 40 mA. In the model we vary the electron density to reach agreement between the discharge current from the model and in the experiment. The model reproduces the dependencies of the reduced electric field and the emission rates on the gas pressure and oxygen concentration. It predicts that an increase of pressure causes an increase of electron density and a decrease of the reduced electric field and the electron temperature. Higher oxygen fractions lead to higher reduced electric fields and lower electron densities.

The work is supported by the European Space Agency under Project I-2021-03399 and the Portuguese FCT - Fundação para a Ciência e a Tecnologia, under projects UIDB/50010/2020 and UIDP/50010/2020.

References

[1] Niemi, K., Waskoenig, J., Sadeghi, N., Gans, T. & O'Connell, D. *Plasma Sources Sci. Technol.* **20**, 055005 (2011).

[2] Stafford, D. S. & Kushner, M. J. *J. Appl. Phys.* **96**, 2451–2465 (2004).

[3] Chen, X. *et al.* *ECS Meeting Abstracts* **MA2021-01**, 880 (2021).

[4] Tejero-del-Caz, A. *et al. Plasma Sources Sci. Technol.* **28**, 043001 (2019).

[5] Alves, L. L., Gousset, G. & Ferreira, C. M. *J. Phys. D: Appl. Phys.* **25**, 1713–1732 (1992).

[6] Dias, T. C. *et al.* A reaction mechanism for oxygen plasmas. Submitted to Plasma Sources. Sci. Technol. (2023).

[7] Viegas, P. *et al. Plasma Sources Sci. Technol.* **30**, 065022 (2021).

Modelling of magnetron plasma using fluid dynamics

Jan Tungli[1], Zdeněk Bonaventura[1]

[1] *Department of Physical Electronics, Masaryk University, Brno, Czech Republic*

In this work, we present simulations of 1D and 2D configurations of a DC magnetron discharge using a fluid model developed in the finite-volume framework OpenFOAM. The model is self-consistent and based on the magnetized drift-diffusion equation for electron transport and Poisson's equation. We also discuss the use of the logarithmic formulation of the drift-diffusion equation. This study explores a computationally efficient approach to modelling magnetron discharges, and contributes to addressing the computational challenges involved in modelling such discharges. Overall, the study aims to further the understanding of magnetron discharges, highlighting the significance of fluid dynamics in modelling magnetized plasmas.

1 Overview

DC magnetron discharges are a powerful industrial tool used to deposit high-quality thin films and coatings [1]. Modelling magnetized plasmas using computational methods is crucial for optimizing industrial processes and gaining insight into fundamental plasma processes. In this context, fluid dynamics provides a valuable approach, producing temporal and spatial resolution of physical quantities, and being computationally less expensive than particle-based methods. However, modelling low-pressure magnetized plasma using fluid dynamics is still challenging due to the longer mean-free path and the numerical difficulty of accounting for the magnetic field effect on electron transport [2, 3].

2 Method

We employ the finite volume method using the open-source C++ framework OpenFOAM to solve Poisson's equation and the magnetized drift-diffusion equation:

$$\frac{\partial n_\mathrm{i}}{\partial t} + \nabla \cdot \left(\hat{\mathbf{T}}_\mathrm{i} \mu_\mathrm{i} \mathbf{E} n_\mathrm{i}\right) - \nabla \cdot \left(D_\mathrm{i} \hat{\mathbf{T}}_\mathrm{i} \nabla n_\mathrm{i}\right) = S_\mathrm{i} \quad (1)$$

where n_i is the density of species i, E is the electric field, μ is the mobility, D the diffusivity, S is the source term, and $\hat{\mathbf{T}}$ is the tensor due to the magnetic field:

$$\hat{\mathbf{T}} = \frac{1}{1+\Omega^2}(\hat{\mathbf{I}} - \hat{\mathbf{\Omega}}_\times + \mathbf{\Omega}\mathbf{\Omega}) \quad (2)$$

with $\mathbf{\Omega} = \mu \mathbf{B}$ where $\mathbf{B}$ is the magnetic field.

We explore the formulation of the drift-diffusion equation in terms of logarithm of number density. In this approach some of the terms must be discretized (in space) explicitly and various choices are present regarding which terms to make implicit. We discuss the numerical benefits of these variations.

We employ the model on 1D and 2D domain discharge with argon gas at low pressures (0.5-5 Pa) with inhomogeneous magnetic field.

3 Acknowledgment

We acknowledge support from TAČR project (FW03010533).

References

[1] Lieberman, M. A. & Lichtenberg, A. J. *Principles of plasma discharges and materials processing* (John Wiley & Sons, Nashville, TN, 2005), 2 edn.

[2] Costin, C., Minea, T. M., Popa, G. & Gousset, G. Fluid modelling of DC magnetrons—low pressure extension and experimental validation. *Plasma Processes and Polymers* **4**, S960–S964 (2007).

[3] Hagelaar, G. J. M., Fubiani, G. & Boeuf, J.-P. Model of an inductively coupled negative ion source: I. general model description. *Plasma Sources Science and Technology* **20**, 015001 (2011).

Modelling radiation using PLASIMO

J.F.J. Janssen[1], J. van Dijk[2]

[1] *Plasma Matters B.V., Eindhoven, The Netherlands*
[2] *Dept. Applied Physics, Eindhoven Univ. Techn., Eindhoven, The Netherlands*

Various approximations exist for estimating the impact of emission and absorption of radiation on a plasma. PLASIMO can offer several of these methods. One of those methods is the net emission coefficient. The optically thick radiation can be considered diffusive. A decay length for the radiation is assumed and the net emission coefficient becomes a source term in the energy equation. The diffusive approximation can be taken one step further by solving for the direction averaged spectral radiance in a spatially resolved manner. In order to fully capture the non-local absorption a ray tracing method is required. In this work these methods are demonstrated and compared.

The equation of radiative transfer is given by

$$\frac{\mathrm{d}I_\nu}{\mathrm{d}s} = j_\nu - \kappa_\nu I_\nu, \tag{1}$$

This equation is difficult to solve in general because the emission (j_ν) and absorption ($\kappa_\nu I_\nu$) of radiation can occur non-locally. For that reason different levels of approximations are made that each have their own balance between speed and accuracy. Three of these approximations are discussed in more detail. The capabilities of these PLASIMO [1] models are demonstrated and compared.

The diffusive approximation is used as formulated by Lowke [2]. In this approximation the radiation losses can be represented in the form of a net emission coefficient (NEC) which can be used as a source term in the energy equation. Lowke defined the NEC as

$$S_R = \int B_\nu \kappa_\nu \exp\left(-\kappa_\nu R\right), \tag{2}$$

with R the radius of the isothermal sphere that is considered. The advantage is that this calculation method is very fast. The disadvantage is that the absorption is local and only controlled by the parameter R.

The diffusive approximation can be improved by considering spatial dimensions. This removes the need for a parameter R. A series expansion in terms of spherical harmonics can be applied to the spectral radiance. By truncating the series expansion to first order and considering a non-scattering medium the system of equations can be written as [3]

$$\nabla \cdot \vec{q_\nu} = \kappa_\nu \left(4\pi B_\nu - G_\nu\right) \tag{3}$$

$$\nabla G_\nu = -3\kappa_\nu \vec{q_\nu}. \tag{4}$$

In order to capture the non-local effects fully the formal solution to the radiative transfer equation must be solved. For a non-scattering medium in thermal equilibrium it is given by [3]

$$I_\nu\left(\tau_\nu\right) = I_\nu(0)\exp\left(-\tau_\nu\right) + \int_0^{\tau_\nu} B_\nu\left(\tau'_\nu\right)\exp^{-\left(\tau_\nu - \tau'_\nu\right)}\mathrm{d}\tau'_\nu, \tag{5}$$

with the optical depth given by

$$\tau_\nu = \int_o^s \kappa_\nu \mathrm{d}s. \tag{6}$$

Equation (5) contains the correct non-local behavior. It is also more difficult to solve. In PLASIMO a raytracing approach is used [1].

References

[1] van Dijk, J., Kroesen, G. M. W. & Bogaerts, A. Plasma modelling and numerical simulation. *Journal of Physics D: Applied Physics* **42**, 190301 (2009). URL `http://stacks.iop.org/0022-3727/42/i=19/a=190301`.

[2] Lowke, J. *Journal of Quantitative Spectroscopy and Radiative Transfer* **14**, 111 – 122 (1974).

[3] Modest, M. F. *Radiative Heat Transfer* (Elsevier, 2013).

Multi-fluid modeling of a weakly-ionized confined plasma: Ion-neutral collision term

A. Berger[1,2], A. Alvarez Laguna[1], T. Magin[2] and A. Bourdon[1]

[1] *Laboratoire de Physique des Plasmas, CNRS, Ecole Polytechnique, Palaiseau, France*
[2] *Aerospace and Aeronautics Dpt., von Karman Institute for Fluid Dynamics, Rhode-Saint-Genèse, Belgium*

The present work focuses on the modeling of the collision term in the momentum conservation equations in a plasma. We study the effect of using a kinetic-derived collision term compared to the simplified one often used. We found an inconsistency in the high-velocity asymptotic behaviour between the two terms, which has a not negligible quantitative on a the macroscopic behaviour of the plasma (shown via the edge-to-center density ratio, i.e., h_l factor).

In the framework of weakly-collisional plasma modeling, the collision terms of fluid models are of paramount importance and have a significant influence on the plasma dynamics. This motivates a proper derivation of these terms from the Boltzmann kinetic equation.
The computation of the collision term of the first moment equation (the momentum conservation) has been done [1] and compared to the simplified collision term widely used in the low-temperature community [2]. We found the same asymptotic behavior in the low-Mach number regime, but the high-Mach number asymptotic behavior differs by a factor. Furthermore, the ion-neutral total cross-section (isotropic plus charge-exchange) is usually considered constant, which is a fairly good approximation in the high-Mach regime, but not in the low-Mach regime (where the cross-section almost scales as the inverse of the velocity), as can be seen figure 1a. This approximation has a quantitative influence on the collision term and on the plasma dynamics.
To illustrate its impact, the two terms has been implemented in an isothermal multi-fluid one-dimensional simulation of a plasma between two walls [3]. The solver considers 5 equations: the density and momentum conservation equations of the ions and the electrons, and the Poisson equation. We found that in the intermediate and high density regimes, the variation of the edge-to-center density ratio (or h_l factor) with the collisionality can differ largely depending on the collision term considered (see figure 1b).

References

[1] Benilov, M. S. A kinetic derivation of multifluid equations for multispecies nonequilibrium mixtures of reacting gases. *Physics of Plasmas* **4**, 521–528 (1997).

[2] Chabert, P. & Braithwaite, N. *Physics of radio-frequency plasmas* (Cambridge University press, 2011).

[3] Alvarez Laguna, A. *et al.* An asymptotic preserving well-balanced scheme for the isothermal fluid equations in low-temperature plasmas at low-pressure. *Journal of Computational Physics* **419**, 109634 (2020).

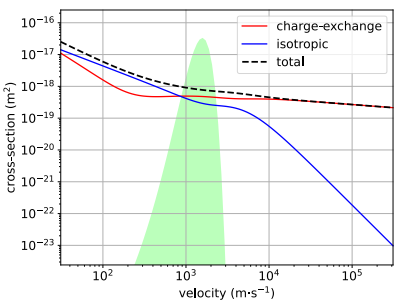

(a) Variation of the Argon ion-neutral cross-section with the velocity. The green area represent a typical Maxwellian velocity distribution function of ions.

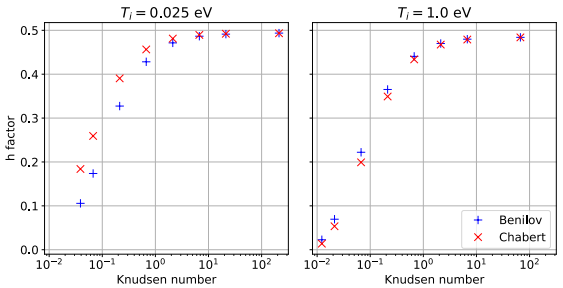

(b) Variation of the h factor with the ion Knudsen number. Data points are otained from simulations using either the properly derived collision term (Benilov) or the simplified one (Chabert).

Effect of multi-tip reactor parameters on energy efficiency using the electrical model equivalent to corona discharge

Karim Saber [1], Alyen Abahazem [1,3] Nofel Merbahi [2] and Mohammed Yousfi [2]

[1] *Materials and Renewable Energies Laboratory, Physics Department, Cité Dakhla BP 8106, Ibn Zohr University, Agadir, Morocco*
[2]*LAPLACE UMR 5213-CNRS, 118 Route de Narbonne, Bât. 3R2, 31062 Toulouse Cedex 9, Paul Sabatier University, France*
[3]*LASDIS, CRMEF-SM, Avenue Mly Abdellah, BP 106, Inezgane, Morocco*

Abstract

This work is devoted to study the effect of certain reactor parameters of a multi-tip-plane configuration on the electrical behavior of the corona discharge in the case of a two-tip-plane configuration, in dry air, for a frequency of 1 kHz and a pulse width of 1µs, at atmospheric pressure, by fixing the inter-electrode distance and the applied voltage. We studied the effect of the inter-tip distance (from 5 to 20 mm) on the delivered power and the useful power which were calculated using the parameters of the electrical circuit equivalent to this discharge. In addition we compared the energy efficiency of the plasma for different distances mentioned above. We have found that the reactor loses a large amount of energy for a small inter-tip distance due to the mutual effect between the tips. This lost energy decreases gradually with increasing inter-tip distance. We have also deduced that beyond a certain inter-tip distance the reactor doesn't lose any energy by mutual effect. Moreover, we have realized the same study but this time by increasing the tip number for a given inter-tip distance. The results obtained in this work are interpreted based on the images taken by the ICCD camera during the discharge.

Keywords: Corona discharge; inter-tip distance; tip number; discharge power; delivered power; Plasma energy efficiency.

Benchmark of particle-in-cell simulations of a Penning-type discharge: Preliminary results

L. Garrigues[1], G. Fubiani[1], J. P. Boeuf[1], A. T. Powis[2], W. Villafana[2], I. Kaganovich[2], Y. Raitses[2], F. Petronio[3], A. Alvarez-Laguna[3], A. Bourdon[3], P. Chabert[3], G. Bogopolsky[4], B . Cuenot[4], O. Vermorel[4], D. Sydorenko[5], M. Papahn Zadeh[6], A. Smolyakov[6], F. Cichocki[7], P. Minelli[7], F. Taccogna[7], D. Eremin[8], L. Xu[8], A. Denig[9], K. Hara[9], P. Q. Elias[10], E. Bello Benitez[11], A. Marin[11], E. Ahedo[11], M. Merino[11], P. Fajardo[11], Z. Donko[12], P. Hartmann[12], M. Turner[13], M. Reza[14], F. Faraji[14], A. Knoll[14], P. Parodi[15], and T. Magin[15]

[1] *LAPLACE, Université de Toulouse, CNRS, INPT, UPS, Toulouse, France*
[2] *Princeton Plasma Physics Laboratory, Princeton, NJ 08540, United States of America*
[3] *LPP, CNRS, Sorbonne Université, École Polytechnique, Institut Polytechnique de Paris, 91120 Palaiseau, France*
[4] *CERFACS, 42, Avenue Gaspard Coriolis, 31057 Toulouse, France*
[5] *University of Alberta, Edmonton, Alberta T6G 2E1, Canada*
[6] *Department of Physics and Engineering Physics, University of Saskatchewan, 116 Science Place, Saskatoon SK S7N 5E2, Canada*
[7] *Institute for Plasma Science and Technology (ISTP), CNR, 70126 Bari, Italy*
[8] *Ruhr University Bochum, Universitaetsstrasse 150, D-44801 Bochum, Germany*
[9] *Stanford University, Stanford, CA, 94305, United States of America*
[10] *DPHY, ONERA, Université Paris-Saclay, F-91123 Palaiseau - France*
[11] *Equipo de Propulsión Espacial y Plasmas, Universidad Carlos III de Madrid, Leganés 28911, Spain*
[12] *Wigner Research Centre for Physics, Wigner FK, Konkoly-Thege M. 29-33, Budapest, 1121, Hungary*
[13] *School of Physical Sciences and National Center for Plasma Science and Technology, DCU, Dublin 9, Ireland*
[14] *Imperial College London, Exhibition Rd, South Kensington, London, SW7 2AZ, United Kingdom*
[15] *Von Karman Institute for Fluid Dynamics, Aeronautics and Aerospace Department, Belgium*

The Penning-type discharge belongs to the $E \times B$ family of plasma devices where electrons are magnetized and ions are weakly magnetized or unmagnetized. In a Penning cell, an axial magnetic field, whose magnitude is a few hundreds of Gauss, is generated with the use of permanent magnets or coils that surround a cylindrical anode. A DC electric field is applied between the anode and the cathode planes located at the end of the plasma column. The primary electrons are injected at one end of the column.

These discharges operate in the pressure range below a few mTorr, and are used in a large number of applications [1]. Plasma densities are in the range of $10^{16} – 10^{18}$ m^{-3} and electron temperature between 1 to 10 eV [2]. Coherent structures whose frequency and wavelength are on the order of a few kHz and a few centimetres develop in the direction of the drifting electrons perpendicular to the radial electric and axial magnetic fields. Attempts to characterize the effect of plasma parameters on the structure of the instability and the mechanisms responsible for its formation have been proposed in Ref. [3] using particle-in-cell (PIC) simulations.

In the last few years, the community of partially magnetized low temperature plasmas scientists has federated around the LANDMARK project [4] to propose a set of reference benchmarks with the aim of demonstrating the accuracy of numerical solutions [5], [6]. The new test case that we propose is in 2D and corresponds to the radial-azimuthal simulation plane of the rotating spoke in a collisionless Penning discharge. Electrons and ions are injected from a central region. The magnetic field is uniform and perpendicular to the simulation domain. More details about initial conditions can be found in Ref. [4].

At this conference, preliminary results of the time-averaged profiles of charged particles densities, electron temperature as well as spoke rotation frequencies calculated by 15 research groups worldwide will be shown.

References

[1] Handbook of Ion Sources, edited by B. Wolf, CRC Press (1995).
[2] Y. Raitses *et al*., *International Electric Propulsion Conference*, Hyogo-Kobe, Japan July 4–10, 2015, pages IEPC–2015–307, 2015.
[3] A. T. Powis *et al.*, Phys. Plasmas **25**, 072110 (2018).
[4] Low temperature magnetized plasma benchmarks (LANDMARK) project, https://www.landmark-plasma.com/.
[5] T. Charoy *et al.*, Plasma Sources Sci. Technol. **28**, 105010 (2019).
[6] W. Villafana *et al.*, Plasma Sources Sci. Technol. **30**, 075002 (2021).

ECR simulations on unstructured meshes

R.H.S. Budé[1], J. van Dijk[1], D.A. van Ameijde[1], I. Harzing[1], T.O. Goedkoop[1], D. Mihailova[2]

[1] *Dept. Applied Physics, Eindhoven Univ. Techn., Eindhoven, The Netherlands*
[2]*Plasma Matters B.V., Eindhoven, The Netherlands*

A Maxwell equation solver is implemented and used to simulate Electron Cyclotron Resonance (ECR) heating of plasmas. The code supports simulations on unstructured, triangular and tetrahedral meshes, in 2D, "2.5D" and 3D. The effect of the effective collision frequency is studied, and it is found that its effect on the total power absorbed in the plasma is minimal, confirming observations from literature.

1 Introduction

ECR heating is a microwave-based plasma heating method that is used to heat plasmas ranging from industrial plasmas to fusion plasmas. Studying how the electromagnetic waves propagate through the plasma, and where they get absorbed, is done using a numerical code for solving the time-harmonic Maxwell's equations. Support for unstructured, triangular meshes is achieved due to the use of vector finite elements for the discretization [1] [2]. Elements up to third order have been implemented. It is found that higher order elements exhibit faster convergence and higher accuracy.

2D cylindrical and Cartesian coordinate systems, and since recently 3D systems, are supported. Furthermore "2.5D" simulations are made possible by assuming a plane-wave continuation of the electromagnetic fields in the perpendicular direction [3]. The code has been added as a module to the plasma modelling framework PLASIMO [4].

2 Effective Collision Frequency

The anisotropy of ECR is modelled by the relative permittivity not being a scalar, ϵ_r, but a tensor: $\bar{\bar{\epsilon}}_r$. For an ECR plasma, this tensor is the Stix tensor [5]. Without damping term of some sort, the terms in this tensor will have singularities in the resonance zone. The introduction of a collision frequency, for example the electron-neutral collision frequency, removes the singularities, but the resonance zone is still thinner than observed in experiments.

Therefore, an "effective collision frequency" ν_{eff} is often used, typically of the order 1GHz [6]. This is orders of magnitude higher than any physical collision frequency in the plasma (these are of the order 10-100MHz), but it restores the width of the resonance zone to widths that are more in line with experimental observations. The effective collision frequency possibly reflects non-collisional particle-wave effects, like Landau damping or cyclotron damping.

Additionally, the smoother resonance zone is easier to resolve, and poses less strict requirements on the mesh density. Numerical experiments seem to indicate that there is a range of effective collision frequencies, where the total absorbed power by the plasma is only weakly dependent on the value of ν_{eff}, confirming the observation made in [6].

3 Outlook

The addition of non-axisymmetric modes could allow an extension of the model to also include hot plasma's. This model could then for example be used to study the propagation of microwaves in, for example, ECRH or ICRH (Ion Cyclotron Resonance Heating) in nuclear fusion reactors.

This activity is co-funded by PPS-contribution Research and Innovation of the Ministry of Economic Affairs and Climate Policy (The Netherlands), and ASML.

4 References

[1] T. Rylander, "MATLAB: FEM with Triangular Edge Elements," in *Computational Electromagnetics*, New York, Springer, 2013, pp. 130-137.

[2] J. P. Webb, "Hierarchical Scalar and Vector Tetrahedra," *IEEE Transactions on Magnetics,* vol. 49, no. 2, pp. 1495-1498, 1993.

[3] N. V. Venkatarayalu, "Efficient computation of Maxwell eigenmodes in axisymmetric cavities using hierarchical vector finite elements," *International Journal of Numerical Modelling: Electronic Networks, Devices and Fields,* 2010.

[4] "The PLASIMO project," Plasma Matters, [Online]. Available: https://plasimo.phys.tue.nl/.

[5] T. H. Stix, "Waves in a Cold Uniform Plasma," in *Waves in Plasmas*, New York, American Institute of Physics, 1992, pp. 25-40.

[6] G. J. M. Hagelaar, "Modelling of a dipolar microwave plasma sustained by electron cyclotron resonance," *J. Phys. D: Appl. Phys.,* p. 194019, 2009.

Determination of the atomic oxygen density distribution in an RF-driven He/O_2 microplasma jet at atmospheric pressure using an efficient 2D hybrid simulation method

M. Vass[1,2], D. Schulenberg[1], Z. Donkó[2], I. Korolov[1], P. Hartmann[2], J. Schulze[1] and T. Mussenbrock[1]

[1] *Chair of Applied Electrodynamics and Plasma Technology, Ruhr University Bochum, Germany*
[2] *Wigner Research Centre for Physics, Budapest, Hungary*

The spatial distribution of the atomic oxygen density is investigated in an RF-driven atmospheric pressure microplasma jet operated in helium with a 0.5% admixture of oxygen, driven by a single frequency waveform of $f = 13.56$ MHz frequency and $V_{\mathrm{rms}} = 250$ V root mean square voltage, based on an efficient spatially 2D hybrid simulation method, where chemical reactions, as well as the effect of the gas flow, are accounted for. The results show good agreement with measured experimental results.

1 Introduction

Radiofrequency (RF) driven micro-atmospheric pressure plasma jets are widely used for various plasma processes, such as surface manufacturing (e.g. sterilization) and plasma medicine (e.g. wound healing), mostly due to the effective generation of certain radical species [1]. In order to optimize the generation of these species, a thorough understanding of the underlying mechanisms is needed, which can be accomplished based on numerical simulations. In this work we investigate the spatial distribution of the atomic oxygen density in the COST reference microplasma jet [2] operated in a He/O_2 mixture excited by a single frequency waveform.

2 Simulation method and results

The simulation method is based on a hybrid (fluid+kinetic) scheme, where charged as well as neutral species are described by a fluid model, by solving the (2 dimensional) continuity equation based on the drift-diffusion approximation, as well as Poisson's equation. The effect of the gas flow (assuming a Poiseuille flow) is included in the equations. In order to capture kinetic effects in case of the electrons, a separate Monte Carlo Collision (MCC) module is used, where electron impact rates are calculated based on the electric field provided by the fluid model. These rates then serve as sources in the respective fluid equations. Chemical reactions, based on reaction rate coefficients, are accounted for in the fluid module. The two modules are run in an iterative way until convergence in the species densities is achieved.

The discharge model is that presented in [3]: there are 7 charged species, including electrons, positive ions (He^+, O^+, O_2^+) and negative ions (O^-, O_2^-, O_3^-), and 8 neutral species (He^*, O, $O(^1D)$, $O_2(v = 1-4)$, $O_2(a^1\Delta_g)$, $O_2(b^1\Sigma_g)$, O_3, O_3^*) considered, with 19 electron impact reactions and 91 chemical reactions.

The COST-jet is assumed to have two plane-parallel electrodes with a gap length of $L_x = 1$ mm, and a nozzle length of $L_z = 30$ mm. The pressure is $p = 10^5$ Pa. The operating gas is a mixture of 99.5% He and 0.5% O_2. The driving waveform is a single harmonic with $f = 13.56$ MHz and $V_{\mathrm{rms}} = 250$ V. The conditions are chosen such that they agree with previous experimental measurements of atomic oxygen based on Two photon Absorption Laser Induced Fluorescence (TALIF) spectroscopy [4]. The simulation results show a good agreement with the experimental data, verifying the saturation of the atomic oxygen density along the discharge channel for different gas flow values.

References

[1] Adamovich, I. *et al. J. Phys. D: Appl. Phys.* **55**, 373001 (2022).

[2] Golda, J. *et al. J. Phys. D: Appl. Phys.* **49**, 084003 (2016).

[3] Liu, Y. *et al. Plasma Sources Sci. Technol.* **30**, 064001 (2021).

[4] Steuer, D. *et al. J. Phys. D: Appl. Phys.* **54**, 355204 (2021).

Insights on Hall effect thruster using Xe Collisional Radiative Model

T. Ben Slimane[1], A. Leduc[1] and L. Schiesko[1], Anne Bourdon[1], Pascal Chabert[1]

[1] Laboratoire de Physique des Plasmas (LPP), CNRS, Sorbonne Université, Ecole polytechnique, Institut Polytechnique de Paris, 91120 Palaiseau, France

A neutral Xe collisional radiative model based on the 6s and 6p levels was developed and validated against other models available in the literature and Langmuir probe measurements. It was able to reproduce similar kinetic trends with respect to the electron temperature. Optical emission measurements on a mid-power Hall effect thruster were then performed for different voltages at the anode and different Xe injection flows, allowing to scan of the plume along three axes: axial, lateral, and radial. An optimization strategy based on 15 neutral lines was used to predict the electron temperature from the collected spectra. A comparison between the temperature profiles between Particle-in-Cell simulations and the predicted results yields a fairly good agreement in terms of trends and order of magnitude.

1 Introduction

Hall effect thrusters have become very popular in recent years since they offer a large range of specific impulses, a wide range of electric power as well as a huge flexibility in flight configurations. Still, compact and non-invasive tools to study the plasma discharge are still needed today in order to easily characterize ground facility effects on the performance of HETs. In this work, we implement optical emission spectroscopy and couple it with collisional radiative modeling (CRM), in order to non-invasively estimate the plasma parameters for different operating regimes of the thruster.

2 Collisional Radiative Model

The collisional radiative model developed in this work is based on and validated against the work of Karabadhzac et al.[1]. It solves the non-linear steady-state balance equations of the 1s and 2p levels of Xe by taking into account electron impact excitation, spontaneous emission as well as absorption using Mewe approximation[2]. The model yields the densities of excited species from which synthetic spectra are generated and compared with experimental spectra to determine which input values of the model generate the best fit for experiments.

3 Experimental setup and results

Optical emission spectroscopy (OES) and Langmuir probes (LP) were conducted on the plume of a laboratory Hall thruster for different operating conditions of the thruster (anode flow and anode voltage). Comparison between the LP and OES measurements showed a very good agreement between the two methods. Axial and radial scans highlighted that the simplified CRM and OES are able to correctly predict axial and radial characteristics of the HET plume, mainly a high electron temperature in the thruster channel that increases linearly, from 24eV to 30eV for a voltage range between $80 - 180$V. The electron density profile in the plume highlights an exponential decrease with the distance, consistent with a Boltzmann isothermal model and axisymmetric simulation results[3].

References

[1] Karabadzhak, G. F., Chiu, Y.-h. & Dressler, R. A. Passive optical diagnostic of Xe propelled Hall thrusters. II. Collisional-radiative model. *Journal of Applied Physics* **99**, 113305 (2006). URL `https://aip.scitation.org/doi/10.1063/1.2195019`.

[2] Mewe, R. Relative intensity of helium spectral lines as a function of electron temperature and density. *British Journal of Applied Physics* **18**, 107 (1967). URL `https://iopscience.iop.org/article/10.1088/0508-3443/18/1/315/meta`.

[3] Domínguez Vázquez, A. *Axisymmetric simulation codes for hall effect thrusters and plasma plumes.* Doctoral Thesis (2019). URL `https://e-archivo.uc3m.es/handle/10016/30603`. Accepted: 2020-06-11T07:23:12Z.

Surrogate collisional radiative models for fluorocarbon plasmas from optical diagnostics data using deep autoencoders

G. Daly[1,2], J. Fieldsend[1], G. Hassall[2] and G. Tabor[1]

[1] *Faculty of Environment, Science and Economy, University of Exeter, UK*
[2] *Oxford Instruments Plasma Technology, UK*

We have created a deep generative model of plasma in an industrial ICP plasma etcher for use as a surrogate model. The plasma etcher was instrumented and a large dataset of 812,500 spectra and images in Ar, O_2, CF_4/O_2 and SF_6/O_2 was collected. This dataset was used to train a deep autoencoder as a generative model using electrode powers, pressure and gas flows as inputs. The generative model can produce synthetic data at 10,000s of points in 10 seconds with good accuracy. The models and data are open source and are available for users to test.

First principle plasma and collisional radiative models are very useful, but the complex chemistries in industrial plasma etching can make it difficult to create an accurate reaction set for the model, and new materials, like GaN in compound semiconductor devices and NbTi in quantum devices, make this even more arduous. An alternative approach is to gather experimental data of the desired processing chemistry and train a machine learning model in place of the plasma model and collisional radiative model. This type of approach has been used to form surrogate models of sputtering simulation data [1, 2], but not with large experimental datasets.

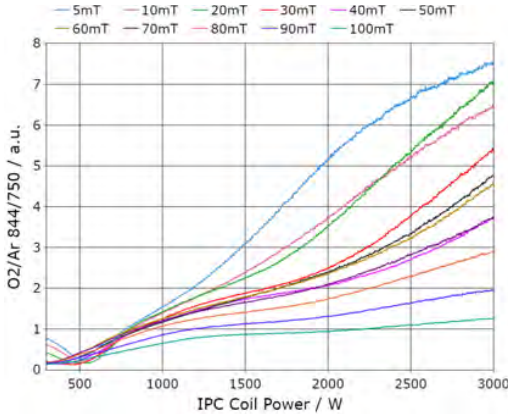

Figure 1: 844.6 nm / Ar 750.4 nm line ratio, in Ar/O_2 at 5-100 mT sweeping from 400-3000 W.

We have trained a deep autoencoder on a large data set of 812,500 spectra and images gathered in an Oxford Instruments PP100 ICP etcher in Ar, O_2, CF_4/O_2 and SF_6/O_2. Autoencoders do not require labelled data, the model takes an image and spectra pair as an input and learns to reconstruct them at the output, it has a bottleneck that forces it to learn a lower-dimensional latent-representation of the data. The second half of the model, the decoder, is a generative model and projects from the latent space back into the real measurement space. We trained a neural network that maps from the tool input space (powers, pressures, gas flows) to the latent space, turning it into an empirical collisional radiative model.

This model can generate 1000s of spectra in seconds, across the entire operating space of the plasma tool, to carry out synthetic experiments as shown in figure 1. This type of generative model architecture is very versatile and additional variables from other diagnostics can be added, from smaller datasets, as additional inputs or outputs without retraining the large autoencoder.

The models, weights and demo code are available here and a colab notebook of the demo can be run by anyone here, the data is available at https://doi.org/10.5281/zenodo.7704879.

References

[1] Gergs, T., Borislavov, B. & Trieschmann, J. Efficient plasma-surface interaction surrogate model for sputtering processes based on autoencoder neural networks. *Journal of Vacuum Science & Technology B* **40**, 012802 (2022).

[2] Gergs, T., Mussenbrock, T. & Trieschmann, J. Physics-separating artificial neural networks for predicting initial stages of Al sputtering and thin film deposition in Ar plasma discharges. *Journal of Physics D: Applied Physics* (2023).

Laser–induced photo-detachment diagnostic for interrogating pulsed ECR–driven plasmas: Application to H^- and D^- negative ions

M. Mitrou[1, 2], S. Béchu[2] and P. Svarnas[1]

[1] *High Voltage Lab., Electrical & Computer Eng. Dept., University of Patras, Rion-Patras 26504, Greece*
[2] *Université Grenoble Alpes, CNRS, Grenoble INP (Institute of Engineering), LPSC-IN2P3, 38000 Grenoble, France*

The present work is devoted to an experimental setup tailored to study time-resolved processes relative to negative ion formation in ECR-driven plasmas. It refers to a laser-induced electron photo-detachment system synchronized with H_2 and D_2 ECR-plasmas being sustained by 2.45 GHz bursts in the kHz range. The system is combined with electrostatic probe time-resolved measurements and information is obtained both on the formation path and the yield enhancement of H^- and D^- negative ions.

1 Introduction

The study of H^- and D^- negative ions relevant to the accelerator and fusion applications, may be supported by considering transient kinetics within the corresponding plasmas. This concept is here tested by: (i) generating electron cyclotron resonance (ECR) H_2 and D_2 plasmas, sustained by 2.45 GHz microwave bursts; and (ii) interrogating them by means of time-resolved photo-detachment (PD) and electrostatic probe (EP) techniques.

2 Experimental setup and method

H_2 and D_2 plasmas are produced in the ECR-driven SCHEME-II+ reactor, which is designed to study volume-produced H^- and D^- negative ions with respect to surface-enhanced production of ro-vibrationally excited molecules [1].

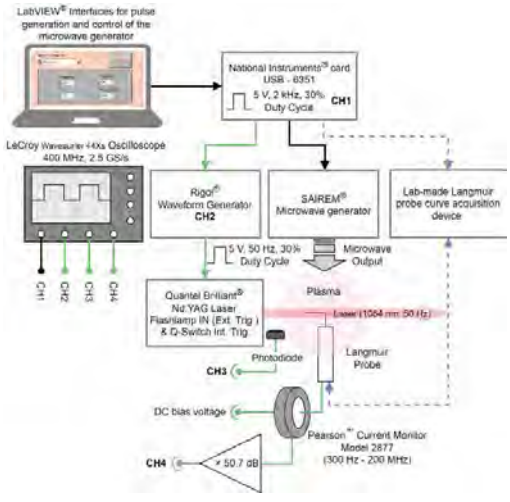

Figure 1. Generation of ECR-plasma bursts and scheduling for time-resolved PD and EP measurements.

Microwave power (150 W) is delivered from a solid-state 2.45 GHz generator and chopped to form bursts (repetition rate 2 kHz; pulse width 150 μs). Laser-induced photo-detachment [2] (50 Hz) and electrostatic probe acquisition are both synchronized with the microwave bursts as explained in Fig. 1. Measurements are carried out at 1.6 Pa and 75 mm downstream of the midplane of the ECR zone. Data are averaged over 100 and 1000 periods of the bursts for the EP and the PD experiments, respectively.

3 Results and Conclusion

Fig. 2 demonstrates indicative results from the D_2 plasma, i.e., the signal of the electrons photo-detached from the D^- negative ions.

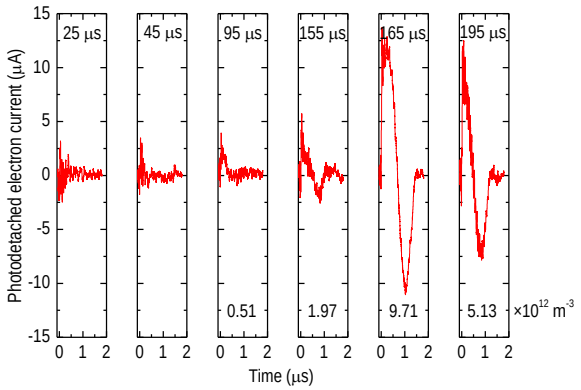

Figure 2. Representative time-resolved photo-detachment signals. Insets: corresponding time points of the acquisition and absolute D^- ion densities. The latter are calculated after factoring in the corresponding time-specific electron densities from the time-resolved probe I-V curves.

The above results stress the enhanced negative ion yield in the post-discharge phase (>150 μs). This may be attributed to the rapid decay of energetic electrons, atomic population, and positive ions involved in destruction reactions, along with the formation of vibrationally excited molecules of long lifetime [3] involved in the main volume production reaction of the H^- and D^- ions, i.e., dissociative attachment.

References

[1] Béchu, S. *et al.* J. Quant. Spectr. Radiat. Transfer **257**, 107325 (2020).
[2] Bacal, M. Rev. Sci. Instrum. **71**, 3981 (2000).
[3] Mosbach, T. *et al.* Plasma Sources Sci. Technol. **7**, 75-81 (1998).

Theoretical and experimental analysis of 2p states kinetics in barrier discharge in argon

T. Hoder[1], L. Kusýn[1], A. P. Jovanović[2], P. Bílek[3],
D. Loffhagen[2], Z. Navrátil[1], D. Prokop[1], M. Stankov[2] , M.M. Becker[2]

[1] *Department of Physical Electronics, Faculty of Science, Masaryk University, Brno, Czechia*
[2] *Leibniz Institute for Plasma Science and Technology (INP), Greifswald, Germany*
[3] *Department of Pulse Plasma Systems, IPP CAS, Prague, Czechia*

The development of new diagnostic methods for non-equilibrium low temperature plasma investigations or the validation of computer simulation models requires, in the best case, joint experimental and theoretical efforts. In this contribution, we investigate the barrier discharge in atmospheric pressure argon experimentally using a time correlated single photon counting enhanced optical emission spectroscopy (OES) and theoretically using a spatially two-dimensional (2D) fluid-Poisson model with extended reaction kinetics scheme. We analyse the development of all ten 2p states (Paschen notation) in the discharge. Based on the results of both experiment and modelling, we propose a possible tool for plasma diagnostics.

1 General

Typically, the discharge mechanisms responsible for the generation of atmospheric pressure plasmas lead to their highly transient behaviour with strong gradients on sub-millimetre and sub-nanosecond scales. These plasmas, generated for example by barrier, corona, or spark discharges or such in nanosecond pulsed or jet discharges, are useful in many application-oriented fields of research. Particularly, the interest is focused on plasmas in gases like air or argon, which have an exclusive position both in nature and technology. For a proper understanding of such plasmas, closely linked diagnostics and modelling approaches are necessary.

While in air or nitrogen, OES based methods for the electric field determination are in use [1], this is not the case for argon at atmospheric pressure. In this contribution, we investigate the barrier discharge in atmospheric pressure argon experimentally using an optical emission spectroscopy and theoretically using a time-dependent 2D fluid-Poisson model with an extended reaction kinetics scheme. We analyse the development of all ten 2p states (Paschen notation) in the discharge and propose a possible tool for non-invasive reduced electric field (E/N) determination.

2 Experiment and model, first results

The experimental setup is an asymmetric barrier discharge with only one electrode covered by a dielectric material [2]. The electrodes are half-spherical with a curvature of 2 mm. Alumina is used as the dielectric. The gap is 1.5 mm. A high-voltage pulse is applied to the powered electrode using an Eagle Harbor Technology nanosecond pulser with a rise time of about 40 ns and an amplitude of 5600 V at a repetition frequency of 10 kHz. The same setup was investigated using a 2D fluid-Poisson model [2] employing an extended reaction kinetics scheme [3].

Comparing results obtained by experiment and modelling, we observe quantitative differences in many observables, which are worth of further detailed research. At the same time, several qualitative signatures are consistent and may enable an estimation of the reduced electric field in different discharge phases. Especially, selected line intensity ratios of certain 2p states show a detectable sensitivity on the electric field development in the discharge.

Acknowledgement

This research has been funded by Czech Science Foundation under contract no. 21-16391S and supported by the project LM2023039 funded by the Ministry of Education, Youth and Sports of the Czech Republic. Furthermore, the work was partly funded by the Deutsche Forschungsgemeinschaft (DFG, German Research Foundation)—project numbers 368502453, 407462159 and 466331904.

References

[1] Goldberg, B., Hoder, T., Brandenburg R. Electric field determination in transient plasmas: in-situ & non-invasive methods. Plasma Sources Sci. Technol. **31**, 073001 (2022).

[2] Jovanović, A.P., Loffhagen, D., Becker M.M. Streamer–surface interaction in an atmospheric pressure dielectric barrier discharge in argon. Plasma Sources Sci. Technol. **31**, 04LT02 (2022).

[3] Stankov, M., Becker, M.M., Hoder, T., Loffhagen, D. Extended reaction kinetics model for non-thermal argon plasmas and its test against experimental data. Plasma Sources Sci. Technol. **31**, 125002 (2022).

Development of optical diagnostics to study neutral species in low-pressure iodine plasmas: application within a gridded thruster.

B. Esteves[1,2], C. Blondel[1], A. Alvarez-Laguna[1], A. Bourdon[1], P. Chabert[1] and C. Drag[1]

[1] *Laboratoire de Physique des plasmas, Centre national de la recherche scientifique, Sorbonne Université, Université Paris-Saclay, Observatoire de Paris, École polytechnique, Institut polytechnique de Paris, route de Saclay, F-91128 Palaiseau cedex, France*

[2] *Safran Spacecraft Propulsion, 27208 Vernon, France*

Molecular iodine is a promising propellant for future plasma thrusters. For this reason, it is critical to understand the basic physics and chemistry of low-pressure iodine plasma discharges. In this work, we use optical absorption methods (with one or two photons) to measure the density of iodine molecules, I_2, and the density and the temperature of the two first levels of iodine atoms, noted $I(^2P^\circ_{3/2})$ and $I(^2P^\circ_{1/2})$. The diagnostics have been developed in an iodine cell where the pressure ranges from 1.5 Pa to 27 Pa before being applied to an ion-gridded thruster where the pressure is typical of electric propulsion applications (between 0.1 and 2 Pa). These measurements will be used to validate chemistry models of iodine plasmas.

1 Optical diagnostics

The optical absorption diagnostics performed on different iodine atomic levels are schematically represented in Figure 1. They allow to measure the density and the temperature of the two first levels of iodine atoms. While absorption measurements (ABS) are line-of-sight integrated, TALIF is local [1].

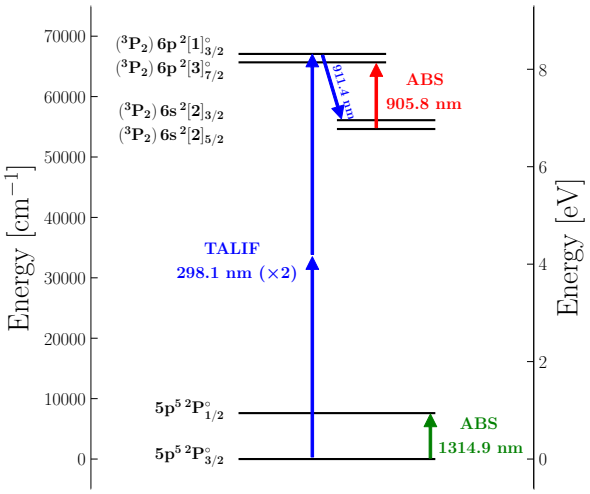

Figure 1: Energy diagram of the atomic iodine levels used in this work. The optical diagnostics are schematically represented by arrows.

For molecules, the absorption spectra may be more difficult to interpret due to the population distribution of the different rotational and vibrational levels. This can be circumvented by setting the excitation wavelength in a region where absorption leads to molecular dissociation (above 20000 cm^{-1} for iodine).

2 Results

1D spatial profiles of density and atomic temperature were obtained along the thrust axis confirming the quasi-total dissociation at the core of the plasma and the presence of very strong gradients with pressure as predicted by measurements previously performed on the charged particles [2]. The density of the $I(^2P^\circ_{1/2})$ level is found to be a significant fraction (about 30 %) of the total atomic density, although the energy difference with the $I(^2P^\circ_{3/2})$ ground level is nearly 1 eV. At 15 mTorr, the atomic temperature could reach more than 1500 K, evidencing the strong heating properties of dissociation processes.

References

[1] Esteves, B., Blondel, C., Chabert, P. & Drag, C. Two-photon absorption laser induced fluorescence (TALIF) detection of atomic iodine in low-temperature plasmas and a revision of the energy levels of I I. *Journal of Physics B: Atomic, Molecular and Optical Physics* **56**, 055002 (2023).

[2] Esteves, B. *et al.* Charged-particles measurements in low-pressure iodine plasmas used for electric propulsion. *Plasma Sources Science and Technology* **31**, 085007 (2022).

RF Plasma source characterization for an EM cavity

P. A. Mendes Rossa[2], J. Oliveira[1], D. Hachmeister[1], J. Brotankova[3], H. Fernandes[1]

[1] *Instituto de Plasmas e Fusão Nuclear, Instituto Superior Técnico, Universidade de Lisboa, Portugal*
[2]*Instituto Superior Técnico, Universidade de Lisboa, Portugal*
[3]*Faculty of Nuclear Sciences and Physical Engineering, Czech Technical University, Prague, Czech Republic*

As part of a remote-controlled experiment included in the advanced laboratory at IST, a RF source is used in order to fill an electromagnetic cavity with a suitable plasma. By doing so, the refractive index is altered according to the plasma dispersion relation and consequently there exist a shift in the resonant frequency of the cavity, allowing the determination of the plasma electron density. The user can vary some parameters and have access to the results in real-time or check then back later, via a browser (on a PC or mobile phone).

1 Introduction

Remote Controlled Laboratories (RCLs) as an educational resource started to emerge in the beginning of this century. Nonetheless only by recent COVID times strong evidence of its real significance came up. In fact, RCLs were already out there but lacking in visibility.

elab, a remote controlled laboratory at IST, Lisbon, come to live precisely by the year 2000 and since then has served various physic experiments. Recently, with contributions from IAEA and Fusenet, two remote experiments have been deployed on the advanced laboratory, namely a Langmuir probe and an Electromagnetic (EM) Cavity. Both are based on a low frequency (50 kHz, 3 W) RF powered plasma source.

2 The Electromagnetic Cavity

An EM Cavity can be considered as a portion of a waveguide and its electromagnetic behaviour applies. The cavity being used is made of a copper cylinder with an anti-corrosive skin protection of nickel. The cylinder tops consist of an aluminium mesh with a spacing less than one-tenth of the microwave wavelength used in the experiment. A spring fastened to the opposite side of the vacuum window holds the mesh in place and are used to impose the RF power via a cold cathode fluorescent light (CCFL) inverter that generates a Penning discharge inside the cavity, ionizing the gas. Presently He, Ar and N_2 are at disposable. The whole cavity lies between two Helmholtz coils that generate a magnetic field of 1.4 mT per Ampere, up to a maximum of 20mT.

2.1 Dispersion relation on a magnetized plasma

The Appleton–Hartree equation applies for the EM propagation of waves in plasmas and the resonance of modes will depend on the wavelength and frequency for given dimensions. Due to the boundary constraints, the wavelength is fixed and so, for different refractive indexes related to various plasma densities and cyclotronic frequencies, we will have a different resonant frequency. For the most fundamental TM_{010} mode it gives the following equation:

$$n_e = \frac{8\pi^2 \epsilon_0 m_e}{e^2} f_{010} \Delta f \qquad (1)$$

3 Main results

The presented results in this section have been obtained for three different nobel gases at different pressures. For each of the available gases (Ar, He, N_2) we performed a background pressure variation from when the RF discharge starts producing ionization to its disappearance due to high pressure, for the imposed RF power, figure 1.

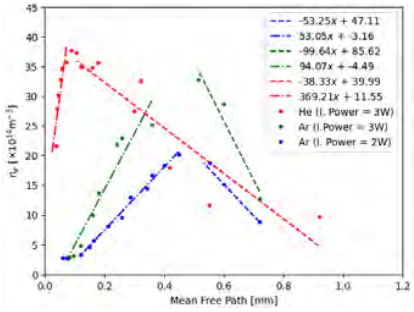

Figure 1: Electron density in function of the mean free path of Ar and He.

Acknowledgements

This work has been supported by IAEA through a research agreement within the IAEA Research Contract No. 22750. on 'Network of Small and Medium Size Magnetic Confinement Fusion Devices for Fusion Research. IPFN activities received financial support from 'Fundação para a Ciência e Tecnologia' through Projects UIDB/50010/2020 and UIDP/50010/2020 and by Grants PD/BD/150408/2019 and PD/BD/150413/2019. It has also benefited from the Fusenet association sponsorship and from the project Laboratoř horkého plazmatu a fúzní techniky PlasmaLab@CTU' CZ.02.1.01/0.0/0.0/16_017/0002248.

Optical tweezers technique for electric field strength and fluctuation measurements in plasma using a fine particle

T. Sato[1], K. Kamataki[1] ,K. Tomita[2], P. Yiming[1], D. Yamashita[1], N. Yamashita[1], N. Itagaki[1], K. Koga[1,3] and M. Shiratani[1]

[1] *Kyushu University Information Science and Electrical Engineering, Japan*
[2] *Hokkaido University, Japan*
[3] *National Institutes for Natural Sciences, Japan*

We propose a measurement method of electric field vector in plasma sheath region by a fine particle trapped with optical tweezers. Experimental results show this measurement method has a high sensitivity (~0.1V/cm) and a high spatial resolution (micro meter order).

1 Introduction

Plasma processing is mainly used to manufacture micro- and nano-electronics devices. The measurement of electric field in micro- and nano- meter order space in plasma sheath region is important for improving plasma processing of materials. For example, small changes and fluctuations of electric field have a significant impact on etching and deposition into high aspect ratio micro- and nano-structure. It is essential to develop highly sensitive diagnostic methods on the sheath electric field. The purpose of this study is to evaluate electric fields strength and fluctuation in Ar plasma using a fine particle trapped with laser tweezers [1].

2 Experimental Setup

Figure 1 shows the diagram of experiment setup. A plasma reaction vessel was set up in an epi-illumination microscope. This vessel had a metal mesh grounded electrode and a ring-shaped powered electrode, which was placed on the sapphire glass under the vessel. The point at $(r, z) = (0\mu m, 0\mu m)$ was set as the center of the sapphire window as shown in fig.1. A radio-frequency voltage of 13.56 MHz was applied between the electrodes to generate plasma. When an acrylic particle of 10, 15, 18, 20 μm in diameter (density 1.20 g/cm^3) was introduced into the plasma, it was suspended near the plasma/sheath boundary above the powered ring electrode. This single particle was trapped in plasma with optical tweezers. When it was moved horizontally with the laser, we measured the levitation position. We deduced electric field at the levitation position from the horizontal and vertical balances of forces on an optically trapped particle. Force balances on a fine particle in plasma were as follows :

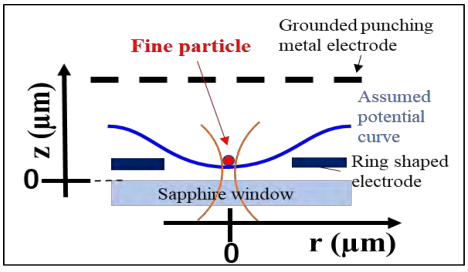

Fig. 1 Diagram of experimental setup

(horizontal balance) $Q_p E_r = F_{ray\_r}$, and (vertical balance) $mg = Q_p E_z + F_{ray\_z}$, where Q_p is the particle charge, mg is the gravity, E_r and E_z are the strength of horizontal and vertical electric field, F_{ray_r} and F_{ray_z} are the force of the laser on the particle, respectively. F_{ray_r} and F_{ray_z} were obtained from an ray optical model [2], and Q_p was deduced from Orbital Motion Limited(OML) model considering ion collision[3].

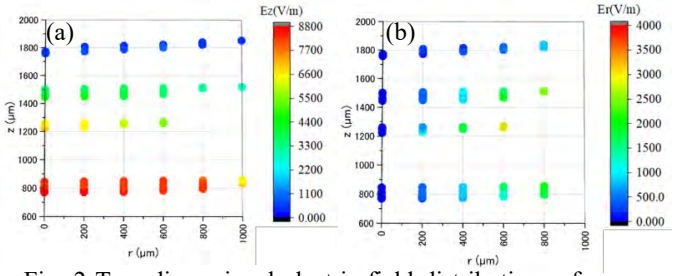

Figs.2 Two dimensional electric field distributions of (a) E_z and (b) E_r.

3 Results and Discussion

By changing the particle size (= gravity force), the measurement region in the plasma sheath can be selected and expanded. Figures 2 show 2D distributions of E_z and (b)E_r. These results show that decreased from the plasma sheath region to the bulk of the plasmathe effect of ion drag force. We will discuss the detail at the conference.

Acknowledgements

This work was partly supported by JSPF KAKENHI (Grant No. JP20H00142) and JSPS Core-to-Core Program (Grant No. JPJSCCA2019002).

References

[1] A. Ashkin, Biophys. J. 61 (1992) 569.
[2] Philip h. Jones, et al., Optical Tweezers Principles and Applications, 22 (Cambridge university press, 2015).
[3] S. A. Khrapak, et al., Phys. Rev. E., 72 (2005) 016406.

Spatiotemporally resolved electric field and temperatures in positive streamers

L. Kusýn[2,1], Siebe Dijcks[1], Petr Bílek[3], Sander Nijdam[1], Tomáš Hoder[2]

[1] *Eindhoven University of Technology, Eindhoven, The Netherlands*
[2] *Department of Physical Electronics, Faculty of Science, Masaryk University, Brno, Czech Republic*
[3] *Institute of Plasma Physics of the Czech Academy of Sciences, Prague, Czech Republic*

Large centimeter-wide highly reproducible positive streamers are investigated in synthetic air and pure nitrogen at pressures ranging from 33 to 266 mbar. The time-resolved emission spectroscopy of the streamer heads is used to observe the temporal and spatial development of the first negative system (FNS, $B^2\Sigma_u^+ \rightarrow X^2\Sigma_g^+$) of N_2^+ and the second positive system (SPS, $C^3\Pi_u \rightarrow B^3\Pi_g$) of N_2. We have determined the rotational and vibrational temperatures of these species and applied the intensity ratio technique to determine a reduced electric field E/N. E/N resolved with sub-millimeter and sub-nanosecond resolution then provides high-resolution insight into the electric field distribution in the streamer head.

1 General

The non-equilibrium nature of streamers and their strong local electric fields make them of interest in various applications. There are methods of measuring E/N directly and indirectly for plasmas and streamer-like discharges. However, it has been proven difficult to apply these measurement techniques to transient and stochastic phenomena like a streamer discharge, which is exacerbated by the low active species densities found in these types of plasmas. In this work, the method of the intensity ratio of FNS and SPS emissions is applied to quantify the electric field in the streamer head with high spatio-temporal resolution.

2 Method & results

A streamer discharge with high reproducibility is achieved by placing two disk electrodes 10 cm opposite of each other with a 1 cm needle protruding from the powered electrode. The electric field distribution in the streamer head for synthetic air and pure nitrogen is determined from the intensity ratio of vibrational transitions SPS(2-5) and FNS(0-0). The emissions of these transitions were recorded by an ICCD camera and processed by *massiveOES* software. This allowed for a separation of individual vibronic transitions and determination of intensities (surfaces under the vibrational bands) used for the intensity ratio method. The procedure is conducted with a temporal resolution of 500 ps and a sub-millimeter spatial resolution resulting in a series of 2D distribution plots at various pressures.

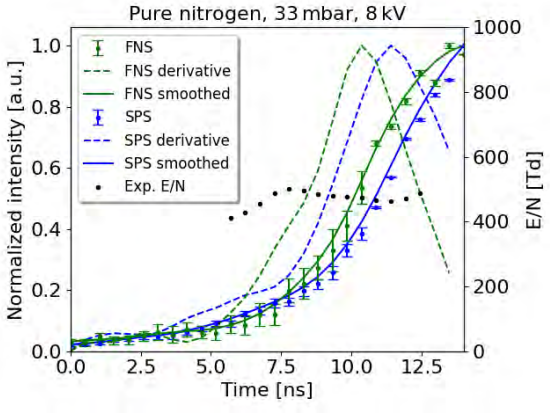

Figure 1: Measured intensities of FNS(0-0) and SPS(2-5), their derivatives and determined E/N.

Acknowledgement

This research (SD & SN) is part of the project 'Let CO2 Spark' (with project number 15052) of the research programme Open Technology Programme which is (partly) financed by the Dutch Research Council (NWO). LK and TH were supported both by the Czech Science Foundation under contract no.21-16391S and Project LM2023039 funded by the Ministry of Education, Youth and Sports of the Czech Republic. PB was supported by the Czech Science Foundation (Project No. 15-04023S) and by the Strategy AV21 project.

1D TALIF of atomic oxygen in the effluent of a CO_2 microwave discharge

A. Meindl, A. Hecimovic and U. Fantz

Max Planck Institute for Plasma Physics, Boltzmannstrasse 2, 85748 Garching, Germany

Atomic oxygen in the effluent of a CO_2 microwave discharge is investigated via TALIF with 1D axial resolution. The results display a late onset of ground state oxygen atoms in the effluent of the plasma indicating the importance of considering metastable states when attempting to understand the chemical conditions unfolding post-discharge.

Motivation

For the purposes of CO_2 conversion via volumetric plasma processes, understanding the post-discharge regime is equally important to understanding the discharge itself, since the ability to retain the conversion achieved in the discharge is limited by recombination in the effluent [1]. The focus of this study is the investigation of the effluent of CO_2 plasma created in a surfaguide setup in the pressure range between 1 mbar and 5 mbar with flow rates between 74 sccm and 370 sccm and 600 W to 1200 W of absorbed microwave powers. Within this parameter space the discharge is characterized by high specific energy inputs (SEI) resulting in high CO_2 conversions (up to 90 %) driven by direct dissociation through electron collisions, thus splitting the CO_2 into CO and metastable O (^1D) atoms [2].

Experiment

The effluent of the CO_2 plasma is investigated via TALIF of oxygen atoms in the electronic ground state ($2p^4\,{}^3P_2$).

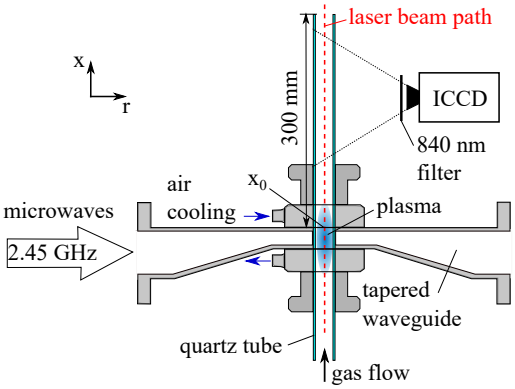

Figure 1: Schematic of the plasma source and the TALIF detection apparatus.

A dye laser system provides ns-pulses with tunable wavelength around 225 nm. The experimental setup is detailed in Fig. 1. Multiple different radial positions within the cylindrical quartz tube are investigated for each plasma condition. Figure 2 depicts the axially and spectrally resolved data acquired for one measurement. The collected data allows for determination of 1D resolved translational temperatures and absolute number densities of ground state oxygen atoms through calibration with xenon. The observed late onset of ground state atomic oxygen in the effluent underlines the importance of considering metastable excited states when attempting to model the post-discharge kinetics.

References

[1] Hecimovic et al. *Journal of CO2 Utilization* **57**, 101870 (2022).

[2] Fridman, A. *Plasma Chemistry* (Cambridge University Press, 2008).

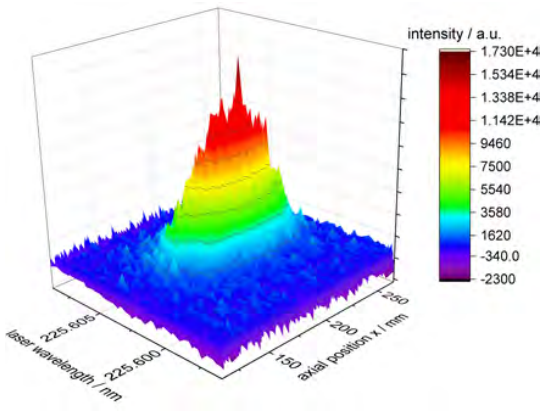

Figure 2: Spectrally and axially resolved TALIF signal.

Estimation of vibrational temperatures of CO_2 in dielectric barrier discharges by deep ultraviolet absorption spectroscopy

K. Sasaki[1], Y. Maniwa[1], and K. Shiratsuchi[1]

[1] *Division of Applied Quantum Science and Engineering, Hokkaido University, Sapporo, Japan*

We tried to estimate the vibrational temperature of CO_2 by deep ultraviolet absorption spectroscopy. The principle of the method is based on the fact that the absorption wavelength of CO_2 is elongated if its vibrational temperature is higher than room temperature. The vibrational temperature estimated by deep ultraviolet absorption spectroscopy was compared with that determined by laser Raman scattering.

1 Introduction

Recently, the vibrational temperature of CO_2 attracts much attention in conjunction with gas conversion processes using plasmas. A method for measuring the vibrational temperature of CO_2 is infrared absorption spectroscopy, but conventional Fourier transform spectrometers are not applicable to various plasma sources due to absorption by CO_2 in air. Laser Raman scattering is an alternative, but only the vibrational distribution of the bending mode can be deduced directly from the Raman scattering spectrum. In this work, we tried simple absorption spectroscopy. It is known that CO_2 at room temperature is transparent in the visible-ultraviolet wavelength range, and it has optical absorption only in vacuum ultraviolet. On the other hand, CO_2 at elevated temperatures has optical absorption in deep ultraviolet. The shift of the absorption wavelength to the longer side is caused by the transition from vibrational excited states of the electronic ground state. The absorption cross section has been measured using CO_2 at thermodynamic equilibrium [1]. Since the same cross section is expected for nonequilibrium CO_2 (CO_2 with different rotational and vibrational temperatures), it is possible to estimate the vibrational temperature of CO_2 in plasmas by measuring the absorption spectrum.

2 Experiment

The light source for absorption spectroscopy was a cw laser-produced plasma with continuum optical emission. It was close to an ideal point source, and a perfectly collimated light path was obtained using a lens. The dielectric barrier discharge source was composed of a tungsten rod connected to a high-voltage power supply, a quartz tube with an inner diameter of 4 mm, and a ring electrode connected to the electrical ground. The rod electrode was placed at the centre of the quartz tube, and the ring electrode was attached on the outside. CO_2 was fed from the top of the quartz tube via a mass flow controller. The collimated lamp light was transmitted just below the exhaust side of the quartz tube. An optical filter with the transmission at a deep ultraviolet wavelength range was inserted between the lamp and the discharge source. The transmitted lamp light was guided to a spectrograph equipped with a cooled CCD array, and the spectra with and without the discharge were compared to deduce the absorption spectrum.

3 Results and discussion

Since the optical emission intensity of the lamp was rather weak in the deep ultraviolet wavelength range (185-210 nm), it was necessary to develop a method to eliminate the influence of the stray light in the spectrograph. The spectrum was composed of absorptions by CO_2 and ozone. The absorption spectrum of ozone was fitted well with the known absorption cross section, and the absorption spectrum of CO_2 was obtained by subtracting the ozone spectrum. The absorption spectrum of CO_2 was converted to the absorption cross section with the help of the Lambert-Beer low, as shown in Fig. 1. The absorption cross sections at various temperatures [1] are also shown in the figure. According to the comparison shown in Fig. 1, the vibrational temperature of CO_2 was estimated to be 450-550 K. The vibrational temperature thus estimated was roughly consistent with the bending-mode vibrational temperature determined by laser Raman scattering.

This work was supported by JST CREST Grant No. JPMJCR19R3.

References

[1] O. Venot, et al., A&A **609**, A34 (2018).

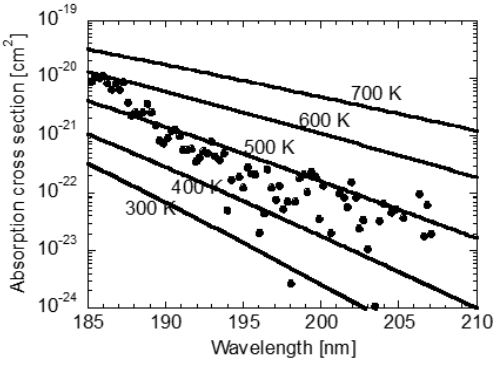

Figure 1. Absorption cross section of CO_2 ejected from a dielectric barrier discharge, and its comparison with absorption cross sections in literature [1].

Microwave discharges under thermal control for generation of nitric oxide

Y. Zhao, V.A. Sterie and G.D. Stancu(*)

Laboratoire EM2C, CNRS, CentraleSupélec, Université Paris-Saclay, 3, rue Joliot Curie, 91192 Gif-sur-Yvette cedex, France

(*) gabi-daniel.stancu@centralesupelec.fr

Capillary and jet microwave discharges were employed to generate nitric oxide (NO) in mixtures of air and argon at atmospheric pressure. Time and space resolved quantum cascade laser absorption spectroscopy (QCLAS) was used to characterize NO densities and temperatures *in-situ* and in plasma effluents. The discharge thermal control has proven to largely extend the plasma working domain, to significantly increase the NO density and to reduce its energy cost. These non-equilibrium discharges have shown here a high versatility for nitric oxide generation, with efficiencies comparable to top literature sources.

Over the last two decades, nitric oxide has received a special attention by the plasma community. As an environmental pollutant released by combustion systems, many investigations were focused on its reduction. Recognized to play a key role in regulation of biological processes, studies were also performed for wound healing and sterilization applications. Furthermore, its plasma generation efficiency was investigated for medical usage and for fertiliser production. The fixation of atmospheric nitrogen by nitric oxide plasma synthesis is currently seen as a complementary approach to the Haber-Bosch process [1].

Here two microwave (mw) discharge configurations with powers below 100 W, frequencies in the range 2.4 ÷ 2.5 GHz and at atmospheric pressure, were employed. Namely, a capillary plasma was generated in argon/air gas mixtures and a jet plasma was produced in dry air. Mid-IR quantum cascade laser absorption spectroscopy [2] was used to measure NO absolute density and gas temperature using *in-situ* and *ex-situ* arrangements.

In the *in-situ* configuration, the Abel inversion of lateral absorbances was employed to determine NO density and temperature across the jet at about 2000 K. A White multi-pass cell was used downstream of plasmas to measure NO in chemically frozen conditions and at room temperature.

Using the thermal resistance concept, a discharge thermal control system was designed to significantly increase the plasma heat transfer across the capillary. Applying an external airflow on the capillary surface was found to reduce the plasma gas temperature up to a factor two. The pressure and the electron density were also significantly changed [3]. Here, the plasma working domain was extended from 10 % to 40 % air/argon molar ratios, as shown in Figure 1. The nitric oxide density and flowrate were increased near one order of magnitude, reaching a maximum of 7.1×10^{16} cm^{-3} (0.3 % molar fraction) and 7.2 sccm, respectively. Consequently, the energy cost per NO molecule was lowered by one order of magnitude (i.e. 160 eV/molec). Larger molar fractions of up to 2 % were generated using the mw jet configuration in air at 2000 K. The energy cost estimated to about 40 eV/molec is comparable with top literature results obtained by atmospheric discharges, e.g. [4]. Moreover, recent studies [5] have shown that the power coupled to mw capillary plasmas is significantly lower than the values given by classical measurement methods, hence even lower energy costs are expected.

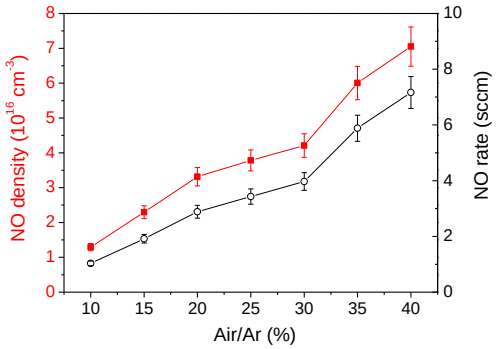

Figure 1. Nitric oxide density and flow rate as a function air/argon molar ratio.

Acknowledgments: This research was founded by Labex LaSIPS, University Paris-Saclay *Thermoplas* project RD 73.

References

[1] B.S. Patil, Q. Wang, V. Hessel, J. Lang, *Catalysis Today* **256** (2015) 49

[2] M. Simeni Simeni, C.O. Laux, G.D. Stancu, *J. Phys. D: Appl. Phys.* **50** (2017) 274004

[3] F. Coquery, *PhD Thesis*, CentraleSupélec, Université Paris-Saclay (2021)

[4] N. Britun, V. Gamaleev, M. Hori, *Plasma Sources Sci. Technol.* **30** (2021) 08LT02

[5] F. Coquery, O. Leroy, T. Minea, G.D. Stancu, *Plasma Sources Sci. Technol.* **31** (2022) 055003

P2-28

3D Particle-in-Cell simulation of the E×B electron drift instability in Hall thrusters

Gwenael Fubiani[1], Laurent Garrigues[1] and Willca Villafana[2]
[1]LAPLACE, Université de Toulouse, CNRS, Toulouse, France
[2]Princeton Plasma Physics Laboratory, Princeton, New Jersey 08540, USA.

Corresponding author: gwenael.fubiani@cnrs.fr

Kinetic drift instabilities are the likely cause for the anomalous electron transport in Hall-effect thrusters (HETs). This work is a continuation of previous efforts to model drift waves in HETs using a Particle-In-Cell (PIC) with Monte Carlo (MCC) algorithm [1]. The latter demonstrated the occurrence of an Electron Cyclotron Drift type Instability (ECDI) which transitions into a modified Ion-Acoustic Wave (IAW). The model had a couple of simplifying assumptions in order to speed-up the calculation and pinpoint the mechanisms leading to the formation of the instability. The electron transport was decoupled from ionization and neutral transport, collisions with neutrals were neglected, the magnetic field had solely an axial profile and the simulation domain was 2D (axial-azimuthal plane). In this work, we perform a similar kind of calculation but in 3D including the walls in the radial direction. We use a 3D PIC-MCC model parallelized using both OpenMP and MPI. The simulation domain includes a section of the canal and the plume. We will analyse: (1) the characteristics of the instability and the anomalous transport versus the discharge power, (2) the effect of the magnetic field strength on the plasma properties and lastly, (3) we will perform a convergence test showing that the 3D simulation may provide an accurate estimate of the physics at plays in a couple of weeks using a relatively small amount of threads (about 60 days with 44 cores in our example for a numerical resolution of 256×512×192 grid nodes and 280 millions charged macroparticles).

[1] J.P. Boeuf et al., Physics of Plasmas **25**, 061204 (2018)

Topic #8 : low pressure plasmas

Experimental observation of the coupling of low frequency instabilities at different scales in a Hall thruster

Q. Delavière--Delion[1], F. Gaboriau[1], G. Fubiani[1] and L. Garrigues[1]

[1] *LAPLACE – Université de Toulouse – CNRS – INPT - UPS, Toulouse, France*

In the plasma of a Hall thruster, a huge azimuthal electron drift current leads to the formation of numerous instabilities at different frequency scales and propagating in different directions. These instabilities play an important role for the plasma, especially in terms of electronic transport through the magnetic barrier. In this presentation, we are only interested in a few low-frequency instabilities that we have been able to observe experimentally, like the breathing mode, the ion transit time oscillations (ITTO) and the rotating spokes. The interdependencies between these different instabilities were studied as a function of the discharge parameters.

Introduction

In a Hall thruster, an axial electric field E and a radial magnetic field B are imposed through an ionisation channel. The application of these two fields perpendicular to each other generates an electron current in the E×B (azimuthal) direction. This important electronic current results from an efficient ionization of the gas, but is also a source of energy for the development of numerous instabilities in the plasma.

These instabilities have been experimentally observed over a large frequency range (from kHz to GHz) [1] [5]. Despite the latter theoretical progress made, the interdependence of these oscillations at different scales makes these phenomena particularly complex and difficult to understand, as they are difficult to simulate, although some numerical simulations manage to reproduce certain features of these instabilities [3,4]. Some of these instabilities are responsible for the anomalous electron transport through the magnetic barrier [4]. They are also responsible of global fluctuations of the plasma that can have harmful consequences. Therefore, it is necessary to better understand the mechanisms governing these instabilities in order to better control them.

Experimental setup and diagnostics methods

The study was carried on the experimental thruster ID-Hall-2, developed at Laplace laboratory and derived to the ID-Hall-1 prototype [5], and focused on low frequency instabilities (from 10^3 to 10^6 Hz).

These oscillations were studied using different diagnostics such as physical probes and fast imaging techniques, via different methods including wavelet analysis.

Results and discussions

The study of the plasma revealed the coexistence and interdependence of at least three kinds of instabilities with different wavelengths and different propagation directions (axial and azimuthal).

The existence of at least three distinct low-frequency oscillation regimes as a function of the discharge voltage was highlighted. It was shown that one of the transitions between regimes occurs when the frequency of one of the harmonics of the breathing mode oscillations becomes a multiple of the frequency of the fast oscillations, which could lead to a resonance explaining the doubling of the discharge current amplitude.

The ion energy distribution functions were also measured in both integrated and over time, and different behaviours were observed in each of the previously identified regimes, pointing out the ITTO.

Instabilities moving azimuthally with a speed 10 times lower than the E×B current has been observed (rotating spokes) and are under studying. Their impact on the electronic transport must be estimated in their existence regime.

Acknowledgments

Q. DD has benefited from a PhD funding from the French Ministry of Research. This work is supported by the CNES agency.

References

[1] E. Y. Choueiri, Plasma oscillations in Hall thrusters, Physics of Plasmas (2001)

[2] J. P. Boeuf, L. Garrigues, E × B electron drift instability in Hall thrusters: Particle-in-cell simulations vs. theory, Physics of Plasmas (2018)

[3] W. Frias, A. I. Smolyakov, Long wavelength gradient drift instability in Hall plasma devices. I. Fluid theory, Physics of Plasmas (2012)

[4] J.-P. Boeuf, Tutorial: Physics and modeling of Hall thrusters, Journal of Applied Physics (2017)

[5] A. Guglielmi, F. Gaboriau and J.P. Boeuf, Simultaneous measurements of axial motion and azimuthal rotation of non-uniformities (spokes) in Hall thruster, Physics of Plasma (2022)

Characterization of a low-pressure microwave plasma in multisource configuration for surface decontamination applications

Y. Fermi, T. Maho and P. Guillot

DPHE Laboratory, Toulouse University, INU Champollion, Albi, France

1 Introduction

The decontamination of surfaces is a barrier against the transmission of pathogens between individuals, especially in medical field. A pass-through is a decontamination apparatus used in cleanroom to transfer an object from a "common environment" to a controlled environment. They usually work with H_2O_2 which have specific drawbacks linked to toxicity. Due to their non-toxicity, safety, and suitability for the treatment of heat sensitive materials, decontamination processes based on plasma have received great attention in recent years [1]. This study consists of low pressure plasma characterizations to define optimal operating conditions in terms of homogeneity and plasma characteristics. The aim is to evaluate if low pressure plasma can be applicable to a pass-through chamber.

2 Experimental setup

Our experimental device consists of a vacuum chamber (diameter of 46 cm, height of 26 cm) filled by synthetic air (fig. 1). The plasma can be excited either by a microwave ECR source (Aura-Wave SAIREM) or a collisional coaxial plasma source (Hi-Wave SAIREM). Both are powered by a solid-state generators operating at 2.5 GHz up to 200 W in a pressure range of 1-40 Pa. The plasma is first generated in one source configuration and next in three sources configuration.

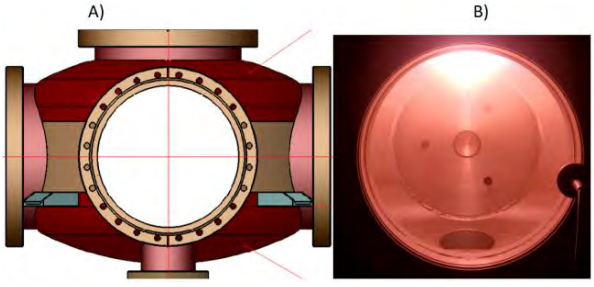

Figure 1. Schematic of the vacuum chamber (A) and plasma discharge in one source configuration (B).

3 Plasma characterization

Optical emission spectroscopy characterization has been carried out using a high-resolution monochromator (SpectraPro HRS-750) coupled to an ICCD camera (Pi-Max-4). Measurements have been realized to obtain 2D emission distributions of N_2 (356 nm), N_2^+ (390 nm) and O I (777 and 844 nm) as a function of pressure (from 1 to 40 Pa), and injected power (from 50 to 175 W). A comparison of simulated and experimental distribution has been done in three sources configuration. In this case, calculated distributions for three sources are deduced from one source experimental distribution (fig. 2).

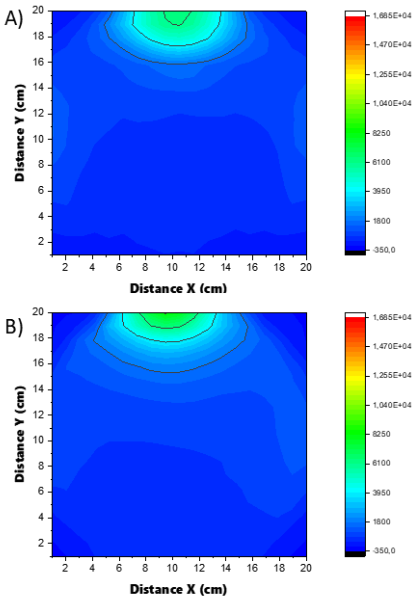

Figure 2. Simulated distribution (A) and experimental distribution (B) of O (777 nm) in three sources configuration (Aura-Wave, 5 Pa, 3x100W).

These results will be presented as well as the plasma characteristics calculated from the optical spectra. Gas temperature was estimated from the rotational temperature of N_2 (C, v'=0) → N_2 (B, v''=2) with SPECAIR software. Electron density is calculated from stark broadening of H_β (486 nm).

Acknowledgement

The authors want to thank Region Occitanie for financial support (SAS-PLAS-BIO project).

References

[1] Rossi, F. Low pressure plasma discharges for the sterilization and decontamination of surfaces. New J. Phys. 11 115017.

Improved negative ion source extraction efficiency using highly emissive inverse sheath for NBI heating in fusion

G. Sun[1], W. Yang[2], J. Chen[3], H. Sun[4], B. Guo[5], S. Zhang[6], Y. Wang[4], X. Yang[1], A. Sun[1], and G. Zhang[1]

[1] *School of Electrical Engineering, Xi'an Jiaotong University, Xi'an, China*
[2] *College of Science, Donghua University, Shanghai 201620, People's Republic of China*
[3] *Sino-French Institute of Nuclear Engineering and Technology, Sun Yat-sen University, Zhuhai 519082, China*
[4] *Ecole Polytechnique Fédérale de Lausanne (EPFL), Swiss Plasma Center (SPC), CH-1015 Lausanne, Switzerland*
[5] *Centrum Wiskunde & Informatica (CWI), Amsterdam, The Netherlands*
[6] *Laboratoire de Physique des Plasmas, CNRS, Ecole Polytechnique, France*

Negative hydrogen ion (H^-) sources employed in neutral beam injection (NBI) system are subject to extraction efficiency issue due to the considerable H^- volumetric losses. Here we propose to improve the H^- extraction by activating the electronegative inverse sheath in front of the H^- production surface, which features zero sheath acceleration for H^- with a negative sheath potential opposite to the classic sheath. With inverse sheath formed, produced H^- exhibits smaller gyration, shorter transport path, less destructive collisions, and higher extraction probability than the existing space-charge limited (SCL) sheath. Formation of the electronegative inverse sheath and the SCL sheath is studied by the continuum, kinetic simulation, and qualitative agreement between simulation and derived analytical model is achieved. The inverse sheath is always coupled with a plasma consisting only hydrogen ions with approximately zero electron concentration, reminiscent of the ion-ion plasma reported in previous NBI experiments.

1 Background and modelling

For future high-power fusion reactors such as ITER and DEMO, neutral beam injection (NBI) is crucial to provide sufficient heating and current drive. Negative hydrogen ion (H^-) source is widely employed in the NBI system due to the high neutralization efficiency of H^- at high energy levels. The maximum delivered current density of surface-produced H^- is however limited by the space charge effect, where a space-charge limited (SCL) sheath is assumed to be formed in front of the H^--emitting surface. The SCL sheath strongly accelerates H^- which undermines its extraction efficiency. This contribution is thus motivated and aims at addressing this issue with alternative sheath structure in the extraction region of negative ion source.

A 1D1V continuum, kinetic simulation model is constructed to simulate the H^- extraction region in the negative ion source for NBI heating, Fig. 1. Constant H^- emission flux is injected from the grid electrode and the source region represents plasmas transported from the expansion region. The code evolves the velocity distribution functions of H^+, H^-, and electron according to the Boltzmann kinetic equation and BKG collision operator is chosen for H^+ charge exchange collision.

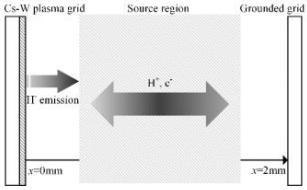

Fig. 1. Schematic of H^- source and the plasma extraction region.

2 Results and conclusions

The observed electronegative inverse sheath near the H^--emitting surface features negative plasma potential relative to wall and hence no H^- acceleration. The bulk plasma is mainly formed by H^+ and H^-, Fig. 2. The formation of the inverse sheath instead of the widely-believed SCL sheath is due to the H^+ charge exchange collision, which creates cold H^+ trapped in the SCL sheath potential well and eventually destroys the entire SCL sheath. Electrons are not confined by the inverse sheath, therefore steady-state electron concentration is low.

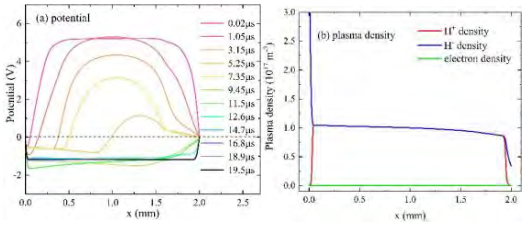

Fig. 2. Inverse sheath potential and plasma density.

The extraction efficiency of created H^- decreases with the H^- energy when injected to plasma, as higher initial energy leads to larger Larmor radius and longer transport path, hence more volumetric losses. The feasibility of using inverse sheath to improve H^- extraction is supported by previous NBI experiments where similar ion-ion plasma associated with the inverse sheath was reported [1].

References

[1] Schiesko L et al. Plasma Physics and Controlled Fusion **53** 085029 (2011)

Investigating the spatial distribution of nitrogen plasma species using saturated cavity ring-down spectroscopy

C. Kniebe-Evans[1], R. Peverall[1], S. D. A. Rogers[1,2], A. L. Vitos[1], and G. A. D. Ritchie[1]

[1] *Department of Physical &Theoretical Chemistry,University of Oxford., United Kingdom*
[2] *Wolfson Atmospheric Chemistry Laboratory, Department of Chemistry, University of York, United Kingdom*

Saturated cavity ring down spectroscopy is utilised to determine number densities and gas temperatures of key trace species $N_2^+(X)$ and $N_2(A)$ in a low pressure ICP. Depending on plasma conditions, ion number densities of ≈ 1×10^{10} cm^{-3} and translational temperatures ≈ 1000 K for $N_2^+(X)$ are observed. The bulk-plasma rotational and vibrational temperatures of $N_2(A)$ have been determined to be ≈525 K and ≈5000 K respectively in experiments conducted at 300 W and 100 mTorr. The studies are extended into the plasma-surface boundary layers to quantify absolute number densities as a function of height above a non-driven electrode. A clear decrease in absolute $N_2^+(X)$ (v = 0) number density is observed as the electrode is approached, with a more gradual decrease for the $N_2(A)$ metastable species.

Saturated cavity ring-down spectroscopy (sat-CRDS) is an absolute, high resolution, calibration-free experimental technique for sensitive measurements of plasma species number densities and temperatures. Selective rotational lines and vibrational bands within the N_2^+ ($A\,^2\Pi_u \leftarrow X\,^2\Sigma_g^+$) and the N_2 ($B\,^3\Pi_g \leftarrow A\,^3\Sigma_u^+$) electronic transitions have been studied in a low pressure inductively coupled nitrogen plasma.

Numerically verified methods have been implemented to quantify optical saturation effects and allow absolute number densities to be determined. In the plasma bulk, experiments conducted across a matrix of pressure (10−100 mTorr) and rf powers (200−400 W) return maximum ion number densities of ≈ 1×10^{10} cm^{-3}. Translational temperatures lie in the range 650−1400 K and 550−1000 K for $N_2^+(X)$ and $N_2(A)$ respectively. The bulk-plasma vibrational temperature of $N_2(A)$ has been determined to be ≈5000 K and the bulk-plasma rotational temperature ≈525 K (at 300 W, 100 mTorr). Trends in ion translational temperature with plasma pressure and rf power are compared to those observed for $N_2(A)$. The sat-CRDS data is supported by previous CEAS measurements. [1]

To effectively probe the plasma-surface boundary region of the plasma with sub-mm resolution, a novel 'wavelength switching' experimental technique is used and absolute number densities as a function of height above the non-driven electrode are quantified. Recorded number densities for $N_2(A)$ are an order of magnitude greater than for $N_2^+(X)$, with maximum bulk values of ≈ 1×10^{11} cm^{-3}. A clear decrease in $N_2^+(X)$ (v = 0) number density is observed as the electrode is approached, with a weaker effect observed for the $N_2(A)$ metastable species. This consolidates (with greater spatial resolution) previous work by Woodcock et al.[2] where the acceleration of ions towards the driven electrode in a CCP chamber was resolved by the use of LIF. Further height profiles are obtained to explore spatial differences in number density as a function of bias voltage applied to the non-driven electrode.

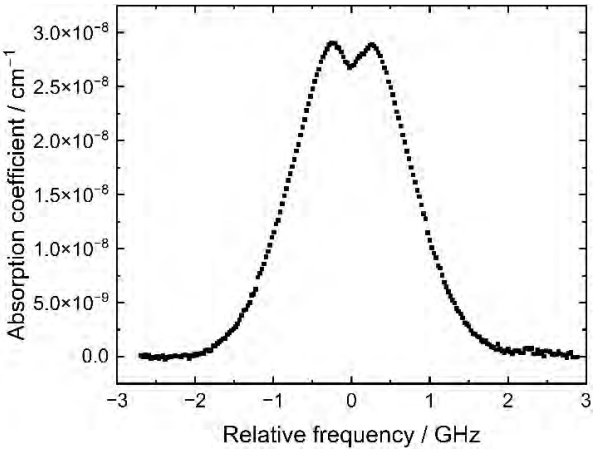

Figure 1: N_2^+ ($A \leftarrow X$) ((2,0) band) saturated absorption profile recorded under conditions of 300 W rf power and 50 mTorr pressure for the $^pP_{22}(7.5)$ transition, showing a prominent Lamb dip.

References

[1] Bakowski B, Hancock G, Peverall R, Ritchie G A D, Thornton L J. Characterization of an inductively coupled N2 plasma using sensitive diode laser spectroscopy. J.Phys D: Appl. Phys. **37**, 2064 (2004).

[2] Woodcock B K, Busby J R, Freegarde T G M, and Hancock G. Doppler spectroscopic measurements of sheath ion velocities in radio-frequency plasmas. Journal of Applied Physics **81**, 5945 (1997).

Experimental investigation of oscillations in a magnetic nozzle

Davide Maddaloni[1], Jaume Navarro-Cavallé[1], Mario Merino[1], and Filippo Terragni[2]

[1] *Equipo de Propulsión Espacial y Plasmas (EP2), Universidad Carlos III de Madrid, Leganés, Spain*
[2] *G. Millán Institute and Department of Mathematics, Universidad Carlos III de Madrid, Leganés, Spain*

Oscillations within the plume of a Helicon Plasma Thruster (HPT) prototype are experimentally collected, analyzed, and discussed. The data is gathered by means of an array of fluctuating Langmuir probes displaced and experimental dispersion diagrams are recovered. Results show a different oscillatory behavior depending on the analyzed position and operating regime.

1 Introduction

Electrodeless Plasma Thrusters (EPTs) [1, 2] promise several improvements over mature electric propulsion devices. Namely, the absence of electrodes, whose erosion gradually affects the performances, would bring extended lifespans, potentially allowing for longer space missions. However, performances of such type of thrusters are still poor [3]. Turbulence, oscillations, and instabilities, which are known to exist in other devices such as Hall effect thrusters, are commonly invoked as plausible explanations for their poor efficiency.

2 Methodology

This work aims at exploring and characterizing the existence of oscillations in the magnetic nozzle of a HPT, by measuring the floating potential of an array of time-resolved probes. This setup allows to resolve the wavenumber components both in the azimuthal and the axial direction, and frequencies up to 50 MHz. Data are collected at several distinct axial and azimuthal positions within the plume and for three different mass flow rate conditions: 5 SCCM, 10 SCCM, and 20 SCCM.

3 Results

Experimental dispersion diagrams are recovered by means of the PSD2P (Two-Points Power Spectral Density) technique [4]. A prominent broadband azimuthal oscillation in the diamagnetic drift direction in the 0–200 kHz range displays at the side of the plume, with a noticeable cross-power contribution in the 40–80 kHz range [5, 6]. Plasma parameters such as density, density gradient, and electron temperature are recovered from time-averaged data, allowing to reconstruct the analytical dispersion relation for the drift wave and compare it with the experimental one, providing a justification for the nature of the oscillation [7]. Additionally, milder fluctuations of different nature are visible along the centreline, close to the thruster nozzle, below 5 kHz.

References

[1] Navarro-Cavallé, J., Wijnen, M., Fajardo, P. & Ahedo, E. Experimental characterization of a 1 kw helicon plasma thruster. *Vacuum* **149**, 69–73 (2018).

[2] Jarrige, J., Elias, P., Cannat, F. & Packan, D. Characterization of a coaxial ecr plasma thruster. In *44th AIAA Plasmadynamics and Lasers Conference, San Diego* (2013).

[3] Ahedo, E. Plasmas for space propulsion. *Plasma Physics and Controlled Fusion* **53**, 124037 (2011). URL `http://stacks.iop.org/0741-3335/53/i=12/a=124037`.

[4] Beall, J., Kim, Y. & Powers, E. Estimation of wavenumber and frequency spectra using fixed probe pairs. *Journal of Applied Physics* **53**, 3933–3940 (1982).

[5] Hepner, S., Wachs, B. & Jorns, B. Wave-driven non-classical electron transport in a low temperature magnetically expanding plasma. *Applied Physics Letters* **116**, 263502 (2020).

[6] Takahashi, K., Charles, C. & Boswell, R. W. Wave-driven electron inward transport in a magnetic nozzle. *Scientific reports* **12**, 20137 (2022).

[7] Swanson, D. *Plasma Waves, 2nd Edition* (IOP Publishing, Bristol, UK, 2003).

Simulating Transformer Coupling and kHz Pulsing in a Toroidal Wave Heated Remote Plasma Source

Scott J. Doyle[1], Amanda Larson[2], Guy Rosenzweig[2], Ilya Pokidov[2], James Gunn[2], and Mark J. Kushner[1]

[1]*Electrical Engineering and Computer Science Department, University of Michigan, Ann Arbor, MI 48109-2122, USA*
[2]*MKS Instruments, 90 Industrial Way, Wilmington, MA 01887, USA*

In this work, control of the spatio-temporal dissociation and ionisation in a simulated transformer-coupled radio-frequency remote plasma source was achieved through the development of a novel transformer surface current model. Simulations were performed employing the Hybrid Plasma Equipment Model. The location of maximum induced power was found to vary with respect to the applied current frequency, with higher frequencies (> 1 MHz) depositing power adjacent to the solenoid antennae, while lower frequencies (< 1 MHz) more effectively coupled power through the transformer ferrites. Synchronous and asynchronous KHz pulsing of the two solenoid winding currents was also investigated. The demonstrated capability to control the spatial power deposition and dissociation fraction of molecular gases in remote plasma sources via geometric and electrical methods, is important to equipment design.

Remote plasma sources facilitate the production of neutral radicals for use in materials processing reactors, which themselves cannot withstand exposure to charged species and radiative fluxes. In this paper, results from 2D fluid/Monte-Carlo simulations of a novel transformer-coupled radio-frequency toroidal plasma source are presented for discharges in argon and NF_3 at pressures of a few Torr. The development of a new transformer surface current model is discussed, and the impact of transformer geometry on the induced electric field topology is presented. The degree to which the applied power, current frequency, and pulsing frequency alter the steady-state dissociation, ionisation fraction, and neutral species transport is addressed. Complete dissociation of 500 sccm of NF_3 was observed for applied powers above 300 W, and neutral fluorine fluxes ranging $1x10^{17\text{-}18}$ (cm^{-2} s^{-1}) were obtained for powers in the range 0.1 – 1 kW. Control of the spatio-temporal inductive power deposition was studied for varying applied current amplitude and frequency, where high frequencies (> 1 MHz) result in narrower regions of dissociation adjacent to the inboard wall. The application of synchronous and asynchronous kHz pulses will also be discussed with respect to the neutral radical transit and recombination timescales. Neutral gas and surface heating are included in the model, and the degree to which surface recombination of neutral radicals may be mitigated is also addressed.

This work was supported by MKS Instruments, US Department of Energy Office of Fusion Energy Sciences and US National Science Foundation.

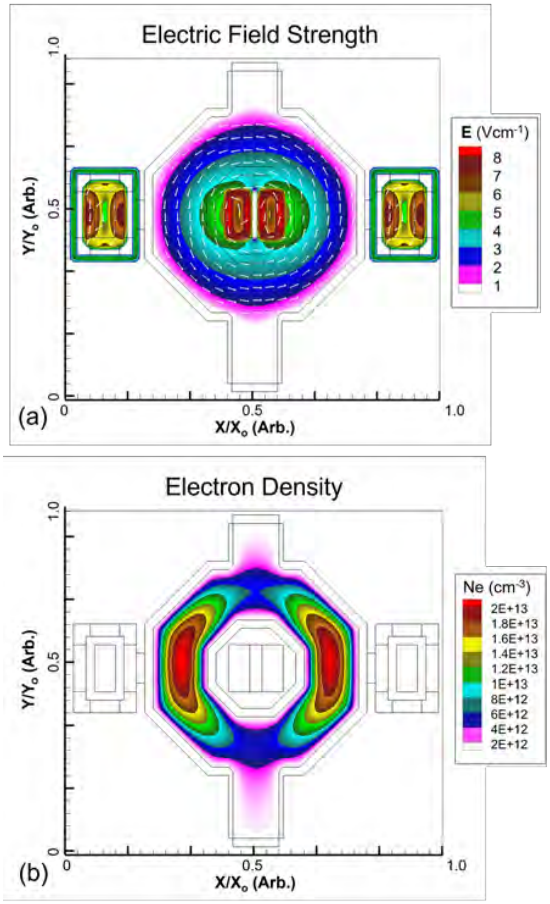

Figure 1 – Top-down view of a simulated toroidal remote plasma source showing (a) the total transformer-coupled electric field strength and orientation (arbitrary vector arrow scale) and (b) the phase-averaged electron density for a 1 kW, 400 kHz discharge in 1 Torr of argon.

Leaky wave discharges in a printed transmission line

L. Fuster[1,2,3], R. Pascaud[3], T. Callegari[1] and P. Hoffmann[2]

[1] *LAPLACE, Université de Toulouse, France*
[2] *CEA, DAM, CEA-Gramat, France*
[3] *ISAE-SUPAERO, Université de Toulouse, France*

This communication presents the mechanism of power coupling between a steady-state plasma discharge and a microwave signal guided in a suspended microstrip line. The propagation of the microwaves is analytically explored in the case of a uniform Argon plasma at 10 Torr. A preliminary study without plasma allows to show that the propagation modes may be of two different types: surface waves and leaky waves. Although the mode in the line without plasma at 3 GHz is a surface wave, the microwave power appears to be coupled to the discharge through a leaky wave.

1 General

With the improvement of power electronics and the emergence of powerful microwave sources, the necessity of developping supllies in order to protect the receiver systems becomes more and more important. A new topology of plasma-based limiter (see fig. 1) that can handle high-power threats has thus been proposed, and the interaction between the discharge and the microwave has first been studied both experimentally and numerically [1]. In this communication we present an analytical exploration of the microwave/plasma coupling mechanism.

2 Modal analysis

The propagation of electromagnetic signals in inhomogenous media has been well studied in the area of antennas [2]. For our work, the Maxwell's equations have been analytically solved in a 2D geometry (see fig. 1), and a modal analysis of the line has been completed. Two differents types of propagation can occur in this topology: surface waves and leaky waves. Although the structure of the line looks like a surfatron's one, the elctromagnetic power is coupled to the plasma through leaky waves and not surface waves.

References

[1] Fuster, L. *et al.* Plasma-based microwave power limitation in a printed transmission line: a self-consistent model compared with experimental data. *Plasma Sources Science and Technology* **31**, 025009 (2022).

[2] Balosso, O., Sokoloff, J. & Bolioli, S. Brief overview about surface wave theory and applications. In *2012 15 International Symposium on Antenna Technology and Applied Electromagnetics*, 1–7 (2012).

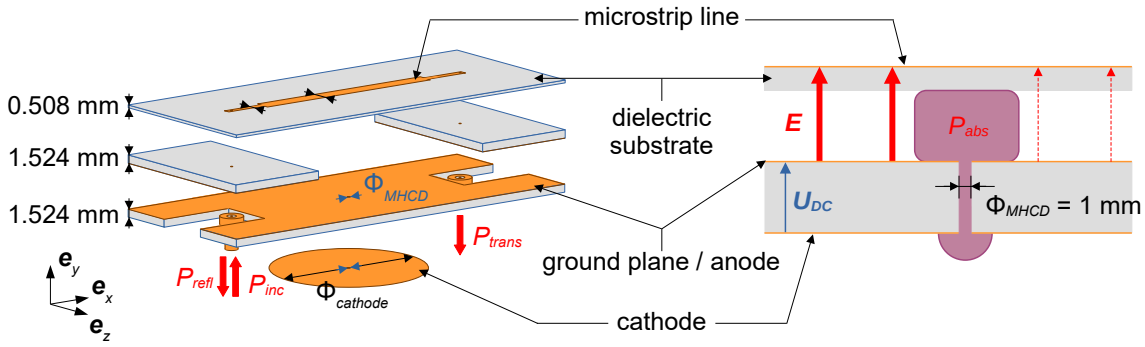

Figure 1: Topology of the microstrip transmission line integrating a Micro Hollow Cathode Discharge.

Effect of pulse repetition frequency on reactive oxygen species production in a pulsed He + H_2O plasma

Benjamin Harris[1], Erik Wagenaars[1]

[1] *York Plasma Institute, School of Physics, Engineering and Technology, University of York, York, UK*

The pulse repetition frequency of a ns-pulsed pin-to-pin He+H_2O discharge is varied to determine its influence on the densities of reactive oxygen species. The plasma is simulated using a 0D plasma-chemical kinetics model. Short-lived radical and electron densities are found to increase with repetition rate due to a reduced afterglow period, leading to higher densities at the start of the next pulse. For species with longer lifetimes, e.g. H_2O_2 and O_3, the dependence is more complex. These species are mainly formed during the afterglow, meaning their density depends on the availability of parent species and on the afterglow duration. This means that pulse repetition frequency is not a simple control parameter and detailed modelling is needed for accurate control of species densities using repetition frequency.

1 Introduction

Nanosecond-pulsed helium plasmas with admixtures of water vapour are known to generate a multitude of reactive species, including OH, H_2O_2, and O_3, that relevant for applications. In this study, the effect of pulse repetition frequency on the overall plasma chemistry is investigated through modelling for a pin-pin discharge of constant pulse duration.

2 Methodology

The plasma is modelled using the zero-dimensional chemical kinetics model GlobalKin, with a He+H_2O chemistry set [1,2]. The plasma is generated in He gas with 0.25% water, using a negative voltage pulse with an amplitude of 2.3 kV, a rise time of 3 ns and a duration of roughly 80 ns [3].

3 Results and discussion

Species densities are analysed after several pulses when all species have reached equilibrium. It is found that the densities of species with short lifetimes, such as O, H, OH, and e^-, increase consistently with pulse frequency. An example of this is shown in the case of OH, in Figure 1.

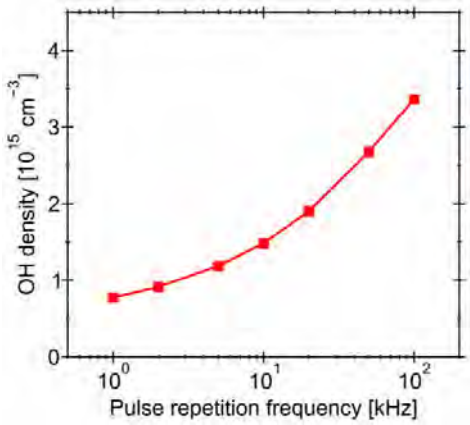

Fig.1: OH density as a function of pulse frequency

Longer-lived species, e.g. H_2O_2 and O_3, exhibit a more complex relationship with the frequency, such as that shown for H_2O_2 in Figure 2.

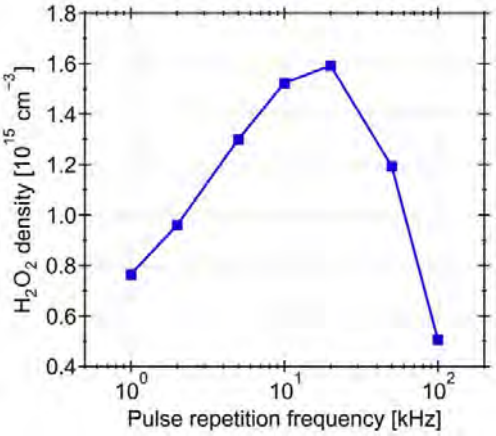

Fig.2: H_2O_2 density as a function of pulse frequency.

Despite the density of OH having a positive relationship with pulse frequency and the dominant reaction producing H_2O_2 being the three-body recombination of two OH radicals, the density of H_2O_2 peaks at 20 kHz and decreases steeply at higher frequencies. Reaction pathway analysis shows that this is because of a reduced afterglow time, during which the H_2O_2 production mainly occurs and an increased gas temperature. It shows that pulse repetition frequency is not a simple control parameter for optimising radical production. Reaction pathways change with frequency and detailed modelling is needed for accurate control.

References

[1] A. M. Lietz and M. J. Kushner, J. Phys. D: Appl. Phys., **49** 425204 (2016).

[2] A. Brisset *et al.* , J. Phys. D: Appl. Phys., **54** 285201 (2021).

[3] B. Harris, E. Wagenaars, J. Phys. D: Appl. Phys. submitted (2023).

Cylindrical SDBD of well-defined expansion area for standardized studies

K. Giotis[1,2], P. Svarnas[1], M. Mitrou[1,3], K. Gazeli[2], G. Lombardi[2] and S. Béchu[3]

[1]*Univ. of Patras, Electrical & Computer Eng. Dept., High Voltage Lab., 26 504 Rion, Patras, Greece*
[2]*Univ. Sorbonne Paris Nord, LSPM, CNRS, 8 UPR 3407, F-93430 Villetaneuse, France*
[3]*Univ. Grenoble Alpes, CNRS, Grenoble INP (Institute of Engineering), LPSC-IN2P3, 38000 Grenoble, France*

The present work lies in the field of atmospheric-pressure surface dielectric-barrier discharges (SDBDs). A tailored experimental cylindrical setup is presented, by which the SDBD expansion area is well defined, avoiding any underside discharge. Preliminary electrical and optical emission results are reported.

1. Introduction

Surface dielectric-barrier discharge (SDBD) is a special case of DBD, in that there exists at least one path along which the two electrodes may be linked through the dielectric barrier exclusively, i.e., without the inclusion of air gap. The incentive for SDBD studies rises from the various cutting-edge applications [1]. Most of the relative setups refer to planar geometries where, depending on how adeptly (ineptly) is encapsulated the lower electrode, the involvement of the underside discharge to the setup operation is to a large (small) extent eliminated [2]. Herein, an underside-discharge-free SDBD is considered and suggested for standardized studies.

2. Experimental Setup

The design of the present SDBD reactor and the installed diagnostics (broadband electrical recorders and optical emission spectroscopy, OES) are depicted in Fig. 1. The use of oil of high dielectric strength (> 1 MV cm^{-1}) excludes any plasma formation in the inner-underside surface of the quartz tube.

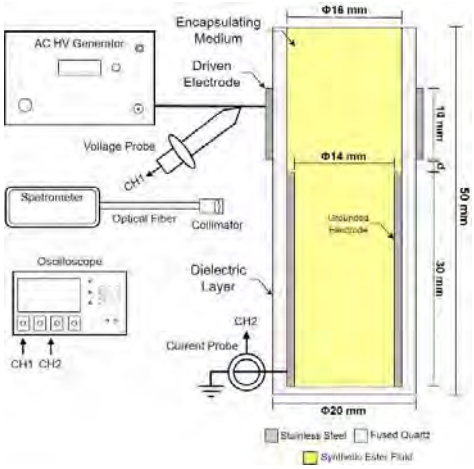

Figure 1. Surface DBD oil-filled reactor and diagnostics.

3. Results – Conclusions

Fig. 2a provides representative voltage and current waveforms, while Fig. 2b the mean power consumed by the DBD, as a function of the applied voltage, for three different interelectrode gaps; *d* in Fig. 1. Firstly,

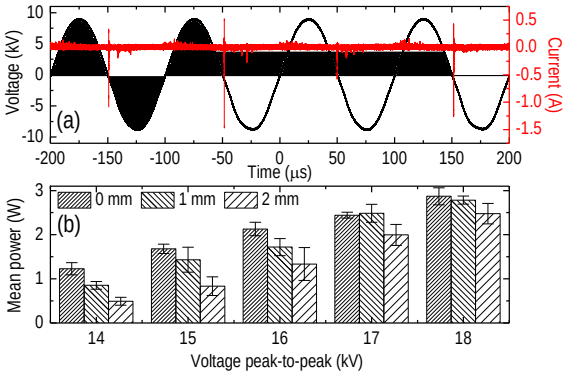

Figure 2. (a) Typical waveforms of the 10 kHz driving high voltage and the induced SDBD current. (b) Mean power versus the applied voltage for three different gaps.

it is suggested that the high current impulses formed during the negative slope of the driving voltage are distinct inherent features of the SDBD and should not mistakenly be attributed to any underside ionization. They are rather related to the release of charge being previously built-up on the dielectric surface. Then, wider gap weakens the discharge for a given applied voltage, and lower power is thus consumed.

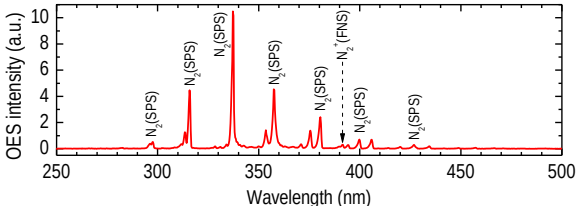

Figure 3. Optical emission spectrum, calibrated in terms of relative spectral efficiency, and species identification.

Finally, Fig. 3 unveils the main emissive species detected in the present SDBD, i.e., N_2 second positive system (SPS) and N_2^+ first negative system (FNS). The latter play a certain role in the electro-fluid-dynamic features of the present SBSD.

References

[1] Leonov S. B. *et al.* Plasma Sources Sci. Technol. **25**, 063001 (2016).
[2] Laurentie J.-C. *et al.* J. Electrostat. **67**, 93 (2009).

Electron density and temperature in a diffuse nanosecond pulse discharge in air at atmospheric pressure

A. Brisset[1], T. guenin[1], P. Tardiveau[1] and A. Sobota[2]

[1] *Université Paris-Saclay, CNRS, LPGP, 91405 Orsay, France*
[2] *Dept. of Applied Physics, Eindhoven University of Technology, PO Box 513, 5600 MB, Eindhoven, The Netherlands*

Preliminary results on the electron properties of a ns diffuse fast ionization wave generated under very strong overvoltage in synthetic dry air were obtained. Both n_e and T_e are investigated by Incoherent Thomson Scattering. n_e is also derived by Optical Emission Spectroscopy from the Stark broadening of excited oxygen lines locally. Most of the volume of the pin-to-plane discharge is quite representative of a quasi-steady state glow discharge characterized by rather homogeneous properties close to the axis with $n_e \sim 10^{15}$ cm^{-3} and T_e ~3 eV within the whole air gap. About 6 ns after the start of the discharge, a sub-millimetric region of strong ionization develops at the pin, which is consistent with the observation of a continuum of emission spreading from the UV to the near-IR spectral range. Within this part of the discharge, n_e reaches values greater than 10^{17} cm^{-3} with an ionization degree higher than 1%. The radiative recombination of nitrogen ions N_2^+ and the three-body recombination of N^+ could explain the continuum.

Plasma sources of large volume and highly stable where discharge properties are relatively uniform are particularly attractive. They can be produced in air by the application of very high overvoltages in the sub-nanosecond range. In the present work, a voltage rise rate of about 50 kV.ns^{-1} is applied in a pin-to-plane electrode configuration which generates the specific features of a diffuse fast ionisation wave. Recently, it was demonstrated that the electric field distribution of the diffuse fast ionisation wave differs from that of low voltage streamer discharges [1]. In particular, the electric field shielding is less efficient under strong overvoltage conditions. The objective of this work is to answer the question: What can be the impact of a specific field distribution obtained at very high overvoltage on the electron properties and how may it differ from streamer discharges characteristics? For that purpose, Thomson scattering is first used to determine electron density and temperature in the main part of the gap down to 1.3 mm from the pin and throughout the 10 ns voltage pulse. Very close to the pin, the mean electron temperature gets higher and the Thomson signal spectrally spreads so that it cannot be suitably deconvoluted. Stark broadening analysis is therefore achieved in that region, where the emission intensity and the oxygen excitation are very high.

Results revealed that the discharge splits into two distinct regions over time, having specific characteristics: the gap and the pin region. The gap region (1-18 mm) is rather homogenous and quite representative of typical non-equilibrium ns discharges with electron densities higher than 10^{15} cm^{-3}. This is an order of magnitude higher than in classical streamers and suggests a strong discharge reactivity at T_{gas} = 300 K.

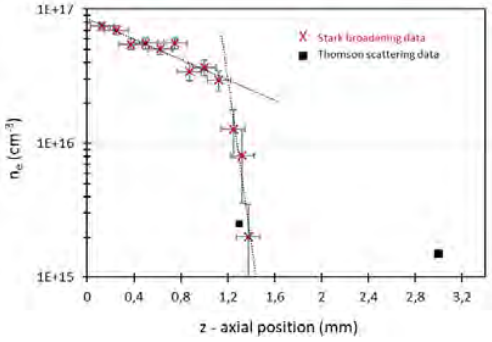

Figure 1: Electron density along the axis of the discharge

The emission is dominated by the first and the second positive systems of molecular nitrogen. From 6 ns onwards, a region of strong ionization develops in the close vicinity of the pin (< 1 mm) with densities close to 5.10^{16} cm^{-3}. There, at the same time as the reduced electric field reaches about 700 Td, lines of atomic nitrogen are detected as well as a continuum emission. A net drop of the electron density along the axis clearly identifies the limit between the two regions of the discharge. The radiative recombination of N_2^+ and N^+ with electrons contribute to the observed continuum of emission spreading from the UV to the near-IR.

References

[1] Brisset A *et al.* PSST 28 (2019) 055016
[2] Shcherbanev S A *et al.* PSST **26** 02LT01

Shape Control of Surface-Launched Plasma Bullets

T. Shirafuji and J.-S. Oh

[1] *Dept. Physics and Electronics, Osaka Metropolitan University, Osaka, Japan*

Surface-launched plasma bullets (SLPBs) can be launched vertically from a planar dielectric plate unlike conventional APPJ. We discuss the method to control the shape of SLPBs by using electrode-shape design. The typical shape of conventional plasma bullets is limited to elongated balls or comets. Our numerical simulation of SLBPs revealed that they can be in the shape of a ring or dome.

1 Introduction

Plasma bullets are generally launched from the nozzle of a DBD tube with helium gas. Recently, we have discovered that plasma bullets can be launched vertically from a planar surface of a dielectric plate if we employ the pulse power with very high dV/dt [1]. We call them surface-launched plasma bullets (SLPBs).

Various possibilities are opened up by eliminating the restriction of "only launching from the nozzle". For example, the SLPBs can hydrophilize the entire inner surfaces of 3D-printed PLA bone-regeneration scaffolds (continuous porous dielectrics) while conventional APPJs cannot [2]. Furthermore, it may be possible to design the shape of the bullets in contrast to the fact that the shape of conventional plasma bullets is limited to elongated balls or comets.

In this study, we investigated the possibility of controlling the shape of a bullet by using a dielectric electrode with a tapered shape.

2. Description of the model

The shape of the reactors examined in this study are shown in **Fig. 1**. The grounded electrode (GND) is on the top and powered electrode (HV) is on the bottom. We examined two bottom-electrode shapes of (a) a planar plate and (b) a tapered plate. The discharge gas was a mixture of 0.1% N_2 and 99.9% He. Applied voltage on the bottom was (15 kV){1−exp(−t/τ)}, where τ was 10 ns. Numerical simulation was performed using an axisymmetric fluid model coupled with Poisson equation and Boltzmann solver (BOLSIG+). Gas-phase reactions in this model were electron impact ionization of He, excitation of He to metastable state, and penning ionization of N_2 by metastable He. Photo ionization was not involved in the model.

3. Results and discussion

Figure 1(a) shows bullet propagation in the case of the planar bottom electrode, in which the bullet is launched from the outer edge of the HV electrode due to the electric-field enhancement at the edge. Resulting bullet is ring-shaped.

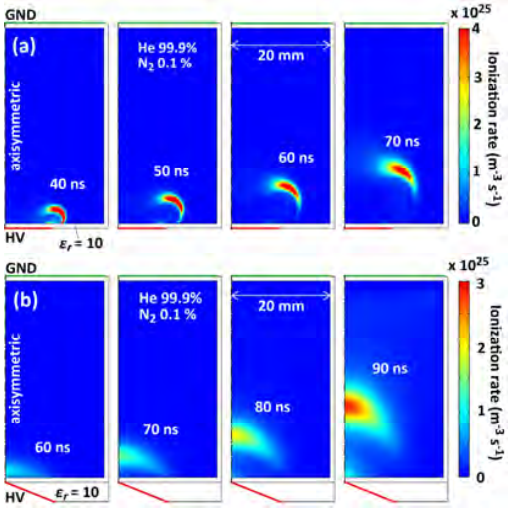

Fig. 1 Generation of SLPBs having different shapes. (a) Ring shaped and (b) dome shaped.

Figure 1(b) shows bullet propagation in the case of the tapered bottom electrode, in which the edge effect is weakened due to thicker dielectric on the outer edge of the bottom electrode. The shape of the launched bullet becomes dome-shaped instead of ring-shaped owing to the weakened edge effect.

The results obtained in this study suggest that sheet-like plasma bullet, which corresponds to large volume atmospheric pressure plasma, may also be possible by properly designing the electrode shape.

Acknowledgments

This work was partly supported by the Grant-in-Aid by JSPS/MEXT, Japan (19H01888, 19K03811, and 20K20913), and the joint usage / research program of center for Low-temperature Plasma Science, Nagoya University.

References

[1] Shirafuji, T. and Oh, J.-S. 11th Int. Conf. Reactive Plasmas / 2022 Gaseous Electronics Conf., ER5.00006 (2022).

[2] Shirafuji, T. et al. 42nd Int. Symp. Dry Process, H-1 (2021).

The influence of non-thermal Ar plasma jet on physicochemical properties of treated liquid

O. Jovanović[1], N. Puač[1] and N. Škoro[2]

[1] *Institute of Physics, University of Belgrade, Pregrevica 118, 11080 Belgrade, Serbia*

We investigated an atmospheric pressure plasma jet (APPJ) that generates a streamer discharge above the liquid sample. In order to create plasma-activated water (PAW), the device was used for treating both distilled and tap water. The working gases were Ar and an admixture of Ar and synthetic air. Optical characterization of the plasma gas phase showed that the streamer discharge, in addition to the excited Ar lines, produces an abundance of reactive oxygen and nitrogen species (RONS) above and in the treated water. The measurement of the physicochemical properties of PAWs showed that different types and concentrations of the measured RONS (H_2O_2, NO_3^-, NO_2^-) were formed in different targets.

1 Introduction

The development of APPJs in recent years has been initiated by applications in various fields, among which are biomedicine [1-2] and plasma agriculture [3]. In these fields, plasma-treated liquids play an essential role [4]. In order to always provide the same treatment conditions, ensure the safety of the target and improve the properties of the treated liquid, a thorough study of these systems is necessary.

Here we will present the results of the influence of parameters such as feed gas, treatment time, sample properties and treated volume on the creation of reactive species in both the gas and liquid phase.

2 Experimental setup

In this work, we employed APPJ with pin electrode configuration that operated in kHz regime. As a working gas we used Ar and Ar+Air and plasma was generated above the liquid sample. Electrical characterization and discharge power measurement were conducted to acquire additional information about the treatments' stability, plasma properties and impact of plasma parameters on PAW. We have used spectrally resolved imaging and optical emission spectroscopy for determination and spatial distribution of excited species created in plasma-liquid interaction. We have treated distilled and tap water samples for different treatment times. After treatments, detailed liquid sample diagnostics including electrical conductivity, temperature, pH and RONS measurement were performed.

3 Results and conclusion

Figure 1 shows recorded optical emission spectra of Ar discharge (gas flow 1slm) from the gas gap between the powered electrode and water surface. The right hand side of Figure 1 represents the discharge structure captured by ICCD with addition of the optical filter (@310nm). A correlation between plasma and liquid properties has been established over a wide variety of plasma parameters and liquid targets. The obtained results demonstrated a link between the formation of RONS in the gas phase and in PAW.

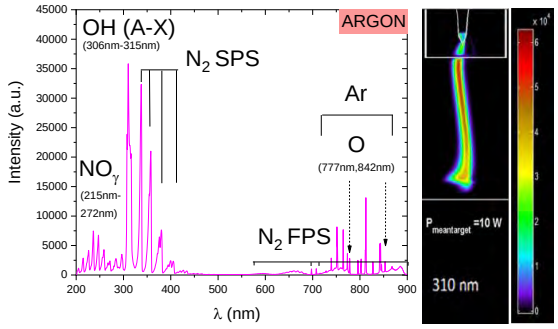

Fig. 1. The obtained optical spectra of Ar plasma above the water sample (left) and the ICCD image of discharge recorded by using 310nm optical filter (right).

Acknowledgment

This work was supported by: The Science Fund of the Republic of Serbia, 7739780, Atmospheric pressure plasmas operating in wide frequency range – a new tool for production of biologically relevant reactive species for applications in biomedicine - APPerTAin- BIOM and by MSTDI Republic of Serbia grant number 451-03-68/2022-14/200024.

References

[1] Kaushik, N. K. et al., Plasma and nanomaterials: Fabrication and biomedical applications. Nanomaterials, 9(1), p98 (2019).

[2] Tomić, S. et al., Plasma-activated medium potentiates the immunogenicity of tumor cell lysates for dendritic cell-based cancer vaccines. Cancers, 13(7), p.1626 (2021).

[3] Puač, N. et al., Plasma agriculture: A rapidly emerging field. Plasma processes and polymers, 15(2), p.1700174 (2018).

[4] Bradu, C. Et al., Reactive nitrogen species in plasma-activated water: generation, chemistry and application in agriculture. Journal of Physics D: Applied Physics, 53(22), p.223001 (2020).

Spatially resolved spectra in an atmospheric pressure DC glow plasma emission with liquid anode

Z. Yang[1], M. García[2] and J. E. Foster[1]

[1] *Department of Nuclear Engineering and Radiological Sciences, University of Michigan, Ann Arbor 40109, United States of America*

[2] *Department of Applied Physics, University of Cordoba, Ed-C2, Campus de Rabanales, Córdoba, 14071, Spain*

Non-thermal atmospheric pressure plasma-liquid interaction has gained lots of interest for its wide application, while the millimetre size and atmospheric pressure cause many trouble and limitation for diagnostics. Although non-invasive optical emission spectroscopy is suitable at this scenario, obtaining the detailed species emission and plasma properties at critical position (sheath, plasma-liquid interface, etc) of an atmospheric pressure plasma is not easy with a fiber which integrates the light at line-of-sight. It has been shown that a Czerny-Turner spectrograph equipped with an intensified charge-coupled device as a detector can acquire a spatial resolved emission spectra by focusing the plasma image directly on slit [1]. Here we present the spatial spectra map of a 1 atm DC glow discharge with liquid anode. Fig.1 depicts a preliminary spatial map of nitrogen emission along the discharge column. The change of the gas temperature along the discharge column is also examined. The goal of this work is to provide insight into discharge structure particularly in the positive column and to assess how such heterogeneity influences self organization at the anode surface.

*This work is supported by the National Science Foundation ECLIPSE program Award No. 2206039.

References

[1] Álvarez, R., M. C. Quintero, and A. Rodero. Spectrochimica Acta Part B: Atomic Spectroscopy 59.5 (2004): 709-721

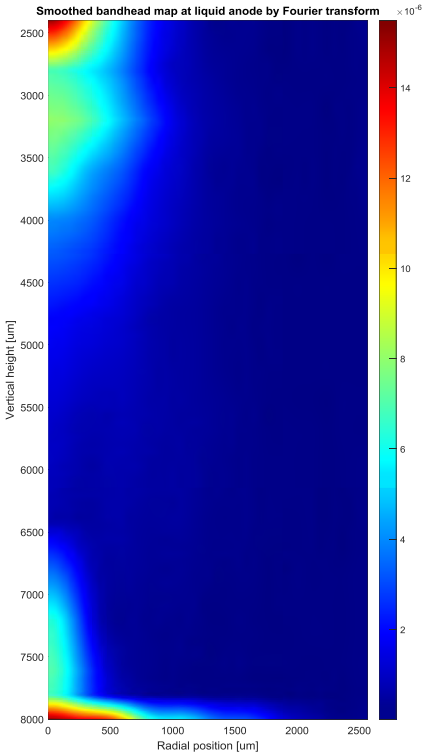

Fig. 1 Axial nitrogen SPS band emission along the plasma column.

XXXV ICPIG, July 9-14, 2023, Egmond aan Zee, The Netherlands Topic number 12, 16

Effluent nozzles in Reverse-vortex-stabilized microwave plasmas for performance enhancement

C. van Deursen[1], H.M.S. van Poyer[2], W.A. Bongers[1], F.J.J. Peeters[3], F.M.A. Smits[4], M.C.M. van de Sanden[1,5]

[1]*DIFFER, de Zaale 20, Eindhoven, The Netherlands*

[2]*University of Antwerp, Prinsstraat 13, Antwerp, Belgium*

[3]*LeydenJar, Emmy Noetherweg 2D, Leiden, The Netherlands*

[4]*Leiden Institute of Physics, Leiden University, The Netherlands*

[5]*TU Eindhoven, EIRES and Dept. Applied Physics, The Netherlands*

Abstract: Efficiency and conversion in a reverse-vortex microwave CO_2 dissociation plasma are enhanced by optimizing the thermal trajectories using a converging diverging nozzle. The nozzle mixes cold, unconverted gas at the edge of the flow with hot, active gas in the middle of the flow. Temperature measurements are taken directly before and after the nozzle and presented to elucidate differences in performance. Measurements show significant improvements in conversion, especially at pressures close to atmospheric pressure (500 – 900 mbar). Temperature measurements at plasma height and at the entry of the nozzle suggest that thermal gradient and good mixing are crucial to performance enhancement.

1 Introduction

Plasma conversion is a promising approach in the search for an efficient way to convert CO_2 into CO. Typical plasma efficiencies for CO_2 plasma conversion processes are around 30 - 35 %, as shown by Snoeckx and Bogaerts in their review. [1] The main cause of these low efficiencies is the high rate of back-reactions according to (R.1) and (R.2), which reform a significant part of the CO_2 dissociated in the plasma.

$$CO + O_2 \rightleftharpoons CO_2 + O \quad \text{(R.1)}$$

$$CO + O + M \rightleftharpoons CO_2 + M \quad \text{(R.2)}$$

Recent work by Hecimovic et. al. show that the efficiency of dissociation plasmas can be improved using a constriction in the effluent path. [2] The constriction acts by forcing the mixing of process gas and, depending on conditions, by lowering the pressure after the nozzle.

2 Experimental

Experiments took place in a vortex-stabilized microwave (MW) reactor equipped with 2.45 GHz magnetron with WR340 waveguide components. A quartz tube is inserted inside the rectangular waveguide to form a resonator. A 3-stub tuner was used to ensure efficient coupling. The reactor was utilized in Reverse-vortex configuration in order to stabilize the plasma and protect the quartz tube. Tangentially mounted injection nozzles with inner diameter 0.9 mm were used to induce the vortex flow. The mixing nozzles were designed as De Laval nozzles and were positioned roughly 8 mm below the waveguide.

3 Results

Plasma conversions and efficiencies were determined using a CompactGC 4.0 gas chromatograph and show marked improvements in energy efficiency, especially at near-atmospheric pressures. Both pressure dependance and flow dependance of the CO_2 plasma decrease by introducing the converging diverging nozzle. Temperature measurements before and after the nozzle reveal that, in the RV case, the nozzle induces a sharp gradient before the nozzle, which could induce additional chemistry within the nozzle itself. This appears to be supported by the post-nozzle measurements, where much lower temperatures are measured than without a nozzle.

3 Conclusion

Effluent nozzles can improve RV CO2 dissociation reactor performance by inducing mixing and, subsequently, inducing additional chemistry within the nozzle itself.

4 References

[1] R. Snoeckx and A. Bogaerts, Chemical Society Reviews, **46**, 19 (2017)

[2] A. Hecimovic, F. A. D'Isa, E. Carbone and U. Fantz, Journal of CO_2 utilization, **57** (2022)

Two-dimensional complex plasma with active Janus particles

V. Nosenko[1]

[1] *Institut für Materialphysik im Weltraum, Deutsches Zentrum für Luft- und Raumfahrt (DLR), D-51147 Cologne, Germany*

A two-dimensional complex plasma containing active Janus particles was studied experimentally. A single layer of micron-size plastic microspheres was suspended in the plasma sheath of a radio-frequency discharge in argon at low pressure. The particle sample used was a mixture of regular particles and Janus particles, which were coated on one side with a thin layer of platinum. Unlike a suspension consisting of regular particles only, the suspension with inclusion of Janus particles did not form an ordered lattice in the experimental conditions used. Instead, the particles moved around with high kinetic energy in a disordered suspension. This is explained by the combination of two driving forces, the photophoretic force and the oppositely directed ion drag force. The mean-squared displacement of the particles scaled as t^{α} with $\alpha = 2$ at small times t indicating ballistic motion and $\alpha \approx 0.56$ at longer times due to the combined effect of the Janus particle propensity to move in circular trajectories and external confinement.

1 Introduction

A complex, or dusty plasma is a suspension of nanometer to micrometer size particles of solid matter in a gas-discharge plasma. The particles become charged due to the collection of electrons and ions from plasma and through their interaction and external confinement self-organize into liquid-like or solid-like structures. Complex plasmas are excellent model systems which allow studying of various plasma-specific and generic phenomena at the level of individual particles. Recently, the scope of complex plasmas as model systems was extended to include active matter systems. An example of active, i.e., self-propelling particles in a complex plasma are the so-called Janus particles, which have two sides of different properties.

2 Experimental results and discussion

The experiments were carried out in a modified Gaseous Electronics Conference (GEC) rf reference cell [1]. Plasma was produced by a capacitively coupled rf discharge in argon at 13.56 MHz. The gas pressure was 1.66 Pa, the discharge rf power was 20 W. The particle sample used in our experiments was a mixture of regular melamine formaldehyde (MF) microspheres and active Janus particles, which were MF microspheres coated on one side with a thin layer of platinum. The particles were injected into the plasma from a manual dispenser mounted in the upper flange. They were suspended in the plasma sheath above the lower rf electrode, where they formed a single layer.

As expected, the regular MF particles formed a two-dimensional triangular lattice (plasma crystal) in our experimental conditions. On the contrary, the suspension of the mixed Janus particles did not crystallize. Instead, the particles energetically moved around colliding with each other, see Fig. 1. The pair correlation function for the mixed Janus particles g(r) indicates a highly disordered (gas-like) state.

The mean-squared displacement MSD of the mixed Janus particles scales as MSD(t) $\propto t^{\alpha}$ with $\alpha = 2$ at small times $t \ll \gamma^{-1}$, where γ is the neutral-gas damping rate for the particles, indicating ballistic motion. Here, the particle inertia is important. At later times, the dynamical exponent $\alpha(t)$ declines, finally reaching the value of 0.56±0.27. We ascribe this to the combined effect of the Janus particle propensity to move in circular trajectories due to a combination of the photophoretic force from the illumination laser and the oppositely directed ion drag force and external confinement.

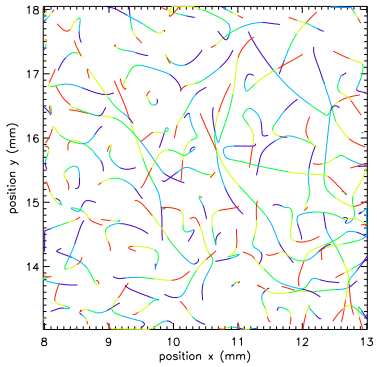

Fig. 1. Trajectories of the mixed Janus particles suspended as a single layer in rf plasma sheath, during 0.6 s (time is color-coded from purple to red).

References

[1] V. Nosenko, Two-dimensional complex (dusty) plasma with active Janus particles, Phys. Plasmas **29**, 123701 (2022).

Investigation of particle charge and interparticle interaction in a plasma

K. Kamataki[1], T. Sato[1], K. Tomita[2], P. Yiming[1], D. Yamashita[1], N. Yamashita[1], N. Itagaki[1] and K. Koga[1,3], M. Shiratani[1]

[1] *Kyushu University Information Science and Electrical Engineering, Japan*
[2] *Hokkaido University, Japan*
[3] *National Institutes for Natural Sciences, Japan*

We experimentally investigated the particle charge in plasma by considering in interaction potential of two charged microparticles. The trajectories of two charged particles in Ar plasma were measured highspeed camera. These results show experimentally the interaction potential of each particle.

1 Introduction

The measurement of sheath electric field in a microscopic space is an important issue for optimizing plasma processing of materials. A lot of different techniques have been developed for the measurement of electric fields in plasmas. Dusty plasmas serve as a unique and commonly used model system to probe plasma environments [1]. One technique to manipulate micro-particles is an optical trap, often named as optical tweezers [2]. we have investigated sensitive measurements of electric field in plasma using a fine particle trapped by the optical tweezers technique. Here, the charge on the particles is a crucial parameter for deriving electric field. However, few reports have been published on determination of the charge on a fine particle in a plasma. In this study, we have investigated measurements of the charge on single fine particle in Ar plasma using central collision experiments [3] of charged fine particles by considering interaction potential of two charged microparticles.

2 Experimental Setup

A plasma reaction vessel was set up in an epi-illumination microscope. This vessel had a metal mesh grounded electrode and a ring-shaped powered electrode, which was placed on the sapphire glass under the vessel. A radio-frequency voltage of 13.56 MHz was applied between the electrodes to generate plasma. When an acrylic particle of 20 μm in diameter (density 1.20 g/cm^3) was introduced into the plasma, it was suspended near the plasma/sheath boundary above the powered ring electrode.

When we put another particle, the collision process was occurred by releasing optical trapped single particle as shown in fig.1.

3 Results and Discussion

The trajectories of two charged particles are mainly determined by the electrical potential around each particle. From the trajectories the relative velocity v_p and the center-to-center distance d of the two particles are extracted. Figures 2 show time evolutions of (a) distance between two particles and (b) kinetic energy of particles system. During the collision, the distance repeatedly increased and decreased, and then, it became constant. The kinetic energy of these particles system was eventually reduced to zero. On the other hand, the interaction potential becomes large. It includes three effects: electrostatic repulsion, attraction due to ion shadowing, and neutral shadowing resulting in attraction or repulsion [4,5]. We will discuss the detail at the conference.

Acknowledgements: This work was partly supported by JSPF KAKENHI (Grant No. JP20H00142) and JSPS Core-to-Core Program (Grant No. JPJSCCA2019002).

References

[1] S. Nunomura, *et al*., Phys. Rev. Lett., 84, 5141 (2000).
[2] A. Ashkin, Biophys. J., **61**, 569 (1992).
[3] U. Konopka, *et al*., Phys. Rev. Lett., **79**, 1269 (1997).
[4] S. A. Khrapak, *et al*., Phys. Rev. E., **64,** 046403 (2001).
[5] S. A. Khrapak, *et al*., Contrib. Plasma Phys., **49,** 3, 148 (2009).

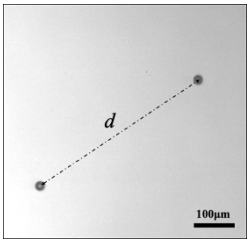

Fig.1 Snapshot of two fine particles which are levitated in a plasma.

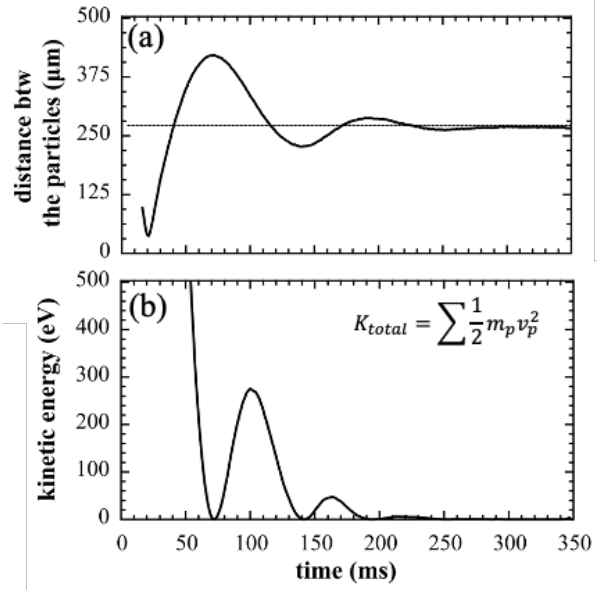

Fig. 2 Time evolutions of (a) distance between two particles and (b) kinetic energy of particles system

Optimization of nanoparticle growth in RF discharge plasma.

Y. Ussenov[1], M. Shneider[1], S. Yatom[2], and Y. Raitses[2]

[1] *Department of Mechanical and Aerospace Engineering, Princeton University, Princeton, USA*
[2] *Princeton Plasma Physics Laboratory, Princeton University, Princeton, USA*

The aim of this work is to optimize the growth process of the nanoparticles in capacitively coupled radio frequency discharge (CCRF) argon/acetylene plasma for further study of the laser-stimulated electron photodetachment effect from the surface of the particles. Dust particles have been grown at different ratios of Ar/C_2H_2 mass flow and 300 – 600 mTorr pressure range for constant 10 W RF power. The particle growth and trapping efficiency were monitored by measuring the DC self-bias voltage change and laser beam light scattered from the nanoparticle cloud.

1 Introduction

Nanometre-sized dust particles can grow in plasma spontaneously during processes such as etching and deposition or can be synthesized with the aim to produce nanoparticles with predefined properties [1]. The diagnostics of the dust particle charge and information on the charging dynamics are crucial not only for the optimization of the nanoparticle synthesis process but also for a deep understanding of the interaction between particles and surrounding plasma. Laser-stimulated electron photodetachment (LSPD) is one of the unique approaches for the study of the charging dynamics, which can be used for in situ measurement of the particle charge in saturation regime if the shift in electron density could be measured precisely and the other particle properties as size and density are known [2]. The theory developed for LSPD from charged metallic nanoparticles in non-thermal plasma shows that threshold laser wavelength for photoelectric effect from particle surface depends not only on the size and material but also on the charge acquired by the nanoparticles (due to the Schottky effect) [3]. In this work, we show the results of the optimization of the carbonaceous nanoparticle growth process in argon/acetylene CCRF plasma.

2 Experiment and Results

Two parallel-plate stainless steel electrodes with 100 mm in diameter and with a 38 mm discharge gap were located in the centre of the cylindrical shape vacuum chamber. 10 W RF power was applied to the bottom electrode by the 13.56 MHz generator through the automatic L-type matching box. Argon with a small amount of acetylene was fed by the mass flow controllers, while the pressure in the plasma chamber was monitored by the convection gauge. Dust particle formation and further growth are controlled by monitoring the discharge DC self-bias voltage. The light scattered from 5 mW, He-Ne (633 nm) laser sheet was used to visually detect the nanoparticle cloud formation and its trapping. Dust particles have been grown at different ratios of Ar/C_2H_2 mass flow rate and 300 – 600 mTorr range for constant 10 W RF power. The results were confirmed by the almost 70% change in the discharge DC self-bias voltage, which is the consequence of the free electron absorption by the nanoparticles after the charging. The nanoparticle growth at lower RF power shows the suppression in grain nucleation while increasing the power to 20 W leads to the deposition of the diamond-like/amorphous carbon films on the surface of the electrodes. The laser light scattered from particles confirms the formation of the “void” in the central region of the dust cloud and the accumulation of the larger particles at the edge of the plasma boundary due to the ion drag force.

3 Acknowledgement

This contribution supported by the U.S. Department of Energy through contract DE-AC02-09CH11466.

4 References

[1] Boufendi L, Jouanny M. Ch., Kovacevic E., Berndt J, and Mikikian M, Dusty plasma for nanotechnology. J. Phys. D: Appl. Phys. 44 174035 (2011).

[2] Staps J.A., Donders M.J.T., Platier B., Beckers J., In-situ measurement of dust charge density in nanodusty plasma, J. Phys. D: Appl. Phys. 55 08LT01 (2022)

[3] Shneider M. N., Raitses Y., Yatom S., Laser-stimulated photodetachment of electrons from metal nanoparticles in plasma, Bulletin of the American Physical Society, BO07.00010 (2022)

Non-equilibrium nitrogen incorporation into ZnO films by rf-magnetron sputtering: stabilization of amorphous phase and noteworthy local structure in crystalline phase by solid phase crystallization

Hisato Yabuta[1], Zhiyuan Shen[1], Yuta Mido[1], Hiroyuki Setoyama[2], Ichiro Hirosawa[2], Naho Itagaki[1]

[1] *Graduate School of Information Science and Electrical Engineering, Kyushu Univ., Fukuoka, Japan*
[2] *Kyushu Sychrotron Light Research Center, Tosu, Saga, Japan*

Annealing of amorphous N-incorporated ZnO films deposited by rf sputtering method supplies high quality polycrystalline ZnO films. We revealed that these films showed notable highly coherent local structure.

1 Introduction

To obtain high quality polycrystalline films, the crystallization process from an amorphous phase by annealing (so-called "solid phase crystallization") is an effective way because polycrystalline films (e.g., poly-Si [1]) through this process often show better crystallinity and conductivity than ones crystallized during deposition on substrates heated to high temperature. However, this method is hardly applicable for ZnO due to difficulty in forming amorphous phase of it even on non-heated substrates.

Recently, we succeeded in obtaining amorphous ZnO films by nitrogen (N) incorporation using non-equilibrium rf-sputtering process [2]. Since the solubility of N into ZnO is extremely low [3], such a non-equilibrium deposition process is suitable for stabilizing N-incorporated ZnO (abbreviated as ZnON) phase. Then the solid phase crystallization from the amorphous ZnON films with desorbing N_2 gas by heating was demonstrated, resulting in relatively highly crystallized polycrystalline ZnO films with flat surface achievable. Furthermore, we discovered that Al-doped ZnO conductive thin-films deposited on the ZnO thin layer through solid phase crystallization process as a buffer layer showed higher conductivity than ones without the buffer layer or with an ordinary ZnO layer [2].

In order to reveal the mechanism of this high-quality crystallization process, we studied local structure of as-deposited and annealed ZnON films.

2 Experimental

Amorphous ZnON films (100 nm) were deposited on non-heated quartz glass substrates by rf magnetron sputtering using two ZnO ceramic targets in Ar/N_2 (20/80) mixed gas atmosphere (0.35 Pa) with supplied rf power to each target of 100 W. Then, the ZnON films were annealed in air at 400°C and 600°C for 3 hours in an electric furnace for crystallization.

Measurements of x-ray absorption fine structure (XAFS) for local structure analysis of the ZnON fims were carried out in Kyushu Sychrotron Light Research Center. Zn-K edge XAFS spectra for the ZnON films and a standard ZnO sample (commercial ZnO powder diluted in boron nitride powder) were collected by the conversion electron yield method and the transmission method, respectively, in ambient atmosphere at room temperature.

3 Results and discussion

Figure 1 shows the oscillation spectra extracted from the Zn-K XAFS spectra of the as-deposited and annealed ZnON films with that of a standard ZnO powder sample. Surprisingly, oscillation in the spectra of the annealed ZnON (crystallized ZnO) films clearly remain in high wavenumber region (beyond 13 $Å^{-1}$), which may imply that a more ordered structure was formed in the crystallized ZnO by the solid phase crystallization from amorphous ZnON than those by conventional methods.

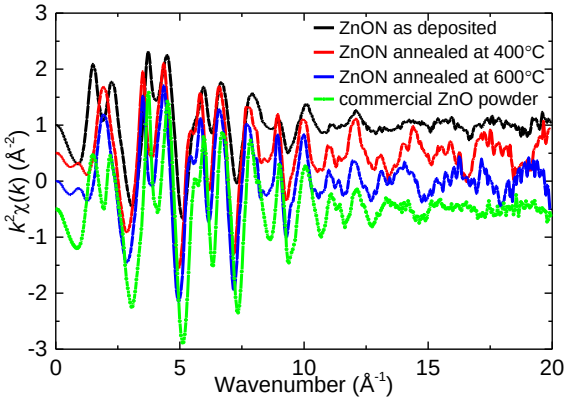

Fig. 1. Zn-K XAFS oscillation spectra of ZnON films.

References

[1] G. Harbeke et al., Appl. Phys. Lett. **42**, 249 (1983).
[2] N. Itagaki et al., Appl. Phys. Express **4**, 011101 (2011).
[3] T. Yamamoto, Thin Solid Films **420**–**421**, 100 (2002).
[4] A. Tsukazaki et al., Nat. Mater. **4**, 42 (2005).

Control of ion trajectory in high aspect ratio trenches by using amplitude modulated rf discharges

I. Nagao[1], Y. Yamamoto[1], K. Kamataki[1], T. Okumura[1], N. Yamashita[1], H. Kiyama[1], N. Itagaki[1], K. Koga[1,2] and M. Shiratani[1]

[1] *Graduate School of Information Science and Electrical Engineering, Kyushu Univ. Fukuoka, Japan*
[2] *National Institute of Natural Sciences(NINS), Tokyo, Japan*

We controlled ion trajectory in high aspect ratio (HAR) trenches in amplitude modulated (AM) rf plasma. Ion energy distribution function (IEDF) and ion angular distribution function (IADF) were simulated using a particle-in-cell/Monte Carlo collision (PIC-MCC) model. AM rf discharges offers control of ion flux and ion energy incident on the sidewalls of trenches.

1. Introduction

Nanometer-scale pattering and processing are required to achieve miniaturization and three-dimensional stacking of the state-of-the-art semiconductor devices.

Silicon oxide (SiO_x) thin films are widely used as dielectric layers. The films are often fabricated by plasma-enhanced chemical vapor deposition (PECVD). Normally, SiO_x film deposition on HAR trenches using PECVD leads to rather poor step coverage and poor film qualities. In our previous study, we demonstrated better step coverage for trench structures by applying AM rf discharges to TEOS-PECVD [1]. We also showed numerically that ion energy distribution function (IEDF) and ion angular distribution function (IADF) on the electrode surface were controlled by the AM rf discharge method [2,3]. However, effects of the AM discharge method on ion trajectory in HAR trench structures has not been investigated. Therefore, in this study, we investigated ion trajectory in HAR trenches in AM rf plasma using simulation.

2. Simulation

We employed particle-in-cell/Monte Carlo collision (PIC-MCC) simulation [4] to simulate Ar capacitively coupled rf discharge plasma between two parallel plate electrodes. The pressure was kept at 10 mTorr. The upper electrode was applied by RF voltage waveform with a voltage amplitude of 200 V and a frequency of 13.56 MHz and the lower electrode was grounded. For AM rf discharges, AM frequency was 10 kHz and AM level was set to 30 and 50%. IEDFs and IADFs on the surface of lower electrode were evaluated. Using the results of IEDFs and IADFs, we evaluated depth dependence of ion flux and ion energy incident on the sidewalls of trenches with AR 25 (h = 100 μm in depth and 4 μm in width).

3. Results and discussion

Figure 1 shows the depth dependence of the ion energy in the direction vertical to the sidewall of the trench for CW and AM discharges. The ion energy for AM discharges is higher than the energy for the CW one at around h = 20~70 μm. Moreover, there are higher flux of ions incident on the trench side walls for AM discharges than CW one (not shown). These results are closely related with larger full width of half maximum (FWHM) of IADF for AM discharges than CW one. Details will be discussed at the conference.

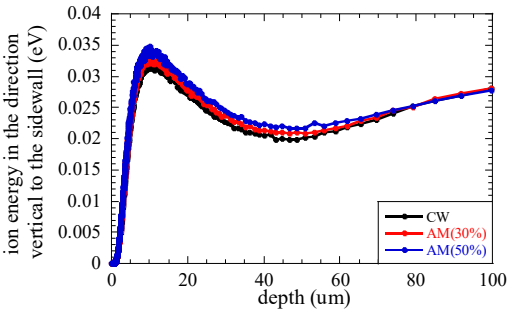

Fig. 1. Depth dependence of ion energy in the direction vertical to trench sidewalls.

Acknowledgements

This study was partly supported by JSPS KAKENHI Grant No. JP20H00142 and JSPS Core-to-Core Program Grant No. JPJSCCA2019002.

References

[1] K. Kamataki, et al., Proc. of 42nd International Symposium on Dry Process (DPS) G1 (2021).
[2] K. Abe, et al., Jpn. J. Appl. Phys. **60**, 106003 (2022).
[3] I. Nagao, et al., MRS Advances, **7**, 911 (2022).
[4] Z. Donko, et al., Plasma Sources Sci. Technol. **30**, 095017 (2021).

Studies on changes in surface morphology of materials under plasma environment and their potential applications in field emission

Jayashree Majumdar[1], John H. Booske[2] and Sudeep Bhattacharjee[1]

[1] *Dept. of Physics, Indian Institute of Technology Kanpur, Kanpur, Uttar Pradesh, 208016, India*
[2] *Dept. of Electrical and Computer Engineering, University of Wisconsin-Madison, Madison, WI 53706, USA*

Surface components of satellites (or, objects in space) and plasma facing components in reactors are exposed to high fluxes of energetic ions. When such surfaces are bombarded by inert gaseous ions, atomically heterogeneous patterned surfaces are produced. The understanding of the growth mechanism process of these structures and their subsequent use as field emitters is important for their sustainable re-utilization in electronics and material processing industries.

1 Introduction

Metallic (or, metallic alloy-based) surfaces of satellites or similar objects facing the external ion-exposed regions in space, as well as plasma facing components in plasma chambers and nuclear reactors, are exposed to high fluxes of energetic ion beams. This causes erosion of surface atoms, accompanied by their redistribution, and subsequently, patterned surface formation. The investigation of the growth mechanism of such surfaces is beneficial to determine their longevity as well as to find their potential applications in vacuum electronics and material processing industries for scientific and technological benefits, instead of disposing them altogether as waste materials.

2 Experimental setup

Positive ions extracted from a microwave generated plasma (~10^{11} cm^{-3} density) produced inside a magnetic multicusp, are made to impinge on the sample floated at high voltage (cf. Fig. 1 (a)). The ion irradiated structured surface is then mounted on a custom fabricated parallel plate setup with a 2 mm gap for field emission current measurement. The set ups are kept inside a stainless-steel vacuum chamber (10^{-7} Torr base pressure) [1,2].

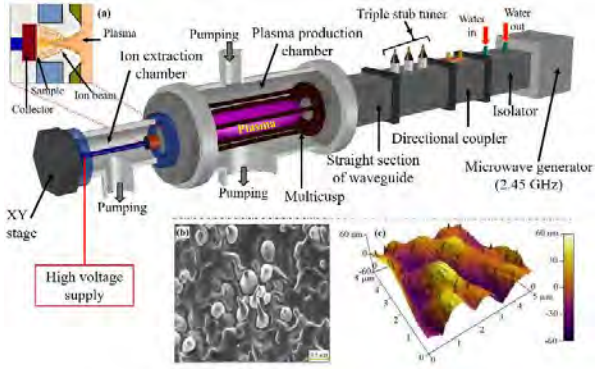

Figure 1: (a) Schematic of the experimental setup. (b) SEM and (c) AFM analysis of surface structures obtained on Cu irradiated by a 4.81×10^{15} $cm^{-2}s^{-1}$ flux of 2 keV Kr ions.

3 Results

A wide variety of atomically heterogeneous self-organized structures are produced when metallic samples such as Al, Ti and Cu are bombarded by inert gaseous ions such as He (flux = 1.1×10^{16} $cm^{-2}s^{-1}$), Ar (flux = 6.47×10^{15} $cm^{-2}s^{-1}$) and Kr (flux = 4.81×10^{15} $cm^{-2}s^{-1}$). Analysis employing surface characterization tools such as SEM and AFM (cf. Fig.1 (b) and 1 (c)) reveal formation of highly porous surfaces. Thus, due to an increase in surface emission area and field-enhancing morphology, these surfaces are excellent candidates for efficient field emission sources. Corresponding on which field emission characterization experiments were performed to identify an optimized range of ion beam fluences.

The experiments were supported by theoretical modelling, where the conical structures were represented as rotationally symmetric hyperbolas. The local field at the apex and the emission current was calculated over an array of uniformly sharp emitters, varying the number density of emitters and a distribution factor associated with spread of tip radii [3]. In parallel, the results were validated by COMSOL simulations, where a statistical distribution of uniformly arranged arrays of field emitters represented experimentally obtained protrusions. The effect of of implanted ions was approximately modeled by a layer over the conical emitter structures.

References

[1] Majumdar, J. and Bhattacharjee, S. Journal of Applied Physics **132**, 083304 (2022)
[2] Majumdar, J. and Bhattacharjee, S. Frontiers in Physics **9**,674928 (2021)
[3] Jensen, K. L. *et al.* Journal of Vacuum Science & Technology B: Microelectronics and Nanometer Structures Processing, Measurement, and Phenomena **14**, 1942 (1996)

Coverage control of carbon nanoparticles on substrate using capacitively coupled plasma chemical vapor deposition

K. Koga[1], S. Ono[2], T. Okumura[1], K. Kamataki[1], N. Yamashita[1], N. Itagaki[1], and M. Shiratani[1]

[1] *Faculty of Information Science and Electrical Engineering, Kyushu Univ., Fukuoka, Japan*
[2] *Graduate School of Information Science and Electrical Engineering, Kyushu Univ., Fukuoka, Japan*

Deposition control of nanoparticles in plasmas is a fundamental topic of plasma nanotechnology for realizing practical applications of nanoparticles. We succeeded in controlling the coverage of carbon nanoparticles (CNPs) deposited on substrates using capacitively coupled plasma chemical vapor deposition (CVD), which has been widely employed in large area deposition. From TEM images, deposited CNPs were classified into two size groups. The mean size of the smaller CNP group is around 5 nm and that of the lager CNP group is around 25 nm. We succeeded in controlling the coverage of CNPs with discharge duration without unexpected agglomeration.

1 Introduction

Carbon nanoparticles (CNPs), also known as carbon nanospheres, have unique features such as high surface area, excellent electrical conductivity, and high thermal conductivity, making them attractive for applications such as catalysis, energy storage, electrochemical reactions. To synthesize and deposit CNPs, control of size without unexpected agglomeration and uniform deposition on large area are issues to realize further improvement of nanotechnology using CNPs. Plasma processes are one of the promising methods to synthesize and deposit CNPs because they can produce the CNPs with fewer impurity and control the agglomeration by utilizing the charging of CNPs [1].

In this study, we have examined CNP synthesis and deposition using a capacitively coupled plasma CVD which can be employed large area deposition and is method with high affinity to semiconductor front-end processes.

2 Experimental

The experiments were performed using a capacitvely coupled plasma CVD reactor [2]. A mesh powered electrode was set 115 mm above a grounded substrate holder. Ar and CH_4 mixture gas was introduced from the top of chamber at 19 sccm and 2.6 sccm, respectively. The total pressure was kept at 0.3 Torr. Discharge frequency was 28 MHz and the discharge voltage was 280 Vpp. Observation of CNPs were carried out with a high-resolution transmission electron microscope (TEM) (JEOL, JEM-2010).

3 Results and Discussion

For synthesis of CNPs using the plasma CVD, unexpected agglomeration occurs in the gas stagnation region of the reactor, and resulting agglomerates are transported to the substrate. To prevent the agglomeration, we employed a pulsed discharge in this study, with a cycle of 1 min ON and 1 min OFF, and control the amount of deposited CNPs with the number of cycles.

Figure 1 shows TEM images of CNPs deposited on a grid mesh for TEM. We measured size distribution of CNPs by measuring the diameter of CNPs in TEM images. The deposited CNPs were classified into two size groups. The mean size of the smaller CNP group is around 5 nm and that of the lager CNP group is around 25 nm. The deposited CNPs has similar size distribution for each discharge cycle. We obtained the coverage of CNP on the substrate surface C_p using the following formula.

$$C_p = \pi \left(\frac{d_p}{2}\right)^2 n_p$$

where d_p and n_p is size (diameter) and area number density, respectively.

These results indicate we succeeded in controlling CNP deposition without unexpected agglomeration using the capacitively coupled plasma CVD.

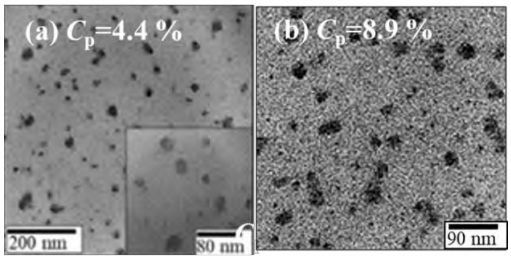

Fig. 2. TEM images of CNP deposition for (a) 20 cycles and (b) 30 cycles.

References

[1] S. Nunomura, et al., Phys. Plasmas **15** (2008) 080703.
[2] Sung-Hwa Hwang, et al., Thin Solid Films **729** (2021) 138701.

Chondro-like particles in the plasma environment: formation mechanisms and properties

D. Batryshev[1], S. Orazbayev[1,2], B. Kyrykbay[1], A. Baikaliyev[1], S. Ussenkhan[1,2], A. Utegenov[1,2], Ye. Ussenov[2,3], M. Gabdullin[1], T. Ramazanov[2]

[1] *Kazakh-British Technical University, Almaty, Kazakhstan*
[2] *IETP, Al-Farabi Kazakh National University, Almaty, Kazakhstan*
[3] *Currently at the Department of Mechanical and Aerospace Engineering, Princeton University, Princeton, USA*

In this work the formation of chondro-like particles with the method of gas-phase synthesis in a plasma environment using metal- and silicon-containing precursors (HMDSO, Ferrocen, etc.) was investigated. The experiment was performed in a vacuum facility where plasma was generated using a capacitive radiofrequency discharge. After synthesis, the structural, morphological, and chemical compositions of the particles deposited on the substrate were analyzed using SEM (scanning electron microscopy), XRD analysis, and Raman spectroscopy. A physical interpretation of the obtained experimental data is presented.

The study of the formation of chondro-like particles in the plasma medium is one of the relevant and interesting areas of research in astrophysics. Chondro-like particles are microscopic grains, which are considered to be precursors of planets and other cosmic bodies. These particles form in stellar clouds and spread throughout space, including Earth's atmosphere, where they can interact with plasma.

There are several possible scenarios of chondro-like formation, such as shock waves, planetesimals collisions, dissipation of magnetohydrodynamic turbulence, nebular lightning, and others [1-3]. However, none of these theories can explain the exact mechanism of particle formation, but one widely accepted hypothesis is that they are formed in a plasma environment.

The formation of chondro-like particles in the plasma environment is studied in experiments on the ground and on board of ISS [4-5]. These experiments investigate the interactions between cosmic dust and plasma under different conditions, such as different temperatures, pressures, and gas compositions. The results of these studies can contribute to refining our understanding of the processes occurring in stellar clouds, as well as help us understand the origin and evolution of planets and other cosmic objects.

In the present work, to study the formation of chondro-like particles, an experimental setup was developed to create a plasma environment using a capacitive radiofrequency discharge at different parameters (pressure, power, types of gases and precursors, etc.) in the following procedures: initially, air is evacuated from the vessel and a deep pressure (10^{-7} torr) is established using an HiCube turbomolecular pump. An inert gas was used as the plasma-forming gas. After plasma ignition, the precursor stream (organosilicon compounds), HMDSO and Ferrocen (metallocene vapour) along with inert gas were fed into the chamber. Particle synthesis will proceed by nucleation, coagulation and agglomeration of primary particles. The process of particle growth was monitored and controlled by methods such as current and voltage oscillography, self-bias voltage measurements, probe diagnostics, optical emission spectroscopy, etc. After synthesis, the particles were deposited on a substrate for further analysis by SEM, XRD analysis, and Raman spectroscopy.

References

[1] Russel, S., Connolly Jr., H.C., Krot, A.N Chondrules: Records of protoplanetary disk processes. In: Cambridge Planetary Science, Cambridge University Press (2018)
[2] Alexander, C. M. O., Grossman, J. N., Ebel, D. S. & Ciesla, F. J The formation conditions of chondrules and chondrites. Science **320**, 1617–1619 (2008)
[3] Horány, M., Morfill G., Goertz C.K., Levy E.H. Chondrule formation in lightning discharges. Icarus **114**, 174–185 (1995)
[4] A. Morlok. Chondrules born in plasma? Simulation of gas–grain interaction using plasma arcs with applications to chondrule and cosmic spherule formation. Meteoritics& Planetary Science **47**, 2269–2280 (2012)
[5] Dominik Spahr, Tamara E. Koch et al, A chondrule formation experiment aboard the ISS: microtomography, scanning electron microscopy and Raman spectroscopy on Mg2SiO4 dust aggregates. Physics and Chemistry of Minerals **5** (2022)

Controlled guiding and focusing of intense plasma ion beams by micro-glass capillaries beyond the self-focusing limit

Sushanta Barman and Sudeep Bhattacharjee

Department of Physics, Indian Institute of Technology, Kanpur, 208016, India

Micro-glass capillaries have become an important tool in the lossless guiding and focusing of ion beams. The key mechanism of ion beam guiding and self-focusing is based on distributions of charged patches on the capillary inner wall induced by the incident beam. However, in focusing intense ion beams through micro-glass capillaries, the space charge force dominates the self-focusing force, which sets a self-focusing limit. Therefore, focusing of ion beams beyond this self-focusing limit is a challenge. In this work, we experimentally demonstrate a new technique in which externally applied electric fields control the dynamics of charge patches and focus the beam beyond its self-focusing limit, which helps to obtain high intensity sub-micron beams.

1 Introduction

Guiding charged particles through micro-glass capillaries has many applications, such as cell surgery, beam steering, nanopore fabrication, and single biopolymer detectors [1]. The self-organized charged patches induced on the capillary inner wall, guides the beam along the tilt angle of the capillary and focuses without changing their initial charge state and energy [2]. However, the space charge force dominates the self-focusing force for high-current ion beams, which sets a self-focusing limit [3]. As a result, it is challenging to reduce the beam size below the capillary outlet diameter. Furthermore, the transmitted beams sometimes become unstable due to the blocking of particles by excessive charge patches and charge discharges, which limits the application of such systems.

In this work, we experimentally demonstrate controlled guiding and focusing of high-current ion beams by micro-glass capillaries and obtain sub-micron beams by overcoming the self-focusing limit. The dynamics of the charge patches are controlled by employing multiple electrodes on the outer surface of the capillary and biasing them with electric potentials.

2 Experimental

Ar ion beams are extracted from a plasma ion source based on electron cyclotron resonance, where the plasma is generated using microwaves of frequency 2.45 GHz and confined in an octupole magnetic multicusp [3]. A compact electrostatic lens (EL) system is employed to extract the ions from the plasma [4]. The schematic diagram of the system is shown in Fig. 1(a). Experiments are performed to obtain stable transmission of Ar ion beams having energy 9 keV through straight (outlet diameter 860 µm) and tapered (outlet diameter 45 µm) capillaries of length ~ 17 mm. The transmitted beam currents are measured using a Faraday cup. To measure the beam size, spots are created on poly methyl methacrylate (PMMA) thin films (thickness ~100 nm) and analyzed using optical microscope and scanning electron microscope (SEM). The evolution of the charge patches and hence, the self-focusing function of the capillary is controlled by applying different biasing voltages to the attached electrodes (L_1 and L_2), as shown in Fig. 1(b)-(c).

Further, particle-in-cell simulations are performed to understand the phenomenon. Experimental and simulation results will be presented at the conference.

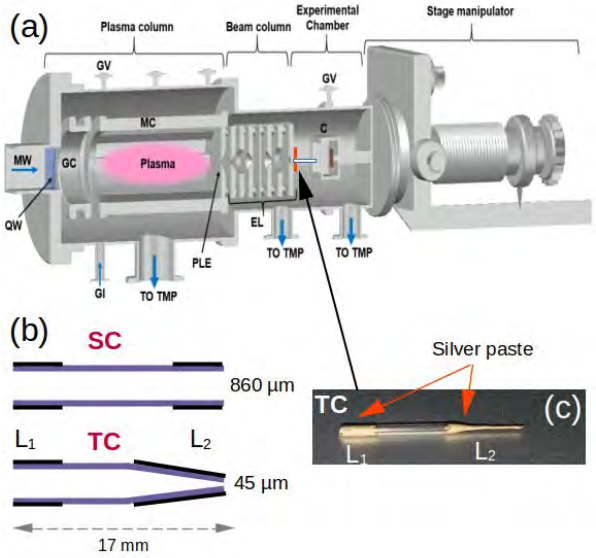

Figure 1. (a) Schametic diagram of the microwave plasma-based ion beam system [3]. (b) Schametic diagram of straight (SC) and tapered (TC) capillaries. (c) Digital picture of a tapered capillary.

References

[1] Ikeda, T. et al., Applied Physics Letters **109**, 133501 (2016).

[2] Paul, S. et al., Applied Physics Letters **101**, 223508 (2012).

[3] Maurya, K. S. et al., Journal of Physics D: Applied Physics **52**, 055205 (2018).

[4] Barman, S. et al., Plasma Research Express **4**, 025003 (2022).

Superhydrophobic surfaces production by PECVD method

S.S.Usenkhan[1], B.Kyrykbay[1], A.T.Zhunisbekov[2], A.U.Utegenov[1,2], S.A.Orazbayev[1,2] and T.S. Ramazanov[2]

[1] *Institute of Applied Sciences and Information Technologies, Almaty, Kazakhstan*
[2] *National Nanotechnology Laboratory of Open Type, Al-Farabi Kazakh National University, Almaty, Kazakhstan*

The work presents the results of a complex study of superhydrophobic surfaces obtained by the PECVD method in RF discharge plasma with gas mixtures (Ar/HMDSO and Ar/TEOS). In this experiment, superhydrophobic surfaces were obtained by deposition of nanoparticles on glass and silicon substrates by atmospheric plasma of Ar/HMDSO and Ar/TEOS gas mixtures. In order to compare surfaces with high hydrophobicity produced by the method their contact angles were studied. The dependence of changes in the contact angle on the storage time of the samples under normal conditions shows that samples obtained in Ar/HMDSO plasma jet at atmospheric pressure are much better preserved.

1 General

Superhydrophobic coatings are applied to the surface of the objects to provide them with water-repellent properties. Currently, superhydrophobic surfaces are the subject of an investigation by various research groups due to their unique properties, such as self-cleaning, anti-icing, anti-fog, anti-frictional properties, and oil-water separation.

The superhydrophobic surface repels water so that a spherical drop easily rolls over the surface. It is usually characterized by a high contact angle (> 150°) and a low angle of inclination or hysteresis with a small contact angle (< 10°).

Although there are several methods for producing hydrophobic surfaces, which differ in the types of surface modification, all these processes are rather complicated technologically and show bad reproducibility. Therefore, most of the methods used in industry are expensive and applicable only on small, flat surfaces or a limited range of materials [1].

1.1 Experimental setup

As mentioned above, in this work superhydrophobic surfaces were synthesized by plasma jet at atmospheric pressure. In the plasma jet, the argon-HMDSO gas mixture was used as the main working gas for igniting the plasma. In paper [2] it is shown a diagram of the experimental setup, which consists of a quartz glass tube (the length – 70 mm, the inner diameter – 3 mm, and the outer diameter – 10 mm) wrapped in a sheet of copper used as a grounding electrode. A 13.56 MHz high-frequency power supply (Seren-R301) was connected to an electrode located inside a quartz tube for igniting a plasma jet. The gas flow was controlled by the above-mentioned mass flow controller. The experiments were carried out with different parameters of the plasma (discharge power, the flow rate of the gas mixture, etc.). The range of the atmospheric discharge power was 10–200 W. The working gas Ar/CH4 was injected into the tube. After applying a high-frequency voltage to the electrodes, the plasma ignites, and nanoparticles are synthesized in chemical reactions by the action of a well-known mechanism.

1.2 Results

The work was carried out on a complex study of superhydrophobic surfaces obtained by PECVD methods in RF-discharge plasma with gas mixtures (Ar/HMDSO and Ar/TEOS). The synthesized superhydrophobic surfaces were deposited on the surface of silicon and glass substrates. The results of the experimental study showed that the contact angle varies in a range of 140°-165° and highly depends on the plasma parameters. It was determined that with an increase in the number of cycles of particle deposition, the contact angle also increases. Finally, the changes in the contact angle on the obtained superhydrophobic surfaces as a function of the storage time under normal temperature and pressure conditions were studied. The experimental results showed that the films obtained in Ar/TEOS plasma begin to lose their hydrophobic properties 10 months after deposition, and after 18 months the contact angle drops to 130°. The samples obtained in Ar/HMDSO plasma showed much higher resistance to change. The contact angle of these samples decreased from 160° to 145° after 24 months.

References

[1] S.A. Orazbayev at al, Obtaining of superhydrophobic surface in RF capacitively coupled discharge in Ar/CH4 medium, Appl. Surf. Sci. 472 (2019) 127–134.

[2] Orazbayev S, Zhumadilov R, Zhunisbekov A, Gabdullin M, Yerlanuly Y, Utegenov A and Ramazanov T 2020 Appl. Surf. Sci. 515 146050

Improve adhesion of electrospun nanofibers to plasma-treated polypropylene textile

L. Janů[1], E. Dvořáková[1], K. Polášková[1], M. Buchtelová[1], P. Ryšánek[3], Z. Chlup[4], T. Kruml[4], O. Galmiz[5], D. Nečas[1] and L. Zajíčková[1,2]

[1] *Plasma Technologies for Materials, CEITEC, Brno University of Technology, Brno, Czech Republic*
[2] *Department of Condensed Matter Physics, Faculty of Science, Masaryk University, Brno, Czech Republic*
[3] *Faculty of Science, J.E. Purkyně University, Ústí nad Labem, Czech Republic*
[4] *Institute of Physics of Materials, The Czech Academy of Sciences, Brno, Czech Republic*
[5] *Department of Physical Electronics, Faculty of Science, Masaryk University, Brno, Czech Republic*

The present work studied the adhesion between two parts of composite material, a supporting textile and a polycaprolactone (PCL) electrospun nanofibers (NFs), because good adhesion between composite parts is required in some applications (i. e., wound dressings). However, spunbond polypropylene (PP) textile, often used as the electrospinning support, is hydrophobic, which can prevent NFs from adhering. The adhesion can be improved by plasma treatment of PP textile, which introduces polar functional groups and increases the hydrophilicity. Low-pressure oxygen treatment showed to be the most effective as it enhanced adhesion almost 6×, which was ascribed to the synergic effect of treatment homogeneity with the right ratio of surface functional groups and sufficient wettability. A good agreement between tensile and loop adhesion tests was shown.

1 Methods

The PP textile was treated by low-pressure oxygen discharge or by atmospheric pressure plasma slit jet (PSJ) in argon or argon/nitrogen before electrospinning. PCL NFs were electrospun on plasma-treated PP textiles. The adhesion was evaluated by tensile and loop tests.

2 Results

Both low and atmospheric pressure plasma treatments introduced oxygen-containing polar groups confirmed by XPS. The PP textile was about 10° less hydrophobic after atmospheric PSJ treatments but became highly hydrophilic after low-pressure treatment. The low-pressure treated textile also stayed long-term hydrophilic. Low as well as atmospheric pressure plasma treatments led to an increase in the adhesion between the PP textile and PCL NFs (Figure 1). Low-pressure oxygen treatment enhanced adhesion almost 6×. On the other hand, the adhesion was improved at least twice after atmospheric PSJ treatments. The comparison of tensile and loop tests confirmed a good agreement between both tests.

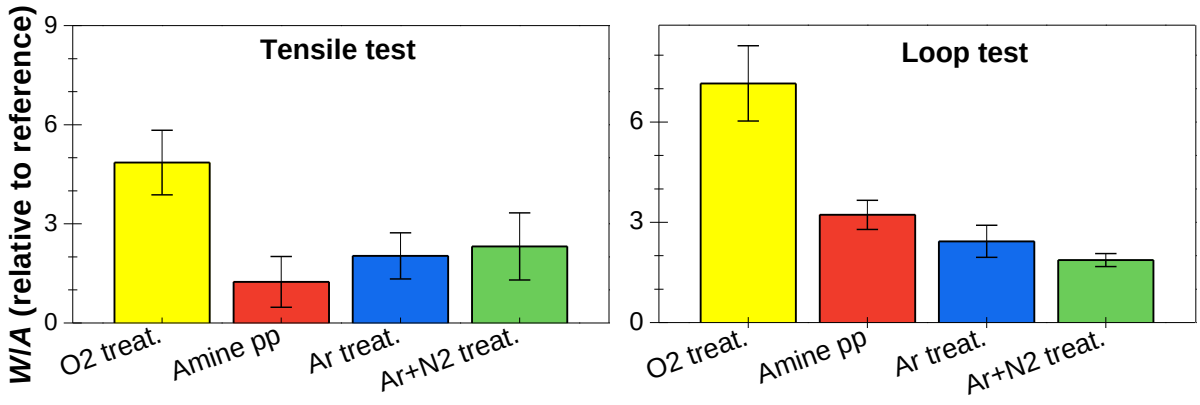

Figure 1: Work per area (W/A) necessary to tear off the PCL NFs by tensile and loop adhesion tests

Bactericidal species in electrically-neutral oxygen radical irradiated solution

H. A. Yamamoto[1], N. Iwata[2], M. Hori[3] and M. Ito[1]

[1] *Department of Electrical and Electronic Engineering, Meijo Univ. Techn., Nagoya, Japan*
[2] *Department of Electronics, Nagoya University, Nagoya University, Nagoya, Japan*
[3] *Center for Low-temperature Plasma Science, Nagoya University, Nagoya, Japan*

Plasma-generated bactericidal effects were investigated using an atmospheric-pressure oxygen-radical generator. To investigate bactericidal species, survival tests of *E.coli* ware performed by radical irradiation to *E. coli* suspended in citrate-phosphate buffer solutions, and oxygen-radical-irradiated citrate-phosphate buffer solution containing DMPO were analysed by ESR. From results of survival tests and analysis, bactericidal species of our methods suggested that OH• and HOO• are not crucial bactericidal species.

1 Introduction

Recently, plasma-in-liquid sterilization is one of the hottest research topics of plasma biology. Luke *et al.* reported that irradiation of helium plasma jet triggers a peroxynitrite (ONOOH) chemistry in aqueous solutions to produce hydroxyl (OH•) radical, and killed *Escherichia coli* (*E. coli*) for their case.[1] Production of ONOOH were catalysed by H^+. Therefore, they reported that the bactericidal effects were stronger at acidic environment. Although the generation pathways for the bactericidal species in liquid have been extensively studied, responsible factors in gas phase are still unidentified due to complexity of NEAPP. Therefore, the identification of key species in gas phase is extremely difficult.

Previously, we developed a non-equilibrium atmospheric-pressure oxygen-radical generator which can selectively irradiate electrically-neutral oxygen radicals such as $[O(^3P_j)]$ and $O_2(^1\Delta_g)$, with densities of 3× and $5\times10^{14}cm^{-3}$.[2] Therefore, individual effect of electrically-neutral radicals on the production of the plasma bactericidal effect can be evaluated.

In the present study, *E. coli*-suspended citrate-phosphate buffer solutions were irradiated using the oxygen-radical generator to evaluate contributions of electrically-neutral oxygen radicals on bacterial death. Electron spin resonance (ESR) analysis was performed to detect OH• and HOO• in oxygen-radical-irradiated solutions.

2 Experimental procedures

A non-equilibrium atmospheric pressure radical generator (Tough Plasma FPA10, FUJI CORP., Japan) was used in this study. Survival test of *E.coli* was performed by 14 min radical irradiation to *E. coli* suspended in citrate-phosphate buffer solutions. *E. coli* was suspended in 3 mL of buffer which pH value are 3 to 7 with a survival number of approximately 1×10^7 CFU/mL, The *E. coli* survival number was measured by a CFU assay. A spin-trapping reagent of 5,5-dimethyl-1-pyrroline-N-oxide (DMPO) was used for detecting free oxygen radical such as OH• and HOO•. 300 μM of DMPO was dissolved into citrate-phosphate buffer solution which pH value are 3 to 7. 1mL of solutions containing DMPO were irradiated using the oxygen-radical generator for up to 2 min. 150 μL of the oxygen-radical-irradiated samples were re-dispensed into a φ1.1-mm ESR quartz tube (Q-Band). ESR signals were measured using an ESR spectrometer (EMXplus, 9.4 GHz, X-Band, Bruker).

3 Results and discussions

ESR signal of DMPO-OH adduct (1:2:2:1) was detected in the solutions containing DMPO irradiated with oxygen radicals. Figure 1 shows that the survival number of *E. coli* and the ratio of intensity for DMPO-OH increased with increasing pH value. An ESR signal of DMPO-HOO adduct was not observed in the oxygen-radical-irradiated solutions. The results indicate that OH• and HOO• have no significant contributions to the *E. coli* death in this study.

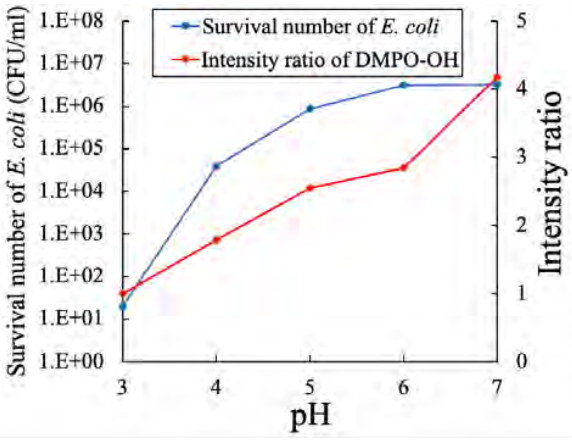

Fig. 1 ESR signal ratios of DMPO-OH and survival number of *E. coli* as a function of pH value.

Acknowledgements

This work was partly supported by a Grant-in-Aid for JSPS-KAKENHI no. JP19H05462 and 22H01213.

References

[1] P. Lukes, et al., Plasma Sources Sci. Technol. **23**, 015019 (2014).
[2] H. Hashizume, et al., Applied Physics Letters, **103**, 153708 (2013).

Carboxyhemoglobin creation in hemoglobin solution following treatment by pulsed DBD kHz plasma jet in Ar-CO_2 for plasma medicine applications

I. Orel[1], E. Mestre[1], S. Dozias[1], T. Gibert[1], R. Motterlini[2] and C. Douat[1]

[1] *GREMI UMR7344 CNRS/Université d'Orléans, Orléans, France*
[2] *INSERM U955, IMRB, Université Paris-Est, Créteil, France*

The present work reports the rates of CO-bind hemoglobin, carboxyhemoglobin, created following treatment of hemoglobin solution by pulsed coplanar-coaxial DBD plasma kHz-jet fed by Argon with CO_2 admixture up to about 1%. In particular, it has been observed that plasma treatment of 3 minutes with an applied voltage of 10 kV and a frequency of 20 kHz fed by 500 sccm Ar and 0.4% CO_2 admixture can transform up to 80% of hemoglobin to carboxyhemoglobin.

1 Introduction

Plasma medicine is a promising field that studies application of various plasmas for medical purposes including sterilization, disinfection, chronic wound healing and others. Non-equilibrium atmospheric pressure plasmas occupy a special niche in medicine thanks to ability to deliver excited, ionized and dissociated species coupled with wide-range emission and electric fields while keeping the plasma close to room temperature. CO molecule is a signaling gasotransmitter specie that plays anti-inflammatory and vasolidatory role but becomes toxic by asphyxiation due to carboxyhemoglobin (COHb) formation at high doses. Although both plasma and CO are known for beneficial effect on medicine, their synergy has not yet been studied [1].

Our previous work had shown that He-CO_2 coplanar-coaxial DBD plasma jet dissociates CO_2 and creates CO in controllable amounts [2], which, combined with localized delivery of a plasma source, would ensure safety of the method. The present communication focuses on quantifying the amount of COHb created in hemoglobin solution after Ar-CO_2 plasma treatment by the same kHz-jet plasma source.

2 Results

Four milliliters of deoxygenated blood hemoglobin solution was placed in a 12-well plate, and the edge of the reactor was immersed at 2 mm depth in the liquid. In such mutual disposition, the outflowing gas stream from the reactor caused the liquid to bubble which ensured homogeneity of the plasma treatment. Special care was taken to prevent O_2 binding by adding sodium dithionite.

Fig. 1 shows absorption spectra of deoxygenated blood hemoglobin solution before and after 3 min kHz-jet plasma treatment with 500 sccm Ar and 0.4% CO_2 with an applied voltage of 10 kV and a frequency of 20 kHz. The percentage of created COHb was calculated based on the absorbance at 420 and 432 nm [3] and equals to 80% for the blue curve of Fig. 1. Influence of other plasma treatment parameters (such as treatment time, CO_2 percentage and others) on COHb formation would be presented as well.

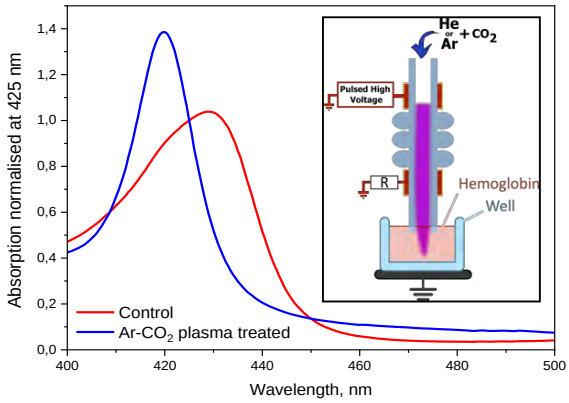

Fig. 1. Absorption spectra normalized at 425 nm of deoxygenated blood hemoglobin solution before (red) and after (blue) 3 min kHz-jet plasma treatment with 500 sccm Ar and 0.4% CO_2 with an applied voltage of 10 kV and a frequency of 20 kHz. Inset: schematics of the kHz-jet.

3 Acknowledgements

The authors thank the French Research Agency, ANR, (MediCO-Plasma | ANR-21-CE19-0005) for research funding. EM thanks the MESRI for founding her PhD thesis.

References

[1] E. Carbone and C. Doaut, "Carbon Monoxide in Plasma Medicine and Agriculture: Just a Foe or a Potential Friend?", Plasma Medicine, **8**-1, (2018).

[2] C. Douat, P. Escot Bocanegra, S. Dozias, É. Robert, R. Motterlini, "Production of carbon monoxide from a He/CO_2 plasma jet as a new strategy for therapeutic applications", Plasma Processes And Polymers, **18:**2100069 (2021).

[3] F. L. Rodkey, T. A. Hill, L. L. Pitts, R. F. Robertson, "Spectrometric measurement of carboxyhemoglobin and methemoglobin in blood", Clinical Chemistry, **25**-1388 (1979).

Paper sheet disinfection and sterilization by non-thermal atmospheric-pressure plasma

Borui Zheng[1], Zhiheng Liu[1], Yi Lei[2], Zhen Cui[1], Minghao Yu[1], Jingrui Luo[1] and Chang Ge[1]

[1] *Xi'an University of Technology, Xi'an, Shaanxi, People's Republic of China*
[2] *Shaanxi Provincial Centre for Disease Control and Prevention, Xian, Shaanxi, People's Republic of China*

The worldwide spread of COVID-19 has increased the importance of preventing the transmission of pathogens through various object surfaces, particularly paper sheets commonly used in education, customs, and administrative agencies. To quickly eliminate pathogens on paper sheets, we designed a grating-shaped dielectric barrier discharge (DBD) plasma actuator and studied its germicidal effect on paper sheets. The experimental results indicated that the plasma actuation voltage and treatment time are positively proportional to the bactericidal rate of Staphylococcus aureus. It was found that plasma discharge could penetrate multiple layers of paper sheets. However, the germicidal efficacy gradually decreased with increasing paper sheets. We compared the germicidal rates of different temperatures and found that temperature plays a particular role in sterilization in the plasma discharge process, but it is not the main influencing factor. The compound effect of temperature, ozone, and active particles in the plasma discharge helps improve germicidal efficacy.

1 Introduction

The COVID-19 pandemic has accumulated over 650 million confirmed cases and 6.6 million fatalities worldwide as of 2021. The pandemic has substantially impacted the global economy, leading to a decrease in the world's collective GDP by approximately two trillion US dollars in 2020. The causative agent of the disease, SARS-CoV-2, is primarily transmitted through person-to-person contact. However, studies have shown that surface transmission is a crucial mode of spread for the novel coronavirus [1]. A study published in the New England Journal of Medicine in 2020 found that the virus can remain viable on cardboard surfaces for up to 24 hours [2]. With the widespread use of paper products in various settings, such as schools, international mail, and documents in customs and government departments, the risk of infectious disease transmission is significant. In 2022, several cases of COVID-19 transmission via mail surfaces were reported in Beijing, highlighting the need for research on paper surface sterilization technology to mitigate the risk of transmission in educational institutions, government departments, and customs.

In this study, we used a self-developed grating-shaped surface dielectric barrier discharge plasma actuator to investigate the germicidal effect of Staphylococcus aureus on paper surfaces while preserving the structural integrity of the treated paper sheets. A simulated field identification test method was used for paper surface disinfection, and the influence of plasma on the germicidal effect on paper sheets under different actuation voltages and treatment times was analyzed. Furthermore, the germicidal efficacy of temperature was compared to gain insights into the mechanism of plasma disinfection and sterilization.

1.2 Conclusion

This thesis systematically studied the characteristics of a grid SDBD plasma actuator. The power of the plasma actuator linearly increased with increasing voltage. The study results indicate a correlation between an increase in actuation voltage and treatment time and a corresponding increase in the germicidal logarithmic reduction The bacterial concentration of Staphylococcus aureus in the positive control group was within the desired range of 5.00 to 6.00. It was observed that the minimum logarithmic reduction was 4.33, achieved when the actuation voltage was 8kV and the treatment time was 5 minutes. This finding meets the established criterion of a minimum log reduction of 3.00, demonstrating a significant decrease in bacterial presence. In the experiment, temperature change impacted germicidal efficacy, but temperature was not the main factor in sterilization. Experiments on different amounts of paper sheets showed that paper sheets could hinder plasma sterilization, but the blocking effect was not apparent with an increasing number of paper sheets.

References

[1]Liu Yuan,et al. 2020,Nature, 582(7813).

[2]Van Doremalen Neeltje,et al. 2020,The New England journal of medicine, 382(16).

Combined effects of cold atmospheric plasma and photocatalysis for indoor air decontamination

T. Vazquez[1], D. Wiedermann[2], M. Palko[2,3], M. Palko[2,3], J. Babic[2], Z. Machala[1]

[1] *Faculty of Mathematics, Physics, and Informatics, Comenius University Bratislava, Slovakia*
[2] *IQ Capital s.r.o., Banská Bystrica, Slovakia*
[3] *Faculty of Mechanical Engineering, Technical University Košice, Slovakia*

We designed and tested a new device for the treatment of polluted indoor air that combines cold atmospheric plasma and photocatalysis technologies. It is targeted to decompose chemical pollutants and pathogenic aerosols containing viruses and bacteria, at high gas flow rates for a real scale use, which is the main challenge of this study. Despite the production of ozone and NOx by the plasma (partially decomposed by the photocatalytic process) the decomposition of chemical pollutants showed promising results. The efficiency depends on the voltage, current and configuration of the plasma, and on the reactor design.

1 Introduction

The recent Covid-19 pandemic showed the deadly impact of a virus spreading mainly airborne and highlighted the importance of a high air quality. Less often emphasized, indoor air environments contain many harmful pollutants (chemical pollutants, bacteria, pathogenic aerosols, tobacco smoke, etc.). These pollutants can contribute to respiratory, cardiovascular, and oncological diseases that might be responsible for an excess of millions of deaths each year [1]. In addition, indoor air pollution has a larger impact on health than outdoor pollution: exposure to harmful compounds is higher indoor than outdoor, and people spend more time indoor. Therefore, achieving a high indoor air quality would be a major advance for public health, and could protect us from a new potential deadly virus pandemic.

In this study, we designed a new device using both cold atmospheric plasma and photocatalysis technologies for the indoor air decontamination. These technologies have shown to be efficient for the decomposition of a wide range of pollutants, and they have also recently proved to be effective for inactivation of viruses such as SARS-CoV-2 [2, 3]. Combining these two techniques may offer a very effective hybrid air decontamination device, as some studies suggest a synergetic effect [4].

2 Device and methods

Our air decontamination device combines a cold atmospheric plasma generated by a surface Dielectric Barrier Discharge (DBD), and a TiO_2 coating which is activated by UV-A LEDs. Several configurations of DBD were designed in order to treat large gas flow rates (< 100 L/min) of polluted air. We studied the effect of each component of the process taken separately (i.e. DBD only, UV only, UV with photocatalytic coating, and their combinations).

To assess the efficacy of the air purification device, we followed a technical norm (AFNOR XP B44-200) that describes the testing methods. It is a single-pass method: the concentration of the pollutant was measured before and after a single-pass through the decontamination device. The tested pollutants were formaldehyde, acetone and acetaldehyde, as representative indoor VOC pollutants.

3 Results

The overall efficacy of the device appeared to be promising given the very short residence time of the pollutant in the reactor (single-pass method and a large gas flow). Several DBD configurations were tested to find out the most efficient for chemical decomposition. We also monitored the concentration of ozone generated by the DBD, which is a strong oxidant of the pollutants but is well decomposed by the photocatalytic process to prevent its outflow from the device. Electrical parameters of the DBD are key components to find the best compromise between the species produced by the plasma, the interaction with the photocatalysis process, and the overall efficiency of the device.

This work was supported by Slovak Research and Development Agency APVV-17-0382, APVV-22-0247, and APVV-20-0566, and a postdoctoral support of Comenius University Bratislava.

References

[1] World Health Organization, WHO guidelines for indoor air quality: selected pollutants, Regional Office for Europe (2010).
[2] H. Mohamed et al, Frontiers in Physics, 9, 683118 (2021).
[3] R. Matsuura et al, Viruses, 13, 942 (2021).
[4] A. Bogaerts et al, J. Phys. D: Appl. Phys., 53, 443001 (2020).

The 2023 status report on the LXCat project

W. Graef[1], D. Boer[2], J. van Dijk[2], M. Hopkins[3], E. Carbone[4], and L. Pitchford[5]
on behalf of the LXCat Team

[1] *Plasma Matters B.V., Eindhoven, The Netherlands*
[2] *Dept. Applied Physics, Eindhoven Univ. Techn., Eindhoven, The Netherlands*
[3] *Sandia Nat'l Lab, Albuquerque, New Mexico, United States of America*
[4] *INRS, Centre Énergie Matériaux Télécommunications, Varennes, Quebec, Canada*
[5] *CNRS & Univ. of Toulouse, Toulouse, France*

An essential ingredient for the simulation of low temperature plasmas (LTPs) is accurate data describing electron and ion collisions with neutrals and their transport. LXCat is an open-access, on-line platform providing such data, as well as services for selecting, plotting, and comparing that data. Details and recent developments of the project are presented, while the LXCat team also aims to contact members of the LTP community for future contributions and participation.

LXCat [1] is an on-line platform for the curation of data needed for modeling the electron and ion components of Low Temperature Plasmas (LTPs). LXCat (`https://lxcat.net`) is open-access and no sign-up is required. The platform is organized in databases which are named and maintained by individual contributors. More than 60 people from around the world participate in this project, either by contributing data or by volunteering time to work on other aspects of the project. The data types available now are electron-neutral or ion-neutral scattering cross sections (also differential), oscillator strengths, and transport parameters (e.g., mobility, diffusion coefficients) and rate coefficients. The LXCat team does not recommend data and hence data for the same process can appear in one or more of the databases. On-line tools are available that allow visitors to search for specific data, plot and compare data from different databases, download data, or use the available complete sets of electron-neutral scattering cross sections in an on-line version of the Boltzmann solver BOLSIG+ [2] to calculate transport and rate coefficients in pure gases or gas mixtures. Recent developments are presented, among which a complete redesign of the platform [3] to better cater to community needs, which will be presented in more detail in another contribution by D.J. Boer, W. Graef et al. The LXCat team is interested in contacting members of the LTP community about data needs and about how people can volunteer to participate in this project.

References

[1] Carbone, E. *et al.* Data needs for modeling low-temperature non-equilibrium plasmas: The lxcat project, history, perspectives and a tutorial. *Atoms* **9** (2021). URL `https://www.mdpi.com/2218-2004/9/1/16`.

[2] Hagelaar, G. J. M. & Pitchford, L. C. Solving the boltzmann equation to obtain electron transport coefficients and rate coefficients for fluid models. *Plasma Sources Science and Technology* **14**, 722 (2005). URL `https://dx.doi.org/10.1088/0963-0252/14/4/011`.

[3] Verhoeven, S., Boer, D., Ali, S., Graef, W. & van Dijk, J. LXCat (2022). URL `https://doi.org/10.5281/zenodo.7381574`.

Nuclear-Spin-Changing Collisions Between H_3^+ and H_2 in an Ion Trap Experiment.

O. E. Hernandez Alvarez[1], S. Rednyk[1], L. Uvarova[1], Š. Roučka[1], P. Dohnal[1], R. Plašil[1] and J. Glosík[1]

[1] *Department of Surface and Plasma Science, Faculty of Mathematics and Physics, Charles University, Prague, Czech Republic*

We present the design and first results of an ion trap experiment for researching nuclear-spin-changing collisions between H_3^+ and H_2. The experiment uses action spectroscopy to observe the rotational population of the trapped H_3^+ ions and to measure the rate coefficients of the nuclear-spin-changing processes. The design of the experiment is guided by a state-to-state kinetic model of the trapped ions.

1 Motivation

In the context of astrochemistry, H_3^+ ions act as universal proton donors [1] and play a significant role in various interstellar processes. The relaxation of the ortho:para ratio of H_3^+ ions, caused by collisions with H_2, is one such process that affects the non-equilibrium populations of H_3^+ and H_2 in the interstellar medium [2]. In this study, we aim to measure the rate coefficients of ortho-para conversion reactions between H_3^+ and H_2, by observing the time evolution of ortho/para H_3^+ populations using a cryogenic 22-pole radiofrequency (RF) ion trap [3].

2 Experiment

The present results were obtained in a cryogenic linear radio-frequency 22-pole trap at 50 K temperature.

To accurately determine the quantum state of H_3^+ ions, we employed Laser Induced Reaction (LIR). In particular we used stimulated second overtone rovibrational transitions of ortho and para H_3^+ to induce the endothermic reaction $H_3^+ + Ar \rightarrow ArH^+ + H_2$, $\Delta H_0 = 0.57$ eV [4].

Our experiment utilized normal H_2 (25% fraction of para-H_2) and para-enriched H_2 (99.5% fraction of para-H_2) produced by catalytic conversion in a para-hydrogen generator as a reactant gas.

3 First Results

The first data, including the time-resolved LIR measurement of H_3^+ nuclear spin population in the ion trap will be presented at the poster. The obtained results concerning the nuclear-spin-changing collisions between H_3^+ and H_2 could help explain the observed non-equilibrium populations of these species in the interstellar medium.

The population of para-H_3^+ ions at trapping times between 115 and 175 ms is probed using a laser pulse at 1381.7311 nm (21.8 mW) power. To remove the ArH^+ ions produced during the injection of H_3^+ ions, we reduce the RF amplitude of the trap to 50 % between 30 and 40 ms trapping times.

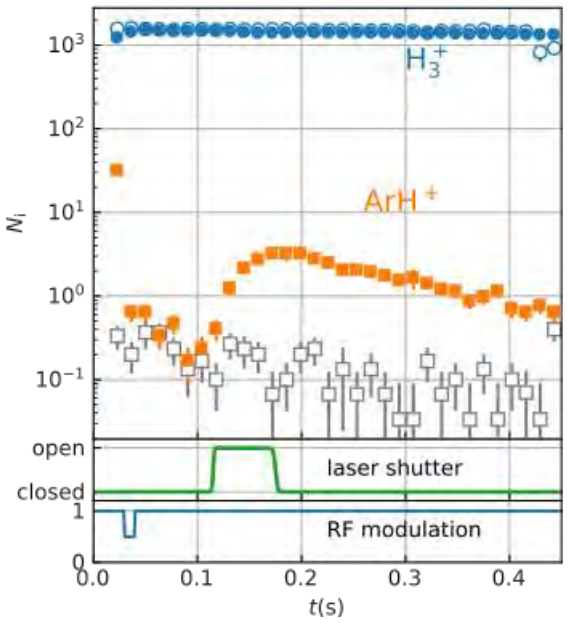

Figure 1: Time evolution of number of ions in trap at 50K.

Acknowledgements

This work was partly supported by the Czech Science Foundation (GACR21-28560S, GACR 22-059358, GACR 23-05439S) and by the Charles University (GAUK 337821, GAUK 332422, GAUK 376721).

References

[1] T. Oka, Proc. Natl. Acad. Sci. USA,103, 12235 (2006).

[2] F. Grussie, M.H. Berg, K.N. Crabtree, Astrophys. J.,759, 21 (2012).

[3] D. Gerlich, Phys. Scr.T59256 (1995).

[4] J. Glosik, Phil. Trans. R. Soc. A (2006) 364, 2931-2942.

Oxygen atom and ozone kinetics in the afterglow of a pulse-modulated DC discharge in pure O_2: an experimental and modelling study

J-P. Booth[1], Shu Zhang[1], O. Guaitella[1], D. Lopaev[2], S. Zyryanov[2], T. Rakhimova[2], D. Voloshin[2], A. Chukalovsky[2], A. Volynets[2], Yu. Mankelevich[2]

[1] *Laboratoire de Physique des Plasma (LPP), CNRS, Sorbonne Universite, École Polytechnique, Institut Polytechnique de Paris, 91120 Palaiseau, France*
[2]*Skobeltsyn Institute of Nuclear Physics, Lomonosov Moscow State University, Russian Federation*

The chemical kinetics of oxygen atoms and ozone molecules were investigated in a fully-modulated DC discharge in pure oxygen gas in a borosilicate glass tube, using cavity ringdown spectroscopy (CRDS) of the optically forbidden $O(^3P_2)\rightarrow O(^1D_2)$ absorption at 630nm. In the afterglow the O atom density decays non-exponentially, indicating a surface loss probability dependent on incident active particle fluxes. Ozone is also measured, from the Chapuis band continuum under the O atom signal. The ozone density passes through a maximum after a few 100ms, then decays slowly. This behaviour can only be modelled by including modified surface processes for O and O_3, and a new kinetic scheme for vibrationally-excited O3 intermediates produced by O + O_3 recombination.

Introduction

Electrical discharges in pure oxygen have been studied for many decades. However, our new measurements of O and O_3 in the afterglow could not be explained by existing models.

Experiment

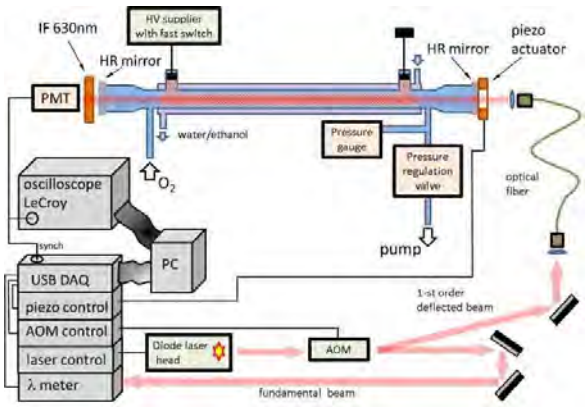

Figure 1 Experimental setup

The experimental setup is shown in figure 1, and described previously [1]. CRDS measurements were made in a dc positive column discharge (0.5-4 Torr, 10-40 mA) in a 2cm ∅ thermostatted borosilicate glass tube, using a tuneable monomode diode laser operating around 630nm. The discharge current was on for 0.2 seconds and off for 0.8 seconds, allowing the build-up to steady-state and the decay in the afterglow to be studied.

Results and discussion

The dynamics of O and O_3 in the afterglow of 40mA discharges are shown in figure 2 at pressures of 0.5 and 4 Torr. Also shown are the results of our 1D(r) fluid model. The experiment results can only be fitted with the following modifications: 1) linear and quadratic terms for O surface recombination, 2) surface production and loss of O_3, 3) kinetics of vibrationally-excited ozone with 7 effective levels, VT transfer and reactions with O and O2a.

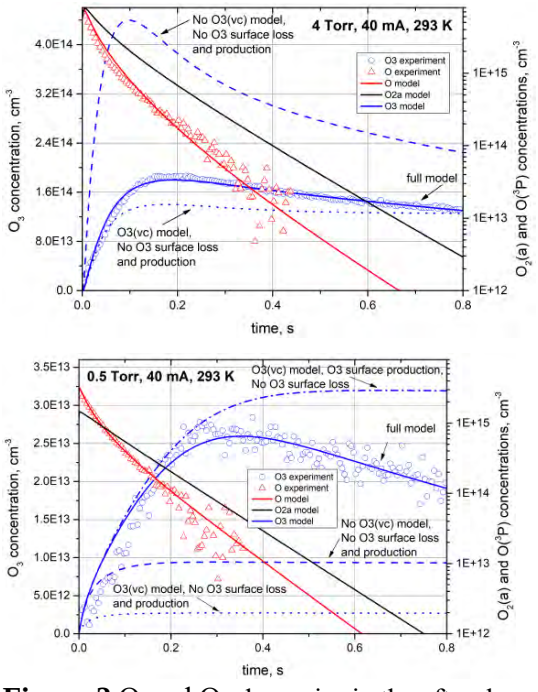

Figure 2 O and O_3 dynamics in the afterglow at 0.5 and 4 Torr O_2

Research supported Federation Plas@par and RSF (project No. 21-72-10040)

[1] J.P. Booth, A. Chatterjee, O. Guaitella, D. Lopaev, S. Zyryanov, A. Volynets, T. Rakhimova, D. Voloshin, A. Chukalovsky, Y. Mankelevich, and V. Guerra, PSST, **31**, 065012, (2022)

Spectroscopy and recombination of H_2D^+ and HD_2^+ ions

M. Kassayová[1], L. Uvarova[1], P. Dohnal[1], D. Hájek[1], R. Plašil[1], Š. Roučka[1] and J. Glosík[1]

[1] *Department of Surface and Plasma Science, Faculty of Mathematics and Physics, Charles University, Prague, Czech Republic*

The aim of this experiment is to measure the recombination rate coefficients of H_2D^+ and HD_2^+ ions for temperatures under 80 K. The time evolution of number densities of idividual nuclear spin states of H_2D^+ and HD_2^+ ions will be measured to obtain the corresponding recombination rate coefficients. The first results will be shown at the conference.

1 Motivation

H_3^+ is one of the most abundantly produced molecular ion in the universe [1] and a key element in the interstellar chemistry. H_2D^+ and HD_2^+ molecules are formed in interstellar gas clouds in collisions of H_3^+ and its deuterated isotopologues with HD molecules and H_2. Both H_2D^+ and HD_2^+ have been detected in the interstellar medium and kinetic models show all four types of H_3^+ present in the interstellar medium [2].

The recombination of H_3^+ and D_3^+ ions has been measured many times [3], but the recombination rate coefficients for H_2D^+ and HD_2^+ are not well known at low temperatures, because of the difficulty to produce plasma containing only a single ion species (either H_2D^+ or HD_2^+) and high rotational excitation ($\sim$ 300 K) in ion storage ring experiments [4].

2 Experiment

The measurements of the recombination rate coefficient of H_2D^+ and HD_2^+ ions with electrons are performed using stationary afterglow apparatus with Cavity Ring-Down Spectroscopy and microwave diagnostics with temperature under 80 K (detailed description can be found in [5]). We probe in situ the number densities of different spin states of both H_2D^+ and HD_2^+ ions. Measuring both ion and electron number densities at the same time, the studied ions H_2D^+ and HD_2^+, do not need to be dominant in afterglow plasma.

3 Acknowledgment

This work was partly supported by the Czech Science Foundation (GACR 23-05439S & GACR 22-059358) and by the Charles University (GAUK 337821 & GAUK 332422).

References

[1] Millar, T. J. Astrochemistry. *Plasma Sources Science and Technology* **24**, 043001 (2015).

[2] Belloche, A. *et al.* Will the starless cores in Chamaeleon I and III turn prestellar? *Astron. Astrophys.* **535**, A2 (2011). 1106.5064.

[3] Plašil, R. *et al.* Stationary afterglow measurements of the temperature dependence of the electron–ion recombination rate coefficients of H_2D^+ and HD_2^+ in $He/Ar/H_2/D_2$ gas mixtures at T = 80–145 K. *Plasma Sources Sci. Technol.* **26**, 035006 (2017).

[4] Petrignani, A. *et al.* Resonant structure of low-energy H_3^+ dissociative recombination. *Phys. Rev. A* **83**, 032711 (2011).

[5] Plašil, R. *et al.* Stationary afterglow apparatus with CRDS for study of processes in plasmas from 300 K down to 30 K. *Rev. Sci. Instrum.* **89**, 063116 (2018).

Simulation and characterization of the interaction of fast quasi-monoenergetic ion beams and deuterium-tritium plasma

J. M. Gil[1], P. R. Beltrán[2], R. Rodriguez[1] and G. Espinosa-Vivas[1]

[1] *IUNAT, Physics Department, Universidad de Las Palmas de Gran Canaria, Spain*
[2] *Instituto de Astrofísica de Canarias (IAC), E-38200 La Laguna, Tenerife, Spain*

In this work we present a model for the calculation of the spatial and temporal temperature field of a compressed DT plasma heated by time dependent and independent fast quasi-monoenergetic Gaussian ion beams. From simulations performed on a wide range of ion beam parameters, we carry out an analysis of the generated hot spot. We focus the study on the influence of the characteristic parameters of the quasi-monoenergetic ion beams (particle density, initial mean energy and energy spread) on the spatial temperature field reached by the heated region at the end of the heating process. The main objective of this work is to characterize as a function of the beam parameters, some relevant properties of the hot spot generated inside the heated region such as length, average temperature or maximum temperature. The results presented in this work were obtained for fully ionized vanadium ion beam in a wide range of ion beam characteristic parameters and for compressed DT plasma conditions.

1 General

Fast ignition (FI) scheme was proposed as an alternative to the standard central ignition of inertial fusion targets [1]. FI scheme intends to reduce the drive requirements by separating target plasma compression and ignition. Due to the large divergences and the high energies found in electron-driven fast ignition experiments and simulations [2], ion-driven fast ignition (IFI) has been taking an increasing interest. IFI scheme offers several advantages, such as generation of collimated beams, well known interaction with the plasma and localized hot spot or energy deposition on compressed deuterium-tritium (DT) plasma. On the other hand, the potential of Maxwellian and Gaussian ion beams to heat fusion target plasma at stagnation state has been extensively investigated [3-6]. There are previous studies of the optimal energies or radius beams for efficient ignition, but they do not perform analysis of the relevant properties of the hot spot. Therefore, detailed analysis about the characteristics of the heated region and hot spot are welcome.

In this work we present a model for the calculation of the spatial and temporal temperature field of a compressed DT plasma heated by time dependent and independent fast quasi-monoenergetic Gaussian ion beams. Furthermore, from simulations performed on a wide range of ion beam parameters, we carry out an analysis of the generated hot spot. We focus the study on the influence of the characteristic parameters of the quasi-monoenergetic ion beams (particle density, initial mean energy and energy spread) on the spatial temperature field reached by the heated region at the end of the heating process. The main objective of this work is to characterize, as a function of the energy spread of the beams, some relevant properties of the hot spot generated inside the heated region such as length, average temperature, maximum temperature and its position. The results presented in this work were obtained for fully ionized vanadium ion beam in a wide range of ion beam characteristic parameters and for compressed DT plasma conditions of interest in the context of the ion fast ignition scheme.

References

[1] M. Tabak, J. Hammer, M. Glinsky, W. Kruer, S. Wilks, J. Woodworth, E. Campbell, M. Perry, Ignition and high gain with ultrapowerful lasers, Phys Plasmas **1**, 1626 (1994).
[2] A.P.L. Robinson et. Al., Nucl. Fusion **54**, 054003 (2014).
[3] J. Fernández, B. J. Albright. F. N. Beg, M. E. Foord, B. M. Hegelich, J. J. Honrubia, M. Roth, R. B. Stephens and L. Yin, Fast ignition with laser-driven proton and ion beams, Nucl. Fusion **54**, 054006 (2014).
[4] J.J. Honrubia and M. Murakami, Ion beam requirements for fast ignition of inertial fusion targets, Physics of Plasmas **22**, 012703 (2015).
[5] S. Gus'kov, N. Zmitrenko, D. Il'in, V. Sherman, Fast ignition when heating the central part of an inertial confinement fusion target by ion beam, J. Exp. Theor. Phys. **119**, 958 (2014).
[6] S. Gus'kov, D. Il'in, V. Sherman, Spatial distribution of the plasma temperatura under ion-beam fast ignition, Plasma Phys Rep **40,** (2014) 572.

Power balance in an anisotropic dipole plasma: thermodynamical insights

Ayesha Nanda and Sudeep Bhattacharjee

Dept. of Physics, Indian Institute of Technology Kanpur, Kanpur 208016, Uttar Pradesh, India

A mathematical model of the power balance is formulated to understand and interpret energy exchange in the language of thermodynamics in a plasma confined by a dipole magnetic field. The measurements using Langmuir probe and wave field probe are carried out by varying neutral pressure and operating power to understand change in energy flux along various directions, resulting in varying internal energy and work done by electrons. The present study focuses on the thermodynamic behaviour of electrons in terms of thermodynamic potentials and polytropic index during plasma heating and power loss mechanisms.

1 Introduction

In plasma, thermodynamics is used to understand key concept of self-organization of particles associated with magneto-fluid couplings and transfer of energy, heat and work. The gas expansion is characterised by a polytropic relation as $PV^{\gamma} =$ const., where P, V and γ are the pressure, volume and the polytropic index. The polytropic index describes the fluid interaction with the surrounding in terms of energy and hence used to model plasma expansion for various application purpose modulating γ. This further helps us to understand plasma heating and expansion in language of thermodynamics. The present study aims to formulate a thermodynamic relation that accounts for experimentally observed parameters in response to plasma heating and energy loss processes with varying pressure and operating power in a dipole field through power balance study.

2 Experimental set-up and diagnostics employed

The schematic of the compact dipole plasma device is shown in Fig. 1 [1]. Langmuir probe and wave field probe are employed for measurements at several accessible spatial position (r, θ, ϕ).

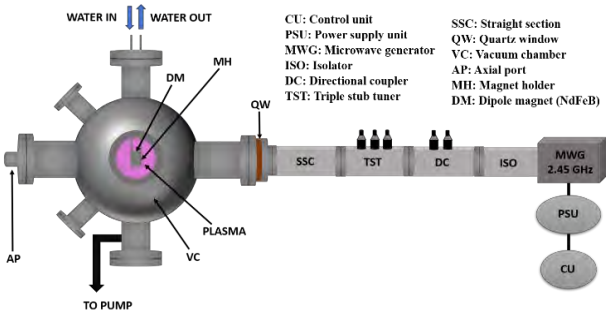

Fig. 1. Schematic of the experimental setup.

3 Theoretical formulations

A mathematical model is formulated from the continuity equation for power balance with net power retention Q_j (= power gain - power loss) along various directions for $j \rightarrow r, \theta, \phi$. Apart from microwave heating by ECR (W_M), particles gain energy by betatron (W_B) and Fermi (W_F) heating in dipole field [2] due to the mirror and curvature drifts resulting in conservation of first and second adiabatic invariants. The power loss happens through diffusion cooling (W_d), charge exchange (W_{cx}) [1], inelastic (W_{in}) and elastic (W_{el}) collision, isotropization (W_{is}) [3] and losses through the walls of the chamber (W_w). Therefore, $Q_j = G_j - L_j$, where G_j $(=W_B + W_F + (W_M)_j)$ and L_j $(=(W_{in})_j + (W_{el})_j + (W_d)_j + (W_{cx})_j + (W_{is})_j + (W_w))$ are the power gain and loss rates respectively. Net power retained is analogous to the heat supplied to the system and hence change in internal energy $dU_j = dQ_j + d(PV)$ can be obtained from first law of thermodynamics. Furthermore, other thermodynamic potentials such as enthalpy, Helmholtz free energy and Gibbs free energy can be determined.

3 Results

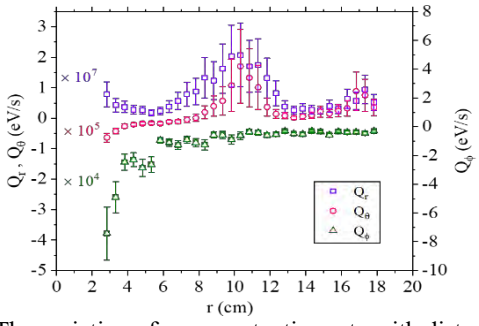

Fig. 2 The variation of power retention rate with distance.

Fig. 2 shows the radial variation of power retention rate in the mid-plane at 2.0 mTorr. The results show that G dominates over L along $\hat{r}$, and the converse is observed along $\hat{\phi}$. Along $\hat{\theta}$, G is lower near the magnet and increases towards the edge.

The detailed study on power balance would be carried out as a function of power and neutral pressure to understand thermodynamics of dipole plasma, and will be presented in the conference.

References

[1] Bhattacharjee, S. *et al.*, Review of Modern Plasma Physics, **6** 16 (2022).

[2] Eriksson, E. *et al.*, Geophysics Research Letter, **47** 085080 (2020).

[3] Nanda, A. *et al.*, Physics of Plasmas, **29** 062105 (2022).

P3-7

PHOTOTHERMIC INFRARED EMISSION OF SPUTTERING TARGETS

Iván Camps, Eduardo García Gallardo, Kassandra Salguero Martínez, Julio César Cruz, Stephen Muhl

Instituto de Investigaciones en Materiales UNAM, CDMX. C.P. 04510, México

In sputtering deposition systems, several factors are commonly varied in order to be produce a coating or thin film, such as working gas, reactive gas, DC/RF power and in some cases heating or biasing of the substrate to obtain a certain crystallinity or to improve certain properties of the deposited materials. Some characteristics of the sputtering setup are usually taken for granted, as for example, the intensity or form of the magnetic field of the magnetron, or the target temperature as “room temperature”. The latter is not entirely stable or constant during most of the sputtering processes and can greatly affect the physical and chemical surface properties of the target and the resulting film. Furthermore, if a reactive atmosphere is used, the bombardment of excited species towards the target, will increase its temperature, and for higher powers this may rise significantly up to a point that can induce chemical reactions, thus changing the electric properties and also the sputtering yield.

In this work we present the results of studies of the photothermic emission in the infrared (IR) of several commonly used sputtering targets: Ti, Ti-O, Al, Al-O, Cr, Ag, and graphite; via thermal imaging using an IR camera. Each of these materials have a unique thermal emissivity, thus we had to perform individual measurements to adjust each emissivity to match the temperature reading from an electric thermocouple. The results are expected to give information for in-situ measurements of the sputtering targets, and the temporal development of the chemical surface reactions during the bombardment processes throughout the coating deposition.

Keywords: IR imagery, magnetron sputtering, emissivity

Corresponding and presenting author:

References:

Acknowledgements: PAPIIT project IG101220

Effects of lower discharge frequency on ion energy distribution function in dual frequency plasma studied by particle-in-cell/Monte Carlo method

J. Lai[1], T. Arima[1], M. Otaka[1], K. Ikeda[1], I. Nagao[1], K. Kamataki[1], D. Yamashita[1], N. Yamashita[1], N. Itagaki[1], T. Okumura[1], K. Koga[1, 2], M. Shiratani[1]

[1]*Kyushu University, 744 Motooka Nishi-ku Fukuoka 819-0387, Japan,*
[2] *National Institutes of Natural Sciences, 4-3-13 Toranomon Minato-ku, Tokyo, 105-0001, Japan*

We investigated effects of lower driving rf frequency on ion energy distribution function (IEDF) in dual frequency (fundamental driving rf frequency is 13.56MHz) capacitively couple radio frequency (CCRF) Ar plasmas studied by one-dimensional particle-in-cell/Monte Carlo collision simulations (PIC-MCCM). We focused on the effect of driving frequency by setting self-bias voltage(Vdc) to 0. These simulation results showed that mean ion energy of dual frequency discharge was at most 16% larger than ones of single discharge (f_{rf} =13.56MHz), which indicated the IEDF could be control through the combination of two frequencies.

1 Introduction

In recent years, there has been a trend towards the adoption of three-dimensional integration of semiconductor devices in pursuit of improved performance [1], which demands the development with more precise processes. For those processes separate control of the ion flux and the ion energy is essential. In traditional discharge methods, it has been difficult to control these two plasmas separately[2]. Thus, we focus on the investigation of control ion by discharge rf frequency. In this study, we investigate the effects of the lower driving frequency on plasma parameters in dual frequency discharges simulated by PIC-MCC method.

2 Experimental

We used a one-dimensional (1d3v) bounded plasma PIC-MCCM simulation to describe CCRF Ar discharges. The two plane parallel electrodes with gap 50 mm were assumed to be infinite. In order to focus on the effect driving frequency, Vdc was set to 0 V. In this study, the dual frequency plasmas were excited by fundamental driving rf frequency f_1 (13.56MHz) and other lower rf frequency f_2 from f_1 /2(6.78MHz) to f_1 /200(0.0678MHz). Numerical simulations for single rf frequency discharge (f_{rf} =13.56MHz) were performed for comparison. In these two simulations, the input peak-to-peak voltage Vpp was 200V and Vdc was 0 V. IEDFs were measured on the surface of rf electrode. Another electrode was grounded. The background neutral gas is uniformly distributed and the gas temperature is 300 K. The pressure is kept at 10 mTorr. The secondary electron emission coefficient is γ = 0.1 in this study.

3 Results and discussion

Figures 1 show (a) the dependence of f_2 frequency on the mean ion energy comparing dual frequency discharge (f_2 = 0.0678 MHz ~ 6.78 MHz) and single frequency discharge and (b) IEDFs of dual frequency discharges (f_2 = 0.226 MHz) and a single-frequency discharge. The result of fig.1 shows that the mean ion energy increases as f_2 becomes less than 1.356 (f_1/10) MHz and has the peak energy at f_2=0.226(f_1/60) MHz with a value of 102.68 eV which is approximately 16% higher than that of a single frequency discharge. The result of fig.2 shows that IEDF of dual frequency discharge have the lower peak energy and the tail extends to higher energy region compared to single frequency discharge . Results for other parameters will be reported in detail in the conference.

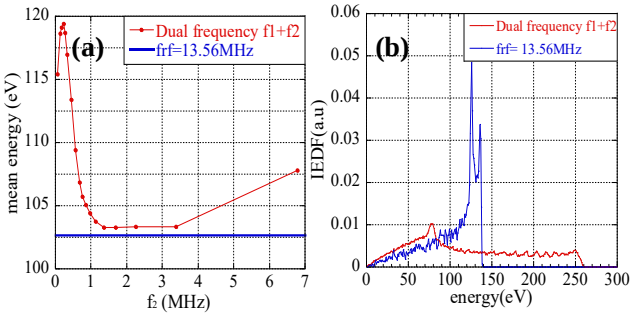

Fig.1 (a) f_2 dependence of mean ion energy from f_1/2 to f_1/200 MHz. (b) IEDF of dual discharge discharges with f_1 13.56+f_2 0.22 6 MHz and single-frequency discharges (f_{rf}=13.56MHz).

Acknowledgements

This work was partly supported by JSPS KAKENHI (Grant No. JP20H00142), JSPS Core-to-Core Program (Grant No. JPJSCCA2019002.

Reference

[1] I. Adamovich,et al., J. Appl. Phys. D, **55**, 373001 (2022).

[3] Z Donk´o1, J Schulze2, B G Heil2,3 and U Czarnetzki2, J. Phys. D: Appl. Phys. **42,** 025205 (2009).

Diamond-coated probes for diagnostics in hot and hazardous plasmas

C. Ioniţa[1], G.S. Xu[2], N. Yan[2], H. Wang[2], V. Naulin[3], J.J. Rasmussen[3], D. Steinmüller-Nethl[4], R.W. Schrittwieser[1]

[1]*Institute for Ion Physics and Applied Physics, University of Innsbruck, Austria*
[2]*Institute of Plasma Physics, Chinese Academy of Sciences, Hefei 230031, China*
[3]*Department of Physics, Technical University of Denmark, Kongens Lyngby, Denmark*
[4]*CarbonCompetence GmbH, Weisstraße 9, Wattens, Austria*

1 Introduction

Plasma probes are handy diagnostic tools, now used even in hot plasmas, e.g. toroidal fusion experiments. Probes can be useful for investigating turbulent fluctuations, and the associated transport in the edge plasma region, in particular in the Scrape-Off Layer (SOL) due to Edge-Localized Modes (ELM) [1].

Inevitably, in such plasmas, probes and their casings are exposed to strong particle fluxes, causing sputtering, over-heating and unwanted chemical reactions. In toroidal experiments this also happens with other Plasma-Facing Components (PFC), such as the inner chamber wall or the divertor plates.

To investigate possibilities to make probes more resilient against such damages, we have tentatively coated two graphite probe casings of the Experimental Advanced Superconducting Tokamak (EAST – Hefei, People's Republic of China) with Ultra-Nano-Crystalline Diamond (UNCD) and tested them in the edge plasma region of EAST [2].

After being coated by UNCD at a Tyrolean company near Innsbruck, the casings were sent back to Hefei, where they were equipped with various graphite probe pins. Then they were inserted frequently even into the near SOL of EAST up to a distance of 15 mm inside the Last Closed Flux Surface (LCFS) in low- and high-confinement regimes (L-mode and H-mode).

Figure 1. (a and b) SEM (Scanning Electron Microscope) of probe surfaces before use: (a) uncoated graphite surface; (b) UNCD-coated surface; (c) Five pin probe head after numerous insertions into EAST SOL and beyond. Red ellipse indicates the spot where UNCD-coating has dropped off; (d) SEM of the spot marked in (c).

2 First results

We found that the UNCD coating was surprisingly effective in preventing sputtering of graphite from the probe casings during insertion. This also strongly reduced the risk of re-deposition of the sputtered-off graphite on the boron nitride isolators between the probe pins and the probe casings by layers of conductive graphite, thereby possibly leading to short circuits or fault currents. Only after numerous insertions into the SOL, first signs of detachment of the UNCD layers were noticed, however, only after removing the probe head from the probe insertion system and handling it in air. See figure 1(c) & 1(d).

3 Outlook

For future applications of UNCD coatings of probes and other PFCs, more homogeneous, thicker and stabler UNCD coatings will be achievable. Our future research efforts will therefore be directed to take advantage of such new coatings and resume the investigations in various types of hot plasmas.

Acknowledgement

This work has been carried out within the framework of the EUROfusion Consortium and has received funding from the Euratom research and training programme 2014–2018 and 2019–2020 under grant agreement No. 633053. The views and opinions expressed herein do not necessarily reflect those of the European Commission.

References

[1] R.W. Schrittwieser et al., *Contrib. Plasma Phys.* **50** (2010) 860-865
[2] C. Ionita et al., *Materials* **13** (2020) 4524.

On surface effects in a capacitive argon discharges

J. T. Gudmundsson[1,2], Janez Krek[3], De-Qi Wen[3,4], E. Kawamura[5], M. A. Lieberman[5], Peng Zhang[3] and J. P. Verboncoeur[3,4]

[1] *Science Institute, University of Iceland, Dunhaga 3, Reykjavik, Iceland*
[2] *Division of Space and Plasma Physics, School of Electrical Engineering and Computer Science, KTH Royal Institute of Technology, Stockholm, Sweden*
[3] *Department of Electrical and Computer Engineering, Michigan State University, East Lansing, Michigan, MI48824, United States of America*
[4] *Department of Computational Mathematics, Science and Engineering, Michigan State University, East Lansing, Michigan, MI48824, United States of America*
[5] *Department of Electrical Engineering and Computer Sciences, University of California, Berkeley, California, CA94720, United States of America*

One-dimensional particle-in-cell/Monte Carlo collisional simulations were performed on capacitive argon discharges in order to explore the role of surface processes. In the intermediate pressure regime (133 Pa) when secondary electron emission from the electrode surfaces is included in the discharge model, the discharge operation transitions from α-mode to γ-mode, and nearly all the ionization is due to secondary electrons. Simulation results compared to experimental measurements in the pressure range 1 – 20 Pa show good agreement when all surface processes are included in the discharge model.

One-dimensional particle-in-cell/Monte Carlo collisional (PIC/MCC) simulations were performed on a capacitive argon discharge in the intermediate pressure regime (133 Pa) for a 2.54 cm gap, driven by a sinusoidal rf current density of 50 A/m^2 at 13.56 MHz. Most of the ionization occurs near the plasma-sheath interfaces, with little ionization within the plasma bulk region. When the excited states, and secondary electron emission due to neutral and ion impact on the electrodes are included in the discharge model, the discharge operation transitions from α-mode to γ-mode, in which nearly all the ionization is due to secondary electrons. Electron impact of ground state argon atoms by secondary electrons contributes about 76 % of the total ionization; primary electrons, about 11 %. [1].

We also explore how the presence of excited state species enhances the plasma density via resonant state photon-induced secondary electron emission and electron induced secondary electron emission on the electrode surface in the pressure range 1 – 20 Pa and 4 cm gap [2]. The simulation results show good agreement with recent experimental measurements [3] in the low pressure range (1 – 10 Pa) while at the higher pressure (20 Pa) the plasma densities from the PIC/MCC simulations are quantitatively higher than observed in the experiments [2] (see Figure 1).

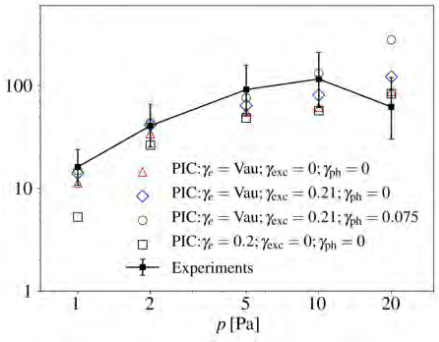

Figure 1: The time-averaged plasma density at the discharge center from kinetic particle-in-cell simulations and experimental measurements, versus the argon gas pressure at a driving voltage of 250 V, driving frequency of 13.56 MHz, and electrode spacing 4 cm, including various surface processes.

References

[1] Gudmundsson, J. T. *et al. Plasma Sources Science and Technology* **30**, 125011 (2021).

[2] Wen, D.-Q. *et al. Plasma Sources Science and Technology* (2023) submitted for publication.

[3] Schulenberg, D. A. *et al. Plasma Sources Science and Technology* **30**, 105003 (2021).

Modeling the extraction of a focused broad ion beam from an inductively coupled plasma source.

K. M. Rettig[1,2], T. Dunger[1], E. Loos[1], M. Nestler[1] and J. Schuster[2]

[1] *scia Systems GmbH, Chemnitz, Germany*
[2] *Fraunhofer Institute for Electronic Nano Systems ENAS, Chemnitz, Germany*

Adjusting properties of a focused broad ion beam to match the requirements of target processes, can be greatly accelerated using simulations. We present a model, capable of calculating ion beam properties based on sources geometries and operation conditions, allowing for prediction and optimization of beam width and ion current. A global model for inductively coupled plasmas is used to obtain plasma parameters from the experimentally applied operation conditions. These parameters are used in a particle-in-cell simulation to numerically calculate the beam extraction from the plasma through a three-grid extraction-system. The resulting simulated ion beam is in good agreement with experimentally observed results.

1 Introduction

By focusing a broad ion beam, it is able to modify the surface of a target locally, which is called ion beam trimming (IBT). Thereby, the ion beam properties must be adjusted to match the according topography error of the semiconductor substrates or optics, which are then used in various applications e. g. augmented reality devices, telescope mirrors or MEMS.

We present a simulation approach to accelerate the development of such adapted focused ion beams. The model is capable of predicting the properties of the plasma and extracted beam, based on sources geometries and applied operation conditions. As a result, the ion beam properties can be adjusted and optimized for target processes and digital prototyping of novel ion beam sources becomes feasible.

To verify the simulation, we experimentally studied the extraction of a focused Ar-ion beam from an inductively coupled plasma (ICP) source through a curved three-grid extraction-system.

2 Simulation model

Ion beam simulation approaches typically require the knowledge of plasma parameters of the investigated system. As plasma diagnostics in an industrial ion source assembly are difficult to realize, we implemented an analytical model for gridded ICP [1]. It utilizes experimentally applied operation conditions to calculate species densities and temperatures in the plasma, which are used as input for the numerical calculation of the beam extraction.

A coupled particle-in-cell (PIC) and direct-simulation Monte-Carlo (DSMC) approach within the code PICLAS [2], simulates the beam formation in the downstream area, including charged and neutral species. To reduce computation time, we used the Boltzmann relation to characterize the electron population in the plasma and to describe space charge compensation (SCC) in the extracted ion beam.

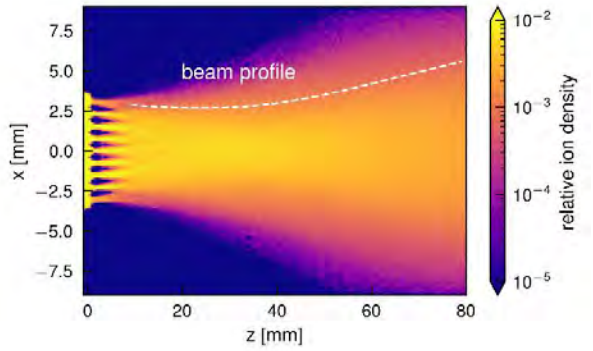

Fig. 1. Projection of the relative ion density in a simulated ion beam and the resulting beam profile.

3 Results

The combined global model and PIC-DSMC approach yields a simulated ion beam, as depicted in Fig. 1, which agrees well with experimentally observed results. A similar qualitative and quantitative behavior in the beam width and extracted ion current is achieved by considering variable extraction-grid transparencies for ions, thus a correct plasma sheath formation, at different applied radio frequency powers. Parameter studies additionally confirm the validity of the simulation approach. Further, the model provides access to the plasma parameters, which otherwise would require complex experimental investigations.

References

[1] Chabert, P. et al. Global model of a gridded-ion thruster powered by a radiofrequency inductive coil. Physics of Plasmas, **19**(7), 073512 (2012).

[2] Fasoulas, S. et al. Combining particle-in-cell and direct simulation Monte Carlo for the simulation of reactive plasma flows. Physics of Fluids, **31**(7), 072006 (2019).

Investigation of self-pulsing discharges in argon at atmospheric pressure

A. P. Jovanović[1], H. Höft[1], D. Loffhagen[1], M. M. Becker[1], and T. Gerling[2,3]

[1] *Leibniz Institute for Plasma Science and Technology (INP), Greifswald, Germany*
[2] *ZIK plasmatis, Leibniz Institute for Plasma Science and Technology (INP), Greifswald, Germany*
[3] *Diabetes Competence Centre Karlsburg (KDK), Karlsburg, Germany*

Understanding the physical processes occurring during and after self-pulsing discharges, such as transient sparks, is very important for optimising plasma sources. For this purpose, a self-pulsing discharge in atmospheric-pressure argon is investigated by means of a time-dependent, spatially one-dimensional (1D) fluid-Poisson model coupled with an equation for the electrical circuit. The model calculations reproduce basic features of the experimentally observed self-pulsing by adapting the properties of this circuit and the applied DC voltage. The spatio-temporally development of charge carriers during the obtained transient spark discharge was analysed to identify the dominant ionic species, which are supposed to be connected to ion-acoustic waves occurring in this type of discharge.

Self-pulsing discharges, such as negative DC corona discharges or transient sparks, have become a good candidate for the efficient production of non-thermal plasmas at atmospheric pressure [1, 2]. In these discharges, the electric circuit limits the current to prevent thermalisation, making them suitable for application. Another interesting aspect of transient spark discharges is the appearance of weak and erratically occurring oscillations of the current signal, since these oscillations were attributed to ion acoustic waves, and their frequency was used to estimate ion densities in argon [3]. Identifying the mechanisms and dominant ions responsible for the excitation of ion acoustic waves could allow using the same procedure for ion density estimation in other discharges as well. Although the experiment provides invaluable information on the discharge behaviour, a combined approach with numerical modelling is often required to fully understand underlying physical processes.

Therefore, a time-dependent, spatially 1D fluid-Poisson model coupled with an electric circuit equation has been used to analyse self-pulsing discharge in atmospheric-pressure argon in a 1.5 mm gap. A detailed description of the model and the solution procedure were recently described in [4].

The current and voltage waveforms and spatio-temporal evolution of ions calculated by the model are shown in Fig. 1. The self-pulsing discharge behaviour in the kHz range is reproduced quite well, i.e. the applied DC voltage drops significantly when a current pulse occurs. An analysis of the relevant charge carriers shows that the Ar^+ ions are locally produced by the direct electron impact ionisation during the initial discharge phase, while Ar_2^+ ions are dominant afterwards (see Fig. 1 (b)). A possible excitation mechanism of ion acoustic waves will be discussed, accompanied by a parametric study of the impact of gap distance and circuit parameters on different discharge modes.

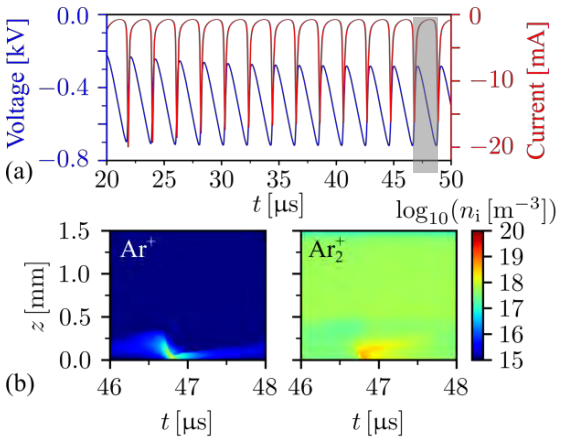

Figure 1. (a) current and voltage waveforms showing the self-pulsing behaviour, (b) spatio-temporal evolution of ion densities during one current pulse (indicated by box in (a)) calculated for gap distance d = 1.5 mm, DC voltage U_0 = -3 kV, resistance R = 1 MΩ and capacitance C = 5 pF.

Acknowledgement

This work has been funded by the DFG (German Research Foundation) – project number 466331904.

References

[1] Bussiahn, R., Brandenburg, R., Gerling, T., Kindel, E., Lange, H., Lembke, N., Weltmann, K.-D., von Woedtke, Th., Kocher, T.: *Appl. Phys. Lett.* **96** 143701 (2010)

[2] Janda, M., Martišovitš V., Machala, Z.: *Plasma Sources Sci. Technol.* **20** 035015 (2011)

[3] Gerling, T., Wilke, C., Becker, M. M.: *J. Phys. D: Appl. Phys.* **54** 085201 (2021)

[4] Jovanović, A. P., Loffhagen, D., Becker, M. M.: https://doi.org/10.48550/arXiv.2212.01288 (2023)

Atmospheric pressure high current diffuse glow-like dielectric barrier discharges in argon

K. van 't Veer[1], D. Mihailova[1] and J. Van Dijk[2]

[1]*Plasma Matters B.V., Eindhoven University of Technology, P.O. Box 513, 5600MB Eindhoven, The Netherlands*
[2] *Dept. Applied Physics, Eindhoven Univ. Techn., Eindhoven, The Netherlands*

The PLASIMO drift-diffusion model is used to study dielectric barrier discharges in argon. The model can describe the plasma over a wide range of conditions. Various discharge regimes and glow-like discharge structures can be observed. Most notably, depending on the conditions, multiple distinct (nonfilamentary) breakdowns can be observed during a single discharge cycle. Each reaction in the model can be assigned one specific role, determining the discharge structure and characteristics. Predicted discharge characteristics were also found in experiments, which exhibit an excellent agreement with the model.

A time dependent 1D drift-diffusion model of a classical parallel plate (double) dielectric barrier discharge in atmospheric argon is used to study high current diffuse glow-like discharges over a wide range of conditions.

The dielectric barrier thickness ranges from 0.1 to 1.5 mm, with dielectric constants of 3.4 to 3.8. The applied voltage ranges from 500 to 2500 V up to 8 kV – depending on the dielectric barriers. The discharge frequencies vary from 50 kHz to 200 kHz.

The model was also used to study dual frequency excitation, i.e., the addition of ca. 200 V at 13.56 MHz on top of the mentioned low frequency (in the order of kHz) [1].

The secondary electron emission coefficients are varied in order to adjust the current and to study the influence of the various ions on the discharge characteristics.

The model solves the continuity equations in the drift-diffusion approximation for 5 species (i.e., electrons, Ar, Ar[4s], Ar^+ and Ar_2^+). Those species interact through 6 reactions. In addition, the model solves the electron energy equation and the poisson equation. The Boltzmann solver BOLSIG+ [2] is coupled and used to calculate the electron mobility and electron impact rate coefficients.

The reaction mechanism is found to capture the plasma behaviour at all aforementioned conditions.

The results of the model are validated by comparison with experimental data at various conditions. At low frequencies the model predicted multiple (nonfilamentary) breakdowns during a single discharge cycle. Based on the model, experiments where conducted that also show the predicted growth of a secondary current peak (cf. Figure 1).

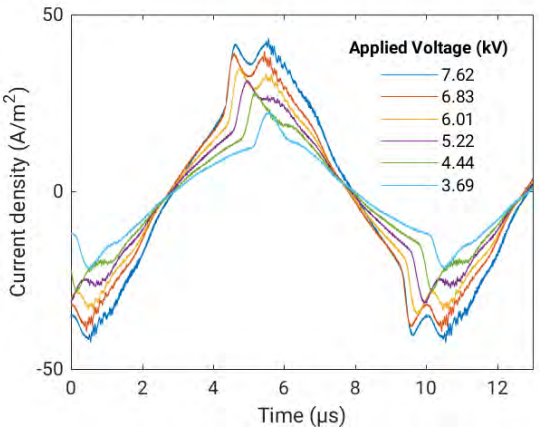

Figure 1: Experimental current characteristics at different sinuisodal applied voltages, showing the gradual growth of a secondary current peak. The discharge frequency is 100 kHz, the dielectric barriers are 1.5 mm with a dielectric constant of 3.8 and the discharge gap is 1 mm.

Acknowledgements

We thank prof. Richard Engeln and dr. Mark Damen for making their dielectric barrier discharge setup available and performing the experiments.

References

[1] Liu, Y., Van 't Veer, K., Peeters, F. J. J., Mihailova, D. B., Van Dijk, J., Starostin, S. A., Van de Sanden, M. C. M. & De Vries, H. W. Numerical simulation of atmospheric-pressure 200 kHz/13.56 MHz dual-frequency dielectric barrier discharges. Plasma Sources Sci. Technol. **27**, 105016 (2018).

[2] Hagelaar, G. J. M. & Pitchford, L. C. Solving the Boltzmann equation to obtain electron transport coefficients and rate coefficients for fluid models. Plasma Sources Sci. Technol. **14**, 722-733 (2005).

Corona modelling for ro-vibrationally resolved spectra analysis in low-temperature hydrogen plasmas

R.C. Bergmayr[1], D. Wünderlich[1], L.H. Scarlett[2], M.C. Zammit[3], I. Bray[2], D.V. Fursa[2] and U. Fantz[1]

[1] *Max Planck Institute for Plasma Physics, 85748 Garching, Germany*
[2] *Curtin Institute for Computation and Department of Physics and Astronomy, Curtin University, Perth, Western Australia 6102, Australia*
[3]*Theoretical Division, Los Alamos National Laboratory, Los Alamos, New Mexico 87545, United States of America*

Corona modelling in combination with emission spectroscopy is a useful tool to derive ro-vibrational distributions and plasma parameters in low-temperature hydrogen plasmas. This contribution discusses corona models based on fully ro-vibrationally resolved MCCC cross sections and focuses on their validation to guarantee an accurate non-invasive diagnostics method.

The rotational and vibrational excitation of the hydrogen molecule (H_2) is crucial for the plasma chemistry and kinetics in low-temperature plasmas, as a change in the ro-vibrational distribution can significantly affect molecular reaction rates [1].

The ro-vibrational distribution of the ground state along with the plasma parameters (e.g. n_e and T_e) in H_2 plasmas can be determined by emission spectroscopy together with population modelling [2]. In comparison to other diagnostics (e.g. laser induced fluorescence), emission spectroscopy features the main advantage that it is non-invasive exploiting naturally emitted radiation [3].

If the radiation field, ionization degree and electron density in a plasma are low and if both the collision reactions between excited states and absorption of photons are negligible, corona models are applicable that balance excitation by collisions from the ground state and spontaneous emission in the form of rate equations. The flexible Yacora code can be used to solve the underlying system of equations [4].

Due to ro-vibrational splitting of the electronic states a corona model for H_2 easily consists of around 1000 (sub-)levels. For all these levels ro-vibrationally resolved cross sections and Einstein coefficients ought to be known. While the Einstein coefficients can be calculated using for instance the Level code [5], as far as cross sections are not available, scaling laws [6] or simplifications [7] have to be accepted at the expense of the accuracy of the models. An example of the latter is a previous Yacora corona model for the Fulcher-α band applying vibrationally resolved cross sections for optically allowed collisions. With this model the ro-vibrational emission band structure could be calculated accurately, while the absolute emission yield was overestimated [7].

This contribution discusses corona models for the visible and vacuum ultraviolet emission spectrum of H_2 applying fully ro-vibrationally resolved MCCC cross sections. The MCCC (molecular convergent close-coupling) method [8] in the adiabatic-nuclei formulation is an ab initio approach for electron scattering problems with the ability to provide accurate ro-vibrationally resolved cross sections also for optically forbidden transition processes.

The model derived spectra can be compared with measured ones from emission spectroscopy. A particular focus of this contribution will be on the validation of the models to further highlight their suitability as part of a non-invasive diagnostic for low-temperature plasmas.

References

1. S. Briefi and U. Fantz, Plasma Sources Sci. Technol. **29**, 125019 (2020).
2. D. R. Bates, A. E. Kingston, and R. W. P. McWhirter, Proc. R. Soc. Lond. A **267**, 297 (1962).
3. U. Fantz, Plasma Phys. Control. Fusion **40**, 1035 (1998).
4. D. Wünderlich, M. Giacomin, R. Ritz, and U. Fantz, Journal of Quantitative Spectroscopy and Radiative Transfer **240**, 106695 (2020).
5. R. J. Le Roy, Journal of Quantitative Spectroscopy and Radiative Transfer **186**, 167 (2017).
6. D. Bruno, B. Zaniol, and I. Mario, Physica Scripta **98**, 15614 (2022).
7. D. Wünderlich and U. Fantz, Atoms **4**, 26 (2016).
8. M. C. Zammit, D. V. Fursa, J. S. Savage, and I. Bray, J. Phys. B: At. Mol. Opt. Phys. **50**, 123001 (2017).

Axisymmetric streamer model in the AMReX environment

I. Simonović[1], D. Bošnjaković[1] and S. Dujko[1]

[1] *Institute of Physics Belgrade, University of Belgrade, Pregrevica 118, 11080 Belgrade, Serbia*

In this work, we have developed an axisymmetric streamer code in the AMReX software framework. The model employed in this code is based on the first-order fluid model with bulk transport coefficients and local field approximation. This code is tested by comparison of its results with the results of the Afivo-streamer code.

Streamers are precursors of arcs and lightning leaders in nature and in plasma technologies [1]. Streamers are used for surface processing, and in plasma medicine for disinfection, and wound healing [1]. Further development of these applications would benefit from a better understanding of streamers through both experiment and modelling.

We have developed an axisymmetric streamer code that is based on the first-order fluid model with bulk transport coefficients. The code is implemented in the AMReX software framework [2]. AMReX is an open source library for numerical calculations with massively parallel, block-structured adaptive mesh refinement. AMReX enables both MPI and OpenMP parallelization, as well as parallelization on graphics processing units. In addition, AMReX comes with inbuilt multigrid solvers and functionality for saving both grid and particle data to checkpoints and to output files for plotting. Although AMReX is implemented in C++, it also has a Fortran interface and Python interface which is under development.

In our model, the time evolution of the number density of electrons is determined by employing the advection-diffusion-reaction equation, while the time evolution of the number densities of positive and negative ions is determined by the reaction equations. Ions are assumed to be stationary for the timescales of our simulations. The spatial dependence of transport coefficients (mobility, diffusion, and rate coefficients for electron impact ionization and attachment) is determined by employing the local field approximation. The total electric field is expressed as the sum of constant and homogeneous applied electric field and the electric field which is generated by space charge. The electric potential of space charge is determined by employing the AMReX inbuilt geometric multigrid solver for solving the Poisson equation. We employ zero Neumann boundary conditions for the number density of electrons at all boundaries. For the electric potential of space charge, we employ zero Neumann boundary conditions at boundaries that are perpendicular to the radial coordinate and zero Dirichlet boundary conditions at boundaries which are perpendicular to the axial coordinate.

We employ the finite volume method for the spatial discretization of the advection-diffusion-reaction equation. Electric field components and electron flux components are defined at cell faces, while the number densities of electrons and ions, the intensity of the total electric field, as well as transport coefficients, are defined at cell centers. We use the Runge-Kutta method for the time integration of this equation. In our code, both 2nd and 4th-order Runge-Kutta methods are supported. The validity of this code is tested by comparing its results to the results of the Afivo-streamer code [1] in a wide range of gases.

Acknowledgments: This work is supported by the Science Fund of the Republic of Serbia, Grant No. 7749560, Exploring ultra-low global warming potential gases for insulation in high-voltage technology: Experiments and modelling EGWIn.

References

[1] Teunissen, J. & Ebert, U. Simulating streamer discharges in 3D with the parallel adaptive Afivo framework. *Journal of Physics D: Applied Physics* **50**, 474001 (2017).

[2] Zhang, W. *et al.* AMReX: a framework for block-structured adaptive mesh refinement. *Journal of Open Source Software* **4**, 1370 (2019).

XXXV ICPIG, July 9-14, 2023, Egmond aan Zee, The Netherlands Topic numbers: 5,10

On stability of negative corona discharges

A. Eivazpour Taher[1,2], N. G. C. Ferreira[1,2], P. G. C. Almeida[1,2], G. V. Naidis[3], M. S. Benilov[1,2]

[1] *Departamento de Física, FCEE, Universidade da Madeira, Largo do Município, 9000 Funchal, Portugal*
[2] *Instituto de Plasmas e Fusão Nuclear, Instituto Superior Técnico, Universidade de Lisboa, 1041 Lisboa, Portugal*
[3] *Joint Institute for High Temperatures, Russian Academy of Sciences, Moscow 125412, Russia*

Stability of negative DC corona discharge is investigated numerically. Atmospheric pressure ambient air in needle-to-plane configuration is treated as an example. Linear stability analysis of the trivial solution, describing the no-discharge situation, has shown that the loss of stability, which happens when the applied voltage equals the corona ignition voltage, occurs on a real eigenvalue. It follows that the negative corona must be stable at low currents. This conclusion was confirmed by investigation of stability of different states of the negative corona discharge against finite perturbations, performed by means of a time-dependent solver. The negative corona is stable against finite perturbations close to its inception as it should. When the current is increased, stability is lost in a time-periodic manner, and the discharge evolves in time into Trichel pulses. Trichel pulses stop appearing with further increase of current, which is an effect already known in the literature, meaning that the stability of a stationary negative corona discharge is regained.

1. Introduction

The appearance of Trichel pulses is an inevitable phenomenon in negative corona discharges in electronegative gases. It is clear that the transition of the discharge between pulseless and pulsed modes is a matter of loss of stability of quasi-stationary negative DC corona discharge. This topic is investigated using as an example a corona in air at atmospheric pressure in a needle-to-plane electrode configuration with 5mm gap [1].

2. The approach

Following [2], a linear stability analysis of the trivial (no-discharge) solution was performed by means of an eigenvalue solver. The trivial solution loses stability when the applied voltage reaches the corona ignition voltage, in agreement with [2]. This occurs on a real eigenvalue, which means that the negative corona must be stable at low currents.

This conclusion was confirmed by investigation of stability of the negative corona discharge against finite perturbations: perturbations in the form of small increments of the applied voltage (about 1V) are imposed and the evolution of the discharge over time is followed by means of a time-dependent solver.

3. Results and discussion

The computed current-voltage characteristics of the stationary negative corona discharge is shown in figure 1. As a perturbation is imposed, the discharge evolves into a stationary state at currents below ~0.2μA (10V above the inception voltage). At higher currents, the discharge becomes unstable and Trichel pulses appear. As the current reaches about 60μA, the Trichel pulses stop appearing, which is an effect already known in the literature; the stationary corona regains stability. The conclusion that the negative corona is stable at low currents is interesting and promises a further insight into the nature of the Trichel pulses.

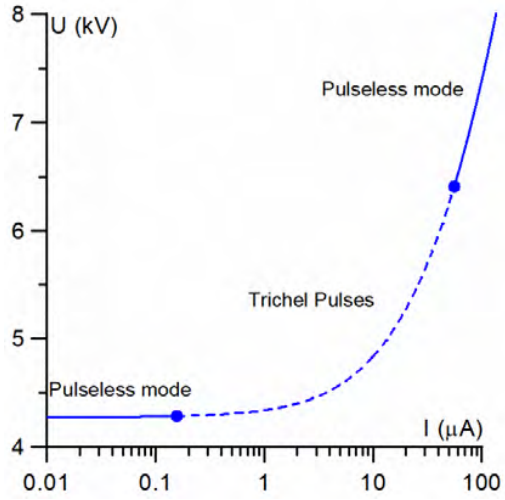

Figure 1: CVC of stationary negative corona discharge. Solid: stable states. Dashed: unstable states (computed by means of a stationary solver). Circles: points of neutral stability.

4. Acknowledgments

The work at Universidade da Madeira was supported by FCT of Portugal under Project Nos. UIDP/50010/2020 and UIDB/50010/2020, and by European Regional Development Fund under Project No. PlasMa-M1420–01-0145-FEDER-000016.

5. References

[1] N. G. C. Ferreira, P. G. C. Almeida, M. S. Benilov, V. A. Panarin, V. S. Skakun, V. F. Tarasenko, and G. V. Naidis, IEEE Trans. Plasma Sci. 48, 4080 (2020).
[2] M. S. Benilov, P. G. C. Almeida, N. G. C. Ferreira, R. M. S. Almeida, and G. V. Naidis, J. Appl. Phys. 130, 121101 (2021).

Estimating the physics of single positive air streamers from measurable parameters

Dennis Bouwman[1], Hani Francisco[1] and Ute Ebert[1,2]

[1] *Dept. Applied Physics, Eindhoven Univ. Techn., Eindhoven, The Netherlands*
[2] *Centrum Wiskunde & Informatica (CWI), Amsterdam, The Netherlands*

We explain how difficult-to-measure parameters (such as the maximum electric field) of positive streamers can be estimated solely from the measurable parameters velocity, radius and length

We present a semi-analytical model for single steadily propagating positive streamers in air. It uses observable parameters to estimate quantities that are difficult to measure. More specifically, based on velocity, radius, length and the applied background field, our model approximates the maximal electric field, the internal electric field, the charge layer width and the ionization degree. They are the key to determining the primary excitations of molecules and the internal currents can be derived from these. We approximate the electron dynamics in different regions of a uniformly-translating streamer head and use conservation laws to determine unknown quantities. We find good agreement (smaller than several tens of percent) with numerical simulations for a range streamer lengths and background electric fields, even if they do not propagate in a steady manner. This is shown in figure 1. Therefore quantities that are difficult to access experimentally can be estimated from easily measurable quantities and our approximations. The theoretical results form a stepping stone towards efficient 1.5D multi-streamer models.

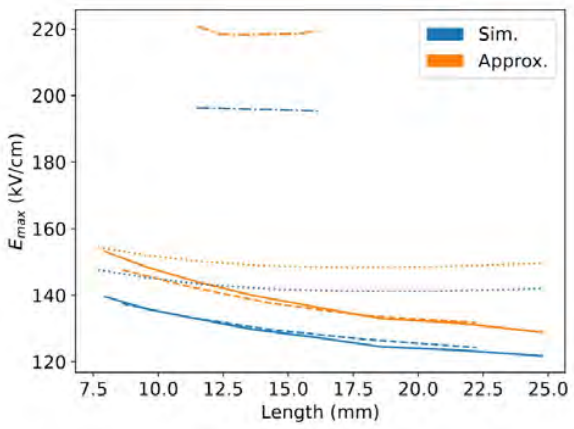

Figure 1: The maximum electric field (Emax) obtained from streamers and our approximation in different background electric fields: 4.5 kV/cm (dash-dot), 10 kV/cm (dashed), 14 kV/cm (solid), 24 kV/cm.

In all cases the agreement is within 20%.

Mass spectrometry of an atmospheric pressure plasma jet interacting with a dielectric surface

L. Chauvet[1], J. Golda[2] and A. von Keudell[1]

[1] *Experimental physics II – Reactive plasmas, Ruhr University of Bochum, Bochum, Germany*
[2] *Research Group – Plasma Interface Physics, Ruhr University of Bochum, Bochum, Germany*

In this work, a dielectric surface is used as a target containing an orifice through which can be sampled the species that are created by a non-equilibrium atmospheric pressure plasma jet and by its interaction with the dielectric surface.

1 Introduction

Over the last decade, the interest for the use of plasma sources grows for a wide range of applications in various fields as analytical chemistry, medicine, decontamination or surface treatment to just mention few examples. Those applications possibly involve an interaction with a surface, affecting the plasma itself in terms of its electric field, its expansion along the surface, the species generated, and the fluid dynamic. Mimicking the conditions in which the plasma will be used in the frame of these applications is crucial, to better understand the mechanisms involved.

In this work, we propose to analyse the species generated when a plasma jet interacts with a 3D printed polyactic acid (PLA) surface by mass spectrometry.

2. Experimental setup

The plasma source is a non-equilibrium atmospheric pressure plasma jet expanding into open air. The source is based on a double dielectric barrier discharge geometry, the high voltage and ground electrodes are both wrapped around the dielectric body as shown on figure 1. This geometry has already been described [1]. The source is fed by a high voltage signal of few kilovolts at 20 kHz. The discharge gas is helium, it flows through the chamber at 1 slm.

The species generated by the jet in ambient air when interacting with a surface are studied with a molecular beam mass spectrometer (MBMS). The maximum pressure needed to operate the mass spectrometer is 10^{-6} mbar. To reach the base pressure, the mass spectrometer is enclosed in a differential pumping stages system with a geometry in line-of-sight. It allows the formation of a molecular beam to measure ions and reactive species sampled from the plasma or its effluent. This system has been described in [2]. The sampling orifice separating the atmospheric pressure from the first stage of the differential pressure interface has a diameter of few tens of μm. A schematic of the system is shown on figure 1. The jet is moveable along the z and y axis allowing to scan the species in the part of the jet propagating along the surface.

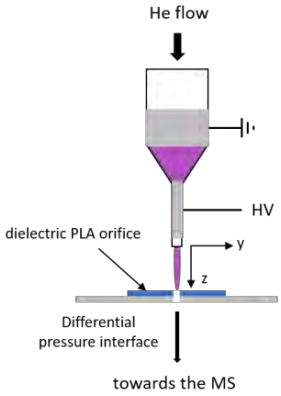

Fig. 1: schematic of the experimental system.

The dielectric PLA orifice has been 3D printed. It has been shaped to adjust to the top of the existing orifice of the differential pressure interface of the MBMS. The dielectric acts as a shield to avoid the discharge arcing and as a dielectric surface on which the plasma impinges.

A multiscalar card can also be coupled to the output signal from the detector of the mass spectrometer and in order to trigger the acquisition on the rising edge of the pulse.

In this work, we propose to evaluate the capability of this system to measure the species from the discharge propagating on the surface. Those measurements are aiming to be temporally resolved.

References

[1] L. Chauvet, L. Thérèse, B. Caillier, Ph. Guillot, Characterization of an asymmetric DBD plasma jet source at atmospheric pressure, J. Anal. At. Spectrom., 29, 2050-2057 (2014).

[2] S. Große-Kreul, S. Hübner, S. Schneider, D. Ellerweg, A. von Keudll, S. Matejcik and J. Benedikt, Mass spectrometry of atmospheric pressure plasmas, Plasma Source Sci. and Technol., 24 (2015) 044008.

Oxygen atom TALIF : temperature dependence of fluorescence quenching

J-P.Booth[1], C.Drag[1], S.Zyryanov[2] and D.Lopaev[2]

[1] *Laboratoire de Physique des Plasma (LPP), CNRS, Sorbonne Université, École Polytechnique, Institut Polytechnique de Paris, 91120 Palaiseau, France*
[2] *Skobeltsyn Institute of Nuclear Physics, Lomonosov Moscow State University, Russia*

The rate constant for the quenching of the 3p ^3P_J level of atomic oxygen (the origin of 844nm fluorescence in 226nm TALIF detection of atomic oxygen) was measured in a DC positive glow discharge in pure O_2 at pressures between 0.5 and 10 Torr and gas temperatures between 300 to 800 K. The quenching rate constant was found to be independent of the gas temperature over the conditions studied.

Introduction

Two-photon Absorption Laser Induced Fluorescence (TALIF), with Xe [1] is widely used to determine absolute atomic oxygen densities. However, collisional fluorescence rate must be known. At atmospheric pressure the lifetime can be below 1 ns, requiring picosecond lasers [2]. If these are not available, it would be useful to be able to make an estimate from the gas pressure and density, but the temperature dependence has not been investigated.

High-resolution TALIF was developed to measure the gas translational temperature in oxygen discharges [3], using a home-built pulsed laser to generate narrow-band 226nm tuneable radiation [4]. Measurements were made in a dc glow discharge in pure oxygen at 0.2 to 10 Torr. HR-TALIF gives the gas translational temperature, the relative oxygen atom density, and the effective lifetime of the fluorescing atoms. Therefore we have all the information necessary to study the pressure and temperature dependence of the quenching processes. The dc discharge operates in flowing O_2 in a 2cm ∅ glass tube [5]. The pulsed UV laser beam (226nm, ~1mJ, 9ns, 20 Hz, spectral width 100MHz [4]) is focussed along the tube axis through a silica window. 844nm fluorescence is collected through the tube wall, detected with a photomultiplier with 850nm filter, and recorded by a numerical oscilloscope.

Results

The temperature increases with discharge current and O_2 pressure (Fig 1), reaching a maximum of 830K. The fluorescence decay rate is plotted as a function of gas density in figure 2. Strikingly, the data fall onto a single line, independent of the gas temperature. A linear fit gives the quenching rate constant, in excellent agreement with Niemi et al. [1] for pure O_2 at room temperature, despite 1) the gas temperature varies 300-850K, 2) the quenching mixture consists of up to 17% O 2p ^3P_J atoms and 8 % O_2 $a^1\Delta_g$ in addition to O_2 X $^3\Sigma_g^+$[5].

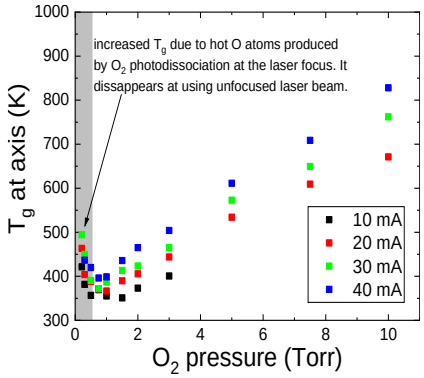

Figure 1 Measured O atom translational temperature.

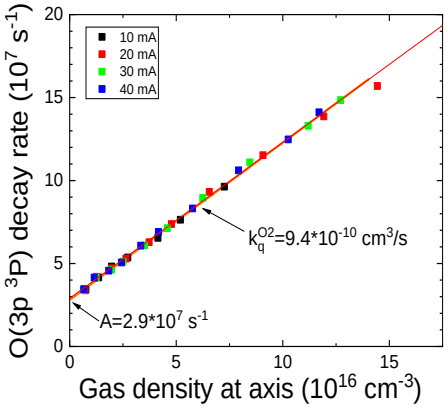

Figure 2 Stern-Vollmer plot of the fluorescence decay rate.

[1] K. Niemi, V. Schulz-von der Gathen, and H.F. Dobele, *PSST,* **14**, 375, (2005)
[2] S. Schröter, J. Bredin, A.R. Gibson, A. West, J.P. Dedrick, E. Wagenaars, K. Niemi, T. Gans, and D. O'Connell, *PSST,* **29**, 105001, (2020)
[3] J.P. Booth, D. Marinov, M. Foucher, O. Guaitella, D. Bresteau, L. Cabaret, and C. Drag, *J. Instrum,* **10**, C11003, (2015),
[4] P. Lottigier, A. Jucha, L. Cabaret, C. Blondel, and C. Drag, *Applied Physics B,* **125**, 14, (2019),
[5] J.-P. Booth, A. Chatterjee, O. Guaitella, J. Santos Sousa, D. Lopaev, S. Zyryanov, T. Rakhimova, D. Voloshin, Y. Mankelevich, N. De Oliveira, and L. Nahon, *PSST,* 115009, (2020)

Diagnosis of spatial distribution of electron temperature and electron density of argon inductively coupled plasma by tomographic optical emission spectroscopic measurement

Yuya Yamashita[1], Kenta Doi[2], Tetsuji Kiyota[3], Keiichiro Asakawa[2], Sotaro Hosoya[1], Wataru Kikuchi[1], Atsushi Nezu[4,1], and Hiroshi Akatsuka[5,1]

[1] *Dept. Electr. Electron. Eng., Tokyo Tech, Meguro-ku, Japan* [2] *Inst. Adv. Tech., ULVAC, Inc., Susono-shi, Japan*
[3] *Strateg. Plan. Dept., ULVAC, Inc., Chigasaki-shi, Japan* [4] *Open Facil. Cent., Tokyo Tech, Meguro-ku, Japan*
[5] *Inst. Innov. Res., Tokyo Tech, Meguro-ku, Japan*

Argon inductively coupled plasma was diagnosed by tomographic optical emission spectroscopy. Tomographic spectra were analyzed based on the collisional-radiation model to obtain the dependence of electron temperature and density on spatial positions. The dependence of those spatially-resolved plasma parameters upon radio-frequency power and gas pressure is discussed by contrasting experimental and electromagnetic field analysis results.

1 General

Recently, tomographic optical emission spectroscopic (OES) measurement has been reported to understand spatial distributions of plasmas. However, there are no reports of tomographic diagnosis taking detailed atomic and molecular processes into account. To achieve a reliable diagnosis, we report a tomographic OES measurement in inductively coupled plasmas (ICP) and analyze them based on the CR model. The diagnosis of the spatial distribution of electron temperature T_e and density N_e was enabled.

2 Experiments

Argon (Ar) plasma was generated by the ICP unit (chamber size ϕ 354 × H 193 mm) as shown in Fig. 1. The pressure p = 0.5 - 10 Pa and 13.56 MHz power P = 200 - 800 W were applied. The dependence of spectral radiance at the window on line-of-sights was measured using a multi-channel spectrometer (M116, Horiba) with 18 fibers with lenses.

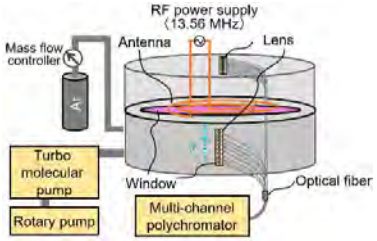

Fig. 1 The schematic diagram of the experimental setup [1].

3 Analysis

In this study, the spectral tomographic calculation was realized by improving the sequential reconstruction program [2]. The dependence of the spectral emission coefficients on the spatial position was obtained. Furthermore, the excited-state density distributions n_i were calculated from line spectra. The Ar CR model [3] is an atomic and molecular process model, which gives n_i as a function of T_e, N_e, atomic temperature T_a, ion temperature T_I, ion density N_I, plasma radius r, p, and electron energy distribution function (EEDF) . In this study, T_e and N_e were diagnosed by the fitting of n_i calculated by the Ar CR model and the experimentally obtained n_i, assuming T_a, T_I, N_I, r, p, and Maxwellian EEDF [1].

4 Results and Discussion

Figure 2 shows the diagnostic results of the spatially-resolved T_e on the y-z plane. T_e was asymmetric to the y-axis. This was caused by the geometry of the antenna, which was clarified by the electromagnetic field analysis conducted separately. While results are not given here due to the limitation of space, the position dependence of T_e and N_e on power and pressure dependencies have already been analyzed. The details will be presented in my presentation, along with an electromagnetic field analysis as a comparison.

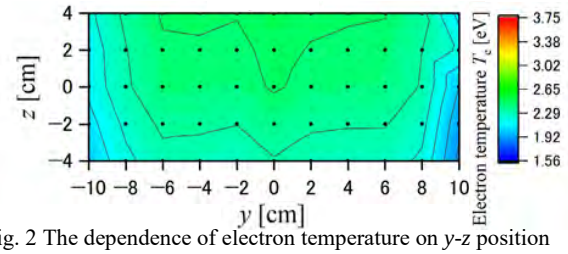

Fig. 2 The dependence of electron temperature on y-z position (pressure p=1Pa, power P=200W) .

Acknowledgment

The authors thank to Mr. Masaki Yokoi and Ms. Yoko Sato of HORIBA STEC, Co., Ltd., Mr. Kengo Yasui, Mr. Takumi Miyaoka, and Mr. Masayuki Sakurai of HORIBA, Ltd. for lending the multi-channel spectrometer and advising on measurements using the spectrometer. This work was supported by JST SPRING, Grant Number JPMJSP2106.

References

[1] Y. Yamashita et al., Ext. Abstr. 70th JSAP Spring Meet. 2023, p.07-007 (2023).
[2] D. R. Ferreira, https://github.com/diogoff/isttok-tomography.
[3] J. Vlcek, J. Phys. D: Appl. Phys., **22**, p.623 (1989).

Electric field analysis of single channel stable streamers using E-FISH

J.H. Laarman, Y. Guo, A.A.A. Limburg, S. Nijdam

Dept. Applied Physics, Eindhoven Univ. Techn., Eindhoven, The Netherlands

In this work, E-FISH's diagnostic ability to determine an absolute electric field is experimentally verified using electrodes with known electric fields, after which these measurements are repeated onto stable, single channel streamers to determine their absolute electric fields.

1 Introduction

Streamer discharges have been researched extensively in recent papers, in which their charge distribution dynamics and electric fields are simulated and measured. However, due to the transient nature of streamers, these phenomena are difficult to analyse. Dijcks et al. [1] have measured streamers using OES and were able to determine the electric field, but have issues in the low-emission, high field region just in front of the streamer. They did not use a recent technique called Electric Field Induced Second-Harmonic generation (E-FISH). This technique allows for a direct electric field measurement anywhere in a plasma using a laser as a probe.

As described in the work of Chng et al., the full length and shape of the electric field have a big influence on the evolution of the E-FISH signal [2], which was previously assumed to be predominantly generated mainly at the focus of the laser beam. Their work shows that this assumption is invalid, which increases the complexity of obtaining the electric field from the SH intensity.

Recent developments on the processing of the E-FISH signal have made this a more viable way of obtaining a direct electric field measurement of a streamer if cylindrical symmetry can be assumed. This will also enable a thorough spatial and temporal scan of the electric field of a streamer, which ideally results in a 2D image of the electric field distribution.

2 Methods

A Nd:YAG laser with a pulse duration of 120 ps is used for the E-FISH setup in order to obtain a high temporal resolution. The repetition rate of the laser is 10 Hz while the pulse energy is on the order of 150 mJ with a Gaussian beam profile with a diameter of 10 mm before focusing.

This laser is focused using a lens with a focal length of 500 mm or higher, such that they can be placed outside the vacuum vessel.

The setup is firstly carefully calibrated using several electrodes of different shapes, including electrodes which have multiple peaks in their electric field.

The E-FISH signal is determined as a function of various focal lengths and position offsets of the laser with respect to these electrodes. This signal is compared to theory using simulations and calibration constants are determined to verify the ability to measure the absolute electric field strength.

After confirming the ability of E-FISH to measure known cylindrically symmetric electric fields, the streamer generation vessel is placed in the setup. A visualisation of a streamer measurement using the vessel can be found in Figure 1. In previous work, this vessel has been used to produce stable, non-branching streamers [1], which can be considered cylindrically symmetric.

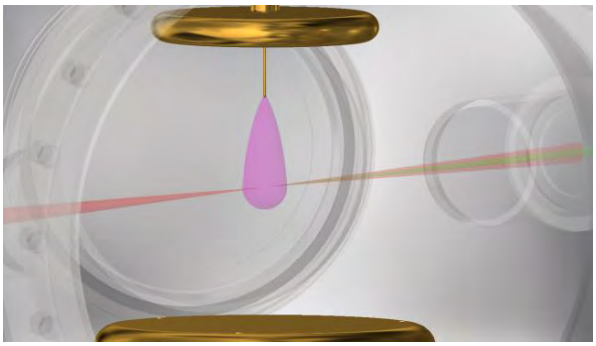

Figure 1: The produced streamer (in purple) causes the generation of a second harmonic in the intersecting laser beam (in red/green).

The same measurement methods, calibration constants and setup parameters and variables are used to obtain the absolute electric field distributions of the streamers.

References

[1] Dijcks et al. High-resolution electric field and temperature distributions in positive streamers. Front. Phys. 1120284 (2023)

[2] Chng et al. Electric field measurements in plasmas: how focusing strongly distorts the E-FISH signal. PSST, 29(12):125002 (2020).

Laser-induced plasma formation in water with up to 600 bar hydrostatic pressure and up to 400 millijoule double-pulse LIBS

M. Henkel[1], M. Siemens[2], R. Methling[1], St. Franke[1], B. Emde[2], J. Hermsdorf[2] and D. Gonzalez[1]

[1] *Leibniz Institute for Plasma Science and Technology (INP), Felix-Hausdorff-Straße 2, 17489 Greifswald, Germany*

[2] *Laser Zentrum Hannover e.V. (LZH), Hollerithallee 8, 30419 Hannover, Germany*

Double-pulse LIBS is a promising technique for deep-sea applications. LIBS measurements in water with up to 600 bar and 400 mJ each pulse were done to select laser parameters which promote optimized spectral line emission from plasma even at elevated pressures, where line broadening until loss of the most spectral information can occur. Optical emission spectroscopy, using a Czerny-Turner spectrometer, has been applied to investigate the dependence of the emitted radiation on laser parameters and hydrostatic pressure. It has been found, that higher laser pulse energies, especially with high water pressure, can also have an adverse effect on the measured spectrum.

LIBS is an established method to analyse material samples with regard to their chemical composition. The possibility of using LIBS underwater makes it particularly interesting for raw material analysis in the deep sea. Double-pulse LIBS is a promising application for this [1], in which a first laser pulse creates a cavity on the material surface to be analysed and a second laser pulse forms the plasma inside the cavity. However, high pressures in the deep sea will have an impact on the plasma and its emission [1, 2].

LIBS measurements in water with a hydrostatic pressure of up to 600 bar and a double-pulse laser with up to 400 mJ each pulse were done to select laser parameters, which promote optimized spectral line emission from plasma even at elevated pressures. Optical emission spectroscopy, using a Czerny-Turner spectrometer, has been applied to study the temporal evolution of the plasma and its emission for different laser parameters. For this purpose, the ratio between continuous and line radiation as well as the line broadening were examined.

Contrary to previous observations in shallow water [3], it could be observed that an increase in the laser pulse energy leads to larger line broadening and a higher continuum-to-line ratio in case of a reduced delay time between the laser pulses, as are necessary at high pressures in water due to the reduced plasma lifetime. For a more detailed study of the dependence of continuum-to-line ratio and line broadening on the laser pulse energies and water pressure, spatially resolved spectra were measured perpendicular to the surface.

This comparative measurements with different laser parameters and water pressures and conclusions for the later application in elevated hydrostatic pressure are shown in this contribution.

References

[1] Emde, B. *et al.* Double pulse laser induced breakdown spectroscopy at 600 bar water pressure. *Procedia CIRP* 94:791–795 (2020).

[2] Thornton, B. & Ura, T. Effects of pressure on the optical emissions observed from solids immersed in water using a single pulse laser. *Applied Physics Express* 4:022702 (2011).

[3] Henkel, M. *et al.* Laser-induced plasma formation in water with up to 400 millijoule double-pulse libs. *to be published* .

Development of a reaction mechanism for CO_2-N_2 plasmas

Chloé Fromentin[1], Tiago Silva[1], Tiago C. Dias[1], Vasco Guerra[1], Omar Biondo[2], Edmond Baratte[3], and Olivier Guaitella[3]

[1] *Instituto de Plasmas e Fusão Nuclear, Instituto Superior Técnico, Universidade de Lisboa, Portugal*
[3] *Plasma Lab for Applications in Sustainability and Medicine – ANTwerp, Belgium*
[2] *Laboratoire de Physique des Plasmas (UMR 7648), CNRS, Univ. Paris Saclay, Sorbonne Université, École Polytechnique, France*

This contribution reports the comparison of simulation results from a 0D self-consistent kinetic model with recent experimental data obtained in low-pressure CO_2-N_2 plasmas. The system of election is a DC glow discharge, operating at a few Torrs and tens of mA in a Pyrex tube of radius 1 cm. The set of measurements provides the gas temperature, vibrational temperatures of CO and the various modes of CO_2, reduced electric field, E/N, and densities of $O(^3P)$, $CO(X^1\Sigma^+)$, $CO_2(X^1\Sigma^+_g)$ and $NO(X^2\Pi_r)$. This work explores the effect of nitrogen addition on CO_2 dissociation under various non-equilibrium plasma conditions. The comparison of the simulation results obtained with the LoKI numerical simulation tool and the experimental data allows the development of a new reaction mechanism, i.e., a set of reactions and rate coefficients validated against benchmark experiments, for CO_2-N_2 plasmas.

1 Introduction

Reducing anthropogenic CO_2 emissions to mitigate climate change is one of the greatest challenges of the century. The conversion of CO_2 into chemicals and energy products using non-thermal plasmas (NTP) via the CCU approach is very promising. The study of CO_2-N_2 NTPs, in particular, is important because N_2 is the main impurity in most CO_2 industrial flue gas and the admixture of N_2 has a beneficial impact on CO_2 decomposition. The aim of this work is to develop a reaction mechanism for CO_2-N_2 plasmas.

2 Experiment and model

A joint experimental and modelling investigation is carried out. The experiments are performed in DC glow discharges, operating at pressures in the range P = 0.6 - 4 Torr and discharge current of 50 mA, in a Pyrex tube of radius 1 cm. These plasma sources are ideal for model validation as they are stable, axially homogenous and accessible to different diagnostics. The set of measurements provides the gas temperature, vibrational temperatures of CO and the various modes of CO_2, reduced electric field E/N, and densities of $O(^3P)$, $CO(X^1\Sigma^+)$, $CO_2(X^1\Sigma^+_g)$ and $NO(X^2\Pi_r)$, obtained by in situ Fourier transform infrared (FTIR) spectroscopy [1] and actinometry [2].

The simulations are done with the simulation tool LoKI (Lisbon KInetics), solving a Boltzmann-chemistry global model [3,4]. The model previously validated for pure CO_2 [5–7] is complemented here with the addition of the electron, vibrational (accounting for 59 vibrational levels) and chemical kinetics of N_2 and the model predictions are compared with measurements in CO_2–N_2 mixtures.

3 Results and discussion

The absolute CO_2 conversion increases with N_2 admixture, both in the experiments and calculations, indicating that N_2 has a beneficial impact on CO_2 splitting. This effect is attributed to the presence of the metastable state $N_2(B^3\Pi_g)$ (creating a new channel for CO_2 dissociation) and to the dilution of dissociation products (limiting the back reactions). The electronically excited state $CO(a^3\Pi_r)$ also influences the plasma chemistry even with the addition of a significant amount of N_2, showing the importance of electronically excited states in the dissociation kinetics.

Acknowledgments

This work was partially supported by the European Union's Horizon 2020 research and innovation programme under grant agreement MSCA ITN 813393, and by Portuguese FCT-Fundação para a Ciência e a Tecnologia, under projects UIDB/50010/2020, UIDP/50010/2020 and PTDC/FIS-PLA/1616/2021.

References

[1] B.L.M. Klarenaar et al., Plasma Sources Sci. Technol. 26 (2017) 115008.
[2] A.S. Morillo-Candas et al., Plasma Sources Sci. Technol. 28 (2019) 075010.
[3] A. Tejero-del-Caz et al., Plasma Sources Sci. Technol. 28 (2019) 043001.
[4] https://nprime.tecnico.ulisboa.pt/loki/
[5] T. Silva et al., Plasma Sources Sci. Technol. 27 (2018) 015019.
[6] M. Grofulović et al., Plasma Sources Sci. Technol. 27 (2018) 115009.
[7] A.F. Silva et al., Plasma Sources Sci. Technol. 29 (2020) 125020.

RF CCPs at intermediate pressure: Dissociation trends in O_2/Ar

S. Zhang[1], G. A. Curley[1] and JP. Booth[1]

[1]*Laboratoire de Physique des Plasmas (LPP), CNRS, Sorbonne Université, École Polytechnique, Institut Polytechnique de Paris, Palaiseau, 91120, France*

We have studied intermediate-pressure (1-10 Torr) RF-CCPs in oxygen/argon mixtures, using cavity ring-down spectroscopy (CRDS) and electrical measurements to determine the oxygen atom densities, the gas temperature, the plasma impedance, and the ion flux. We see a significant increase of the oxygen dissociation fraction with Ar addition, which can be attributed to increased electron density.

1 Introduction

Radiofrequency capacitively coupled plasmas (RF-CCP) operating at intermediate-pressures are significant for many applications, notably PECVD, but have been much less studied than lower pressure RF-CCPs because common diagnostic techniques (such as Langmuir probes) are difficult to use.

2 Experimental Setup

Measurements were made in a highly-symmetric CCP reactor, excited at 13.56 MHz, (aluminium, 50 cm diameter with a 2.5 cm gap) in mixtures from pure Ar to pure O_2, and at pressures from 1 to 8 Torr The ion flux profile is measured with a 9-probe array across half the ground electrode radius. The O density, [O], and gas temperature are determined by monomode laser CRDS at 630 nm, using a setup described previously [1].

3 Results and Discussion

The radially-averaged ion flux to the ground electrode is shown in Fig. 1 as a function of RF power for different Ar fraction at 4 Torr. The ion flux increases with power and decreases with Ar fraction, indicating increasing electron density in both cases.

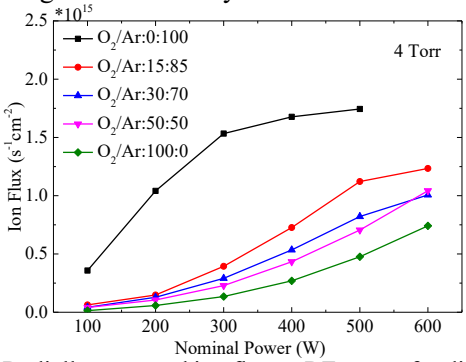

Fig. 1 Radially-averaged ion flux vs RF power for different gas mixtures at 4 Torr.

Fig. 2 (a) shows the O density as a function of O_2 percentage at different RF powers. While [O] increases with RF power as expected, the O density passes through a maximum at around 50% Ar.
Fig. 2 (b) shows the [O]/[O_2] ratio as a function of Ar addition. The dissociation fraction increases with power, but decreases with O_2 percentage, indicating a higher dissociation rate with Ar addition. The variation of [O] with O_2 addition therefore reflects the trade-off between increasing O_2 feedstock and decreasing electron density.

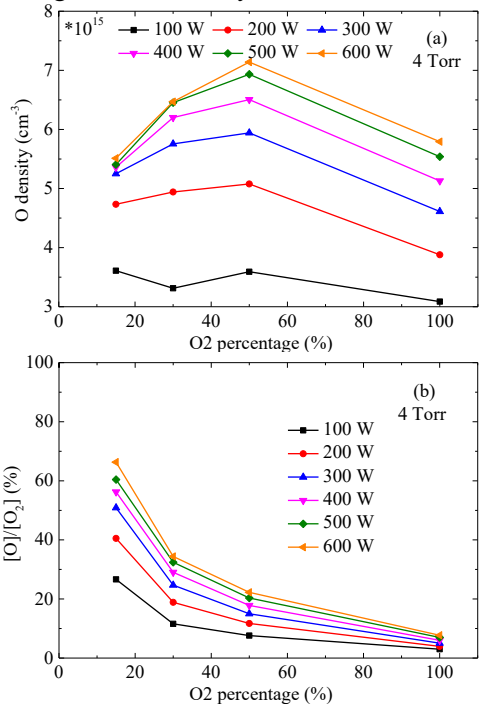

Fig. 2 (a) O density and (b) [O]/[O_2] vs. O_2 fraction for different powers at 4 Torr.

At pressures below 2 Torr, we observe complex trends in the atomic oxygen density, which suggest that energetic ion bombardment can increase the surface recombination coefficient of atomic oxygen, which will be discussed in the poster.

4 Acknowledgements

We thank Applied Materials Corporation and Fédération de Recherche PLAS@PAR for financial support, and SZ thanks China Scholarship Council for a doctoral grant.

5 References

[1] J.P. Booth, A. Chatterjee, O. Guaitella *et al*, Plasma Sources Science and Technology, 31, 065012, (2022)

On working gas rarefaction in high power impulse magnetron sputtering

K. Barynova[1], S. Suresh Babu[1], M. Rudolph[2], J. Fischer[3], D. Lundin[3], and J. T. Gudmundsson[1,4]

[1]*Science Institute, University of Iceland, Dunhaga 3, Reykjavik, Iceland*
[2]*Leibniz Institute of Surface Engineering (IOM), Permoserstraße 15, Leipzig, Germany*
[2]*Plasma and Coatings Physics Division, IFM-Materials Physics, Linköping University, Linköping, Sweden*
[2]*Space and Plasma Physics, School of Electrical Engineering and Computer Science, KTH Royal Institute of Technology, Stockholm, Sweden*

The ionization region model (IRM) is applied to explore the working gas rarefaction in high power impulse magnetron sputtering discharges. The various contributions to working gas rarefaction including electron impact ionization, kick-out by the sputtered species and diffusion, are evaluated and compared for the different target materials.

Working gas rarefaction in HiPIMS discharges was studied, using the ionization region model (IRM)[1], when operated with graphite [2], copper [3], molybdenum, titanium [4], and tungsten [5] targets. For all cases the working gas rarefaction is significant, and is caused by several processes, and that their relative importance varies between different target materials.

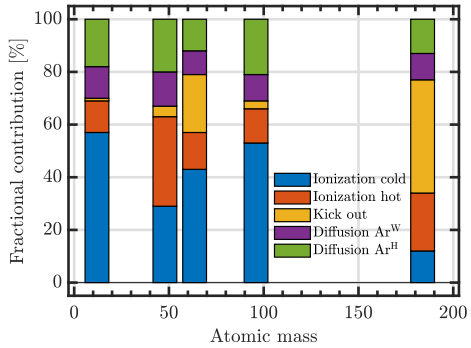

Figure 1: The fractional contribution of the various processes to working gas rarefaction within the ionization region versus the atomic mass. The data is for C (12 amu) ($J_{\mathrm{D,peak}}$ = 1 A/cm^2, t_{pulse} = 50 μs), Ti (47.9 amu) ($J_{\mathrm{D,peak}}$ = 1.0 A/cm^2, t_{pulse} = 100 μs), Cu (63.5 amu) ($J_{\mathrm{D,peak}}$ = 1 A/cm^2, t_{pulse} = 40 μs), Mo (96.0 amu) ($J_{\mathrm{D,peak}}$ = 1 A/cm^2, t_{pulse} = 100 μs), and W (183.8 amu) ($J_{\mathrm{D,peak}}$ = 0.73 A/cm^2 t_{pulse} = 100 μs).

The degree of working gas rarefaction is in the range 36 – 51 % for a discharge with a graphite target and discharge current density in the range 1 – 3 A/cm^2, while it is in the range 40 – 66 % for a discharge with tungsten target and discharge current density in the range 0.33 – 0.73 A/cm^2. Figure 1 shows the fractional contributions to working gas rarefaction versus the atomic mass. In the case of a graphite target, electron impact ionization is the dominating contributor to the working gas rarefaction, with 65 – 69 % contribution, while the kick-out, or sputter wind, has negligible influence, whereas in the case of tungsten target, the kick-out dominates, with 39 – 48 % contribution. The relative role of kick-out by the sputtered species increases, and the relative role of electron impact ionization decreases, with increased mass of the target atoms. The main factor influencing how much each process contributes to working gas rarefaction appears to be the mass of the target species, while it is not clear how the ionization potential and the cohesive energy, that determines the most probable velocity, with which the sputtered particles leave the target, influence the relative contribution of the various terms.

References

[1] Huo, C. *et al. Journal of Physics D: Applied Physics* **50**, 354003 (2017).

[2] Eliasson, H. *et al. Plasma Sources Science and Technology* **30**, 115017 (2021).

[3] Gudmundsson, J. T. *et al. Surface and Coatings Technology* **442**, 128189 (2022).

[4] Rudolph, M. *et al. Journal of Applied Physics* **129**, 033303 (2021).

[5] Suresh Babu, S. *et al. Plasma Sources Science and Technology* **31**, 065009 (2022).

Investigation of radiation of Hg 198 isotope lamp

G.Revalde[1,2], A.Abola[1], N.Zorina[1] and A.Skudra[1]

[1] *Institute of Atomic Physics and Spectroscopy, University of Latvia, Riga, Latvia*
[2] *Institute of Technical Physics, Riga Technical University, Riga, Latvia*

Hg isotope-198 low-pressure discharge lamp spectra in the UV has been studied by the means of a Fourier Transform spectrometer. The real line shapes were calculated using a regularisation method. The structure of Hg II 194.2 nm line was investigated. Optimum operating conditions to ensure an optically thin discharge was found.

1 Introduction

Mercury low-pressure discharge lamps are widely used for different purposes due to the bright radiation in the UV spectral region. However, one of the problems of this discharge is to create optically thin radiation when a narrow resonance line is required, for example in AAS [1]. When Hg lamps are filled with natural mercury, the resonance line is very broad not only because of the isotopic composition of the natural Hg but also due to the self-absorption. In this work, we prepared high-frequency capillary mercury lamps, filled with only one Hg isotope, and studied their spectra in different operation conditions in comparison with a spherical discharge.

2 Experimental

Mercury lamps were produced in our laboratory at the Institute of Atomic Physics and Spectroscopy. Lamps consist of a spherical part (diameter of 10 mm) with a long cylindrical capillary tail [2].

The capillary radius was 500 μm, and the length was about 20 mm. The lamps were filled with the Hg 198 isotope of about 98 % abundance and Xe as a buffer gas. The outer EM field of about 100 MHz /300 MHz was applied to ignite the discharge in the capillary or in the spherical part of the lamp. The spectra were measured by the Fourier spectrometer Bruker IFS HR125 with a spectral resolution of 0.015 cm^{-1}. The spectra were registered from both, the capillary part, and the spherical part. While exciting the discharge from the spherical part, the voltage of the exciting EM field was changed from 7 V to 15 V. The current was kept in the region from 0.4 - 0.8 A.

To recover the real spectral lines, the method elaborated in our laboratory based on Tikhonov's regularisation principle was used [3].

3 Results and discussion

The spectra were recorded in the UV and visible spectral regions depending on operation mode to find the conditions without self-absorption. For example, in fig.1 the Hg II resonance spectral line of 194 nm is shown, emitted from the spherical part of the discharge by the highest voltage. The line has some structure consisting of at least two peaks. Obviously, the other isotopes rise due to the strong self-absorption of the main component. In this work, the optimum conditions were found to minimise the effect of self-absorption.

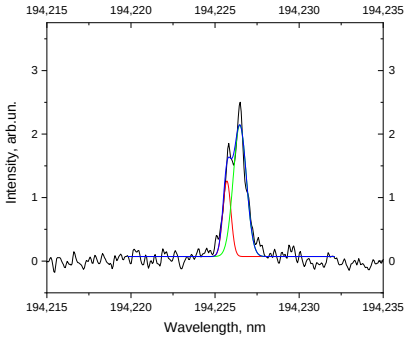

Fig.1. Example of the Hg II 194 nm line, emitted from the spherical part of the lamp. Fitting with Gauss functions is applied to estimate the distance between components.

4 Conclusions

The line spectra of a Hg 198 isotope light source were studied by means of the Fourier Transform spectrometer, as well as the regularisation method to receive the real spectral line shapes. The optimum conditions of lamp operation for optically thin conditions are found.

References

[1] Ganeev A.A., et al. *Spectrochim. Acta* B **58** 879–889 (2003).
[2] Denisova N, et.al. A study of physical processes in microplasma capillary discharges, *Eur. Phys. J. Appl. Phys.* **56**, 24003 (2011).
[3] Zorina, N., Revalde, G., Skudra, A., Validity of the deconvolution method for multicomponent spectral lines, *J. Phys.: Conf. Ser.* **1289,** 012045 (2019)

Acknowledgments

This work was supported by the Latvian Council of Science Project No. lzp-2020/1-0005 and UL IAPS.

Behavior of atomic oxygen in pulsed barrier discharge under sub-atmospheric pressure He/O_2 mixture

Y. Nakagawa, M. Kobayashi and F. Tochikubo

Dept. Elec. Eng. & Comp. Sci., Tokyo Metropolitan Univ., Tokyo, Japan

Sub-atmospheric pressure plasma has a potential to extend the radical lifetime without suppression of radical production, which can increase the radical flux in chemical processes using plasma. In the pure O_2 sub-atmospheric pressure discharges, the atomic oxygen production exhibited a local maximum at 50 kPa. Use of rare-gas mixture is an effective way to improve the radical production efficiency and uniformity of sub-atmospheric pressure plasma. We investigated the behavior of atomic oxygen in pulsed barrier discharge under sub-atmospheric pressure He/O_2 mixture. At 50 kPa, the maximum O production near the cathode was saturated at 50% of O_2 fraction. This is supposed to arise from the balance of electron energy exceeding dissociation threshold and dissociative collision frequency.

1 Introduction

Atmospheric pressure plasma can be applied to various fields including surface modification, chemical synthesis in liquid, and medical treatment. Plasmas in sub-atmospheric pressure, which is slightly reduced from the atmospheric pressure, plasma can extend the radical lifetime with radical production equivalent to atmospheric plasma, leading to increase in radical flux without compromising the diversity of the target[1].

It can be effective to mix a rare gas to the feed gas to increase the average electron energy for improvement of radical production. We investigated atomic oxygen behavior by Two-photon absorption laser induced fluorescence (TALIF)[2] in pulsed barrier discharge under sub-atmospheric pressure He/O_2 mixture.

2 Experimental

A stainless needle anode and a stainless sphere cathode were used for positive pulsed discharge. A borosilicate glass hemisphere was placed on the cathode as a dielectric barrier. The gap length between the needle and the top of cathode was 3 mm. A mixture of He/O_2 was flowed with a rate of 2 SLM in the reactor, and the pressure in the reactor was adjusted to be 50 kPa. A 300-ns-duration pulsed high voltage was applied at 10 pulses/s to the needle. The discharge energy was adjusted to 0.6–0.8 mJ.

The TALIF measurement was conducted using 226 nm pulsed dye laser and the 845 nm fluorescence was detected by a photomultiplier tube after passing optical bandpass filters. The observation volume was W5 × D6.25 × H0.005–0.01 mm^3, where the height was confined by the vertical beam height of the laser.

3 Results and Discussion

The temporal profiles of average O density in the observed volume near the cathode are represented in Fig. 1. The maximum O density $[O]_{max}$ exhibited a saturation near 50% of O_2 fraction, whereas the decay of O density was slowest at 10% of O_2 fraction. The slow decay of atomic oxygen arises from decrease in O_2 density, which strongly affect the O decay via ozone-production reaction, $O + O_2 + M \rightarrow O_3 + M$.

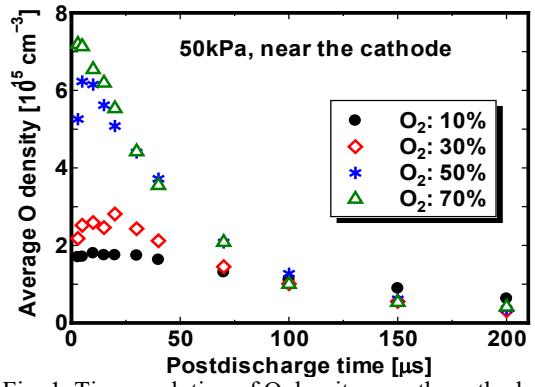

Fig. 1. Time evolution of O density near the cathode.

A possible reason for the saturation in $[O]_{max}$ is as below. With decreasing O_2 fraction (increasing He fraction), the average electron energy and the number of electrons exceeding O_2-dissociation threshold increase. In contrast, collision frequency between electrons and O_2 molecules decreases with decreasing O_2 fraction. Consequently, the total dissociation can be saturated with increasing O_2 as a balance between the effects of electron energy and dissociative collision frequency. More detailed explanation will be described in presentation. Oxygen Fraction below 30% exhibited a lower $[O]_{max}$. This indicates that the decrease in collision frequency was more dominant than increase in electron energy at low O_2 fraction.

References

[1] Y. Nakagawa *et al., J. Appl. Phys.*, **131**, 113304 (2022).

[2] A. V. Klochko *et al., Plasma Sources Sci. Technol.*, 14, 375 (2005)

Interaction of two single-filament, pulsed-operated dielectric barrier discharges

Hans Höft[1], Chiel Ton[2], Tom Huiskamp[2], and Torsten Gerling[3,4]

[1] *Leibniz Institute for Plasma Science and Technology (INP), Greifswald, Germany*
[2] *Department of Electrical Engineering, Electrical Energy Systems, Eindhoven University of Technology, Eindhoven, The Netherlands*
[3] *ZIK plasmatis, Leibniz Institute for Plasma Science and Technology (INP), Greifswald, Germany*
[4] *Diabetes Competence Centre Karlsburg (KDK), Karlsburg, Germany*

A dielectric barrier discharge configuration consisting of two identical single-filament arrangements with a variable radial distance between them was investigated by means of synchronised, fast electrical and optical diagnostics. There seems to be an interaction between these two adjacent, pulsed-driven DBDs, which is supposed to be connected to interplay with the electrical circuit formed by the arrangement.

Dielectric barrier discharges (DBDs) are a common tool to generate a non-thermal, low temperature plasma at atmospheric pressure [1]. The purpose of this study is to investigate the interaction between two defined filaments, since for most DBD arrangements used in practice many filaments occur, while the physical processes within a single filament determine the characteristics of the overall discharge [2].

The DBD configuration used for this experiment consisted of two identical single-filament arrangements, which were investigated by means of synchronised, fast electrical and optical diagnostics. For that purpose, two single, alumina-covered, semi-spherical electrode pairs featuring two 1 mm gaps with a variable distance between them (in this case 14 mm, see Fig. 1 (c)) were put in a stainless-steel chamber flushed with 0.1 vol% O_2 in N_2 at atmospheric pressure. An unipolar positive high-voltage (HV) pulse with approximately 45 ns rise time as shown in Fig. 1 (a) was simultaneously applied to both electrodes (amplitude 10 kV and varying repetition frequencies). The diagnostics consisted of fast voltage and current probes, which were synchronised with an iCCD camera to record individual discharge events like displayed in Fig. 1 (c). The current was measured at the grounded side for each single-filament to calculate the discharge energy and transferred charge for two single-filaments and both filaments combined. Discharge events occur in both gas gaps within few ns as can be seen in Fig. 1 (b) (even if the inception jitter is hundreds of ns), which indicates a coupling of the two single-filament DBDs, which is most likely a result of the interaction in the (parasitic) electrical circuit formed by the arrangement. Therefore, this interaction was investigated to better understand upscaling challenges and opportunities [3], e.g. by using an electrical circuit model and the synchronised single-shot data of the electrical measurements and the corresponding iCCD images.

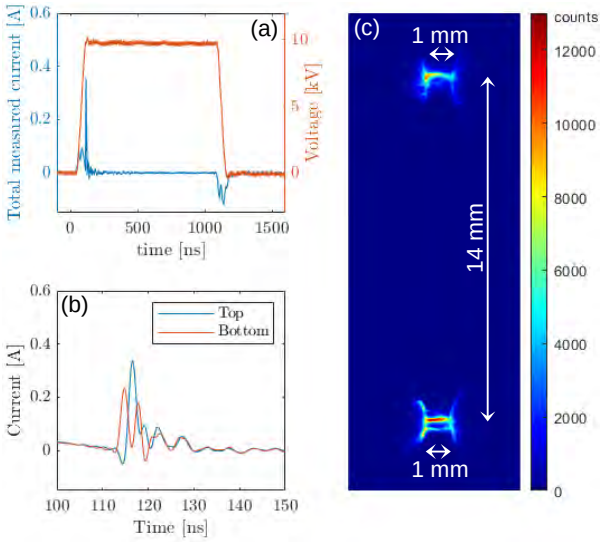

Figure 1. Example of synchronised current and voltage waveforms (a) showing the currents at the top and bottom electrode in detail (b) and the corresponding discharge emission at the rising slope of the HV pulse captured by an iCCD single shot (c) of a double-filament arrangement featuring two 1 mm gaps with 14 mm distance between the fixed filament positions.

Acknowledgement

This work was funded by the DFG (German Research Foundation) – project number 466331904, a grant from the Dutch 3E stichting and the NWO (Dutch Research Foundation) – project number 10029091

References

[1] Kogelschatz, U.: *Plasma Chem. Plasma Process.* **23** 1–46 (2003)
[2] Brandenburg, R.: *Plasma Sources Sci. Technol.* **26** 053001 (2017)
[3] Höft, H., Becker, M.M., Kettlitz, M., Brandenburg, R.: *Plasma Sources Sci. Technol.* **32** 025006 (2023)

On the influence of the gas temperature on electron power absorption in atmospheric pressure radio frequency micro plasma jets

D. Schulenberg[1], M. Klich[2], M. Vass[1,3], Z. Donko[3], J. Klotz[1], N. Bibinov[1], J. Schulze[1], T. Mussenbrock[1]

[1] *Chair of Applied Electrodynamics and Plasma Technology, Ruhr University Bochum, Germany*
[2] *Chair of Theoretical Electrical Engineering, Ruhr University Bochum, Germany*
[3] *Wigner Research Centre for Physics, Budapest, Hungary*

The interplay between background gas temperature and plasma parameters is investigated in a radio frequency (RF)-driven plasma jet at atmospheric pressure, operated with a mixture of helium and nitrogen. Sinusoidal driving voltages with f = 13.56 MHz and different amplitudes (250 V, 300 V, 350 V) are used. Conventional optical emission spectroscopy (OES) and phase resolved OES (PROES) are used to determine nitrogen rotational temperatures and the electron-impact excitation rate into the He I ($^3S_1$) state along the jet's discharge channel, respectively. Depending on the voltage amplitude and gas-mixture, a lateral increase of the gas temperature, which induces an electron heating mode transition from Ω- to Penning-mode, can be detected. The experimental results are supported by both hybrid and particle-in-cell / Monte Carlo collisions simulations (PIC/MCC). The simulations reproduce the same trends as the experimental results, and thus help in understanding the physical details of the observed effects.

1 General

Atmospheric pressure plasmas recently receive increased attention due to their diverse potential applications, for example in catalysis or medicine [1-3]. To allow medical use, a crucial parameter is the temperature of the background gas, which should be low enough to not damage any treated tissue. Previous work has demonstrated that the temperature in the effluent of the plasma source of choice, the COST micro plasma jet [4], stays below 40 °C for standard operating parameters, which makes it suitable for bio-related applications [5]. In the presented work, the interplay between the gas temperature and the dynamics of electrons in the plasma is investigated.

2 Operating conditions and measurements

In this study, sinusoidal driving voltages with amplitudes of 250 V, 300 V, and 350 V are used. The gas is a mixture of 1000 sccm helium and a variable amount of nitrogen (0.5 sccm - 2 sccm). All cases are repeated using ½ of the total gas flow while keeping the He/N_2 ratio constant (500 sccm of He and 0.25 sccm - 1 sccm of N_2).

Time integrated spectra are measured at six evenly spaced positions along the discharge channel using an ESA3000 echelle spectrometer. The 0-1 vibrational band of the second positive system of nitrogen is then used to determine the gas temperature with the rotational distribution in the emission spectrum [6].

PROES measurements of the electron impact excitation rate from the ground state into the He I ($^3S_1$) state reveal the motion of energetic electrons in the plasma within the RF-period. The measurements are taken at the same six positions along the discharge channel as the conventional OES measurements.

3 Results

For most cases, the N_2 rotational temperature increases along the way of the gas through the discharge channel. This effect is proportional to the driving voltage amplitude, and inversely proportional to the N_2 concentration. The PROES measurements show a power absorption mode transition along the discharge channel. The degree of transition from one mode to the other correlates with the increase in N_2 rotational temperature as observed in the OES measurements.

PIC/MCC simulations reproduce the trends of the PROES measurements, and therefore help in understanding the underlying physical mechanisms.

4 Acknowledgement

This work is supported by the DFG in the frame of the SFB 1316 (project A4).

References

[1] A. Bogaerts *et al* 2020 *J. Phys. D: Appl. Phys.* **53** 443001
[2] I. Adamovich *et al* 2022 *J. Phys. D: Appl. Phys.* **55** 373001
[3] M. Laroussi *et al* 2022 *IEEE TRPMS* **6** 127-157
[4] J. Golda *et al* 2016 *J. Phys. D: Appl. Phys.* **49** 084003
[5] S. Kelly *et al* 2015 *J. Phys. D: Appl. Phys.* **48** 444002
[6] P. J. Bruggeman *et al* 2014 *Plasma Sources Sci. Technol.* **23** 023001

Characterization of a plasma system with microwave launcher used for treatment of liquids

N. Škoro[1], N. Babucić[1], K. Kutasi[2], K. Spasić[1] and N. Puač[1]

[1] *Institute of Physics, University of Belgrade, Belgrade, Serbia*
[2] *Wigner Research Centre for Physics, Budapest, Hungary*

In this work we present first steps in characterization of a MW plasma system used for water treatment and PAW creation. We performed spatially resolved optical emission measurements of a MW plasma operating with Ar as working gas and also determined properties of the treated water.

1 Introduciton

In the last decade a new research direction in the scientific field of non-thermal plasmas developed towards treatments of liquid targets. The motivation stems from the fact that plasma-activated liquid (PAL) has versatile applications in plasma medicine and agriculture. PAL contains reactive species with the pH of the solution reduced [1] and consequently have antimicrobial and antibacterial effect with an influence to the cells at different levels. Attaining positive effects in treatments of particular samples using PAL depend on properties which are directly connected to the conditions of the plasma treatment. Thus, for tuning of the PAL properties, among else, different plasma sources should be used [2].

In this regard, this work is a continuation of our plasma activated water (PAW) studies, now involving a microwave (MW) excited plasma. The setup will enable characterization of both the plasma and treated water thus enabling investigation of chemical reactivity properties of PAW.

2 Experimental setup

The plasma is created using an inductively coupled wave launcher and a microwave generator with precise control of an input power. The surface wave launcher is operated using Ar (with flow range 1-7 slm). Plasma is created inside the quartz tube with the plume formed at the tube ending. We analysed recordings of emission originating from different regions of plasma - images that show the spatial structure and optical emission spectra. For determination of reactive nitrogen and oxygen species in PAW colorimetric techniques were used.

3 Results and discussion

Optical measurements showed that the size of the plasma plume protruding depended on operating conditions. These measurements were conducted in order to establish distances from the source where role of reactive species is important which is important for water treatment. The optical spectrum recorded from the active volume of the plasma had lines of several excited species: Ar, O, N_2^+ and OH radical. In Fig. 1 we show change in the line intensity for argon 811 nm line depending on the position along the tube axis for 3 power values. The positions shown in the x-axis are with the respect to the tube ending (x=0) with positive values marking the outside zone.

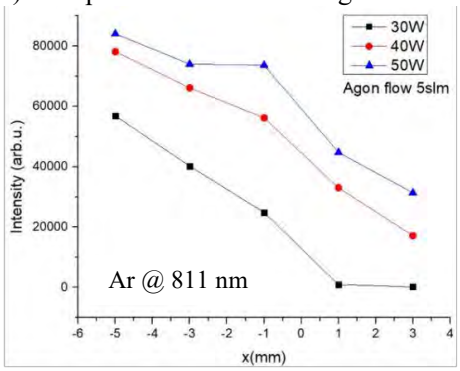

Fig. 1. Spatial change in the Ar 811 nm line intensities along the tube axis for 3 input powers. Ar flow 5 slm.

At a certain position, intensities increase with increasing power. Absence in intensities outside the tube at lower powers is due to reduced length of plasma plume. This type of measurements enables comparison of properties between existing surfatron and the new wave launcher.

Acknowledgment

This work was supported by the Sci. Fund of the RS, no. 7739780 - APPerTAin-BIOM and MSTDI Republic of Serbia grant number 451-03-68/2022-14/200024.

References

[1] Bradu C., Kutasi K., Magureanu M., Puač N., Živković S. Reactive nitrogen species in plasma-activated water: generation, chemistry and application in agriculture. J. Phys. D: Appl. Phys. **53(22)**, 223001 (2020)

[2] Kutasi K., Popović D., Krstulović N., Milošević S. Tuning the composition of plasma-activated water by a surface-wave microwave discharge and a kHz plasma jet. Plasma Sources Sci. Tech. **28(9)**, 095010 (2019)

Plasma-Activated Water (PAW): Sustainable Technology for Wastewater Treatment and its Reuse as a Green Fertilizer

Saeed Kooshki[1], Pankaj Pareek[1], Robin Mentheour[1], Mario Janda[1], Zdenko Machala[1]

[1] [1]*Faculty of Mathematics, Physics, and Informatics, Comenius University Bratislava, Slovakia*

The global water crisis is a significant challenge posed by the rapidly growing world population. By 2050, the UN predicts that nearly six billion people will face water scarcity, and demand for water is expected to surge over the next two decades, particularly in agriculture, which accounts for the largest demand sector, projected to increase by 60% by 2025 [1]. One potential and eco-friendly solution to address water contamination and excessive use in agriculture is the use of Non-Thermal Plasma (NTP) treatment of wastewater. NTP treatment can effectively decontaminate wastewater by enriching it with Reactive Oxygen and Nitrogen Species (RONS), hence producing Plasma-Activated Water (PAW). Such NTP-treated PAW can be reused in agriculture to enhance plant growth and seed germination [2].

In this study, we investigated the effectiveness of NTP as a sustainable technology to treat *Staphylococcus epidermidis* bacteria-contaminated water and to enhance barley seed germination *in vitro* using PAW produced from the plasma treatment of wastewater.

Our results showed that the use of PAW produced from plasma wastewater treatment improved barley seed germination by over 20% compared to tap water (Figure 1). We also investigated the chemical and bactericidal effects induced by NTP on the bacteria suspensions. We found that the inactivation of bacteria suspensions was dependent on pH and Oxidation-Reduction Potential (ORP), which correlated with the chemical RONS changes induced in the PAW. We used Response Surface Methodology (RSM) to determine the optimum plasma treatment time as the main parameter in the experiments to minimize electric power consumption for bulk water treatment. Our findings showed that plasma treatment after the optimum treatment time can reduce Staphylococcus bacteria in water by up to 7 logs (Figure 2). Furthermore, we observed a significant decrease in hydrogen peroxide and nitrite concentrations, as well as pH, after reaching the optimum plasma treatment time.

Overall, our study demonstrates that NTP treatment of wastewater represents an efficient approach for the water recovery for sustainable agriculture.

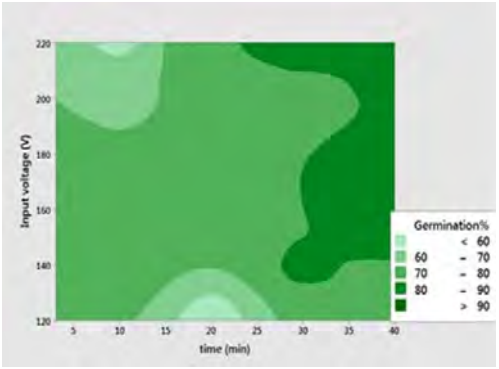

Figure 1. Contour plot of germination % improved by PAW vs input voltage (V) and plasma treatment time (min).

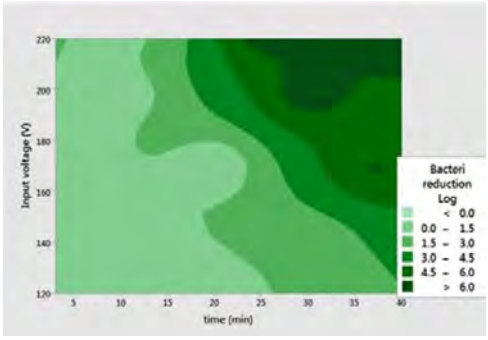

Figure 2. Contour plot of bacterial log reduction by PAW produced at different input voltage (V) and plasma treatment time (min).

This work was supported by Slovak Research and Development Agency APVV-17-0382 and APVV-22-0247, Slovak Grant Agency 1/0822/21, and a postdoctoral support of the Faculty of Mathematics, Physics, and Informatics Comenius University Bratislava.

References

[1] B. Alberto and R. Lorenzo, "Reassessing the projections of the World Water Development Report," *Nature partner journals Clean Water*, 2, 1, p. 15, 2019.

[2] P. Gururani *et al.*, "Cold plasma technology: advanced and sustainable approach for wastewater treatment," *Environmental Science and Pollution Research*, pp. 1–21, 2021.

Microparticle charge in a spatio-temporal afterglow plasma: influence of an externally applied electric field

J.C.A. van Huijstee[1], P. Blom[2] and J. Beckers[1]

[1] *Dept. Applied Physics, Eindhoven Univ. Techn., Eindhoven, The Netherlands*
[2] *VDL Enabling Technologies Group, Eindhoven, The Netherlands*

An interesting and relevant topic in the field of complex plasma physics is the interaction between dust particles and afterglow plasmas. This type of plasma is especially relevant for contamination control applications in high-tech equipment, where there are plasmas present and trajectories (and therefore charge) of contaminating particles need to be precisely controlled. It has been shown that applying an external electric field during the afterglow, greatly influences the residual charge of the particles (collected from the plasma). In this contribution we present experimental measurements of residual particle charges in a spatio-temporal afterglow plasma and investigate the influence of an externally applied electric field thereon.

An interesting and relevant topic in the field of complex plasma physics is the interaction between dust particles and afterglow plasmas. The term afterglow is used here to describe a (region of) plasma in which there is no (more) net ionization. This means that the plasma's power source is removed in either time (temporal afterglow) or space (spatial afterglow), or a combination thereof (spatio-temporal afterglow).

These types of plasma are especially relevant for contamination control applications in high-tech ultra clean equipment, where there are plasmas present and trajectories (and therefore charge) of contaminating particles need to be precisely controlled. A promising new particle contamination control methodology is the so-called plasma seal [1]. In this application, the property that particles are electrically charged by the collection of plasma species is used to filter the contaminating particles from a gas flow using an external electric field. However, due to the plasma shielding such electric fields, deflection of the particles needs to happen in an afterglow plasma. The complication here is that the charge of the particles does not remain constant in the afterglow plasma. Theory predicts that particles will typically have a residual charge distribution around a small negative value, which in some cases can even extend to positive charges.

However, in experiments it has been shown that applying an external electric field during the afterglow phase, greatly influences the residual charge of the particles. In [2] highly positively charged particles were measured when applying a DC bias in a temporal afterglow plasma. In [3] it was also shown that DC electric fields in the temporal afterglow are important for the residual particle charge. However, further experimental data, which is necessary for further development of the theoretical framework, is lacking.

In the experimental setup used in this work, the charge of microparticles is measured after they passed through a spatio-temporal afterglow of an inductively coupled plasma. This is done by visually recording their trajectories in an externally applied electric field between two parallel electrodes. The magnitude of this electric field and the moment when it is applied (relative to the moment the plasma power is terminated) can be controlled. Measurements with varying externally applied DC field are presented.

References

[1] Blom, P., van Huijstee, J., Medini, F., Baade, R. & Beckers, J. Plasma-assisted removal of particles: taming the beast. *Mikroniek* **6**, 15–18 (2021).

[2] Chaubey, N. & Goree, J. Preservation of a Dust Crystal as it Falls in an Afterglow Plasma. *Frontiers in Physics* **10**, 1–9 (2022).

[3] Wörner, L. *et al.* The effect of a direct current field on the microparticle charge in the plasma afterglow. *Physics of Plasmas* **20**, 10–17 (2013).

Ion bombardment on microorganism in dusty plasmas

Kazuo Takahashi[1], Hiroaki Sasaki[2] and Hiroto Tanaka[2]

[1] *Fac. Electrical Eng. & Electronics, Kyoto Institute of Technology, Kyoto, Japan*
[2] *Dept. Electronics, Kyoto Institute of Technology, Kyoto, Japan*

Spores of a microorganism (*Bacillus subtilis var. natto*) were injected into plasmas generated by rf discharges. The spores were levitated in gas phase of the plasmas and also put on surface of an electrode at the bottom. Typically, the spores levitated in the gas phase were inactivated effectively much more than those on the surface. The ion flux onto the spores in the gas phase, which was calculated by the OML theory exceeded one on the surface. This means that ion bombardment contributes to inactivation of the spores.

Plasmas generated by electrical discharges have shown as a tool for sterilization especially on surfaces. This means that gas phase of the plasmas possibly inactivate microorganisms levitating in the air. In this study, living spores of a microorganism (*Bacillus subtilis var. natto*) are introduced to a plasma generated by rf discharge. The discharge was induced by Ne gas introduced at 4 sccm and an rf at 13.56 MHz applied to a parallel-plate electrodes. The spores were levitated in the plasma as the same of a form of dusty plasmas. They were distributed as a cloud located at 8-11 mm of height from the bottom electrode. Survival rate of the spores was evaluated in the plasma. Ion density and electron temperature were measured by a method of double-probe.

Injecting the spores to the plasma, they were levitated and trapped in gas phase of the plasma. They were treated in the gas phase. Conversely, once the spores were trapped, they were transported to surface of an electrode at the bottom. They could be also treated on the surface.

Figure 1 (a) shows survival rates of the spores treated in the gas phase and on the surface. The rates tend to be reduced as a treatment time. Then the spores were efficiently inactivated in the gas phase rather than on the surface. Spatial distributions of Ion density and electron temperature are shown in Fig. 1 (b). The ion density and electron temperature enable to calculate ion fluxes onto the spores in the gas phase and on the surface. The ion flux of the gas phase was derived to be 4.2×10^{15} cm^{-2}s^{-1} by the orbit-motion-limited (OML) theory. On the surface, the spores were irradiated by the ion flux of 2.5×10^{14} cm^{-2}s^{-1} calculated from the Bohm criterion. The ion flux of the gas phase is much larger than that of the surface, which contributes to inactivating the spores.

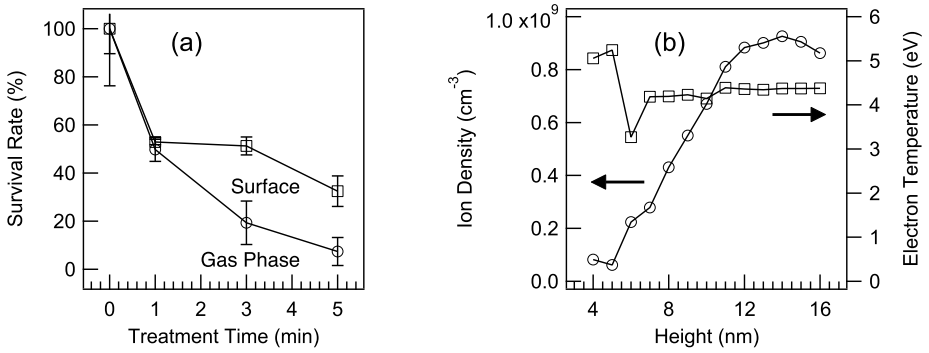

Figure 1: (a) Survival rates of the spores in gas phase and on surface as functions of exposure time. (b) Spatial distributions of ion density and electron temperature as functions of height from the bottom electrode.

Influence of target heating on the growth of Nb coatings during hot magnetron sputtering

K. Leonova[1], D. Depla[2], G. Savorianakis[1], O. Janssens[2], N. Britun[3] and S. Konstantinidis[1]

[1] *Plasma-Surface Interaction Chemistry (ChIPS), University of Mons, Mons, Belgium*
[2] *Department of Solid State Sciences, Ghent University, Ghent, Belgium*
[3] *Center for Low-Temperature Plasma Sciences, Nagoya University, Nagoya, Japan*

In this work, we highlight the important features of a hot magnetron sputtering (HMS) discharge with a Nb target and study their impact on the growth of Nb coatings. Particularly, it is shown that once the target temperature reaches 1900 K, a thermionic emission from the target is stimulated. This phenomenon contributes to increased ionization of sputtered metal flux and is always accompanied by strong thermal radiation from the hot target. Ultimately, it is observed that Nb coatings obtained in the HMS configuration become less porous but have higher intrinsic stress as the target temperature increases up to 2100 K. On the other hand, we observe that if the substrate is exposed to the heated target for a longer time interval, thermal stress reduces and coating density increases. This, in turn, might be beneficial in the need of relatively thick (0.6-1 μm) but dense Nb coatings.

1 Introduction

Within the last decade, hot magnetron sputtering (HMS) has become more attractive to the coating community because of the deposition rate enhancement by an order of magnitude [1] as compared to classical cold magnetron sputtering (CMS). In HMS, the target is thermally insulated from the cathode to prevent magnets damage. The increase in the deposition rate can usually be understood by sublimation of the target. Although, it is negligible for refractory materials such as Nb (i.e. the materials with a melting point above 2500 K) even at high temperatures. Nevertheless, the use of HMS allows researchers to safely apply higher power loads to the magnetron source and thus to reach higher deposition rates.

During HMS with Nb, the target temperature can rise to 1900 K and promote a thermionic emission [2]. This, in turn, affects plasma properties, in particular the production of metal ions, and may change the coating characteristics. The aim of this work is to correlate the discharge parameters, the plasma properties, and the growth of Nb films by HMS.

2 Results

Our experimental data show that when the power density of 20 W/cm^2 is applied to the HMS source, the target temperature rises to 1900 K and the discharge current starts to increase dramatically due to amplification of a thermionic emission. Consequently, the release of additional number of electrons into the discharge contributes to higher ionization of the plasma bulk species, including the sputtered metal atoms. This effect was verified by laser-induced fluorescence, where both ground state Nb neutrals and ions were monitored.

In order to investigate the influence of the observed plasma features onto the film growth, Nb coatings were deposited at different target temperatures and during different deposition times, and then characterized by scanning electron microscopy, X-ray diffractometry (XRD) and ellipsometry. Coatings deposited with a conventional CMS configuration demonstrate a columnar structure with a porosity of 40% and a negligible stress. In contrast, the shift of the XRD peaks illustrates that an internal thermal stress is always noticed for coatings deposited by HMS. This stress can lead to delamination of the coating. It is also observed that the film porosity in this case is only 26%, i.e., lower as compared to the CMS coatings. In addition, it is shown that the longer the substrate is exposed to the heat radiation emanating from the hot target during HMS deposition, the less intrinsic stress is observed and the denser the coating becomes.

Acknowledgments

The work was supported by FNRS (National Fund for Scientific Research) under FRIA (Fund for Research training in Industry and Agriculture) grant FC 41423.

References

[1] Kaziev, A., Tumarkin, A., Leonova, K., Kolodko, D., Kharkov, M., Ageychenkov, D. Discharge parameters and plasma characterization in a dc magnetron with liquid Cu target. Vacuum **156**, 48–54 (2018).

[2] Leonova, K., Britun, N., Konstantinidis, S. Target heating and plasma dynamics during hot magnetron sputtering of Nb. Journal of Physics D: Applied Physics **55(34)**, 345202 (2022).

Deposition characteristics of cumene plasma CVD for high-speed deposition of high-density a-C:H films

Shinjiro Ono[1], Takamasa Okumura[2], Kunihiro Kamataki[2], Naoto Yamashita[2], Naho Itagaki[2], Kazunori Koga[2,3], and Masaharu Shiratani[2]

[1] *Graduate School of Information Science and Electrical Enginnering, Kyushu University, Japan*
[2] *Faculty of Information Science and Electrical Enginnering, Kyushu University, Japan*
[3] *Center for Novel Science Initiatives, National Institutes of Natural Sciences, Tokyo, Japan,*

We have deposited hydrogenated amorphous carbon (a-C:H) films using plasma chemical vapor deposition (CVD) with cumene (C_9H_{12}) as a novel precursor to improve the deposition characteristics. We have measured pressure dependence of the deposition rate and mass density. We found the deposition rate significantly increases from 38 nm/min at 0.02 Torr to 291 nm/min at 0.3 Torr while the mass density decreases slightly. These results suggested that the higher-order carbon molecules are a promising material to increase the deposition rate.

1. Introduction

Carbon films such as a-C:H with high mass density have been widely used for protective coatings applied for automobile, medicine, and semiconductor device manufacturing [1]. To improve the durability of the films, deposition of thick films with high mass density has been required. Energy and flux of ions and radical flux to film surface have been pointed out as important factors for realizing high deposition rate of dense films. Our previous research found that substrate position affected the above film properties in the capacitively coupled plasma chemical vapor deposition system [2]. To increase the deposition rate, ingredient gas molecules which consist of several C atoms has been considered. Here we have studied characteristics of films deposited by plasma CVD using cumene (C_9H_{12}).

2. Experimental setup

The deposition was performed using a capacitively coupled plasma CVD chamber which installed two parallel electrodes. 10 mm × 10 mm Si substrates were set at the center of the lower electrode of 95 mm in diameter connected to a 13.56 MHz rf power supply. C_9H_{12} was introduced using a vaporizer (Vapbox, Kemstream) with Ar as carrier gas from the top of the chamber. Concentration of cumene was 20 % and total pressure was from 0.02 Torr to 0.3 Torr. The total gas flow rate was 100 sccm. The discharge voltage was kept at 600 V_{pp}.

3. Results and discussion

Figure 1 shows the pressure dependence of deposition rate and mass density together with the self-bias voltage V_{dc}. The self-bias voltage increases from -260 V_{dc} for 0.02 Torr to -200 V_{dc} for 0.3 Torr with increasing pressure. The deposition rate increases from 38 nm/min at 0.02 Torr to 291 nm/min at 0.3 Torr. The deposition rate for cumene is much higher than that for CH_4 and C_2H_2. The mass density decreases with increasing the pressure from 1.42 g/cm^3 at 0.02 Torr to 1.12 g/cm^3 at 0.3 Torr. The V_{dc} increases with increasing the pressure. It shows the ion energy decrease with increasing the pressure. Based on the subplantation model [3], the decrease of ion energy and flux ratio of radicals and ions are responsible for the decrease of mass density. However, the increase of deposition rate is much larger than the decrease of mass density. Thus, the ion energy increase by substrate bias would improve the mass density. These results suggest that the cumene plasma CVD is promising to improve deposition characteristics of a-C:H films.

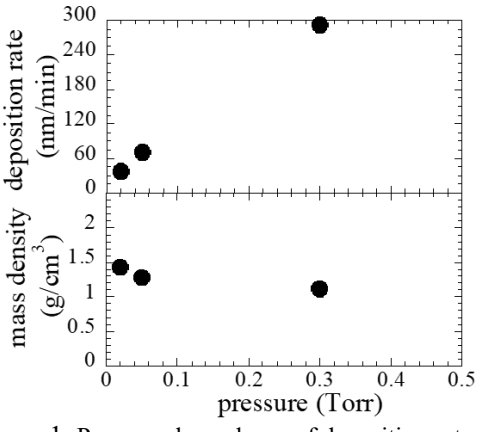

Figure 1. Pressure dependence of deposition rate and mass density. V_{pp} is constant at 600V.

References

[1] J. Vetter, Surface & Coatings Technology journal **257** (2014), 213-240.
[2] S.H. Hwang et al., Thin Solid Films **729** (2021), 138701.
[3] J. Robertson, Materials Science and Engineering R **37** (2002), 129-281.

Effects of Ne mixing on plasma enhanced chemical vapor deposition of a-C:H films using CH_4/Ar/Ne capacitively coupled discharges

K. Ikeda[1], M. Otaka[1], H. Otomo[1,2], T. Arima[1], J. Lai[1], K. Kamataki[1], D. Yamashita[1], T. Okumura[1], N. Yamashita[1], H. Kiyama[1], N. Itagaki[1], K. Koga[1], M. Shiratani[1], T. Shindo[2], S. Tanaka[2], T. Matsudo[2]

[1] *Graduate School and Faculty of Information Science and Electrical Engineering, Kyushu Univ. Japan*
[2] *Tokyo Electron Technology Solutions Limited, Japan*

We investigated effects of Ne mixing on plasma enhanced chemical vapor deposition (PECVD)of a-C:H films using CH_4/Ar/Ne capacitively coupled discharges. Both the film density and the deposition rate are maximum at a Ne mixing ratio of 15%. Simulation results suggest that ion induced surface reactions plays a key role in deposition.

1. Introduction

Hydrogenated amorphous carbon (a-C:H) films have many applications due to their favourable mechanical properties. Ferreira, et al. showed that harder a-C:H films realized by adding Ne to Ar magnetron sputtering plasma [1]. So far, few studies have been reported on effects of Ne mixing on the quality of a-C:H films deposited by PECVD. In this study, we have investigated effects of Ne mixing on PECVD of a-C:H films using CH_4/Ar/Ne capacitively coupled plasma (CCP).

2. Experimental

Experiments were performed using a CCP reactor. Plasma generated between two parallel plate electrodes (85 mm in diameter and 26 mm in gap between them) by supplying rf voltage (13.56MHz). Total gas flow rate was 15 sccm. Here, 5 sccm of CH_4 and 10 sccm of Ar+Ne were fixed. The Ne mixing ratio (Ne/(Ar+Ne))×100 was varied from 0 to 75%. The pressure was 30 mTorr. The self-bias voltage was -180 V. The film density and thickness were measured by X-ray reflectometry. In addition, SRIM simulations [2] were performed to investigate the effects of Ar and Ne ion irradiation on a-C:H films. The simulation conditions were as follows: a-C:H films with a hydrogen content of 35% and a film density of 1.8 g/cm^3 was bombarded with 1,000,000 Ar^+ or Ne^+ at 100 eV ion incident energy.

3. Results and Discussion

Figure 1 shows effects of Ne mixing ratio on the film mass density and the deposition rate of a-C:H films. The film at Ne mixing ratio 15% has 2.15% increase in film density (1.78 g/cm^3) compared to the film density (1.74 g/cm^3) when deposited without Ne. The deposition rate increases by 3.60% from 2.81 nm/min to 2.91 nm/min at a Ne mixture ratio from 0 to 15%.

SRIM simulated sputtering yields of H and C atoms in a-C:H film by Ne^+ and Ar^+ bombardments as shown in Table.1. Ne^+ ions sputter out more H and C atoms and realize a higher ratio of the sputtering yield H/C than Ar^+ ions. In other words, Ne^+ preferentially reduces H content in films. Such reduction of H content, eventually increases the film mass density. Details will be reported at the conference.

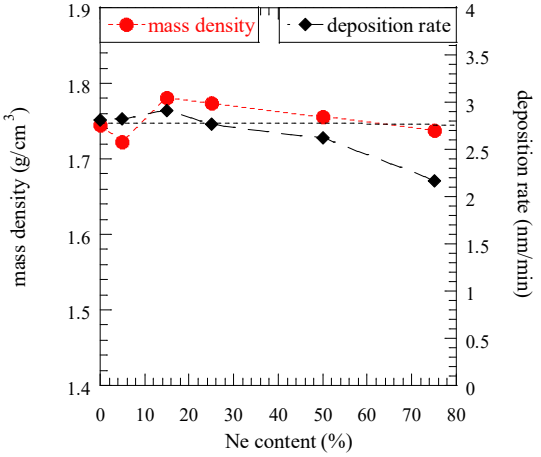

Fig.1 Effects of Ne mixing ratio on film mass density and deposition rate of a-C:H films.

Table.1 SRIM simulation results of sputtering yield of H and C atoms by Ne and Ar ion irradiation.

	H (atom/ion)	C (atom/ion)	H/C
Ne	0.0173	0.00739	2.34
Ar	0.00265	0.00135	1.97

References

[1] F. Ferreira, et al. Diam. Relat. Mater., **98** 107521 (2019).
[2] V. I. Shulga, Appl. Surf. Sci., **439**, 456 (2018).

Effects of electrode geometries and materials on a water purification using the ball lightning discharge

M. Maeyama[1], T. Yokokura[1] and Y. Inada[1]

[1] *Graduate School of Science and Engineering, Saitama Univ., Saitama, JAPAN*

Applying the ball-lightning discharge for water treatment, we conducted experiments of its water treatment performance characteristics and research on improving characteristics.

1 Purpose of this study

The ball lightning discharge[1] that can be generated at the gas-liquid interface under atmospheric pressure (example of the experimental apparatus Fig.1) was used because of its long life, large volume, and ability to generate active species[2]. In order to apply it to waste water treatment, we are conducting experiment of its water treatment performance characteristics and research on improving characteristics.

From previous studies [2], it has been experimentally found that in this water treatment, 1) a large polarity effect, and 2) a decrease in decomposition performance occurs during treatment in the negative polarity. However, there is no report on the influence of electrode shape and material. In this presentation, we will report the results of an experiment conducted with the aim of clarifying these effects experimentally.

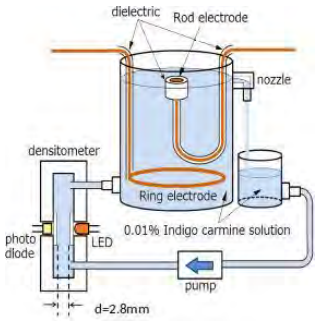

Fig. 1: Experimental setup

2 Experimental Setup

In this study, we also used a circular disk with a hole at its centre as the anode electrode other than circular ring in Fig.1 at the bottom of the container.

3 Results

Fig. 2 shows the change in Indigo-carmine(IC) concentration n_{IC} with the number of discharges($n_{dis.}$) when the Cu-circular-ring is used as the lower electrode. As a result, the IC decomposition rate increases with V_c as the input energy increases, but when V_c is as low as 3 kV or 3.2 kV, the rate of decomposition becomes extremely lower after $n_{dis.}$ = 200 and 150, respectvely.

Fig.3 shows the results when V_c=3.0kV and IC is added after $n_{dis.}$=150. The slopes a of the exponential function ($n_{IC} \propto \exp(-a.n_{dis.})$) are almost the same at $n_{dis.}$=74 and 151 where n_{IC} being a same value. Therefore, it is considered that the decrease of the processing speed after $n_{dis.} > 100$ is because that the concentration of other decomposition products becomes large relatively to the concentration of the particles to be decomposed. details such as the influence of the electrode material will be detailed in the presentation.

This work was supported by JSPS KAKENHI Grant Numbers JP21K04017.

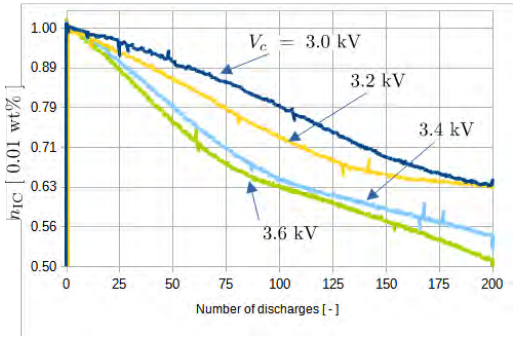

Fig. 2: IC decompositions at V_c=3.0 kV to 3.6kV

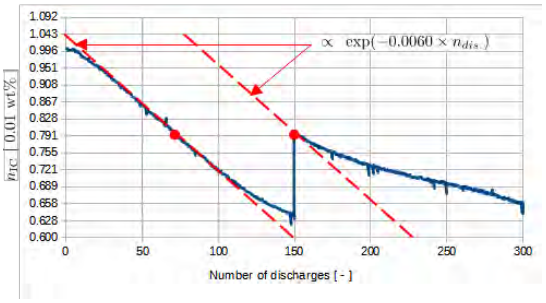

Fig. 3: Comparison of slope n_{IC} at $n_{dis.}$=74 and 151.

References

[1] A. I. Egorov, S. I. Stepanov: Technical Physics, Vol. 47, No. 12, pp. 1584–1586,2002

[2] M. Maeyama, et.al.: JPS Conf. Proc. 1(2014) 015076

Optical emission spectroscopy of a plasma jet for biomedical applications

E. Martines[1], L. Zampieri[1], R. Barni[1] and C. Riccardi[1]

[1] *Department of Physics "G. Occhialini", University of Milano–Bicocca, Milano, Italy*

This contribution describes analyses performed on optical emission spectra obtained from an atmospheric pressure plasma jet for biomedical applications, and shows how different plasma parameters, such as electron temperature and density, and vibrational and rotational temperatures, can be estimated through a careful analysis of the spectral data.

1 Introduction

Atmospheric pressure plasma jets operating at low power levels, typically with helium or argon as main gas, have become a major tool for the studies of biomedical plasma applications ("plasma medicine"). Biological effects are primarily induced by active chemical species produced within the plasma thanks to the dissociation of air molecules mixing with the plasma plume. A proper modelling of the complex chemistry taking place within the plasma requires a knowledge of the plasma parameters. While advanced diagnostic techniques can be used to deduce many of these properties, it is also of interest to have simple methods to make the same kind of estimation. One of the simplest diagnostic techniques which can be used is Optical Emission Spectroscopy (OES). This is also relatively cheap if a compact spectrometer is used. The present contribution describes some of the advancements that our group has made in developing reliable methods to interpret emission spectra obtained on plasma jets.

2 Experimental setup

The spectra analysed in this contribution have been obtained with an Avantes AvaSpec-ULS4096CL-EVO compact spectrometer, capable of measuring spectra from 200 to 1100 nm with a resolution of 0.3 nm. The optical system consisted in a 6-mm diameter lens with 8.7 mm focal length, focused within the plasma jet, so that light from a spot with 0.5 mm diameter could be collected and sent to the spectrometer through an optical fibre. The spectrometer was calibrated using a calibration lamp.

3 Analysis of the helium and argon lines

The population of helium and argon excited states derives from a balance between excitation, which we consider solely due to electron impact, and decay, due to either spontaneous emission, electron impact or impact with heavy species (neutrals, ions, excimers).

Electron impact excitation rate coefficients starting from the ground state and from metastable states have been evaluated from cross sections [1], assuming a Maxwellian distribution function (in the future it is planned to evaluate the distribution function using a Boltzmann equation solver).

Decay process rate coefficients have been evaluated using the detailed balance principle for electron impact and using expressions found in the literature for heavy species impact [2,3]. A comparison of the different processes led to the understanding that electron impact decay is not sufficient to model the system, and that in particular collisions with ground state neutrals are a major player in the overall balance. Electron density and temperature at different positions in the plasma jet and for different power supply options were evaluated from line ratios, using the expressions described above. The photon escape factor was not considered and will be the object of future studies.

4 Analysis of the molecular nitrogen lines

The spectral lines related to the second positive system of the neutral nitrogen molecule were fitted using an expression which includes the rotational and vibrational excited states, assuming a Maxwellian distribution of these states. The rotational and vibrational temperatures were thus estimated. The values were also compared to similar estimates made in two other atmospheric pressure plasma, namely a surface DBD and a low power arc. As expected, the rotational temperatures found in the biomedical plasma jet were lower than in the other plasmas.

5 Conclusions

OES is potentially a powerful tool for the analysis of atmospheric pressure plasma jets for biomedical applications. Here we have described a first step towards a full use of its potential, and some experimental results which have been obtained.

References

[1] Ralchenko, Yu., *et al.*, Atom. Data Nucl. Data Tables **94**, 603 (2008).

[2] Zhu, Xi-Ming and Pu, Yi-Kang, J. Phys. D: Appl. Phys. **43**, 015204 (2010).

[3] Lee, Wonwook, *et al.*, Phys. Plasmas **27**, 073502 (2020).

Zeeman AAS – a means to assess mercury pollution in the environment through artefacts of wild birds

A. Abola[1], A. Rimsa[1,2], Z. Brike[1], R. Veilande[1], G. Revalde[1,3]

[1]*Institute of Atomic Physics and Spectroscopy, University of Latvia, Riga, Latvia*
[2]*Institute of Biology, University of Latvia, Riga, Latvia*
[3]*Riga Technical University, Riga, Latvia*

In this work, we present our research in the framework of a project dedicated to mercury concentration measurements in wild birds, mostly black storks, in Latvia, using a Zeeman atomic absorption spectrometer (AAS). Our data consist of measurements of several hundred artefacts. Here we compare the results based on their type, temporal and territorial distribution.

1 Introduction

Various artefacts of living organisms are often used as a means for assessment of environmental pollution. For birds, those are, for example, feathers, eggs, faeces and food remains. If the bird species are endangered (like black storks in Latvia), non-invasive sample-gathering methods are preferable, to diminish the disturbance as much as possible.

It is well known, that mercury and its compounds are all deemed toxic. Its organic species methylmercury is formed in aquatic environments and is often recognized by its ability to bioaccumulate. It is one of the reasons why birds that feed in water bodies, such as rivers, ponds, etc. are at risk of higher mercury intake. In our case – more than 90% of a black stork's diet consists of fish and other smaller water animals [1].

In this work, we measure total mercury concentrations in eggshells, membranes and feathers of several wild birds nesting in Latvia. Bulk of the data consists of black stork artefacts.

2 Experiment

Measurements were done by atomic absorption spectrometer with Zeeman background correction, coupled with thermal combustion attachment. Our spectrometer uses a capillary mercury isotope high-frequency electrodeless lamp as its light source.

The use of pyrolysis means that no specific sample pretreatment is required, thus ensuring less possible sample contamination. This method allows fast real-time measurements, and the results are obtained in a timeframe of a couple of minutes.

Eggshell samples were gathered over a time period of almost 20 years from nesting sites all over the territory of Latvia. Only hatched, failed and discarded eggs and their shells were collected. Some feathers were also gathered.

3 Results and Discussion

Our results showed that all artefacts of fish-eating wild birds nesting in Latvia contain some mercury.

Similarly, to our previous work [1] we confirmed that mercury concentration levels in eggshells are lower than in the membranes.

The mercury concentration in eggshells was from 2 ng/g (limit of the detection for experimental setup) up to 70 ng/g, with an average value of 15 ng/g.

The concentration in membranes was in the range of 10 ng/g and 1900 ng/g, although the highest values were more like exceptions. The average value for membranes was about 200 ng/g.

When separated by the year of laying, eggshell and membrane data show, that the overall differences in concentrations between years are small.

The current small data pool of Hg concentrations in feathers indicates that they have a potential to complement our study.

There is an ongoing investigation on the spatial distribution of the data acquired, as this is a complex matter to analyse due to the bird feeding patterns and waterbody distribution, as well as possible sources of mercury, such as beaver ponds, peat bogs etc.

A thorough analysis of territorial and temporal analysis requires more complementary data.

Acknowledgments

This work was supported by the Latvian Council of Science project No. lzp-2020/1-0005 and ESF project No. 8.2.2.0/20/I/006.

References

[1] Abola A. et al Assessing Mercury Pollution Using Black Stork Eggshells, Environment. Technologies. Resources. Proceedings of the 13th International Scientific and Practical Conference, p.12-16 (2021).

Nitric oxide radicals penetrates into fibroblast cells to promote proliferation

Yasumasa Mori[1], Kazane Oguri[1], Naoyuki Iwata[2], Tomiyasu Murata[3], Masaru Hori[4] and Masafumi Ito[1]

[1] *Department of Electrical and Electronic Engineering, Meijo University, Japan*
[2] *Department of Electronics, Nagoya University, Japan*
[3] *Faculty of Pharmacy, Meijo University, Japan*
[4] *Center for Low-temperature Plasma Science, Nagoya University, Japan*

We have investigated whether nitric oxide radical (NO•) generated from plasma penetrates into fibroblast cells to promote the proliferation. c-PTIO, which reacts with NO• into c-PTI and NO_2•, was employed to scavenge NO• only. c-PTIO and c-PTI were detected using electron spin resonance (ESR) spectroscopy. NO• irradiated the solution dissolving c-PTIO. As a result, the c-PTI signal became stronger and the c-PTIO signal became weaker as the irradiation time increased. The result and another result for uptakes of NO• in cells suggest that NO• diffuses and reacts with the cells in the solution or reacts at the surface of the solution, penetrates in the fibroblast cells to promote the proliferation of fibroblast cells.

1. Introduction

Medical applications of non-equilibrium atmospheric-pressure plasmas (NEAPP) currently attract great attention. Previously, we reported that NEAPP contributes to proliferation promotion of mouse fatal fibroblasts (NIH3T3). [1] Fibroblasts play an important role to maintain the structural integrity of skin tissue. This technique is considered to be useful to accelerate preparation of skin for graft. Nitric oxide (NO•) was identified as a promotion species in gas phase. However, it has been widely reported that NO• reacted with water molecules and produced longer-lived reactive oxygen and nitrogen species (RONS) such as nitrate (NO_2^-) and nitrite (NO_3^-). Therefore, the direct promotion species for the fibroblast was still unclear.

In this study, we have investigated whether NO• penetrates into fibroblast cells to promote the proliferation using a radical generator and carboxy-PTIO(c-PTIO). c-PTIO reacts with NO• to form c-PTI and NO_2•. c-PTIO and c-PTI were detected using electron spin resonance (ESR). Moreover, the uptake of NO• in the cells were investigated using fluorescent probes.

2. Experimental Procedures

3.3 mM of c-PTIO was dissolved in a DPBS solution. 1 mL of the c-PTIO solution was dispensed on a watch glass. The samples were irradiated using an atmospheric-pressure radical source (Tough plasma, FPA10, Fuji Co., Ltd.). [2] The total gas flow rates were set at 4.0 slm, 0.3 slm, and 0.7 slm for Ar, O_2, and N_2, respectively.150 μL of the radical-irradiated c-PTIO solutions was dispensed in a ϕ 1.1-mm ESR quartz tube (Q-Band). ESR signals were measured using an ESR spectrometer (EMXplus, 9.4 GHz, X-Band, Bruker).

3. Results and Discussion

Figure 1 shows ESR signals of the radical-irradiated c-PTIO solution. The ESR signals of c-PTIO, indicated by the solid circles (#), were observed both in the radical-irradiated and unirradiated c-PTIO solutions. The ESR signals of c-PTI, indicated by the solid inverse triangles (*), were detected only in the radical-irradiated c-PTIO solutions. The ESR intensity ratios of c-PTIO was reduced with the longer radical irradiation time, whereas that of c-PTI was inversely increased. The result and another result for uptakes of NO• in cells suggest that NO• penetrates in the fibroblast cells to promote the proliferation of fibroblast cells.

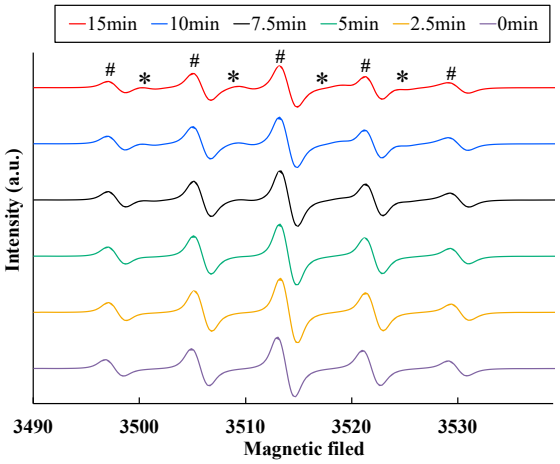

Fig. 1 ESR spectra of the radical-irradiated c-PTIO solutions.

Acknowledgments

This work was supported by a JSPS KAKENHI [grant numbers 19H05462 and 19H01889].

References

[1] Y. Hori, et al., Plasma Process Polym. **18**, 2000225 (2021).
[2] H. Hashizume, et al., Appl. Phys. Lett. **103**, 153708 (2013).

Permeation characteristics of hydrogen peroxide through biological membranes by applying electric field

Yuta Iwata[1], Kosuke Takami[1], Ippei Yagi[1], Kosuke Tachibana[2], Akinori Oda[3], Takehiko Sato[4] and Satoshi Uchida[1]

[1] Tokyo Metropolitan Univ., Tokyo, Japan, [2] Oita Univ., Oita, Japan, [3] Chiba Inst. Technol., Chiba, Japan, [4] Tohoku Univ., Miyagi, Japan

In plasma medicine, behaviour of reactive oxygen species in vivo is an important factor. Particularly, membrane permeation of reactive oxygen species could be controlled by only electrical operation. The aim of this study is to clarify the effects of electric fields and charges on cell membrane permeability. In this paper, changes in potential of mean force and permeability coefficient of POPC lipid membrane in response to H_2O_2 by applied electric field were investigated with molecular dynamics simulations. Consequently, the PMF decreased, and the permeability coefficient increased with electric field.

1 Introduction

Recently, stable generation technology of cold atmospheric plasma (CAP) has been established, and its medical applications are rapidly developing. In plasma medicine, electrical, chemical, and optical effects are intricately involved [1]. However, the balance of influences and interactions among these multiple factors are complicated. In particular, electrical effects such as electric fields and currents have not been understood well. In this work, the potential of mean force (PMF) and membrane permeation coefficient of hydrogen peroxide (H_2O_2) under an applied electric field were derived from the results of molecular dynamics (MD) simulations of intermolecular interactions. The effects of the electric field on membrane transport were also discussed.

2 Analysis Method

In order to construct a typical lipid bilayer containing H_2O_2, we selected POPC (1-Palmitoly-2-oleoyl-sn-glycero-3-phosphocholine), a phospholipid that mainly forms cell membranes. The present calculation conditions were as follows. The pressure was set to 1 bar and the temperature to 303 K. The time step was 2 fs. The equilibration time and sampling time were 100 ns and 5 ns, respectively. The applied electric field was varied from 0 V/nm to 0.4 V/nm. Umbrella sampling method was adopted to apply artificial bias potentials to obtain statical data in high energy regions, which tend to be lacking [2]. The present simulations were performed with the MD software Amber20.

3 Results and Discussion

Figure 1 shows the PMF as a function of distance from the centre of POPC membrane. The PMF at the centre of the membrane decreased with an increase in the electric field. The energy barrier in the positive polarity region became smaller than that in the negative one. The PMF decreased rapidly above 0.3 V/nm. The change in membrane permeability coefficients is shown in Table 1. The permeability intensified with the electric field. Rapid increase occurred at 0.3 V/nm. This is because H_2O_2 can move freely through a breakdown channel of cell membrane generated by the electric field. Although the overall permeability of the membrane at 0.1 V/nm was higher than that at 0 V/nm, the permeability might decrease due to the existence of a high energy barrier in the negative polarity region.

4 Conclusion

The potential barrier was affected by the application of an electric field. This result must be important as basic data for the permeability of membranes. The possibility of permeability control by plasma irradiation was also shown quantitatively.

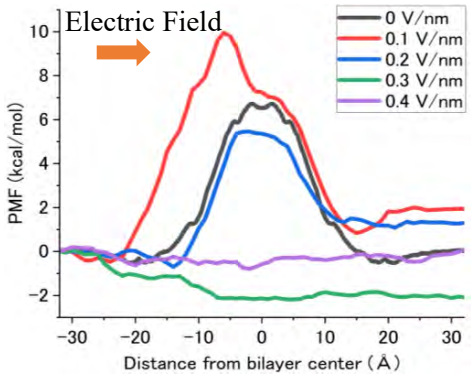

Fig. 1. PMF through the membrane.

Table 1. Membrane permeability coefficients.

Condition	Permeability coefficients (cm/s)
0 V/nm (H_2O_2)	1.33×10^{-3}
0.1 V/nm (H_2O_2)	7.22×10^{-3}
0.2 V/nm (H_2O_2)	6.24×10^{-2}
0.3 V/nm (H_2O_2)	1.89×10^{1}
0.4 V/nm (H_2O_2)	1.46×10^{1}

References

[1] Kong, M. G., Kroesen, G., Morfill, G., Nosenko, T., Shimizu, T., and Zimmermann, J. L., Plasma medicine: an introductory review. New Journal of Physics **11**, 1-35 (2009).

[2] Kumar, S., Rosenberg, J. M., Bouzida, D., Swendsen, R. H., & Kollman, P. A., The Weighted Histogram Analysis Method for Free-Energy Calculations on Biomolecules. I. The Method. Journal of Computational Chemistry **13**, 1011-1021 (1992).

XXXV ICPIG, July 9-14, 2023, Egmond aan Zee, The Netherlands Topic number 17

Treatments of cancer tumors in mice using streamer discharge

R. Ono[1], K. Wada[1], R. Ito[1], D. Okada[1], A. Komuro[1] and H. Yanai[2]

[1] *Dept. Advanced Energy, The Univ. Tokyo, Tokyo, Japan*
[2] *Dept. Inflammology, Research Center for Adv. Sci. & Technol., The Univ. Tokyo, Tokyo, Japan*

We have used streamer discharge for cancer treatment in mice. Our previous studies showed that the streamer discharge can induce an abscopal effect, which is a remote antitumor effect on tumors distant from the discharge-treated tumor (K. Mizuno, J. Phys. D, 50, 12LT01, 2017). This effect can be induced even when the discharge is not irradiated to the tumor but to normal tissue (R. Jinno, J. Phys. D, 55, 17LT01, 2022). Long-term (more than weeks) and systemic antitumor effects have also been demonstrated using the streamer discharge (K. Mizuno, IEEE Trans. Rad. Plasma Med. Sci., 2, 353, 2018). In the present study, some recent progresses on the cancer treatment in mice using streamer discharge are presented including studies on (1) contribution of adaptive immunity and the effect of irradiation site in the abscopal effect induced by normal tissue treatment, (2) inhibition of local recurrence, and (3) combination effects of streamer discharge with immune checkpoint inhibitors.

1 Introduction

Our previous studies have shown that the pulsed streamer discharge is effective for cancer treatment in mice. The streamer discharge can induce a remote antitumor effect, called abscopal effect [1]. Plasma treatment of one tumor in mice with two tumors induced an antitumor effect even on the other untreated tumor. This abscopal effect can be induced even when the discharge is irradiated to normal tissue (not tumor) [2]. The antitumor effect induced by streamer discharge is systemic and kept for more than weeks after the plasma treatment [3]. These results suggest that the streamer discharge activates antitumor immunity in mice. In the present study, some recent progresses on the cancer treatment in mice using streamer discharge are presented.

2 Experimental setup

A tumor-bearing mouse is put on a grounded plate under anesthesia. The repetitive pulsed streamer discharge (25 kV, 20 ns, 100 pps) is generated from a rod electrode with semispherical tip to the mouse. Humid oxygen is flowed to the discharge area. The experimental details can be found in [1–3].

3 Results and discussion

3.1 Normal tissue treatment

To study if the abscopal effect induced by normal tissue treatment is caused by adaptive immunity, immunodeficient mice (SCID and hairless mice) were used. The back of the mice having colon-26 cancer tumors in their right limb was irradiated using the streamer discharge for 10 min/day for five days, but the abscopal effect was not observed. This suggests that the abscopal effect is related to T cell-derived adaptive immunity.

Next, wild type mice were used, but the irradiation site was changed from the back to the stomach. The abscopal effect was observed, indicating that the abscopal effect is not limited to irradiation of specific site of normal tissue.

3.2 Inhibition of local recurrence

We examined whether the plasma irradiation of resection sites of incompletely resected B16F10 melanoma tumors in the right limb of mice inhibits local recurrence. The tumor resected site was irradiated using the streamer discharge for 10 min. Then, the skin was sutured, and the local recurrence was observed. The results showed that the plasma irradiation increases the recurrence-free survival probability by approximately 2 times.

3.3 Combination effects with ICI

We examined whether the plasma irradiation of tumor can enhance the antitumor effects of immune checkpoint inhibitors (ICI). Although the results are not yet decisive and additional experiments are needed, the results suggested that the plasma irradiation may be able to enhance the antitumor effects of ICI.

References

[1] Mizuno, K. et al., Anti-tumor immune response induced by nanosecond pulsed streamer discharge in mice. J. Phys. D: Appl. Phys. **50**, 12LT01 (2017).
[2] Jinno, R. et al., Antitumor abscopal effects in mice induced by normal tissue irradiation using pulsed streamer discharge plasma. J. Phys. D: Appl. Phys. **55**, 17LT01 (2022).
[3] Mizuno, K. et al., Plasma-induced suppression of recurrent and re-inoculated melanoma tumors in mice. IEEE Trans. Radiat. Plasma Med. Sci. **2**, 353 (2018).

Bactericidal activity against *Listeria* spp using Plasma Activated Water

Ana Sainz-García[1], Elisa Sainz-García[1], Félix González-Gallarta[2], Alpha Verónica Pernía-Espinoza[1], Rodolfo Múgica-Vidal[1], Ignacio Muro-Fraguas[1], Ana González-Marcos[1], Paula Toledano[3], Yolanda Sáenz[3], Fernando Alba-Elías[1] rod ana paula

[1]*Department of Mechanical Engineering, University of La Rioja, La Rioja, Spain*
[2]*Department of Chemistry, University of La Rioja, La Rioja, Spain*
[3]*Center for Biomedical Research of La Rioja (CIBIR), La Rioja, Spain*

This work studies the effect of Plasma Activated Water on bacterial inactivation using different hole-setting (number and distribution). A fluid simulation software has been used to know the size, shape and behaviour of bubbles for each hole-configuration.

1. Aim of the work

According to the Food and Agriculture Organization of the United Nations (FAO) the concept "One Health" has been implemented in medical and agri-food fields during the past years. The objective is to balance and optimize the health of ecosystems, animals and humans since they are closely linked [1]. In this regard, there are bacteria such as *Listeria* spp. that could inhabit in all of this field and cause several problems; for instance, food-borne illnesses [2].

This work studies Plasma Activated Water (PAW) generated by an atmospheric pressure cold plasma jet system with dielectric barrier discharge. The PAW used was generated by bubbles method (b-PAW). For generating b-PAW, two gas flows (60-80 slm) and several 3D printed pieces with different hole-configurations (number and distance among holes) were used. *Listeria* spp was chosen as the target bacterium, microbiological experiments were carried out after putting in contact each b-PAW with 10^8 CFU/mL (30 min, 60 min, 2 h, 4 h, 6 h and 24 h). The general objective was to know which b-PAW reached the higher inactivation against *Listeria* spp. However, that objective was divided into two specific ones. The first one was related to how the number of holes (12 or 48) affects the bactericidal activity of b-PAW and the second one related to which are the effects of the distance among holes in terms of bacterial reduction (symmetrical or random hole-configuration). Chromatographic, UV-vis and colorimetric methods were used for reactive species characterization (NO_2^*, NO^*, OH^*, NO_2^-, NO_3^-). Moreover, other parameters such as temperature, oxidation-reduction potential (ORP), electrical conductivity (EC) and pH were also analysed.

Finally, in order to understand inactivation results, bubbles simulations were performed using a fluid-dynamic software (Ansys-Fluent).

2. Results of the work

In terms of bactericidal activity, after 24 h of contact (b-PAW/bacterium) total inactivation was reached regardless the b-PAW studied.

Regarding the first objective, it was suggested higher bacterial reductions when the 3D piece with the maximum number of holes was used. That could be explained due to the fact that the higher the number the holes, the wider the surface interaction air-water when generating b-PAW. It was also showed after fluid dynamic simulation a stronger turbulence with 48 holes compared to 12 holes which is known to increase reactive species diffusion. On the other hand, the research suggested a better bacterial inactivation when using an equal distance among the holes. In this case, simulation illustrated bubble aggrupation after random distances among holes. Besides, since the latest setting reduced the surface interaction air-water the inactivation achieved was lower.

3. Acknowledgments

This work was supported by National Grant PID2019-105367RB-C21 and PID2020-113658RB-C2. The author Ana Sainz-García is thankful to the program of pre-doctoral contracts for contracts for the training of research staff funded by Spanish Ministry of Science and Innovation.

References

[1] Food and Agriculture Organization of the United Nations. OneHealth [Internet]. 2023. [Cited 2023 March 27]. Available from: https://www.fao.org/one-health/en#:~:text=A%20hub%20of%20technical%20knowledge,change%20adaptation%20and%20mitigation%20efforts%3B.

[2] World Health Organization. Listeriosis [Internet]. 2018. [Cited 2023 March 27]. Available from: https://www.who.int/es/news-room/fact-sheets/detail/listeriosis.

Coupling of a non-thermal plasma to a membrane process for the treatment of n-hexane

P. Trad[1], N. Blin-Simiand[1], F. Gerardin[2], M. Heninger[3], P. Jeanney[1], and S. Pasquiers[1]

[1] *Univ. Paris-Saclay, CNRS, Laboratoire de Physique des Gaz et des Plasmas, Orsay, France*
[2] *PROCEP, INRS, Vandœuvre-lès-Nancy, France*
[3] *Univ. Paris-Saclay, CNRS, Institut de Chimie Physique, Orsay, France*

Low concentrations of n-hexane in air stream are treated by non-thermal plasma. A packed-bed reactor filled with alumina beads shows an improvement in the treatment of this hydrocarbon, and a better oxidation of the molecule compared to a DBD reactor. However, even in this case, n-hexane is not completely degraded by plasma for reasonable energy conditions. From the perspective of an industrial application with a more complete treatment, this reactor is coupled to a PDMS membrane that allows the separation of n-hexane molecules from a polluted air stream.

1 Introduction

The treatment of VOC, volatile organic compounds, is a major concern for work safety issues. Methods such as oxidation by non-thermal plasmas [1], and membrane separation [2] are known for the treatment of VOC. However, the coupling of these two techniques has not been examined to date.

In a first step, two coaxial cylindrical plasma reactors are used to treat the n-hexane: a DBD and a packed bed (PB) reactor made of a glass tube filled with alumina beads. The plasma is generated using the same high-voltage pulsed power supply with a repetition frequency of 500 Hz. Gas analysis is made at the exit of the reactor with O_3 and CO_2 detectors, gas phase chromatography and high-resolution mass spectrometry (CI-FTICR) which allows real-time measures of a large range of molecules.

In a second step, a PB reactor/membrane coupling is studied using a PDMS membrane (50 µm) in order to separate the n-hexane from the air stream. In this configuration, the stream of n-hexane that passes through the membrane is treated by the plasma, and then reinjected into the membrane module, forming a loop between the plasma and the membrane. Gas analysis is performed by gas chromatography coupled with mass spectrometry.

2 Results

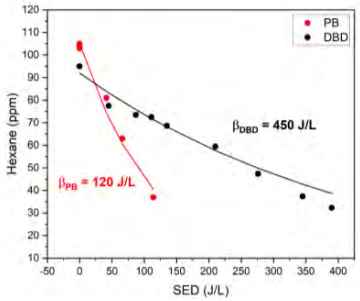

Fig. 1: residual n-hexane at the exit of the PB and DBD reactors as a function of energy density.

The use of the PB reactor improves the treatment of n-hexane: the factor β, the characteristic energy consumed per unit of volume, is 120 J/L, compared to 450 J/L with the DBD, for the treatment of 100 ppm of n-hexane in an air flow of 0.5 L/mn. By-product formation, such as formaldehyde and acetaldehyde, also decreases, going from several ppm with the DBD to less than 1 ppm with the PB reactor. However, this decrease cannot be only attributed to the plasma since there is an adsorption effect on the alumina that should be considered. When the PB reactor is coupled to the PDMS membrane process, the recovery rate, *i.e.* the percentage of VOC transferred through the membrane, is measured. It allows us to evaluate the performance of this coupling compared to that already obtained with the combination of membrane and catalytic oxidation. This study requires the elimination of ozone between the plasma reactor and the membrane in order to ensure that no oxidation takes place in the membrane module influencing the recovery rate.

3 Conclusion and prospects

PB reactors are more efficient for the treatment of n-hexane. But in order to eliminate the adsorption effect that is observed, a study with glass beads replacing alumina beads is planned. When the packed-bed reactor is coupled to the PDMS membrane process, first results show that a good recovery rate is achieved compared to other membrane coupling methods, but ozone must be eliminated at the plasma reactor outlet.

References

[1] Veerapandian et al. Abatement of VOCs Using Packed Bed Non-Thermal Plasma Reactors: A Review. *Catalysts* 7(4):113 (2017).

[2] Gérardin et al. A photodriven energy efficient membrane process for trace VOC removal from air: First step to a smart approach. Chemical Engineering Journal, Volume 419 (2021).

Cold plasma therapy applied to non-small cell lung cancer: deciphering the relevant plasma parameters to induce antitumor effects

K. Géraud[1], S. Marmier[2], M. Soulier[1], H. Decauchy[1], I. Cremer[2] and T. Dufour[1]

[1] *LPP, Sorbonne Université, CNRS, École Polytechnique, Paris, France*
[2] *Team Inflammation, Complement and Cancer, INSERM UMRS1138 Centre de Recherche des Cordeliers (CRC), Sorbonne Université, Université Paris Cité, Paris, France*

Owing to their physico-chemical properties, cold atmospheric plasmas (CAP) represent a promising option to be used as an adjunct/alternative to current anti-cancer treatments. In recent years, LPP and CRC laboratories have been developing new therapeutic approaches for the treatment of non-small cell lung cancer (NSCLC). Experimental campaigns on immunocompetent mouse models have shown a significant reduction in tumour volumes after five plasma treatments as well as abscopal effects.

1 Context

NSCLC is asymptomatic in the early stages of its development and therefore diagnosed late, driving to a 5-year survival rate of about 20% in France [1]. Although systemic treatments (chemotherapy, targeted therapy and immunotherapy) work quite well in the early stages, non-responders are a major problem in the later stages (only 30% for immunotherapies) [2]. In this context, LPP and CRC laboratories (Paris, France) have developed new therapeutic approaches to treat non-small cell lung cancer (NSCLC) by plasma. Reactive oxygen species (ROS) generated by plasma are assumed to activate cellular mechanisms such as oxidative stress, capable of initiating tumour immunogenic cell death resulting in the activation of antitumoral immune responses [3].

2 Plasma Sources

The therapeutic effects of two plasma sources are compared on NSCLC: ORJET (dielectric capillary with Outer Ring electrodes, generating a plasma JET) and DBD-Med (Dielectric Barrier Device with gas flowing through Mesh counter-ElectroDe). Both are supplied in helium and operate in the following conditions: 3-5 kV, 10-20 kHz, 1-10%. The power deposited by the two sources is determined by electrical measurements and the production of reactive species is measured by optical emission spectroscopy and mass spectrometry.

3 Results

First, safety of the two plasma sources is demonstrated by assessing the absence of electrical hazard using targets mimicking electrical response of human body. Besides, temperature measurements achieved by infrared camera indicate values lower than 30 °C While the ORJET source promotes the formation of reactive nitrogen species (N_2*, N_2^+) the DBD-Med source creates in addition reactive species of oxygen (especially O, OH). The role of these species is discussed.

Experimental campaigns carried out on immunocompetent murine models have shown that subcutaneously injected tumours exposed to CAP are smaller in size compared to those in the control groups. After five treatments of 10 minutes every 2 days, tumour volumes are approximately twice smaller than tumour volumes from control groups. Preliminary results about immunology will be introduced. Besides, we show that cold plasma treatment induces an abscopal effect. For this, each mouse is injected simultaneously with NSCLC tumour cells in the left flank and in the right flank. While only the right flank is treated by CAP, it is observed that the two tumours decrease in size following the same kinetics. The abscopal effect appears as a beneficial response to cold plasma therapy and it is thought to be mediated by the immune system, potentially causing shrinkage or eradication of tumors outside the radiation field.

4 References

[1] Pujol, J.-L. *et al.* Lung Cancer in France. *Journal of Thoracic Oncology* **16**, 21–29 (2021).
[2] Zarogoulidis, K. *et al.* Treatment of non-small cell lung cancer (NSCLC). *Journal of Thoracic Disease* **5**, (2013).
[3] Mitra, S. *et al.* Impact of ROS Generated by Chemical, Physical, and Plasma Techniques on Cancer Attenuation. *Cancers* **11**, 1030 (2019).

Mechanism of molecular introduction into plant cells using plasma treatment

Y. Ikeda[1], Y. Hamada[1], R. Ueshima[1], Y. Kido[2], H. Kaya[3], T. Yaeno[3] and M. Jinno[1]

[1] *Graduate School of Science and Engineering, Ehime University, Ehime, Japan*
[2] *Pearl Kogyo Co. Ltd., 3-8-13, Osaka, Japan*
[3] *Graduate School of Agricultural Sciences, Ehime University, Ehime, Japan*

We have successfully edited genomes in plant cells using discharge plasma treatment[1]. In this study, we report the mechanism of molecular introduction into plant cells by plasma treatment with fluorescent molecules of a similar size as the genome editing system. Using an endocytosis inhibitor, we found that the molecules are introduced into plant cells by endocytosis same as in the case of animal cells. We also observed the cell wall surface of plasma-treated plant cells using SEM and found that plasma treatment forms pore on the cell wall surface large enough for the molecules of the genome editing system to pass through. These results suggest that the mechanism of molecular introduction into plant cells is as follows. Plasma creates pathways in the cell wall for the molecule to reach the cell membrane. Molecules that reach the membrane are taken up into the cell by endocytosis induced by the plasma.

1 Introduction

Genome editing technologies are expected to improve crop breeding. However, the introduction of molecules into plant callus is blocked by the cuticula, intercellular material, and cell wall, which are absent in animal cells. In this study, the surface of the tobacco callus after plasma treatment was observed by SEM, and the introduction mechanism was investigated.

2 Experimental setup

The tobacco (*Nicotiana tabacum*) callus was used as a target plant cell. The callus was placed in a 3.5 cm dish. Plasma treatment was carried out at a distance of 1 mm from the electrode tip to the callus. The applied voltage was a sinusoidal 11 kVpp. After the treatment, 10 µl of FITC-dextran (250 kDa: Sigma Aldrich) solution (10 µg/µl) was dropped into the cells, left to stand for a specific time, washed, and observed treated callus under a fluorescence microscope (MVX10: Olympus). FE-SEM observed the callus freeze-dried from t-butanol after plasma treatment. In addition, comparative experiments with an inhibitor (ES9-17: Sigma Aldrich) were performed to investigate the contribution of endocytosis.

3 Result and Discussion

The SEM and fluorescence images of the callus after plasma treatment are shown in Fig.1. We observed the cell wall surface of plasma-treated plant cells using SEM and found that plasma treatment forms pores on the cell wall surface large enough for the molecules of the genome editing system to pass through. The fluorescence observation results are shown in Fig.2. The inhibition of endocytosis reduces the fluorescence intensity of FITC-dextran. Based on these results, the mechanism of molecular introduction into plant cells is as follows. The electrical and chemical stimulation of the plasma breaks down the cell wall, resulting in pores. The pores are the entry pathway for molecules to reach the cell membrane. Molecules that reach the cell membrane are taken into the cell by endocytosis.

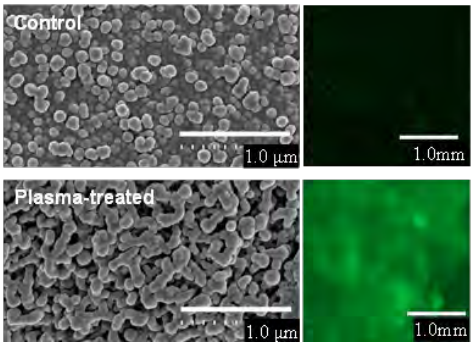

Fig.1 SEM observation results (left) and fluorescence observations after FITC-dextran introduction treatment (right).

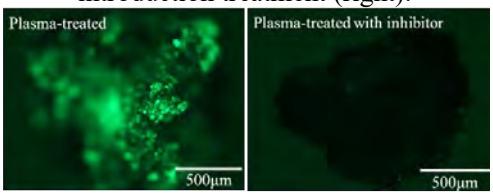

Fig.2 Results of molecular introduction into tobacco callus treated with endocytosis inhibition.

Acknowledgment

Part of this work was supported by JSPS KAKENHI 17H01068 and 15H00896.

References

[1] Jinno, M. Japanese Journal of Applied Physics, **60** (3) (2021).

Measurement of electric field, UV photons, and long-lifetime reactive species generated by atmospheric pressure air plasma for plasma bio applications

T. Okumura[1], S. Tsuboyama[2], Y. Tagawa[1], T. Nakao[1], T. Anan[1], H. Tanaka[1], K. Kamataki[1], N. Yamashita[1], N. Itagaki[1], P. Attri[1], K. Koga[1,3], M. Shiratani[1], K. Kuchitsu[2]

[1] *Kyushu University, Fukuoka, Japan,*
[2] *Tokyo University of Science, Tokyo, Japan*
[3] *National Institutes of Natural Sciences, Tokyo, Japan*

Dielectric barrier discharge (DBD) plasma has attracted much attention as a novel environmental-friendly process for inducing plant responses. DBD plasma generates reactive species, ions, photons, and electric fields which affect the plant growth. Here we report measurements of these factors which allow us to discuss correlation between these factors and plant response quantitatively.

1 Introduction

Plasma irradiated seeds show interesting responses such as germination enhancement, growth promotion, increasing harvest yield [1-3]. So far, the response was discussed with the amount of reactive oxygen and nitrogen species (RONS) such as H_2O_2, NO_x^- while the plasma generates RONS, UV, and electric field [4,5]. The comprehensive study, taking these factors into account, is important to reveal plasma-induced plant response. The aim of this study is to provide the absolute amount of these factors generated by atmospheric pressure air plasma for plasma bio applications.

2 Experimental

Plasma was generated by a scalable dielectric barrier discharge (SDBD) plasma device [6]. The applied voltage was varied from 0 to 7.8 kV, and the frequency was 15 kHz. The environment during plasma irradiation was set at a temperature of 22°C and a humidity of 45%Rh. Three-dimensional electric field was measured by Pockels effect with changing distance *y* using Pockels cell (SEIKOH GIKEN, CS-1403), LiNbO3 of 1.5 × 2.5 mm with 8 μm thickness, placed in a polymer box of W6.0 × D23.5 × H5.5mm [7]. We also examined plasma irradiation to plant samples which is *Marchantia polymorpha* gemmae as model plant. Samples were placed upon a paper filter with 240 μL of ultra-pure water-absorbed paper filter of 25 mm × 25 mm in a petri dish below SDBD electrode during the plasma irradiation for 10 s. The distance between electrode and sample *y* was 3 mm. After plasma irradiation, samples were cultured for 10 days, and size and fresh weight of samples were obtained.

3 Results and discussion

Phenotype analysis showed that the size and fresh weight of samples increase by plasma irradiation up to 4.7 kVpp and above which that decrease, indicating that plasma irradiation allows us to control *Marchantia polymorpha* growth. The electric field decreased as the distance y from the electrode increased from 15 mm to 200 mm. Fig. 1 shows the electric field intensity at 3 mm by synthesizing the values in three-dimension. Fig. 1 was obtained by extrapolation based on the approximation curve obtained from the distance dependence of the electric field strength of each applied voltage. Fig. 1 shows that the electric field increases from 3.63 to 40.1 kV/m as the applied voltage increases from 1.68 to 7.80 kVpp. In the conference, we will comprehensively provide the absolute amount of particle species by plasma irradiation including RONS and ultraviolet light fluxes. The above results are important parameters for reproducing the plasma irradiation effect.

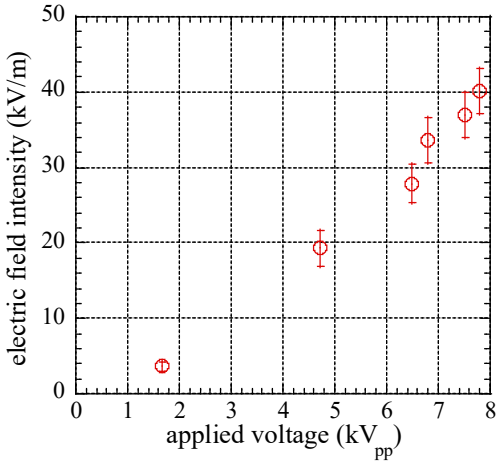

Fig 1. Electric field intensity at 3mm below the electrodes.

References

[1] P. Attri et al., Processes 8, 1002 (2020).
[2] P. Attri et al., Jpn. J. Appl. Phys. 60 (2021).
[3] P. Attri et al., Agronomy 12, 1–22 (2022).
[4] T. Okumura et al., Sci. Rep. 12, 12525 (2022).
[5] F. Tochikubo, & T. H. Teich, Jpn. J. Appl. Phys., Regul. Pap. Short Notes Rev. Pap. 39, 1343–1350 (2000).
[6] K. Koga et al., Appl. Phys. Express 9, 016201 (2016).
[7] K. Kamataki et al., AIP Advances 12, 085220 (2022).

The inhibitory effect of volume dielectric barrier discharge on phytopathogenic fungi

P.F. Ambrico[1], P. R. Rotondo[2], C. Rotolo[2], D. Aceto[1], M. Ambrico[1], G. Dilecce[1], F. Faretra[2] and R.M. De Miccolis Angelini[2]

[1] *CNR – Institute for Plasma Science and Technology, Dipartimento Interateneo di Física - Uniba – 70126 Bari – Italy*
[2] *Department of Soil, Plant and Food Sciences, University of Bari - 70126 Bari, Italy*

The study evaluated the inhibitory effect of cold plasma on fungal conidial germination using a square wave modulated plasma with a duty cycle of 20% at atmospheric pressure. The efficacy of the treatment was influenced by different factors such as total treatment time, applied voltage, medium composition and different cellular structure of the analysed fungi. The inhibitory effect increased with exposure time and decreased with fungal complexity. The uniformity of the plasma and agarized medium were also important factors. Complete inhibition of conidial germination was achieved for all tested species at different treatment times.

1 Introduction

Low-temperature plasma has potential as a sustainable and eco-safe technology for controlling microbial growth in food and agricultural products [1,2]. This is due to charged particles, reactive oxygen (ROS) and nitrogen (RNS) species present in the plasma that can damage the microorganisms cell membrane, resulting in loss of function and structure, and cell death. Target microorganisms have varying levels of sensitivity to plasma treatments, depending on their characteristics, such as cytology, morphology, and growth. Previous studies showed a differential response of fungal species to plasma [2]. To further investigate the observed differences, VDBD treatments on conidial germination of phytopathogenic fungi (*Alternaria alternata*, *Aspergillus carbonarius*, *Botrytis cinerea*, *Fusarium graminearum* and *Monilinia fructicola*) were performed.

2 Experimental

The VDBD reactor is made of a double barrier DBD, using the nickel metallic electrode (ϕ = 6 mm) screen printed on two circular alumina plates (ϕ = 25.4 mm) place at a distance of 6 mm. The samples were disposed on the grounded electrode. Burst of two 5 kHz AC HV waveform were supplied at a rep rate of 500 Hz. Conidial germination assays for *B. cinerea*, *M. fructicola*, *A. alternata* and *F. graminearum* were performed using Water Agar (WA) while for *A. carbonarius* different agarized media were used: Agar Glucose (AG), Malt Extract Agar (MEA) and Potato Dextrose Agar (PDA).

2 Results and conclusions

The VDBD is the richest plasma environment in terms of antimicrobial agents, being the samples exposed directly to radiation (UV/VIS/NIR), direct impact of ions and electrons, radical and atomic species. Plasma induced N_2 emission evidenced strong electric field and a fast thermal heat shock (lasting hundreds of μs). The electrical response of the discharge apparatus was depending on the agarized medium used.

In vitro studies on WA showed (figure 1) that *B. cinerea* and *M. fructicola* with unicellular conidia and similar melanin content, showed similar behaviour and sensitivity to the treatment. *F. graminearum* and *A. alternata*, both having multicellular conidia, were more resistant to the plasma treatment showing different sensitivity likely due to a different content in melanin. Inhibition of *A. carbonarius* conidia on different agarized media was influenced by the complexity and composition of the medium used, being PDA the artificial medium that more hindered the plasma treatment (data not shown).

In conclusion, low temperature plasma could be useful in the control of fungal species but different factors can influence antimicrobial activity, and treatment conditions must be carefully chosen to reach a complete decontamination.

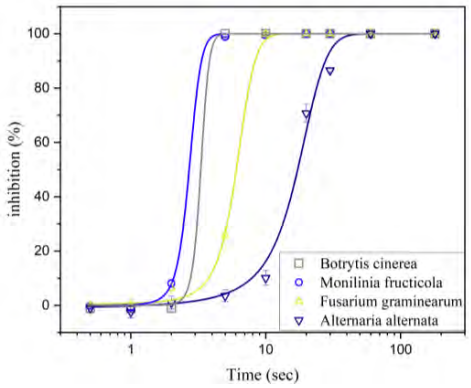

Figure 1. Response of different fungal species on WA.

References

[1] Ambrico P F, et al, *J. Phys. D. Appl. Phys.* (2017) **50** 305401

[2] Ambrico P F, et al, *Sci. Rep.* (2020) **10** 1–17

Determination of antibacterial effectiveness rate of plasma activated physiological saline (PAIS) solution (0.9% NaCl)

A. Uygun Oksuz [1], S.N. Kutlu[2], Lutfi Oksuz[3] and A. Güleç[4]

[1] *Department of Chemistry, Faculty of Arts and Sciences, Suleyman Demirel University, Isparta, Turkey*
[2] *Biomedical Device Technologies, Uluborlu Selahattin Karasoy Vocational School, Isparta University of Applied Sciences, Isparta, Turkey*
[3] *Department of Physics, Faculty of Arts and Sciences, Suleyman Demirel University, Isparta, Turkey*
[4] *Biomedical Engineering, Faculty of Technologies, Isparta University of Applied Sciences, Isparta, Turkey*

Plasma active liquids are one of the safest methods of applying plasmas to biological tissues. Many of the studies in the literature are on PAW, PAM, PAPBS and PARL. So, in this study, the antibacterial activity of physiological saline (0.9% NaCl) isotonic solution treated with atmospheric pressure plasma (cold plasma) was investigated. An intra-oral microbial sample was used to determine the antibacterial ability. It has been observed that the hydrogen peroxide, nitrite and nitrate products formed in PAIS vary both according to the plasma exposure time and according to the storage condition of PAIS. In the period after plasma treatment, the pH changes in the PAIS continued for a certain period of time and then became stable.

1 General

Plasma activated distilled/deionized/tap water (PAW), plasma activated medium (PAM), plasma activated phosphat buffer (PAPBS), plasma activated ringer lactate solution (PARL), plasma activated isotonic saline (PAIS) can be summarized as plasma activated liquids (PALs) studied in the literature. Recently, plasma activated saline solutions (PASs) that can be used as antibacterial agents have been attracting great interest. In some cases, simple buffer solutions have shown a selective cytotoxic effect even greater than PAW (tap) [1]. The antibacterial effectiveness of PAW has been found to be lower in some studies compared to saline solutions. Because saline solutions contain different types of reactive oxygen and nitrogen species (RONS) than PAW, depending on the type of saline. For example, if there are chlorine ions in the solution, hypochlorous acid (HOCl) may form, which Yang et al. detected ClO in the PAS [2]. It is known that neutrophils from defence system cells show antimicrobial activity by forming HOCl via myeloperoxidase. It has been found that HOCl in high concentrations has a cytotoxic effect on some types of microorganisms that can develop drug resistance. Despite all these data, one of the least researched liquids in PASs is isotonic saline containing 0.9% NaCl.

2. Material and Methods

Argon was used as a plasma gas. The gas flow rate was maintained at 6-7 L/min during plasma exposure. Borosilicate material with a wall thickness of 1 mm, a diameter of 3 mm, a length of 15 mm was used as a discharge tube. The power supply with a frequency of 50 kHz, 6 kV was used to perform the discharge. The plasma treatment time was determined between 1-10 min. Samples were stored at room temperature, +4 ºC and -20 ºC. Oral culture was propagated in glass tubes in an incubator at 37 °C in Luria Bertani (LB) growth medium. At the end of the incubation, microorganisms were cultivated at a concentration of 10^6 cell/mL for each group. Each group was treated with PAIS for 1 min. The process steps are shown in the Figure 1.

3. Results

It has been observed that the hydrogen peroxide, nitrite and nitrate products formed in PAIS vary both according to the plasma exposure time and according to the storage condition of PAIS. In the period after plasma treatment, the pH changes in the PAIS continued for a certain period of time and then became stable.

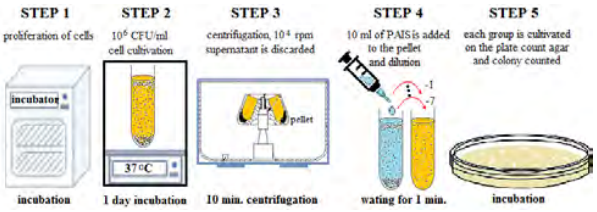

Figure 1. steps of process.

References

[1] Sampaio, A. D. G., Chiappim, W., Milhan, N. V. M., Botan Neto, B., Pessoa, R., & Koga-Ito, C. Y. (2022). Effect of the pH on the Antibacterial Potential and Cytotoxicity of Different Plasma-Activated Liquids. International Journal of Molecular Sciences, 23(22), 13893.

[2] Yang, L., Niyazi, G., Qi, Y., Yao, Z., Huang, L., Wang, Z., ... & Liu, D. (2021). Plasma-Activated Saline Promotes Antibiotic Treatment of Systemic Methicillin-Resistant Staphylococcus aureus Infection. Antibiotics, 10(8), 1018.

Nonthermal plasma regeneration and repetitive use of deactivated catalysts

R. Cimerman[1], J. Kšanová[1], L. Satrapinskyy[2] and K. Hensel[1]

[1] *Division of Environmental Physics, Comenius University, Bratislava, Slovakia*
[2] *Department of Experimental Physics, Comenius University, Bratislava, Slovakia*

Nonthermal plasma regeneration of deactivated catalysts was investigated at ambient and elevated temperatures and compared with ozone regeneration. A level of catalyst regeneration strictly depended on the catalytic material and gas temperature. Regenerated catalysts were reused in several cycles and the obtained results were compared with those of non-regenerated ones.

1 Introduction

A catalyst deactivation, i.e., the loss of catalytic activity and/or selectivity over time, is generally one of the major and inevitable concerns in conventional as well as plasma catalysis. After a decrease of catalyst activity, the catalyst can be regenerated (restored, reactivated), used for another application, recycled, or discarded [1]. From the economic and environmental point of view, the first option is the most appropriate.

It is well known that nonthermal plasma can create highly reactive environment even at ambient conditions. In this sense, a potential of nonthermal plasma generated by atmospheric pressure dielectric barrier discharge (DBD) for regeneration of deactivated catalysts was investigated.

2 Experiment and analysis

The experimental procedure consisted of two steps. Firstly, plasma catalytic removal of a model volatile organic compound (toluene) or polycyclic aromatic hydrocarbon (naphthalene) was employed using packed-bed DBD reactors in synthetic air as a carrier gas [2, 3]. The reactors had a cylindrical coaxial geometry and were packed with various catalysts (TiO_2, Pt-, Pd-γAl_2O_3, $BaTiO_3$). Decomposition of the model compounds resulted in formation of various gaseous and solid compounds (products) often found as carbon containing deposits on surface of the catalysts. These solid deposits were responsible for deactivation of catalysts and decrease of their activity over time.

Secondly, the deactivated catalysts were regenerated using the packed-bed DBD reactors of the same geometry in oxygen as a carrier gas at ambient (25°C) or elevated (100°C) temperatures for 2 hours. Besides, in order to evaluate a role of ozone in the regeneration process, the catalysts were also regenerated by ozone from an ozonator.

Regeneration led to formation of gaseous oxidation products (CO_2, CO and HCOOH) and temporal evolution of their concentrations was monitored by infrared absorption spectroscopy FTIR. Surface of the catalysts was analysed by scanning electron microscopy SEM and optical microscopy. In addition, the thermogravimetric analysis TGA of the catalysts was also performed.

3 Results

The results showed that the concentrations of the oxidation products rapidly increased, reached maxima and then gradually decreased with time. Moreover, efficiency of the catalyst regeneration depends predominantly on the used catalytic material, i.e., its dielectric constant. It determines not only an interaction between catalyst and plasma, but also an exhibiting discharge mode (surface or localised filamentary mode). Surface analysis of the catalysts proved oxidation and partial removal of solid carbon deposits. Efficiency of catalyst regeneration was higher with nonthermal plasma compared to ozone regeneration alone and depended on gas temperature.

Finally, some of the regenerated catalysts were reused and tested for the removal of toluene by plasma catalysis in three repetitive cycles. The results showed that regenerated catalysts exhibited higher efficiency of toluene removal than non-regenerated ones. This effect was the most evident for Pt/γAl_2O_3, and then for TiO_2.

This work was supported by grants of Slovak Research and Development Agency APVV-20-0566 and Slovak Grant Agency VEGA 1/0822/21.

References

[1] Argyle, M. D., Bartolomew, C. H. Heterogeneous catalyst deactivation and regeneration: A review. Catalysts **5**, 145–269 (2015).

[2] Cimerman, R., Račková, D., Hensel, K. Tars removal by non-thermal plasma and plasma catalysis. J. Phys. D: Appl. Phys. **51**, 274003 (2018).

[3] Cimerman, R., Cíbiková, M., Satrapinskyy, L., Hensel, K. The effect of packing material properties on tars removal by plasma catalysis. Catalysts **10**, 1476 (2020).

Plasma assisted decontamination of food packaging

Filippo Capelli[1,5], Ana Sainz-García[2], Caterina Maccaferri[1], Francesco Tomelleri[1], Giulia Laghi[1], Fernando Alba-Elías[2], Vittorio Colombo[1,3,4,5], Matteo Gheradi[1,4], Romolo Laurita[1,3]

[1]*Department of Industrial Engineering, Alma Mater Studiorum - University of Bologna, Bologna, Italy*
[2] *Department of Mechanical Engineering, University of La Rioja, La Rioja, Spain*
[3]*Interdepartmental Centre for Industrial Research Health Sciences and Technologies, Alma Mater Studiorum - University of Bologna, Ozzano dell'Emilia, Italy*
[4]*Interdepartmental Centre for Industrial Research Advanced Mechanical Engineering Applications and Materials Technology, Alma Mater Studiorum - University of Bologna, Bologna, Italy*
[5]*Almaplasma S.r.l., Bologna, Italy*

This work examines the relation between bacterial inactivation and the various parameters which defines a surface dielectric barrier discharge plasma treatment, particular effort has been put in analysing the chemical composition of the atmosphere produced by the plasma discharge into the reactor.

1 Aim of the work

Cold plasma technology is well spread in the industry world and permeates different application fields. From a research point of view one of the most promising contexts is the food-agro one; this fact is highlighted by the increasing number of scientific papers published in recent years in this field.

Plasma processes have a high degree of flexibility and might be used in the food-agro field for different purposes, such as increasing seeds germination, surface modification, nutrient extraction; nevertheless, the main topic which connects this field and plasma is decontamination processes.

One of the main lessons that the COVID-19 pandemic has taught the world is the importance of decontaminating living and non-living surfaces to reduce the spread of diseases [1]. The global market has a major importance in the spread of diseases: goods could be transported across countries before being sold to customers with little if any attention to possible contamination of the packaging. Moreover, plasma processes could be exploited to directly decontaminate the foods, this type of treatments aim to clean goods to reduce the chance of spoilage, increasing shelf-life of fresh foods and therefore reducing waste.

This work examines the relation between the decontamination efficacy of a SDBD (Surface Dielectric Barrier Discharge) plasma treatment on materials typically used in the food packaging industry and the concentrations of reactive species produced by the plasma discharge.

2 Results

In literature there are many papers assessing the relation between the surface power density (SPD) and the chemical composition of air plasma [2, 3]; a low SPD leads to an atmosphere enriched with ozone, while a high SPD produces an atmosphere dominated by nitrogen oxides. Optical absorption spectroscopy was performed to analyse the concentration of ozone and nitrogen dioxide during treatments. Multiple tests were performed varying the axial line of sight to observe the diffusion of ozone and nitrogen dioxide inside the 18 L closed treatment volume.

Two different operating conditions were tested varying the SPD absorbed by the SDBD; tests were performed varying treatment time from 10 to 30 minutes. In addition, the effect of a mixed atmosphere inside the reactor was evaluated using or not a fan.

Biological results were obtained with *Staphylococcus epidermidis* (ATCC 12228), a Gram-positive bacterium. The plasma system, developed by AlmaPlasma srl, was used to treat polypropylene contaminated sample, inactivation of approximately 2 logarithmic reductions were obtained with a 30-minute treatment.

3 Acknowledgment

This activity received funding from the PlasTher COST Action CA20114.

4 References

[1] F. Capelli et al., Appl. Sci. 11, 4177 (2021).
[2] E. Simoncelli et al., Plasma Sources Sci. Technol. 28, 95015 (2019).
[3] M. J. Pavlovich, et al., Plasma Sources Sci. Technol. 23, 6 (2014).

Prediction of plasma process conditions via machine learning

K. Kamataki[1], F. L. Chawarambwa[1], D. Yamashita[1], N. Yamashita[1], T.Okumura[1], N. Itagaki[1], K.Koga[1,2], M. Shiratani[1]

[1] *Graduate School and Faculty of Information Science and Electrical Engineering, Kyushu Univ. Japan*
[2] *National Institutes of Natural Science, Japan*

Plasma processes demand many external parameters to be tuned. For the better tuning, process data of plasma suppering of amorphous ITO films is analyzed by two methods: support vector machine (SVM) and ensemble learning method: gradient boosting decision tree (GBDT). These analyses are useful not only for identifying key external parameters and suggesting better experimental conditions, but also for giving predictive insights into experimental results.

1. Introduction

In semiconductor manufacturing, plasma processes of CVD, sputtering, and etching, play central roles. These processes have dozens of tuning parameters and multiple objective variables for product evaluation. Relations between the tuning parameters and objective variables are highly complicated and thus are hard to be interpreted. Since plasma process has a non-linear relationship between these tuning parameters and plasma parameters and a complex relationship between the plasma and material interface/property of material, to identify important experimental tuning parameter for the quick production of the desired material requires considerable efforts by well-established researchers and can be a bottleneck of the research and development. In this study, the estimation of key tuning parameter in plasma process is partially overcome by utilizing the state-of-the-art ensemble learning algorithm. We used one of the ensemble learning, gradient boosting decision trees (GBDT) [1], for estimating feature importance. Moreover, we perform classification and regression analysis for crystallinity and mobility of a-ITO film in order to predict the optimal sputtering conditions for fabricating high mobility a-ITO/In_2O_3 film. For classification of crystallinity, support vector machine (SVM) [2] is used.

2. Method

N_2/Ar flow ratio, which is the feature of NMA, ranges from 0 % to 12.5 %. The vertical position of the substrate is controllable in 55-115 mm of target-substrate distance (d(T-S)). The substrate temperature varies from room temperature (~30 ℃) to 300 ℃. The sputtering target was ITO or In_2O_3. These four parameters (N_2/Ar, d(T-S), T_S, target) are used as the features which means the variables for training predictive models and performing predictions.

3 Results and Discussion

we discuss classification between amorphous and crystal films. For the classification of crystallinity, we used SVM with radial base function kernel which was non-linear, and logistic regression model which was linear. SVM in machine learning is supervised learning models with associated learning algorithms that analyze data used for classification and regression analysis. Figure 1 shows the results of SVM for ITO films. The number of all labels is 124, and 89 of which are amorphous and 35 are crystalline. These results show the classification is successful and films tend to become amorphous when N_2/Ar flow ratio and d(T-S) increase. The trained classification model is useful for predicting the crystallinity of not measured data and future experiment with probability as confidence level. Moreover, GBDT model show the key parameter for good film fabrication. We will discuss details at the conference.

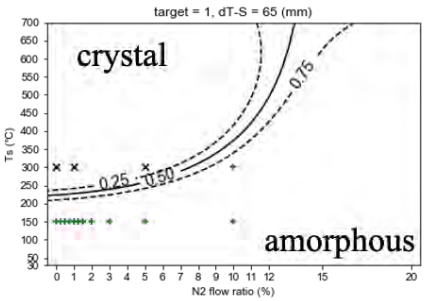

Fig1. SVM results (ITO films, dT-S=65mm, n= 124)

Acknowledgements

This work was partly supported by JSPS KAKENHI (Grant No. JP20H00142), JSPS Core-to-Core Program (Grant No. JPJSCCA2019002).

References

[1] J. H. Friedman, The Annals of Satistics, **29**, 5 1189 (2001).
[2] H. Liu, H. Motoda, IEEE Intell. Syst. their Appl., **13**, 2, 26 (2005).

Stabilize Voltage and Transmit Power by Atmospheric-Pressure Plasma Jet in Streamer Mode

Po-Hsien Chiu and Jong-Shinn Wu*

Department of Mechanical Engineering, National Yang Ming Chiao Tung University, Hsinchu, Taiwan

The atmospheric-pressure plasma jet (APPJ) has many applications but is rarely used in the power source although APPJ itself requires high voltage. This study analysed the electrical properties of the APPJ device with a simple structure. The ambient air was pumped into the APPJ device and charged by an AC power source to produce plasma. It is found that when the discharge is streamer, the voltage amplitude of the powered electrode is similar while different power is applied, and thus APPJ has the potential to serve as the voltage stabilizer. Further, streamer can transmit power to the receiver electrode with the moving ions in the air flow for a longer distance than arc while the same voltage is applied, and thus APPJ has the potential to be developed to transmit power wirelessly.

1. INTRODUCTION

The electrical discharges can be used to transmit electricity directly. The electrical discharges are categorized into streamer-like plasma, spark discharges, and arc discharges [1]. However, the prior researches are not enough to provide information to use APPJ to transmit power or stabilize voltage.

2. EXPERIMENTAL METHODS

The APPJ was driven by an AC power supply. The voltage and current signals on the powered electrode and the receiver electrode were measured in the points P1 and P2 shown in Fig. 1, respectively.

3. RESULTS AND DISCUSSION

Refer to Fig. 2, with the air pumped into the APPJ device, the discharge from the powered electrode moved downward but curved to the tip of the receiver electrode. Without air flow, none of arc, spark or streamer was produced. It implies that the ions in the air flow were media to carry electrons. Further, while the distance d between electrodes was short enough, the arc or the spark were generated without the air flow. However, the discharge was dominated by the streamer if the air flow was provided.

Fig. 3 shows when the discharge is streamer, the voltage amplitude of the powered electrode is similar while different power is applied. Thus, the APPJ device can be used as the voltage stabilizer when the point near the powered electrode (P1 shown in Fig. 1) is connected to provide the power output.

Further, the measurement of the voltage and current in the point near the receiver electrode (P2 shown in Fig. 1) shows that the receiver electrode received power from the powered electrode. Thus, streamer can transmit power wirelessly.

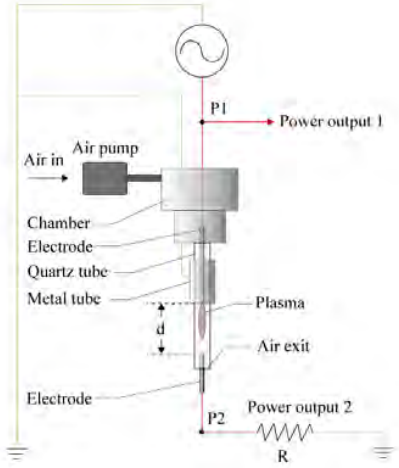

Fig. 1. Experimental setup for using an APPJ.

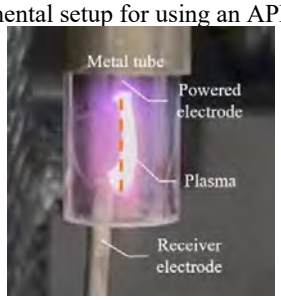

Fig. 2. The discharge in the stream mode.

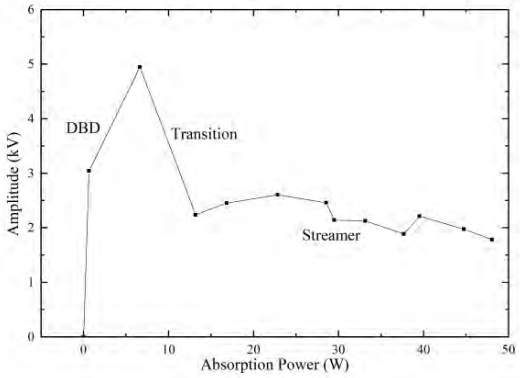

Fig. 3 The voltage amplitude as a function of the absorption power the powered electrode.

References

[1] B. R. Locke and S. M. Thagard, Analysis and review of chemical reactions and transport processes in pulsed electrical discharge plasma formed directly in liquid water, vol. 32, 2012, pp. 875-917.

Microscopic properties of xenon plasmas in a wide range of plasma conditions

G. Espinosa-Vivas, R. Rodríguez and J.M. Gil

IUNAT, Physics Department, Universidad de Las Palmas de Gran Canaria, Spain

In this work, we present a systematic study of microscopic properties of xenon plasmas such as average ionization, charge states distributions, emissivities and opacities in a wide range of plasma conditions covering local and non-local thermodynamic regimes. These properties can be useful for radiation-hydrodynamic simulations of these plasmas and for their spectroscopic diagnostics in the field of high energy density plasmas.

1 General

Xenon is an element of current interest in the field of high energy density plasmas since it is commonly used, for example, in experiments of laboratory astrophysics [1-4] and extreme ultraviolet lithography [5,6]. For the radiation-hydrodynamics simulations of these plasmas or their spectroscopic diagnostics, it is useful to have a predictive numerical model of the microscopic properties of xenon. However, this is not an easy task due to the complexity of the low charge ion stages of this element.

In this work, we present numerical simulations of microscopic properties of xenon plasmas such as the average ionization, the charge state distributions, the emissivities and the opacities in a wide range of plasma conditions, with electron temperatures from 1 to 1000 eV and mass densities between 10^{-6} and 10^{-1} gcm^{-3}. Since these conditions cover both equilibrium and non-equilibrium thermodynamic regimes, the calculations were performed using a collisional-radiative model that includes the common atomic processes in thermal plasmas such as collisional excitation and de-excitation, collisional ionization and three-body recombination, autoionization and electron capture, spontaneous decay and radiative recombination. This collisional model is implemented in the computational package MIXKIP/RAPCAL [7]. As the number of configurations and transitions of low charge xenon ions is very high (with open 4d subshells) and the study carried out was made in a wide range of plasma conditions, the atomic data were obtained in the relativistic detailed configuration account. For this purpose, the FAC code was used [8]. In order to group detailed transition lines, the unresolved transition array formalism has been used [9].

Acknowledgments

This work was supported by the Spanish Government through the Project PID2019-110678GB-I00.

References

[1] Koenig, M. et al. Radiative shocks: An opportunity to study laboratory astrophysics. Phys. Plasmas **13**, 056504 (2006).

[2] Falize, E. et al. High-energy density laboratory astrophysics studies of accretion shocks in magnetic cataclysmic variables. High Energy Density Phys. **8**, 1 (2012).

[3] Osterhoff, J., Symes, D., Edens, A., Moore, A., Hellewell, E. and Ditmire T. Radiative shell thinning in intense laser-driven blast waves. New J. Phys. **11**, 023022 (2009).

[4] Keilty, K., Liang, E., Ditmire, T. Remington, B., Shigemori, K.and Rubenchick, A. Modeling of laser-generated radiative blast waves. Astrophys. J. 538, 645 (2000).

[5] Chkhalo, N.I. and Salashchenko, N.N. Next generation nanolithography based on Ru/Be and Rh/Sr multilayer optics. AIP Advances **3**, 082130 (2013).

[6] Velik, V.P., Kalmykov, S.G., Mozharov, A.M., Petrenko M.V. and Sasin, M.E. Features of experimental spectra of the laser plasma with a dense xenon gas-jet target in the extreme ultraviolet range. Tech. Phys. Lett. **43**, 1001 (2017).

[7] Rodríguez, R., Espinosa, G. and Gil, J.M. MIXKIP/RAPCAL: A Computational Package for Integrated Simulations of Large-Scale Atomic Kinetics and Radiation Transport in Non-Local Thermodynamic Equilibrium Plasmas. Commun. Comput. Phys. **30**, 602 (2021).

[8] Gu, M.F. The flexible atomic code. Can. J. Phys. **86**, 675 (2008).

[9] Bauche, J., Bauche-Arnoult, C. and Klapisch, M. Transition arrays in the spectra of ionized atoms. Adv. At. Mol. Phys. **23**, 131 (1988).

Inelastic momentum transfer cross-sections from inelastic differential cross-sections for electron-impact excitation in Helium and in Argon

R.J. Carman[1] and R.P. McEachran[2]

[1] *Dept. of Physics and Astronomy, Macquarie University, Sydney, Australia*
[2] *Research School of Physics, Australian National University, Canberra, Australia*

A comprehensive set of state-specific inelastic momentum transfer cross-sections associated with electron-impact excitation will be reported for both helium and argon gases. These cross-sections have been evaluated from the underlying differential cross-sections for excitation which have been calculated using the relativistic distorted wave (RDW) method over a broad range of incident electron energies up to E=5000eV.

For the rare-gases, the inelastic momentum transfer cross-sections associated with electron-impact excitation and ionisation have not been studied extensively to date, although they are expected to play an important role in modelling electron transport in plasmas with improved accuracy [1]. These cross-sections are particularly important for characterising the behaviour of energetic plasma electrons (E=10-1000eV) generated in fast transient pulsed discharges, electron-beam plasmas [2] or tokamaks [3].

For plasma modelling purposes, an inelastic momentum transfer cross-section $Q_{mj}(E)$ is required to be defined as a smooth, continuous function of the electron energy starting at the excitation/ionisation thresholds (e.g. E_{ex} for excitation), and this task is dependent on the availability of full differential cross-sections (DCS) $\sigma_j(E,\theta)$ (in cm^2/sr) between θ=0-180°.

The momentum transfer cross-section for electron excitation collisions is given by [4]:

$$Q_{mj}(E) = \int_0^{\pi} \left(1 - (1 - E_{ex}/E)^{1/2} \cos\theta\right) \sin\theta \, \sigma_j(E,\theta) d\theta$$

.

In this work, the differential cross-sections for excitation have been calculated using the relativistic distorted wave (RDW) method which was originally developed in [5] and then applied to the excitation of the $6s[1/2]_1$ and $6s[3/2]_1$ states of Xenon between 30-80eV. The method was subsequently used to treat excitation processes in Argon, Krypton and Xenon up to 500eV [6].

Although the original version of the RDW method required that the ground and excited state wavefunctions be determined in a single multi-configuration Dirac-Fock (MCDF) calculation, a modified version of the RDW method has been used here which allows for the ground and excited state wavefunctions to be determined in separate MCDF calculations, thereby giving a more accurate representation of both atomic states. Furthermore, the numerics of this new code have been modified so that it can accommodate incident energies greater than 2000eV (up to 5000eV), and incident electron orbital angular momentum greater than 100 au.

In this paper, the DCS's from the RDW calculations will be directly compared to existing experimental and theoretical DCS data sets [4][7][8] for selected electron energies up to E=500eV.

Finally, state-specific inelastic momentum transfer cross-sections for both helium (10 excited states) and argon (26 excited states) will be presented and compared to experimentally derived values, where available from the literature. To our knowledge, this is the first time inelastic momentum cross-sections for individual excited states with coverage of a broad range of electron energies (11-5000eV) have been evaluated for any of the rare gases.

References

[1] T. Makabe, R. White, J. Phys. D: Appl. Phys. **48** 485205 (2015)
[2] Special issue on Fast Pulse Discharges, Plasma Sources Sci. Tech. **26**, 020201 (2017)
[3] B.N. Breizman, P. Aleynikov, E.M. Hollmann and M. Lehnen, Nucl. Fusion **59** 083001 (2019)
[4] N.T. Padial, G.D. Meneses, F.J. Paixao, and Gy. Csanak, Phys. Rev A **23** 5, 2194-2212 (1981)
[5] T. Zuo, R.P. McEachran, A.D. Stauffer, J. Phys. B, **24** 2853 (1991)
[6] T. Zuo, R.P. McEachran, A.D. Stauffer, J. Phys. B, **25** 3393 (1992)
[7] M.A. Khakoo, O. Zatsarinny and K. Bartschat, J. Phys. B: At. Mol. Opt. Phys. **44** 015201 (2011)
[8] R. Ward, D. Cubric, N Bowring, G C King, F.H. Read, D.V. Fursa, I. Bray, O. Zatsarinny and K. Bartschat, J. Phys. B: At. Mol. Opt. Phys. **44** 045209 (2011)

Effects of impurities on beam-plasma interaction and hot spots properties in fast ignition nuclear fusion

P.R. Beltrán[1], J.M. Gil[2], R. Rodríguez[2] and G. Espinosa-Vivas[2]

[1]*Instituto de Astrofísica de Canarias (IAC), E-38200 La Laguna, Tenerife, Spain*
[2] *IUNAT, Physics Department, Universidad de Las Palmas de Gran Canaria, Spain*

In this work we analyze the influence of the impurities and their abundances on the beam-plasma interaction and on the properties of the resulting heated plasma in the context of fast ignition scheme in inertial fusion. Three kinds of beams and impurities, which are common in this context, are considered. The study is carried out using a 1D spatial-temporal numerical model to simulate the slowing down of an ion beam in the plasma target and the heating of the plasma.

1 General

Fundamental research in ion beam-plasma interaction is essential to advance in the understanding of high energy density plasmas. This interaction is expected to occur at a future confinement fusion power plant in the ion fast ignition (IFI) scheme. In IFI, the fusion process is decoupled: the fuel is compressed with a laser system and then a short beam with high energy is focused on one side of the fuel, heating it and starting ignition. Therefore, a precise knowledge of the energy deposition of the beam in the target plasma is required to design this scheme [1]. The small spherical target contains the fuel which is typically made up of deuterium-tritium (DT) although it is possible to find traces of impurities due to the detached components from the ablator material. Therefore, it is a priority to analyze the influence of these impurities in this system.

The aim of this work is to study the interaction between an ion beam and a plasma fuel of DT with impurities and also the resulting heated plasma and its properties. For this purpose, we use a spatial-temporal numerical model to simulate the stopping of an ion beam in a plasma target, as well as the plasma heating process. Three kinds of beams have been considered (p^+, C^{6+} and V^{23+}) in a wide range of kinetic energies and number of particles. The ion beam is assumed as perfectly collimated, cylindrical and monoenergetic with constant flux impacting on a radial direction on the plasma, so the interaction beam-target can be described as 1D [2]. With respect to the plasma, we have considered a compressed sphere of DT fuel with a 50 μm radius, with temperature and density homogeneous distributions, and three kinds of common impurities (C, Cu and Au) at different concentrations. It is assumed that the time of the interaction is considerably shorter than the characteristic hydrodynamic times and thus, the plasma heating can be considered as isochoric. Therefore, the change in the plasma temperature depends exclusively on the energy deposited by the beam projectiles, since the mechanical work and conduction can be neglected [3]. The energy by the beam deposited is obtained in a classical dynamic context by means of the calculation of the stopping power of the plasma [4]. With this numerical model, we calculate the temperature field after the interaction, and we define a region of special interest named hot spot. From the distribution of temperatures, we extract key parameters such as the maximum temperature and its position and the length and the mean temperature (of both the heated region and the hot spot), analyzing the influence of the different impurities and their concentrations in these properties.

Acknowledgments

This work was supported by the Spanish Government through the Project PID2019-110678GB-I00.

References

[1] Tabak, M. et al. Ignition and high gain with ultrapowerful lasers. Phys. Plasmas **15,** 1626-1634 (1994).

[2] Gasparyan O.R. Gus'kov, S. Yu., Il'in, D. V. J., Sherman, V. E., Zmitrenko, N. V. Mathematical modeling of the heating of a fast ignition target by an ion beam. Russ. Laser Res. **34**, 33-40 (2013).

[3] Atzeni, S., Meyer-ter-Vehn, J. The Physics of Inertial Fusion: Beam-plasma interaction, hydrodynamics, hot dense matter. Oxford University Press (2004).

[4] Beltrán, P.R., Gil, J.M. Rodríguez, R. Espinosa, G. Barriga-Carrasco, M.D. Simulation of the ion-beam plasma interaction processes for point-like ions in doped DT plasmas. X-Ray Spectrom. **49**, 173-176 (2020).

Simulation of negative ion mobility at atmospheric pressure in O_2 by Monte Carlo method using rate coefficients of ion-molecule reactions

Y. Okuyama[1] and H. Sugawara[2]

[1] *Department of Engineering for Innovation, National Institute of Technology, Tomakomai College, Hokkaido, Japan*
[2] *Graduate School of Information Science and Technology, Hokkaido University, Hokkaido, Japan*

Simulations of ion drift were carried out using rate coefficients and ion mobility at atmospheric pressure in O_2 with a little amount of H_2O. The simulation results were compared with experimental ones to investigate the influence of transition ion species by ion−molecule reactions on several ion mobilities. As the results, ion mobility was changed by rate coefficients because dominant ions are depended on them sensitively.

1 Introduction

The study of ion−molecule reactions and transport coefficients such as mobilities and diffusion coefficients has been carried out in low pressures for collecting fundamental data of discharge plasmas. Recently, these fundamental data are required also for investigations of atmospheric plasma discharges.

The authors investigated the effects of a small amount of H_2O on negative ion mobility in O_2 at atmospheric pressure. As the results, simulation data using estimated values of rate coefficients and ion mobilities were in good agreement with experimental one[1].

In this paper, we describe the influence of ion−molecule reactions on several ion mobilities.

2 Simulation method and conditions

Monte Carlo simulations were carried out using mobility of electrons, that of the ions obtained in the measurements, and rate coefficients of ion-molecule reactions[1]. Fig. 1 shows ion-molecule reactions in O_2 with H_2O. Energy of initial electron is 0 eV. The rate coefficients k_{12} through k_{65} and ion mobilities used were taken from the literature[1-4].

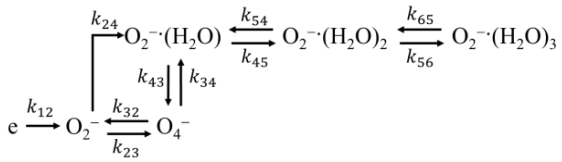

Fig. 1. Ion−molecule reactions in O_2 with H_2O.

3 Results and discussions

Fig. 2 a) shows ion mobility against H_2O concentration varying with rate coefficient k_{45}. In Fig. 2 b), simulation results are fitted to experimental one using estimated values of the rate coefficients and mobilities. The gradients of mobility against H_2O concentration are changed by variation of k_{45} due to transition of dominant ion species such as $O_2^-\cdot(H_2O)_n$ as shown in Fig.1.

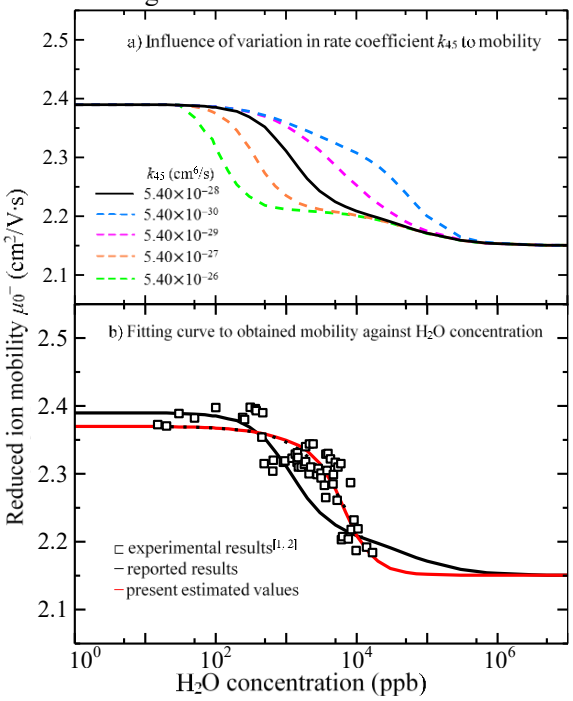

Fig. 2. Negative ion mobility in O_2 with H_2O.

Acknowledgement

This work was supported by JSPS KAKENHI GRANT Number 19K14974.

References

[1] Y. Okuyama, Y. Yasuzawa and H. Sugawara: Electr. Eng. Japan **216**, DOI:10.1002/eej.23413 (2023) (to be published).
[2] F. C. Fehsenfeld, E. E. Ferguson and D. K. Bohme: Planet. Space Sci. **17** (1969) 1759–1762.
[3] N. G. Adams, D. K. Bohme, D. Dunkin, F. C. Fehsenfeld and E. E. Ferguson: J. Chem. Phys. **52** (1970) 3133–3140.
[4] M. L. Huertas, J. Fontan and J. Gonzalez: Atmos. Environ. **12** (1979) 2351–2362.

XXXV ICPIG, July 9-14, 2023, Egmond aan Zee, The Netherlands Topic number 4

Plasma acceleration in the magnetic nozzle

A.Smolyakov[1], A.Sabo[1], M. Jimenez[1], A. Chapurin[1], M. Tyushev[1], P. Yushmanov[2], S. Putvinski[2]

[1]*University of Saskatchewan, 116 Science Place, Saskatoon, SK, S7N 5E2 Canada*
[2]*TAE Technologies, 19631 Pauling, Foothill Ranch, CA, 92610 USA*

We present our recent analytical and simulation results on the mechanisms and characteristics of transonic acceleration of plasma flows in the magnetic nozzle driven by the plasma pressure, rotation, and azimuthal magnetic field. Analytical results from fluid theory are compared with results using hybrid, and fully kinetic simulations models. Further extension is on electromagnetic effects which occur when plasma flow velocity approaches the Alfven velocity. Pecularities of Alfven, slow, and fast magnetosonic point singularities in transonic solutions and their possible connections to the detachment processes are discussed.

Plasma flow and acceleration in the magnetic nozzle with converging-diverging magnetic configuration are important for applications in electric propulsion [1] and fusion systems such as open mirrors and tokamak divertors [2]. Finite plasma pressure in the non-monotonic magnetic field, with a local maximum, results in quasineutral plasma acceleration to supersonic velocities similar to Laval nozzle effect in gas dynamics [3]. This mechanism is modified by the magnetic field when plasma pressure becomes anisotropic [4]. We present our recent results obtained with analytical theory and numerical simulations. The kinetic effects obtained with quasineutral hybrid model with kinetic ions and isothermal Boltzmann electrons are compared with full kinetic simulations including the kinetic ions and electrons and full Poisson equation. Further modifications occur due to plasma rotation and electromagnetic effects. The latter are important when plasma velocity becomes comparable to the Alfven velocity as it occurs in the outer (plume) part of the diverging magnetic field where the magnetic field is low. Magnetic field and plasma rotation also offer additional sources of free energy to drive plasma acceleration. Electromagnetic effects including azimuthal magnetic field and plasma rotation, i.e., coupling with Alfven wave dynamics, are investigated with a fluid model highlighting some similarities with the problem of magnetically driven flows in astrophysical jets and winds. The roles of the Alfven, slow, and fast magnetosonic point singularities in plasma acceleration are discussed.

References

[1] Longmier, B. W., E. A. Bering, M. D. Carter, L. D. Cassady, W. J. Chancery, F. R. C. Diaz, T. W. Glover, N. Hershkowitz, A. V. Ilin, G. E. McCaskill, C. S. Olsen and J. P. Squire (2011). "Ambipolar ion acceleration in an expanding magnetic nozzle." *Plasma Sources Science & Technology* **20**(1): 015007.

[2] Togo, S., T. Takizuka, D. Reiser, M. Sakamoto, N. Ezumi, Y. Ogawa, K. Nojiri, K. Ibano, Y. Li and Y. Nakashima (2019). "Self-consistent simulation of supersonic plasma flows in advanced divertors." *Nuclear Fusion* **59**(7): 076041.

[3] Smolyakov, A. I., Sabo, A., Yushmanov, P., & Putvinski, S. (2021). On quasineutral plasma flow in the magnetic nozzle. *Physics of Plasmas, 28*(6), 060701.

[4] Sabo, A., Smolyakov, A., Yushmanov, P., & Putvinski, S. (2022). "Ion temperature effects on plasma flow in the magnetic mirror configuration." *Physics of Plasmas* **29**(5): 052507.

[5] Jimenez, M., Smolyakov, A., Chapurin, O., & Yushmanov, P. (2022). "Ion kinetic effects and instabilities in the plasma flow in the magnetic mirror." *Physics of Plasmas* **29**(11): 112117.

The LisbOn KInetics simulation tools

A. Tejero-del-Caz[1,2], T. C. Dias[1], V. Guerra[1], M. Lino da Silva[1], L. Marques[3], N. Pinhão[1], C.D. Pintassilgo[1,4] and L.L. Alves[1]

[1] *Instituto de Plasmas e Fusão Nuclear, Instituto Superior Técnico, Universidade Técnica de Lisboa, Lisboa, Portugal*
[2] *Departamento de Física, Facultad de Ciencias, Universidad de Córdoba, Campus de Rabanales, Spain*
[3] *Centro de Física das Universidades do Minho e do Porto, Universidade do Minho, Braga, Portugal*
[4] *Departamento de Engenharia Física, Faculdade de Engenharia, Universidade do Porto, Portugal*

The LisbOn KInetics tools comprise a suite for plasma chemistry simulations (LoKI) and a Monte Carlo code for electron kinetics simulations (LoKI-MC). This contribution presents a status report of the LoKI/LoKI-MC tools and is intended to also receive comments and suggestions from the low-temperature plasmas community, in preparation of the release of LoKI as open-source code.

The LisbOn KInetics tools [1] comprise a suite for plasma chemistry simulations (LoKI) and a Monte Carlo code for electron kinetics simulations (LoKI-MC), developed / consolidated resorting to the well-grounded scientific foundations of the Portuguese group N-PRiME.

LoKI, written in MATLAB adopting an ontology that separates tools and data, couples two main calculation blocks: a Boltzmann solver (LoKI-B) [2,3] and a Chemical solver (LoKI-C).

LoKI-B (released as open-source code [4] licensed under the GNU GPL v3.0) solves the space independent form of the two-term electron Boltzmann equation for non-magnetised non-equilibrium low-temperature plasmas, excited by DC/HF electric fields or time-dependent (non-oscillatory) electric fields from different gases or gas mixtures. The tool addresses glow plasmas, using a stationary description for DC fields, a Fourier time-expansion description for HF fields, and a time-dependent description for time-varying fields. LoKI-B handles the electron kinetics in any complex gas mixture, describing first and second-kind electron collisions (with anisotropic effects for elastic and rotational encounters) with any target state, characterized by any user-prescribed population.

LoKI-C solves the system of zero-dimensional (volume average) rate balance equations for the most relevant charged and neutral species in the plasma, receiving as input the kinetic schemes for the gas/plasma system under study. LoKI-C uses several modules (i) to describe the mechanisms (collisional, radiative and transport) controlling the creation / destruction of species, namely various transport models for charged and neutral particles; (ii) to self-consistently calculate the gas temperature, by solving a gas/plasma thermal model; and (iii) to fully couple volume and surface kinetics.

LoKI-MC (released as open-source code [5] licensed under the GNU GPL v3.0) solves the electron kinetics for plasmas excited by uniform DC electric fields from different gas mixtures, using Monte Carlo techniques independent from the two-term approximation [6]. The code, written in C++, follows an object-oriented structure and a data organization similar to LoKI-B, including as output the electron velocity distribution function and related macroscopic parameters. Recently, the LoKI-MC formulation was extended to further include AC/time-dependent electric fields [7], as well as DC magnetic fields [8].

Presently, the development of LoKI comprises: (i) the development of LoKI-B++, the C++ version of LoKI-B; (ii) the inclusion of an additional heating operator in LoKI-B, describing the combined ohmic-stochastic interaction of electrons with the applied electric field; (iii) the time-dependent coupling between LoKI-B and LoKI-C. LoKI is planned to be fully released as open-source code in the near future.

Acknowledgements

This work was supported by the Portuguese FCT - Fundação para a Ciência e a Tecnologia, under projects 2022.04128.PTDC, UIDB/50010/2020 and UIDP/50010/2020.

References

[1] nprime.tecnico.ulisboa.pt/loki/
[2] Tejero-Del-Caz, A. *et al.* Plasma Sources Sci. Technol. **28**, 043001 (2019).
[3] Tejero-del-Caz, A. *et al.* Plasma Sources Sci. Technol. **30**, 065008 (2021).
[4] github.com/IST-Lisbon/LoKI
[5] github.com/IST-Lisbon/LoKI-MC
[6] Dias, T. C. *et al.* Computer Physics Communications **282**, 108554 (2023).
[7] Dias, T. C. and Guerra, V. Assessment of time-locality assumptions on the modelling of nanosecond-pulsed discharges. XXXVth ICPIG (2023).
[8] Pintassilgo, C. D. *et al.* Effect of the magnetic field on the electron kinetics under AC/DC electric fields. XXXVth ICPIG (2023).

Effect of the magnetic field on the electron kinetics under AC/DC electric fields

C. D. Pintassilgo[1,2], T. C. Dias[1], V. Guerra[1]

[1] *Instituto de Plasmas e Fusão Nuclear, Instituto Superior Técnico, Universidade de Lisboa, Portugal*

[2] *Departamento de Engenharia Física, Faculdade de Engenharia, Universidade do Porto, Portugal*

This work focus on the electron kinetics under AC/DC electric and DC magnetic fields, using the Monte Carlo solver LoKI-MC. The implementation of the magnetic field is benchmarked against results available in the literature and new calculations in different conditions are proposed to be used as benchmark for the community. Moreover, while in a DC electric field adding a magnetic field is detrimental for the electron energy, under an AC electric field, the present results confirm the increase of the electron energy due to resonance conditions caused by the magnetic field.

Electrons play a major role in the reactivity of low-temperature plasmas (LTP), since they transfer the energy gained from the electric field to the heavy species through various collisional channels. Thus, an accurate solution of the electron kinetics is necessary for a precise description of an LTP.

The LisbOn KInetics Monte Carlo solver (LoKI-MC) [1] was recently developed by our group, aiming to provide the community a general and flexible electron kinetics solver that does not depend on the two-term approximation. Some interesting features are the straightforward insertion of gas internal levels, anisotropic scattering and inclusion of the thermal motion of the gas molecules.

The first version of LoKI-MC addressed only configurations with constant electric field and null magnetic field [1]. Here, we extend the formulation to AC/DC electric fields together with DC magnetic fields. The implementation of this significant feature requires an extensive benchmark/verification.

The purpose of this work is threefold: (i) verify LoKI-MC against previous independent benchmark calculations, reinforcing the confidence on the present code and on the past calculations; (ii) extend the set of benchmarks available in the literature to consider the influence of other physical parameters, specially in conditions of coexistent AC electric fields and DC magnetic fields; (iii) gain insight into the underlying physics of the electron swarm kinetics in these configurations, with special emphasis on the phenomenon of electron-cyclotron resonance.

With respect to point (i), LoKI-MC passed with distinction several benchmark tests available in the literature, using the well-known Reid-ramp and Lucas-Saelee gas models, and this will be shown in the conference. Figures 1 and 2 concern the points (ii) and (iii) above mentioned. Figure 1 presents the electron mean energy ($\langle\epsilon\rangle$) and reduced Townsend coefficient (α/N) in N_2 for DC electric and magnetic fields. An increase of the magnetic field significantly reduces the fraction of high-energy electrons, leading to a decrease of $\langle\epsilon\rangle$ and α/N. Figure 2 shows $\langle\epsilon\rangle$ in Ar for an AC electric field and a DC magnetic field, and different AC frequencies. In this case, when the cyclotron frequency is near the excitation angular frequency, the magnetic field may increase the electron energy due to the well-known electron-cyclotron resonance, where there is an enhancement of electron acceleration caused by a synchronization of the cyclotron motion with the electric field.

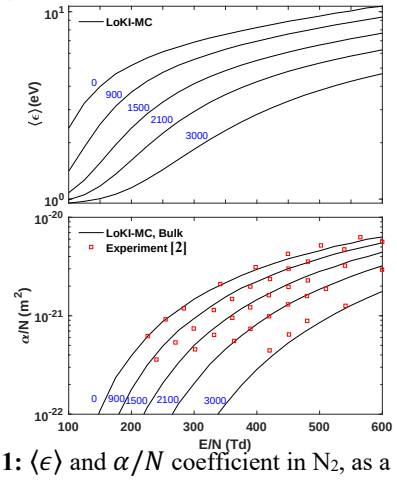

Figure 1: $\langle\epsilon\rangle$ and α/N coefficient in N_2, as a function of *E/N* (DC) and varying *B/N* from 0 to 3000 Hx.

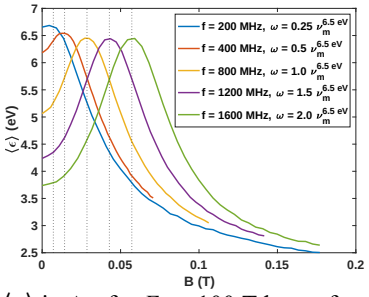

Figure 2: $\langle\epsilon\rangle$ in Ar, for E_{rms}=100 Td, as a function of B and varying the AC frequency of *E*.

Acknowledgements

This work was supported by the Portuguese FCT - Fundação para a Ciência e a Tecnologia, under projects PTDC/FISPLA/1616/2021, MIT-EXPL/ACC/0031/2021 UIDB/50010/2020 and UIDP/50010/2020, and grant PD/BD/150414/2019.

References

[1] Dias, T. C., Tejero-del-Caz, A., Alves, L. L., Guerra, V. Comput. Phys. Commun. **282**, 108554 (2023).

[2] Heylen, A., Dargan, C.L., Int. J. Electronics, **35**, 433 (1973)

Comparison of 1D particle-in-cell simulations with Langmuir probe measurements of a low-pressure inductively-coupled discharge

N. Lequette[1], B. Esteves[1], A. Alvarez Laguna[1], A. Bourdon[1] and P. Chabert[1]

[1] *Laboratoire de Physique des Plasmas, CNRS, Ecole Polytechnique, 91128, Palaiseau, France*

Due to the large computational cost of particle-in-cell (PIC) simulations, full-domain 3D simulations are in most cases unfeasible, in particular regimes. For this reason, approximations that allow for reducing the dimensionality, while reproducing the important physics, are required. In this work, we propose a model for the loss of charged particles in directions that are not simulated. This loss model is implemented into a 1D code of an inductively-coupled plasma (ICP) discharge in a cuboidal chamber. The simulated electron density and temperature profiles are compared with Langmuir probe measurements along the thrust axis of an ion-gridded thruster with xenon for pressures below 5 mTorr.

1 Motivation

PIC simulations are a valuable tool, complementary to experiments, to analyze the discharge characteristics of non-equilibrium plasmas. However, as these simulations rely on cross-sectional data and numerical methods with numerical noise and discretization error as well as on geometrical simplifications, they require validation against experimental data. In this work, we will validate our PIC simulations against Langmuir probe measurements performed along the main axis of the PEGASES thruster running on xenon [1].

2 Simulation characteristics

The simulation code used in this work is a 1D electrostatic PIC with Monte Carlo collisions. We simulate the main axis of the thruster, from the heating antenna at $x = 0$ to the extraction grids at $x = 13$ cm. The ICP power source is modeled by applying a transverse electric field near the antenna, with a magnitude matching the experimental absorbed power. We propose a method to include particle loss on the walls in the plane that is perpendicular to the simulated direction. This model is inspired by previous 2.5D simulations [2]. For ions, a collision frequency is introduced to model the Bohm fluxes on the walls, with

$$\nu_{\mathrm{L}} \;=\; h_{2\mathrm{D}} u_{\mathrm{B}} \left(\frac{2}{\mathrm{L}_y} + \frac{2}{\mathrm{L}_z} \right), \qquad (1)$$

where $h_{2\mathrm{D}}$, the 2D edge-to-center ratio is computed following [3].

3 Comparison

We compare our PIC simulations to a set of electron density and temperature measurements along the thrust axis with pressures ranging from 0.3 to 3.5 mTorr, and an input power of 50 W. In Fig. 1, we show that the PIC code captures the measured electron temperature which shows the potential of the dimensionality-reduction model to mimic the surface-to-volume ratio of the actual device.

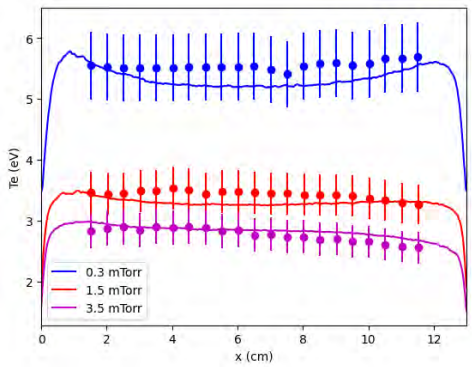

Figure 1: Simulated (line) and measured (dots) electron temperatures for 3 neutral pressures.

References

[1] Esteves, B. *et al.* Charged-particles measurements in low-pressure iodine plasmas used for electric propulsion. *Plasma Sources Sci. Technol.* **31**, 085007 (2022).

[2] Fubiani, G. & Boeuf, J. P. Plasma asymmetry due to the magnetic filter in fusion-type negative ion sources: Comparisons between two and three-dimensional particle-in-cell simulations. *Physics of Plasmas* **21**, 073512 (2014).

[3] Lucken, R. *et al.* Edge-to-center plasma density ratios in two-dimensional plasma discharges. *Plasma Sources Sci. Technol.* **27**, 035004 (2018).

A physics-informed neural network to accelerate Montecarlo streamer simulations

A. Malagón-Romero[1], M. Bayo[2] and A. Luque[2]

[1] *Centrum Wiskunde & Informatica (CWI), Amsterdam, The Netherlands*
[2] *Instituto de Astrofísica de Andalucía (IAA), Granada, Spain*

Lightning and laboratory sparks produce X-rays by accelerating free electrons to high energies [1-3]. These discharges are populated by thousands of streamers, plasma channels that grow by ionizing the air due to a high electric field at their tip. Hypothetically, a fraction of electrons near the streamer tip could be accelerated to relativistic energies, resulting in the emission of X-rays. The acceleration process fluctuates owing to the probabilistic nature of particle interactions. Montecarlo simulations are well-suited to modeling some aspects of streamer discharges but also are inherently noisy. Attempting to simulate a computationally feasible number of particles results in excessive streamer branching and high electric fields that spoil simulation results. To address these issues, we present a neural network that can reduce the noise in a Montecarlo simulation by mapping between noisy particle data and the underlying physical quantities. But this mapping alone cannot produce results that, combined with a Montecarlo streamer code, can lead to stable streamer simulations. To achieve numerical stability, we enforce the conservation of fundamental physical quantities into the neural network itself. By reducing the number of particles required to infer the physics, this approach aims to mitigate the computational burden of Montecarlo simulations and enable the investigation of phenomena that were previously inaccessible numerically.

[1] Cooray, V. et al. (2009). On the possible origin of X-rays in long laboratory sparks. *Journal of Atmospheric and Solar-Terrestrial Physics*, *71*(17-18), 1890-1898.
[2] Moore, C. B. et al. (2001). Energetic radiation associated with lightning stepped-leaders. *Geophysical Research Letters*, *28*(11), 2141-2144.
[3] Dwyer, J. R. et al. (2003). Energetic radiation produced during rocket-triggered lightning. *Science*, *299*(5607), 694-697.

First-principles simulation of optical emission spectra for low-pressure argon plasmas and its experimental validation

F. J. Arellano[1], M. Gyulai[2,3], Z. Donkó [1,3], P. Hartmann[3], Ts. V. Tsankov[4], U. Czarnetzki[4] and S. Hamaguchi[1]

[1] *Center for Atomic and Molecular Technologies, Osaka University, Osaka, Japan*
[2] *Eötvös Loránd University, Budapest, Hungary*
[3] *Institute for Solid State Physics and Optics, Wigner Research Centre for Physics, Budapest, Hungary*
[4] *Ruhr University Bochum, Faculty of Physics and Astronomy, Experimental Physics V, Germany*

A particle in cell simulation is combined with a collisional-radiative model to reproduce the emission spectra of a capacitive discharge in argon via first-principle calculations. Comparison with experimental measurements shows good agreement up to 20 Pa. The discrepancy at higher pressures is attributed to processes involving metastable atoms.

1 General

Emission spectra in a combination with a collisional-radiative model (CRM) are often used for the experimental characterization of low-temperature plasmas. The CRM requires external inputs such as the distribution function of the electrons (EEDF). Here we obtain the EEDF for capacitively-coupled argon plasmas from first-principle simulations via one-dimensional particle-in-cell (PIC) code. The results are coupled to a global CRM that then provides the emission intensities of various atomic lines. Comparison with experimental spectra allows analysis of the reliability of this approach.

2 Methods

The CRM of Siepa et al [1] has been modified to work with EEDFs obtained from the PICit! code [2]. The inputs for the models – gas pressure and temperature as well as voltage waveform – are obtained from experiments. The computed intensities are compared to experimental ones obtained in the Budapest v.3 Cell capacitively coupled plasma source [3].

3 Discussions

The comparison of experimental with computed results for the emission intensities shows reasonable agreement up to 20 Pa (fig. 1). At higher pressures an increasing deviation is observed. Detailed analysis suggests as a possible reason for this deviation the increasing importance of the metastable states of argon in the ionization processes above 20 Pa as revealed from the CRM. This is also in accordance with the general expectation for an increase in the density of these states with the pressure. However, the present PIC model does not include collisional processes with the metastable species. A verification of this hypothesis is needed.

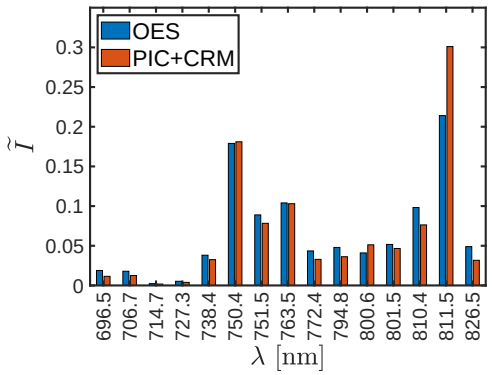

Figure 1: Measured (OES) and calculated (PIC+CRM) emission intensities of selected Ar I lines at 4 Pa.

References

[1] Siepa, S. *et al. J. Phys. D: Appl. Phys.* **47**, 445201 (2018).

[2] Derzsi, A. *et al. Plasma Sources Sci. Technol.* **31**, 085009 (2022).

[3] Horváth, B. *et al. Plasma Sources Sci. Technol.* **29**, 055002 (2020).

Two-dimensional electrostatic instabilities in Hall thrusters

F. Petronio[1,2], A. Alvarez Laguna[1] A. Bourdon[1] and P. Chabert[1]

[1] *Laboratoire de Physique des Plasmas (LPP), CNRS, Sorbonne Université, Ecole Polytechnique, Institut Polytechnique de Paris, 91120 Palaiseau, France*
[2] *Safran Spacecraft Propulsion, 1 Avenue Hubert Curien, 27200 Vernon, France*

This work presents theoretical and simulation results on the physics of low-temperature low-pressure magnetized plasmas in the radial-azimuthal and axial-azimuthal planes of a Hall thruster (HT). We focus on analyzing the instabilities in HTs, which strongly impact device lifetime, to explain the origin of their growth and highlight their role in the anomalous transport of electrons, which directly affects the thruster's performance.

This work presents a theoretical study on plasma instabilities and their impact on discharge physics and Hall thruster (HT) performance. A 3D dispersion relation (DR) is derived using a linear perturbation approach to understand the development of instabilities. By simplifying the global DR, we recovered the 1D and 2D dispersions of the most relevant instabilities for a plasma in the HT configuration [1, 2]. The importance of the instabilities relies in their relationship with the anomalous electron transport in the axial direction, which is strongly influenced by the azimuthal modes [3]. Synchronous oscillations of the azimuthal electric field and plasma density produce a so called friction force that accelerates the electrons, reducing their residence time in the discharge chamber.

Theoretical results are compared with the results of Particle-in-Cell (PIC) simulations, and radial-azimuthal simulations led to the formalization of a criterion for the growth of the Modified Two-Stream Instability (MTSI) and an evaluation of its contribution to anomalous transport. The axial-azimuthal simulations allowed for the characterization of the Ion Transit-Time Instability (ITTI), a better understanding of its growth, and its effect on the population of low-energy ions in the plasma plume. Additionally, these simulations explained the propagation of the ion acoustic wave (IAW) in the discharge, which starts in the central part of the thruster channel and propagates toward the cathode and anode. In the Figure below we show the comparison of a spectral map from PIC and the IAW DR.

References

[1] Petronio, F., Charoy, T., Alvarez Laguna, A., Bourdon, A. & Chabert, P. *Physics of Plasmas* (2023). URL `https://doi.org/10.1063/5.0119253`.

[2] Petronio, F., Charoy, T., Alvarez Laguna, A., Bourdon, A. & Chabert, P. *Physics of Plasmas* (2023). URL `https://doi.org/10.1063/5.0119255`.

[3] Lafleur, T., Baalrud, S. D. & Chabert, P. *Physics of Plasmas* (2016). URL `https://doi.org/10.1063/1.4948496`.

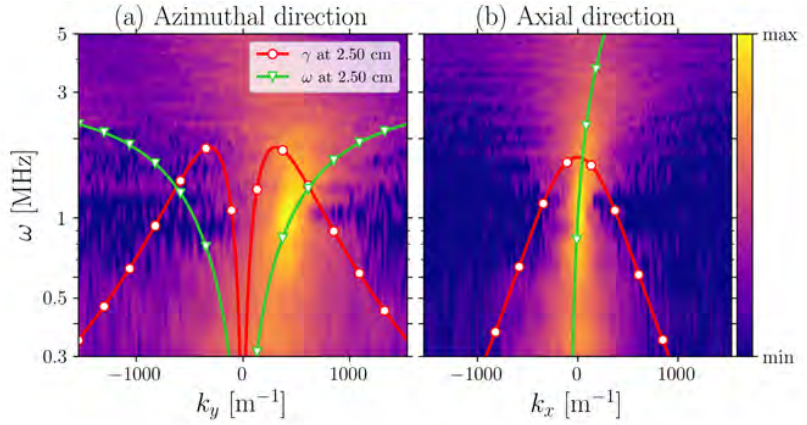

Figure 1: Spectra from PIC simulations compared to analytic DR of IAW.

Spatial distribution of vibrational and rotational temperatures of N_2 ICP by tomographic optical emission spectroscopic measurement

K. Yoneda[1], Y. Yamashita[1], K. Doi[2], T. Kiyota[3], K. Asakawa[2], K. Ishi[1], A. Nezu[4] and H. Akatsuka[1,5]

[1] *Dept. Elec. Electron. Eng., Tokyo Tech., Tokyo, Japan,* [2] *Inst. Adv. Tech., ULVAC, Inc., Susono, Japan*
[3] *Strateg. Plan. Dept., ULVAC, Inc., Chigasaki, Japan,* [4] *Open Facil. Cent., Tokyo Tech, Tokyo, Japan*
[5] *Inst. Innov. Res., Tokyo Tech, Tokyo, Japan*

Nitrogen inductively coupled plasma of its discharge pressure of ~ 1 Pa was measured by tomographic optical emission spectroscopy to understand the spatial distribution of vibrational and rotational temperatures. The spatial distribution of vibrational and rotational temperatures of N_2 and N_2^+ were diagnosed by spectral fitting.

1 Introduction

To gain a better understanding of discharges specific to molecular gases, it is important to investigate the characteristics of nitrogen plasma, as a typical example. In inductively coupled plasma (ICP), which is applied to semiconductor etching processes, it is crucial to understand the spatial distribution of rotational temperature that approximates the gas temperature. For this purpose, tomographic optical emission spectrometry (OES) was applied to examine the spatial distribution of the vibrational temperature T_v and rotational temperature T_r of N_2(1PS, 2PS) and N_2^+(1NS) excited states in nitrogen plasma in this study.

2 Experiments

The discharge apparatus applied in this study was the same that Y. Yamashita *et al.* will report for their Ar-ICP in this conference [1]. A nitrogen plasma was generated with its discharge pressure of 1 Pa and an input power of 300 W. 18 fibers with lenses, 8 on the outside of the side window of the chamber and 10 on the outside of the top window, were attached to the chamber window, and the spectral radiance on the window surface was measured with a multichannel spectrometer (M116, manufactured by Horiba, Ltd.).

3 Data analysis

In this study, the spatial distribution of the spectral emission coefficient was obtained from the spectral radiance by using a tomography analysis program that is an improvement of the sequential reconstruction program [2]. Furthermore, T_v and T_r of N_2 2PS (370−385 nm), 1NS (410−430 nm), and 1PS (635−655 nm) were determined by theoretical fitting procedures, respectively [3].

4 Results and discussion

Figure 1 shows the spatial distribution of T_r of 2PS, 1PS and 1NS. Concerning 2PS and 1PS, T_r increased from the negative to the positive direction of the y-axis (chamber diameter). It can be considered that this is due to the structure of the ICP chamber in which the gas inlet is located on the $-y$ side. On the other hand, T_r of 1NS decreased outward from the center of the y-axis. This is found to be correlated with the electromagnetic field distribution, which indicates the ion motion is reflected on the T_r of 1NS.

Acknowledgment

The authors thank Mr. M. Yokoi and Ms. Y. Sato of HORIBA STEC, Co., Ltd., Mr. K. Yasui, Mr. T. Miyaoka, and Mr. M. Sakurai of HORIBA, Ltd. for lending the multi-channel spectrometer and advising on measurements using the spectrometer.

References

[1] Yamashita, Y. *et al.* In *XXXV ICPIG* (2023).

[2] Carvalho, P. *et al.* *Fusion Eng. Des.* **85**, 266–271 (2010).

[3] Akatsuka, H., Kawano, H., Naoi, K., Matsuura, H. & Nezu, A. *Jpn. J. Appl. Phys.* **56**, 056102 (2017).

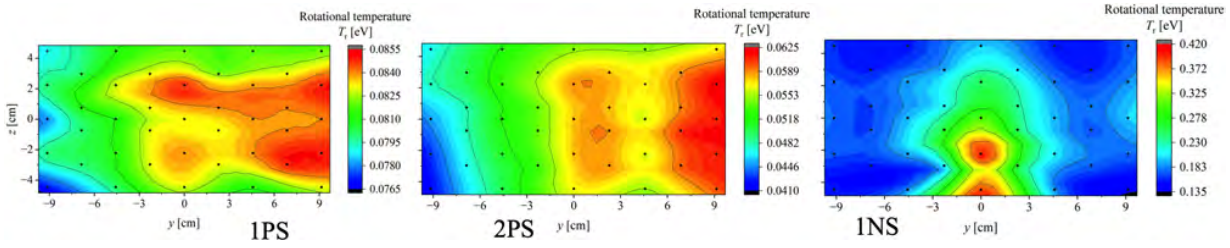

Figure 1: Spatial distributions of rotation temperature of 1PS, 2PS, and 1NS.

A Numerical Algorithm to Restore the Electric Field Distribution from E-FISH Signals

I.D. van de Haar[1], A.A.A. Limburg[1], Y. Guo[1], and S. Nijdam[1]

[1] *Dept. Applied Physics, Eindhoven Univ. Techn., Eindhoven, The Netherlands*

E-FISH is a diagnostic which can be used to determine the electric field in a plasma non-intrusively. However, determination of the electric field from the measurement data is complicated due to the effect of the regular phase shift and Gouy phase on the E-FISH signal. The aim of this research is to develop an algorithm which fits the electric field to the E-FISH signal including the different phase effects for cylindrically symmetric field distributions. With this algorithm all components of the electric field vector can be calculated in a 2-dimensional plane.

1 Introduction

Electric Field Induced Second Harmonic Generation, E-FISH, can be used to measure the electric field in a plasma. The diagnostic is based on a nonlinear optical phenomenon which can only occur in centrosymmetric mediums in the presence of an external electric field – like the plasma electric field. In this process, a second harmonic signal is generated from incident laser light. The known relation between the intensity of the second harmonic generated signal (E-FISH signal) and external electric field can be used to determine the electric field. While obtaining an E-FISH signal is described as a simple and straightforward process, the interpretation of the results is more difficult. Factors like the phase mismatch and the Gouy phase complicate the determination of the electric field significantly. These factors are ignored in current papers using E-FISH.

Two different methods to describe the relation between the external electric field and intensity of the E-FISH signal are used. The first approach uses a trial function for the amplitude of the electric field in order to solve the Maxwell equations. This approach has been applied in the works of Chng [1] and Nakamura [2] and has been based on a derivation by Boyd [3]. On the other hand, the second approach uses the Hankel transform, which puts the equations in wave-vector space. This method has been used by Van der Schans [4] and Pleijers [5]. Although both methods restore the electric field while taking the effect of using a focused Gaussian beam into account, the relation these methods obtain is different.

The goal of this research is the development of an algorithm that can restore the electric field from an E-FISH signal, including the different phase changes.

2 Algorithm

The E-FISH signal can be considered as a line integral along the path of the incident laser beam. With the focused Gaussian beam shape of the laser, specific asymmetry is added to this signal. Since the impact of the Gaussian beam on the E-FISH signal can be described, this asymmetry can be removed from the signal of a cylindrically symmetric electric field. Cylindrical symmetry is required to be able to use only one scan perpendicular to the field. In the algorithm, this is done by least squares fitting a piecewise polynomial to the E-FISH signal which takes the asymmetry introduced by the phase shift and Gouy phase into account. Thus, the x-, y-, and z-components of the electric field can be calculated. The two different methods described in the introduction will both be considered to determine which method is better suited as a field restoration technique.

References

[1] Chng, T. L., Starikovskaia, S.vetlana M. Starikovskaia, and Marie-Claire Schanne-Klein, M. "Electric field measurements in plasmas: how focusing strongly distorts the E-FISH signal." Plasma Sources Science and Technology 29.12 (2020).

[2] Nakamura, S., et al. "Electric-field-profile measurement along a probing laser path based on electric-field-induced second-harmonic generation." Physical Review A 104.5 (2021).

[3] Boyd, R. W. “Nonlinear optics”. Academic press, 2020. P130-P135.

[4] van der Schans, M. “Experiments on the physics of pulsed plasma jets”. PhD Technische Universiteit Eindhoven, 2018. Ch7.

[5] Pleijers, R. F. E. "A numerical and experimental investigation on the physics of E-FISH when using a focused Gaussian probing beam." Master Thesis TU/e (2021).

Challenges of ps-TALIF measurements using a streak camera

L. Invernizzi[1], C. Y. Duluard[1], H. Höft[2], K. Hassouni[1], G. Lombardi[1], K. Gazeli[1] and S. Prasanna[1]

[1] *Laboratoire des Sciences des Procédés et des Matériaux, LSPM, CNRS, Université Sorbonne Paris Nord, UPR 3407, F-93430 Villetaneuse, France*

[2] *Leibniz Institute for Plasma Science and Technology (INP), Felix-Hausdorff-Str. 2, 17489 Greifswald, Germany*

In this work, the peculiarities of TALIF measurements of H-atom densities using a picosecond laser and a streak camera were investigated. H-atom densities were probed in low- and atmospheric-pressure plasmas. However, an unavoidable distortion of the actual TALIF signal was observed, even for optimal time ranges, preventing the accurate, straightforward measurement of the effective lifetime of H atoms. Consequently, H-atom density measurements will be inaccurate if no precautions are taken for the extraction of the actual TALIF signal. To overcome this issue, a study of the influence of the time range on the TALIF properties was carried out, and a mathematical procedure was developed to determine the actual effective lifetimes of H-atoms.

1 Introduction

Two-photon Absorption Laser Induced Fluorescence (TALIF) has been employed to determine absolute densities of reactive atomic species (such as H, O and N) in plasmas [1-2]. The knowledge of their absolute density is essential for implementing plasmas in real applications. Particularly, the study of collisional plasmas may be simplified when using picosecond (ps) excitation and detection systems. In fact, classic ns-TALIF, PMTs and ICCD cameras reach their detection limits when used to capture ultrafast signals (time scales: few ps - 100s ps). In this case, ps-TALIF and streak cameras become advantageous as their temporal resolution can reach down to few ps.

However, the correct use of a streak camera is not straightforward, since it requires a careful consideration of its peculiarities and use of signal processing methods for accurately extracting actual TALIF signals to determine correct atomic densities in reactive plasmas. Otherwise, the effective lifetime of probed species can be largely misinterpreted if no precautions are taken during the uncorrected TALIF signal recording and post-processing procedures.

In this work, a methodology is presented to perform H-atom fluorescence signal measurements with a streak camera in two reactive plasmas: *(i)* low-pressure H_2 microwave plasma, and *(ii)* pulsed atmospheric pressure He plasma jet.

2 Results

The choice of the time range (TR) of the streak camera allows for the temporal discrimination of the fluorescence photons with a larger or smaller sweeping rate. Its choice has a strong impact on the temporal resolution and thus on the measured TALIF profiles. The modification of the actual TALIF signal is visualised in Figure 1, showing the same TALIF measurement for different TR from 10 to 500 ns. This distortion is additionally linked to a variable instrumental function (IF) of the streak camera which distorts the actual TALIF signal.

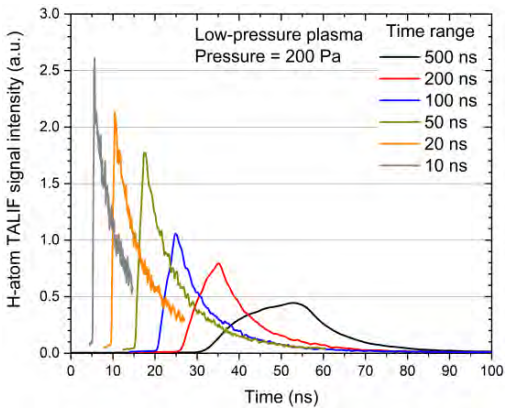

Figure 1: Measured, uncorrected ps-TALIF profiles for H atoms using different time ranges.

Even for an optimal TR that can be intuitively chosen from Figure 1 to capture TALIF (e.g., 50 ns), the time constant of the corresponding exponential decay cannot be accurately determined without a consideration of the IF of the streak camera. This study proposes a detailed procedure for *(i)* measuring the IF, *(ii)* determining the correct TR to capture the raw TALIF, and *(iii)* extracting the actual TALIF by deconvolving the IF from the raw TALIF signal.

This work was funded by the ANR ULTRAMAP project (ANR-22-CE51-0020) and the IDF regional project SESAME DIAGPLAS.

References

[1] Stancu G.D. *Plasma Sources Sci. Technol.* **29** 054001 (2020).

[2] Gazeli K. *et al., Plasma* **4** 145-71 (2021).

Experimental characterization of a Kr-Cl DBD lamp for surface irradiance distribution study including simple photon transfer simulation

A. Baraze[1,2], S. Allix[2] and Ph. Guillot[1]

[1] *Plasma Diagnostics laboratory, Toulouse University, INU Champollion, Albi, France*
[2] *LabScience, Amboise, France*

This work is based on the study of a Kr-Cl excimer lamp which generates radiation at 222 nm, in the UVC band. First, the spectral characteristics of the lamp were studied as a function of the electrical parameters of the power supply. Next, irradiance measurements were carried out for different distances between the lamp and the surface and for different injected power. From the 2D mapping of the irradiance on the surface, an integration allows to obtain the irradiance profile. In parallel, a simple photon transport model based on the Monte Carlo method has been done to estimate distribution profiles on the surface. Simulations are carried out according to the number of initial excited states and according to the distance between the lamp and the surface. The experimental and theoretical results are then compared.

1 Introduction

The decontamination of surfaces by ultraviolet (UV) radiation is an alternative method to processes using chemicals. The biocidal effectiveness of UVC radiation (220 nm – 280 nm) has been widely demonstrated. They cause mutations in the genome (DNA) of the cell, thus blocking its development.

The final aim is to use a Kr-Cl excimer lamp which generates biocidal radiation at 222 nm, in the UVC band, to carry out biological decontamination of solid surfaces. First, a focus has been made on the irradiance distribution on the surface.

2 Experimental characterizations

The plasma source is a Kr-Cl excimer lamp (Oliscié, Toulouse) based on DBD coaxial configuration (length 200 mm, internal diameter 20 mm, external diameter 50 mm) coupled to a pulsed power supply. Three injected powers have been investigated in this study (20, 30 and 40 W). For the measurements of emission spectra, a Princeton Instrument SpectraPro HRS-750 coupled to PIMAX4 ICCD has been used. An irradiance meter (Opsytec) coupled to a calibrated UVC detector (210-310 nm) was used for irradiance measurements (mW/cm^2). Irradiance distribution at the surface (400 mm x 300 mm) was measured with a spatial resolution of 5 mm. These measurements were obtained for several distances between plasma lamp and detector surface (10, 20, 30, 40 and 50 mm).

3 Modelling

The initial excited states from the plasma are located inside a ring defined by the internal and external diameters of the lamp. Initial coordinates and angle for the direction of the radiation are determined randomly (Monte Carlo). For all the excited states, the simulation provides the % of photon impacts on the reference surface and a statistical distribution. This distribution is transformed into a profile so that the simulation results can be compared with the experimental irradiance profile as a function of the power and of the distance between the lamp and the surface.

Acknowledgement

The authors want to thank the Research National Agency (ANR, France) for financial support.

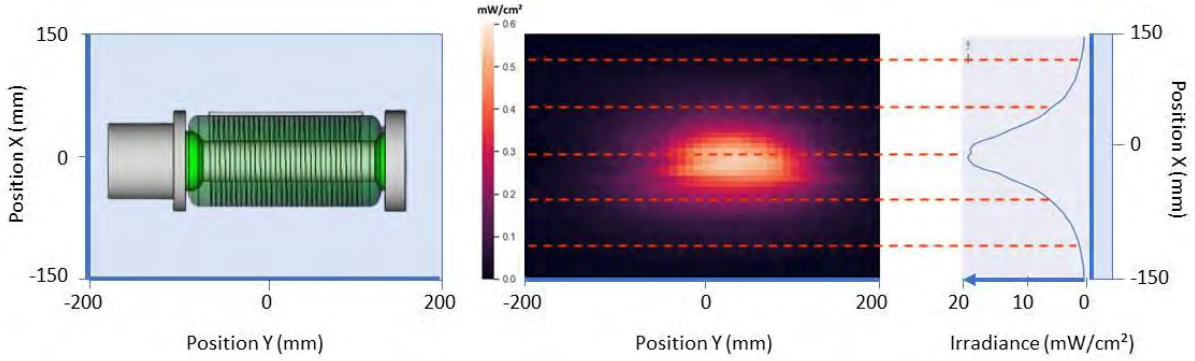

Figure 1. Plasma source at 10 mm of the surface, experimental irradiance on the surface (mW/cm^2) and irradiance profile by integrating along X axis.

Time-resolved absolute density of atomic oxygen in the early afterglow of a nanosecond CO_2 plasma

Z. Shu[1], G.V. Pokrovskiy[1] and S.M. Starikovskaia[1]

[1] *Laboratoire de Physique des Plasmas (LPP), CNRS, Sorbonne Université, Université Paris-Saclay, Observatoire de Paris, PSL Université, École Polytechnique, Institut Polytechnique de Paris, 91120 Palaiseau, France*

This work presents experimental measurements of parameters of plasma in CO_2 nanosecond capillary discharge at moderate (units and tens of mbar) pressure. Electric current, reduced electric field and specific deposited energy are measured for each discharge pulse. The temporal density distribution of O atoms in the early afterglow was measured by TALIF technique. A numerical modelling was developed to compare with the experimental results.

1 Introduction

In low temperature nonequilibrium plasmas, the dominating channel of CO_2 conversion is usually the dissociation of mixture molecules by electron impact under high electric field and high deposited energy, which can be provided by nanosecond discharges. It is important to apply time-resolved measurements of major species like atomic oxygen in the CO_2 discharges to understand the dynamic processes.

2 Experimental setups and methods

The nanosecond discharge was initiated in the capillary tube with 2.0 mm of internal diameter and 52.89 mm of inter-electrode distance. High-voltage pulses (9 kV of amplitude, 30 ns of FWHM and 10 Hz of frequency) were delivered via the coaxial cable. CO_2 under 19.5 mbar flowed at rate of 10 sccm so that each discharge was initiated in the new gas portion.

Two-photon absorption laser-induced fluorescence (TALIF) was used to measure the absolute density of atomic oxygen in the afterglow. The ground-state O atoms were excited by a 225.7 nm focused laser pulse (10 Hz of frequency, 7 ns of FWHM) and 845 nm fluorescence signal was detected by a photomultiplier (PMT). TALIF calibration was taken by Xe under the pressure of 2 mbar.

3 Results

The measured electrical parameters of the CO_2 discharge in Figure 1 show that the reduced electric field reaches 700 Td and the specific deposited energy is almost 1 eV/particle immediately after the first nanosecond pulse.

Rotational temperature was taken from $N_2(C^3\Pi_u, v = 0)$ emission spectrum by adding 10% N_2 into CO_2. It shows a fast gas heating process from 300 K to 1400 K in the first 1.5 µs.

The TALIF measurements, as shown in Figure 2, indicate a temporal profile of $O(3p\ ^3P_{0,1,2})$ effective decay rates between 0.3 to 0.9 ns^{-1} and $O(2p^4\ ^3P_2)$ absolute density between 10^{16} to 10^{17} cm^{-3}, which gives the dissociation rate up to 20 % in a single pulse.

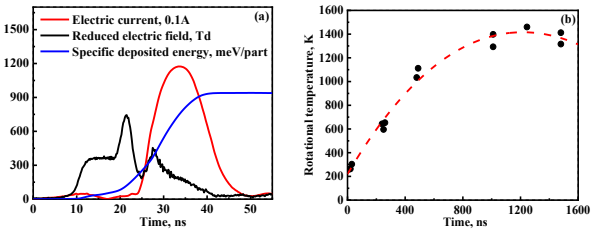

Figure 1. (a) Experimental profiles of the electric current, reduced electric field and specific deposited energy in the first high voltage pulse. (b) Measured rotational temperatures in high voltage pulses and early afterglow.

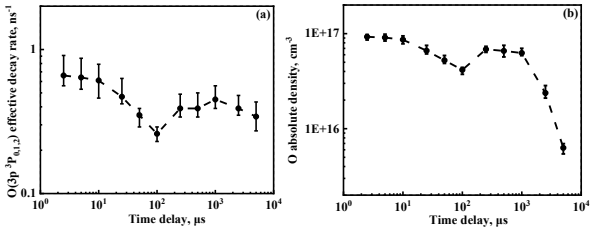

Figure 2. (a) Measured temporal $O(3p\ ^3P_{0,1,2})$ effective decay rates. (b) Calculated temporal absolute densities of ground-state O atom in the afterglow. The error bars reflect the stochastic scattering from experiment to experiment.

Acknowledgements

The work was partially done in the framework of activity of E4C Interdisciplinary Center of IPP.

References

[1] Pokrovskiy, G. V., PhD Thesis "Dissociation of carbon dioxide in pulsed plasma at high electric fields: role of energy exchange with electronically excited species", l'Institut Polytechnique de Paris (2021).

[2] Pokrovskiy, G. V., Popov, N. A., & Starikovskaia, S. M. Fast gas heating and kinetics of electronically excited states in a nanosecond capillary discharge in CO_2. Plasma Sources Science and Technology, **31(3)**, 035010. (2022).

Fluorescence (LIF) measurement of atomic antimony concentration in a planar dielectric barrier discharge

W. Khan , P. Dvořák and M. Mrkvičková

Dept. of Physical Electronics, Faculty of Science, Masaryk University, Brno, Czech Republic

The concentration of atomic antimony (Sb) was measured in a planar dielectric barrier discharge (DBD) used as an atomizer, i.e., as a device used in analytical chemistry to decompose volatile analytes. In this work, the ability of the DBD to decompose the antimony hydride (SbH_3) was studied by measurement of the concentration and spatial distribution of free Sb atoms. The DBD was ignited at atmospheric pressure in argon with an admixture of hydrogen. Single photon absorption laser-induced fluorescence (LIF) intensity of atomic antimony was used for Sb detection. LIF calibration was realized by Rayleigh scattering. The concentration of atomic Sb was around 10^{17} m^{-3}, which was stable during the discharge period. Dependences on gas composition, discharge power, and position in the DBD were measured. The results contribute to the understanding of Sb atomization in DBD and demonstrate the ability to use DBD as a source of free analyte atoms.

LIF measurement was performed and evaluated according to the methods described in [1]. We used a partially saturated regime to increase the signal-to-noise ratio of the LIF signal. The measurement was calibrated by Rayleigh scattering on air. A planar DBD-based T-shaped atomizer (shown in Fig. 1) with rectangular optical arm was employed, and a quartz tube was sealed to the center of the optical arm, where

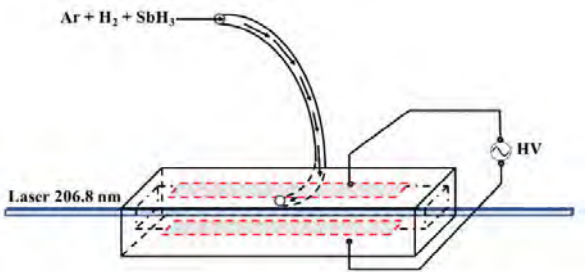

Fig.1 The dielectric barrier discharge atomizer.

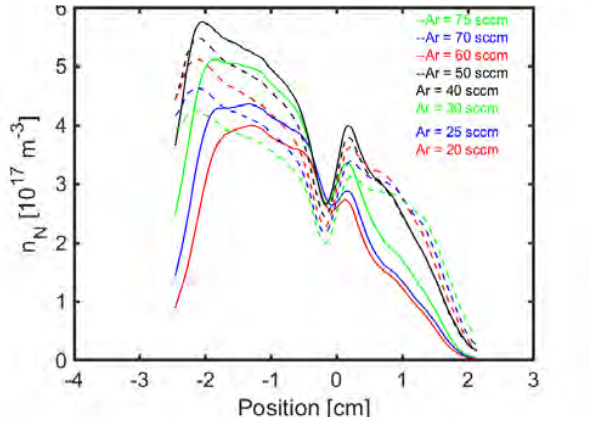

Fig. 2 The Spatial profile of atomic Sb concentration along the axis of DBD for different argon flow rates with fixed power supply.

Ar and H_2 were fed with a flow rate of 50 sccm and 16 sccm, respectively. A trace of antimony hydride (SbH_3, 20 ppb) was added to the supplied gases. The laser beam passed through the atomizer where the DBD-plasma was sustained (the inner dimensions of the optical arm are 7 mm × 3 mm × 75 mm), then the laser beam excites the atomized Sb.

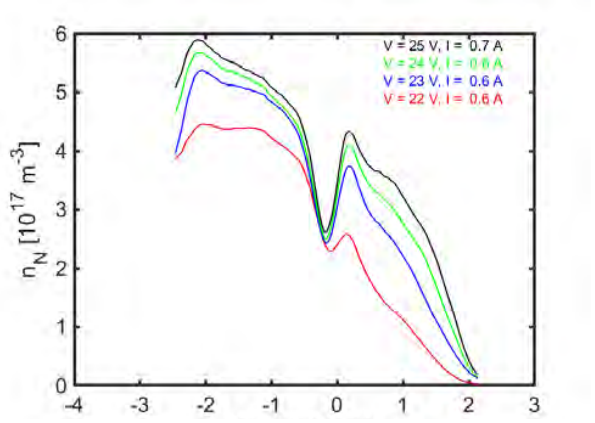

Fig. 3 The Spatial profile of atomic Sb concentration along the axis of DBD for different power with fixed argon flow rate (50 sccm). Shown voltage and current values were measured on the power generator before the amplification.

Examples of the spatial distribution of free Sb atoms are shown in Fig. 2 and 3, where the zero indicates the atomizer's center (an inlet). The concentration of free Sb atoms was around 10^{17} m^{-3}, which shows the ability of DBD as a source of free Sb atoms. Free atoms were spread throughout the active discharge. The Optimum Ar flow rate for Sb detection was around 40 sccm, as shown in Fig 2. The dependence on supplied voltage is shown in Fig 3.

Acknowledgment: This research has been supported by the Czech Science Foundation under Contract 23-05974K and by the Project LM2018097 funded by the Ministry of Education, Youth and Sports of the Czech Republic.

References: [1]. Mrkvičková, M., Dvořák, P., Svoboda, M., Kratzer, J., Voráč, J. and Dědina, J. Combustion and Flame, **241**, 112100 (2022).

Absorption properties of Laser Induced Plasma

D. Dojić[1], M. Skočić[1] and S. Bukvić[1]

[1] *University of Belgrade, Faculty of physics POB 368, 11000 Belgrade, Serbia*

Absorption of the Nd:YAG first harmonic (1064 nm) laser pulse was measured during plasma formation on a copper target. A probe, CW He-Ne laser was applied side-on for absorption measurements in plasma. The absorption coefficient is deduced from absorption profile of the He-Ne laser line using inverse Abel transform. It is shown that absorption coefficient has maximum next to the copper target, immediately after terminating of the laser pulse. The amount of the laser pulse energy absorbed by the plasma is proportional with incident energy of the laser pulse.

1 General

It is known that during plasma formation, in the experiments with powerful laser pulses, only a part of the laser pulse energy reaches the target [1], while the rest of the energy is absorbed or scattered by the plasma, so called 'shielding effects'. In this investigation we propose the method suitable for quantitative determination of the plasma shielding caused by absorption of the laser radiation.

Plasma was created by focusing a strong pulsed (FWHM = 5.6 ns) radiation from Nd:YAG laser, at 1064 nm, on the copper target. A probe, CW He-Ne laser was illuminating plasma side-on. A part of He-Ne radiation passes through the plasma and falls onto the entrance slit of the spectrograph. Measuring the laterally resolved He-Ne laser line at 632.8 nm with and without plasma, we are able to calculate a lateral profile of optical depth in the plasma. Inverse Abel transformation was used for deducing radial profile of the shielded He-Ne laser radiation. This procedure is repeated for different axial position (z) in the plasma. Assuming that inverse bremsstrahlung is dominant process in laser pulse energy shielding, it is possible to calculate energy of the Nd:YAG laser pulse absorbed on its whole path through the plasma. In this way, values for absorption coefficient were determined for different experimental conditions.

The measurements are conducted for different moments in the respect of the beginning of the laser pulse. The experimental results clearly show that the absorption reaches a maximum immediately after terminating of the laser pulse (Fig. 1.) and next to the copper target (Fig. 2.). These findings are consistent with some previously published numerical studies [2].

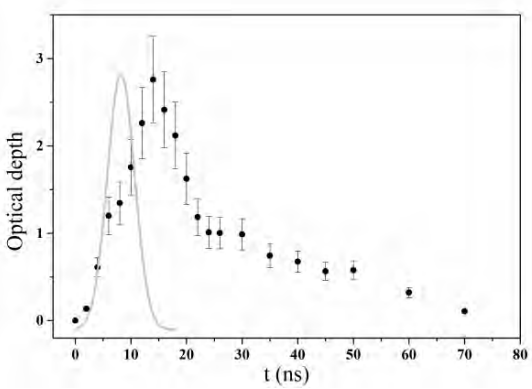

Fig. 1. Optical depth (black circles) as a function of time for 5350 J/cm^2 laser fluence. Grey line represents a time profile of the laser pulse.

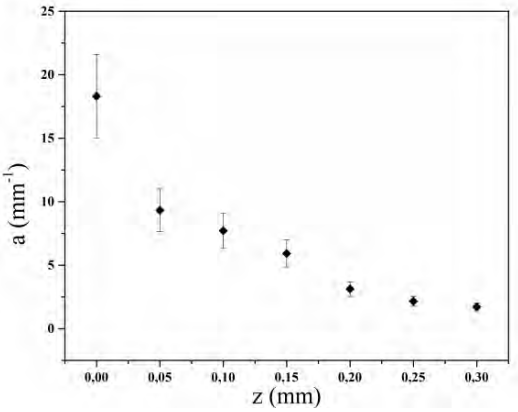

Fig. 2. Absorption coefficient along z axis recorded for delay time of 16 ns. Laser fluence was 5350 J/cm^2.

References

[1] Singh, R. K. and Narayan J. Pulsed-laser evaporation technique for deposition of thin films: Physics and theoretical model. Physical Review B **41** (13), 8843-8859 (1990).

[2] Bogaerts, A., Chen, Z., Gijbels, R., Vertes A. Laser ablation for analytical sampling: what can we learn from modeling? Spectrochimica Acta B **58**, 1867-1893 (2003).

Relevance of N_2 addition in the ion composition of C_2H_2 glow discharges

I. Tanarro[1], R. J. Peláez[1], M. Jiménez-Redondo[1,2], and V. J. Herrero[1]

[1] *Instituto de Estructura de la Materia (IEM-CSIC), Serrano 123, 28006 Madrid, Spain*
[2] *Present address: Max-Planck-Institute for Extraterrestrial Physics, Gießenbachstraße 1, 85748, Garching, Germany*

Drastic effects of small proportions of N_2 in the ion composition of C_2H_2+Ar plasmas have been observed in a RF discharge. Slight N_2 increments causes global increases of negative ions and a depletion of the positive ones, but with very different tendencies for ions that contain N or not; and it is more evident in the case of anions. Noticeably, several of the ions detected are among the scarce ones found in the interstellar media (ISM). Besides, this study can shed some light on the basic processes in the anion chemistry of C_2H_2 plasmas devoted to dust generation, which nowadays present some controversy.

1 General

From the ~250 molecules identified till now in the ISM or circumstellar shells, C and H containing species are dominant, and C_2H_2 is one of the most abundant ones. Besides, up to 45 of these molecules contain C-N chemical bonds [1]. The CN radical was the first N-bearing molecule discovered in space (in 1940), HCN is ubiquitous, and ions such as CN^-, $C3N^-$, $C5N^-$, HC_3NH^+, $NCCNH^+$, and $HCNH^+$ have been identified in star forming regions. CN bonds are of prime importance in prebiotic chemistry; and interstellar dust is assumed to be an efficient catalyst for the synthesis of complex organic molecules. Besides, the atmosphere of Titan, the satellite of Saturn most studied by astrophysicists, is rich in these compounds and a complex chemistry occurs in its ionosphere.

Low pressure glow discharges containing C_2H_2 and N_2 are efficient laboratory systems to generate and characterize many of the cyanide species of interest in astrophysics. They can be also good factories of carbonaceous deposits that resemble interstellar dust [2].

In this work, plasmas of C_2H_2+Ar+N_2 are used to study and identify the neutrals and ions of both signs produced before the onset of dust formation. A plethora of $C_xH_yN_z$ charged species is found, whose concentrations strongly depend of the relative concentrations of the parent precursors.

2 Experimental

The experimental set-up was described elsewhere [3]. Briefly, it consists in a capacitively coupled RF 13.56 MHz discharge reactor with different flanges for gas input and exit, two differentially pumped mass spectrometers for neutrals and ions, respectively, a Langmuir probe, and windows for optical emission spectroscopy and light scattering.

Flow rates (in sccm) up to 2 C_2H_2, 0.4 Ar and 0.4 N_2 are applied. The discharge was modulated at 100 Hz, at an effective power of 50 W, allowing the extraction of anions during the off part of the cycles. In that case, the extraction hood of the mass spectrometer is set at +24 V and it is grounded for cations.

3 Results

The study shows that N_2 addition to the C_2H_2+Ar plasma, even in very small proportions, produces a dramatic effect in the relative concentrations of the different ions; whose compositions have been assigned with ref. [4].

Particularly, a rise of the relative N_2 concentration from 2% to 6% with respect to C_2H_2 increases CN^-, C_3N^-, C_5N^- or C_7N^- by a factor > 10, whereas ions without nitrogen like C_4H^-, C_6H^-, C_8H^- or $C_{10}H^-$ decrease. Noticeably, these eight anions are among the very few detected in the ISM until now. Furthermore, some of the $C_xH_yN_z^-$ mixed anions increase by tens or even hundreds times.

Conversely, the effect of N_2 addition on positive ions is an overall decrease in their concentrations approximately by a factor of 10, but with a larger effect on $C_xH_y^+$ species than on N containing cations. Among them, ions such as $C_3NH_2^+$, $C_2N_2H^+$ or $C_5NH_2^+$ have been detected too in the ISM.

4. Aknowledgements

This work has been funded by the Ministerio de Ciencia e Innovación of Spain under grant PID2020-113084GB.

References

[1] https://cdms.astro.uni-koeln.de/classic/molecules
[2] Herrero, V. J. et al, I. Structure and evolution of interstellar carbonaceous dust. Insights from the laboratory. Front. Astron. Space Sci. **9**:1083288 doi: 10.3389/fspas.2022.1083288
[3] Jiménez-Redondo, M. et al. Ionic Polymerization in Cold Plasmas of Acetylene with Ar and He. J. Phys. Chem. A **123**, 8135-8147 (2019).
[4] https://webbook.nist.gov/chemistry/

A reaction mechanism for oxygen plasmas

T. C. Dias[1], C. Fromentin[1], L. L. Alves[1], A. Tejero-del-Caz[1,2], T. Silva[1] and V. Guerra[1]

[1] *Instituto de Plasmas e Fusão Nuclear, Instituto Superior Técnico, Universidade de Lisboa, Portugal*

[2] *Departamento de Física, Facultad de Ciencias, Universidad de Córdoba, Campus de Rabanales, Spain*

This work presents a reaction mechanism for oxygen plasmas, *i.e.*, a set of reactions and corresponding rate coefficients that are validated against benchmark experiments. The kinetic scheme is validated in a DC glow discharge for gas pressures of 0.2-10 Torr and currents of 10-40mA, using the LisbOn KInetics (LoKI) simulation tool. The comparison comprises the gas temperature, the reduced electric field and the densities of the main species in the discharge. The results show that oxygen atoms play a dominant role in gas heating, via recombination at the wall and quenching of $O_2(X,v)$ vibrations and O_2 electronically-excited states.

Low-temperature oxygen-containing plasmas have been used in a manifold of applications, due to the inherent ability to produce highly reactive species. The potentiality comes together with great complexity and, although these plasmas were vastly studied, important details of its kinetics remain uncertain. Modelling may play a key role to better understand O_2 discharges.

The kinetic scheme describing the interactions between the heavy species and their connection with the electrons is one of the pillars of low-temperature plasma modelling. Therefore, the definition of a *reaction mechanism* is mandatory to make sensible modelling predictions of the system under study.

In this work, we leverage on recent experimental data [1-3] to develop a reaction mechanism for oxygen plasmas. The positive column of a DC glow discharge is used as validation system and is described using the self-consistent 0-D model LoKI [4,5]. The calculations of the gas temperature (T_g), the reduced electric field (E/N) and the densities of the main species – $O(^3P)$, $O_2(X)$, $O_2(a)$ and $O_2(b)$ – are benchmarked with success against experiments.

The calculation of T_g is done with a self-consistent thermal model accounting for the energy released in volume and wall reactions, the heat losses due to thermal conduction and the gas-to-wall convection transfer. The model predictions agree well with the measurements. This agreement is of upmost importance, since many rate coefficients are temperature dependent.

The self-consistent calculation of E/N also agrees with experiment. This indicates that the charge balance, which includes ion formation and ambipolar diffusion (with corrections due to O^- ions), is adequately described in the model.

The present reaction mechanism captures very well the trends and values of the densities of the four main species in the discharge. Figure 1 shows the comparison against experiment of $[O_2(a)]$ and $[O_2(b)]$ for a current I = 30 mA. The addition of a 3-body quenching of $O_2(a)$ [6], $O_2(a)+O_2(X)+O(^3P)\rightarrow 2O_2(X)+O(^3P)$ (R1), and the introduction of a reactive temperature-dependent component in the 2-body quenching of $O_2(b)$ [3], $O_2(b)+O(^3P)\rightarrow O_2(X)+O(^3P)$ (R2), are instrumental to obtain a good agreement with experiments. The densities of $O(^3P)$ and $O_2(X)$ are highly correlated, and the production of $O(^3P)$ is mainly ruled by electron-impact dissociation and the destruction by recombination at the surface. Therefore, the good agreement of $[O(^3P)]$ relies on the values of the recombination probabilities, in this case the experimental values are considered.

It is argued that a new paradigm for the development and validation of kinetic schemes for plasma chemistry should be adopted, based on the comparison against standard validation tests.

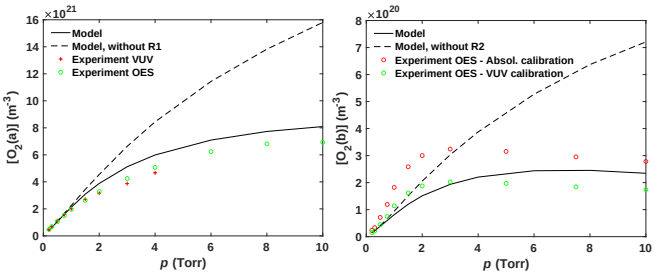

Figure 1: Comparison between experimental [1-3] and modelling results of $[O_2(a)]$ and $[O_2(b)]$, for I = 30 mA.

Acknowledgements

This work was supported by the Portuguese FCT - Fundação para a Ciência e a Tecnologia, under projects PTDC/FISPLA/1616/2021, UIDB/50010/2020, UIDP/50010/2020 and grant PD/BD/150414/2019, and ESA under project I-2021-03399.

References

[1] Booth, J. P. *et al.* Plasma Sources Sci. and Technol. **28**, 5, 055005 (2019).

[2] Booth, J. P. *et al.* Plasma Sources Sci. and Technol. **29**, 11, 115009 (2020).

[3] Booth, J. P. *et al.* Plasma Sources Sci. and Technol. **31**, 6, 065012 (2022).

[4] Tejero-del-Caz, A. *et al.* Plasma Sources Sci. and Technol. **28**, 043001 (2019).

[5] Tejero-del-Caz, A. *et al.* The LisbOn KInetics simulation tools, XXXVth ICPIG (2023).

[6] Braginskyi, O. V. *et al.* J. Phys. D, **38**, 3609 (2005)

XXXV ICPIG, July 9-14, 2023, Egmond aan Zee, The Netherlands Topic number 8

Structural and Electrical Enhancement of Radial Homogeneity in Wide Aspect Ratio Capacitively Coupled Plasma Processing Sources

Scott J. Doyle[1], James P. Dedrick[2], and Mark J. Kushner[1]

[1]*Electrical Engineering and Computer Science Department, University of Michigan, Ann Arbor, MI 48109-2122, USA*
[2]*York Plasma Institute, Department of Physics, University of York, Heslington, York, YO10 5DD, UK*
scdoyle@umich.edu

In this work, control of the radial homogeneity in a simulated radio-frequency capacitively coupled plasma source was achieved through structuring of the powered electrode surface and through the application of tailored voltage waveforms. Simulations were performed employing the Hybrid Plasma Equipment Model. Hollow cathode structures were found to be most effective when positioned at high radii and geometrically square. The greatest degree of control was achieved via the application of 'peak' shaped tailored voltage waveforms, enabling a significant 20% variation in the radial homogeneity over the 360 degree phase offset range. Real time control of the radial homogeneity in plasma processing via tailored voltage waveforms allows for the processing of wider area substrates, while maintaining etch and deposit fidelity.

Plasma-assisted manufacturing processes are ubiquitous in modern semiconductor fabrication processes where control of the radial plasma density profile is key to maintaining etch or deposition quality. In this work, 2D fluid/Monte-Carlo simulations are employed to demonstrate and compare two methods for the control of radial uniformity in a collisional (200 Pa, 1.5 Torr argon) radio-frequency capacitively coupled discharge.

Control of the radial uniformity is initially demonstrated by the introduction of a single toroidal cavity into the powered electrode for a 13.56 MHz discharge. Optimal conditions were found for radially wide, but axially shallow, cavities at high radii (~80% of the electrode radius); where plasma densities peak below the cavity but become more uniform towards the centre of the electrode as compared to an unstructured electrode. This effect is then replicated electronically, through the application of `tailored' voltage waveforms, themselves formed via the superposition of 5 harmonics of 13.56 MHz. Variation of the inter-harmonic phase offset enables control of the spatio-temporal ionisation rate across the surface of the electrode, via modulation of the sheath dynamics. The most significant effects are observed towards the outer radial edge of the electrode, where ionisation rates and plasma density peak due to enhanced sheath collapse heating, with a more uniform distribution observed towards the centre of the electrode. Continued enhancement of radial uniformity in plasma-assisted manufacturing reactors enables higher fidelity outputs in existing infrastructure, and presents the capability to maintain current processing quality with increased substrate diameters in next-generation sources.

This work was supported by the US Department of Energy and US Army Research Office.

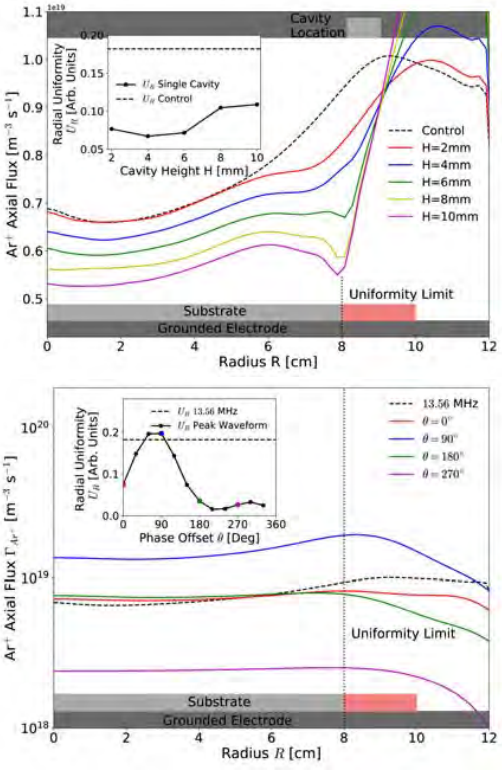

Figure 1 – Simulated radial profiles showing the axial Ar^+ flux incident upon the grounded electrode with respect to (a) the height of a hollow cathode positioned at R=8.6 cm in a 300 V, 13.56 MHz discharge and (b) the inter-harmonic phase offset for a 300 V, 5 harmonic 'peak' tailored voltage waveform. Insets show the respective radial homogeneity, where a homogeneity of 0 represents a flat radial profile.

Self-modulation in arsenic high-frequency electrodeless lamps

A. Abola[1], G. Revalde[1,2]

[1]*Institute of Atomic Physics and Spectroscopy, University of Latvia, Riga, Latvia*
[2]*Riga Technical University, Riga, Latvia*

This work is dedicated to the investigation of the self-modulation regime occurring in high-frequency electrodeless lamps containing arsenic. Self-modulation is a periodical change of spectral line intensity happening under specific circumstances. Its occurrence is influenced by lamp characteristics and voltage applied to the excitation generator. We discuss changes in the intensity of spectral line maxima and the frequency of modulation.

1 Introduction

High-frequency electrodeless lamps (HFEDLs) are bright radiators emitting narrow and intense spectral lines. They have a quite wide range of applications, such as use in scientific devices, for example, atomic absorption and emission spectrometers, use in disinfection, studies of plasma-quartz interactions and other non-invasive plasma processes research.

For HFEDLs of certain fillings, for example, arsenic, selenium and iodine, one can observe two modes of work – stable, with insignificant changes of intensity over a longer time period, and so-called self-modulation, when spectral intensity is changing periodically because of the overheating happening in light bulb. Here we concentrated on the second one.

2 Experiment

HFEDLs used in this work were produced at the Institute of Atomic Physics and Spectroscopy. Lamps were made of SiO_2 glass and filled with arsenic as a "work element" and argon as a buffer gas.

Lamps were excited in the excitation generator coil by an electromagnetic field operating at 100 MHz frequency. The excitation generator voltage was chosen accordingly to observe self-modulation (in the range of 23V-29V).

Spectra of three arsenic resonance spectral lines at 189.0nm, 193.8nm and 197.3nm were recorded by using the spectrometer Jobin Yvon SPEX 1000M (spectral resolution 0.07nm).

3 Results and Discussion

We have investigated two groups of arsenic HFEDLs – with and without side-arm. For the lamps with a side-arm, self-modulation starts at higher voltages – about 27V-29V, for the lamps without a side-arm, the effect starts earlier, as low as 23V-24V. This difference can be explained by the fact that atoms have a tendency to concentrate in cooler places, and as they cannot leave the lamp bulb, overheating happens sooner.

Figure 1 shows an example of the self-modulation process in one of the lamps investigated. Here the excitation generator voltage is 28V, integral intensity changes are observed over 5 minutes and the period of modulation is about 28 seconds. All three spectral lines have a similar integral intensity pattern.

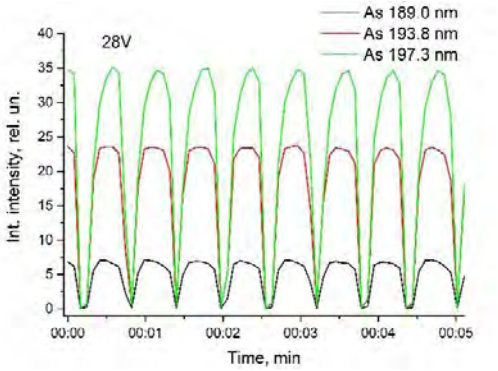

Fig. 1 An example of self-modulating As resonance lines

Our results show that the frequency of modulation is increasing when the excitation generator voltage is augmented. In addition, a slight increase in peak maximum values is also observed.

At the moment we need more data from more light sources, to give conclusions on the repeatability of the effect and its numerical values between lamps of the same build. And there are still data needed to understand what influences the frequency value and tendencies of its changes, as well.

Acknowledgments

This work was supported by the Latvian Council of Science project No. lzp-2020/1-0005 and ESF project No. 8.2.2.0/20/I/006.

Evidence of a significant N-atom metastable population by ns-TALIF in pulsed N_2 microwave plasma

S. Prasanna[1], E. Bisceglia[1], A. Remigy[1], X. Aubert[1], C.Y. Duluard[1], G. Lombardi[1] and K. Hassouni[1]

[1]*LSPM, CNRS, UPR 3407, Université Sorbonne Paris Nord, 99 avenue J.B. Clément, 93430 Villetaneuse, France*

In this work, we will discuss the dynamics of N_2 dissociation in a pulsed MW plasma in the pressure range 20-200 Pa studied using ns-TALIF.

The aim of this work is to investigate quantitatively the nitrogen dissociation in low pressure MW pulsed plasmas. We focus on nitrogen 2.45 GHz microwave plasmas generated by Sairem Hi-wave source working at low pressures (20 – 200 Pa) regime. N-atom density measurements have been performed using ns-TALIF [1] and gas temperature measurements using OES.

Figure 1 shows the transient evolution of the N-atom densities and the plasma emission during the transition between the high and low power phases at a pressure of 100 pa, 20% duty cycle and 10 Hz frequency. The plasma emission is mainly due to the first positive system of the N_2 molecule and closely follows the MW power. However, one can easily observe that the densities of N-atom densities have a rapid increase ($<$ 2ms) immediately after the transition followed by a gradual decrease in N-atom densities. This sudden increase in N-atom densities is referred to as "Surge". A similar phenomenon, named "Crash" has been observed during the transition between low power phase to high power phase where N-atom denisties experience a sharp decrease over a few ms gradually increases. The ratio of surge and crash N-atom densities are as high as 100% at 20 Pa while gradually decrease with pressure (c.f. Figure 2).

Using a 0D-collisional radiative model we demonstrate that these sudden changes of N-atom densities are mainly caused due to the equilibrium dynamics between N-atom and its metastables $N(^2D^o)$ and $N(^2P^o)$ while vibrational mechanisms are negligible for these conditions. Therefore the surge and crash densities is indicative of the significant N-metastables produced during the pulsed plasma process. This could be interesting with respect to improvement of reactivity of N. Finally, we will discuss the potential enhancement of the production of N-atom densities as a function of duty cycle and frequency of plasma pulsation.

References

[1] Bisceglia, E. *et al.* Investigation of n(4s) kinetics during the transients of a strongly emissive pulsed ecr plasma using ns-talif. *Plasma Sources Sci. Technol.* **30**, 095001 (2021). URL `http://iopscience.iop.org/article/10.1088/1361-6595/ac0da1`.

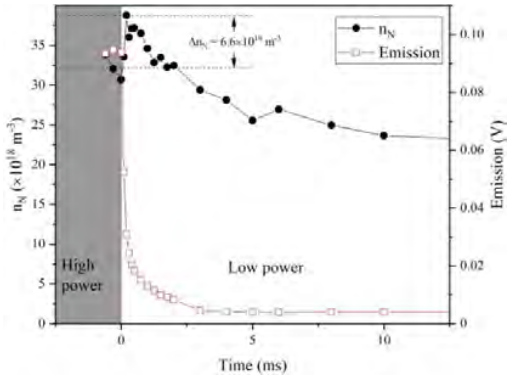

Figure 1: Time-resolved measurement of N-atom density and N2($B^3\Pi_g$) emission around the transition between the high and low power phases at 100 Pa, 0.2 duty cycle, 10 Hz

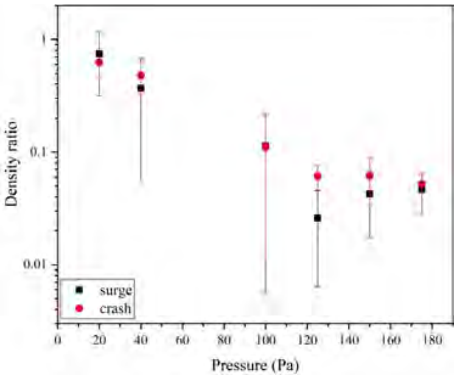

Figure 2: Ratio of surge and crash densities to the N-atom density just before the phase transition observed for Hi-wave plasma source as a function of pressure

Streamer discharge instabilities under repetitive nanosecond pulses

Zheng Zhao, Anbang Sun, and Jiangtao Li

School of Electrical Engineering, Xi'an Jiaotong University, Xi'an, China

Pulse-periodical streamer discharges feature complicated instabilities although discharge stochastics have been significantly reduced. We report our recent investigations on nanosecond repetitively pulsed (NRP) streamer discharge instabilities, from discharge evolution tendencies to important influential factors. New modulation concepts have been proposed regarding the discharge instabilities, i.e., the quantitative charge transport and the organized energy transfer.

1 Background and motivations

Pulse-periodical streamer discharges in open air exhibit complicated instabilities, which critically limit the plasma source consistency and predictability in various applications such as plasma medicine and heat-sensitive material treatment. The discharge memory effects are usually ambiguously utilized to explain why the nanosecond repetitively pulsed (NRP) discharge tends to be intensified [1]. Nevertheless, traditional memory effect frameworks based on free electrons or metastable species could not explain recent evolution tendencies. Meanwhile, modulation methods have not been fully established regarding how to reduce discharge instabilities.

We systematically review our experimental and simulation studies in the recent five years regarding NRP streamer discharge instabilities. Unique and sometimes unexpected evolution phenomena are reported, which inspire one to reconsider NRP discharge mechanisms.

2 Streamer discharge instabilities phenomena under repetitive nanosecond pulses

2.1 NRP streamer discharge mode instability.

The numbers of applied pulses before breakdown (streamer-to-spark transition) are dependent on pulse repetition frequency (PRF) and gas pressure. Meanwhile, with increasing PRF, the interval pulse numbers between two streamer discharge events firstly increase, and then the spark discharge quickly occurs after several voltage pulses. The above tendency is surprising since the streamer is monotonously facilitated if metastable species or free electrons are dominant memory effect agents.

2.2 NRP discharge regime instability.

Traditionally, the NRP discharge is categorized into the corona, glow, and spark regimes. The NRP spark regime would be consistent once it is formed due to excessive heat. However, we observed a unique periodical NRP discharge regime transition, which is characterized by periodical spark quenches and reestablishments. Periodical NRP spark quenches are probably initiated with the streamer 'detour' and accelerated by the thermal-ionization instability when the equivalent operation point enters the right leg of the power transfer curve.

2.3 Effects of the gas composition and gas flow.

Effects of electronegative gas compositions on NRP discharges are compared. The number of applied pulsed for the streamer-to-spark transition decreases in the low-PRF region with increasing the O_2 concentration, which is in contrast to the consensus that the electron attachment capability of O_2 molecules would hinder the streamer propagation and increase the insulation capability. Moreover, an interesting streamer bending pattern towards the gas inlet has been observed, despite higher densities of charge remnants at the downstream side.

2.4 Effect of the solid surface.

NRP streamer discharges propagating along the gas/solid interface are investigated. Principal results qualitatively support those surface streamer and flashover behaviors dominated by the electric field distribution, volume and surface memory effects (interactions and bidirectional transformations).

2.5 3D simulations of streamer propagation with the pre-existing plasma patches.

A 3D steamer simulation was performed based on *Afivo-streamer* framework with different pre-existing plasma patches in the gas gap. The streamer detour could only occur with pure plasma patches and not be observed with neutral plasma patches. This observation challenges previous explanations that the neutral plasma patch may provide the electric field shielding effect.

3 Summary and perspectives

Streamer discharge instabilities under repetitive nanosecond pulses are induced by charge and energy relaxations. Two modulation concepts have been proposed regarding discharge instabilities, i.e., the quantitative charge transport (e.g., DC offset) and the organized energy transfer (e.g., waveform tailoring to reach more vibrational excitations).

References

[1] Nijdam S, Teunissen J, Ebert U. The physics of streamer discharge phenomena. Plasma Sources Science and Technology **29**, 103001 (2020).

XXXV ICPIG, July 9-14, 2023, Egmond aan Zee, The Netherlands Topic number 9

The electron power absorption mechanism due to the sheath motion in a microwave-driven plasmaline discharge

D. Eremin

Institute of Theoretical Electrotechnics, Ruhr University Bochum, Bochum, Germany

It is argued that there is an electron power absorption mechanism in a MW-driven surface wave plasmaline discharge, which is alternative to the commonly assumed plasma resonance. The new mechanism is related to the electron energization by the sheath motion taking place in CCP discharges driven at RF frequencies.

1 Introduction

Surface wave plasma discharges sustained in the microwave frequency range are known due to their ability to produce large-area plasmas with high densities [1]. A particular case of such a discharge exploited for societal needs is a modified plasmaline discharge driven at 2.45 GHz, producing plasmas with densities up to a few 10^{18} m^{-3}, which generate fluxes of particles to be deposited on PET bottles to reduce their gas permeability [2]. The electromagnetic energy is fed to such a discharge through a coaxial line-like setup, with a central metal rod and a plasma ignited at the surface of a dielectric encasing the rod, the plasma being the second electrode [3].

One of the crucial aspects for understanding any plasma discharge is the conversion of field energy into kinetic energy of plasma particles, typically electrons. Despite its importance, this topic is not fully understood and needs further investigation. A common assumption for unmagnetized microwave-driven discharges is that the dominant power absorption mechanism is related to the excitation of plasma waves in the vicinity of the resonance point where the driving frequency matches the local plasma frequency (also known as "plasma resonance") [4]. However, the considered surface discharge features a significant sheath formed at the dielectric surface, with the sheath width being modulated with the driving frequency.

2 The numerical model

Due to the driving frequency exceeding the elastic moment transfer frequency and the energy relaxation length being comparable to the system size for the typical pressures used for the operation of the plasmaline discharge in question, a kinetic and nonlocal description, taking into account electron inertia, is required. To meet this need, in this work we employed a fully electromagnetic, energy- and charge-conserving implicit PIC code [5,6]. Such an algorithm allows one to overcome the time step limitation inherent to explicit EM PIC codes, which is required to resolve a lightwave traversing a cell, and the cell size limitation needed to resolve the Debye length. Another numerical acceleration factor comes from massive parallelization on GPU using a 2D generalization of an algorithm described in [7].

3 Discussion

The simulation results demonstrate that the surface modes are generated as standing waves, which causes nonuniformities of the electron density, temperature, and ionization rate along the plasmaline. However, owing to the high frequency, the wavelength is much smaller than the system size, and the corresponding patterns have many nodes. Due to the diffusive character of the neutral transport, the corresponding nonuniformities are substantially smeared out close to the reactor walls. Two electron heating mechanisms can be identified – the first one occurring close to the plasma resonance locations (because of the nonuniform plasma density profile, there are two of those), and the second one due to the repulsion of the electrons at the sheath edge by its potential during the expansion phase, which generates beams of energetic electrons propagating toward the plasma bulk. The latter mechanism is similar to the one occurring in conventional CCP discharges driven at RF frequencies (see, e.g., [6]).

References

[1] M. Moisan and Z. Zakrzewski 1991 J. Phys. D: Appl. Phys. 24 1025
[2] M. Deilmann et al 2008 J. Phys. D: Appl. Phys. 41 135207
[3] E. Räuchle 1998 J. Phys. IV 08 7-99
[4] S.V. Bulanov et al 1990 Phys. Rep. 186 1
[5] D. Eremin 2022 J. Comp. Phys. 452 110934
[6] D. Eremin et al "Modeling of very high frequency large-electrode capacitively coupled plasmas with a fully electromagnetic particle-in-cell code" arXiv:2212.08836v2 [physics.plasm-ph]
[7] P. Mertmann et al 2011 Comp. Phys. Comm. 182 2161

Generating non-filamented argon plasma columns at atmospheric pressure using a surfatron consuming low 2.45 GHz microwave power

M. C. García[1], J. Amaro-Gahete[2], A. Rodero[1], and F.J. Romero-Salguero[2]

[1] *Grupo de Física de Plasmas: Diagnosis, Modelos y Aplicaciones (FQM-136)*
Edificio A. Einstein (C-2), Campus de Rabanales. Universidad de Córdoba, 14071 Córdoba, Spain
[2] *Departamento de Química Orgánica, Instituto Químico para la Energía y el Medioambiente (IQUEMA), Facultad de Ciencias, Universidad de Córdoba, Campus de Rabanales, 14071 Córdoba, Spain*

A new procedure to generate 2.45 GHz plasmas under atmospheric pressure conditions by using a surfatron device and powers as low as 50 W is presented. The modified design allows non-filamented argon plasmas to be sustained. The reactor also makes it possible to maintain plasmas containing relatively high proportions of water and so generate larger amounts of OH^* species. This new configuration extends the applicability of microwave-induced plasmas as new experimental conditions can be run. Thus, the methylene blue (MB) degradation in aqueous solutions has been evaluated under different initial dye concentrations and plasma flow conditions.

1 Plasma reactor

A surfatron was used to couple energy coming from a 2.45 GHz power supply to generate argon plasmas within a quartz tube using powers from 50 W. For this purpose, the electromagnetic field configuration created by the surfatron was altered by introducing in the tube a small rectangular-shaped Si(100) wafer (4 mm × 20 mm × 300 μm) (see **Fig. 1**). Thus, a strong electric field was established at the edges of the silicon strip and a plasma column was formed. Unlike usual surfatron experiments, neither plasma was observed inside the surfatron nor plasma filamentation took place. The reactor also allowed stable maintenance of plasmas with moderate fractions of water, thus favouring the generation of OH reactive species.

In this work, we have studied the generation of excited species in this reactor when different amounts of water were dragged through the main gas. The power was set at 105 W and, in a primary gas line, the argon flow rate was adjusted at 700 sccm. A secondary feeding argon line bubbling through water was also used with argon flow rates set from 750 to 1550 sccm.

Figure 1. Argon plasma column.

2 Plasma characterization

OES techniques were used for plasma diagnosis. A Czerny-Turner type spectrometer of 1 m focal length (with a 1200 grooves/mm holographic grating and a photomultiplier as a detector) was used for the analysis of the plasma emission.

2.1. Plasma excited species

The main emission of this plasma corresponded to Ar I lines, although spectra also revealed the presence of both water and air (through OH, H, and N_2 excited species) (see **Fig. 2**). OH^* species were particularly copious increasing in quantity as the argon flow rate bubbling through water raised.

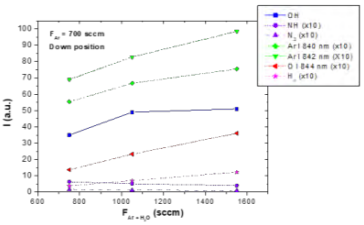

Figure 2. Excited species evolution.

2.2. Electron density and gas temperatures

The electron density and the gas temperature were measured from the collisional broadening of some atomic lines (H_β line and Ar I 840 nm, respectively) ranging from $n_e = (3.5\text{-}5.8)\cdot 10^{20}$ m^{-3} and T_g = 1000-1500 K.

3 MB degradation

This plasma configuration was applied to degradation of MB from aqueous solutions at high dye concentrations. An almost total conversion of 96% was achieved at flow rate of 1550 sccm obtaining a remarkable kinetic constant in the dye degradation process of 0.1598 min^{-1} and energy yield of 0.0401 g/kWh.

Acknowledgements

Authors thank the FEDER program, the Spanish Ministry of Science and Innovation (PID2020-112620GB-I00, PID2020-114270RA-I00, TED2021-130124A-I00, and PDC2022-133973-I00 Grants) and Junta de Andalucía (ProyExcel_00492).

Discharge sustained by HF cathode for fluorescent lamp applications

Q. Gutierrez[1] A. Lacoste[1] A. Bés[1] L. Simonot[2]

[1] *Laboratoire de Physique Subatomique et de Cosmologie (CRPMN), Grenoble, France*
[2] *Institut PPrime, Poitiers, France*

The cathode hybrid discharge where the conventional DC cathode is substituted by a microwave cathode has advantageous characteristics for the application to mercury-free fluorescent lamps. These advantages result from the suppression of the cathodic fall and will be presented through the electrical, electromagnetic and optical characteristics of such a discharge.

1 Introduction

DC discharge consists of two electrodes set at both extremities of a sealed glass tube after being filled with a gas. When applying a DC voltage, the discharge is ignited and sustained through the electrons generated at the cathode [1] either by thermionic emission (in hot-cathode operating mode) or ion bombardment (in cold-cathode operating mode). Hot-cathodes are commonly used as electron guns in cathode ray tubes and laboratory equipment such as electron microscopes, but also as an electron source in fluorescent tubes with a good emission efficiency. However, for the lighting application, the high temperature of the cathode (> 1000 K) limits its lifetime and prevents the use of reactive gases with respect to the electrode. The cold-cathodes, widely used in many application fields, relay on the emission of secondary electrons resulting from the bombardment by high energy ions. The concomitant sputtering of the electrode as well as the loss of a large part of the energy (~30%) in the cathodic fall for the acceleration of the ions exclude the use of this type of discharge for applications such as fluorescent lamps.
A solution circumventing both the ion bombardment and the heating of the cathode is the use as an electron source an HF cathode added or instead of the DC voltage [2,3]. Thus, the discharge can be operated in HF or in hybrid DC-HF power supply.

2 HF cathode discharge

Our work concerns firstly the study and the electrical and electromagnetic characterization of a hybrid discharge where the HF supply of one of the electrodes is superimposed on the DC voltage. The I-V characteristics obtained in such configuration are shown in Fig. 1 for an argon (1 Torr) discharge and several HF powers. For a direct comparison with a conventional cold-cathode DC discharge, a ballast resistor R_b = 23 kΩ is integrated into the electrical circuit. Fig. 1 reveals a large decrease in discharge voltage (V_d), from ~500 V to 50-75 V when adding microwave power, signifying the suppression of cathodic fall. It can be also observed that to obtain an equivalent DC current of a few mA, less than 1 W is enough for the HF cathode plasma, and for a weak variation of the DC discharge voltage, the discharge current increases with the microwave power.

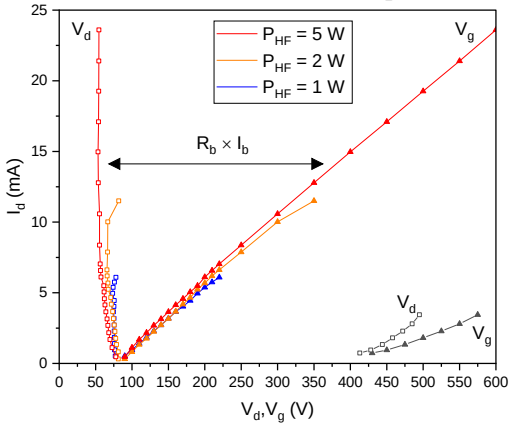

Fig. 1. I-V curve of hybrid discharge (in colors) and DC discharge (black) with a ballast resistor of 23.3 kΩ. Current are plotted as a function of Vg (full triangle) and as a function of Vd (open circles) at 1 Torr in pure Argon.

Under hybrid discharge conditions, *i.e.*, low voltage, the ballast resistance is no longer required and, in its absence, the I-V characteristics are modified. We will therefore present their dependence of the HF power and interelectrode distance, their photon production energy efficiency and the comparison with a microwave cathode discharge free of DC voltage.

3 Conclusion

Based on the presented work and on previous studies on HF discharges sustained in argon-sulphur [3], it appears that HF cathode discharges could operate with UV emitters such as S_2 or N_2/O_2 for the elaboration of mercury-free fluorescent lamps**.**

References

[1] J. T. Gudmundsson and A. Hecimovic. Plasma Sources Sci. Technol. , 26(12), 123001 (2017)
[2] P Baële, A Lacoste and J Pelletier J. Phys. D: Appl. Phys. 52 395202 (2019).
[3] P Baële, A Bés, A Lacoste,and J Pelletier J. Phys. D: Appl. Phys. 52 32LT02 (2019)

Nanosecond Surface Dielectric Barrier Discharge: Experimental study of high-pressure streamer to filament transition with varying gas composition

V. Lafaurie[1], S. Starikovskaia[1]

Laboratory of Plasma Physics, UMR764, Ecole Polytechnique, Palaiseau, France[1]

In high-pressure nanosecond surface dielectric barrier discharges (nSDBD) it is common to observe two different type of discharge development: a diffuse (or streamer) mode and a filamentary mode [1]. In this study, the effects of photoionisation and electronegativity of the gas mixture on the transition voltage were compared for a wide range of pressures and concentrations. In the positive polarity, it was found that photoionisation played a stabilising role on the diffusive discharge for all studied pressures, while electronegativity appeared to reduce the threshold for transition at lower pressures. In the negative polarity, the photoionisation effect was no longer observable while the filament threshold was lowered for more electronegative mixtures. Fundamental understanding of these processes is of great importance in many applications, most of all in plasma-assisted combustion [2-3].

1. Introduction

A common feature of high-pressure nSDBD is the two different discharge propagation modes that exist depending on the pressure and applied voltage, referred to here as the diffuse/streamer mode and the filament mode. A transition point was defined as the voltage for which formation of 2 to 5 filaments is observed in the first 12 ns of the discharge.

2. Experimental set-up

In this study, a 20 mm diameter round high-voltage electrode was used. It rests on a 0.3 ± 0.1 mm PVC sheet, held in place on the 50 mm diameter mass electrode by a similarly sized layer of silicon adhesive. Single-shot HV pulses of positive and negative polarities, 20 ns in duration (FWHM), 2 ns rise time and 20-60 kV on HV electrode are produced by FID Technology pulsers.

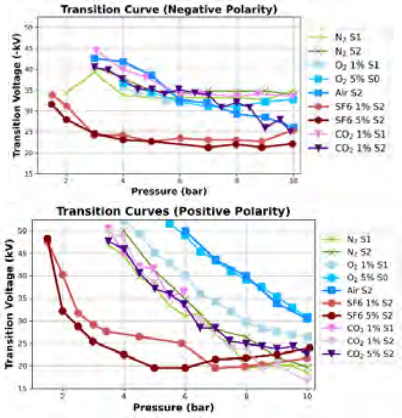

Figure 1: Transition curves in positive and negative polarities for different gas compositions

3. Results

The transition curves obtained for varying gases are shown in Figure 1. Looking at the positive polarity and using N_2 as the reference, the addition of fractions of O_2 to the mixture appears to increase the transition voltage for a given pressure. This can be attributed to photoionisation of the O_2 by electronically excited N_2. Indeed, in N_2:O_2 mixtures ionization of O_2 molecules occurs due to the absorption of the emission produced by highly excited N_2 and N-atoms, both produced by direct electron impact [5,6]. For comparison, measurements with CO_2 fractions cannot be differentiated from N_2 transition. At the negative polarity, all curves for N_2:O_2 mixtures and CO_2 are collapsed together.

Finally, looking at the highest possible electronegativity, that is at the SF_6 fractions, the transition voltage is noticeably lower than all other mixtures in both polarities. It is of importance to note that in the highest pressures, the SF_6 discharges are immediately in filamentary mode, no diffuse mode existing and no discharge lighting before the transition. The trend of transition is somewhat maintained although shifted left, and the addition of even 1% of SF_6 is sufficient to still transition at pressures where, in pure N_2, it would be impossible to get a filament.

4. Acklowledgements

The work was partially supported by the French General Directorate of Armaments (DGA) under the EP-DGA convention, PPRINCE Project.

References

[1] Ding, Ch, et al. "Fine structure of streamer-to-filament transition in high-pressure nanosecond surface dielectric barrier discharge." Plasma Sources Science and Technology 31.4 (2022): 045013.

[2] Starikovskaia S et al. Surface discharges: possible applications for plasma-assisted ignition and electric field measurements. In48th AIAA Aerospace Sciences Meeting Including the New Horizons Forum and Aerospace Exposition (2010) (p. 1587).

[3] Kosarev INet al. A nanosecond surface dielectric barrier discharge at elevated pressures: time-resolved electric field and efficiency of initiation of combustion. Plasma Sources Science and Technology. 2012 Jul 31;21(4):045012.

[4] Zheleznyak M Bet al. Photoionization of nitrogen and oxygen mixtures by radiation from a gas discharge. High Temp. **20** (1982) 357.

[5] Pancheshnyi S. Photoionization produced by low-current discharges in O_2, air, N_2 and CO_2. Plasma Sources Sci. Technol. **24** (2015) 015023.

Study of Townsend Dielectric Barrier Discharge in CO_2

C. Bajon[1], S. Dap[1], A. Belinger[1], O. Guaitella[2], T. Hoder[3] and N. Naudé[1]

[1] *LAPLACE, Université de Toulouse, CNRS, INPT, UPS, Toulouse, France*
[2] *Laboratoire de Physique des Plasmas, Ecole Polytechnique, Route de Saclay, F-91128, Palaiseau Cedex, France*
[3] *Department of Physical Electronics, Faculty of Science, Masaryk University, Kotlářská 2, 61137 Brno, Czech Republic*

Generally, dielectric barrier discharges work in the filamentary regime at atmospheric pressure, especially in the CO_2 atmosphere. However, we discovered for the first time that obtaining diffuse Townsend discharges under specific conditions is possible. Electrical characteristics, iCCD imaging and optical emission spectroscopy results have highlighted a clear difference between this regime and a classical filamentary discharge.

1 General

Faced with the need to lower greenhouse gas emissions to limit global temperature evolution, studies on CO_2 conversion have gained interest. Non-equilibrium plasmas, and especially Dielectric Barrier Discharges (DBD), present an exciting way for CO_2 conversion at atmospheric pressure. Under these conditions, DBD generally work in the filamentary regime. However, for the first time, we can obtain a diffuse discharge in CO_2 DBD.

2 Experimental set-up

The DBD under study is a classical plane-to-plane electrode configuration powered by sinusoidal high voltage. An alumina plate covers each electrode. The atmospheric pressure inside the vessel is maintained, and a gas flow may be imposed at the entrance of the discharge cell.

3 Results

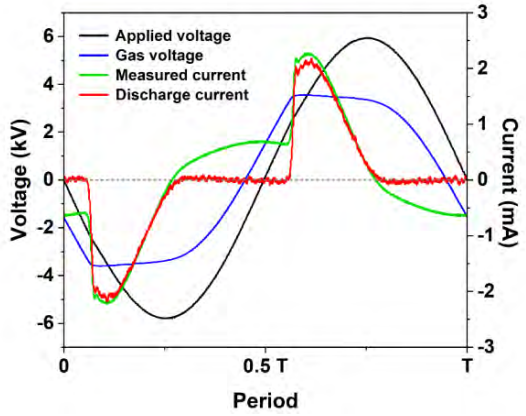

Fig. 1: Oscillogram of a diffuse DBD in CO_2 at atmospheric pressure (gas gap = 1 mm).

Fig. 1 shows the oscillogram of the discharge. The measured current shows only one peak per half period, characteristic of a diffuse discharge. This discharge is compared to a filamentary discharge in CO_2. ICCD images of the light emitted during a half period for both regimes are proposed in Fig. 2. The light is located on the anode side for the diffuse discharge, whereas it crosses the gap for the filamentary discharge. Moreover, the gas gap voltage remains almost constant during the discharge in Fig. 1. These results demonstrate that this diffuse discharge works in the well-known Townsend regime. Indeed, similar electrical and optical characteristics were observed for Atmospheric Pressure Townsend Discharges (APTD) in N_2 [1,2]. The mechanism responsible for the Townsend breakdown appears to be related to surfaces, as in air [3,4]. In addition, the first optical emission spectroscopy results show a difference between both discharge regimes and provide a basis for discussing the mechanisms involved in CO_2 DBD.

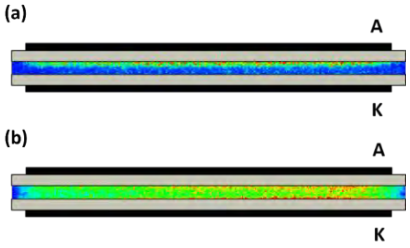

Fig. 2: iCCD images of a diffuse discharge (a) and a filamentary discharge (b) in CO_2 (exposure time = half of the period).

References

[1] F. Massines, P. Ségur, N. Gherardi, C. Khamphan, A. Ricard, Surface and Coatings Technology 174–175 (2003) 8–14.
[2] C. Tyl, X. Lin, M.C. Bouzidi, S. Dap, H. Caquineau, P. Ségur, N. Gherardi, N. Naudé, Journal of Physics D: Applied Physics 51 (2018).
[3] N. Osawa, A. Takashi, Y. Yoshioka, R. Hanaoka, Eur. Phys. J. Appl. Phys. 61 (2013) 24317.
[4] A. Belinger, S. Dap, N. Naudé, J. Phys. D: Appl. Phys. 55 (2022) 465201.

Effect of charge accumulation on the ionized gas propagation in atmospheric pressure plasma jet

J. S. Lim[1], E. H. Choi[1]

[1] *Plasma Bioscience Research Center (PBRC), Kwangwoon Univ., Seoul, Republic of Korea*

Propagation of ionized gas behavior is interesting field in the atmospheric pressure plasma. In the atmospheric pressure capillary plasma jet, initial plasma generated between the electrodes and propagate following the guided capillary tube for gas outlet. Although, ionized gas escape from the high electric field region between the electrodes, still propagate forward to the nozzle of the gas outlet as a streamer. The guided capillary tube which consists of dielectric material can be accumulated the charge from the pre ionized gas. The electric field from this charge accumulation and residual charge from the pre-discharge could be affect to the propagating ionized gas for their kinetic energy. In this report, we applied the bipolar and unipolar voltage for the accumulated charge difference by pre-ionization, and report the effect of charge accumulation to the propagating ionized gas behavior for speed and electron temperature variation.

1 Introduction

Propagation of ionized gas behavior is interesting field in the atmospheric pressure plasma. In the capillary plasma jet, initial plasma generated between the electrodes and propagate following the guided capillary tube for gas outlet. Although, ionized gas escape from the high electric field region between the electrodes, still propagate forward to the nozzle of the gas outlet. The guided capillary tube which consists of dielectric material can be accumulated the charge from the pre-ionized gas. The accumulated charge vicinity of the electrodes can reduce the breakdown voltage by compensate the potential at the bipolar voltage. Also, the electric field from accumulation and residual charge can be affect to the propagating ionized gas for their kinetic energy. [1,2] In this report, we applied the bipolar and unipolar voltage for the accumulated charge difference by pre ionization and report the effect of charge accumulation to the propagating ionized gas behavior for speed and electron temperature variation.

2. Experimental setup

The plasma jet was based on the capillary quartz tube for the ionized gas flow guidelines. Syringe needle tip which inserted into the quartz tube as aa gas inlet and copper clip surround the quartz outline were used to high voltage electrode and grounded electrode, respectively. The 3 lpm of pure Ar gas (99.999%) was used for the discharge. High voltage invertor used for plasma jet operation for unipolar and bipolar voltages with 50 kHz sinusoidal wave. To measure the behavior of ionized gas propagation, ICCD (intensified charge-coupled device, PIMAX4) was used with 50 ns gate width. The Ar collisional radiative model using optical emission spectrum were used to the evaluation of temporal electron temperature distribution of ionized gas propagation.

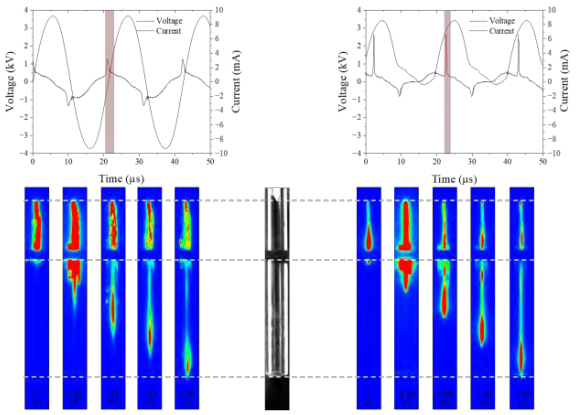

Figure 1. Propagation of ionized gas in the atmospheric pressure Ar plasma jet with applied bipolar (left) and unipolar (right) voltage.

References

[1] Jing Li, Bingying Lei, Jing Wang, Boping Xu, Shuang Ran, Yishan Wang, Tongyi Zhang, Jie Tang, Wei Zhao and Yixiang Duan. Atmospheric diffuse plasma jet formation from positive-pseudo-streamer and negative pulseless glow discharges. Communications physics **4**, 64(2021)

[2] Erdinc Karakas, Mehmet Arda Akman and Mounir Laroussi. The evolution of atmospheric-pressure low-temperature plasma jets : jet current measurements. Plasma Sources Science and Technology **21,** 034016 (2012)

P4-31

Breakdown characterization in device with dielectric spacer in air at 1 atm

Rui Almeida[1,2], Pedro Almeida[1,2], George Naidis[3], Mikhail Benilov[1,2]

[1] *Departamento de Física, FCEE, Universidade da Madeira, Funchal, Portugal*
[2] *Instituto de Plasmas e Fusão Nuclear, Instituto Superior Técnico, Universidade de Lisboa, Lisboa, Portugal*
[3] *Joint Institute for High Temperatures, Russian Academy of Sciences, Moscow, Russia*

In this work we study the dependence of the ignition and breakdown voltages with regard to the proximity of a dielectric surface to the active discharge path. The studied device consists of two disc electrodes with a dielectric disc spacer. Non-stationary breakdown modeling results show that in some configurations the calculated ignition voltages must be unstable and therefore physically unrealizable.

1 Introduction

For each device in an ionizable medium it is possible to calculate, through the stationary resonance method [1], a certain minimum voltage that when applied to it, would produce a stationary low current discharge across it. We designate it as the ignition voltage (IV) or self-sustainment voltage. If the discharge is stable, then at a voltage higher or equal to the IV, the discharge will undergo a non-stationary transition to a regime with a high current discharge between the electrodes. The lowest voltage that brings about this transition is called the breakdown voltage (BDV). In this work we study the dependence of the IV and BDV on the proximity of a dielectric surface to the active discharge path.

2 The Model

The studied device consists of a dielectric disc spacer, in-between two disc electrodes with radius 7.5 mm in dry air at atmospheric pressure. We employ 2D axi-symmetric numerical modelling of transport and conservation of one positive species, electrons and three negative ions. The Poisson equation and equations for photoionization source terms are solved. The model is described in detail in previous work [1].

3 Results and discussion

The dependence of the IV was investigated against different: dielectric radii, secondary electron emission (SEE) coefficients and boundary conditions over the dielectric surface, by means of the resonance method [1].

Results show that (i) the IV doesn't depend on the dielectric permittivity, that (ii) the dielectric SEE coefficient has just a negligible effect on the IV, (iii) that applying the boundary condition of vanishing normal component of electric field or of vanishing normal component of current density doesn't affect the IV much, that (iv) the proximity of the dielectric surface substantially affects the IV, and that (v) the discharge path goes from being semicircular for the retracted dielectric, to start clinging to the surface as the dielectric radius comes close and exceeds the electrode radius. An attempt is made to explain all these results.

The dependence of the BDV was investigated using time-dependent simulations, for three dielectric radii (***R***), two dielectric constants (ε_D) and against two initial surface charge distributions, using the model described in [1] with the boundary condition of surface charge accumulation on the dielectric surface. For this non-stationary study, we considered as initial conditions for the electric field the Laplace solution and low 'no discharge' densities for the species and vanishing photoionization terms.

	$\varepsilon_D = 1$		$\varepsilon_D = 12$		
R(mm)	***U***(kV)	Outcome	***U***(kV)	Outcome	***IV***(kV)
3	≤ 9.5	Extinction	≤ 9.5	Extinction	9.9
3	≥ 10.0	Breakd.	≥ 10.0	Breakd.	
7.5	≤ 9.0	Extinction	≤ 11.5	Extinction	6.8
7.5	≥ 9.5	Breakd.	≥ 12.0	Breakd.	
8.2	≤ 14.0	Extinction	≤ 8.5	Extinction	11.5
8.2	≥ 14.5	Breakd.	≥ 9.0	Breakd.	

Table: BDV defined to within 0.5 kV. Case where there was no initial surface charge on the dielectric.

An attempt is made to explain the results obtained in the table, where it is noted that for ***R***=8.2 mm, the BDV (9kV) is lower than the IV (11.5kV), indicating that the device has no stable discharge. In this latter case no conduction channel is observed and the triple junctions play an important role. It was also observed that the existence of an initial surface charge distribution over the dielectric surface, lowers the BDV.

Acknowledgments

This work was supported by European Regional Development Fund through the program Madeira 2014–2020 under Project No. PlasMa-M1420-01-0145-FEDER-000016 and FCT of Portugal under Project No. UIDP/50010/2020 (UMa).

References

[1] Benilov, M. S. et al, Journal of Applied Physics **130**, 121101 (2021).

Effects of rf power and potential of water jet on quantum yield of laser-induced desolvation in inductively coupled plasma

Y. Inagaki[1] and K. Sasaki[1]

[1] *Division of Applied Quantum Science and Engineering, Hokkaido University, Sapporo, Japan*

We measured the pulsed current which was originated from laser-induced desolvation of hydrated electrons in a micrometer-size water jet immersed in a low-pressure inductively coupled plasma. The pulsed current represented the quantum yield of the laser-induced desolvation. The effect of the rf power on the quantum yield was examined at various potentials of the water jet. The quantum yield decreased with the rf power, but the magnitude of the decrease was dependent on the water jet potential.

1 Introduction

Hydrated electrons are generated by plasma-liquid interaction. However, there have been limited reports on the detection of hydrated electrons in liquids interacting with plasmas. The difficulty is caused by the fact that hydrated electrons generated by the plasma irradiation are localized in a narrow region with a thickness of several nanometers below the plasma-liquid interface. To overcome the difficulty, we have developed a method to detect hydrated electrons in the interfacial region [1]. Hydrated electrons in the interfacial region are converted to free electrons when they are irradiated with laser beam having a photon energy exceeding the solvation energy. Free electrons produced by the desolvation are transported to the gas phase. In the present work, we tried to detect hydrated electrons in a micrometer-size water jet immersed in a low-pressure plasma.

2 Experimental methods

Figure 1 shows a schematic of the experimental setup. A NaOH aqueous solution was squirted through a plastic tube into a vacuum chamber. The length and the inner diameter of the plastic tube were 1.5 cm and 75 μm, respectively. The water jet had a filament-like shape with a length of approximately 2 cm in vacuum, and it was dispersed into droplets in the downstream. The pressure of water vapor in the chamber was 7-9 mTorr. We added helium to realize a total pressure of 100 mTorr. Inductivity coupled plasmas were generated. The water jet was irradiated with the 4th harmonics of Nd:YAG laser pulses. A dc voltage was applied between the electrical ground and the solution in the reservoir. The pulsed current through the water jet was measured by the voltage across the resistor of 50 Ω.

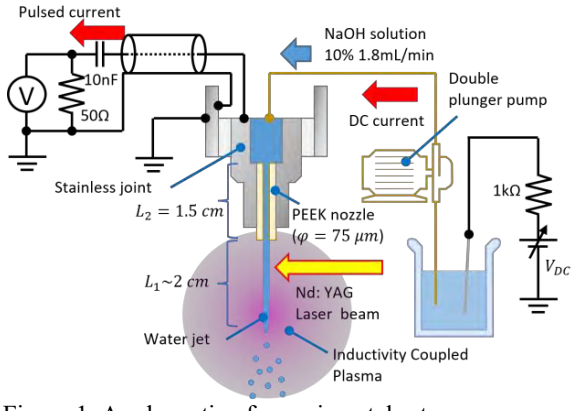

Figure 1. A schematic of experimental setup.

3 Results and Discussion

Figure 2 shows the amplitude of the pulsed current, which represents the quantum yield of laser-induced desolvation, as a function of the rf power. The bias voltage was adjusted between -150 and +150 V. It is noted that the potential of the water jet was lower than the bias voltage in the case of the positive bias due to the voltage drop between the water reservoir and the top of the water jet. Despite the increase in the fluence of electrons and ions irradiated onto the water jet, the quantum yield decreased with the rf power. However, the magnitude of the decrease was dependent on the bias voltage. Since a higher production rate of hydrated electrons is expected at a higher fluence, the decrease in the quantum yield with the rf power may be caused by the greater densities of scavengers for hydrated electrons.

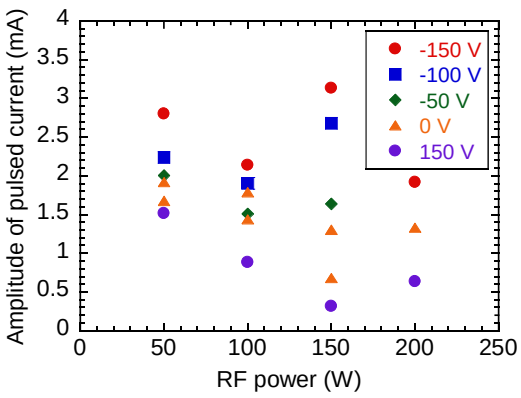

Figure 2. The amplitude of the pulsed current as a function of the rf power at various bias voltages.

References

[1] Y. Inagaki, and K. Sasaki, Plasma Sources Sci. Technol. **31**, 03LT02 (2022)

Electrical potential and luminescence distribution measurements of repetitive surface dielectric barrier discharges in N_2 and O_2 mixture gases

T. Uemura[1], A. Komuro[2], and R. Ono[2]

[1] *Dept. Electrical Engineering, The Univ. Tokyo, Tokyo, Japan*
[2] *Dept. Advanced Energy, The Univ. Tokyo, Tokyo, Japan*

We measured the spatiotemporal variations of electrical potential of surface dielectric barrier discharges in nitrogen and oxygen mixture gas using the Pockels effects. The results show that the geometrical parameters of the surface discharge such as the length and width of the filament change in different oxygen concentration. For the positive half cycle of AC voltage, the positive filaments become thicker and branch less as the oxygen concentration increases. On the other hand, for the negative half cycle, the propagation distance of the negative polarity discharge increases, and the uniformity decreases with decreasing oxygen concentration. In addition, the result shows that the charge distribution differs from the luminescence of the discharge, which indicates that the diffusion rates of the charges are different depending on the charge polarities.

1 Introduction

Dielectric barrier discharge (DBD) has already been used in industrial applications such as surface treatment [1], ozonizers [2], and in recent years there has been much research on airflow control [3]. DBD has a mechanism whereby an external electric field is canceled by the accumulation of charge on the dielectric surfaces between the electrodes when an external electric field is applied, and the discharge is sustained even at atmospheric pressure. In particular, understanding the charge distribution on the dielectric surface is important to reveal the physical characteristics of Surface-DBD (SDBD). In this study, the effect of gases on the potential distribution on the dielectric surface in SDBD at AC voltages was investigated. Nitrogen, oxygen, and synthetic air (nitrogen: oxygen = 4:1) were used, and discharge emission was measured as well as potential distribution.

2 Experimental setup

The Pockels effect [4], a type of optical technique, was used to measure the surface potential. The Pockels device used 1 mm thick BGO crystals, copper tape for the high-voltage electrode, and a transparent conducting (ITO) film for the ground electrode.

3 Results and discussion

When a positive voltage was applied, the potential distribution became clear filaments, but when a negative voltage was applied, the potential distribution became uniform. Since discharge luminescence was also measured almost in agreement with the potential distribution, we believe that the geometric characteristics of the potential distribution due to the difference in polarity can be explained by the different direction of electron movement depending on the polarity of the electrodes. Analysis of the positive polarity filaments showed that they became thicker and less branched with increasing oxygen concentration. Next, the discharge propagation distance for negative polarity increased with increasing nitrogen concentration. As the nitrogen concentration increased, the residual positive charge generated a strong electric field when a negative polarity voltage was applied, and a negative filament-like discharge was observed. As a result, the uniformity of the potential distribution was lost and random geometrical characteristics were noticeable. Finally, at negative polarity, the coincidence between the discharge luminescence and the potential distribution was not as good as at positive polarity, possibly indicating a difference in the diffusion rates due to carriers.

References

[1] Morent R, et al. Surface treatment of a polypropylene film with a nitrogen DBD at medium pressure, *Euro. Phys. J. Appl. Phys.*, **43**, 289-294 (2008).
[2] Jodzis S and Marcel Z, Energy efficiency of an ozone generation process in oxygen. Analysis of a pulsed DBD system, *Vacuum,* **155**, 29-37 (2018).
[3] Uemura T, et al. Flow control around a pitching oscillation circular cylinder using dielectric barrier discharge plasma actuator *J. Phys. D: Appl. Phys.*, **56**, 125202 (2023).
[4] Tanaka D, et al. Two-dimensional potential and charge distributions of positive surface streamer, *J. Phys. D: Appl. Phys.*, **42**, 075204 (2009).

Needle-to-liquid DC and AC dielectric barrier discharges in atmospheric air: electrical characteristics and chemical analysis

L. Alomari[1], T. Orriere[1], C. Batiot-Dupeyrat[2], B. Teychene[2] and E. Moreau[1]

[1] *Institut PPRIME, Université de Poitiers, Poitiers, France*
[2] *Institut de chimie des Milieux et des Matériaux de Poitiers (IC2MP), Université de Poitiers, Poitiers, France*

This abstract presents experimental results on DC and AC dielectric barrier discharges ignited between a high voltage needle and water (gap = 2 mm). The electrical and chemical aspects of these two configurations are investigated, with the aim of optimizing a plasma reactor for wastewater treatment. The chemical diagnosis consists in the addition of a chemical dye (potassium iodide, KI) into the water, allowing the track of the production of reactive species.

1 General

Plasma-liquid interactions have become an increasingly important subject in recent years due to their key role in chemical applications, such as wastewater treatment [1]. Indeed, the production of reactive chemical species can oxidize a large variety of waterborne chemical contaminants. However, improving the quality of a plasma reactor for water purification is actually limited by the good understanding and characterization of all processes occurring at plasma-liquid interface. It's within this context that the contribution of our project fits. The study consists firstly in testing several types of discharges with different electrical, chemical and electrohydrodynamic (EHD) characteristics. We will focus here only on the electrical and chemical aspects of two types of plasma discharges: the DC discharge and the sinusoidal AC dielectric barrier discharge (DBD).

2 Method

In both the DC and DBD configurations, the high voltage electrode is a tungsten needle placed above an optical glass tank, filled with the liquid to be treated (20 mL) with a constant gap of 2 mm. The ground electrode is a platinum ring placed inside the liquid at the bottom of the tank in the DC discharge, and a piece of copper tape symmetrically placed under the tank in the DBD. Potassium iodide (KI) is used as a chemical tracer in the liquid phase. For instance, iodide ions (colorless) are oxidized to iodine (yellow to brown color) in the presence of reactive species [2]. The correlation between the iodine concentration and the in-situ grey levels of the treated solution provide a visual estimation of the plasma efficiency and the mixing degree due to EHD effects.

3 Results and perspectives

Interestingly, in both DC and DBD configurations, several discharge regimes are identified, depending on the value of the input parameters. Let us look for example at the case of a DC discharge (figure 1). In the AB section of the figure, the discharge is localized in a small ionization region around the needle tip. This is the "corona regime". After the gas breakdown phenomenon (point B), ionized channels repeatedly strike out from the high voltage electrode through the gas. We also observe a sudden increase in current and a drop of discharge voltage. This is the "transition regime" (section BC). Finally, from point D a luminous stable glow discharge occupies the entire gap between the tip and the liquid surface, the discharge is then in the "normal glow regime". In the case of the DBD, similar regimes have been observed. Chemical measurements show that the DBD configuration is more efficient in terms of reactive species production associated to lower energy consumption, with an optimal frequency of 1000 Hz in the frequency range from 50 to 4000 Hz.

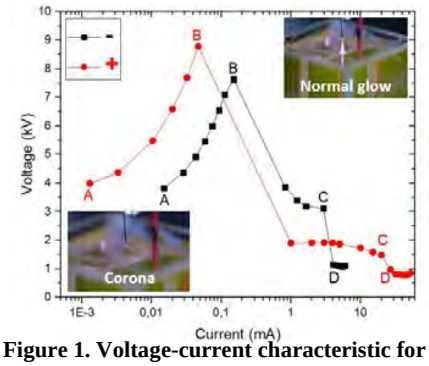

Figure 1. Voltage-current characteristic for negative and positive DC at a gap of 2 mm.

A third type of plasma discharge is currently investigated: the nanosecond-pulsed DBD. Moreover, the EHD flow generated in the liquid phase will also be characterized as it has a major influence on the transportation of reactive species. Results of flow characterization will also be presented during the conference.

4 References

[1] A. Barjasteh *et al.*, Appl. Sci. **11** (2021) 3372.
[2] K. Tachibana and K. Yasuoka, J. Phys. Appl. Phys. **53** (2020) 125203.

Behaviour of interstellar dust analogues under interstellar conditions

R. J. Peláez[1], B. Mate[1], M. Jiménez-Redondo[1,2], R. Carrasco-Herrera[1], D. Iancu[3], M. Straticiuc[3], I.C. Gerber[4], I. Mihaila[4], I. Topala[5], I. Tanarro[1] and V. J. Herrero[1]

[1] *Instituto de Estructura de la Materia (IEM), CSIC, Serrano 121-123, 28006 Madrid, Spain*
[2] *Max Planck Institut für Extraterrestrische Physik, Gießenbachstraße 1, 85748 Garching, Germany*
[3] *Horia Hulubei National Institute for Physics and Nuclear Engineering, Reactorului 30, Magurele, Romania*
[4] *Integrated Center of Environmental Science Studies in the North-Eastern Development Region (CERNESIM), Alexandru Ioan Cuza University of Iasi, Carol I 11, 700506 - Iasi, Romania*
[5] *Faculty of Physics, Alexandru Ioan Cuza University of Iasi, Blvd. Carol I, No. 11, 700506 - Iasi, Romania*

In this work, we present selected results from recent years that focus on the astrophysical properties of carbonaceous interstellar dust analogues produced in the cold plasma lab at IEM-CSIC. We produce thin film deposits or porous structures. In both cases, we have experimentally simulated the effects of Cosmic Rays and interstellar UV field energetic processing. Additionally, we have analysed the desorption energy of volatiles on the dust analogues, and we have estimated their active surface.

1 Introduction

Since the discovery of the 3.4 μm IR band in the diffuse interstellar medium, several materials have been proposed as possible carriers of this band. Among these materials, hydrogenated amorphous carbon (HAC) has been found to be the most likely candidate. Cold plasmas are well-suited for producing this type of material in the laboratory [1].

2 Carbonaceous production by plasmas

We employ RF discharges to produce HAC analogues of interstellar dust, using light hydrocarbons mixed with other buffer gases as precursors [2,3]. Different diagnostic techniques (MS, OES, light scattering, Langmuir probe…) allow us to characterize the plasmas in situ, and the deposits are analysed ex situ by FTIR and SEM. We have the capability to generate deposits in thin films (inductively coupled plasmas with CH_4-He mixtures [2]) or produce porous structures (capacitively coupled plasmas with C_2H_2-Ar mixtures [3]). The C:H ratio and, above all, the volume density of the two carbonaceous analogues, change significantly.

3 Interstellar conditions

3.1 Cosmic rays

Destruction rates of the 3.4 μm band are estimated under UV, high energy ions and keV e^- irradiation that simulate the effects of interstellar UV field or cosmic rays.

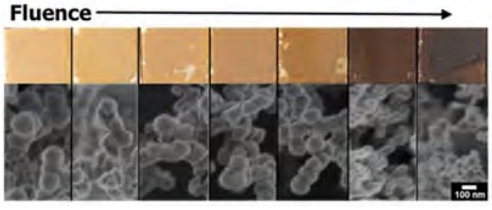

Color and morphology variation of dust under 1 MeV C^+ ion irradiation at different fluences. ($0 \rightarrow 10^{15}$ ions/cm^2).

In the case of ion irradiation, the Tandetron 3 MV Accelerator facility in Bucharest is used [4]; while a high-vacuum low-temperature chamber in the ice laboratory at IEM_CSIC is used for electron and UV irradiations [5]. In both cases, the intensity of the 3.4 μm band decreases with fluency. The effect of energetic processing as a function of the sample's porosity/density is currently under research.

3.2 Binding energies and specific surface area

The interaction of volatile species such as N_2, CO, CH_4, and CO_2 with HAC is highly relevant in the dense clouds of the interstellar medium. In our laboratory, the desorption energies of these molecules deposited on HAC at cryogenic temperatures is investigated using thermal programmed desorption (TDP) [5]. The results suggest that the interaction of volatiles with the aromatic substructure of HAC is stronger than that with the aliphatic part.

Finally, the effective surface areas of these highly porous materials are studied by depositing on them a varying number of CO monolayers at 20 K and analysing the spectra by grazing-angle reflection absorption infrared spectroscopy (RAIRS).

4. Acknowledgements

This work has been funded by the MCIN of Spain under grant PID2020-113084GB.

References

[1] Herrero V J et al Front. Astron. Space Sci. **9**:1083288, (2022).
[2] Peláez, R. J., et al. PSST **27**, 035007 (2018).
[3] Jiménez-Redondo, M., et al. J. Phys. Chem. A. **123**, 8135–8147 (2019).
[4] Burducea I, et al. Nucl Instrum Methods Phys Res B. **359:**12 (2015).
[5] B. Maté et al. MNRAS **490** 2936 (2019).

Photodetachtment experiments on Plasma Confined Micro-Particles

G.B. Klaassen[1], P.P.M. Blom[2] and J. Beckers[1]

[1] *Dept. Applied Physics, Eindhoven Univ. Techn., Eindhoven, The Netherlands*
[2] *VDL Enabling Technologies Group B.V, Eindhoven, The Netherlands*

We propose a set of experiments utilizing the detachment of plasma charge accumulated by a micro-particle confined in the plasma sheath, by exposure to a UV light source. By measuring the changes in the height of the micro-particle above the electrode and by obtaining natural frequency of the particle-plasma system, certain properties such as particle charge and the electric field profile are expected to be determinable.

1 Introduction

Micrometer sized particles exposed to a plasma accumulate a negative charge due to the higher mobility of electrons compared to that of ions. Because of this charge, the particles can be confined in the plasma which has a higher electrical potential than its surroundings. Especially in the plasma sheath region, micro-particles can be used as electrostatic probes to measure properties which are unobtainable with traditional measurement techniques.

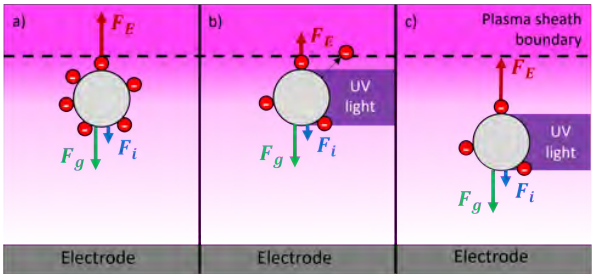

Figure 1: Figure 1.a depicts a representation of a micro-particle with attached electrons, confined in the plasma sheath by a balance between the electrostatic force F_E, gravity F_g and the ion-drag force F_i. When UV light interacts with the particle (figure 1.b), some of the electrons are detached and the electrostatic force, which is the product of the charge and the electric field, decreases. This results in a net force towards the electrode. The position of the particle changes until the forces reach a new equilibrium (figure 1.c).

2 Photodetachment on micro-particles

In this work we propose a set of experiments in which the charge accumulated on a micro-particle is partially removed using ultra violet (UV) light. The micro-particle will be confined a certain height above the electrode where the electrostatic force balances the gravity and ion drag force. When the magnitude of the charge of the particle is decreased with exposure to UV light, the magnitude of the electrostatic force (the product of the particle charge and the local electric field) decreases accordingly. This will disturb the force balance and the particle is expected to change its position until a new equilibrium in the forces is achieved at a new position closer to the electrode, where the electric field is stronger. This idea is depicted in figure 1.

3 Proposed experiments

In this work we propose two experiments using the principle of photodetachment of electrons from a micro-particle confined in the plasma sheath.

Particle oscillation: When exposed to UV light, the height of the particle above the electrode will change. As long as this displacement is relatively small, compared to the size of the sheath (typical $1 - 10mm$), the particle is expected to return to its original position once the UV light is turned off as the charge returns to its initial value. By pulsing the UV light, the particle is expected to oscillate between these positions. These oscillations are dependent on the pulse frequency, from which a natural frequency of the particle can be derived. This natural frequency relates to the charge of the particle, which is otherwise difficult to obtain without altering the plasma.

Electric field profile: The relation between the intensity of the UV light and the number of detached electrons is linear as long as a small portion of the initial electrons remain. By incrementally increasing the intensity of the UV light in this linear regime, and measuring the height of the particle at each step, the relative strength of the electric field can be determined at each position. Combined with the charge of the particle determined from the particle oscillation, quantitative results of the electric field in the plasma sheath can be obtained.

First Mirror cleaning in ITER Edge Thomson Scattering diagnostic system using 40.68-MHz discharge in hydrogen

C. Rijnsent[1], C. Meekes[1], M. van Putten[1], J. van Veldhoven[1], E. Yatsuka[2], M. Yokoyama[2], L. Moser[3], M. Bassan[3], E. van Beekum[1], A. Ushakov[1] and T. Hatae[2]

[1] *TNO, Stieltjesweg 1 2628 CK, Delft, Netherlands*
[2] *National Institutes for Quantum Science and Technology, 801-1 Mukoyama, Naka, Ibaraki, Japan*
[2] *ITER Organization, Route de Vinon-sur-Verdon, CS 90 046, 13067 St. Paul Lez Durance Cedex, France*

ITER optical diagnostics for advanced machine control use first mirrors (FM). Contaminants as thick as 5-10 nm produced during operation may distort optical signals. FM performance is maintained by periodic cleaning in radio-frequency plasma. Ion physical sputtering of W may introduce damage to mirrors, thus H_2-plasma is studied considering physical and chemical effects at lower power and lower ion energies. Sputtering of W/W-oxide films at the rate of 3-8 nm/h is confirmed in a set of exposures. X-ray photoelectron spectroscopy shows changes in tungsten concentration and in oxidation state of films. Films' properties and cleaning mechanisms in hydrogen plasma are discussed.

1 Introduction

Optical diagnostic systems of the ITER tokamak use first metal mirrors (FM) to collect optical signals. FMs are expected to be contaminated during tokamak operation with the First Wall, Divertor and construction materials. The ITER Edge Thomson scattering (ETS) diagnostic uses relatively large FMs [1]. To restore their performance, mirror cleaning based in a 40.68 MHz discharge is foreseen. Among the contaminants, W is difficult to clean due to its high atomic mass. Physical sputtering in plasma produced in inert gas clean W/W-oxides [2-3]. However, the risk of simultaneous damage to the FM and the construction components increases. This work considers cleaning of W in H_2-plasma in the ETS FM prototyping setup (Fig. 1) [3], where power in plasma and ion fluxes on the FM vary. For cleaning tests at 5 Pa, ions with the energies of 170-200 eV and fluxes of $5 \cdot 10^{18}$ ions$\cdot m^{-2} \cdot s^{-1}$ were produced.

2 Experiments

Sputtered samples were installed on the FM surface (the inset of Fig. 1) having a 20-nm-thick layer of W/W-oxide on top of a 200-nm-thick Mo-layer. Ion energies/currents were controlled by a Retarding Field Ion Energy Analyzer. X-ray Photo-electron Spectroscopy measured samples' compositions before and after the tests to understand variations of C, O, W and Mo. It showed that O and W concentrations reduce with time. The 20-nm-thick W-layer was cleaned within 3 hours. Variation of components (WC, WO_3, W-metal) with exposure duration was also studied. WO_3 reduction may be assumed during W-metal removal. The sputtering rate was estimated in the range of 3-8 nm/h using optical interferometry in 6-8 locations on the FM (Fig.2). Ways to improve sputtering uniformity are discussed.

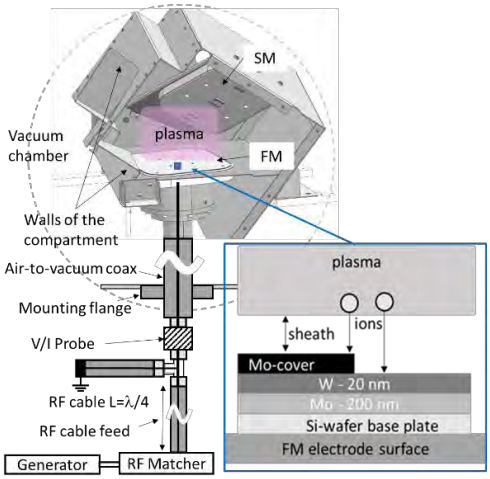

Fig. 1. Experimental setup prototyping ETS FM compartment and the sample composition (inset).

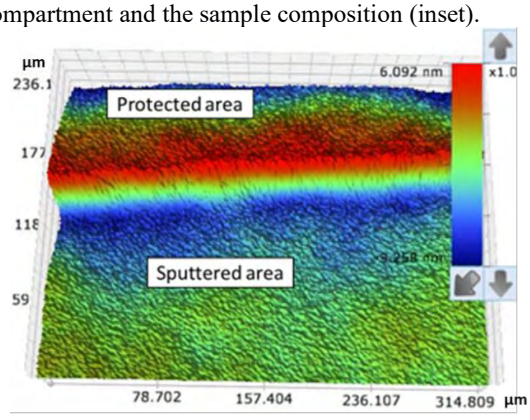

Fig. 2. Interferometry picture of the step between the sputtered/non-sputtered parts of the W-coating after the exposure in H_2-plasma.

3 References

[1] Bassan M et al J. Instrumentation **11** C01052 (2016)
[2] Dmitriev A et al Fusion Eng. Des. **146** 1390 (2019)
[3] Ushakov A et al Phys. Scr. **98** 015604 (2023)

Sputter deposition of low resistive 30-nm-thick ZnO:Al films using ZnO seed layers grown via solid-phase crystallization

Yoshiharu Wada[1], Zhiyuan Shen[1], Hisato Yabuta[1], Naoto Yamashita[1], Takamasa Okumura[1], Kunihiro Kamataki[1], Haruki Kiyama[1], Kazunori Koga[1,2], Masaharu Shiratani[1], and Naho Itagaki[1]

[1] *Graduate School of Information Science and Electrical Engineering, Kyushu University, Fukuoka, Japan*
[2] *National Institutes of Natural Science, Tokyo, Japan*

ZnO seed layers have been synthesized by sputter deposition of ZnON films in Ar/N_2 atmosphere followed by air annealing, which enable us to grow highly conducting transparent ZnO:Al films. We found that the amount of N atoms incorporated into films governs the degree of crystallization of the ZnON films and eventually affect both the crystal quality and electrical properties of the subsequently grown ZnO:Al films. Using the seed layers grown via annealing of fractionally crystallized ZnON films, ZnO:Al films with significantly low resistivity of 4.7×10^{-4} Ω·cm are obtained even when the thickness is small of 30 nm.

1. Introduction

ZnO:Al films are promising alternatives to In_2O_3:Sn (ITO) transparent electrodes because of the wide band gap (3.4 eV), the high doping efficiencies, and the material abundance. The resistivities of ZnO:Al films, however, are higher than that of ITO one, especially when the thickness is less than 100 nm, limiting their use in displays where sufficiently high transparency to the human eye is required. Recently, we have developed novel seed layers fabricated via solid phase crystallizaiton (SPC), the ZnO:Al resistivity on which are significantly low of the order of 10^{-4} Ω·cm [1,2]. SPC is known to be a powerful method to achieve high crystal quality because crystal growth proceeds under thermal equilibrium conditions. Though this method was hardly applicable to ZnO due to the difficulty in forming the amorphous phase, we have realized it by making ZnO incorporate N atoms during sputtering deposition in Ar/N_2 atmosphere where the non-equilibrium nature rather works well for the amorphization. Here, aiming to further reduce the resistivity of ZnO:Al films, we synthesize new seed layers prepared via solid phase crystallization of not amorphous (a-) but fractionally crystallized (fc-) ZnON films. They are expected to lead to higher crystal quality since the crystal nucleation and the subsequent growth are controlled independently during the crystal growth.

2. Experimental

First, 10-nm-thick seed layers were prepared on quartz glass substrates by sputtering deposition of ZnON in Ar/N_2 at room temperature, followed by air annealing at 400–600°C for 3 hours. Then 30-nm-thick ZnO:Al films were deposited by sputtering on the seed layers in Ar at 200°C.

3. Results and discussion

Figure 1 shows atomic force microscope (AFM) images of the seed layers grown from fc- and a-ZnON films. Here the degree of ZnON crystallinity was controlled by controlling the amount of N atoms incorporated into the films. The seed layers grown from fc-ZnON has more uniform grain sizes, attributed to the shorter period of nucleation occurring. In fact, we observed the activation energy of crystal growth during SPC of fc-ZnON is about the half of that of a-ZnON, indicating that no nucleation occurred and crystals just grew originating from nuclei embedded in the fc-ZnON during SPC. Using such seed layers, we successfully obtained 30-nn-thick ZnO:Al films with the resistivity of 4.7×10^{-4} Ω·cm, much lower than that without seed layers (12.5×10^{-4} Ω·cm) and even lower than that with seed layers prepared from a-ZnON films (8.3×10^{-4} Ω·cm). This improvement was brought about by the improved crystal quality of ZnO:Al films on the seed layers (Fig. 2).

This work was supported by JSPS KAKENHI Grant Numbers JP21H01372, JP21K18731, and JP22H05000.

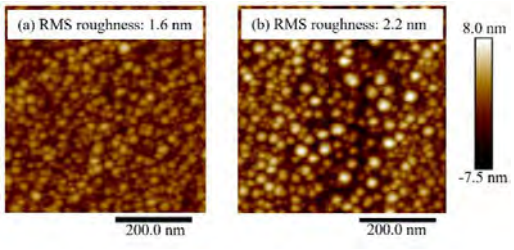

Fig. 1. AFM images of seed layers prepared through SPC of fc-ZnON (a) and a-ZnON (b) films.

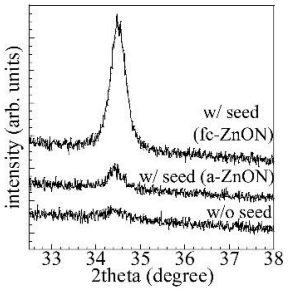

Fig. 2. XRD spectra of ZnO:Al films on seed layers.

[1] N. Itagaki et. al., Appl. Phys. Express 4, 011101 (2011).
[2] I. Suhariadi et. al., ACS Appl. Nano Mater. 3, 2480 (2020).

Pseudomorphic growth of $(ZnO)_x(InN)_{1-x}$ films on ZnO substrates by magnetron sputtering using $Ar/N_2/O_2$ discharges

R. Narishige[1], Y. Nakano[1], N. Yamashita[1], K. Kamataki[1], T. Okumura[1], H. Kiyama[1], K. Koga[1,2], M. Shiratani[1], H. Yabuta[1], and N. Itagaki[1]

[1] *Graduate School of Information Science and Electrical Engineering, Kyushu University, Fukuoka, Japan*
[2] *National Institutes of Natural Science, Tokyo, Japan*

$(ZnO)_x(InN)_{1-x}$ (hereafter ZION) films have been epitaxially grown on 0.9%-lattice mismatched ZnO substrates at room temperature to 450°C by magnetron sputtering, where the chemical compositions are tailored using $Ar/N_2/O_2$ discharges. We observed a change in growth mode from Volmer-Weber (VW) to Stranski-Krastanov (SK) one with an increase of substrate temperature and pseudomorphic growth of the films on the substrate below 150°C. Atomically-flat films showing significantly small full-width at half maximum of x-ray rocking curve (0.07°) have been successfully grown at the critical temperature of 150°C, where secondary nucleation due to both In-N dissociation and insufficient adatom migration is suppressed.

1. Introduction

We have developed novel semiconductors, $(ZnO)_x(InN)_{1-x}$ (hereafter ZION), the tuneable band gaps (1.5–3.4 eV) and the high exciton binding energies (30–60 meV) of which make them promising materials for optoelectronic devices [1]. A major challenge for this system is to achieve high crystal quality avoiding thermal dissociation of In-N bond that generally occurs above 550°C. Recently, we have succeeded to grow epitaxial ZION films by magnetron sputtering on ZnO substrates at 450°C through precise control of O and N atomic fluxes to the substrates, the densities of which in the plasma were measured by vacuum ultraviolet absorption spectroscopy [2, 3]. They actually show high crystal quality but at the same time have polycrystalline structures and large root-mean-square roughness (R_q) around 4 nm, probably due to still somewhat high temperature that causes In segregation and thus secondary nucleation. Here, we demonstrate growth of atomically flat ZION films at precisely controlled temperature where we suppress bond dissociation leading to In segregation while keeping sufficient migration of surface adatoms.

2. Experimental

ZION films were deposited on 0.9%-lattice mismatched ZnO substrates by radio-frequency magnetron sputtering in $Ar/N_2/O_2$ atmosphere of 0.50 Pa. ZnO and In targets were used. The substrate temperature (T_s) was room temperature (RT) to 450°C.

3. Results and discussion

Figure 1 shows atomic force microscope (AFM) images and (002) plane x-ray rocking curves (XRC) of ZION films on O-polar substrates. We observed significantly smoother surfaces, smaller full width at half maximum (FWHM) of XRC, and lower diffraction angles of the films deposited below 150°C, all of which indicate two-dimensional (2D) pseudomorhic growth, that is, SK growth of ZION films. At 450°C, on the other hand, films grow in 3D mode from the initial stages (VW mode), which is because In-N dissociation and thus secondary nucleation occur even at 450°C being supplied an additional thermal energy from plasma. We also found that at RT, XRC shows a low-intense but broad peak of FWHM = 0.3° other than the sharp peak. The broad one presumably reflects 3D islands originated from secondary nuclei, where insufficient adatom migration leads to the secondary nucleation. In conclusion, pseudomorphic growth of ZION with atomically flat surfaces and small XRC-FWHM of 0.07° have been successfully grown at 150°C, where secondary nucleation due to both In-N dissociation and insufficient adatom migration is suppressed.

This work was supported by JSPS KAKENHI Grant Numbers JP21H01372, JP21K18731, and JP22H05000.

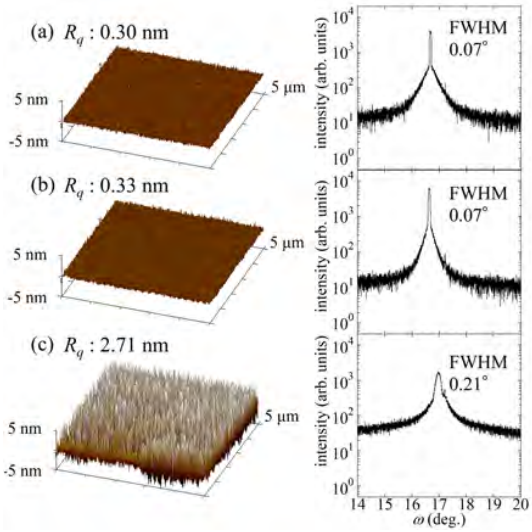

Fig. 1. AFM images and (002) XRC of ZION films fabricated at T_s = RT (a), T_s = 150°C (b), T_s = 450°C (c).

[1] N. Itagaki, et al., Mater. Res. Express, 1, 36405 (2014).
[2] R. Narishige et al., Jpn. J. Appl. Phys., 60, SAAB02 (2021).
[3] K. Matsushima et al., IEEE Trans. Plasma Sci. 45, 323 (2017).

Sputter epitaxy of $Zn_{1-x}Mg_xO$ films on lattice-mismatched sapphire substrates utilizing ZnO(N)/MgO buffer layers fabricated by Ar/N_2 and Ar/O_2 discharges

T. Yunoue[1], K. Yataka[1], N. Yamashita[1], D. Yamashita[1], T. Okumura[1], K. Kamataki[1], H. Kiyama[1], K. Koga[1, 2], M. Shiratani[1], H. Yabuta[1], N. Itagaki[1]

[1] *Graduate School of Information Science and Electrical Engineering, Kyushu University*
[2] *National Institutes of Natural Sciences*

We have synthesized new buffer layers using Ar/N_2 and Ar/O_2 discharges, ZnO(N)/MgO, which allow us to grow high-quality epitaxial $Zn_{1-x}Mg_xO$ films even on 18%-lattice mismatched sapphire substrates. The crystal quality of ZnO(N) layers is drastically improved on O-polar MgO layers, where the polarity is controlled by both the MgO layer thickness and O_2 flow rate ratio during the sputtering deposition. The smallest full-width at half maximum of (002)-plane x-ray rocking curve of the ZnO(N) layers is 0.03°, about an order of magnitude smaller than that of ZnO(N) layers on MgO layers with non-controlled polarity.

1. Introduction

$Zn_{1-x}Mg_xO$ have attracted attention as materials for optoelectronic devices due to the wide band gaps (3.3–4.5 eV) and the large exciton binding energies (60–99 meV). Recently, we have succeeded to grow single crystalline $Zn_{1-x}Mg_xO$ films on cost-effective but 18%-lattice mismatched sapphire substrates using ZnO(N) buffer layers [1,2]. The latter are synthesized using Ar/N_2 sputtering, where surface adsorption-desorption behaviours of N atoms are controlled to make the buffers have relaxed three-dimensional (3D) ZnO islands. On the buffers, 3D $Zn_{1-x}Mg_xO$ islands first grow, and they finally coalesce to form 2D single crystalline layers in Ar/O_2 sputtering atmosphere. Here, aiming to further improve the crystal quality of $Zn_{1-x}Mg_xO$ films, we synthesize new buffer layers, ZnO(N)/MgO, where MgO layers are deposited prior to the ZnO(N) layers. Since the surface migration of cation atoms during film growth is enhanced on O-polar surfaces of wurtzite materials, and the polarity can be controlled by inserting a-few-nm-thick MgO layers between the materials and sapphires [3], the combination of lattice-relaxed ZnO(N) layers and polarity-controlled MgO layer is expected to bring about $Zn_{1-x}Mg_xO$ films with unprecedented high crystal quality.

2. Experimental

All layers were deposited by radio frequency magnetron sputtering. First, MgO layers with the thickness (d_{MgO}) of 1–5 nm were deposited on c-plane sapphire substrates at 800ºC in Ar/O_2 of 0.70 Pa. Next, 270–570-nm-thick ZnO(N) layers were deposited on the MgO layers at 780ºC in N_2/Ar of 0.35 Pa.

3. Results and discussion

Figure 1 shows the x-ray rocking curves (XRC) of the wurtzite (002) plane of the ZnO(N) layers. We found that inserting MgO layers of d_{MgO}=1–2 nm leads to drastic improvements in the out-of-plane alignment of ZnO(N) layers. This is probably because the MgO layers provides O-polar surfaces, enhancing the migration of cation atoms during the film growth and thus suppressing defect formation. On MgO layers of $d_{MgO} \geq 3$ nm, however, ZnO(N) layers show large full width at half maximum of the XRC, which are almost same as that of ZnO(N) films directly deposited on sapphires. This deterioration observed at large d_{MgO} is attributed to the phase transition of MgO from wurtzite to rocksalt and thus to polarity change from O- to cation-polar surfaces. Effects of ZnO(N)/MgO layers as well as O_2 flow rate ratio during MgO deposition on $Zn_{1-x}Mg_xO$ film quality will be reported at the conference.

This work was supported by JSPS KAKENHI JP21H01372, JP21K18731, and JP22H05000.

[1] N. Itagaki, et al., *Sci. Rep.*, **10**, 4669, 2020.
[2] D. Takahashi, et al., *MRS Adv.*, **7**, 415–419, 2022.
[3] H. Kato, et al., *Appl. Phys. Lett.*, **84**, 4562, 2004.

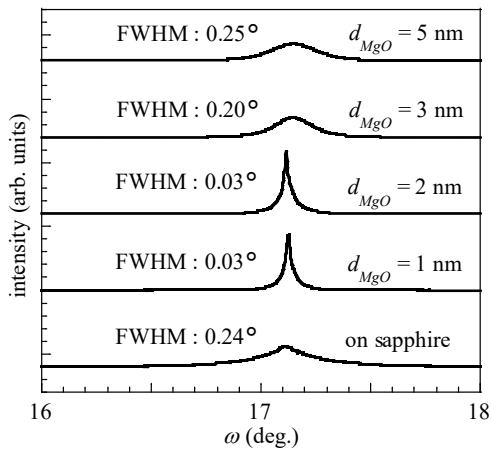

Fig. 1. XRC of (002) plane ZnO(N) buffer layers fabricated on MgO layers with various thickness.

Atomic layer etching of SiN films with CF_4/H_2 surface modification and H_2/N_2 plasma exposure

Shih-Nan Hsiao[1], Makoto Sekine[1] and Masaru Hori[1]

[1]*Center for Low-temperature Plasma Sciences, Nagoya Univ., Nagoya, Japan*

Cyclic atomic layer etching of SiN with high selectivity to SiO_2 using a CF_4/H_2 surface modification followed by exposure to H_2/N_2 plasma is presented. To understand the surface reactions and etching mechanism that occurred during the process, *in situ* attenuated total reflectance Fourier transformation infrared spectroscopy (ATR-FTIR) and spectroscopic ellipsometry (SE) were used. In the modification step, the hydrofluorocarbon film was deposited on top of the SiN films by the CF_4/H_2 plasma with an H_2 concentration of 85 %. Subsequently, the modification layer was removed by exposure to the H_2/N_2 plasma. The etch amount per cycle of the SiN can be controlled by the composition of the feeding gas in the etching step. The hydrogen-rich layer was formed not only during CF_4/H_2 surface modification but also in the etching step. On the other hand, the high N_2 content resulted in the reconfiguration of hydrogen that is already present in the SiN film and led to a decrease of etch amount of SiN. Furthermore, the selectivity of SiN against SiO_2 can be manipulated by varying the composition of the H_2/N_2 plasma in the etching step.

1 Introduction

The miniaturization of electronic devices requires the development of novel nanofabrication techniques with high precision and low damage in the semiconductor industries. Atomic layer etching (ALE) is a promising approach that allows for accurate and well-controlled removal of thin films in nanoscale. ALE has been widely studied for several materials, including Si related materials, oxides, nitride, etc [1]. In this work, we present an approach for the ALE of SiN with high selectivity to SiO_2 using hydrofluorocarbon deposition and H_2/N_2 plasma exposure. The relationship between etch amount per cycle (EPC) and surface reactions during the process is also discussed based on the results of surface structure and film thickness variations using *in-situ* monitoring techniques.

2 Experimental

The reactor used for ALE is equipped with a capacitively coupled plasma on top electrode with a frequency of 100 MHz. The SiN and SiO_2 films, prepared by plasma-enhanced chemical vapor deposition, were used in this work. In the surface modification step, a mixture of CF_4 and H_2 gases with H_2 concentration of 85 % was used. In the etching step, H_2 or a mixture of H_2 and N_2 with different ratios were used. The surface structure and thickness variation during etching were monitored with in situ ATR-FTIR and SE.

3 Results and summary

Figure 1 shows the real time thickness change of the SiN and SiO_2 films exposure to H_2 plasma, after the surface modification (deposition) by CF_4/H_2 plasma. The horizontal and vertical dash line indicate the thickness before deposition half-cycle and time duration for the films exposure to the H_2 plasma. Note that the absolute thickness after surface modification is meaningless due to a single layer, i.e., SiO_2 or SiN optical model was used to estimate total thickness of the films. As observed, the self-limiting etch reactions with an EPC of 3.6 nm/cycle for SiN and 0.4 nm/cycle for SiO_2 were achieved. The hydrogen-rich layer was formed not only in the surface modification step but also in the initial stage of the etching step with pure H_2 plasma. On the contrary, the high N_2 additives resulted in the reconfiguration of hydrogen, which is already present in the SiN. The reconfiguration of surface structure affects the layer formation in the following step, i.e., etching. This is also associated with the observed EPC which depends on the composition of H_2/N_2 plasma in the etching step.

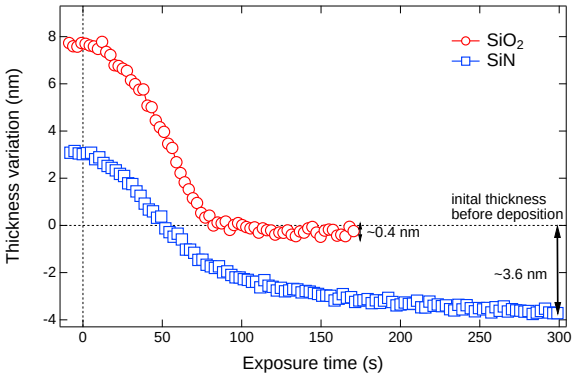

Figure 1. Real time thickness variation of SiN and SiO_2 as a function of H_2 plasma exposure using *in situ* SE.

References

[1] Kanarik, K. J. *et al*., *J. Phys. Chem. Lett*., **9**, 4814 (2018)

Temperature-friendly remote atmospheric pressure plasma source for plasma activation of materials

J. Feng, R. Krumpolec, A. Jamaati Kenari, L. Zahedi, S. Sihelník, M. Stupavská, M. Černák, D. Kováčik

Department of Physical Electronics, CEPLANT—R&D Center for Plasma and Nanotechnology Surface Modifications, Faculty of Science, Masaryk University, Kotlářská 2, 611 37 Brno, Czech Republic

A novel temperature-friendly remote atmospheric pressure plasma source based on diffuse coplanar surface barrier discharge (DCSBD) technology is reported and used for surface activation of polymer materials, in particular rough ionoplast used as an interlayer for production of high-performance laminated safety glass. The presented remote plasma source is capable to generate plasma plume in ambient air and N_2 environments when using N_2 as the working gas was used. The discharge characteristics of the DCSBD-based remote plasma source was studied for various parameters such as power input, gas flow rate, and discharge electrode geometry. As measured, the temperature load of this new plasma system is significantly less than of similar plasma devices. The results of plasma surface modification of model-like ionoplast interlayer show its effectivity and potential for effective activation and adhesion improvement of rough and structured surfaces and even temperature sensitive materials.

Plasma surface modifications play important role in modern technologies for surface processing of materials. Low-cost, chemical free, fast-throughput and effective scalable plasma technologies working at atmospheric pressure are preferred by industry.

Diffuse coplanar surface barrier discharge (DCSBD) technology has been widely used in glass activation, polymer and textiles modification, as well as for treatment of e.g., seeds and plants.

High power density, plasma uniformity, robustness and virtually unlimited lifetime of the electrode system and capability to generate scalable atmospheric pressure plasma in all technically important gases make DCSBD very versatile technology for large area plasma surface modification of materials.

DCSBD generates atmospheric plasma of high-power density of ~ 100 W.cm-3 due to the fact that it is generated as a thin film of plasma of effective thickness ~ 0.3 mm. This makes DCSBD very effective source for plasma surface modification of flat sheets and flexible foils/textiles. Considering the limited active distance of the plasma, the conventional DCSBD system is not suitable for the modification of materials with rough and structured surface [1-3]. Therefore, plasma sources generating remote afterglow plasma are more suitable for such surface. Commercially available plasma systems generating atmospheric plasma are however highly localized (plasma jets) or generate highly nonuniform plasma not suitable for temperature sensitive materials (gliding arc).

Therefore, based on DCSBD technology a new source of atmospheric remote plasma especially suitable for treatment of rough, curved and structured surfaces was designed for effective plasma modification at effective treatment distance 1-20 mm.

This new DCSBD-based system suitable for remote plasma surface modification was studied for plasma activation and adhesion improvement of ionoplast polymer interlayer used as model like material. Such material with rough surface is used for production of high-performance laminated safety glass products.

As observed, the adhesion and surface wettability of plasma-modified ionoplast interlayer surface was significantly improved after short plasma treatment time of 5 seconds.

The results show that the plasma generated by the remote plasma source put very low thermal load on the sample – material surface temperature is less than 55 degC even for long treatment times. Basic comparison between the new source of remote plasma and conventional surface DCSBD plasma as well as similar commercial plasma systems generating remote plasma was done and will be presented.

References

[1] Pei X. K., *et al,* Discharge modes of atmospheric pressure DC plasma jets operated with air or nitrogen. J. Phys. D: Appl. Phys. **51**, 3384001 (2018).

[2] Talviste, R., *et al,* Effect of DCSBD plasma treatment on surface properties of thermally modified wood. Surf. Interfaces **16**, 8 (2019).

[3] Černák, M., *et al,* Generation of a high-density highly non-equilibrium air plasma for high-speed large-area flat surface processing. Plasma Phys. Control. Fusion **53**, 124031 (2011).

Nonthermal plasma impact on NaCMC/glauconite suspension properties

E. Grządka[1], E. Godek[1], U. Maciołek[1], G. Słowik[1],
M. Kwiatkowski[2], P. Terebun[2], D. Zarzeczny[2], J. Pawłat[2]

[1] *Faculty of Chemistry, Institute of Chemical Sciences, Maria Curie-Skłodowska University, Poland*
[2] *Institute of Electrical Engineering and Electrotechnologies, Lublin University of Technology,Poland*

In this study, atmospheric pressure plasma generated in a glidearc reactor was used to enhance colloidal suspensions' stability and to explore mechanisms taking place at the interface, changes in chemical bonding, surface texture and composition. A clay mineral (glauconite, GT) and polysaccharide-based polymer (sodium salt of carboxymethyl cellulose, NaCMC) were used as substrate materials.
Reactive species generated in plasma caused oxidation of GT surface and decrease in the volume of pores. Interaction of -OH groups from GT surface with the carboxylate ion of NaCMC took place.

1 Introduction

Presently, many cosmetic and pharmaceutical formulations utilize natural mineral clays. These materials have been known for many years for their versatility and stabilization properties while used in multiphase dispersed systems. Besides cosmetology-oriented properties such as cleansing, exfoliating, nourishing, pigmenting, etc.; they can enhance organoleptic properties of the products. Many unique properties of clays are related to the electric charges present on the particles' surface. In cosmetic applications clays are often combined with other non-toxic, natural compounds: polysaccharides, forming colloidal suspensions. The goal of this work was to enhance adsorptive properties and stability of polymer/solid suspensions, which are ones of the key issues in cosmetic products by means of non equilibrium plasma.

2. Experimental set-up and results

Glidearc reactor (GAD) [1] with two copper electrodes (f=50 Hz, 230 V RMS voltage (primary windings), 3,72 kV maximum. voltage (secondary windings)) utilized air (440 L/h) as a substrate gas. (GT: $(K,Na,Ca)(Fe,Al,Mg)_2[(OH)_2/(Al,Si)_4O_{10}] \times nH_2O$, glauconite) of natural origin [1] and NaCMC (sodium salt of carboxymethyl ether of cellulose) were used as adsorbent and adsorbate, respectively.
Samples made of GT with and without addition of NaCMC in different concentrations (50-500 ppm) were placed in a glass container and treated with GAD for 10 minutes while stirred. The highest temperature of samples after plasma treatment did not exceed 36°C. The effect of GAD treatment on stability of the aqueous GT and GT/NaCMC suspensions (Fig.1) was investigated using Shimadzu UV-2600 UV–Vis spectrophotometer at 500 nm wavelength for 16 h. For the aqueous GT suspensions without the polymer, the changes are noticeable but rather insignificant. For the adsorbent/adsorbate system, plasma increased NaCMC adsorption on the glauconite surface and improved the stability via the electrosteric stabilization. Microscopic analyses depicted changes in surface structure with larger diameters but smaller volumes pores after plasma treatment.

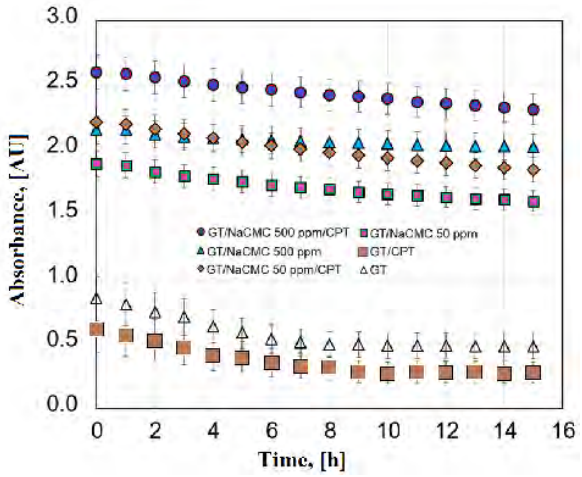

Fig. 1. Non thermal plasma impact on stability of the GT and GT/NaCMC suspensions, pH=6.5-7.

References

[1] Pawłat, J., Terebun, P., Kwiatkowski, M. Tarabová, B., Kovalová, Z., Kučerová, K., Machala, Z., Janda, M., Hensel K. Evaluation of Oxidative Species in Gaseous and Liquid Phase Generated by Mini-Gliding Arc Discharge. Plasma Chem Plasma Process. **39**, 627–642 (2019).
[2] Godek, E., Grządka, E., Maciołek, U., Bastrzyk, A. Influence of zwitterionic CAPB on flocculation of the aqueous cationic guar gum/glauconite suspensions at various pH. Int. J. Mol. Sci. **22**, 12157 (2021).

Relation between Spatial Distribution of Optical Emission Intensity and SiO_2 Film Property in TEOS-PECVD

Y. Yamamoto[1], I. Nagao[1], A. Yamamoto[1], K. Kamataki[1], D. Yamashita[1], T. Okumura[1], N. Yamashita[1], N. Itagaki[1], K. Koga[1,2], and M. Shiratani[1]

[1] *Graduate School and Faculty of Information Science and Electrical Engineering, Kyushu Univ. Japan*
[2] *National Institutes of Natural Science, Japan*

We investigated the relation of information from spatial distribution of optical emission intensity of TEOS plasma and film properties of silicon dioxide (SiO_2) which were fabricated by plasma-enhanced chemical vapor deposition (PECVD). These results showed that there was a good agreement between the gradient of Hα emission intensity and the deposition rate. These information by in-situ measurement were used to estimate the contribution of precursor for SiO_2 deposition.

1. Introduction

The semiconductor front-end manufactures must have superb efficient analytical methodologies and tools to analyse process parameters, plasma parameters and product quality efficiently and rapidly. However, many process parameters (e.g. gas flow, rf power, gas pressure etc.) determine the various plasma parameters (e.g. electron density, its temperature, ion energy distribution function etc.), which in turn determine the thin film quality. Therefore, determining the optimum process parameters to achieve the desired film properties is very costly. In this study, we have proposed a method to predict some film qualities of silicon dioxide (SiO_2) from information of plasma emission distribution in the plasma enhanced chemical vapor deposition (PECVD) using TEOS/O_2/Ar plasma.

2. Experimental

The experiments were performed using the parallel-plate capacitively coupled rf discharge reactor [1]. The discharge frequency was 13.56 MHz and the power was 40W. For obtain information of plasma parameters, we measured emission intensity profiles of Hα (656.4 nm) by a high-speed camera (Photron, Mini-100) with interference filters. We investigated the dependence of deposition rate of SiO_2 film and Hα emission intensity distribution between electrodes on oxygen flow rate. Here, the flow rates of TEOS, Ar and O_2 were 10, 50, and 10~100 sccm, respectively.

In TEOS-PECVD, Hα excitation line is a proof of the TEOS molecule dissociation [2]. In general, this intensity is proportional to the radical density in the region of constant electron temperature [3]. Assuming that Hα intensity is the density of precursor for deposition, its gradient of emission intensity indicates the radical flux to the substrate. N. Itabashi et al. showed the deposition rate is proportional to the density gradient of radicals SiH_3 near the substrate in RF silane plasma [4].

3 Results and Discussion

Figure 1 shows the relationship between the deposition rate of SiO_2 film and the gradient of Hα emission intensity to the substrate. The correlation coefficient between them was 0.87. This result indicates that the Hα gradient is proportional to deposition rate and can be one of indicators that predict the deposition rate by in-situ measurement. Results for other parameters will be reported in detail in the conference.

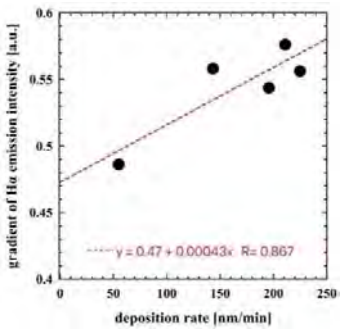

Fig. The relationship between deposition rate and gradient of emission intensity of Hα

Acknowledgements

This work was partly supported by JSPS KAKENHI (Grant No. JP20H00142), JSPS Core-to-Core Program (Grant No. JPJSCCA2019002) and collaborative research with KIOXIA corp..

References

[1] K. Kamataki *et al.*, AIP adv., **12**, 085220 (2022).
[2] M. A-. Firouzjah *et al.*, J. Non-Crist. Solids., **368**, 86 (2013).
[3] J. Tanaka *et al.,* J. Vac. Sci. & Technol. A, **25,** 2, 353 (2007).
[4] N. Itabashi *et al*., Jpn. J. Appl. Phys., **29**, 3, L505 (1990).

Challenges in obtaining uniform distribution of core shell Tin nanoparticles using dc magnetron sputtering plasma.

Munaswamy Murugesh[1] and Koichi Sasaki[1]

[1]*Division of Applied Quantum Science and Engineering, Hokkaido University, Sapporo, Japan*

Energy management is one of the critical areas of focus in the recent years. Current research findings are related to the phase changing materials development that are useful in thermal energy management. The key challenges include deposition on liquid droplets and its uniformness. DC magnetron sputtering plasma coupled with rf plasma techniques were employed to obtain core shell tin (Sn) particles. The diameters of the synthesized particles were in the order of 100 nm covered with the shell films (carbon). Combination of carbon and tin were considered based on the melting points, which are 3550 ºC and 231.9 ºC respectively. SEM, TEM and energy dispersive spectroscopy were used to characterize core shell particles.

1 Introduction

The energy management is a common interest in the recent years with increasing awareness over sustainable development goals. Particularly, with phase changing materials (PCM) for thermal storage have gained wide attention from recent decades [1]. Effective methods and technologies can actively contribute addressing the crises of limited reserves of naturally available fossil fuels and concerns over global warming/greenhouse gas emissions. Thermal energy storage can be achieved by cooling, heating, melting, solidifying, or vaporizing a material with the energy becoming available as heat when the process is reversed. Generally, they can be classified as latent heat thermal energy storage or sensible heat thermal storage [2]. Latent heat storage method is considered as one of the efficient methods of thermal energy storage; it relies on the storage material absorbing or releasing heat as it undergoes a solid to liquid, solid to solid or liquid to gas change or vice versa.

Among available technologies, plasma processing to generate core shell nanoparticles has its advantages in developing shell over melted liquid core material. In current investigations, rf plasma is used to obtain melted liquid tin droplets that are developed from sputtering using dc magnetron plasma under vacuum conditions. Especially the challenges in developing uniform core/shell of the particles are discussed.

2 Materials and Methods

The main steps in this process were sputtering of tin atoms (and its growth) using dc magnetron sputtering followed by heating and collection. A ring electrode, which was connected to an rf power supply at 13.56 MHz, was installed at the bottom of the vacuum chamber, and it was used for producing capacitively coupled rf plasma; used for storing and heating the particles. A positively biased electrode was placed inside the ring rf electrode, and it was used for collecting nanoparticles.

3 Results and Discussion

Main discussion of this findings are the challenges such as the porosity, uniform distribution of shell and core area of the particles. The core region is the melted Sn material covered by carbon in the shell area which is shown in figure 1.

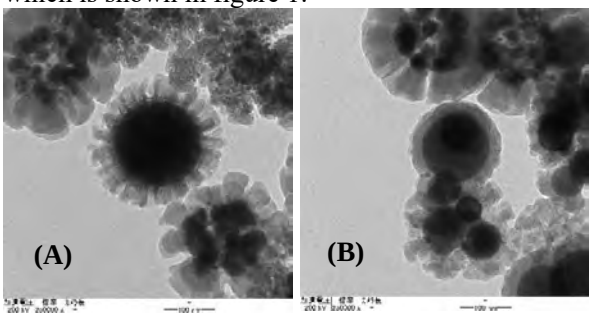

Figure 1. Porosity and non-uniform distribution can be seen in both (A) and (B) (TEM).

Further surface morphology can be observed from the SEM imaging data shown in figure 2. The uneven surface distribution can be observed across.

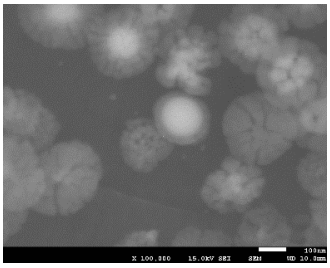

Figure 2. Surface morphology of particles (SEM)

4 Conclusions

From the spherical nature of the core area, material melting can be inferred. Uneven distribution challenge is observed across many discharge conditions, further longer evacuation for vacuum preparation will be tested in further investigations.

References

[1] C.Y. Zhao & G.H. Zhang, Review on micro-encapsulated PCMs: Fab, Char & Appls., Renwble & Sust. Engy. Revws, 15 (8), 3813-3832 (2011).

[2] Kinga. P and Krzysztof. P, Phase change materials for thermal energy storage, Prog. in Matl. Science, 65, 67-123 (2014).

Plasma processing of Al-doped zinc oxide thin films using powder targets

T. Ohshima[1], H. Kawasaki[1], Y. Hibino[1], T. Ihara[1], Y. Yagyu[1], T. Satake[1,2]

[1] *Dept. Electrical and Electronics Eng., National Institute of Technology, Sasebo College, Nagasaki, Japan*
[2] *Graduate Dept. Division of Applied Information Sciences, Sojo Univ., Kumamoto, Japan*

Aluminum-doped zinc oxide (AZO) thin films were prepared by sputter deposition using a mixed powder target of aluminum Oxide (Al_2O_3) and zinc oxide (ZnO). The bulk density of the powder target can be varied depending on the pressing pressure. AZO thin films were prepared using powder targets with different bulk densities ranging from 0.898 to 3.00 g/cm^3. The structural, electrical, and optical properties of the AZO thin films were examined, and the relationships between the target bulk density and film properties were investigated. X-ray diffraction measurements revealed c-axis ZnO (002) diffraction peaks. Hall effect measurements showed the carrier density and hole mobility increasing as the bulk density of the powder target increased. When the bulk density of powder is 3.00 g/cm^3, the AZO thin film showed the lowest resistivity of 1.35×10^{-3} Ω · cm. UV-visible spectroscopy measurements showed that the average transmittance in the visible light region exceeded 80% for the AZO thin films.

1 Introduction

The sputtering method is one of the most important thin film deposition technic, which has been put to practical use in a wide range of fields from research and development to semiconductors, automobiles, and optics. While high-density solid targets are generally used, we have proposed the sputtering method using powder targets [1]. In this paper, we fabricated Al-doped zinc oxide (AZO) thin films, a transparent conductive material, using mixed powder targets with different bulk densities, measured their structural, optical, and electrical properties, and investigated the effect of target density on film properties.

2 Experimental setup

The mixed powder target was prepared by rotating and mixing powders with ZnO:Al_2O_3=98:2 wt% in a V-shaped vessel. After the mixed powder was filled into the target holder, the pressing pressure of the press machine was varied to prepare the mixed powder targets with different densities. AZO thin films were prepared on Si(100) and sapphire substrates at room temperature, Ar 0.38 Pa, RF 100 W, and 60 min, using RF magnetron sputtering equipment. AZO thin films were characterized using X-ray diffract meter system, Hall effect measurement system, and UV-visible spectrophotometer.

3 Experimental Results

Figure 1 shows the relationship between the bulk density of the powder target and the thickness of the deposited AZO thin films as a function of pressing pressure of the powder. The bulk density of the powder target increases in proportion to the pressing pressure, and saturates above the pressing pressure of 30 kN. Agglomeration of powder targets occurs during the mixing process, and it is believed that the bulk density of agglomerated powders saturates even with increased pressure. The deposited AZO thin film also increased in thickness with increasing pressing pressure when the pressing pressure was small, and saturated in the film thickness when the pressing pressure exceeded a certain magnitude. Increasing the bulk density of the powder target flattens the surface of the target, reducing voids and increasing the number of particles ejected from the target, resulting in a larger film thickness.

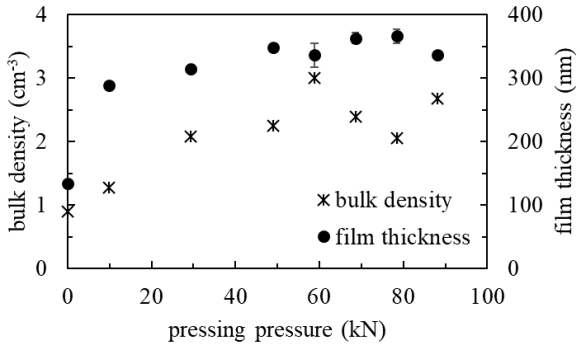

Fig.1 Dependence of the bulk density of the powder target and the film thickness of the deposited films on the pressing pressure.

Acknowledgments

This work was supported by JSPS KAKENHI Grant Number JP20K03921.

References

[1] T. Ohshima, T. Maeda, Y. Tanaka, H. Kawasaki, Y. Yagyu, T. Ihara and Y. Suda: J. Appl. Phys., **55**(1S), 01AA08 (2015).

Cold plasma systems for bioaerosol decontamination: comparison between a Rotating Dielectric Barrier Discharge plasma source and a commercial device

P. Isabelli[1], K. De Baerdemaeker[2], F. Devlieghere[2], M. Gherardi[1], R. Laurita[1,3]

[1]*Department of Industrial Engineering, Alma Mater Studiorum - University of Bologna, Bologna, Italy*
[2] *Research Unit Food Microbiology and Food Preservation, Department of Food Technology, Safety and Health. Ghent University, Ghent, Belgium*
[3]*Interdepartmental Centre for Industrial Research Health Sciences and Technologies, Alma Mater Studiorum - University of Bologna, Ozzano dell'Emilia, Italy*

The airborne transmission of pathogens is considered one of the most dangerous ways of spreading diseases such as health-acquired infections (HAIs) and, more recently, the spread of the SARS-CoV-2, especially indoors. This study presents a Rotating Dielectric Barrier Discharge (RDBD) plasma source to inactivate bioaerosol containing *Staphylococcus epidermidis*. The results show that the RDBD plasma source can achieve bacterial inactivation levels higher than 3.6 Log_{10} CFU, comparable to those obtained with a commercial device with similar ozone concentrations. Moreover, it is proven that the applied voltage does not affect bacterial inactivation when using comparable average discharge power and ozone concentrations.

1 Aim of the work

The spread of infections in indoor environments, mainly in healthcare, is a great issue with substantial social, health, and economic impacts. The most recent example is the spread of the SARS-CoV-2 virus, which has significantly affected people's lives, highlighting society's difficulties in containing the virus. The microorganisms transmission modes can differ, but airborne one is considered the primary mechanism linked to the diffusion of HAIs and SARS-CoV-2; indeed, micrometer droplets (<5 µm – droplet nuclei) containing pathogens can remain suspended in the air for a long time, and travel for long distances being dangerous if inhaled by people [1][2][3]. Several methods to decontaminate air from pathogens (e.g., filters, UV lamps, chemical or gas spray) are commonly employed indoors. However, the impressive number of infections during the pandemic and the consistently high number of HAIs show how much work is needed in the air quality field. Cold atmospheric plasmas (CAPs), thanks to their blend of bioactivate agents (electrons, ions, UV rays, and reactive oxygen and nitrogen species), represent a promising technology to contrast airborne transmission of pathogens and thus decontaminate the indoor air, reducing the risk of spreading HAIs or viruses such as SARS-CoV-2 [4][5]. The aim of this study is to develop a new system based on CAP technology to decontaminate the air of medium-small rooms from airborne pathogens. The development of a particular DBD source architecture, called Rotating DBD (RDBD) plasma source, is presented to treat air contaminated with *S. epidermidis* bioaerosol inside a test chamber. Its antimicrobial efficacy was evaluated under different operating conditions. The ozone concentration produced by the RDBD plasma source inside the chamber was monitored using optical absorption spectroscopy (OAS). The antimicrobial capacity and ozone production of the RDBD plasma source were compared with those of a commercial air purifier based on CAP (Jonix Cube device).

2 Results

Using different operating conditions, the RDBD plasma source exerts a logarithmic reduction more significant than 3.6. These results are comparable to those obtained with the Jonix Cube device but with an airflow rate of 3.5 times higher. The inactivation levels of *S. epidermidis* and corresponding ozone concentrations produced by the two devices inside the test chamber show that ozone is a key species in obtaining a high degree of bacterial inactivation. Moreover, the microbial inactivation results obtained by applying different operating conditions highlight that the applied voltage does not directly affect microbial inactivation.

3 Acknowledgments

The authors acknowledge the COST Action CA19110 (PlAgri) for their support.

References

[1] C.C. Wang et al.,373, (2021)
[2] A.S. Collins, Preventing Health Care-Associated Infections, Patient Safety and Quality: An Evidence-Based Handbook for Nurses (2008)
[3] N. van Doremalen *et al.*, N Engl J Med, 382, 1564-1567, (2020)
[4] A. Bisag et al., Plasma Process. Polym.,17, (2020)
[5] A. Bisag et al., Plasma Process. Polym.,19, (2022)

Unraveling surface effects for improving the germination of barley seeds: from drying to air plasma treatments

A. Perea-Brenes[1,2], A. Gómez-Ramírez[1,3], C. López-Santos[1,4], M. Oliva-Ramírez[1,3], R. Molina[5], J. Cotrino[1,3], J.L. García[2], M. Cantos[2], A. R. González-Elipe[1]

1 Nanotechnology on Surfaces and Plasma Laboratory, Institute of Materials Science of Seville (CSIC-US), Seville, Spain.

2 Departament of Plant Biotechnology, Institute of Natural Resources y Agrobiology of Seville (CSIC), Seville, Spain.

3 Departamento de Física Atómica, Molecular y Nuclear, Universidad de Sevilla, Seville, Spain.

4 Departamento de Física Aplicada I, Escuela Politécnica Superior, Universidad de Sevilla, Seville, Spain.

5 Department of Biological Chemistry, Plasma Chemistry Group, Institute of Advanced Chemistry of Catalonia (CSIC), Barcelona, Spain

1 General

The effects that plasma treatment achieves on seed germination are now well recognized. The surface of seeds becomes hydrophilic after the air plasma action, however this need not be directly related to an improvement in germination due to an increase in the water uptake capacity. [1] In this work, we present an analysis of the main factor involved in the germination of mature barley seeds subjected to atmospheric air plasma treatments and, for comparison, to a mild drying and a hydrogen peroxide (H_2O_2) treatments at ambient temperature. Short plasma treatment times were used to study the effects on germination, in petri dish and in substrate as well as on the surface contamination in *in vitro* conditions. Analysis of the water uptake has been carried out by different methodologies for the plasma treated seeds compared with dried ones: exposure to water vapor, immersion in liquid water and monitoring on a microbalance in presence of humid environment. Furthermore, the content of peroxo-type species incorporated in the seeds after their plasma treatment was evaluated in order to support the central hypothesis of this work: the fact that peroxo-type species can affect abscisic acid (ABA), an agent responsible for the seed dormancy and, consequently, in the germination rate. Chemical and morphological changes in the treated barley seeds were studied with techniques such as Scanning electron microscopy (SEM) or X-ray photoelectron spectroscopy (XPS). The results indicate an increase in germination rate and decrease in contamination level upon plasma treatment without a correlated increase in the water uptake capacity. By contrast, the formation of reactive oxygen and nitrogen species (ROS and RONS) can affect the ABA factor and enhance the germination rate of barley seeds (Figure 1).

Keywords: Air Plasma, Barley seed, Germination, Contamination, Water uptake, Abscisic acid, H_2O_2, RONS.

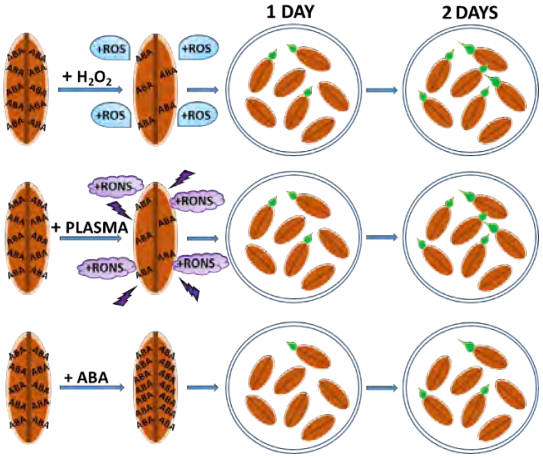

Figure 1: Scheme showing the effect of H_2O_2 and plasma treatments in the generation of RONS and the affectation of ABA as responsible for the acceleration of the germination rate. From left to right: the removal of ABA molecules after the incorporation of RONS species produce a decrease in the concentration of ABA within the seeds and the triggering of germination evidenced by an increase of the germination rate.

References:

[1] Randeniya, L.K., de Groot, G.J.J.B. (2015) Non-Thermal Plasma Treatment of Agricultural Seeds for Stimulation of Germination, Removal of Surface Contamination and Other Benefits: A Review, *Plasma Process. Polym.* 12, 608.

Fractal Dimension of cathode spots in a Vacuum Arc Thruster

E. Michaux[1], A.E. Vinci[1] and S. Mazouffre[1]

[1] *ICARE, CNRS, Orléans, France*

The fractal dimension of cathode spots occurring in the discharge of a high-current vacuum arc thruster (VAT) are determined according to the Minkowski-Bouligand method. Photographs taken during operation of a 30 W VAT allowed observation of spots distribution over the surface depending on the cathode material. A machine learning model as well as a heuristic analysis permit to highlight that work function, cohesive energy and ionization energy of the cathode material are the main driver in the magnitude of fractal dimension and total surface area covered by the spots.

1 Intro

Recent spacecraft propulsion technology for microsatellites rely on triggering an electrical discharge between two electrodes. Those systems, called Vacuum Arc Thrusters (VAT), ionize the cathode material, accelerate and eject it at high velocity, leading to thrust generation in the opposite direction. This technology presents inherent advantages regarding miniaturization, simplicity and reliability through the use of a solid metal propellant. In order to gain a more detailed insight into the formation of the arc, its dynamics and the subsequent plasma acceleration mechanism, probing in depth the physics of VATs and gathering data is needed. Such investigation is also necessary to propose more efficient solutions with longer lifetime able to meet the requirements of a wide range of space missions.

2 Experimental setup, methods and results

Experiments were conducted with the PJP thruster, a pulsed 30-W VAT developped by the french company COMAT. The thruster was equipped with a copper anode and various metallic cathode materials, allowing a maximum of 2 to 4 kA to flow during a discharge. Overall, for each pulse, a few J were released over 25 µs. The background pressure achieved during operation was about 10^{-6} mbar. A camera has been set outside the vacuum chamber, facing the thruster, permitting to photograph the plasma emission areas, also called cathode spots, in the course of the operation. The exposure time was set to 1 s so that all the light emitted during a pulse was captured by the camera sensor. Example of a photograph taken with a titanium cathode is presented in Figure 1.

Patterns in which the cathode spots organize turn out to be ramified, very luminous and present a fractal structure [1] that vary from one pulse to another. The fractal dimension of these patterns has been assessed with the Minkowski-Bouligand method. This dimension as well as the surface covered by the spots appear to significantly vary depending on the cathode material.

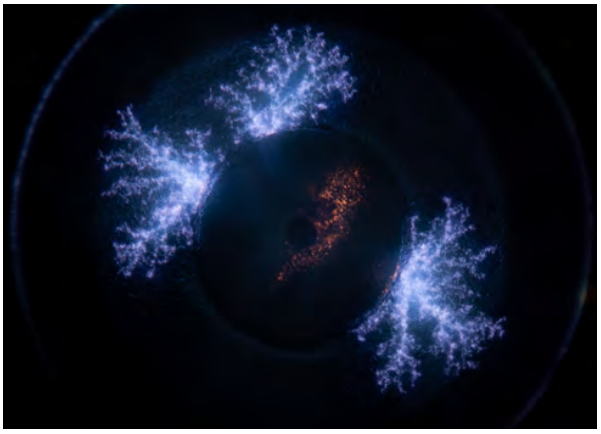

Figure 1: Photograph of spot distribution during a PJP discharge with a titanium cathode.

In order to determine a relation between the material properties and the fractal dimension D, an approach based on machine learning as well as a heuristic approach have been developed. These two analysis were performed on more than 400 images and 6 different materials, outlining that the cohesive energy, the ionization energy and the work function of the material are the main drivers in the change of D.

References

[1] Anders, A. The fractal nature of vacuum arc cathode spots. *IEEE Transactions on Plasma Science* **33**, 1456–1464 (2005).

Sensitivity of *Deinococcus radiophilus* and *Escherichia coli* to UVC radiation generated by a plasma lamp combined with phosphors

A. Baraze[1,2], C. Muja[1], T. Maho[1], F.P. Sainct[1], S. Allix[2] and Ph. Guillot[1]

[1] *DPHE Laboratory, INU J.F. Champollion, Univesity of Toulouse, Albi, France*
[2] *LabScience, Amboise, France*

1 Introduction

UV-C technology is one of established "no-touch" decontamination technologies that can be used to deal with maintaining clean surfaces. Historically, the germicidal UV-C lamp containing mercury emit a monochromatic emission at 254 nm but several other types of lamps such as excimer lamps can be used to obtain UV-C emissions [1]. In this study we use the emission of a Kr-Cl DBD lamp to excite phosphors that will generate a polychromatic UV-C emission (225 – 330 nm).

The aim of this study is to assess the sensitivity profiles of *D. radiophilus* and *E. coli* strains to the polychromatic UV-C exposure and to compare these profiles with their sensitivity to the monochromatic light (at 222 nm and 254 nm).

2 Experimental setup

In this work we have used a cylindrical Kr-Cl DBD lamp (Oliscié, Toulouse) producing an UV emission at 222 nm. The lamp was coupled with three different phosphors to obtain polychromatic UV-C emissions (figure 1). A Hg lamp producing a monochromatic UV emission at 254 nm was used for comparison.

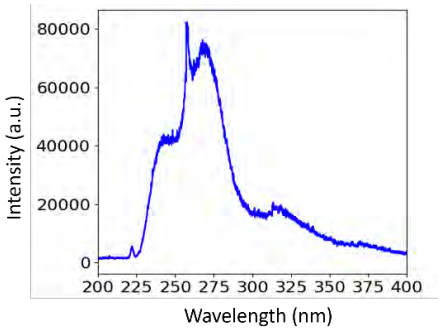

Figure 1. Emission spectra of the phosphors combined with the Kr-Cl DBD lamp

3 Physical characterisation of the setup

Optical emissions of the lamp and of each couple lamp – phosphor were assessed using an optical spectrometer (Princeton Instrument SpectraPro HRS-750). The irradiance was measured using an irradiance meter (Opsytec, Ettlingen).

4 Decontamination efficiency

E. coli K12 (ATCC 47076) and *D. radiophilus* (ATCC 27603) were inoculated separately on sterile coupons and dried in a laminar flow hood before exposure. After the UV treatment the coupons were transferred in maximum recovery media. The microorganisms' survival was assessed using the plate count method on Tryptic Soy Agar for *E. coli* (figure 2) and TGYM medium for *D. radiophilus*. Colony counting was made after incubation at 32°C for 72 hours for *D. radiophilus* and at 37° C for 24 hours for *E. coli*.

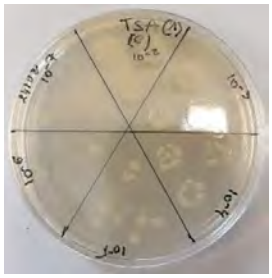

Figure 2. *E. coli* on TSA agar plate

In parallel the survival was also assessed using XTT method [2]. The generation of sub lethally injured cells was assessed by plating on selective media and by repair methods [3]. Finally, the degradation of DNA was examined by pulsed field gel electrophoresis.

References

[1] Wladyslaw Kowalski. Ultraviolet Germicidal Irradiation Handbook, Springer, (2009).
[2] Courti I. et al. Impact of Bacterial Growth Phase on Liquid Decontamination Efficiency Using Atmospheric Pressure Plasma **11**, 85-104 (2021).
[3] Wu VC. A review of microbial injury and recovery methods in food. Food Microbiol **25,** (2008).

Development of a novel plasma device for cancer treatment and irradiation effects on the hepatoblastoma-derived cell, Hep G2

Y. Yagyu[1], Y. Baba[2], T. Ohshima[3], Y. Hibino[1], K. Moriyama[1]
T. Satake[1], T. Ihara[1], H. Kawasaki[1] and N. Hayashi[2]

[1] *Dept. of Electrical and Electronic Engineering, National Institute of Tech. Sasebo College, Sasebo, Japan*
[2] *Dept. of Advanced Energy Science and Engineering, Kyushu Univ., Fukuoka, Japan*
[3] *Graduate School of Engineering, Nagasaki Univ., Nagasaki, Japan*

Low-temperature atmospheric pressure plasma irradiation of cancer cells is expected to be a novel minimally invasive cancer therapy. In this study, we developed a non-equilibrium atmospheric pressure plasma device aiming to establish in vivo cancer therapy method by separating the liquid and gas phases with porous membrane sheet. The characteristics of the plasma device and the effects of reactive species on hepatoblastoma-derived cells, Hep G2, were verified. The plasma device could easily generate plasma in the liquid phase. It is found that mainly due to reactive oxygen species through the porous membrane induced cell death of Hep G2.

1 Introduction

Low-temperature plasma irradiation of cancer cells is expected to be a novel minimally invasive cancer therapy [1, 2]. In this study, we have developed a plasma apparatus for the purpose of irradiating plasma in vivo by separating the liquid and gas phases. The verification of the characteristics of the plasma device and the effects of reactive species generated by a non-equilibrium atmospheric pressure plasma on hepatoblastoma-derived cell, Hep G2.

2 Methods

Hepatoblastoma-derived cell line, Hep G2 (JCRB1054), was used in this study. The Hep G2 cells were cultured in D-MEM with 10% fetal bovine serum (BioWest S.A.S) and penicillin-streptomycin solution (FUJIFILM Wako Pure Chemical Corp.) in the 5% CO_2 incubator set at 37°C . Hep G2 cells were adjusted to 1.0×10^5 cells/ml, placed in 96-well plates at 100µl each, and pre-cultured for 24h. The supernatant of the culture medium was removed and treated with a plasma device (Fig 1). The ambient gases were air, nitrogen, and oxygen, and the treatment time is from 0s to 60s. After plasma treatment, 100 µl of culture medium was added immediately, and the cells were incubated for 24h. The number of viable cells was measured using cell counting kit-8 reagent (Dojindo Laboratories Co., Ltd.). The absorbance was measured with an absorption microplate reader (MTP-320, Corona Electric Co., Ltd.).

3 Results and Discussion

The plasma device could easily provide active species generated by plasma even in the liquid phase. Death cells of Hep G2 cells tended to increase with plasma irradiation period in oxygen and air (Fig. 2). In the case of nitrogen gas, the cell viability was over 90%. The results suggest that cell death is induced by reactive oxygen species, and the reactive nitrogen species are not the main factor in cell death.

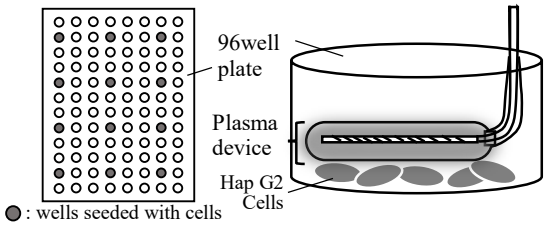

Fig.1. Experimental setup of plasma treatment

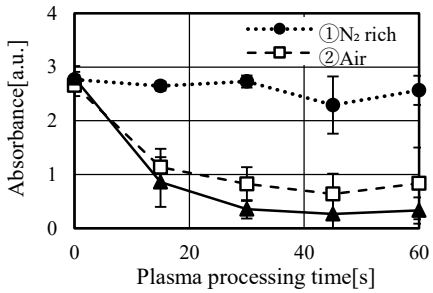

Fig .2. Relationship of viable cells and ambient gases

4 Conclusion

We developed a non-equilibrium plasma device with porous membrane sheet for separating the liquid and gas phases. It was suggested that reactive oxygen species through the porous membrane to Hep G2 cells is the main factor of inducing cell death.

References

[1] G. Fridman et al. Plasma Process. Polym., 5, 503 (2008)
[2] K. Sato et al. J. Clin. Biochem. Nutr., 65, 8 (2019)

Deactivation efficiency analysis of airborne microorganisms using a Dielectric Barrier Discharge (DBD) based plasma system

Ramavtar Jangra, Kiran Ahlawat and Ram Prakash

Department of Physics, Indian Institute of Technology Jodhpur, Jodhpur, India, 342030

In this study, the deactivation efficiency analysis of airborne microorganisms has been carried out using a self-made DBD based plasma system. The developed system produces negative ions predominantly dominated by hydroxyl radicals as well as positive ions in the environment similar to mother nature. The analysis is done for the reduction of total microbial counts (TMCs), total fungal counts (TFCs), and deactivation of *E. coli* bacteria and MS2 bacteriophage in an enclosed environment of sizes up to 1,000 ft^3. Much higher efficiencies for the deactivation of TMCs and TFCs are recorded (i.e., more than 99%) during continuous operation. Also, around 5 log reduction of the *E. coli* bacteria and MS2 bacteriophage is achieved in just 60 minutes of continuous operation of the device at optimized parameters and system has shown more than 99.999% efficiency in much shorter time.

1 Introduction

People spend the majority of their time (roughly 90%) indoors because most of the world's population lives in cities and expanding villages. Contrary to popular belief, indoor air pollution is far higher than outdoor air pollution[1]. Also, the newly emerged SARS-CoV-2, influenza virus can transmit through air[2]. Hence, deactivating harmful airborne microorganisms that exist in enclosed environments and are transmitted at longer distances need better strategy. Here, we report a self-made DBD plasma-based system, which deactivates airborne microorganisms quite effectively.

2 Experimental Setup

An experimental setup was established to analyse the electrical and operational performance of the developed DBD plasma system. A bipolar pulsed power supply is utilized to produce the plasma discharge. The DBD plasma discharge continuously generates the negative and positive charged ions, measured by an air ion counter. A portable ozone monitor, with a precision of 1 ppb, was used to measure the concertation of ozone produced. Air quality probes and toxic gas probes were used to measure the different parameters of air quality monitoring.

3 Results and Conclusion

The developed DBD based cold plasma system, successfully produces negative ions predominantly dominated by hydroxyl radicals and positive ions in the indoor environment with balanced concentration. The concentrations are such that they can produce local fields similar to the bond energy of the chemical bonds of the harmful pathogens in the environment for faster deactivation. Also, the generated positive and negative ions can instantaneously bond on the surface of substances such as bacteria, fungi, viruses, and allergens, becoming cold-plasma detergent ions which break down the proteins on the surface of such pathogens. The developed system is tested in the enclosed environment on numerous factors like reduction of TMCs, TFCs (see figure 1) and deactivation of *E. coli* and MS2 bacteriophage (see table 1). The ozone concentration and other air quality monitoring parameters are within the permissible limit.

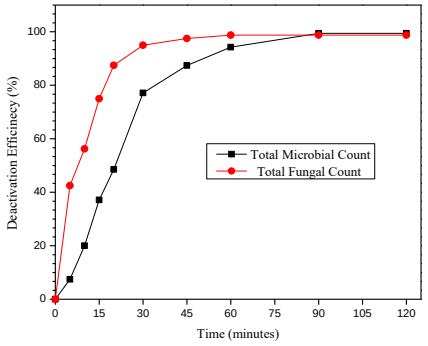

Figure 1: Reduction of TMCs and TFCs.

Table 1: Deactivation of *E. coli* and MS2 phage

Tested Contaminates	Initial Concentration	Final Concentration
E. coli bacteria	9.55×10^4 cfu	2 cfu (after 60 min)
MS2 Phage	1.40×10^5 pfu	1 pfu (after 30 min)

4 References

[1] J.M. Samet, Ann. Intern. Med. **116**, 175 (1992).

[2] K. Nissen, J. Krambrich, D. Akaberi, T. Hoffman, J. Ling, Å. Lundkvist, L. Svensson, and E. Salaneck, Sci. Rep. **10**, 1 (2020).

Acknowledgements

RJ and KA acknowledge UGC for providing fellowship during PhD program. RP acknowledges SERB for providing funding under project No. S/SERB/RP/20200082.

Nonthermal Plasma Interactions with Microplastics in a Polymer-Water Matrix

R.Z. Walker[1] and J.E. Foster[1]

[1] *Dept. Nuclear Engineering and Radiological Sciences, Univ. of Michigan, Ann Arbor, MI, United States*

The ecological damage associated with the accumulation of microplastics waste particularly in the oceans is a rapidly growing environmental problem. Nonthermal plasma treatment offers new recycling opportunities for plastics depolymerization, thus showing potential for addressing the plastics waste problem by augmenting either conventional methods or direct depolymerization. This work aims to review active research aimed at plasma-based depolymerization as well as report on recent in-house research aimed at depolymerization using direct plasma interaction with solid particles and plasma treatment of polymers in a liquid solution. Surface modifications inferred using FTIR, depolymerization products observed in OES, and liquid phase products determined using mass spectrometry are reported.

1 General

Plastic waste is a growing environmental concern, due largely to the low current recycling rates (<10%) coupled with increasing production. Plastic degradation in the environment is relatively slow (decades) and thus it accumulates in the environment. The additives added to plastics that make them more resistant to breakdown are toxic and thus as plastics degrade in the environment, contaminants leach out. Especially concerning is the proliferation of plastics in aqueous environments, as weathering driven by mechanical processes and UV from solar driven photochemical degradation leads to the formation of micro- and nanoplastics, which can be readily uptaken through the food chain. There is growing interest in waste “upcycling” (chemical recycling) where plastics are converted into either their monomer constituents or other high value products. Current methods of chemical recycling, such as pyrolysis, are still limited in that they are energy intensive and produce gaseous and solid waste products.

It is well known that nonthermal plasma surface treatment can modify polymer surfaces, in the nm to um depth range, to produce useful functional groups (e.g. making traditionally hydrophilic polymers hydrophobic)[1]. Depending on the plasma environment and polymer being modified, selectivity via the control of which functional groups are added is possible. It has also been observed that hotter nonthermal plasmas, such as an AC dielectric barrier discharge (DBD) reactor, are capable of complete depolymerization of polymers into useful solid, liquid, and gaseous phase products [2]. Therefore, nonthermal plasma offers a compelling approach to the plastics problem: both in terms of surface functionalization and complete depolymerization.

These nonthermal plasma in contact with water are capable of producing reactive oxygen and nitrogen species, UV light, and solvated electrons capable of functionalizing and depolymerizing plastic substrate in solution, including microplastics.

This work focuses on characterizing the functional groups and depolymerization processes observed for plasma treated polymers in solution, both as microplastics and water soluble polymers. Preliminary results, shown in Figure 1, demonstrated surface modifications of a polypropylene (PP) microplastic mixture with water treated with an AC plasma jet. These functional groups are similar to those seen previously in De Geyter [1] for a medium pressure air plasma DBD discharge. This work uses FTIR to observe polymer surface functional groups as well as determine products produced in the liquid phase. Plasma discharge properties and water chemistry are also tracked.

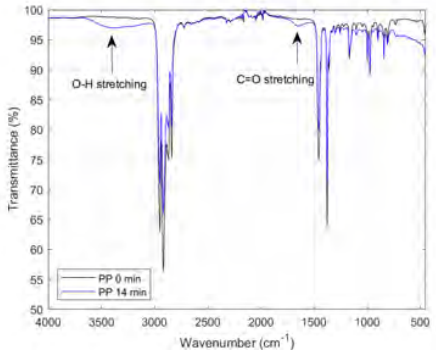

Figure 1. ATR-FTIR transmittance of PP samples treated by an AC plasma jet showing O-H and C=O stretching modifications of the polymer surface.

Acknowledgements

This work was supported by NSF GRFP, DOE: DE-EE0009945 and DE-SC0022189.

References

[1]De Geyter, N., Morent, R., & Leys, C. Surface and Interface Analysis **40**, 608-611 (2008).

[2]Yao, L., King, J., Wu, D. et. al. Nature Communications **13**, 885 (2022).

Combining diagnostics for characterizing antibacterial effect of a cold atmospheric plasma source

L. Zampieri[1], R. Agus[2], L. Ibba[2], C. Riccardi[1], I. Furno[2], M. Zuin[3], G. De Masi[3], L. Cordaro[3], R. Cavazzana[3] and E. Martines[1]

[1] *Università degli Studi di Milano-Bicocca, Dept. of Physics "G. Occhialini", Milano, Italy*
[2] *Ecole Polytechnique Fédérale de Lausanne (EPFL), Centre de Recherches en Physique des Plasmas, Lausanne, Switzerland*
[3] *Consorzio RFX, Padova, Italy*

In the characterisation of an atmospheric pressure plasma jet acting on a biological substrate, a synchronised multidisciplinary approach is needed; multiple diagnostics should be combined. Moreover, given the complexity of the system, it is of fundamental importance to keep constant all the external parameters which can affect the interaction. In this work the plasma, the treated liquid substrate and the biological effects are analysed using a fixed setup, obtaining a set of fully comparable data. The results shows clear trends in the reactive species and in the biological effects, which can be correlated to help the understanding of the involved reactions.

Following the large growth in plasma medicine of the last years, a wide landscape of different plasma sources is now available in the various research groups. Different layouts, power levels, application methods, gases and peculiar characteristics make each source unique. At the same time, a large variety of different diagnostics has been proposed to characterize the apparatus. The absence, however, of a standardized analysis protocol leads to important difficulties in comparing the various plasma sources; moreover, the different diagnostics are typically applied in very different experimental conditions, resulting in not easily correlatable data. As a results, it is hard to properly reconstruct the activated biochemical chain.

In the process of optimising the plasma sources, it is of fundamental importance to recognise which agents have the key role in triggering the aimed effects. It is therefore of interest to correlate physical parameters of the source with the production of reactive oxygen and nitrogen species and the biological consequences. A contribution to this project is here proposed using a helium pulsed plasma jet, originally developed in Consorzio RFX in Padova (Italy) [1], and in collaboration with EPFL in Lausanne (Switzerland).

A variety of diagnostics has been applied on the same setup, which involves the treatment for 10 minutes of 6 ml of deionized water. The jet has been electrically characterized, describing the voltage and current waveforms and the power as a function of the different tunable parameters. In-situ Fourier Transform Infrared spectroscopy (FTIR) is performed to observe the variations in the production of ozone and nitrous species in the gas phase between the nozzle and the water surface. Using photochemical surveys, the presence of peroxides, nitrates, nitrites and ozone in the water after the treatment has been described. Finally, the killing of *E. coli* suspended in water has been described using CFU counts. Particular attention is paid to use a unique experimental setup to perform all the measurements, allowing for a straightforward comparison of the results.

The correlations between the measurements from the different diagnostics, combined on the same source in the same experimental setup, shows promising results in contributing to outline the pathway which leads from plasma to disinfection. Following them, the tunable parameters of the source can be connected to the final biological effects, allowing for an effective optimization of the jet.

References

[1] De Masi, G. *et al.* Plasma coagulation controller: A low-power atmospheric plasma source for accelerated blood coagulation. *Plasma Medicine* **8** (2018).

Discharge space expansion in single-phase atmospheric pressure gliding arc discharge

O. V. Prysiazhna[1], K. Yamauchi[2], F. Mitsugi[3], M. Yamazato[4], H. Kawasaki[5], M. Shiratani[6], H. D. Stryczewska[7], T. Baba[8] and S. Aoqui[1]

[1]*Dept. of Computer and Information Sciences, Sojo Univ., Japan*
[2]*Graduate School of Eng., Sojo Univ., Japan*
[3]*Faculty of Advanced Science and Technology, Kumamoto Univ. Japan*
[4] *Faculty of Eng., Univ. of the Ryukyus, Japan*
[5] *Dept. of Electrical and Electronic Eng., National Institute of Tech., Sasebo College, Japan*
[6]*Graduate School of Information Science and Electrical Eng., Kyushu Univ., Japan*
[7] *Dept. of Electrical Eng. and Electrotechnology, Lublin Univ. of Tech., Poland*
[8] *HyBridge Co.,Ltd., Japan*

Gliding arc discharge (GAD) is expected to have a wide range of applications as a non-thermal equilibrium atmospheric pressure discharge with a very simple configuration. However, the narrow discharge space and non-stationarity are problems. In this study, we developed a device using twisted electrodes that can expand the discharge space without losing the simplicity of GAD.

1 Introduction

Gliding Arc Discharge (GAD), discovered by A. Czernichowski, is one of the newest types of atmospheric discharges. GAD has unique characteristics compared to other Types of atmospheric discharges. One of the main characteristics is that the discharge power is not a high-current discharge close to thermal equilibrium like ICP or DC arc, nor is it a high-voltage, low-current discharge like DBD or corona discharge. In other words, the neutral gas temperature during discharge is sufficiently low. Atmospheric pressure discharge with these characteristics is rarely found. When considering how to apply this GAD, the possibility of large-scale processing in an agricultural field can be seen in terms of the wide range of power adjustment. On the other hand, GAD is a non-thermal equilibrium and non-steady state discharge, and the principle of intermittent discharge characteristics is a severe limitation in its application. In other words, GAD is completely different from ordinary AC arc in that the discharge path in the discharge space between electrodes is arc extinguishing for a long time, and most of the introduced gas passes through during the arc extinguishing process. However, several innovations have been proposed to efficiently supply the introduced gas to the discharge space. As an example, we have developed a GAD system with a multiphase power supply. We have developed a GAD system that uses 3-, 6-, and 12-phase power supplies, which considerably improves the problem of non-steady state. However, 6-phase and 12-phase power supplies are special and inhibit the simplicity of GAD. As another improvement, the tornado type, in which gas is introduced from the tangential direction of the reaction tube, was also proposed. In this study, we developed a twisted-electrode GAD that can suppress the bare flow of gas as much as possible while taking advantage of the simplicity that is a characteristic of the original GAD.

2 Experiment

The electrodes were prepared at 180° and 360° twist angle. Fig. 1 shows the electrode structure for the 180° case. Fig. 2 shows the discharge measurement system. The discharge path was measured using the high-speed camera Phantom V1210.

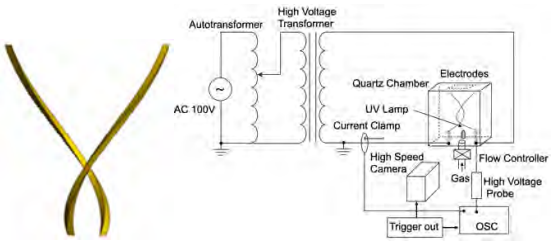

Fig. 1 Electrode structure Fig.2 Equipment Configuration

The discharge paths taken at 1000 fps from different angles of 90° degrees are shown in Fig. 3. The discharge path was rising while twisting.

Fig. 3 Discharge path captured at low speed 1000 fps